Preface

The extensive research devoted to the physics of compound semiconductors and semimetals during the past decade has led to a more complete understanding of the physics of solids in general. This progress was made possible by significant advances in material preparation techniques. The availability of a large number of compounds with a wide variety of different and often unique properties enabled the investigators not only to discover new phenomena but to select optimum materials for definitive experimental and theoretical work.

In a field growing at such a rapid rate, a sequence of books which will provide an integrated treatment of the experimental techniques and theoretical developments is a necessity. An important requirement is that the books contain not only the essence of the published literature, but also a considerable amount of new material. The highly specialized nature of each topic makes it imperative that each chapter be written by an authority. For this reason the editors have obtained contributions from ten to fifteen scientists to provide each volume with the required detail and completeness. Much of the information presented relates to basic contributions in the solid state field which will be of permanent value. While this sequence of volumes is primarily a reference work covering related major topics, the volumes will also be useful in graduate courses.

Because of the important contributions which have resulted from studies of the III–V compounds, the first few volumes of this series are devoted to the physics of these materials: Volume 1 reviews key features of the III–V compounds, with special emphasis on band structure, magnetic field phenomena, and plasma effects. In Volume 2, the emphasis is on physical properties, thermal phenomena, magnetic resonances, and photoelectric effects, as well as radiative recombination and stimulated emission. This volume is concerned with optical properties, including lattice effects, intrinsic absorption, free carrier phenomena, and photoelectronic effects. Volume 4 will include thermodynamic properties, phase diagrams, diffusion, hardness, and phenomena in solid solutions as well as the effects of strong electric fields, hydrostatic pressure, nuclear irradiation, large impurity concentrations, and nonuniformity of impurity distributions on the electrical and other properties of III–V compounds.

The editors are indebted to the many contributors and their employers who made this series possible. They wish to express their appreciation to the Bell and Howell Company and the Battelle Memorial Institute for providing the facilities and the environment necessary for such an endeavor. Thanks are also due to the U.S. Air Force Offices of Scientific Research and Aerospace Research, whose support has enabled the editors to study many features of compound semiconductors. The assistance of Rosalind Drum, Martha Karl, Eleanor Quinan, and Inez Wheldon in handling the numerous details concerning the manuscripts and proofs is gratefully acknowledged. Finally, the editors wish to thank their wives for their patience and understanding.

May, 1967

R. K. WILLARDSON
ALBERT C. BEER

List of Contributors

Numbers in parentheses indicate the pages on which the authors' contributions begin.

H. E. BENNETT, *Michelson Laboratory, China Lake, California* (499)

RICHARD H. BUBE, *Department of Materials Science, Stanford University, Stanford, California* (461)

MANUEL CARDONA, *Brown University, Providence, Rhode Island* (125)

JOHN O. DIMMOCK, *Lincoln Laboratory, Massachusetts Institute of Technology, Lexington, Massachusetts* (259)

H. EHRENREICH, *Division of Engineering and Applied Physics, Harvard University, Cambridge, Massachusetts* (93)

H. Y. FAN, *Purdue University, Lafayette, Indiana* (405)

MARVIN HASS, *Code 6471, U.S. Naval Research Laboratory, Semiconductor Branch, Solid State Division, Washington, D.C.* (3)

EARNEST J. JOHNSON, *Lincoln Laboratory, Massachusetts Institute of Technology, Lexington, Massachusetts* (153)

B. LAX, *National Magnet Laboratory, Massachusetts Institute of Technology, Cambridge, Massachusetts* (321)

J. G. MAVROIDES, *Lincoln Laboratory, Massachusetts Institute of Technology, Lexington, Massachusetts* (321)

EDWARD D. PALIK, *U.S. Naval Research Laboratory, Washington, D.C.* (421)

H. R. PHILIPP, *General Electric Research Laboratory, Schenectady, New York* (93)

R. F. POTTER, *U.S. Naval Ordnance Laboratory, Corona, California* (71)

B. O. SERAPHIN, *Michelson Laboratory, China Lake, California* (499)

WILLIAM G. SPITZER, *Electrical Engineering Department, University of Southern California, Los Angeles, California* (17)

D. L. STIERWALT, *U.S. Naval Ordnance Laboratory, Corona, California* (71)

GEORGE B. WRIGHT, *Lincoln Laboratory, Massachusetts Institute of Technology, Lexington, Massachusetts* (421)

COPYRIGHT © 1967, BY ACADEMIC PRESS, INC.
ALL RIGHTS RESERVED
NO PART OF THIS BOOK MAY BE REPRODUCED IN ANY FORM, BY PHOTOSTAT, MICROFILM, RETRIEVAL SYSTEM, OR ANY OTHER MEANS, WITHOUT WRITTEN PERMISSION FROM THE PUBLISHERS.

ACADEMIC PRESS, INC.
111 Fifth Avenue, New York, New York 10003

United Kingdom Edition published by
ACADEMIC PRESS, INC. (LONDON) LTD.
24/28 Oval Road, London NW1 7DD

LIBRARY OF CONGRESS CATALOG CARD NUMBER: 65-26048

PRINTED IN THE UNITED STATES OF AMERICA
80 81 82 9 8 7 6 5 4

SEMICONDUCTORS AND SEMIMETALS

Edited by R. K. WILLARDSON
BELL AND HOWELL RESEARCH LABORATORIES
PASADENA, CALIFORNIA

ALBERT C. BEER
BATTELLE MEMORIAL INSTITUTE
COLUMBUS LABORATORIES
COLUMBUS, OHIO

VOLUME 3

Optical Properties of III–V Compounds

1967



ACADEMIC PRESS New York San Francisco London
A Subsidiary of Harcourt Brace Jovanovich, Publishers

CHAPTER 1

Lattice Reflection

Marvin Hass

I. INTRODUCTION 3
II. EXPERIMENTAL TECHNIQUES 3
III. ANALYSIS OF RESULTS 4
IV. EXPERIMENTAL INVESTIGATIONS 8
V. EFFECTIVE IONIC CHARGE 13

I. Introduction

The principal information that can be obtained from a study of the infrared lattice-reflection spectra of the III–V compound semiconductors are the frequencies of the transverse and longitudinal optical modes for long-wavelength vibrations.[1] Aside from their value in lattice-vibration investigations, these particular frequencies are of special interest in that they can be used to calculate an effective charge parameter, which is one quantitative measure of the polar character of the compound. The degree of polar character can be related to the mobility of free carriers in certain temperature ranges.

In this chapter the experimental techniques and analysis will be discussed first. This will be followed by a review of the experimental data of the lattice-reflection spectra of the III–V compound semiconductors and derived quantities. Finally, some comments on the effective charge parameter and its various definitions will be presented.

II. Experimental Techniques

The experimental measurement of the reflectivity is straightforward, and the principal requirement is the availability of reasonably pure single-crystal or polycrystalline material capable of having a face polished with a minimum surface area of about 3 mm × 8 mm (and possibly smaller). The samples should preferably be pure in order to avoid complications due

[1] The propagation vector **k** of long-wavelength modes approaches zero, and in this section only long-wavelength modes will be discussed unless otherwise stated.

to free-carrier reflection discussed in Chapter 9 of this volume. Such specimens are easily prepared for the more common III–V compounds. In the case where the materials are hygroscopic or susceptible to oxidation (e.g., AlSb), surface contamination may impede the measurements. Even in non-hygroscopic materials, surface effects due to polishing may be observed in the reflection spectrum.

The spectral region of interest for III–V compounds extends from about 15 to 60 microns. Measurements out to about 45 microns can be carried out on small prism spectrometers and out to somewhat beyond 200 microns with small grating spectrometers. Commerical double-beam infrared spectrometers for this spectral range have become available.

There are several methods that can be employed to determine the optical constants from the measured reflectivity. The approach most commonly used in the III–V compounds involves measurement of the reflection spectrum at near-normal incidence over a wide spectral range, followed by an attempt to fit the observed data by classical dispersion formulas accounting for the lattice absorption. It will be seen that the general details of the infrared lattice-reflection spectra of the III–V compounds can be accounted for fairly well in this manner, using only a single classical dispersion oscillator. Alternatively, a direct calculation of the optical constants can be obtained by a Kramers–Krönig analysis of the data. Here it is more essential that the absolute reflectivity be known accurately. This approach has more generally been used when the reflection spectrum is more complex, as in the ultraviolet region discussed in Chapter 5. More detailed descriptions of the various methods can be found in the literature.[2,3]

III. Analysis of Results

The reflectivity R of radiation incident normally on a semi-infinite slab of an absorbing material is related to the complex index of refraction $\bar{n} = n - ik$ by

$$R = \left|\frac{\bar{n} - 1}{\bar{n} + 1}\right|^2 = \frac{(n-1)^2 + k^2}{(n+1)^2 + k^2}, \tag{1}$$

where n is the ordinary index of refraction and k is the extinction coefficient. For purposes of comparison with a model, it is convenient to express the optical constants n and k in terms of the real and imaginary parts of the complex index of refraction $\bar{\varepsilon} = \varepsilon_1 - i\varepsilon_2$. In analogy with the situation in a nonabsorbing medium where $n = \varepsilon^{1/2}$ (both n and ε real), in an absorbing

[2] T. S. Moss, "Optical Properties of Semiconductors," Chap 2. Butterworth, London and Washington, D.C., 1959.

[3] W. G. Spitzer and D. A. Kleinman, *Phys. Rev.* **121**, 1324 (1961).

medium the same relation can be used with both $\bar{n}$ and $\bar{\varepsilon}$ complex. Consequently, on squaring it can be seen that

$$n^2 - k^2 = \varepsilon_1 \tag{2a}$$

$$2nk = \varepsilon_2 . \tag{2b}$$

An alternative approach involves expressing n and k in terms of a susceptibility χ and conductivity σ instead of ε_1 and ε_2 as is done in Chapter 9 of this volume in discussing free-carrier reflection.

In order to deduce a relation between the complex dielectric constant $\bar{\varepsilon}(\omega)$ and the long-wavelength lattice frequencies it is convenient to employ a model involving one or more damped harmonic oscillators. In the case of the III–V compound semiconductors the experimental data, to a good approximation, can be expressed in terms of the parameters of only one oscillator. However, this situation is not true in general for other materials, e.g., the alkali halides. The relations can be developed following a general macroscopic approach given by Born and Huang.[4] For a diatomic cubic crystal that is large compared to the wavelength of electromagnetic radiation of the frequency of the optical modes, the following macroscopic equations can be written in the harmonic approximation:

$$\ddot{\mathbf{w}} = b_{11}\mathbf{w} + b_{12}\mathbf{E} - \gamma\dot{\mathbf{w}}, \tag{3a}$$

$$\mathbf{P} = b_{21}\mathbf{w} + b_{22}\mathbf{E}. \tag{3b}$$

Here $\mathbf{w}$ represents a generalized relative displacement of the positive ions with respect to the negative ions during a long-wavelength optical vibration and is given by $(\overline{M}N)^{1/2}(\mathbf{u}_+ - \mathbf{u}_-)$ where $\mathbf{u}_+$ and $\mathbf{u}_-$ are the displacements of the positive and negative ions from their equilibrium position, $\overline{M}$ is the reduced mass equal to $M_+M_-/(M_+ + M_-)$, and N is the number of ion pairs per unit volume. The vectors $\mathbf{P}$ and $\mathbf{E}$ are the dielectric polarization and electric field in the medium appearing in Maxwell's equations. The phenomenological coefficient b_{11} corresponds to a force constant that will introduce a characteristic resonant frequency ω_0. It can be shown for ions in tetrahedral or higher symmetry sites that $b_{12} = b_{21}$, and this term is essentially proportional to a mean effective ionic charge. The significance of this charge will be discussed in Part V. The factor γ is a damping coefficient introduced in an ad hoc manner. By assuming solutions periodic in the frequency ω with $\mathbf{w} = \mathbf{w}_0 e^{i\omega t}$, $\mathbf{E} = \mathbf{E}_0 e^{i\omega t}$, $\mathbf{P} = \mathbf{P}_0 e^{i\omega t}$ and remembering that the dielectric displacement $\mathbf{D}$ is related to $\bar{\varepsilon}(\omega)$ by

$$\mathbf{D} = \mathbf{E} + 4\pi\mathbf{P} = \bar{\varepsilon}\mathbf{E}, \tag{4}$$

[4] K. Huang, *Proc. Roy. Soc.* (*London*) **A208**, 352 (1951); M. Born and K. Huang, "Dynamical Theory of Crystal Lattices," p. 82. Oxford Univ. Press, London and New York, 1954.

it can be shown in a straightforward manner that the real and imaginary parts of $\bar{\varepsilon}(\omega)$ are given by

$$\varepsilon_1(\omega) = n^2 - k^2 = \varepsilon_\infty + \frac{(\varepsilon_0 - \varepsilon_\infty)[1 - (\omega/\omega_0)^2]}{[1 - (\omega/\omega_0)^2]^2 + (\omega/\omega_0)^2(\gamma/\omega_0)^2}, \tag{5a}$$

$$\varepsilon_2(\omega) = 2nk = \frac{(\varepsilon_0 - \varepsilon_\infty)(\gamma/\omega_0)(\omega/\omega_0)}{[1 - (\omega/\omega_0)^2]^2 + (\omega/\omega_0)^2(\gamma/\omega_0)^2}, \tag{5b}$$

where the characteristic frequency ω_0 can be associated with the transverse optical frequency for long-wavelength phonons, ε_0 is the static or low-frequency dielectric constant measured at a frequency low compared to ω_0, and ε_∞ is the high-frequency dielectric constant measured at a frequency high compared to ω_0. In this approximation the contributions arising from free-carrier and bound-carrier absorption are not considered. Usually the experimental conditions can be chosen so that this approximation can be fulfilled.[5–5b]

The real and imaginary parts of $\bar{\varepsilon}(\omega)$ defined by Eqs. (5) are shown in Fig. 1 as a function of the reduced frequency ω/ω_0. It will be noted that there is a maximum in $\varepsilon_2(\omega)$ very close to ω_0. The reflectivity corresponding to the various values of the damping parameter is also shown in Fig. 1. The dominant feature of this reflection spectrum is a region of strong reflection extending from ω_0 up to a frequency ω_1 given by

$$(\omega_1/\omega_0)^2 = \varepsilon_0/\varepsilon_\infty . \tag{6}$$

It is possible to show that ω_1 corresponds to a longitudinal frequency for long-wavelength phonons; relation (6) was first demonstrated by Lyddane *et al.*[6]

The problem then reduces to a question of fitting the experimental data in terms of the parameters ω_0, ω_1, ε_0, ε_∞, and γ. The first four of these are not independent, being related by Eq. (6). Often the value of ε_∞ can be obtained from index-of-refraction data in the appropriate high-frequency region. In principle, ε_0 could also be obtained directly. However, free-carrier dispersion at low frequencies prevents use of standard dielectric-constant techniques, and the best values of ε_0 are generally obtained by fitting reflection spectra. In choosing the best fit to the data, use is made of

[5] The case of combined free-carrier and lattice reflection involves a more complicated analysis, which will not be discussed here. Experimental data and analysis for this case have been carried out for InSb by R. B. Sanderson, *J. Phys. Chem. Solids* **26**, 803 (1965).

[5a] Unpublished results for InSb have been obtained by R. Geick.

[5b] The interaction of plasmons with longitudinal branch phonons in GaAs is revealed quite well in the Raman results of A. Mooradian and G. B. Wright, *Phys. Rev. Letters* **16**, 999 (1966).

[6] R. H. Lyddane, R. G. Sachs, and E. Teller, *Phys. Rev.* **59**, 673 (1941).

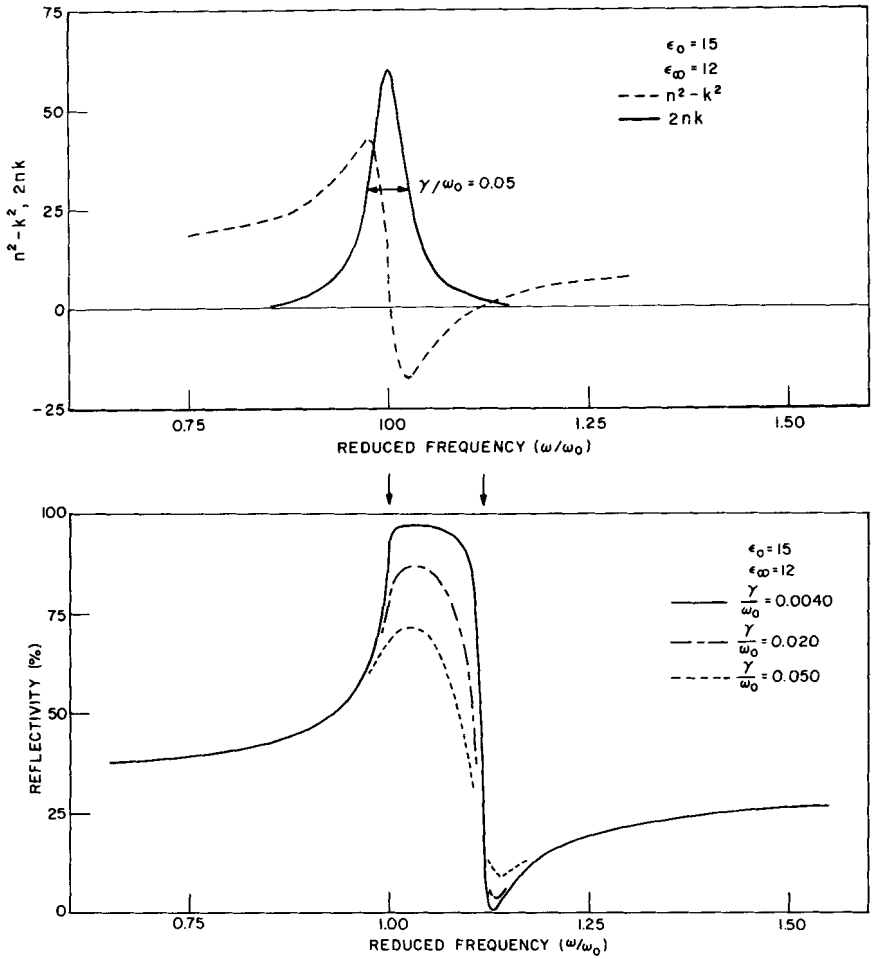


FIG. 1. (top) Calculated real ($n^2 - k^2$) and imaginary ($2nk$) parts of the complex dielectric constant for a single classical dispersion oscillator as a function of the reduced frequency. (bottom) Calculated reflectivity for a single classical dispersion oscillator for various values of the reduced damping constant as a function of the reduced frequency. The arrows at the top of the chart indicate the position of the transverse optical (ω_0) and longitudinal optical (ω_l) frequencies for long-wavelength vibrations.

the fact that the reflectivity is high between ω_0 and ω_l. The evaluation of the best parameters is facilitated by use of calculations carried out on an electronic computer. However, fairly good values can often be estimated by visual inspection of the data.

The expressions for the optical constants deduced in this manner can also be used to analyze the transmission spectrum under certain conditions.

The maximum in $\varepsilon_2(\omega)$ is very close to ω_0, and this corresponds to a strong absorption band. Such strong absorption bands near ω_0 can also be observed in the transmission spectra or reflection spectra of thin layers. If such measurements are carried out at oblique incidence, then ω_1 can also be revealed.

IV. Experimental Investigations

The existence of a reflection spectrum of a III–V compound characteristic of polar cystals was first reported by Spitzer and Fan and by Yoshinaga and Oetjen for InSb.[7] The room-temperature spectra of relatively pure material showed an essentially temperature-independent region of high reflectivity attributed to the polar lattice vibrations, and a region of high reflectivity at lower frequencies that moved to still lower frequencies as the temperature (and resulting carrier concentration) was decreased. The temperature-dependent region is attributed to free-carrier reflection, which is discussed in Chapter 9 of this volume. Studies on the compounds InAs, InP, GaAs, GaSb, and AlSb by Picus *et al.*[8] indicated a similar reflection spectrum, presumably due to lattice vibrations. The compounds InSb, InAs, GaAs, and GaSb were studied at low temperature and at higher resolution by Hass and Henvis,[9,10] and these data were subjected to a classical dispersion analysis to deduce ω_0 and ω_1. The room-temperature lattice-reflection spectrum for GaP has been reported and analyzed by Kleinman and Spitzer,[11] for AlSb by Turner and Reese,[12] for GaAs by Iwasa *et al.*,[13] and for BN by Gielisse *et al.*[14] Furthermore, ω_0 and ω_1 can also be determined by studying the single-phonon infrared transmission or reflection spectrum of thin layers; such measurements have been carried out for GaAs by Iwasa *et al.*[13] and for InSb by Wagner.[15] Infrared investigations of the lattice frequencies of the alloy systems $GaAs_ySb_{1-y}$ and $GaAs_yP_{1-y}$ have also been

[7] W. G. Spitzer and H. Y. Fan, *Phys. Rev.* **99**, 1893 (1955); H. Yoshinaga and R. A. Oetjen, *Phys. Rev.* **101**, 526 (1956).

[8] G. S. Picus, E. Burstein, B. W. Henvis, and M. Hass, *J. Phys. Chem. Solids* **8**, 282 (1959).

[9] M. Hass and B. W. Henvis, *J. Phys. Chem. Solids* **23**, 1099 (1962).

[10] M. Hass, unpublished measurements and analysis.

[11] D. A. Kleinman and W. G. Spitzer, *Phys. Rev.* **118**, 110 (1960).

[12] W. J. Turner and W. E. Reese, *Phys. Rev.* **127**, 126 (1962).

[13] S. Iwasa, I. Balslev, and E. Burstein, *in* "Physics of Semiconductors" (Proc. 7th Intern. Conf.), p. 1077. Dunod, Paris and Academic Press, New York, 1964.

[14] P. J. Gielisse, S. S. Mitra, J. N. Plendl, R. C. Griffis, L. C. Mansur, R. Marshall, and E. A. Pascoe, *Phys. Rev.* (to be published).

[15] V. Wagner, Thesis, University of Freiburg, Germany, 1965.

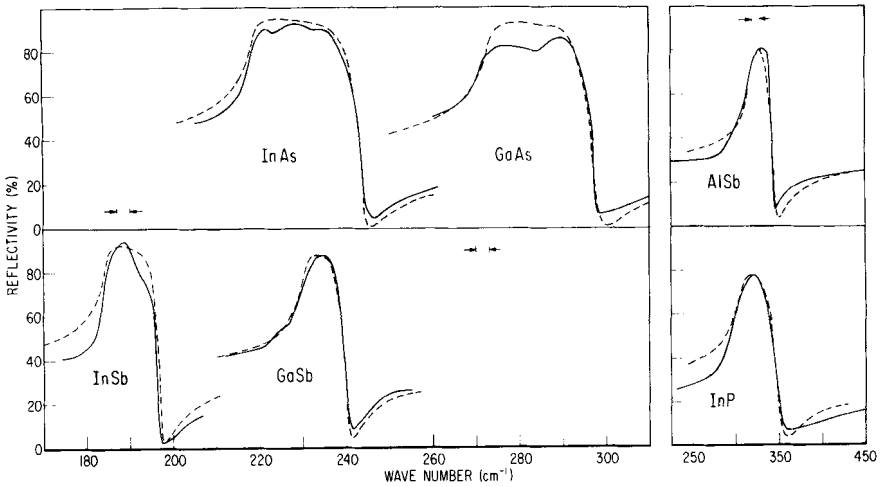


FIG. 2. Lattice reflection spectra of various III–V compound semiconductors. The solid line is experimental; the dashed line is the calculated fit for a single classical dispersion oscillator. The samples of InSb, InAs, GaAs, and GaSb were measured at liquid-helium temperature, whereas AlSb and InP were measured at room temperature. (After Hass and Henvis.[9])

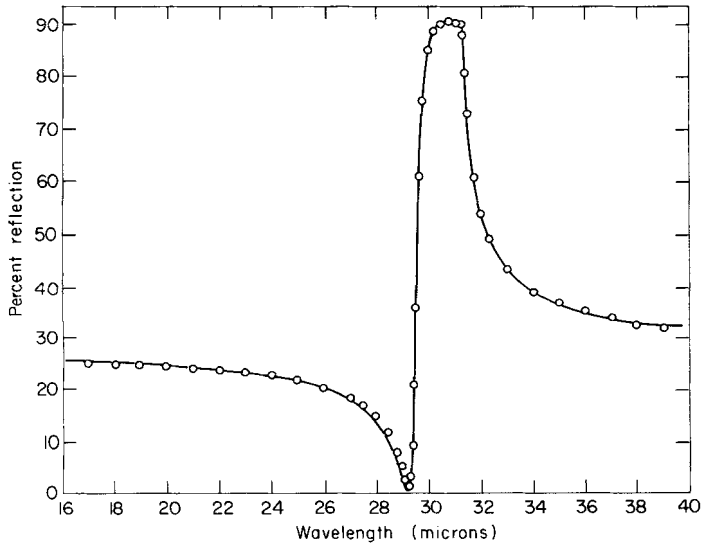


FIG. 3. Lattice-reflection spectrum of AlSb. Data are shown by points, and the calculated fit for a single classical dispersion oscillator by the solid line. (After Turner and Reese.[12])

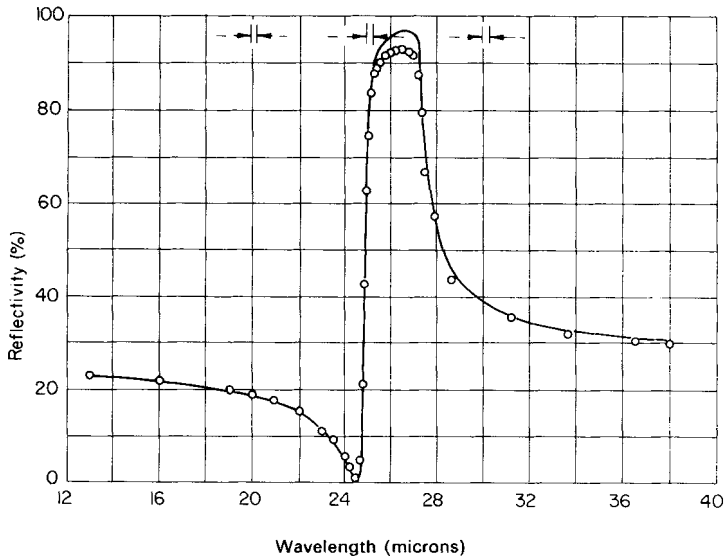


FIG. 4. Lattice reflection spectrum of GaP. Data are shown by points, and the calculated fit for a single classical dispersion oscillator by the solid line. (After Kleinman and Spitzer.[11])

reported.[15a] Absorption corresponding to ω_0 for BP is also believed to have been observed in transmission.[16] In all of the compounds except InSb, the carrier concentrations were sufficiently low that free-carrier reflection at room temperature can be neglected.

The lattice-reflection spectra for these compounds are shown in Figs. 2–4, along with the reflection spectra calculated by fitting the data to a single dispersion oscillator. It can be seen by comparison of the calculated and experimental curves that satisfactory results can be obtained using only a single dispersion oscillator. This is in marked contrast to the situation for the alkali halides, where use of only one oscillator is not adequate. The small discrepancy from perfect agreement in the III–V compounds may be due in part or whole to surface effects. It has been observed in the case of GaP[11] that the maximum reflectivity can be increased by etching the surface.

The results of the analysis yield the best values of $\bar{\nu}_0$, $\bar{\nu}_1$, and γ, where $\bar{\nu} = \omega/2\pi c$. Although the approximate values can be estimated by inspection

[15a] R. F. Potter and D. L. Stierwalt, in "Physics of Semiconductors" (Proc. 7th Intern. Conf.), p. 1111. Dunod, Paris and Academic Press, New York, 1964; H. W. Verleur and A. S. Barker, Jr., *Phys. Rev.* **149**, 715 (1966); Y. S. Chen, W. Shockley, and G. L. Pearson, *Phys. Rev.* **151**, 648 (1966).

[16] B. Stone and D. Hill, *Phys. Rev. Letters* **4**, 282 (1960).

TABLE I

TRANSVERSE AND LONGITUDINAL FREQUENCIES FOR LONG-WAVELENGTH PHONONS

Compound	Reference	Type of measurement	Temperature	$\bar{\nu}_0$ (cm^{-1})	$\bar{\nu}_1$ (cm^{-1})	γ/ω_0 [$\omega_0 = 2\pi c\bar{\nu}_0$]
InSb	9	Reflection	Helium	184.7 ± 3	197.2 ± 2	<0.01
—	5	Reflection	100°K	183.0	193.3	0.007
—	5	Reflection	300°K	179.1	190.4	0.016
—	5a	Reflection	300°K	180.2 ± 0.5	191.3	≤0.015
—	15	Transmission	300°K	180.2 ± 0.1	189.2	0.024 ± 0.002
InAs	9	Reflection	Helium	218.9 ± 3	243.3 ± 2	<0.01
InP	10	Reflection	Room	307.2 ± 3	348.5 ± 2	~0.01
—	22a	Raman	Room	303.7 ± 0.3	345.0 ± 0.3	—
—	22a	Raman	Helium	308.2 ± 0.3	349.5 ± 0.3	—
GaSb	9	Reflection	Helium	230.5 ± 3	240.3 ± 2	<0.01
GaAs	9	Reflection	Helium	273.3 ± 3	297.3 ± 2	<0.01
—	13	Transmission	Helium	272.4 ± 0.5	294.2 ± 0.5	—
—	13	Transmission	296°K	268.2 ± 0.5	290.5 ± 0.5	0.007
—	13	Reflection	296°K	268.2 ± 0.5	291.5 ± 0.5	0.007
—	18	Neutron	296°K	267 ± 3	285 ± 6	—
—	22a	Raman	Room	268.6 ± 0.3	291.9 ± 0.3	—
	22a	Raman	Helium	273.1 ± 0.3	296.4 ± 0.3	—
GaP	11	Reflection	300°K	366.3 ± 0.7	401.9 ± 0.7	0.003 ± 0.0005
—	22a	Raman	Room	367.3 ± 1	403.0 ± 0.5	—
—	22a	Raman	200°C	359.3 ± 1	397.0 ± 0.5	—
—	22a	Raman	Helium	365.6 ± 1	403.0 ± 0.5	—
—	22	Raman	20°K	366	402	—
AlSb	12	Reflection	300°K	318.8 ± 0.5	339.6 ± 0.5	0.0059 ± 0.0005
—	22a	Raman	Room	318.9 ± 0.5	339.9 ± 0.5	—
—	22a	Raman	Helium	323.4 ± 0.5	344.4 ± 0.5	—
BP	16	Transmission	Room	826	—	—
BP	14	Reflection	Room	820	835	—
BN	14	Reflection	Room	1065	1340	—

of the data, the exact values have been arrived at with the aid of electronic computers. The best results are shown in Table I. The frequencies $\bar{\nu}_0$ and $\bar{\nu}_1$ can be deduced fairly well. However, it is sometimes difficult to establish a good value of γ because this parameter depends upon an accurate measurement of the maximum reflectivity.

In an ideal crystal, γ/ω_0 would be very small. In a real crystal, the major contribution to γ/ω_0 is generally attributed to mechanical anharmonicity. In the case of the alkali halides, where anharmonicity is expected to be greater from other evidence, the values of γ/ω_0 are an order of magnitude higher[17] than in the III–V compounds that have been measured. In addition

[17] G. O. Jones, D. H. Martin, P. A. Mawer, and C. H. Perry, *Proc. Roy. Soc.* (*London*) **A261**, 10 (1961).

to the fundamental absorption, which can be well described by a single classical oscillator for the III–V compound semiconductors, there are also weaker absorption bands at other frequencies not described by this analysis. However, when these bands are relatively weak compared to the fundamental absorption, they will not be revealed in the reflection spectrum, except in special cases. The weaker bands are easily seen in the transmission spectrum of thick sections; these are discussed in detail in Chapter 2 of this volume.

It is of some interest to compare the reflection method for obtaining the transverse and longitudinal frequencies with other methods. The frequencies obtained from single-phonon infrared transmission and inelastic neutron scattering[18] are also shown in Table I. Fairly accurate indications of the frequencies can be obtained also by critical-point analysis of the multiphonon transitions as revealed by infrared transmission[19] or spectral emittance.[20] In addition, tunneling[21] and photoconductivity[21a] measurements are sensitive to the value of the longitudinal frequency. Measurements of the first-order Raman spectrum using a laser source for excitation appear

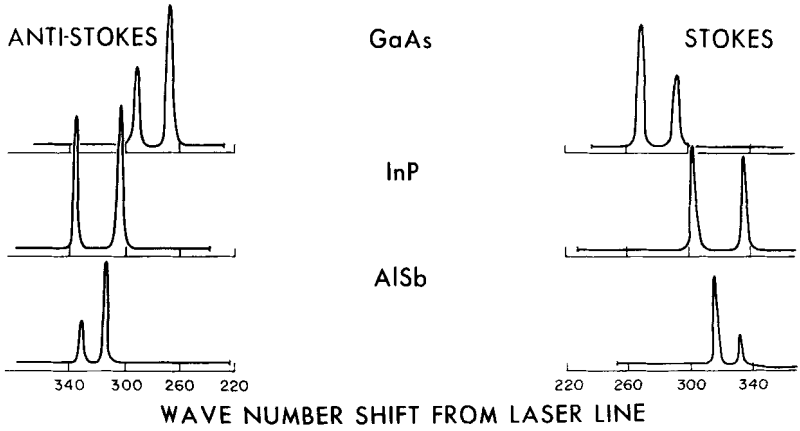


FIG 5. Raman spectra of GaAs, InP, and AlSb at room temperature. (After Mooradian and Wright.[22a])

[18] G. Dolling and J. L. T. Waugh *in* "Lattice Dynamics" (R. F. Wallis, ed.), p. 19. Macmillan (Pergamon), New York, 1965.

[19] W. G. Spitzer, "Multiphonon Lattice Absorption," Chapter 2 of this volume; F. A. Johnson, *Progr. Semicond.* **9**, 179 (1965).

[20] D. L. Stierwalt and R. F. Potter, "Emittance Studies," Chapter 4 of this volume.

[21] R. N. Hall and J. H. Racette, *J. Appl. Phys.* **32**, 2078S (1961).

[21a] W. Engeler, H. Levinstein, and C. Stannard, Jr., *Phys. Rev. Letters* **7**, 62 (1961).

to give quite accurate values of the transverse and longitudinal frequencies.[22,22a] Such measurements can be undertaken for crystals whose symmetry is such as to allow a first-order Raman effect and where a suitable source of exciting radiation is available in a spectral region in which the crystal is sufficiently transparent. The first III–V compound to be studied in this manner was GaP.[22] The compounds GaAs, InP, and AlSb, in addition to GaP, have been reported by Mooradian and Wright.[22a] Some of their results are shown in Fig. 5. The Raman spectra have the advantage of not requiring any extensive analysis as definite bands corresponding to the desired frequencies are observed.

V. Effective Ionic Charge

The degree of polar character in an ionic crystal can be defined in a number of ways.[23] One convenient approach that has been employed for ionic crystals is based on the concept of an effective ionic charge e^*, which can be defined from a classical treatment of the dielectric polarization due to lattice vibrations. This effective charge enters into the macroscopic phenomenological equations (3) in the terms for $b_{12} = b_{21}$. This can be seen more explicitly in the following way: In the case of a long-wavelength transverse (t) mode, the internal electric field $\mathbf{E}$ defined in Eq. (3b) vanishes, so that

$$\mathbf{P}_T = b_{21}\mathbf{w}_t = \left[\left(\frac{\varepsilon_0 - \varepsilon_\infty}{4\pi}\right)^{1/2} \omega_0 \left(\frac{\overline{M}}{N}\right)^{1/2}\right](\mathbf{u}_{t+} - \mathbf{u}_{t-})N = Ne_B^*(\mathbf{u}_{t+} - \mathbf{u}_{t-}) \tag{7}$$

in which use is made of the relation $b_{12} = b_{21} = (\varepsilon_0 - \varepsilon_\infty/4\pi)^{1/2}\omega_0$, which arises in the derivation of Eq. (5) given by Born and Huang.[4] The term in the square brackets in Eq. (7) can be set equal to an effective charge denoted as e_B^* (for Born) so that the polarization can be expressed as a product of a mean charge and a displacement.

Similarly, for a long-wavelength longitudinal (l) mode, $\mathbf{D} = \mathbf{E}_l + 4\pi\mathbf{P}_l = 0$ so that

$$\mathbf{E}_l = -4\pi\mathbf{P}_l = -4\pi(b_{21}\mathbf{w}_l + b_{22}\mathbf{E}_l) = -4\pi b_{21}\mathbf{w}_l/(1 + 4\pi b_{22}),$$
$$\mathbf{E}_l = -4\pi\left[\left(\frac{\varepsilon_0 - \varepsilon_\infty}{4\pi}\right)^{1/2} \frac{\omega_0}{\varepsilon_\infty} \left(\frac{\overline{M}}{N}\right)^{1/2}\right](\mathbf{u}_{l+} - \mathbf{u}_{l-})N = -4\pi Ne_C^*(\mathbf{u}_{l+} - \mathbf{u}_{l-}), \tag{8}$$

[22] M. V. Hobden and J. P. Russell, *Phys. Letters* **13**, 39 (1964); J. P. Russell, *J. Physique* **26**, 620 (1965).

[22a] A. Mooradian and G. B. Wright, *Solid State Commun.* **4**, 431 (1966).

[23] The theory of dielectric polarization and the effective charge has been discussed in greater detail by F. Stern, *Solid State Phys.* **15**, 300 (1963); and by E. Burstein *in* "Phonons and Phonon Interactions" (T. A. Bak, ed.), p. 276. W. A. Benjamin, New York, 1964.

in which use is made of the relation $b_{22} = (\varepsilon_\infty - 1)/4\pi$. The quantity in the square brackets is denoted as e_C^* (after Callen) in analogy to e_B^*. An effective charge relation of this type was first derived by Lyddane *et al.*[6] and later by Callen[24] in a different way. The relation (8) indicates that an electric field is associated with a long-wavelength longitudinal mode, and the intensity of this field can be calculated from a knowledge of the charge e_C^*. This field can interact with free carriers, and in certain temperature ranges this interaction dominates the various contributions to the mobility.[25] The values of e_C^* and e_B^* are shown in Table II.

TABLE II

DIELECTRIC CONSTANTS AND EFFECTIVE CHARGES

Compound	Reference	Dielectric constants		Effective charge		
		ε_∞ High frequency	ε_0 Low frequency	e_C^*/e	e_S^*/e	e_B^*/e
InSb	9	15.68[a]	17.88[b]	0.16	0.42	2.5
InAs	9	11.8[c] ± 0.1	14.55[c] ± 0.3	0.22	0.56	2.6
InP	10	9.61[a]	12.37[b]	0.26	0.66	2.5
GaSb	9	14.44[a]	15.69[b]	0.13	0.33	1.8
GaAs	13	11.10	13.13[b,d]	0.20	0.51	2.2
GaP	11	8.457 ± 0.2	10.182[b] ± 0.2	0.24	0.58	2.0
AlSb	12	9.880 ± 0.2	11.212[b]	0.19	0.48	1.9
BN	14	4.5	7.1	0.56	1.14	2.5

[a] Determined from index-of-refraction data collected in Ref. 2, p. 224. Error is of the order of tenths of a unit.

[b] Usually $\varepsilon_0 - \varepsilon_\infty$ is reported and can often be established to hundredths of a unit. Absolute error in ε_0 is of the order of tenths of a unit. Low-temperature values are given when available.

[c] O. G. Lorimor and W. G. Spitzer, *J. Appl. Phys.* **36**, 1841 (1965).

[d] Direct measurement on semi-insulating GaAs gives $\varepsilon_0 = 12.53 \pm 0.26$ according to K. G. Hambleton, C. Hilsum, and B. R. Holeman, *Proc. Phys. Soc. (London)* **77**, 1147 (1961).

The effective charges e_B^* and e_C^* can also be termed the macroscopic transverse and longitudinal charges, respectively. The macroscopic nature stems from the fact that the macroscopic electric field is involved in the derivation. In the microscopic treatment it is necessary to consider the effective electric field acting on an ion. For sites of tetrahedral and higher symmetry, the effective field E_{eff} is given by

$$\mathbf{E}_{eff} = \mathbf{E} + 4\pi\Gamma\mathbf{P}/3, \tag{9}$$

[24] H. B. Callen, *Phys. Rev.* **76**, 1394 (1949).

[25] H. Ehrenreich, *J. Phys. Chem. Solids* **2**, 131 (1957).

in which Γ is a constant that can be set equal to unity for nonoverlapping ions. This assumption is believed to hold fairly well for typically ionic crystals. With the aid of Eq. (9) and the microscopic equations of motion and dielectric polarization, the well-known Szigeti expression for a microscopic effective charge can be obtained,[26,27] provided $\Gamma = 1$:

$$\frac{e_S^*}{e} = \left(\frac{\varepsilon_0 - \varepsilon_\infty}{4\pi}\right)^{1/2}\left(\frac{\bar{M}}{N}\right)^{1/2}\left(\frac{3\omega_0}{\varepsilon_\infty + 2}\right). \tag{10}$$

(This is often alternatively expressed as a distortion parameter that is defined as e_S^*/Ze, where Z is an assumed formal charge of the ions.) The value of e_S^*/e for typically ionic compounds such as the alkali halides is close to unity, which is expected for singly charged ions. This suggests that the assumptions involved in the derivation of e_S^*/e for the alkali halides and similar compounds are fulfilled. On the other hand, in the case of the III–V compound semiconductors, the binding is believed to involve a large amount of covalent character because of the similarity in properties to the group-IV semiconductors. As a result, the assumptions involved in the derivation of Eq. (10) may not be fulfilled. As mentioned above in the derivation of Eq. (10), it is assumed that the Lorentz polarization factor Γ can be set equal to unity. The validity of this assumption in the case of the III–V compounds has been questioned by Brodsky and Burstein,[28] who pointed out that the valence-electron wave functions of the III–V compounds can be regarded as extended in space, rather than localized as in typically ionic compounds. Consequently, Γ can be less than unity. In the limiting case of setting $\Gamma = 0$, the expression analogous to e_S^* is numerically equal to e_B^*. The values of e_B^* are several times higher than e_S^*, as shown in Table II. Some calculations of Γ for various electron distributions carried out by Guertin and Stern[29] show this effect in a more quantitative way. Some experimental evidence supporting the conjecture of Brodsky and Burstein has been presented.[30] However, additional evidence on this point would be desirable.

Another complication lies in the concept that there are several different mechanisms contributing to a microscopic effective charge such as that defined by Eq. (10). In typically ionic crystals the major contribution to

[26] B. Szigeti, *Trans. Faraday Soc.* **45**, 155 (1949).

[27] M. Born and K. Huang, "Dynamical Theory of Crystal Lattices," p. 112. Oxford Univ. Press, London and New York, 1954.

[28] M. H. Brodsky and E. Burstein, *Bull. Am. Phys. Soc.* 7, 214 (1962). See also E. Burstein, Ref. 23.

[29] R. F. Guertin and R. Stern, *Phys. Rev.* **134**, A427 (1964).

[30] D. Gill and N. Bloembergen, *Phys. Rev.* **129**, 2398 (1963).

e_S* can be regarded as arising from charged ions. Thus, for the monovalent alkali halides, e_S* is about 0.7 to 1.0e. Here the deviations from an exact multiple of the unit electronic charge are small, but not negligible. In the case of more covalently bonded crystals, it is possible that the factors causing the deviation are larger. Consequently, caution should be exercised in discussing the physical significance of e_S* for the III–V compounds.[31]

While being aware of these difficulties, it is nevertheless interesting to compare the effective charges given in Table II with those obtained by other methods. On the basis of common ideas of chemical bonding, it is usual to consider the limiting cases of "ionic" and "covalent" bonding in which the former implies a charge configuration of $A^{3+}B^{3-}$ (A is the group-III element) and the latter implies $A^{-}B^{+}$.[32] If the electronic configuration is assumed to be similar to the group-IV element semiconductors, then a large degree of covalent character is expected, resulting in a small and possibly negative charge on the group-III atom. The data for e_S* are in accord with this view, although the sign of the charge on the atoms cannot be established from the infrared measurements. Other measurements, such as electron distributions from X-ray scattering piezoelectric constants, and magnetic resonance, appear to indicate similar results.[32] However, there are difficulties in relating these other measurements to an effective charge as well. Further experimental and theoretical investigations may help to provide additional insight into the relation among these various measures of ionic character.

[31] W. Cochran, *Nature* **191**, 60 (1961).

[32] C. Hilsum *in* "Physics of Semiconductors" (Proc. 7th Intern. Conf.), p. 1127. Dunod, Paris and Academic Press, New York, 1964; C. Hilsum *in* "Semiconductors and Semimetals" (R. K. Willardson and A. C. Beer, eds.), Vol. 1, Chap. 1. Academic Press, New York, 1966.

CHAPTER 2

Multiphonon Lattice Absorption

*William G. Spitzer**

I. INTRODUCTION 17
II. LATTICE ABSORPTION IN SEMICONDUCTORS 18
1. *Optical Absorption* 18
2. *Lattice Absorption* 19
III. MEASUREMENTS AND DATA 31
3. *Silicon* 31
4. *Germanium* 35
5. *Diamond* 36
6. *Silicon Carbide* 38
7. *Germanium–Silicon Alloys* 41
8. *Gallium Arsenide* 43
9. *Gallium Phosphide* 48
10. *Gallium Antimonide* 49
11. *Indium Arsenide* 51
12. *Indium Antimonide* 52
13. *Indium Phosphide* 56
14. *Aluminum Antimonide* 56
15. *Cadmium Sulfide (Wurtzite)* 57
16. *Zinc Sulfide (Wurtzite and Zinc Blende)* 61
17. *Zinc Selenide (Wurtzite)* 61
IV. CRITICAL-POINT ANALYSIS 62

I. Introduction

In recent years there has been considerable activity concerned with the measurement of the infrared properties of crystals. Some of this effort has been directed towards utilizing the measurements of optical absorption by the lattice to gain information concerning the phonon spectrum of the material. Along with the use of slow-neutron scattering experiments to deduce the phonon spectrum and with the availability of theoretical models, such as the shell model,[1] which give reasonable agreement with neutron work, the infrared methods are an integral part of an over-all study in phonon spectroscopy.

* Supported by the Technical Advisory Committee of the Joint Services Electronics Program.

[1] W. Cochran, *Advan. Phys.* **9**, 387 (1960); also see Ref. 3.

Stimulation has been provided by the measurement of a large number of electrical and optical effects that depend upon processes involving phonon participation. The semiconductors, including the III–V compounds, have proved to be very fruitful materials in many of these investigations, and it may be anticipated that optical studies will continue to provide basic information.

In the present discussion it will be assumed that the reader has available the chapter[1a] on the theory of lattice dynamics and is familiar with the chapter immediately preceding this one on the infrared reflection spectra of III–V compounds. Part II will discuss phonon branches, temperature dependence of lattice absorption, conservation laws, multiphonon absorption mechanisms, selection rules, analysis of data, phonon systematics, and the experimental method. Part III will contain a discussion of data, analysis, and phonon energies where available, for a number of materials.

Although the present purpose is to review the work on III–V compounds, the group-IV elements and II–VI compounds are so similar that some of them have also been included. Indeed, the original work in the detailed analysis of multiphonon absorption processes in semiconductors, which has served as a basis for much of that which has followed, was the work of F. A. Johnson[1b] for silicon. Part IV will discuss the most recent attempts to analyze the detailed structure of the absorption curves with the aid of selection rules governing the matrix elements for optical absorption. This analysis, referred to as "critical-point analysis of the infrared spectrum," yields energy values for the phonon branches at specific points in the Brillouin zone. This discussion will be curtailed, since much of the work done in this area is preliminary and has not, at the time of this writing, been published.

II. Lattice Absorption in Semiconductors

1. Optical Absorption

Optical absorption in semiconductors can be related to a variety of different mechanisms. Photon absorption with electronic transitions from the valence band to states in the conduction band can take place if the photon energy $h\nu \geqslant E_g$, where E_g is the minimum energy between the valence and conduction bands. For the materials of interest in the present case, $0.17 \lesssim E_g \lesssim 6$ eV. This absorption is determined by the energy-band structure of the material and hence is characteristic of that material.

The photon energy for Mott-type exciton absorption is close to that for band-to-band absorption—i.e., $h\nu \gtrsim E_g - E_B$, where E_B is the binding energy of the hole-electron pair which, for these materials, is small compared

[1a] To be published in a future volume of this series (see D. A. Kleinman).

[1b] F. A. Johnson, *Proc. Phys. Soc.* (*London*) **73**, 265 (1959).

to E_g. Phonons will be of concern in these processes if the transitions are indirect, i.e., if the electron crystal momentum $\hbar k$ between the initial and final states changes by more than the photon momentum. In the present cases, where the primary interest is in lattice absorption, the measurements are restricted by the above processes to $h\nu < E_g$. In general this restriction is not a serious one because the photon energies of interest in all cases are much less than E_g.

Free-carrier absorption involves transitions of "free" electrons or holes between states in the same band (intraband absorption) or states in different bands (interband absorption). The intraband absorption generally has a spectral dependence of the form ν^{-p}, where $1.5 \lesssim p \lesssim 3.5$. This absorption depends upon the free-carrier concentration and generally decreases with decreasing carrier concentration. It is therefore possible, at least in principle, to reduce the absorption from free carriers by improving purity or by compensation until this absorption is small compared to that which we wish to measure. It is also possible to obtain absorption bands associated with the presence of impurities or defects. These bands will be discussed later in this section.

The remaining type of absorption commonly observed in semiconductors is that due to the lattice—that is, the interaction of the radiation with the vibrational motion of the crystal lattice. Experimentally, this type of absorption can manifest itself in two spectral regions, distinguished from one another principally by the magnitude of the absorption. For those materials of interest here that are compounds there is a region of intense optical absorption in the infrared. Because of the high absorption, transmission measurements are difficult, and the reflectivity is often measured. In this region the reflectivity shows the well-known residual-ray (or reststrahlen) behavior discussed in Chapter 3. The elemental diamond-type semiconductors do not have this region of intense absorption. However, all semiconductors show a number of weaker absorption bands characteristic of the material and independent of impurity and carrier concentrations. Because these bands are weaker, they have little effect on the reflectivity and are amenable to study by the use of conventional transmission measurements. For the diatomic crystals these bands have been investigated primarily for $E_g < h\nu < h\nu_1$, where ν_1 is the frequency of the residual-ray absorption band. It is the transmission measurement and interpretation of these lattice absorption bands that will be of primary interest in this section.

2. Lattice Absorption

a. Phonon Branch

The diamond and zinc blende structures have two atoms per primitive cell, and therefore there are six branches in the vibrational spectrum.

Usually frequency vs. wave-vector plots are given along certain symmetry directions, and the branches are usually classed as transverse or longitudinal and acoustical or optical depending upon whether the long-wavelength modes have polarizations transverse to or along the wave vector $\mathbf{q}$ and whether for these modes the two atoms (or ions) of the cell vibrate in or out of phase with one another. Therefore, the branches may be characterized as two TO (transverse optical), and one LO (longitudinal optical), two TA (transverse acoustical), and one LA (longitudinal acoustical). When $\mathbf{q} \to 0$, the acoustical modes reduce to rigid translations of the lattice, and hence the frequencies $\omega(\mathbf{q}) \to 0$. For the diamond structure the optical modes become degenerate near $\mathbf{q} = 0$, whereas for a zinc blende crystal this degeneracy between the LO and the TO modes is lifted. If the longitudinal and transverse optical frequencies near $\mathbf{q} = 0$ are ω_l and ω_t, respectively, then they are related by the Lyddane–Sachs–Teller[2] expression

$$\frac{\omega_l}{\omega_t} = \left(\frac{\varepsilon_0}{\varepsilon_\infty}\right)^{1/2}, \tag{1}$$

where ε_∞ and ε_0 are the limiting values of the dielectric constant on the high- and low-frequency sides of the residual-ray band, respectively. For the diamond and zinc blende structures the two TO branches and the two TA branches are each degenerate in the [100] and [111] directions. In addition the LO and LA branches in the diamond structure are degenerate

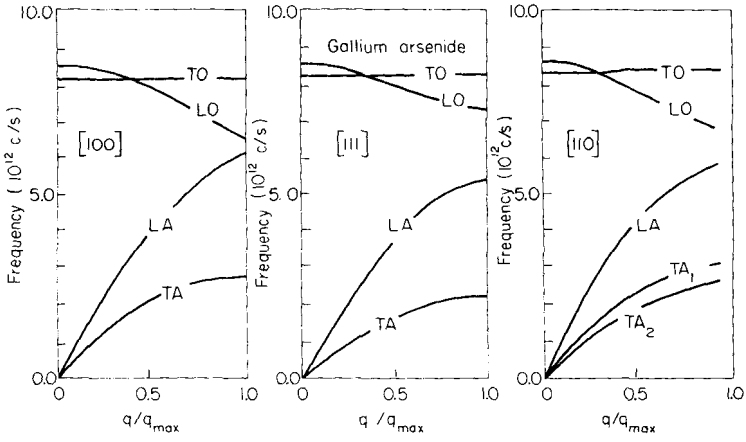


FIG. 1. The calculated phonon dispersion curves for GaAs. (After Johnson and Cochran.[3])

[2] R. H. Lyddane, R. G. Sachs, and E. Teller, *Phys. Rev.* **59**, 673 (1941).

at the zone edge in the [100] direction. Examples of curves calculated[3] for the [100], [111], and [110] directions for gallium arsenide are shown in Fig. 1.

b. Temperature Dependence and Conservation Laws

Lattice absorption is a process in which there is absorption of energy from the radiation field by the lattice. The net probability of photon absorption will be proportional to the probability of photon absorption with emission of a phonon of energy $\hbar\omega(\mathbf{q}_i)$less that of emission of a photon with phonon absorption. The first term is proportional to $[1 + n(\mathbf{q}_i)]$ and the second to $n(\mathbf{q}_i)$, where $n(\mathbf{q}_i)$ is $[\exp(\hbar\omega(\mathbf{q}_i)/kT) - 1]^{-1}$. Full specification of $n(\mathbf{q}_i)$ requires a knowledge of $\omega(\mathbf{q}_i)$ and hence the phonon branch. Where processes involve the emission and absorption of more than one phonon, each of the above terms becomes the product of probabilities. Thus, if two phonons are involved the net probability of photon absorption is proportional to

$$\text{Case I,} \qquad [1 + n(\mathbf{q}_1)][1 + n(\mathbf{q}_2)] - n(\mathbf{q}_1)n(\mathbf{q}_2) \tag{2}$$

or

$$\text{Case II,} \qquad [1 + n(\mathbf{q}_1)]n(\mathbf{q}_2) - n(\mathbf{q}_1)[1 + n(\mathbf{q}_2)], \tag{3}$$

depending upon whether the photon absorption is with emission of two phonons (Case I) or with emission of one phonon and the absorption of another (Case II). The extension to three phonons is obvious and gives

$$[1 + n(\mathbf{q}_1)][1 + n(\mathbf{q}_2)][1 + n(\mathbf{q}_3)] - n(\mathbf{q}_1)n(\mathbf{q}_2)n(\mathbf{q}_3), \tag{4}$$

$$[1 + n(\mathbf{q}_1)][1 + n(\mathbf{q}_2)]n(\mathbf{q}_3) - n(\mathbf{q}_1)n(\mathbf{q}_2)[1 + n(\mathbf{q}_3)], \tag{5}$$

or

$$[1 + n(\mathbf{q}_1)]n(\mathbf{q}_2)n(\mathbf{q}_3) - n(\mathbf{q}_1)[1 + n(\mathbf{q}_2)][1 + n(\mathbf{q}_3)]. \tag{6}$$

In addition to the above factors, the absorption will be proportional to a matrix element expressing the transition probability. If this term is assumed to be nearly temperature independent, then the dependence of the absorption on temperature will be controlled by the $n(\mathbf{q})$ terms. As will be seen, this assumption appears to be in reasonably good agreement with experiment.

Regardless of the coupling mechanism between the radiation field and the phonons, the absorption process is subject to the conservation laws of energy and wave vector. Therefore, if the photon has energy $\hbar\omega$ and wave

[3] F. A. Johnson and W. Cochran, *Proc. Intern. Conf. Phys. Semicond., Exeter, 1962* p. 498. Inst. of Phys. and Phys. Soc., London, 1962.

vector $\mathbf{k}$, then

$$\hbar\omega = \sum_{i=1}^{n} (\pm)\,\hbar\omega(\mathbf{q}_i) \tag{7}$$

and

$$\mathbf{k} = \sum_{i=1}^{n} (\pm)\mathbf{q}_i + A\mathbf{K}, \tag{8}$$

where $\mathbf{K}$ is a reciprocal lattice vector, $\mathbf{q}_i$ is the wave vector of the phonon of frequency $\omega(\mathbf{q}_i)$, and A is a positive or negative integer or zero. If $n = 1$ or 2, $A = 0$; if $n = 3$, $A = \pm 1$ or 0. The plus signs in (7) and (8) are used for phonon emission and the minus signs for absorption.

From the above considerations, a one-phonon process will have

$$\omega = +\,\omega(\mathbf{q}), \tag{9}$$

$$\mathbf{k} = \mathbf{q}, \tag{10}$$

and

$$\alpha\ (\text{absorption coefficient}) \propto [1 + n(\mathbf{q})] - n(\mathbf{q}) = 1. \tag{11}$$

Since $|\mathbf{k}| = 2\pi/\lambda$, where $\lambda \gtrsim 1$ micron and $|\mathbf{q}_{\max}|$, i.e., $|\mathbf{q}|$ at the zone edge, is of the order of π/a, where a is lattice constant, condition (10) becomes equivalent to $\mathbf{q} \approx 0$. Near $\mathbf{q} = 0$, $\omega(\mathbf{q})$ can assume values appropriate to each of the branches; however, only the transverse optic branch possesses an electric moment capable of coupling to the radiation field, and hence,

$$\hbar\omega(\mathbf{q}) = \hbar\omega_t. \tag{12}$$

For two-phonon processes we have (Case I)

$$\hbar\omega = \hbar\omega(\mathbf{q}_1) + \hbar\omega(\mathbf{q}_2), \tag{13}$$

$$\mathbf{k} = \mathbf{q}_1 + \mathbf{q}_2 \approx 0, \tag{14}$$

and

$$\alpha \propto [1 + n(\mathbf{q}_1)][1 + n(\mathbf{q}_2)] - n(\mathbf{q}_1)n(\mathbf{q}_2) = 1 + n(\mathbf{q}_1) + n(\mathbf{q}_2) \tag{15}$$

or (Case II)

$$\hbar\omega = \hbar\omega(\mathbf{q}_1) - \hbar\omega(\mathbf{q}_2), \tag{16}$$

$$\mathbf{k} = \mathbf{q}_1 - \mathbf{q}_2 \approx 0, \tag{17}$$

and

$$\alpha \propto [1 + n(\mathbf{q}_1)]n(\mathbf{q}_2) - n(\mathbf{q}_1)[1 + n(\mathbf{q}_2)] = n(\mathbf{q}_2) - n(\mathbf{q}_1). \tag{18}$$

Equations (13), (14), and (15) are for summation absorption, since the sum of the phonon frequencies must equal the photon frequency. Equations (16), (17), and (18) represent difference absorption, since $\omega = \omega(\mathbf{q}_1) - \omega(\mathbf{q}_2)$. Since $n(\mathbf{q}) \to 0$ as $T \to 0$, the difference absorption becomes small at low temperatures. These same considerations may be extended to higher-order (three-phonon, etc.) processes.

c. Absorption Mechanisms for Multiphonon Bands

The preceding discussion explains some of the characteristics of multiphonon absorption; however, it does not explain why there is absorption. In the zinc blende crystals the mechanism of interaction for the phonons with the radiation field can be the anharmonic part of the crystal potential. The role of this mechanism in gallium phosphide has been considered in detail by Kleinman.[4] The interaction is via the dipole moment of the fundamental resonance—i.e., the transverse optical mode near $\mathbf{q} = 0$. The absorption (two-phonon, summation) is a process in which a photon is absorbed and two phonons are created with the fundamental as an intermediate state.

Because of symmetry the fundamental resonance in the group-IV semiconductors has no dipole moment and is infrared inactive. Therefore, the anharmonic mechanism will be inoperative in these cases. Lax and Burstein[5] have pointed out a mechanism that explains multiphonon absorption in these materials and may also have some importance in the zinc blende crystals. In this case the phonons interact directly with the radiation field through terms in the electric moment of second order (or higher) in the atomic displacements. The order of the term corresponds to the number of phonons involved. According to Lax and Burstein, the second-order terms in the electric moment may be visualized as the result of one vibrational mode inducing charges on the atoms while the second vibrational mode causes these charges to vibrate, thus producing an electric moment that can couple to the radiation field.

d. Symmetry and Selection Rules

The two-phonon absorption is actually a continuum absorption. If $\hbar\omega(\mathbf{q}_1)$ is the phonon energy at $\mathbf{q} = \mathbf{q}_1$ for one phonon branch and $\hbar\omega(\mathbf{q}_2)$ the energy at $\mathbf{q} = \mathbf{q}_2$ for the same or a different branch, then where $\mathbf{q}_1$ and $\mathbf{q}_2$ are varied throughout the zone, summation absorption can occur for all $\hbar\omega$ given by $[\hbar\omega(\mathbf{q}_1) + \hbar\omega(\mathbf{q}_2)]_{\text{minimum}} \leqslant \hbar\omega \leqslant [\hbar\omega(\mathbf{q}_1) + \hbar\omega(\mathbf{q}_2)]_{\text{maximum}}$ subject to the conditions of Eqs. (13) and (14). The total absorption at $\hbar\omega$

[4] D. A. Kleinman, *Phys. Rev.* **118**, 118 (1960).
[5] M. Lax and E. Burstein, *Phys. Rev.* **97**, 39 (1955).

will be given by the sum of the contributions from every pair of branches. Selection rules will modify the preceding somewhat in that combination of phonons from the same or different branches in certain regions of the zone may be forbidden.

At this point it is reasonable to inquire as to the origin of the peaks in the absorption spectrum. The two-phonon absorption is usually written as the product of a matrix-element term, which is a function of $\mathbf{q}$, times Eq. (2). This product must be summed over all states in the two branches. If the matrix element is not a strong function of $\mathbf{q}$, then we might expect the absorption to be large at summation energies where the branches have large numbers of states within a small energy range. The density of states of $\mathbf{q}$ space is constant, and hence the number of states in a volume of $\mathbf{q}$ space of radius q is proportional to q^3. The states that will be most influential will be near the zone edge unless the dispersion is large in this region. Also it may be noted in Fig. 1 that the branches tend to become flat near the zone edges, giving rise to strong peaks in a curve of density of states $N(\omega)$ vs. ω. Such curves may be calculated[3] by uniformly distributing a large number of states to represent the theoretical $\omega(\mathbf{q})$ vs. $\mathbf{q}$ curves as in Fig. 1 for all directions in $\mathbf{q}$ space and then summing states over frequency intervals. This procedure gives a single-phonon density-of-states curve. Of more importance here are the two-phonon density-of-states curves, since the matrix element must be summed over both branches. In this case the density of states $N(\omega)$ appropriate to summation absorption may be calculated as above if one first combines the states in the branches according to $\omega(\mathbf{q}_1) + \omega(\mathbf{q}_2)$ where $\mathbf{q}_1 + \mathbf{q}_2 = 0$. Also at the zone edge in certain symmetry directions[6,7]—i.e., [100], [111], and [$1\frac{1}{2}0$]—the slope of ω vs. $\mathbf{q}$ is zero for some branches. At these points of zero slope, which are called critical points and hereafter referred to as the X, L, and W points, respectively, it is anticipated that there will be critical points in the two-phonon densities of states and hence, at the corresponding summation energies, structure in the absorption.

Birman[8,9] has recently deduced the selection rules for electric-dipole-allowed two- and three-phonon processes for the diamond and zinc blende structures at the X, L, and W critical points and at the critical point $\mathbf{q} = 0$ (Γ point). These rules modify the density-of-states discussion somewhat because combinations of phonons from some branches in certain regions of the zone may be forbidden. The two-phonon selection rules listed in Tables I and II were determined from a space-group analysis. The symbols

[6] L. Van Hove, *Phys. Rev.* **89**, 1189 (1953).
[7] J. C. Phillips, *Phys. Rev.* **104**, 1263 (1956).
[8] J. L. Birman, *Phys. Rev.* **127**, 1093 (1962).
[9] J. L. Birman, *Phys. Rev.* **131**, 1489 (1963).

TO(X), LO(L), etc., represent the frequency or energy of the branch at the indicated point in the zone. Therefore, in Table II, TO(Γ) and LO(Γ) are what we have previously called ω_t and ω_l. Where LO and LA are degenerate, the letter L is used, and at the W point in the zinc blende case the transverse modes are not degenerate and hence the subscripts 1 and 2 in Table II.

TABLE I

INFRARED ALLOWED PROCESSES IN THE DIAMOND STRUCTURE

Two-phonon processes
TO(X) + L(X)
TO(X) + TA(X)
L(X) + TA(X)
TO(L) + LO(L)
TO(L) + TA(L)
LO(L) + LA(L)
LA(L) + TA(L)
TO(W) + L(W)
TO(W) + TA(W)
L(W) + TA(W)

TABLE II

INFRARED ALLOWED PROCESSES IN THE ZINC BLENDE STRUCTURE

Two-phonon processes
2LO(Γ), LO(Γ) + TO(Γ), 2TO(Γ)
2TO(X), TO(X) + LO(X), TO(X) + LA(X), TO(X) + TA(X)
LO(X) + LA(X), LO(X) + TA(X)
LA(X) + TA(X)
2TA(X)
2TO(L), TO(L) + LO(L), TO(L) + LA(L), TO(L) + TA(L)
2LO(L), LO(L) + LA(L), LO(L) + TA(L)
2LA(L), LA(L) + TA(L)
2TA(L)
$TO_1(W)$ + LO(W), $TO_1(W)$ + LA(W)
$TO_2(W)$ + LO(W), $TO_2(W)$ + LA(W)
LO(W) + LA(W), LO(W) + $TA_1(W)$, LO(W) + $TA_2(W)$
LA(W) + $TA_1(W)$, LA(W) + $TA_2(W)$

e. Analysis of Data and Systematics of the Phonon Energies

It has been observed that the principal peaks in the absorption will be closely related to major peaks in the density-of-states curve. Since there are four vibrational energies at the critical points X and L [for the diamond structure only three at X since $\mathrm{LO}(X) = \mathrm{LA}(X)$], we would hope to be able to interpret the gross features of the absorption curve—i.e., the main peaks—in terms of combinations of four frequencies called characteristic TO, LO, LA, and TA phonons, the temperature dependence of these peaks to be given by equations such as (2)–(6). As will be seen, in many cases the experimental results are in agreement with this expectation. In some cases[3] the density of states calculated from theoretical curves such as Fig. 1 indicate major peaks at four energies, in reasonable agreement with the characteristic phonon energies obtained from absorption. The selection rules given in the previous section are used, but in a less direct manner than in the critical-point analysis of Part IV. For the diamond lattice, in the two-phonon case of Table I, TO + TO is forbidden at all three critical points, and therefore any TO + TO band should be weak. In fact all two-phonon combinations in which the phonons do not come from distinct branches are forbidden.

It has been observed in some materials that four frequencies will not suffice to represent the data, and five or six frequencies must be used. This indicates that the joint density-of-states curve may have resolved maxima arising, perhaps, from a branch having different, nearly constant energies at different regions of $\mathbf{q}$ space. For example, as will be noted in the analysis of the GaP absorption, it was necessary to use two TA energies to fit the observed data. The TA_1 and TA_2 frequencies are close to the values of $\mathrm{TA}(X)$ and $\mathrm{TA}(L)$ obtained by Johnson as discussed in Part IV.

In those cases where four frequencies suffice, they usually may be ordered as TO, LO, LA, and TA in order of decreasing frequency as indicated by the zone-edge values of the curves of Fig. 1. For convenience TO, LO, etc., will be used to represent the characteristic phonons, and phonon energies at specific points will be given as $\mathrm{TO}(\Gamma)$, $\mathrm{LO}(X)$, etc. In all of the present cases the optical modes are larger than the acoustical ones, and LA > TA. However, there has been some doubt in the past as to whether LO or TO was larger in some of the partially polar compounds. Keyes[10] noted a semiempirical relation between the ratio LO/TO and the Szigeti[11] effective charge e^*, where e^* is given by

$$\frac{e^*}{e} = \left[\frac{\pi(\varepsilon_0 - \varepsilon_\infty)mv_t^2}{Ne^2}\right]^{1/2}\left(\frac{3}{\varepsilon_0 + 2}\right), \tag{19}$$

[10] R. W. Keyes, *J. Chem. Phys.* **37**, 72 (1962).
[11] B. Szigeti, *Trans. Faraday Soc.* **45**, 155 (1949).

where ε_0 and ε_∞ are as defined in Eq. (1), N is the concentration of ion pairs, and m is the reduced mass of the ion pair. For $e^* = 0$, LO(Γ) = TO(Γ) and LO < TO at the zone edge. As e^* increases, the LO energy increases near $\mathbf{q} = 0$ relative to the TO energy, apparently causing the entire LO branch to move up relative to the TO branch. Therefore, at sufficiently large e^* the value of LO near the zone edge can be larger than TO. Keyes observed that if the two highest characteristic phonon frequencies were labeled LO and TO in the proper order for the various materials, then $(\mathrm{LO/TO})^2$ is a linear function of e^{*2}. This observation has been checked by Mitra[12] and by Marshall and Mitra[13] for a large number of materials, and as indicated in Fig. 2 the data are reasonably consistent with the relation. At $e^* = 0.7$ the LO and TO values are equal.

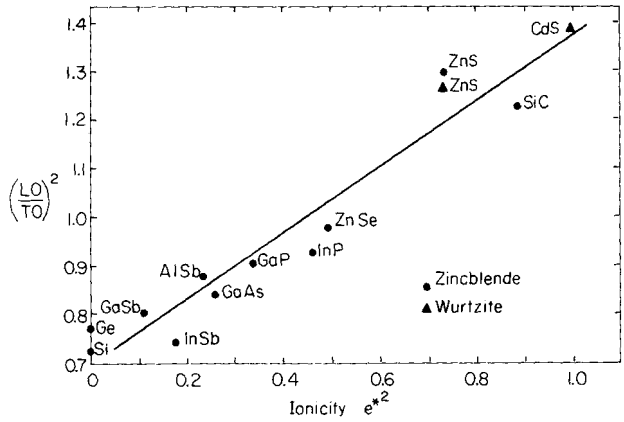


FIG. 2. The ratio $(\mathrm{LO/TO})^2$ as a function of the Szigeti effective charge e^*. (After Marshall and Mitra.[13])

The theory of the one-dimensional, diatomic, linear chain[14] leads to a ratio of the frequencies at the zone edge of $\omega_1/\omega_2 = (M_1/M_2)^{1/2}$ where ω_1 is the optical mode, ω_2 the acoustical mode, and M_1 and M_2 the heavier and lighter masses, respectively. This led Marshall and Mitra to investigate $(\mathrm{LO/LA})^2$ vs. M_1/M_2 for the IV, III–V, and II–VI systems with the results shown in Fig. 3.

Another relation that has been found to be valid for the materials studied here is the Brout sum rule,[15] which states that the sum of the $\omega_b^2(\mathbf{q}_i)$ for

[12] S. S. Mitra, *Phys. Rev.* **132**, 986 (1963).
[13] R. Marshall and S. S. Mitra, *Phys. Rev.* **134**, A1019 (1964).
[14] S. S. Mitra, *Solid State Phys.* **13**, 32 (1962).
[15] R. Brout, *Phys. Rev.* **113**, 43 (1959).

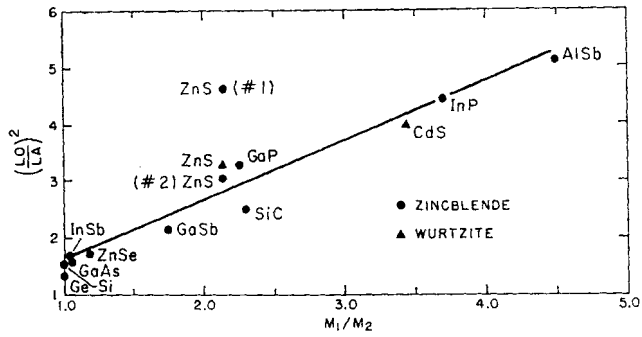


FIG. 3. The effect of mass difference on the separation between the optical and the acoustical branches. (After Marshall and Mitra.[13])

all b branches at a given $\mathbf{q}_i$ is a constant independent of $\mathbf{q}_i$. Thus, for example,

$$2\mathrm{TO}^2(\Gamma) + \mathrm{LO}^2(\Gamma) = 2\mathrm{TO}^2 + \mathrm{LO}^2 + \mathrm{LA}^2 + 2\mathrm{TA}^2, \tag{20}$$

where the factor of 2 comes from the degeneracy of the transverse branches. This relation was originally derived for an ionic model employing Coulomb attractive forces and nearest-neighbor repulsion. More recently it has been shown[16] that this relation should also hold for more generalized force models. The application of the Brout sum is summarized in Table III. It must be remembered, however, that in this case and in the other phonon-energy relationships considered, the various characteristic phonon energies are related to gross peaks in the density of states for the phonon branches, and are not necessarily phonon values at particular positions in $\mathbf{q}$ space. For this reason the quantitative agreement obtained in Table III is impressive.

Other aids in determining frequency assignments for the absorption spectra are the relative magnitude of the absorption peaks, their temperature dependence, and the frequency of the absorption band. The absorption associated with two-phonon processes is expected to be larger than that for three-phonon processes, and so on. The temperature dependence was discussed previously. Since, for curves of the type illustrated by Fig. 1, LO(Γ) is the maximum phonon energy, the high-frequency cutoff of the absorption for an n phonon process will be nLO(Γ). The LO(Γ) value can be obtained from TO(Γ)—i.e., ω_t—with Eq. (1) or from Raman spectra measurements.

[16] H. B. Rosenstock, *Phys. Rev.* **129**, 1959 (1963).

TABLE III

CHARACTERISTIC PHONON ENERGIES AND THE BROUT SUM RULE[a] APPLIED TO A NUMBER OF MATERIALS[b]

Semiconductor	$\nu_t = TO(\Gamma)$ (cm^{-1})	$\nu_l = LO(\Gamma)$ (cm^{-1})	TO (cm^{-1})	LO (cm^{-1})	LA (cm^{-1})	TA (cm^{-1})	$2TO^2(\Gamma) + LO^2(\Gamma)$ ($10^6\ cm^{-2}$)	$2TO^2 + LO^2 + LA^2 + 2TA^2$ ($10^6\ cm^{-2}$)
C (diamond)	1337	1337	1275	1161	991	750	5.364	6.707
Si	510	510	482	413	333	139	0.780	0.784
Ge	300	300	280	247	215	65	0.270	0.272
SiC	793	970	770	851	540	363	2.199	2.465
GaAs	273	297	262; 255	234	188	70	0.237	0.234
GaP	366	402	378	361	197	115; 66	0.430	0.472
GaSb	231	240	215	193	134	49	0.164	0.152
AlSb	318	345	316	297	132	65	0.321	0.314
InP	307	351	329	318	150	62	0.312	0.348
InSb	185	197	179	155	118	43	0.107	0.106
ZnSe (cubic)	210	250	208	212	162	87	0.151	0.173
ZnS (cubic)	312	390	298	339	155	93	0.347	0.334
CdS (wurtzite)	241	305	261; 238	295	149	79; 70	0.209	0.245

[a] Equation (20).

[b] The data of this table were taken from the compilations of Refs. (12) and (13).

f. Experimental Measurements

The methods generally used are essentially the same, although materials have been measured by a number of investigators. The quantity desired is the linear absorption coefficient α as a function of photon energy from the fundamental absorption edge to the reststrahlen region and beyond if possible. This is usually obtained from measurements of the transmission and reflection. Stierwalt and Potter[17] have reported some very interesting measurements of the infrared spectral emittance of several different materials. This method possesses a distinct advantage over the usual transmission-reflection measurements for nearly transparent samples in that small absorption coefficients can be measured without using very thick samples. A discussion of this method is given by Stierwalt and Potter in Chapter 3.

Assuming the measurements to be limited to $\omega > \omega_t$, then the low photon-energy limit of the transmission measurement will be determined by the thickness of the samples that are prepared, how low a transmission can be accurately measured, the spectral purity of the monochromator, and, in the diatomic case, the magnitude of the background absorption arising from the fundamental (single-phonon) resonance as compared to the multiphonon processes. As $\omega \to \omega_t$, the strong fundamental resonance will tend to dominate the absorption and make the combination bands increasingly difficult to measure. It should be mentioned that some combination bands can occur for $\omega < \omega_t$. This requires frequencies sufficiently removed from ω_t so that the fundamental absorption can again be small. In general this means far-infrared spectroscopy, and little work has been done here.

Since infrared instrumentation covering most of the desired spectral range, from approximately 1 to 50 microns, is commercially available, the major experimental difficulty in the measurement often lies in the samples themselves. There are a number of cases in which bands of strength comparable to the combination absorption have been observed, but these bands vary from sample to sample of the same material. These bands are the result of the presence of impurities or defects in the crystal. Examples are oxygen[18] and nitrogen[19] in silicon, oxygen in germanium,[18] and nitrogen in diamond.[20] One band in gallium arsenide has been observed by H. Hrostowski and W. G. Spitzer to vary from sample to sample,

[17] D. L. Stierwalt and R. F. Potter, *Proc. Intern. Conf. Phys. Semicond., Exeter, 1962* p. 513. Inst. of Phys. and Phys. Soc., London, 1962. Also see Chapter 3 of this volume.

[18] W. Kaiser, P. H. Keck, and C. F. Lange, *Phys. Rev.* **101**, 1264 (1956).

[19] W. Kaiser and C. Thurmond, *J. Appl. Phys.* **30**, 427 (1959).

[20] W. Kaiser and W. L. Bond, *Phys. Rev.* **115**, 857 (1959).

although the impurity has not been identified. Also, it has been proposed[21] that one band observed in a copper-compensated gallium phosphide sample is an impurity band.

The absorption in these cases is attributed to different causes. Oxygen in silicon produces a pair of absorption bands that are related to the Si–O bond. The presence of nitrogen in diamond—i.e., Type I diamond—produces bands that were originally[19] thought to be related to the C–N bond; however, recent evidence[22] points out that the bands can be interpreted as single phonon bands normally forbidden by crystal symmetry. In support of this view it has been pointed out[22] that irradiated diamond has absorption bands at the same energies. Irradiated silicon also has absorption bands[23,24] that have been interpreted as one-phonon absorption bands allowed near the defects introduced into the crystal. Although these impurity or defect bands are an interesting subject, we shall confine ourselves primarily to those bands that are allowed in a pure, well-ordered crystalline state. In those systems where purity is a problem, several samples of different impurity content should be measured to establish the bands' independence of the impurity.

III. Measurements and Data

3. Silicon

Silicon is a material without a first-order electric moment, and therefore the multiphonon absorption will occur by the Lax and Burstein mechanism.[5] The first measurements of lattice absorption in germanium and silicon semiconductors were those of Lord,[25] Briggs,[26] and Collins and Fan.[27] The Collins and Fan measurements of the room-temperature absorption for silicon and germanium are indicated in Fig. 4. Within the limitations of the material available at that time, it was demonstrated that the rather complicated-looking spectra were indeed characteristic of the material. However, particularly for the case of silicon, this latter conclusion had to be modified because of the high oxygen content of all the early silicon crystals.

[21] D. A. Kleinman and W. G. Spitzer, *Phys. Rev.* **118**, 110 (1960).
[22] S. D. Smith, J. R. Hardy, and E. W. J. Mitchell, *Proc. Intern. Conf. Phys. Semicond., Exeter, 1962* p. 529. Inst. of Phys. and Phys. Soc., London, 1962.
[23] H. Y. Fan and A. K. Ramdas, *J. Appl. Phys.* **30**, 1127 (1959).
[24] M. Balkanski and W. Mazerewics, *J. Phys. Chem. Solids* **23**, 573 (1962).
[25] R. C. Lord, *Phys. Rev.* **85**, 140 (1952).
[26] H. B. Briggs, *J. Opt. Soc. Am.* **42**, 686 (1952).
[27] R. J. Collins and H. Y. Fan, *Phys. Rev.* **93**, 674 (1954).

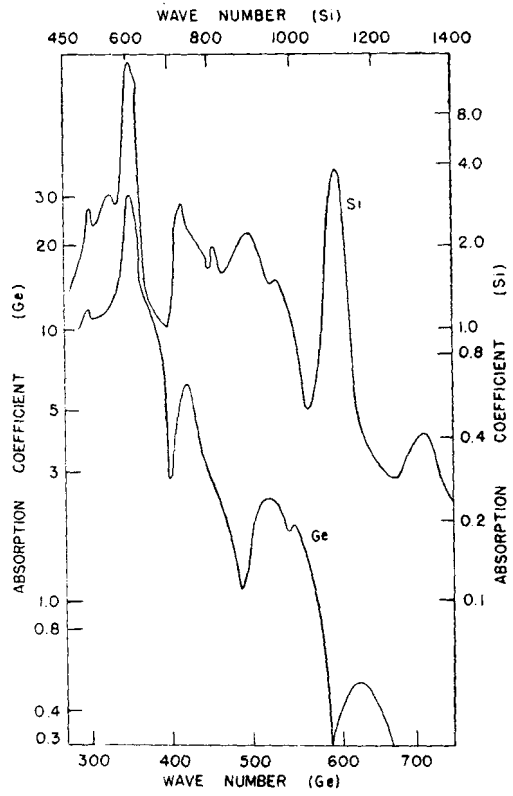


FIG. 4. Lattice absorption in germanium and silicon. (After Collins and Fan.[27])

The measurements of Collins and Fan were repeated in greater detail by Johnson,[1b] who used oxygen-free silicon; his results are shown in Fig. 5. Reductions of the bands[18] near 1100 cm^{-1} and 530 cm^{-1} are evident. Brockhouse[28] used the silicon data of Collins and Fan to show that the absorption bands were amenable to a multiphonon interpretation. Johnson used his own data in the first detailed attempt to analyze the absorption in terms of characteristic phonons. Four characteristic phonon energies were used, and the fit of experimental and calculated absorption-peak positions along with the observed and calculated temperature dependence is indicated in Table IV(a). As can be seen, the fit is quite impressive, particularly when one recalls the assumption involved in using just four characteristic phonon energies. The LO + TA energy is perhaps the only exception to this excellent agreement. Johnson has attributed this exception to

[28] B. N. Brockhouse, *J. Phys. Chem. Solids* **8**, 400 (1959).

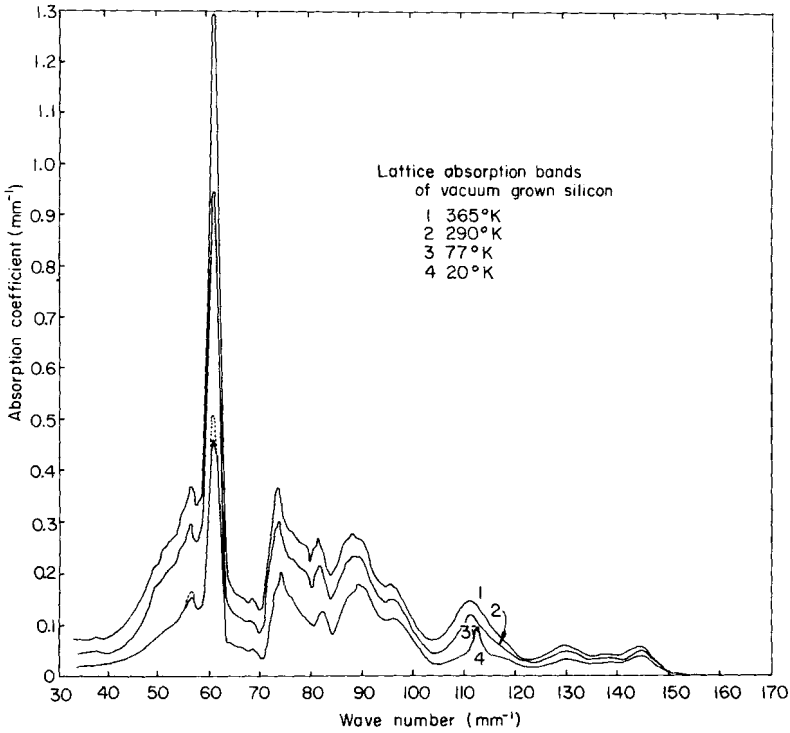


FIG. 5. Lattice absorption of vacuum grown silicon. (After Johnson.[1b])

the forbiddeness of this combination at the L point where the TA energy is considerably less than at the X point.

These phonon energies can be compared with those obtained in other ways. Data are available,[29,30] in the present case, from slow-neutron scattering experiments. Although direct comparison is difficult without doing a joint density-of-states calculation, the neutron values are in reasonable agreement with those given here, except possibly for LA. The neutron values of $\mathrm{LA}(L) = 0.0469\,\mathrm{eV}$ and $\mathrm{LA}(X) = 0.0509\,\mathrm{eV}$ are both substantially higher than the $\mathrm{LA} = 0.0414\,\mathrm{eV}$ value obtained here. This objection, however, is removed by the critical-point analysis made by Johnson and discussed in Part IV.

Theoretical calculations of the phonon curves[3] for silicon have been made by using the shell model with a nearest-neighbor approximation.

[29] B. N. Brockhouse, *Phys. Rev. Letters* **2**, 256 (1959).

[30] G. Dolling, Paper presented at the Symposium on Inelastic Scattering of Neutrons in Solids and Liquids, Chalk River, Ontario, September, 1962. Results quoted by F. A. Johnson, *Progr. Semicond.* **9**, 179 (1965).

TABLE IVa

PHONON ASSIGNMENTS IN SILICON

Peak energy (eV)	Phonon assignment[a]	Assignment energy (eV)	Observed temperature dependence[b]				Calculated temperature dependence			
			20°K	77°F	296°F	365°K	20°K	77°K	296°K	365°K
0.1795	3TO	0.1794	1	1	1.3	1.6	1	1	1.33	1.64
0.1708	2TO + LO	0.1709	1	1	1.4	1.7	1	1	1.41	1.72
0.1614	2TO + LO	0.1624	1	1	1.45	1.9	1	1	1.45	1.85
—	2TO + LA	0.1610	—	—	—	—	1	1	1.49	1.93
0.1195	2TO	0.1196	1	1	1.3	1.5	1	1	1.22	1.40
0.1111	TO + LO	0.1111	1	1	1.3	1.5	1	1	1.27	1.46
0.1015	TO + LA	0.1012	1	1	1.3	1.6	1	1	1.35	—
0.0917	LO + LA	0.0927	1	1	1.5	1.8	1	1	1.44	—
0.0756	TO + TA	0.0756	1	1.1	1.05	1.65	1	1.1	1.25	1.72
0.0702	LO + TA	0.0671	1	1.1	2.0	2.6	1	1.1	2.37	2.91
0.0461	TO − TA	0.0440 (?)	0	0	0.75	1.0	0	0.06	0.73	1.0

[a] TO = 0.0598 eV, LO = 0.0513 eV, LA = 0.0414 eV, TA = 0.0158 eV.

[b] The indicated temperature dependence is the ratio of the measured absorption to that at 20°K. The TO–TA peak uses the 365°K absorption for the normalization.

TABLE IVb

COMPARISON OF CHARACTERISTIC PHONON ENERGIES OBTAINED BY DIFFERENT METHODS

Assignment	From two-phonon bands	One-phonon bands irradiated silicon	Calculated
TO	0.0598 eV	0.0603	0.061
LO	0.0513	0.0517	0.054
LA	0.0414	0.0414	0.038
TA	0.0158	—	0.016

The values for the characteristic phonon energies based on the peaks of a density-of-states curve calculated from the theoretical ω vs. $\mathbf{q}$ curves are given in Table IVb. The agreement is quite good, although it has been pointed out that the model tends to make the TO branch too flat.

Also listed in Table IVb are the values[23,24] obtained from irradiated silicon. The removal of crystal symmetry in the neighborhood of the defect allows the normally forbidden single-phonon absorption to become optically active, and the radiation field becomes capable of coupling to phonons of any $\mathbf{q}$ value. Therefore, the absorption again will reflect the density-of-states curve, and peaks are observed at the characteristic phonon frequencies. The agreement here again is quite good.

4. GERMANIUM

Like silicon, germanium does not have an infrared-active fundamental vibration but does show a large number of multiphonon absorption bands as seen in Fig. 4. The phonon spectrum of germanium was investigated by Brockhouse and Iyengar[31] by using the slow-neutron scattering techniques. These authors showed that the absorption bands in germanium are compatible with a multiphonon model when the neutron values for the zone-boundary phonon energies were used.

It is unfortunate and somewhat surprising that detailed measurements and characteristic phonon assignments for germanium are not yet available in the literature. Measurements by Fray *et al.* are to be published shortly and have been referred to by Johnson and Cochran.[3] A comparison of the characteristic phonon energies and the peaks in the calculated density-of-states curve is given in Table V. The density-of-states curve was obtained from the theoretical ω vs. $\mathbf{q}$ curves[32] for germanium, which are known to be

[31] B. N. Brockhouse and P. K. Iyengar, *Phys. Rev.* **111**, 747 (1958).
[32] W. Cochran, *Proc. Roy. Soc.* (*London*) **A253**, 260 (1959).

in reasonable agreement with the neutron data in the [100] and [111] directions.

TABLE V

GERMANIUM PHONON ENERGIES

Assignment	Phonon energies deduced from assignment (eV)	Peaks in calculated density-of-state curve (eV)
TO	0.0350	0.0350
LO	0.0305	0.0299
LA	0.0225	0.0226
TA	0.0095	0.0084

5. DIAMOND

Smith *et al.*[22,33] have measured two- and three-phonon combination bands in type-IIa diamond. Type-IIa diamond has absorption bands between 2 and 6 microns, which are common to all diamonds, and is transparent elsewhere in the infrared. The results of their measurements are

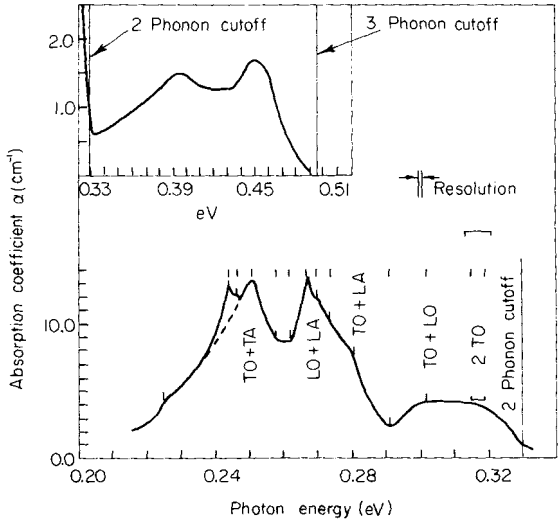


FIG. 6. Two- and three-phonon absorption in diamond. (After Smith *et al.*[22])

[33] J. R. Hardy and S. D. Smith, *Phil. Mag.* **6**, 1163 (1961).

shown in Fig. 6, and the assignments for six two-phonon summation bands in terms of four phonons are given in Table VI. The only case where excellent agreement is not obtained is for the LO + TA band. This difficulty has already been noted for the same band in silicon. Before any neutron-scattering data were available for diamond, a value for the TA phonon energy of 0.063 eV was deduced[22] from specific-heat data. Smith *et al.* point out that this value for TA, as compared to their value of 0.093 eV, and the absence of the strong TO + TA peak seen in silicon indicate large changes in the TA value for different directions in **q** space. A glance at Table III shows that the Brout sum rule is poorly satisfied for diamond. Comparison of the zone-edge characteristic phonon energies among the different materials in this table indicates that the TA frequency in diamond is unusually large.

The additional absorption bands observed[22] in type-I and irradiated type-II diamond have been attributed to one-phonon absorption similar to that described for the irradiated silicon (see Section 2,*e*). If the bands

TABLE VIa

DIAMOND CHARACTERISTIC PHONON ASSIGNMENTS

Observed energy of feature (eV)	Assignment and phonon energies[a] (eV)	Calculated energy (eV)
0.319–0.315	2TO	0.316
(Shoulder)	2 × 0.158	—
0.302	TO + LO	0.302
(Peak)	0.158 + 0.144	—
0.281	TO + LA	0.281
(Shoulder)	0.158 + 0.123	—
0.267	LO + LA	0.267
(Peak)	0.144 + 0.123	—
0.251	TO + TA	0.251
(Peak)	0.158 + 0.093	—
0.244	LO + TA	0.237
(Peak)	0.144 + 0.093	—

[a] TO = 0.158 eV, LO = 0.144 eV, LA = 0.123 eV, TA = 0.093 eV. Two-phonon cutoff at 0.330 eV = 2 × 0.165 eV, or twice the Raman energy.

are interpreted in this way, then the photon energies of the absorption peaks compare favorably with the characteristic phonon energies as shown in Table VI b . These authors have also performed a point-group analysis of their data. The results of this analysis are discussed in Part IV.

TABLE VIb

CHARACTERISTIC PHONON ENERGIES OBTAINED FROM DIFFERENT MEASUREMENTS

Assignment	Two-phonon bands (eV)	Type-I single-phonon bands (eV)	Irradiated type-II single-phonon bands (eV)
TO	0.158	0.159	0.159
LO	0.144	0.148	0.148
LA	0.123	0.125	0.125
TA	0.093	—	—

6. SILICON CARBIDE

Silicon carbide is known to exist in a large number of crystallographic modifications including a zinc blende cubic one known as the β form. Much of the research on silicon carbide has been on the hexagonal 6H modification, which has twelve atoms per unit cell. In all forms of SiC the Si–C distance is 1.89 Å, and each atom has four nearest neighbors of the other type at regular tetrahedral positions.

Two independent reflectivity measurements [34,35] of ω_t and the Szigeti effective charge have been reported for the hexagonal 6H, and the results are in good agreement with one another. Only a slight difference was noted[35] for ω_t when the incident electric vector was polarized parallel to and perpendicular to the c axis. Moreover, transmission measurements[36] on very thin films of β SiC again showed very nearly the same ω_t value. Therefore, these different modifications of SiC show very little difference from one another in their single-phonon spectra. However, they differ widely from the materials considered thus far in that they possess a strong, infrared-active fundamental absorption band.

The combination bands for a hexagonal SiC sample as measured by Spitzer *et al.*[35] are given in Fig. 7. Transmission measurements for the β form in the same spectral region indicate that, as in the single-phonon absorption, very little difference exists between the cubic and hexagonal modifications. It may be noted, however, that the absorption peaks, after subtracting out a reasonable estimate of the background absorption, are an order of magnitude greater than the peak values in silicon, germanium, and diamond.

[34] J. Lely and F. A. Kröger *in* "Halbleiter und Phosphore" (Vorträge des intern. Kolloquiums 1956 in Garmisch–Partenkirchen), p. 514. Vieweg, Braunschweig, and Wiley (Interscience), New York, 1958.

[35] W. G. Spitzer, D. A. Kleinman, and D. Walsh, *Phys. Rev.* **113**, 127 (1959).

[36] W. G. Spitzer, D. A. Kleinman, and C. J. Frosch, *Phys. Rev.* **113**, 133 (1959).

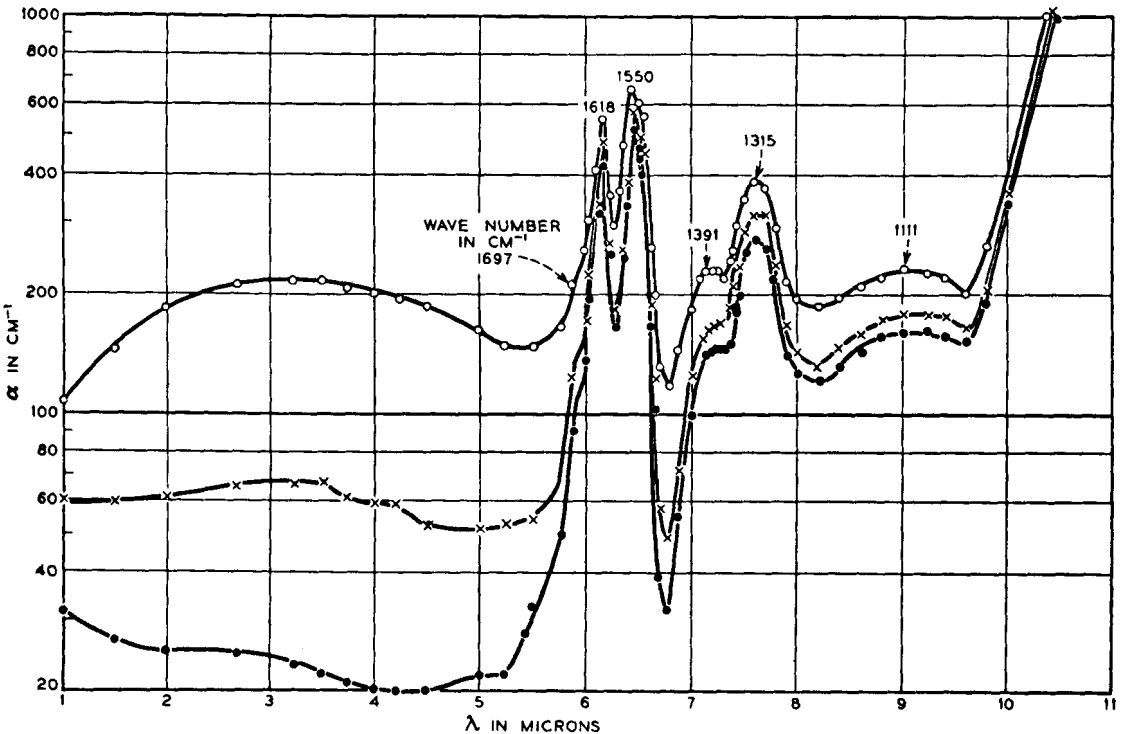


FIG. 7. Absorption coefficient as a function of wavelength of α–II SiC. The three curves are for regions of a specimen with different impurity concentration. (After Spitzer *et al.*[35])

Patrick and Choyke[37] made combination-band transmission measurements for two different hexagonal modifications and again the two modifications gave, within the experimental accuracy, identical results. The optical data are shown in Fig. 8, and the summary of the summation bands and characteristic phonon energies is given in Table VII. It therefore seems reasonable to assume that the density-of-states curves do not change in any major way in considering the various SiC modifications. It may be noted from Table VII that the highest phonon energy is called LO, since $e^* = 0.94$ and, according to Keyes' observation, the LO branch should lie above the TO branch at the zone edge.

In a later study of exciton recombination. Choyke and Patrick[38] suggested that the fine structure seen in the hexagonal 6H modifications' 2 TO and TO + LO bands (see Fig. 8) could be explained in terms of optical

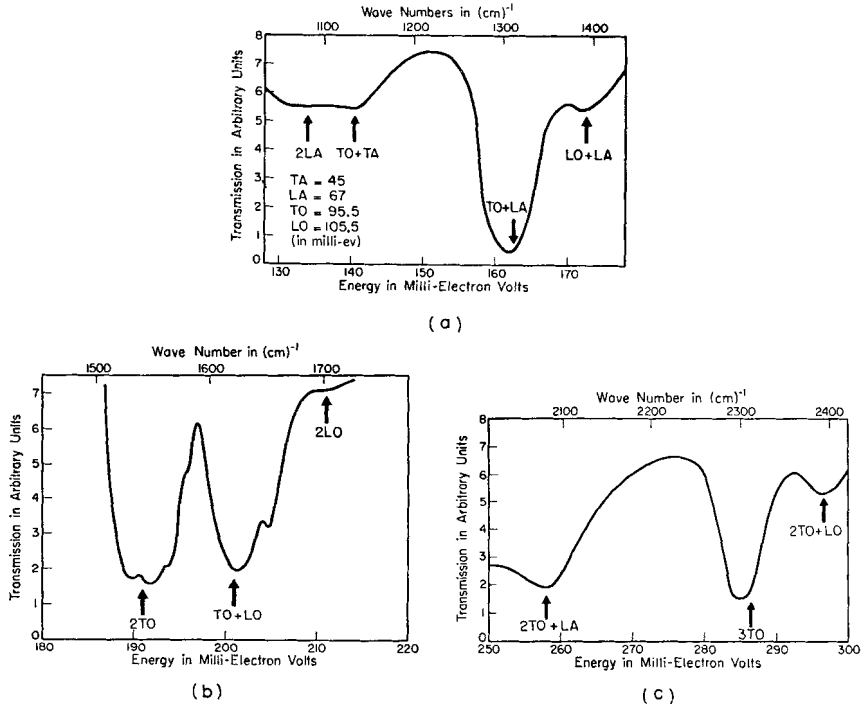


FIG. 8. (a) Two-phonon optical-acoustical summation bands. Arrows point to the energy values calculated by using the four assigned phonon energies. (b) Two-phonon optical-optical summation bands. Arrows point to calculated values. These are the strongest bands. (c) Three-phonon summation bands. These bands are relatively weak. (After Patrick and Choyke.[37])

[37] L. Patrick and W. J. Choyke, *Phys. Rev.* **123**, 813 (1961).
[38] W. J. Choyke and L. Patrick, *Phys. Rev.* **127**, 1868 (1962).

phonons observed in the recombination studies. These phonons originate near $\mathbf{q}_c = 2\pi/c$, $4\pi/c$, and $6\pi/c$ in an extended zone model, where c is the lattice constant along the hexagonal axis.

TABLE VII

COMPARISON OF OBSERVED AND ASSIGNED SUMMATION-BAND ENERGIES FOR SiC

Observed peaks		Assignment using TA = 45, LA = 67, TO = 95.5, LO = 105.5	
(cm^{-1})	(10^{-3} eV)	(10^{-3} eV)	Branches
—	—	134	2LA
1135	140.7	140.5	TO + TA
1308	162.1	162.5	TO + LA
1390	172.3	172.5	LO + LA
1548	191.9	191	2TO
1622	201.1	201	TO + LO
1700	210.7	211	2LO
2080	257.8	258	2TO + LA
2300	285.1	286.5	3TO
2390	296.3	296.5	2TO + LO

7. GERMANIUM–SILICON ALLOYS

An interesting study[39] of lattice vibration spectra of germanium-silicon alloys was recently reported by Braunstein. In this study combination-band spectra were measured throughout the alloy range from pure germanium to pure silicon, and spectra for a number of samples are given in Fig. 9. However, as discussed by the author, the gross features of the spectra suggest that results may be characteristic of pure germanium and silicon aggregates rather than a true disordered alloy. The feature that suggests this interpretation is the lack of sensitivity of the silicon- and germanium-like summation bands on composition. In fact the TO + TA germanium band approaches but does not merge with the equivalent silicon-like band, and it is possible to observe both bands in the same specimen in the 70–80 mole % silicon range.

The insensitivity of band position to alloy composition is indicated by the data of Table VIII. Extrapolation of the germanium-like TO + TA values to pure silicon would give a value of $\sim 410\,cm^{-1}$ as compared to the $610\,cm^{-1}$ value for the silicon-like TO + TA band. In the 76 mole % silicon, both TO + TA bands are observed with a separation of $\sim 200\,cm^{-1}$.

[39] R. Braunstein, *Phys. Rev.* **130**, 879 (1963).

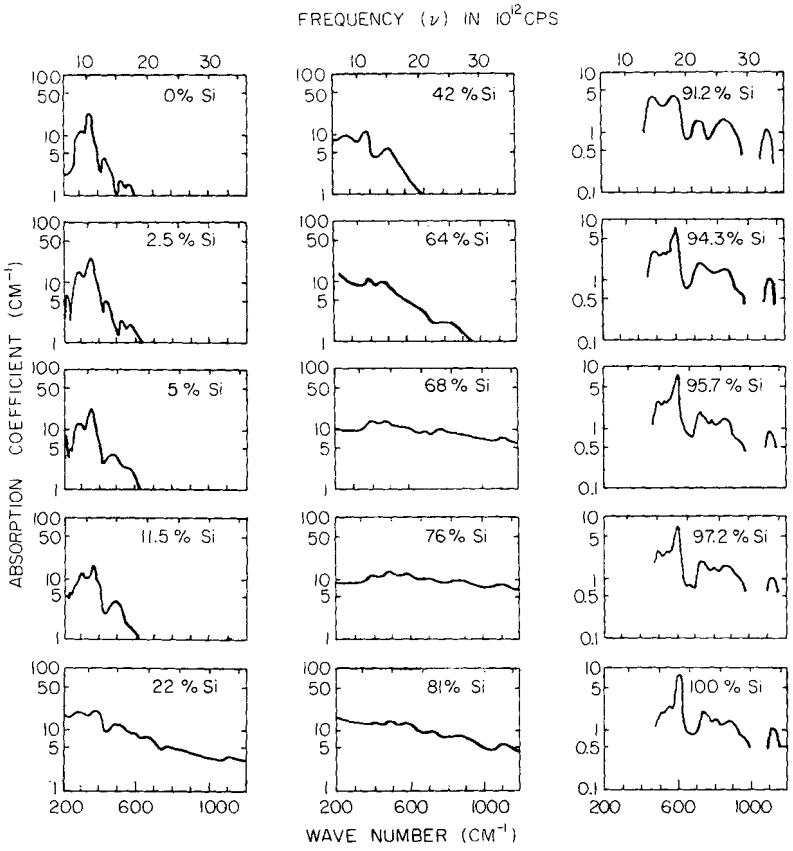


FIG. 9. Lattice absorption in germanium–silicon alloys. (After Braunstein.[39])

Braunstein obtains a set of three characteristic phonon energies from the values of Table VIII by assuming the degeneracy of the LO and LA branches at the zone edge (true at points W and X but not at L) for the pure materials and the alloys. A plot of these energies is shown in Fig. 10, where the dashed region connecting the curves is arbitrary. In fact the dashed region cannot be correct for the present case, since, as just pointed out, the phonon energies from the two sides do not merge. It may be noted that the characteristic phonon energies given here for pure silicon are in poor agreement with those of Johnson[1b] which were based on a much more extensive analysis. However, this is not expected to alter the qualitative features of the results.

In addition to the lattice bands discussed above, two new bands were observed—one in the germanium-rich material and the other in the silicon-rich material. Neither of these bands is present in the pure material, and

TABLE VIII

TWO-PHONON SUMMATION BANDS IN Ge–Si ALLOYS

Germanium-like			
Mole % Si	TA + LA (cm^{-1})	TA + TO (cm^{-1})	LA + LO (cm^{-1})
0	300 (0.0382)[a]	343 (0.0426)[a]	421 (0.0522)[a]
2.5	281	346	425
5.0	281	350	469
11.5	292	355	483
22.0	292	371	492
42.0	288	388	510
64.0	—	394	—
68.0	—	400	—
76.0	—	400	—
81.0	—	406	—
Silicon-like			
Mole % Si	TA + TO (cm^{-1})	LA + TO (cm^{-1})	TO + LO (cm^{-1})
68.0	558	690	781
76.0	598	723	860
81.0	598	712	850
91.2	598	738	875
94.3	604	738	875
95.7	606	733	871
97.2	609	740	875
100.0	610 (0.0756)[a]	741 (0.0918)[a]	885 (0.1098)[a]

[a] Values in parentheses are in eV.

they grow in intensity as the composition is changed away from the pure material. These are impurity bands, and their temperature dependence is similar to that of the two-phonon bands close by and thus suggests a second-order moment mechanism. This behavior may be contrasted with the temperature independence of the one-phonon band[23] in irradiated silicon. The impurity band in almost pure silicon is at 506 cm^{-1} or 0.0626 eV, as compared with the TO values of 0.0598 eV and 0.0603 eV of Table IVb. No bands with a one-phonon temperature dependence were observed in any of the samples.

8. GALLIUM ARSENIDE

Gallium arsenide is the first of the III–V compounds considered here, and like the rest of the compounds of this class it crystallizes in the zinc

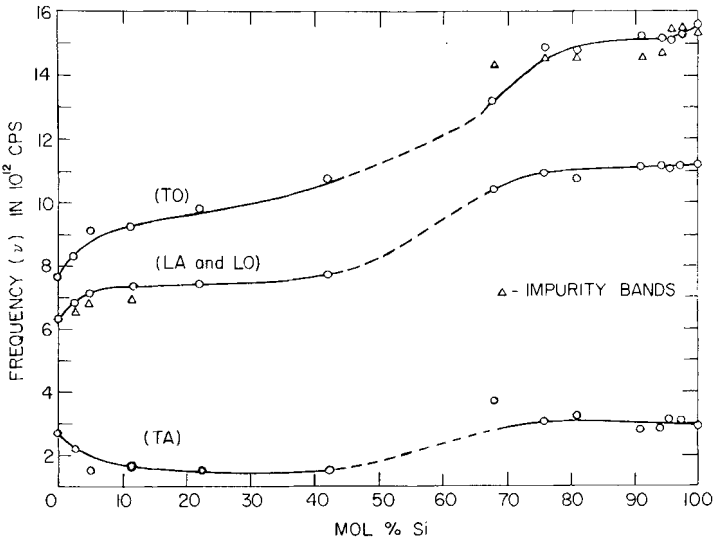


FIG. 10. Phonon frequencies as a function of Ge-Si alloy composition. (After Braunstein.[39])

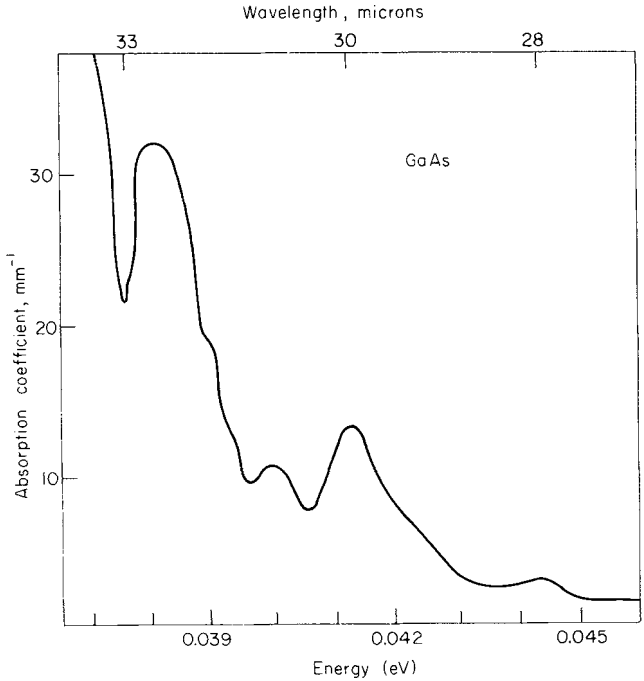


FIG. 11a. Lattice absorption coefficient of high-resistivity *n*-type GaAs vs. wavelength from 28 to 35 microns. (After Cochran *et al.*[40])

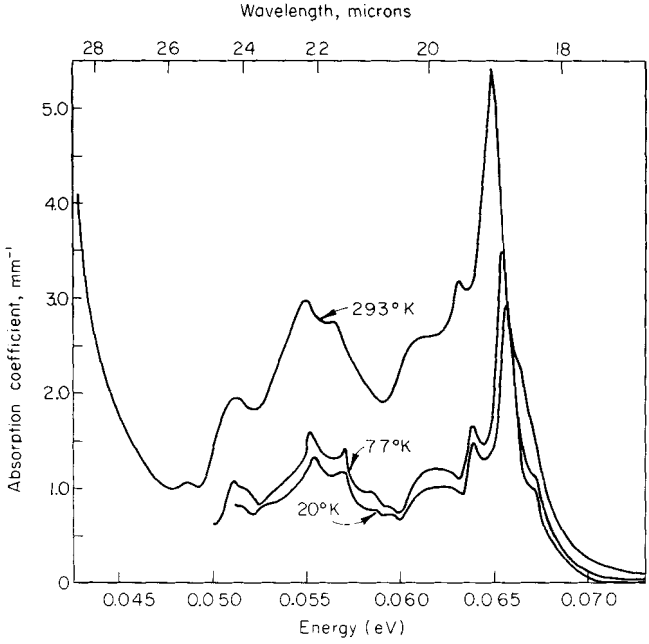


FIG. 11b. Lattice absorption coefficient of high-resistivity *n*-type GaAs vs. wavelength from 18 to 28 microns at 20°, 77°, and 293°K. (After Cochran *et al.*[40])

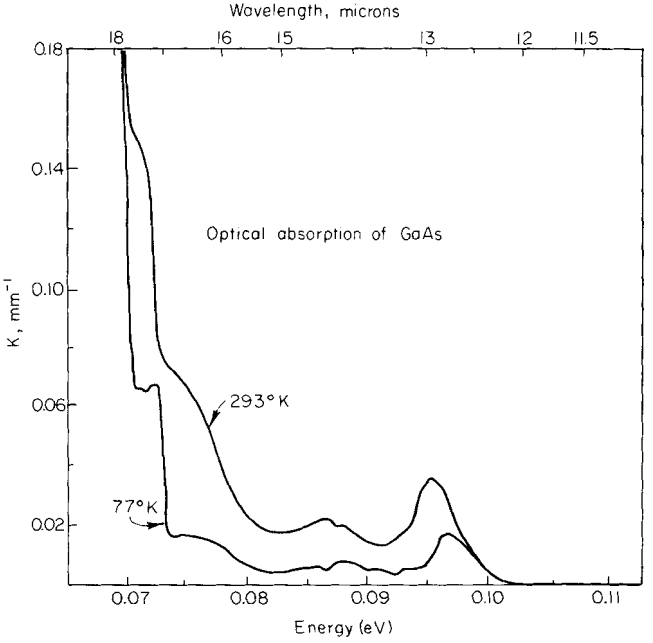


FIG. 11c. Lattice absorption coefficient of high-resistivity *n*-type GaAs vs. wavelength from 10 to 18 microns at 77° and 293°K. (After Cochran *et al.*[40])

TABLE IX

CHARACTERISTIC PHONON ENERGIES AND ASSIGNMENT FOR GaAs

Position (eV)	Assignment
0.0955	$\begin{matrix}\mathrm{TO_1 + TO_2 + TO_2}\\ 0.0324 + 0.0316 + 0.0316\end{matrix}$
0.0885	$\begin{matrix}\mathrm{TO_1 + TO_1 + LA}\\ 0.0324 + 0.0324 + 0.0237\end{matrix}$
0.0860	$\begin{matrix}\mathrm{TO_2 + TO_2 + LA}\\ 0.0316 + 0.0316 + 0.0228\end{matrix}$
0.0735	$\begin{matrix}\mathrm{TO_1 + TO_1 + TA}\\ 0.0324 + 0.0324 + 0.0087\end{matrix}$
0.0716 (?)	$\begin{matrix}\mathrm{TO_2 + TO_2 + TA}\\ 0.0316 + 0.0316 + 0.0084\end{matrix}$
0.0648	$\begin{matrix}\mathrm{TO_1 + TO_1}\\ 0.0324 + 0.0324\end{matrix}$
0.0631	$\begin{matrix}\mathrm{TO_2 + TO_2}\\ 0.0316 + 0.0316\end{matrix}$
0.0612	$\begin{matrix}\mathrm{TO_1 + LO}\\ 0.0324 + 0.0288\end{matrix}$ or $\begin{matrix}\mathrm{TO_2 + LO}\\ 0.0316 + 0.0296\end{matrix}$
0.058	$\begin{matrix}\mathrm{LO + LO}\\ 0.029 + 0.029\end{matrix}$
0.0565	$\begin{matrix}\mathrm{TO_1 + LA}\\ 0.0324 + 0.0241\end{matrix}$
0.0548	$\begin{matrix}\mathrm{TO_2 + LA}\\ 0.0316 + 0.0232\end{matrix}$
0.0510	$\begin{matrix}\mathrm{LO + LA}\\ 0.0288 + 0.0222\end{matrix}$
0.048 (?)	$\begin{matrix}\mathrm{LA + LA}\\ 0.024 + 0.024\end{matrix}$
0.0413	$\begin{matrix}\mathrm{TO_1 + TA}\\ 0.0324 + 0.0089\end{matrix}$
0.0398	$\begin{matrix}\mathrm{TO_2 + TA}\\ 0.0316 + 0.0082\end{matrix}$
0.038	$\begin{matrix}\mathrm{LO + TA}\\ 0.029 + 0.009\end{matrix}$

blende structure and has an infrared-inactive fundamental resonance. Detailed absorption data from 1000 cm^{-1} to 300 cm^{-1} wave numbers and at different temperatures have been given by Cochran *et al.*[40] The absorption coefficient as a function of photon energy is given in Fig. 11. Sixteen peaks observed were interpreted in terms of five characteristic phonon energies indicated in Table IX as TO_1, TO_2, LO, LA, and TA. It has been pointed out,[41] moreover, that the same peaks plus the ones seen in Fig. 11 at ~0.067, ~0.053, and 0.0444 eV could be explained with another set of five characteristic phonons. The two different phonon assignments are given in Table X where that due to Cochran *et al.* is called assignment 1.

TABLE X

TWO DIFFERENT SETS OF CHARACTERISTIC PHONON ENERGIES FOR GaAs

	Assignment 1		Assignment 2		
	ν (cm^{-1})	E (eV)		ν (cm^{-1})	E (eV)
TO_1	262	0.0324	ν_1	262	0.0324
TO_2	255	0.0316	ν_2	247	0.0306
LO	239–232	0.0296–0.0288	ν_3	207	0.0256
LA	195–180	0.0241–0.0222	ν_4	181	0.0224
TA	73–68	0.0090–0.0082	ν_5	127	0.0157

The comparison between the predicted and observed temperature dependencies for the absorption bands is equally good for the two assignments.

This lack of uniqueness in the characteristic phonon energies has also been noted for other cases (see InP, CdS, and ZnS), and in the absence of more infrared data such as the low-energy-difference bands we must resort to other considerations in order to make a choice between the assignments. It must be recalled that neither assignment may be totally correct because of the assumptions involved in attempting to fit all peaks by using exactly or nearly exactly the same few phonon energies. However, assignment 2 does not possess the low-energy TA phonon predicted by the shell-model calculation given in Fig. 1 and confirmed by neutron scattering[42] as in Fig. 12. Also the systematics of the phonon energies for the IV, III–V, and II–VI compounds tend to favor assignment 1. Assignment 2 gives $(LO/TO)^2 = 0.66$, which is in poor agreement with the data of Fig. 2.

[40] W. Cochran, S. J. Fray, F. A. Johnson, J. E. Quarrington, and N. Williams, *J. Appl. Phys.* **32**, 2102 (1961).

[41] W. G. Spitzer, *J. Appl. Phys.* **34**, 792 (1963).

[42] J. L. Waugh and G. Dolling, *Phys. Rev.* **132**, 2410 (1963).

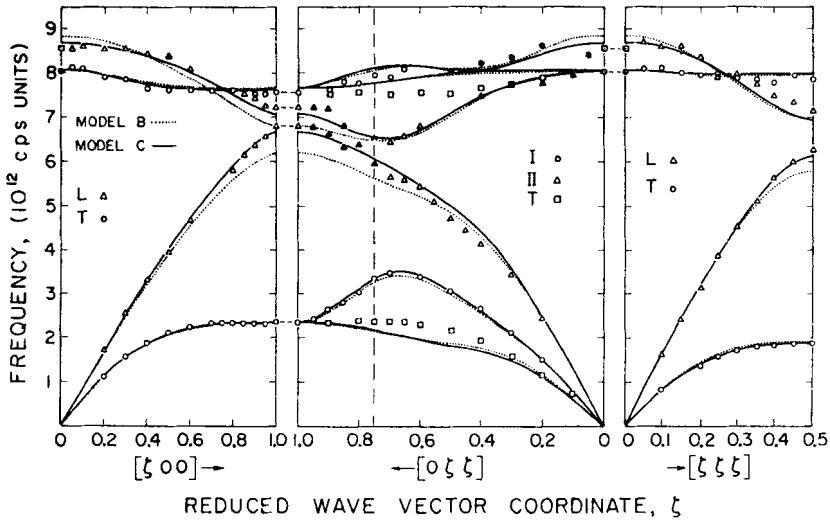


FIG. 12. Neutron scattering results for the phonon curves of GaAs. (After Waugh and Dolling.[42])

9. GALLIUM PHOSPHIDE

The absorption coefficient for gallium phosphide from 1000 to 400 cm^{-1} wave numbers was determined by Kleinman and Spitzer.[21] The samples had sufficient free-electron absorption that in order to obtain accurate measurements of the lattice absorption it was necessary to reduce the carrier concentration by compensation. Within the accuracy of measurement the copper diffusion did not alter the lattice absorption. The room-temperature absorption coefficient of a copper-diffused sample is shown in Fig. 13, where α is the measured absorption coefficient and α_f is that calculated as being due to the single-phonon absorption band. Nine two-phonon bands were explained in terms of five characteristic phonon energies. Because of the large energy difference between the two higher- and the three lower-energy phonons it was assumed that the two were optical and the three acoustical. Although LO(Γ) > TO(Γ), it appears from the photon systematics that TO > LO near the zone edge. The proposed assignment is given in Table XI. One band, located at 604 cm^{-1}, did not fit into the assignment scheme and was assumed to be an impurity band. Attempts to identify the impurity as oxygen were unsuccessful.

As noted in the SiC discussion, the two-phonon absorption in the partially polar materials is approximately an order of magnitude larger than that of silicon, germanium, and diamond. It was shown[21] that the integrated absorption for the optical-optical mode combination bands is $\int \alpha \, d\lambda = 7 \times 10^{-3}$ for GaP, 2×10^{-2} for SiC, and 6×10^{-4} for Si. The value for Si

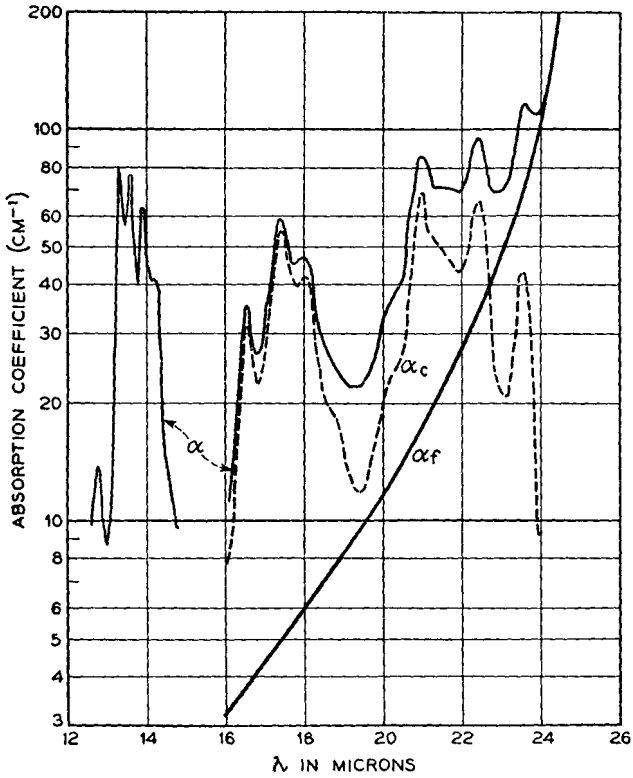


FIG. 13. The experimental absorption coefficient α, the absorption coefficient for the fundamental resonance α_f, and the absorption coefficient for the combination bands $\alpha_c = \alpha - \alpha_f$. (After Kleinman and Spitzer.[21])

already includes a factor of 2 to take into account the difference in selection rules between the diamond and zinc blende cases. This difference in integrated absorption was taken as evidence for the importance of the anharmonic mechanism in the first two cases, and led Kleinman[4] to a detailed consideration of the anharmonic model for GaP.

10. GALLIUM ANTIMONIDE

A particularly nice demonstration of the use of compensation as a technique for reducing free-carrier absorption, thus enabling lattice band measurements to be made, is provided by GaSb. Pulled GaSb crystals normally have a large net acceptor concentration, $\sim 10^{17}/\text{cm}^3$. The infrared transmission spectrum for a 0.032-in thick sample is given by curve A in Fig. 14. Hrostowski and Fuller[43] diffused Li into the sample with the

[43] H. Hrostowski and C. S. Fuller, *J. Phys. Chem. Solids* **4**, 155 (1958).

TABLE XI

SUMMARY OF COMBINATION BANDS IN GaP[a]

λ (microns)	ν (cm^{-1})	Assignment[b]	$\nu_{expected}$ (cm^{-1})	f_{exp}	f_{theor}
12.75	784	3 phonon	—	—	—
13.25	755	TO + TO	756	1.3	1.4
13.55	738	LO + TO	739	1.4	1.4
13.85	722	LO + LO	722	1.3	1.4
(14.15)	707	—	—	—	—
16.55	604	—	—	1.5	—
17.40	575	TO − LA	575	1.5	1.5
17.90	559	LO + LA	558	1.6	1.5
(18.60)	538	—	—	—	—
(20.3)	493	TO + TA_1	493	1.8	1.5
20.95	477	LO + TA_1	476	1.6	1.5
22.40	446	TO + TA_2	444	1.6	1.6
23.50	426	LO ± TA_2	427	~1.5	1.6

[a] λ (microns) and ν (cm^{-1}) are the wavelength and wave number of the observed absorption bands. The third column gives the assignments of the bands. The $\nu_{expected}$ is determined from the assignment and the phonon values given at the bottom of the table. f_{exp} is the ratio of α_c (200°C) to α_c (25°C), and f_{theor} is the predicted ratio calculated according to Eq. (15).

[b] TO = 378, LO = 361, LA = 197, TA_1 = 115, TA_2 = 66.

result that transmission became as given by curve B. Bands were observed at frequencies given in Table XII. Mitra[12] has interpreted these measurements with four characteristic phonons, and the assignments are also indicated in Table XII.

TABLE XII

PHONON ASSIGNMENTS IN GaSb

Absorption peak energy		Characteristic phonon assignment	Calculated position
(eV)	(cm^{-1})		(cm^{-1})
0.0302	244	LO + TA	244
0.0310	250	2LO − LA	252
0.0359	240	LO + 2TA	291
0.0404	326	LO + LA	327
0.0434	350	TO + LA	349
0.0508	410	TO + LO	408
0.0532	429	2TO	430
0.0625	504	TO + LO + 2TA	506

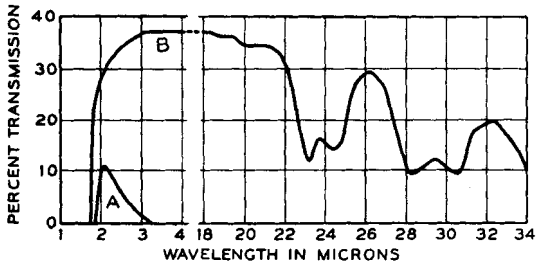


FIG. 14. The room-temperature absorption spectra of GaSb: (A) before and (B) after compensation by lithium diffusion. Sample thickness is 0.032 in. (After Hrostowski and Fuller.[43])

11. INDIUM ARSENIDE

Measurements of the room-temperature multiphonon lattice absorption bands of InAs were reported by Oswald[44] in a study of the mixed crystal system $In(As_yP_{1-y})$. Unfortunately, the measurements were not sufficiently detailed to permit characteristic phonon assignments. Figure 15 shows some recent room-temperature data of Lorimor and Spitzer[45] on a single-crystal sample of *n*-type InAs. The absorption bands are similar to those

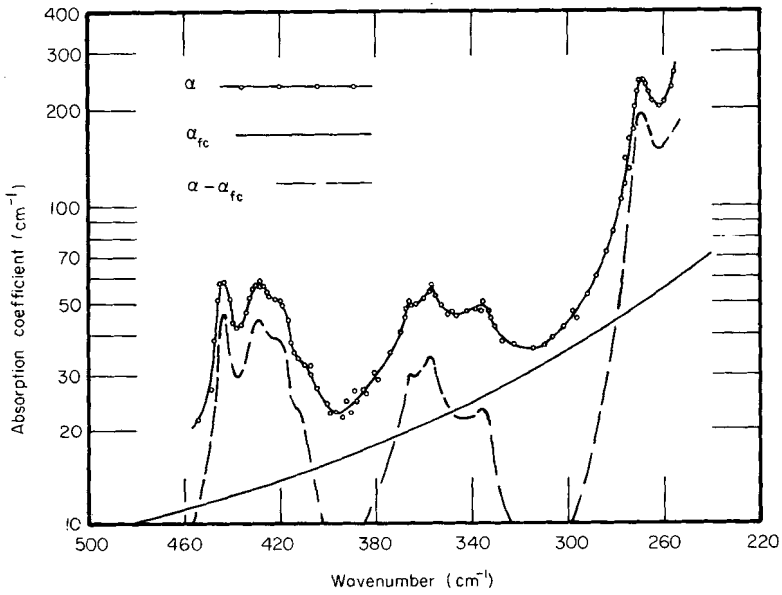


FIG. 15. Room temperature infrared absorption of InAs. The small circle indicates the experimental data. The solid curve without points is the estimated free carrier absorption. The dashed curve gives the multiphonon absorption. (After Lorimor and Spitzer.[45])

[44] F. Oswald, *Z. Naturforsch.* **14a**, 374 (1959).
[45] O. G. Lorimor and W. G. Spitzer, *J. Appl. Phys.* **36**, 1841 (1965).

observed in other III–V compounds and are probably lattice bands. The rapid rise in the absorption observed at the low energy is due to the fundamental[46] located at $TO(\Gamma) = 219\,cm^{-1}$.

The observed bands can be interpreted in terms of four characteristic phonon energies as indicated in Table XIII. These phonon values should be regarded as tentative because measurements on different samples and at low temperature have not yet been made. The assignment, however, does seem to be consistent in that a $TO_1 + TO_2$ is not observed, which is to be expected if the values come from high density-of-states regions at

TABLE XIII

PHONON ASSIGNMENTS IN InAs

Absorption peaks (cm^{-1})	Assignment[a]	Calculated peak position (cm^{-1})
444	$2TO_1$	444
428	$2TO_2$	428
419	$TO_1 + LO$	418
409	$TO_2 + LO$	410
366	$TO_1 + LA$	365
357	$TO_2 + LA$	357
336	$LO + LA$	339

[a] $TO_1 = 222\,cm^{-1}$, $TO_2 = 214\,cm^{-1}$, $LO = 196\,cm^{-1}$, $LA = 143\,cm^{-1}$, $TA = ?$

different $\mathbf{q}$. Also the lack of a 2 LO band is consistent with the weakness of $TO_1 + LO$ and $TO_2 + LO$ bands compared to the 2 TO_1 and 2 TO_2 bands.

The choice of TO_1, TO_2, LO, and LA rather than TO, LO, LA, and TA is dictated largely by the phonon energies. If the second assignment is used, poor agreement is observed for the Brout sum rule, whereas the first assignment gives good agreement (6% or better) if $TA \gtrsim LA/2$. With the exception of diamond, this latter condition is reasonably well followed by all the materials given in Table III. The assignment used is also in fair agreement with the predictions of Figs. 2 and 3. (See Ref. 17 for recent spectral emittance measurements and a critical-point analysis for this material.)

12. INDIUM ANTIMONIDE

The original observation of some of the combination bands of InSb was made by Spitzer and Fan.[47] Detailed measurements over a large frequency

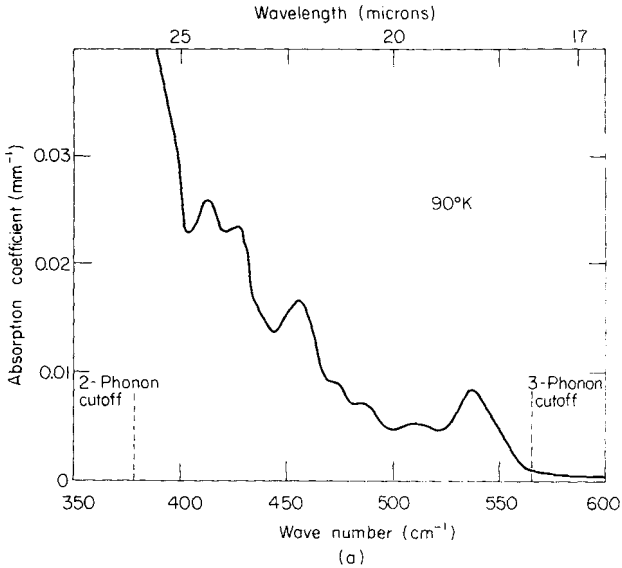
[46] M. Hass and B. W. Henvis, *J. Phys. Chem. Solids* **23**, 1099 (1962).
[47] W. G. Spitzer and H. Y. Fan, *Phys. Rev.* **99**, 1891 (1955).

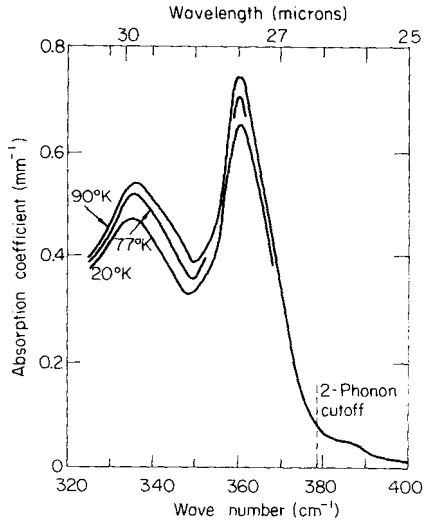
TABLE XIV

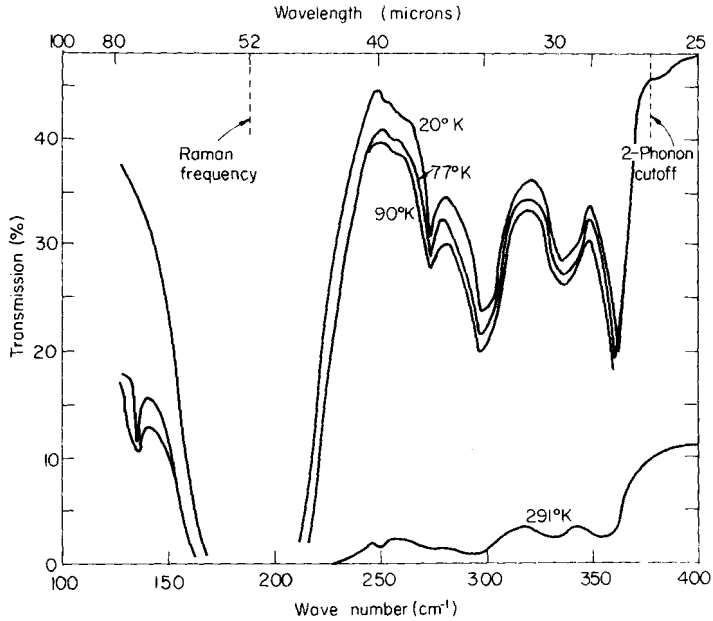
CHARACTERISTIC PHONON ASSIGNMENT IN InSb

Absorption-peak position (cm^{-1})	Observed relative intensity			Assignment[a]	Calculated peak position (cm^{-1})	Calculated relative intensity		
	20°K	77°K	90°K			20°K	77°K	90°K
538	—	—	—	3TO	537	—	—	—
513	—	—	—	2TO + LO	513	—	—	—
488	—	—	—	TO + 2LO	489	—	—	—
475	—	—	—	2TO + LA	476	—	—	—
456	—	—	—	3LO or TO + LO + LA	465 or 442	—	—	—
426	—	—	—	2LO + LA	428	—	—	—
413	—	—	—	TO + 2LA	415	—	—	—
360.5	1	1.08	1.13	2TO	358	1	1.07	1.12
336	1	1.10	1.15	TO + LO	334	1	1.09	1.15
297	1	1.14	1.25	TO + LA	297	1	1.16	1.24
274	1	1.17	1.26	LO + LA	273	1	1.18	1.27
136	0	0.8	1	TO − TA	136	0.06	0.83	1
85.5	—	—	—	2TA	86	—	—	—

[a] TO = 179 cm^{-1}, LO = 155 cm^{-1}, LA = 118 cm^{-1}, TA = 43 cm^{-1}.


Wavelength (microns)
25
20
17
Absorption coefficient (mm⁻¹)
0.03
0.02
0.01
0
90°K
2-Phonon cutoff
3-Phonon cutoff
350
400
450
500
550
600
Wave number (cm⁻¹)
(a)


Wavelength (microns)
30
27
25
Absorption coefficient (mm⁻¹)
0.8
0.6
0.4
0.2
0
90°K
77°K
20°K
2-Phonon cutoff
320
340
360
380
400
Wave number (cm⁻¹)
(b)



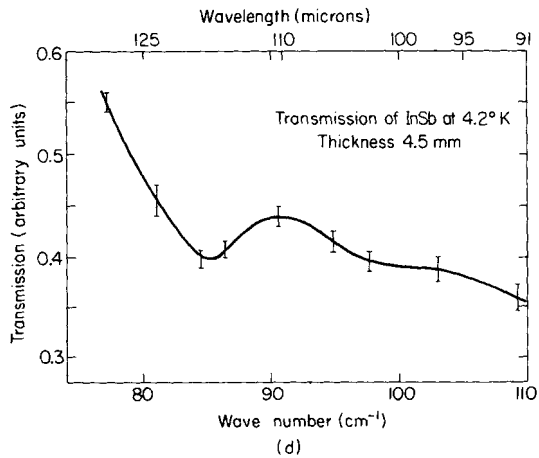


FIG. 16. (a) Absorption coefficients for indium antimonide in the range 600 to 350 cm^{-1}. (b) Percentage transmissions for indium antimonide in the range 400 to 320 cm^{-1}. (c) Absorption coefficients for indium antimonide in the range 400 to 100 cm^{-1}. (d) Transmission of indium antimonide in the range 110 to 75 cm^{-1}. (After Fray *et al.*[48])

range, from 600 to 77 cm^{-1}, and as a function of temperature from 291° to 20°K have been reported by Fray *et al.*[48] The optical measurements, characteristic phonon assignments, and comparison of observed and calculated temperature dependencies are summarized in Fig. 16 and Table XIV. Of noteworthy interest is the observation of the TA + TA band at 85.5 cm^{-1}, which is on the low-energy side of the one-phonon band at TO(Γ) = 181.5 cm^{-1}. As previously observed, this measurement required the use of far-infrared instrumentation.

13. Indium Phosphide

The attempts to assign characteristic phonon energies for this material have been based on an absorption spectrum given by Newman.[49] Although the measurement as shown in Fig. 17 is not very detailed, it does allow a tentative assignment. The assignment given by Mitra[12] does fit the observed bands and is consistent with the phonon systematics discussed in Section 2, *e*. If LO = 318 cm^{-1}, TO = 329 cm^{-1}, LA = 150 cm^{-1}, and TA = 62 cm^{-1}, then the bands at 379, 403, 442, 467, 633, and 658 cm^{-1} would be LO + TA, LO + LA − TA, LO + 2TA, LO + LA, 2LO, and 2TO, respectively. Also the shoulder at ~492 cm^{-1} could be TO + LO − LA. Unfortunately, low-temperature measurements are not available. They would be of considerable aid in checking at least the LO + LA − TA and TO + LO − LA assignments. The LO + LA − TA assignment (band at 403 cm^{-1} or 0.050 eV) is surprising, since it has a higher peak absorption than any of the two phonon bands.

Recent spectral emittance measurements[17] have provided better data. A critical-point analysis for this material is given by Stierwalt and Potter (see next chapter).

14. Aluminum Antimonide

The early measurements of lattice absorption by Turner and Reese[50] were later repeated[51] in much greater detail by the same investigators. They described their results in terms of four characteristic phonon energies. The absorption measurements and a summary of the assignments with the phonon energies are given in Fig. 18 and Table XV. Considering the number of absorption bands fitted, this is an impressive piece of work. Birman[9] has pointed out that upon close inspection there may be some inconsistencies with the zinc blende selection rules. However, in view of the characteristic phonon approximation previously discussed and since

[48] S. J. Fray, F. A. Johnson, and R. H. Jones, *Proc. Phys. Soc.* (*London*) **76**, 939 (1960).
[49] R. Newman, *Phys. Rev.* **111**, 1518 (1958).
[50] W. J. Turner and W. E. Reese, *Phys. Rev.* **117**, 1003 (1960).
[51] W. J. Turner and W. E. Reese, *Phys. Rev.* **127**, 126 (1962).

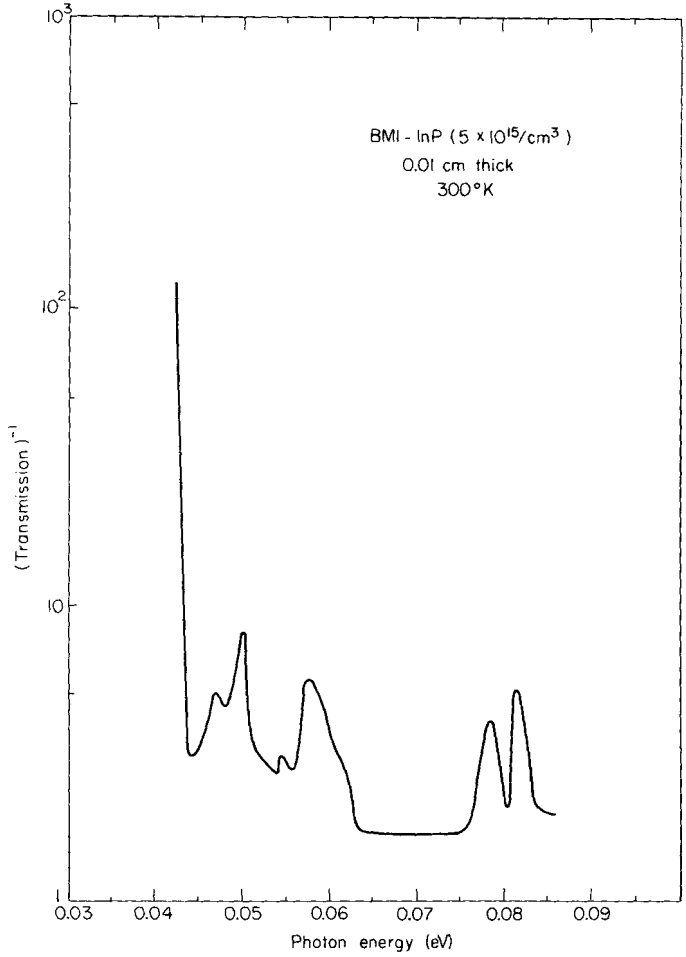


FIG. 17. Absorption spectrum (300°K) of an InP sample in the reststrahlen region. (After Newman.[49])

the selection rules hold only at the specified wave vectors, the work of Turner and Reese is quite impressive.

There is insufficient data available for the other aluminum III–V compounds to attempt even a qualitative assignment.

15. CADMIUM SULFIDE (WURTZITE)

The most recent work on CdS is that of Marshall and Mitra[13] in which they review the previous work done on this material. Balkanski and Besson[52] reported seven absorption peaks between 600- and 400-cm^{-1}

[52] M. Balkanski and J. M. Besson, *J. Appl. Phys.* **32**, 2292 (1961).

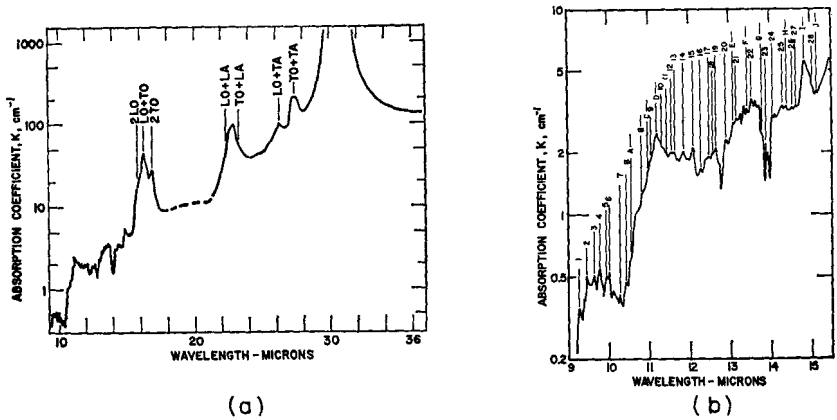


FIG. 18. Absorption coefficient of AlSb at 300°K: (a) In the range 36 to 10 microns. (b) In the range 15 to 9 microns, showing three (letters)- and four (numbers)-phonon recombination bands. (After Turner and Reese.[51])

TABLE XVa

THE FOUR CHARACTERISTIC PHONONS OF AlSb, GIVEN IN DIFFERENT UNITS

Mode	ν (cm^{-1})	(°K)	(eV)
LO	316	454	0.039
TO	297	428	0.037
LA	132	190	0.016
TA	65	93	0.008

TABLE XVb

SUMMARY OF THE TWO-PHONON SUMMATION-BAND DATA FOR AlSb WITH PROPOSED ASSIGNMENT AND OBSERVED AND CALCULATED INTENSITY RATIOS FOR TWO TEMPERATURES

Observed			Assignment	Expected		
λ (microns)	ν (cm^{-1})	f_0		λ (microns)	ν (cm^{-1})	f_c
15.80	633	1.56	2LO	15.82	632	1.55
16.31	613	1.57	LO + TO	16.31	613	1.59
16.81	595	1.70	2TO	16.83	594	1.62
22.33	448	1.91	LO + LA	22.32	448	2.20
23.29	429	2.27	TO + LA	23.31	429	2.23
26.30	380	2.86	LO + TA	26.25	381	2.82
27.50	363	2.83	TO + TA	27.62	362	2.84

TABLE XVc

SUMMARY OF THE THREE- AND FOUR-PHONON COMBINATION BANDS IN AlSb

Band No.	Assignment	Expected		Observed	
		ν (cm^{-1})	λ (microns)	ν (cm^{-1})	λ (microns)
1	3LO + LA	1080	9.26	1081	9.26
2	2LO + TO + LA	1061	9.42	1059	9.44
3	LO + 2TO + LA	1042	9.60	1042	9.60
4	3TO + LA	1023	9.77	1023	9.77
5	3LO + TA	1013	9.87	1012	9.88
6	2LO + TO + TA	994	10.06	996	10.03
7	2TO + LO + TA	975	10.26	975	10.26
8	3TO + TA	956	10.46	959	10.43
A	3LO	948	10.55	949	10.54
B	2LO + TO	929	10.76	928	10.78
C	LO + 2TO	910	10.99	911	10.98
9	2LO + 2LA	896	11.16	896	11.16
D	3TO	891	11.22	893	11.20
10	3LO − TA	883	11.32	883	11.33
11	LO + TO + 2LA	877	11.40	876	11.42
12	2LO + TO − TA	864	11.57	865	11.56
13	2TO + 2LA	858	11.65	858	11.65
14	LO + 2TO − TA	845	11.83	846	11.82
15	2LO + LA + TA	829	12.06	828	12.07
16	3LO − LA	816	12.25	816	12.26
17	LO + TO + LA + TA	810	12.34	809	12.36
18	2LO + TO − LA	797	12.55	795	12.57
19	2TO + LA + TA	791	12.64	792	12.63
20	LO + 2TO − LA	778	12.85	778	12.85
E	2LO + LA	764	13.09	765	13.07
21	3TO − LA	759	13.17	760	13.15
F	LO + TO + LA	745	13.42	745	13.42
22	LO + TO + 2TA	743	13.46	741	13.50
G	2TO + LA	726	13.77	728	13.73
23	2TO + 2TA	724	13.81	725	13.80
24	LO + 3LA	712	14.04	712	14.05
25	2LO + LA − TA	699	14.31	700	14.29
H	2LO + TA	697	14.35	696	14.36
26	TO + 3LA	693	14.43	689	14.52
27	LO + TO + LA − TA	680	14.70	683	14.63
I	LO + TO + TA	678	14.75	675	14.83
28	2TO + LA − TA	661	15.13	661	15.12
J	2TO + TA	659	15.17	660	15.16

TABLE XVI

ASSIGNMENT OF THE ABSORPTION MAXIMA OBSERVED IN CdS IN TERMS OF PHONON COMBINATIONS OF FREQUENCIES

Band No.	Marshall and Mitra[13] (300°K) (cm^{-1})	Balkanski and Besson[52] (77°K) (cm^{-1})	Deutsch[53] (77°K) (cm^{-1})	Marshall and Mitra assignment[a]	Calculated (cm^{-1})
1	308	—	—	$TO_2 + TA_2$	308
2	318	—	—	$TO_2 + TA_1$	317
3	331	—	—	$TO_1 + TA_2$	331
4	340	—	—	$TO_1 + TA_1$	340
a	347	—	—	$TO_1 + TO_2 - LA$	350
5	365	—	—	$LO + TA_2$	365
6	374	—	—	$LO + TA_1$	374
7	387	—	—	$TO_2 + LA$	387
—	—	403	—	—	—
8	410	—	—	$TO_1 + LA$	410
b	421	—	—	$TO_1 + TO_2 - TA_1$	420
c	428	—	432	$TO_1 + TO_2 - TA_2$	429
9	442	—	443	$LO + LA$	444
d	467	—	—	$TO_2 + LA + TA_2$	466
10	478	—	—	$2TO_2$	476
11	498	500	502	$TO_1 + TO_2$	499
e	511	—	—	$2LO - TA_1$	511
12	522	524	562	$2TO_1$	522
13	533	540	—	$LO + TO_2$	533
14	555	562	562	$LO + TO_1$	556
f	571	579	576	$TO_1 + TO_2 + TA_2$	569
15	590	599	598	$2LO$	590
g	628	—	—	$LO + TO_1 + TA_2$	626
h	647	—	—	$TO_1 + TO_2 + LA$	648
i	660	—	—	$2LO + TA_2$	660
j	684	—	—	$LO + TO_2 + LA$	682
k	695	—	—	$LO + TO_1 + 2TA_2$	696
l	715	—	—	$3TO_2$	714
m	730	—	—	$2LO + 2TA_2$	730
—	795	—	—	$LO + TO_1 + TO_2$	794
—	1045 (broad and weak)	—	—	$LO + 2TO_1 + TO_2$	1055
—	1345 (broad and weak)	—	—	$2LO + 2TO_1 + TO_2$	1350

[a] $LO = 295$, $TO_1 = 261$, $TO_2 = 238$, $LA = 140$, $TA_1 = 79$, $TA_2 = 70$.

wave numbers and used four characteristic frequencies. Later, Deutsch[53] made some polarized-light measurements, and he found new absorption peaks that were not consistent with the previously assigned phonon energies. It was also observed[41] that one of the Balkanski and Besson frequencies could be altered and still fit their observed data. The spectral range of measurement has been extended[13,54] to include 1400 to 600 cm^{-1} and 400 to 300 cm^{-1}. It was found that six characteristic energies were necessary; the assignments are given in Table XVI. The temperature dependencies of the two-phonon bands are in reasonable agreement with the expected values, and the characteristic phonon energies fit in well with the systematics of those for the group-IV elements and the III–V compounds.

16. Zinc Sulfide (Wurtzite and Zinc Blende)

In ZnS some reasonably detailed measurements of the multiphonon bands have been made in both the hexagonal and cubic structures, and it would be of interest to compare the characteristic phonon assignment for the two cases. The comparison, however, is hampered by uncertainty in the correct phonon assignment for the cubic modification.

The cubic zinc blende measurements were reported by Deutsch[55] for the wave-number range 10^4 to 417 cm^{-1} and temperatures between 8° and 420°K. A four-phonon assignment was used. Deutsch pointed out that his assignment was not unique. Later these measurements were reinterpreted by Marshall and Mitra[13] in terms of two new four-phonon assignments. The first of their assignments agrees better than the second with the observed peak positions and with the Brout sum rule, but is in poorer agreement with the $(LO/LA)^2$ vs. M_1/M_2 results of Fig. 3. The phonon assignments are summarized in Table XVII.

The hexagonal modification has been measured by Marshall and Mitra,[13] and they found it necessary to use six phonon energies as indicated in Table XVIIc. It is of interest to note that these authors have used $TO_1 + TO_2$ and both $TO_1 + TA_1$ and $TO_1 + TA_2$ assignments, which would be forbidden if the subscripts referred to energies for the same branch at different critical points. Therefore, the two transverse optical energies would indicate a breakdown of the twofold degeneracy of that branch and similarly for the acoustic branch.

17. Zinc Selenide (Wurtzite)

The 300°K absorption spectrum for ZnSe was reported by Aven *et al.*[56] and is given in Fig. 19. The data were treated as in Table XVIII by Mitra,[12]

[53] T. Deutsch, *J. Appl. Phys.* **33**, 751 (1962).
[54] S. S. Mitra, *Phys. Letters* **6**, 249 (1963).
[55] T. Deutsch, *Proc. Intern. Conf. Phys. Semicond., Exeter, 1962* p. 505. Inst. of Phys. and Phys. Soc., London, 1962.
[56] M. Aven, D. T. F. Marple, and B. Segall, *J. Appl. Phys.* **32**, 2261 (1961).

using a four-phonon set to fit six absorption peaks. A noteworthy point with regard to the phonon energies employed is that LO and TO are nearly equal as predicted by Keyes' relation and shown in Fig. 2 where ZnSe has an e^* of 0.7.

IV. Critical-Point Analysis

It has been emphasized in the discussion up to this point that the use of characteristic phonon energies to fit the peaks in the absorption data

TABLE XVIIa

CHARACTERISTIC PHONON ENERGIES IN CUBIC ZnS

Mode	ν (Deutsch) (cm^{-1})	ν No. 1 (cm^{-1})	ν No. 2 (cm^{-1})
LO	379	339	339
TO	297	298	298
LA	263	155	190
TA	228	93	115

TABLE XVIIb

ASSIGNMENT OF THE MULTIPHONON ABSORPTION BANDS IN CUBIC ZnS

Deutsch[55]			Marshall and Mitra[13]			
Observed (cm^{-1})	Assignment	Calculated (cm^{-1})	Assignment 1	Calculated (cm^{-1})	Assignment 2	Calculated (cm^{-1})
431	—	—	LO + TA	432	TO + TA	413
415	—	—	—	—	—	—
455	2TA	456	TO + LA	453	LO + TA	454
491	LA + TA	491	LO + LA	494	TO + LA	488
526	2LA, TO + TA	526	LO + 2TA	525	LO + LA	529
593	2TO	594	2TO	596	2TO	596
605	—	—	TO + 2LA	608	LO + LA + TA	603
642	LO + LA	642	LO + TO	637	LO + TO	637
677	LO + TO	677	2LO	678	2LO	678
733	—	—	LO + TO + TA	731	LO + 2LA	719
823	2TO + TA	822	LO + TO + 2TA	824	LO + TO + LA	827

TABLE XVIIc

ASSIGNMENT OF THE LATTICE ABSORPTION IN HEXAGONAL ZnS IN TERMS OF THE PHONON FREQUENCIES

Band No.	Peak position at 300°K (cm^{-1})	Assignment[a]	Calculated position (cm^{-1})
1	358	$TO_2 + TA_2$	360
2	362	2LA	362
a	374	$2LO - TO_1$	374
3	381	$TO_2 + TA_1$	383
4	390	$TO_1 + TA_2$	391
b	404	$TO_1 + LA - TA_1$	406
5	409	$TO_1 + TA_1$	409
6	419	$LO + TA_2$	419
c	423	$TO + LA - TA_2$	425
7	437	$LO + TA_1$	437
d	450	$TO_1 + TA_1 + TA_2$	452
e	463	$TO_1 + 2TA_2$	464
8	475	$TO_2 + LA$	474
9	487	$TO_1 + TA_1 + TA_2$	483
10	498	$TO_1 + LA$	500
11	526	$LO + LA$	528
f	555	$LO + TO_2 - TA_1$	551
g	571	$TO_1 + LA + TA_2$	572
12	583	$2TO_2$	584
13	612	$TO_1 + TO_2$	610
h	622	$LO + LA + TA_1$	620
14	634	$2TO_1$	636
15	640	$LO + TO_2$	638
16	658	$LO + TO_1$	658
17	694	2LO	692
i	730	$LO + TO_2 + TA_1$	730
j	750	$2LO + TA_1$	750

[a] LO = 346, TO_1 = 318, TO_2 = 297, LA = 181, TA_1 = 92, TA_2 = 73.

depends upon the approximation of the phonon density-of-states curve by a few main peaks. These peaks represent the gross effect on the absorption and are not necessarily representative of a particular phonon. It would be of considerable interest and importance if the values of the phonon energies for specific branches and at specific points could be deduced from the absorption data. From the work of Hardy and Smith[33] on diamond

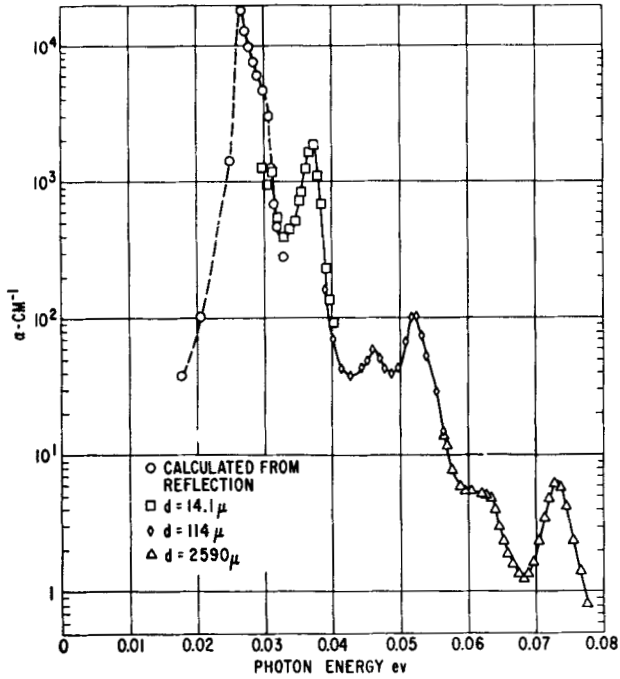


FIG. 19. Absorption coefficient α for ZnSe in the infrared region as a function of photon energy at room temperature. (After Aven *et al.*[56])

TABLE XVIII

CHARACTERISTIC PHONON ENERGIES AND ASSIGNMENTS FOR ZnSe

Peak position (cm^{-1})	Assignment[a]	Calculated position (cm^{-1})
588	2TO + LA	586
501	2LO + TA	503
420	LO + TO	420
371	LO + LA	370
—	TO + LA	374
298	LO + TA	295
—	TO + TA	299
250	LA + TA	249

[a] LO = 208 cm^{-1}, LA = 162 cm^{-1}, TO = 212 cm^{-1}, TA = 87 cm^{-1}.

and some recent work by Johnson[57] for several materials it appears possible to obtain such detailed information from a close inspection of the absorption curves.

Hardy and Smith[33] and Smith *et al.*[22] pointed out that the presence of critical points in an ω vs. $\mathbf{q}$ plot leads to discontinuities in the first derivative of the density-of-states vs. ω curve and hence to kinks or discontinuities of slope in the absorption curve. If critical points are present in two one-phonon branches at the same $\mathbf{q}$, then the corresponding two-phonon branch will also have a critical point. "Accidental" critical points for the two-phonon branch could occur when the two one-phonon branches have the same (if $\mathbf{q}_i - \mathbf{q}_j = 0$) or opposite (if $\mathbf{q}_i + \mathbf{q}_j = 0$) gradients. Omitting the accidental critical points, we then expect the critical points to occur at Γ, X, L, and W for frequencies corresponding to all two-phonon combinations at these points. If allowed by the selection rules of Tables I and II, kinks should be observed in the absorption data at these combination frequencies.

Smith *et al.* have used this approach to make a detailed interpretation of their absorption data for diamond. The results of this critical-point analysis are given in Table XIX in the form of two possible assignments, where it is seen that the indicated features in the absorption are attributed to combinations of single-phonon critical points. The $\mathbf{q}_1 + \mathbf{q}_2 = 0$ condition, of course, rules out any combination of two phonons from critical points at different $\mathbf{q}$'s. It may also be noted that the selection rule that the phonons cannot come from the same branch has been followed. Details of the analysis[22,23] are given by Smith *et al.* The features indicated in Table VI at 0.302, 0.281, and 0.267 eV are not included in Table XIX but are assigned as TO(L) + LO(L), TO(L) + LA(L), and LO(L) + LA(L), since the degeneracy of the longitudinal modes at X and W make the combination of two longitudinal modes forbidden at these points.

Some recent neutron work on diamond by Yarnell *et al.*[58] gives the TA branch along the [100] and [111] directions. These authors give TA(X) = 0.099 eV and TA(L) = 0.069 eV, in good agreement with the TA(X) = 0.105 eV and TA(L) = 0.063 eV values of Table XIX. The second-order Raman effect (two-phonon Raman scattering) has been analyzed by Johnson,[57] and the resulting phonon energies at the critical points are in good agreement with those obtained from the absorption data when TA(W) = 0.116 eV and TA(L) = 0.063 eV are used.

The work done on diamond has been extended to other materials by Johnson.[57] Of particular interest are the results for silicon, since accurate

[57] F. A. Johnson, *Progr. Semicond.* **9**, 179 (1965).

[58] J. L. Yarnell, J. L. Warren, and R. G. Wengel, *Phys. Rev. Letters* **13**, 13 (1964).

TABLE XIX

CRITICAL POINT ANALYSIS FOR DIAMOND

Feature energy (eV)	Assignment and phonon energies (eV)	Calculated energy (eV)	α600/α300[a]	
			Calculated	Observed
(a) 0.258	TO(X) + TA(X)	0.258	—	—
(Kink)	0.153 + 0.105	—	—	—
0.251	TO(W) + TA(W)	0.251	1.17	1.17
(Peak)	0.158 + 0.093	—	—	—
0.244	L(X) + TA(X)	0.244	—	—
(Peak)	0.139 + 0.105	—	—	—
0.225	L(W) + TA(W)	0.224	1.2	1.4
(Kink)	0.131 + 0.093	—	—	—
	or			
	TO(L) + TA(L)	0.221	1.3	1.4
	0.158 + 0.063	—	—	—
	[no TA(Σ) c.p.]			
(b) 0.258	TO(X) + TA(X)	0.258	—	—
(Kink)	0.153 + 0.105	—	—	—
0.251	—	—	—	—
(Peak)	(not associated with c.p.)	—	—	—
0.244	L(X) + TA(X)	0.244	—	—
(Peak)	0.139 + 0.105	—	—	—
0.247	L(W) + TA(W)	0.247	—	—
(Minimum)	0.131 + 0.116	—	—	—
0.274	TO(W) + TA(W)	0.274	—	—
(Kink?)	0.158 + 0.116	—	—	—

[a] Ratio of the absorption coefficients at 600°K to those at 300°K.

absorption measurements, neutron-scattering data, and shell-model calculations are all available for the same material. Johnson's critical-point analysis is given in Table XX. The large amount of structure observed and the accuracy in absorption measurements permit the determination of all branches at each critical point. The importance of having high-resolution measurements for this type of analysis becomes apparent. It is also apparent that this type of analysis requires detailed knowledge of the selection rules. Johnson also related minima in the absorption to forbidden combination

TABLE XX

CRITICAL-POINT ANALYSIS OF INFRARED SPECTRUM FOR SILICON

Position (eV)	Feature[a]	Assignment	Calculated position (eV)
0.1289	m	$O(\Gamma) + O(\Gamma)^b$	0.1288
0.1126	s	$TO(L) + LO(L)$	0.1127
0.1074	s	$TO(X) + L(X)$	0.1024
0.1064	k	$TO(W) + L(W)$	0.1064
0.1040	m	$LO(L) + LO(L)^b$	0.1036
0.1008	k	$L(X) + L(X)^b$	0.1010
0.0985	s	$LO(L) + LA(L)$	0.0985
0.0943	m	$LA(L) + LA(L)^b$	0.0934
0.0915	k	$L(W) + L(W)^b$	0.0918
0.0848	p	$TO(W) + TA(W)$	0.0848
0.0761	s	$TO(X) + TA(X)$	0.0761
0.0756	p	$TO(L) + TA(L)$	0.0757
0.0702	p	$L(W) + TA(W)$	0.0702
0.0697	k	$L(X) + TA(X)$	0.0697
0.0667	k	$LO(L) + TA(L)^b$	0.0666
0.0615	s	$LA(L) + TA(L)$	0.0615
0.0490	m	$TA(W) + TA(W)^b$	0.0486
0.0461	p	$TO(L) - TA(L)$	0.0461

[a] m = minimum, s = shoulder, k = kink, and p = peak.
[b] Forbidden by selection rules of Table I.

energies. A comparison of the phonon energies used to calculate the feature positions in Table XX along with the phonon energies obtained by other methods is given in Table XXI. The over-all agreement, particularly between the infrared and neutron data, is very impressive.

Johnson has also deduced critical-point energies for several of the zinc blende crystals where the available data are sufficiently detailed to permit a critical-point analysis. The results are summarized in Table XXII. In most cases these results are to be regarded as preliminary. Neutron data are not yet available except for GaAs, where the critical-point values are in good agreement with those proposed by Johnson.

It may be observed from Table XXII that the TO and LO assignments at L and X are in agreement with the order for characteristic phonon energies as proposed by Keyes, but the SiC and ZnS are opposite. It therefore becomes of interest to plot $(LO/TO)^2$ as a function of e^{*2} as in Fig. 2, but now for the L and X points independently. Again one obtains graphs

TABLE XXI

CRITICAL-POINT PHONON ENERGIES FOR SILICON[a]

Point	Mode	Infrared absorption	Neutron scattering	Shell model calculated
Γ	O	0.0644	0.0642	0.0617
L	TO	0.0609	0.0607	0.0612
	LO	0.0518	0.0521	0.0557
	LA	0.0467	0.0469	0.0365
	TA	0.0148	0.0142	0.0131
X	TO	0.0569	0.0575	0.0612
	L	0.0505	0.0509	0.0468
	TA	0.0192	0.0186	0.0165
W	TO	0.0605	—	0.0619
	L	0.0459	—	0.0458
	TA	0.0243	—	0.0169

[a] All energies in eV.

TABLE XXII

CRITICAL-POINT ENERGIES OBTAINED FROM INFRARED ABSORPTION IN ZINC BLENDE CRYSTALS[a,b]

Point	Mode	AlSb[c]	GaP	GaAs	InSb	SiC	ZnS[c]
Γ	LO	0.0420	0.0486	0.0355	0.0255	—	0.0454
	TO	0.0399	0.0457	0.0335	0.0235	—	0.0419
L	TO	0.0380	0.0468	0.0326	0.0223	0.1003	0.0398
	LO	0.0289	0.0408	0.0294	0.0199	0.0942	0.0337
	LA	0.0266	0.0346	0.0257	0.0169	0.0688	0.0282
	TA	0.0077	0.0085	0.0073	0.0054	—	—
X	TO	0.0369	0.0447	0.0319	0.0219	0.0961	0.0378
	LO	—	0.0385	0.0296	0.0198	0.0911	0.0341
	LA	—	0.0328	0.0271	0.0177	0.0812	0.0274
	TA	0.0102	0.0144	0.0095	—	0.0416 (?)	—

[a] All energies in eV.

[b] For the values for InAs and InP as obtained from spectral emittance studies, see Chapter 3 by Stierwalt and Potter.

[c] 77°K values.

similar to Fig. 2 if the LO and TO assignments of Table XXII for ZnS and SiC are reversed; however, there is somewhat more scatter in the points, and hence the argument for the reversal is not quite so convincing. The Brout sum rule is followed reasonably well for the phonon values of Tables XXI and XXII. For silicon, the variation among the $\Sigma_i \omega_i^2(\mathbf{q})$ for the different critical points is $\sim 3\%$.

Note added in proof. It has been pointed out by Dr. M. Aven and Dr. D. T. S. Marple that some of the bands in the ZnSe specimen of Fig. 19 may be impurity bands, i.e., localized vibrational modes. In particular the band at 0.037 eV (298 cm^{-1}) is at least in considerable part due to the presence of sulfur. The peak at 0.073 eV (588^{-1}) may also be impurity related. Thus, the analysis of Table XVIII may be questionable. The author wishes to thank Drs. Aven and Marple for pointing out this uncertainty.

CHAPTER 3

Emittance Studies

D. L. Stierwalt and R. F. Potter

I. Introduction 71
II. Experimental Technique 73
III. Experimental Results 76
1. *InAs* 76
2. *InP* 79
3. *InSb (p-Type)* 80
4. *GaSb* 81
5. *GaAs* 81
6. *GaP* 82
7. *AlSb* 82
8. *AlAs* 83
IV. Discussion 83
9. *Reststrahlen Bands* 83
10. *Two-Phonon Processes* 83
11. *Electron-Absorption Effects* 87
V. Summary 90

I. Introduction

When radiation is incident upon the surface of an object, one portion is reflected, another is absorbed, and the remainder is transmitted through the object. If the incident radiation is totally absorbed, the object is known as a blackbody.

The spectral emissive power of such an ideal blackbody—i.e., the power emitted per unit area and per unit wavelength—is given by the Planck equation:

$$W_\lambda(T) = C_1\lambda^{-5}[\exp(C_2/\lambda T) - 1]^{-1}, \tag{1}$$

where $C_1 = 2\pi c^2 h$, $C_2 = hc/k$, h is Planck's constant, k the Boltzmann constant, c the speed of light, λ the vacuum wavelength, and T the absolute temperature.

The flux emitted in the spectral band between λ and $\lambda + \Delta\lambda$ is given by $W_\lambda(T)\,\Delta\lambda$. That portion of the incident radiation which is absorbed by an object can be designated as the spectral absorptance A_λ.

According to Kirchhoff's law, such an object will emit thermal radiation in the amount

$$W_{0\lambda}(T) = E_\lambda W_\lambda(T) = A_\lambda W_\lambda(T), \tag{2}$$

where E_λ (the spectral emittance) $= A_\lambda$ and $W_{0\lambda}(T)$ is the observed thermal radiation at the temperature T. The emittance is defined as the ratio of thermal emission of a body at a given temperature to that of a blackbody at the same temperature and is equal to the absorptance of that body.

Consider a quasi-transparent sample, having plane parallel sides and specular surfaces, in spectral regions where $k/n \ll 1$ ($n^* = n - ik$, which is the complex refractive index). The following approximations hold for the reflectance, transmittance, and absorptance at normal incidence:

$$R = r^2\left[\frac{1 + (1 - 2r^2)\exp(-2\alpha t)}{1 - r^4\exp(-2\alpha t)}\right], \tag{3}$$

$$T = \frac{(1 - r^2)\exp(-\alpha t)}{1 - r^4\exp(-2\alpha t)}, \tag{4}$$

$$E = A = \frac{(1 - r^2)[1 - \exp(-\alpha t)]}{1 - r^2\exp(-\alpha t)}. \tag{5}$$

It is easily seen that

$$A + R + T = 1, \tag{6}$$

where $r = (n^* - 1)/(n^* + 1)$ is the Fresnel reflection coefficient and $\alpha = 4\pi k/\lambda$ is the absorption coefficient, both for normal incidence.

Expressions (3) and (4) have been extensively used for determining the optical properties of solids in many experiments. Equations (2) and (5) suggest a third type of experiment, namely, measuring the spectral emittance. Absorptance studies have been used for opaque samples[1] but only limited experiments have been attempted with quasi-transparent materials such as semiconductors. Moss and Hawkins[2] measured the spectral emittance of InSb and Ge samples for $1.0 < \lambda < 10$ microns at nominal temperatures ($308° < T < 508°$K). More recently, however, the technique has been developed to the point where spectral emittance can be measured for $2.5 < \lambda < 50$ microns and at sample temperatures as low as 77°K.[3]

A large number of III–V compound semiconductor samples have been studied using these techniques. One can study the reststrahlen region,

[1] C. Nanney, *Phys. Rev.* **129**, 109 (1963); M. A. Biondi, *ibid.* **102**, 964 (1956).

[2] T. S. Moss and T. D. H. Hawkins, *Proc. Phys. Soc. (London)* **72**, 270 (1958).

[3] D. L. Stierwalt and R. F. Potter, *Proc. Intern. Conf. Phys. Semicond., Exeter, 1962* p. 513. Inst. of Phys. and Phys. Soc., London, 1962; D. L. Stierwalt, J. B. Bernstein, and D. D. Kirk, *J. Appl. Opt.* **2**, 1169 (1963).

multiple-phonon absorption, free-carrier absorption and edge absorption, in some instances all in the same sample.

This versatility exists in three domains for E_λ values:

(1) $\alpha t \ll 1$. It is seen that for quite transparent samples $E_\lambda \to \alpha t$. Very low absorption coefficients can be and have been measured in this manner.[4]

(2) $\alpha t \gg 1$. At the other extreme, for an opaque sample $E_\lambda \to (1 - r_\lambda{}^2)$. In this instance, information concerning the front-surface reflectance is obtained. This technique is well suited for observing the reststrahlen bands.

(3) In the intermediate situation the absorption coefficient can be obtained from the expression

$$\alpha t = \ln\left(1 + \frac{E}{1 - (E/E_\infty)}\right), \tag{7}$$

where $E_\infty = (1 - r_\lambda{}^2)$. Thus for suitable ratios of E/E_∞, structure in α is directly observed in the emittance spectrum. A secondary item is that the absorption coefficient can be determined with good accuracy from the emittance without precise knowledge of the refractive index for values of $\alpha t \leqslant 2.5$.

II. Experimental Technique

For our emittance measurements we compare radiation from a sample at a given temperature with that from a blackbody at the same temperature. The sample and blackbody are heated or cooled by thermal conduction from the polished aluminum sample holder (Fig. 1). The sample compartment is temperature controlled, well baffled, and painted black. It is assumed that inserting the sample holder and sample or blackbody into the sample compartment has a negligible effect on the blackness of the compartment, and this has been verified experimentally.

The radiation from the sample or the standardizing blackbody is modulated by an opaque chopper wheel. The ac signal from the detector is proportional to the difference between the energy received from the sample or blackbody and that received from the chopper blades. Adding up all contributions to the signal we find

$$S_S = K[E_S W_S + (R_S + T_S)W_R - E_C W_C - R_C W_R], \tag{8}$$

where K is a constant depending on the optics of the instrument and the response of the detector. W_S, W_R, and W_C refer to thermal radiation from a blackbody source at sample, reference, and chopper temperatures, respectively. The reference is the sample compartment, which is normally

[4] D. L. Stierwalt and R. F. Potter, *J. Phys. Chem. Solids* **23**, 99 (1962).

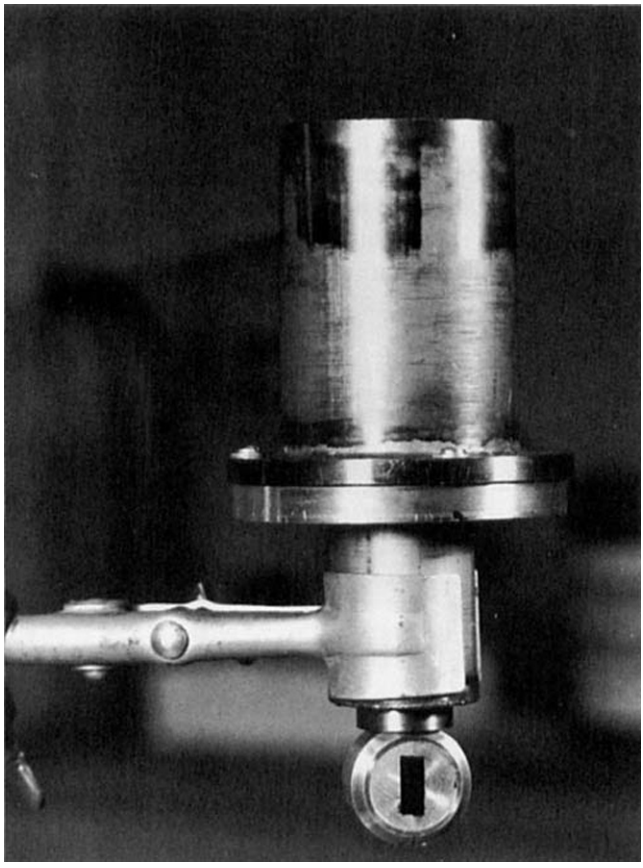


FIG. 1. Liquid-nitrogen cold finger with blackbody inserted in the polished aluminum sample holder.

maintained at 25.0° ± 0.05°C. The first term in the brackets is due to radiation from the sample; the second, radiation from the sample chamber that is reflected and transmitted by the sample. The third and fourth terms are due to radiation emitted and reflected by the chopper blades. Applying Kirchhoff's law, $E + R + T = 1$, Eq. (8) reduces to

$$S_S = K[E_S(W_S - W_R) - E_C(W_C - W_R)]. \tag{9}$$

It is desirable to make the second term in the brackets negligible to simplify data reduction and because the chopper temperature is difficult to measure. For this reason the chopper blades were made of aluminum foil so that E_C would be very small, and the chopper wheel was driven by a

small, efficient motor requiring about 0.1 watt input power. The motor is in good thermal contact with the sample compartment so that very little of the heat from the motor reaches the chopper blades and $W_C - W_R$ is kept small. Checking the system with the sample holder empty ($E_S = 0$) gave no measurable signal, indicating that $E_C(W_C - W_R)$ was indeed negligible.

We thus have

$$S_S = KE_S(W_S - W_R), \tag{10}$$

and for the standardizing blackbody,

$$S_b = K(W_S - W_R). \tag{11}$$

Combining (10) and (11),

$$E_S = S_S/S_b. \tag{12}$$

Note that the sample temperature may be above or below the reference temperature, as long as there is sufficient difference to give a usable signal.

In the modified Beckman IR-3 spectrophotometers used for these measurements, a servo system varies the slit width to maintain constant output from the detector during the spectral scan. The slit and wavelength program with the blackbody in the sample holder is recorded on magnetic tape.

If this program is used to operate the slit and wavelength drives when the sample is in the holder, S_b in Eq. (10) becomes unity; we then have

$$E = S_s, \tag{13}$$

and the spectral emittance is directly recorded on the chart. A block diagram of this system is shown in Fig. 2.

To cover the spectral range from 2 to 44 microns, two instruments are used. One has KBr prisms to cover the 2- to 20-micron region, and the other uses a grating and interference filters from 14 to 44 microns.

For the low-temperature measurements a sample holder was constructed with a well to hold either liquid nitrogen or a mixture of dry ice and alcohol. Normally, the instruments are evacuated to a pressure of about 10^{-2} Torr, but for the low-temperature measurements the sample compartment was evacuated with an ion pump to less than 10^{-6} Torr to avoid contamination of the sample surface. For temperatures from 323° to 500°K a sample holder was made using resistors for heaters and a platinum resistance element as a sensor for the temperature-control circuit. The temperature is monitored by a copper-constantan thermocouple.

The detectors for both instruments are evacuated thermocouples, one having a KBr lens and the other a CsI lens.

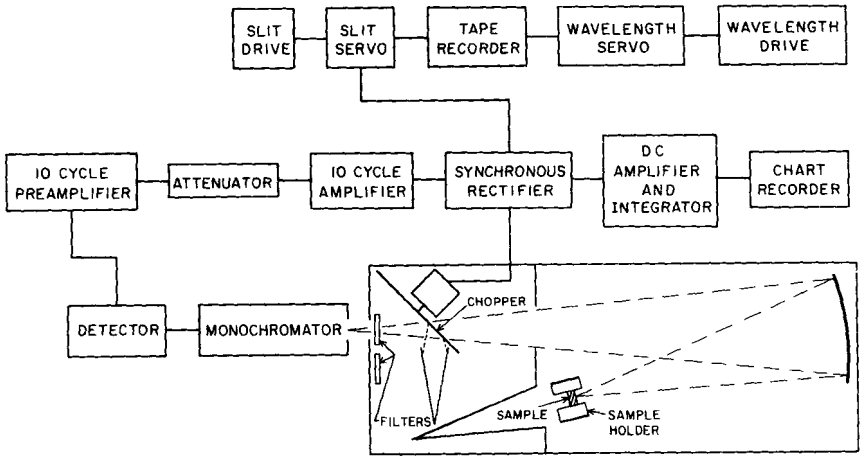


FIG. 2. Block diagram of system for measuring emittance–absorptance. Sample chamber, monochromator, and detector are enclosed in an isothermal evacuated chamber at 25° ± 0.05°C.

III. Experimental Results

1. InAs

Spectral emittance has been used to study a wide variety of optical absorption processes in solids. To date, these processes include transitions across the semiconductor band gap, free-carrier absorption, intervalence-band transitions, multiple-phonon absorption, and the reststrahlen band.[5] Indium arsenide is an excellent example because all of these effects can be seen in its emittance spectra (Fig. 3) and demonstrate the utility of the emittance technique.

For instance, this sample at 77°K is opaque at both the short-wavelength and long-wavelength extremes. Thus the emittance experiment ($E_\infty = 1 - r^2$) provides the data, which would require a measure of reflectance on a sample of nominal size and at zero angle of incidence (the viewing cone is less than 15°). The reststrahlen region is of great importance in establishing the optical vibration frequencies at the Γ point (lattice wave vector $q = 0$).

In the intermediate region ($20 < \lambda < 38$ microns) the multiple-phonon spectrum becomes apparent (Fig. 4). The sample is only partially transparent at these wavelengths; however, detailed structure is observed. It is in this region that the approximations based on $k/n \ll 1$ become useful, so

[5] D. L. Stierwalt and R. F. Potter, *Phys. Rev.* **137**, A1007 (1965).

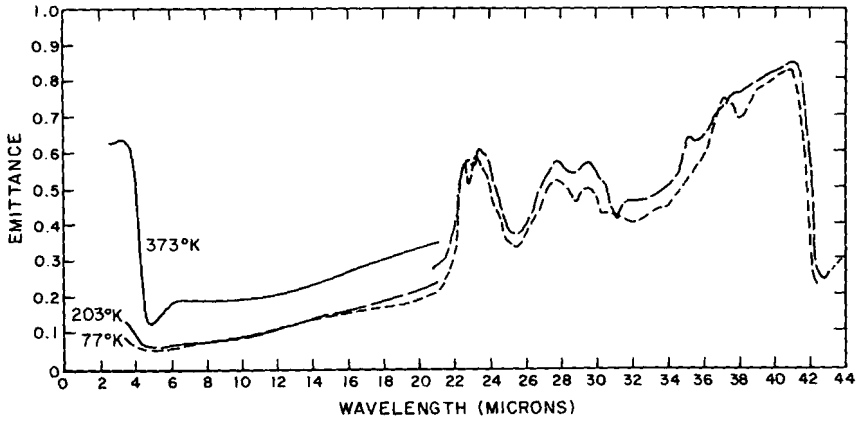


FIG. 3. Emittance spectra of InAs, wavelength region 2.5–44 microns (Stierwalt and Potter[5]).

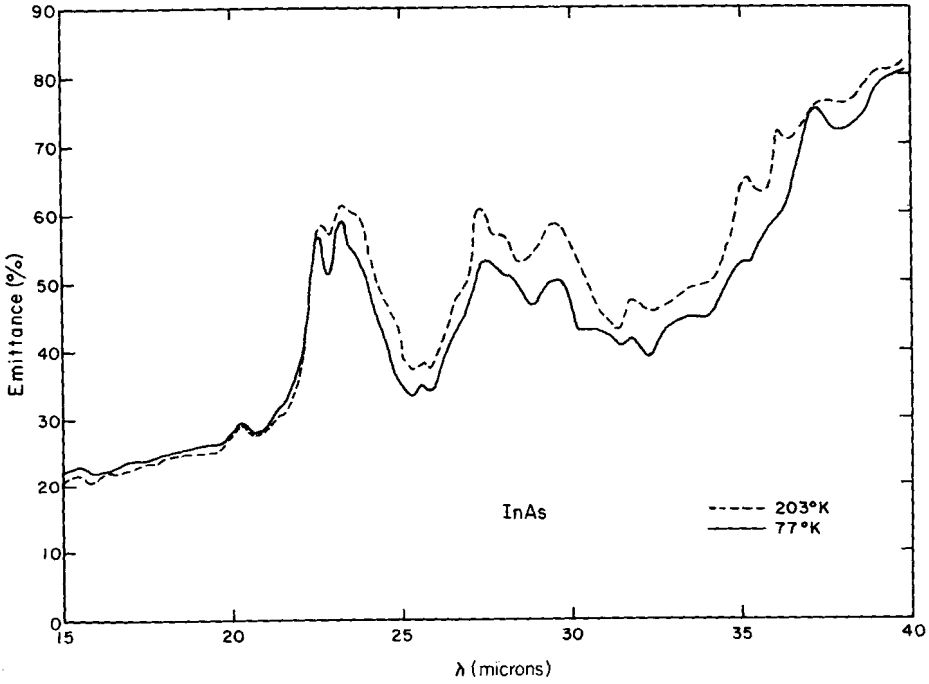


FIG. 4. Spectral-emittance spectra of InAs at 77° and 203°K for the 15–40 micron region. $N_A - N_D \simeq 10^{16}/cm^3$ (Stierwalt and Potter[5]).

that Eq. (7) can be applied to determine the absorption coefficient (Fig. 5).

The spectrum at shorter wavelengths ($6 < \lambda < 20$ microns) is that due to the absorption of light by the free carriers present, in addition to the residual absorption due to the lattice. This sample is p-type with approximately $10^{16}/cm^3$ excess carriers.

The curve in Fig. 3 for a sample temperature of 373°K has two interesting features. At 6.5 microns is seen a peak in absorption that has been attributed to the intervalence light- and heavy-hole band transitions[6]

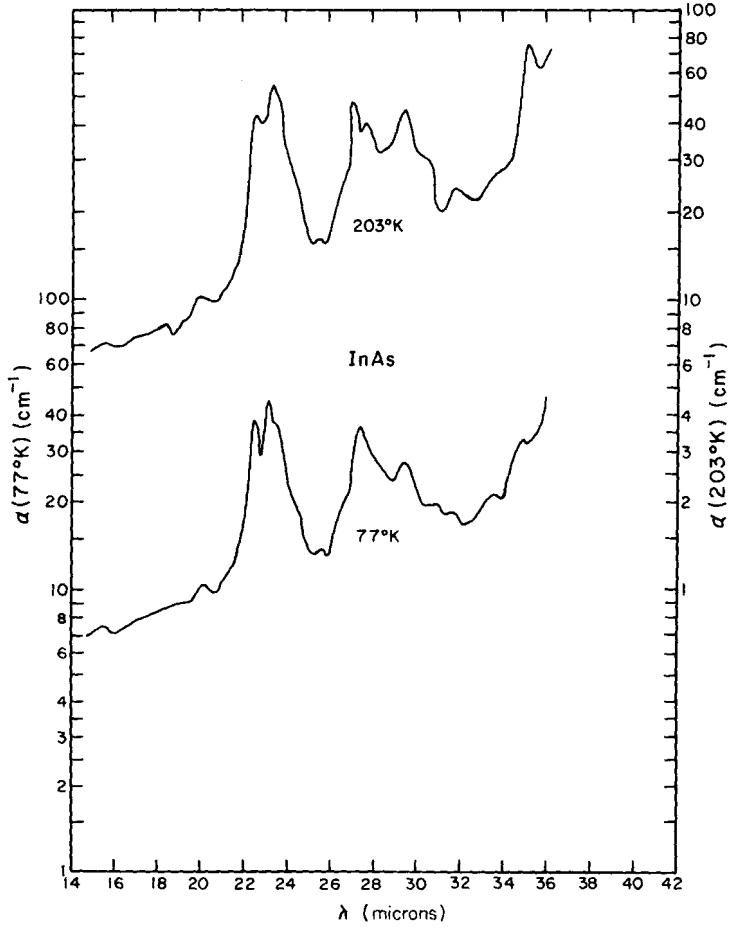


FIG. 5. Absorption coefficient of InAs, based on the spectra of Fig. 4 (Stierwalt and Potter[5]).

[6] J. R. Dixon, *Proc. Intern. Conf. Phys. Semicond., Prague, 1960* p. 656. Czech. Acad. Sci. Prague, 1961; F. Matossi and F. Stern, *Phys. Rev.* **111**, 472 (1958).

(0.19 eV). The direct transitions from the valence band to the conduction band (0.3 eV) can be seen at $\lambda \sim 4.3$ microns.

The measurements do not extend to sufficiently short wavelengths to see the full absorption-edge curve for the two lower temperature runs. However, they indicate a rise in absorption that is consistent with a negative temperature coefficient of the edge value. The 203°K run also has a small peak at $\lambda \sim 6.0$ microns corresponding to the 0.19-eV intervalence-band transition.

The structure, seen at $\lambda > 20$ microns, is attributed to multiple-phonon absorption processes and is discussed below. The spectroscopic detail that can be brought out by this technique extends from the transparent region $\lambda < 20$ microns into the opaque spectral region of the reststrahlen bands.

2. InP

The emittance curves for an InP sample are shown in Fig. 6. The principal structure between 12 and 25 microns is also attributed principally to two-phonon absorption processes.[7] However, the reststrahlen frequencies are such that the entire band can be observed. The emittance curve for the reststrahlen band agrees very well with the reflectance curve for InP as observed by Hass and Henvis.[8] (See Chapter 1.)

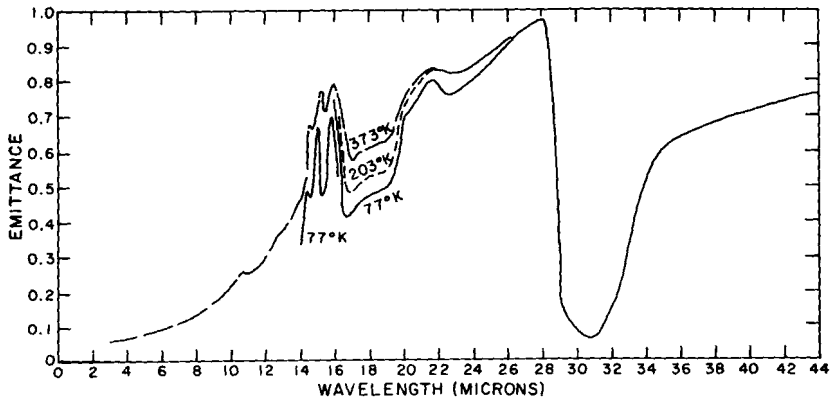


FIG. 6. The spectral emittance of InP; sample thickness was 0.65 mm except for the 14–16 micron region of the 77°K curve, where it was 0.38 mm (Stierwalt and Potter[7]).

[7] D. L. Stierwalt and R. F. Potter *in* "Physics of Semiconductors" (Proc. 7th Intern. Conf), p. 1073. Dunod, Paris and Academic Press, New York, 1964.

[8] M. Hass and B. W. Henvis, *J. Phys. Chem. Solids* **23**, 1099 (1962); D. A. Kleinman and W. G. Spitzer, *Phys. Rev.* **118**, 110 (1960).

3. InSb (p-TYPE)

This sample had such strong hole absorption that no multiphonon effects were observed. The set of curves is shown in Fig. 7. The most striking character of these curves is the behavior at the intrinsic edge. The emittance shows quite clearly the well-known edge shift with temperature.

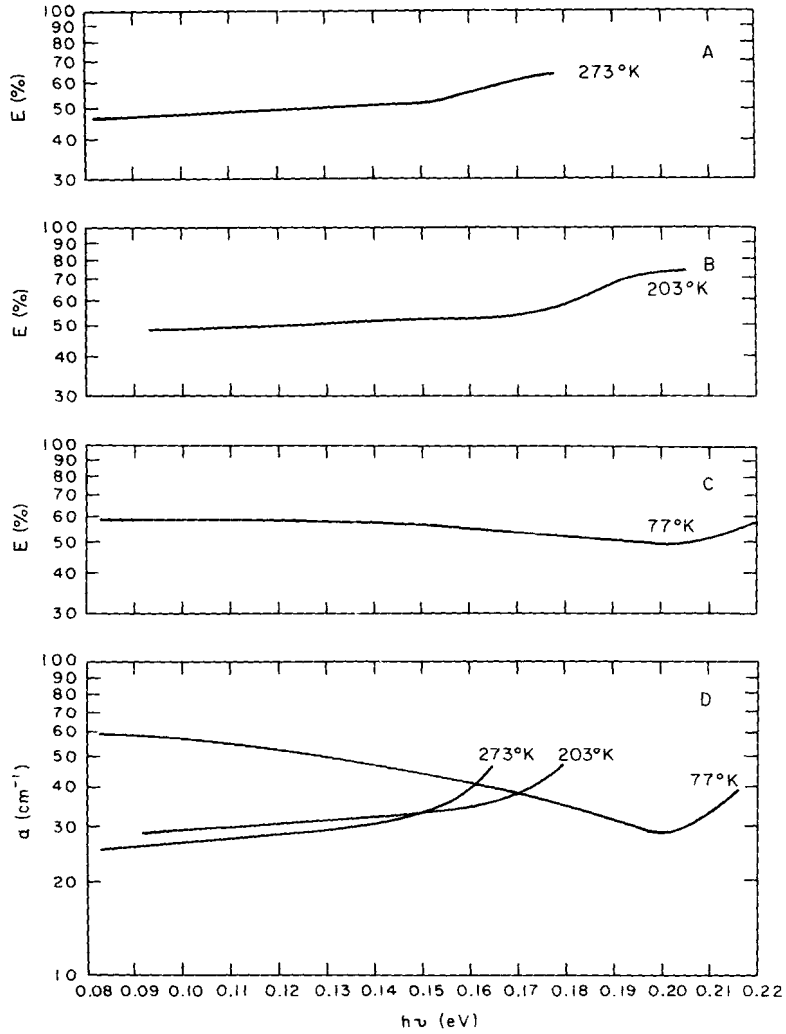


FIG. 7. Spectral-emittance curves for a p-type sample of InSb at 77°K, 203°K, and 273°K are shown in parts A, B, and C. Part D shows the absorption coefficient α for InSb based on the data of A, B, and C. $N_A - N_D \approx 3 \times 10^{16}/\text{cm}^3$.

4. GaSb

Many different types of studies have been made on GaSb, but few absorption studies. An n-type sample, Te doped with 1.1×10^{17} carriers/cm^3, was prepared for emittance measurements. The results for two thicknesses and two temperatures are shown in Fig. 8. The free-carrier absorption is so strong that the sample is opaque in the two-phonon region. In Fig. 9 are shown the absorption coefficients for the two temperatures. The short-wavelength residual absorption has been removed in order to bring out the wavelength dependence. There is a change from a $\lambda^{3.5}$ dependence at 77°K to a $\lambda^{2.9-3.0}$ dependence at 373°K.

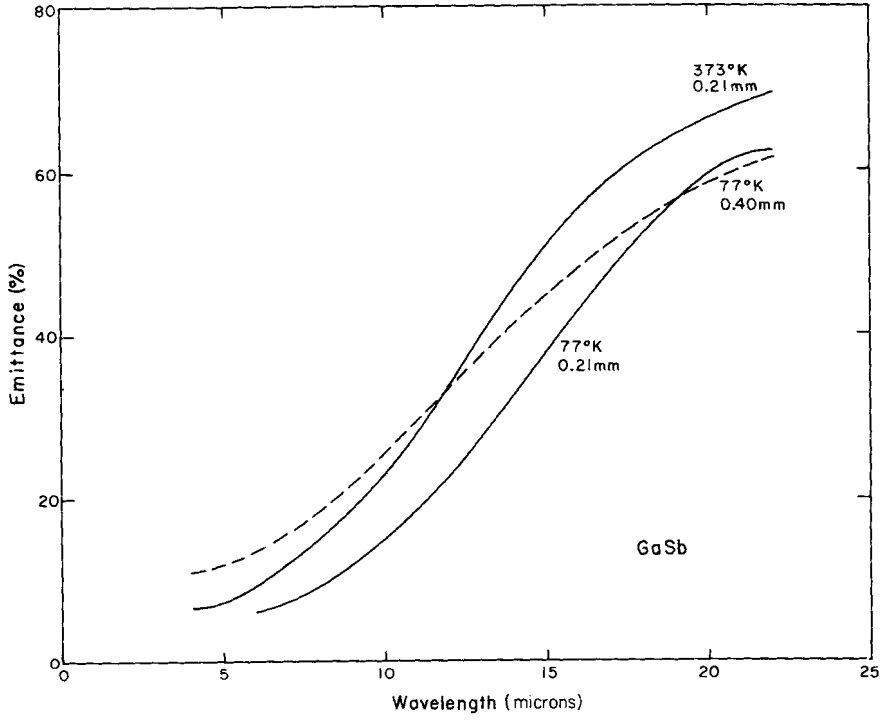


FIG. 8. Spectral-emittance curves for n-type GaSb samples for two temperatures and for two thicknesses. $N_D - N_A \approx 10^{17}$/cm^3, Te doped.

5. GaAs

This material is of interest because its optical properties have been well studied. Cochran *et al.*[9] have measured the multiphonon absorption. The

[9] W. Cochran, S. J. Fray, F. A. Johnson, J. E. Quarrington, and N. Williams, *J. Appl. Phys. Suppl.* **32**, 2102 (1961).

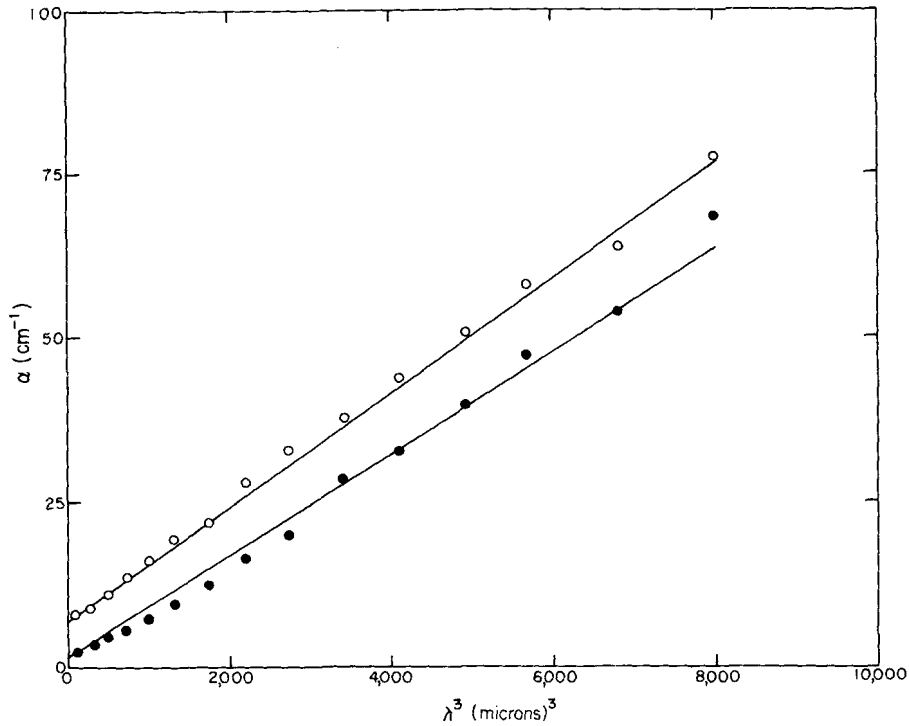


FIG. 9. Absorption coefficient of *n*-type GaSb, based on the data of Fig. 8: open circles, 373°K, solid circles, 77°K.

spectral emittance at 77°K for a sample having 10^{17} carriers/cm^3 is shown in Fig. 10. The two-phonon structure and the reststrahlen band can be seen. Analyses of similar spectra are given in Ref. 8 and by Spitzer.[10]

6. GaP

In the infrared region the sample was so absorbing that no features other than reststrahlen absorption were observed (see Fig. 11).

7. AlSb

A *p*-type sample with 10^{17} carriers/cm^3 was measured. The absorption was so strong that only information concerning the reststrahlen band was obtained (see Fig. 11).

[10] W. G. Spitzer, *J. Appl. Phys.* **34**, 792 (1963).

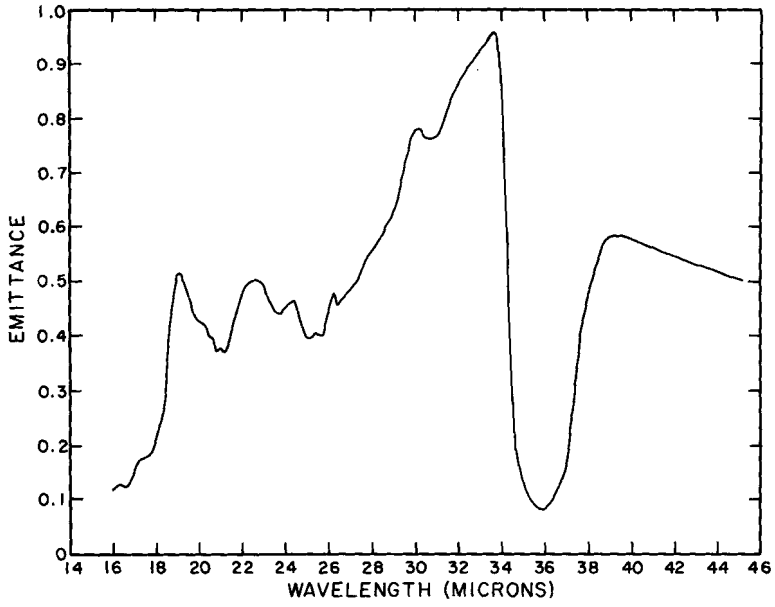


FIG. 10. Spectral-emittance curves for the GaAs sample at 77°K.

8. AlAs

A polycrystalline sample of poor quality was measured. Again only the reststrahlen band information could be obtained (see Fig. 11).

IV. Discussion

9. Reststrahlen Bands

The reststrahlen bands for seven of the eight materials reported here are shown in Fig. 11. All have been reported as measured by reflectance techniques except AlAs. The agreement with previous results is excellent. Because of the poor quality of the AlAs, no attempt was made to analyze the curve. However, reasonable estimates of the transverse optical and longitudinal optical modes at the zone center are $TO(\Gamma) = 0.046$ eV and $LO(\Gamma) = 0.049$ eV. The two compounds InSb and AlP would have bands at wavelengths to the right and to the left, respectively, of those shown.

10. Two-Phonon Processes

Samples of the three compounds InP, InAs, and GaAs exhibited pronounced structure that has been attributed to two-phonon processes.

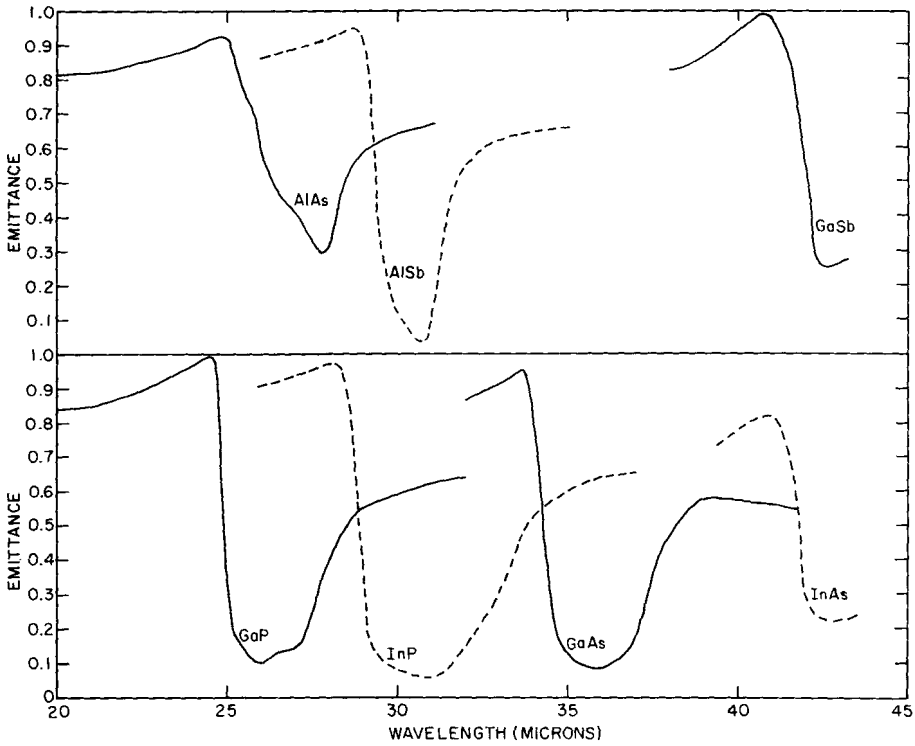


FIG. 11. Emittance curves (77°K) for seven of the eight compound semiconductors described in the text. The AlAs sample had holes and occlusions, which account for the peculiar shape of its curve.

Spectral emittance curves can be especially useful because in the quasi-transparent region they correspond so closely to the absorption. Thus, one can directly observe pertinent features in the experimental data.

Infrared absorption of the indium compounds is of interest because they are not suitable materials for neutron-scattering experiments. Hence, any determinations of the phonon spectrum rely upon optical techniques. Figures 4 and 6 were the first observations reported of the emittance spectra of the two-phonon region for InP and InAs.[5,7] The features used as a basis for assignments are listed in Tables I and II. A critical-point analysis was used for each compound, based on the $\Gamma[000]$, $X[100]$, and $L[111]$ points of the Brillouin zone. Also used were selection rules for dipole transition due to Birman.[11] He gives 21 allowed two-phonon dipole transitions at those points for zinc blende lattices. The spectrum for InP has 13 features,

[11] J. L. Birman, *Phys. Rev.* **131**, 1489 (1963).

TABLE I

PHONON ENERGIES FOR InP

Wavelength (microns)	Energy (eV)	Assignment	Energy (eV)
14.62	0.0848	2LO(Γ)	0.0848
15.24	0.0813	LO(Γ) + TO(Γ)	0.0813
15.93	0.0778	2TO(Γ)	0.0778
16.8	0.0738	2TO(L)	0.0738
—	—	2TO(X)	0.0686
—	—	TO(L) + LO(L)	0.0681
18.7	0.0663	TO(L) + LA(L)	0.0663
19.5	0.0636	TO(X) + LO(X)	0.0636
19.7	0.0629	TO(X) + LA(X)	0.0629
19.9	0.0623	2LO(L)	0.0623
20.5	0.0605	LO(L) + LA(L)	0.0605
21.1	0.0588	2LA(L)	0.0588
21.4	0.0579	LO(X) + LA(X)	0.0579
22.8	0.0544	TO(X) + TA(X)	0.0544
—	—	TA(X) + LO(X)	0.0494
—	—	TA(X) + LA(X)	0.0487
26.0	0.0477	TO(L) + TA(L)	0.0477
—	—	TA(L) + LO(L)	0.0420
—	—	2TA(X)	0.0404
—	—	TA(L) + LA(L)	0.0402
—	—	2TA(L)	0.0216

whereas InAs has 18. The nature of the photon-phonon interaction for the combination modes has been attributed to the interaction of the photon with a fundamental lattice mode in a virtual state, with the final state being the creation of two phonons.[12] Conservation of crystal momentum and energy are maintained. The nature of the transition can be a high order anharmonic interaction or of a dipole transition. The selection rules of Birman are based on symmetry conditions, hence do not depend upon a particular model for the interaction.

In Tables III and IV the phonon assignments are tabulated, and the lattice dispersion curves are given schematically in Figs. 12 and 13. The low-**q** acoustic modes are shown also for comparison. In the case of InP they are based upon a guess for the elastic constants. Measured values were available for InAs.[13]

[12] For a discussion, see M. Balkanski *in* "Physics of Semiconductors" (Proc. 7th Intern. Conf.), p. 1021. Dunod, Paris and Academic Press, New York, 1964.

[13] D. Gerlich, *Bull. Am. Phys. Soc.* **8**, 472 (1960).

TABLE II

TWO-PHONON COMBINATIONS FOR InAs

λ (microns)	Feature	$1/\lambda$ (cm^{-1})	Assignment	$1/\lambda$ (cm^{-1})
20.2	pk	492	2LO(Γ)	492
21.3	sh	467	LO(Γ) + TO(Γ)	467
22.6	pk	442	2TO(Γ)	442
23.2	pk	431	2TO(L)	432
23.6	sh	424	2TO(X)	424
24.5	sh	408	TO(L) + LO(L)	410
25.7	pk	389	2LO(L)	388
26.6	sh	376	TO(X) + LO(X)	376
27.5	pk	364	TO(L) + LA(L)	364
28.0	sh–pk	357	TO(X) + LA(X)	357
29.5	pk	339	LO(L) + LA(L)	342
31.0	sh–pk	322	TO(X) + TA(X)	323
31.8	pk	314	LO(X) + LA(X)	309
33.9	sh–pk	295	2LA(L)	296
35.0	pk	286	TO(L) + TA(L)	289
36.2	—	276	LO(X) + TA(X)	275
37.2	—	269	LO(L) + TA(L)	267
39.3	—	254	LA(X) + TA(X)	256
—	—	—	2TA(X)	222
—	—	—	TA(L) + LA(L)	221
—	—	—	2TA(L)	146

The bottom row of Tables III and IV gives a value of the sum of the squares of the modes at a given value of the crystal-lattice $\mathbf{q}$ vector. This "sum rule"[14] has been found to be generally applicable to the diamond and zinc blende type lattices where

$$\sum_i \omega_i^2(\mathbf{q}) = \text{constant}. \tag{14}$$

The present assignments for InP[7] and InAs[5] also follow this rule within a few percent. Rosenstock[15] has discussed the "sum rule" and shows that lattice dynamics determined by electrostatic forces (Coulomb, etc.) and first-neighbor forces might be expected to follow the rule, whereas contributions from second-neighbor forces would cause a departure from (14) as a function of $\mathbf{q}$. The evidence for InP and InAs is that second-neighbor forces make only a small contribution to the lattice modes.

[14] R. Brout, *Phys. Rev.* **113**, 43 (1959); S. S. Mitra, *ibid.* **132**, 986 (1963); see also Ref. 9.

[15] H. B. Rosenstock, *Phys. Rev.* **129**, 1959 (1963).

TABLE III

PHONON ENERGIES FOR InP

Mode	Critical-point energy (eV)		
	Γ	L	X
LO	0.0424	0.0312	0.0293
TO	0.0398	0.0369	0.0343
LA	—	0.0294	0.0286
TA	—	0.0108	0.0201
Sum rule: $(eV^2) \times 10^4$	48.2	48.0	48.6

TABLE IV

PHONON FREQUENCIES FOR InAs

Mode	Critical-point frequency (cm^{-1})		
	Γ	L	X
LO	246	194	164
TO	221	216	212
LA	—	148	145
TA	—	73	111
Sum rule: $(cm^{-2}) \times 10^{-4}$	15.90	16.40	16.24

11. ELECTRON-ABSORPTION EFFECTS

Emittance studies have not been extensively used for studying free-carrier effects. The data for GaSb of Fig. 8, however, show that it could be very effective in such studies.

The absorption coefficients have a wavelength dependence with a power greater than λ^2, which is what might be expected for the electron-lattice interaction. When α is plotted vs. λ^3 (Fig. 9), the 373°K curve is very nearly linear, whereas the 77°K curve appears to follow a slightly higher power curve. When the same data are plotted (less the short-wavelength absorption) on a log-log graph, the curves have slopes of 2.9 and 3.5, respectively.

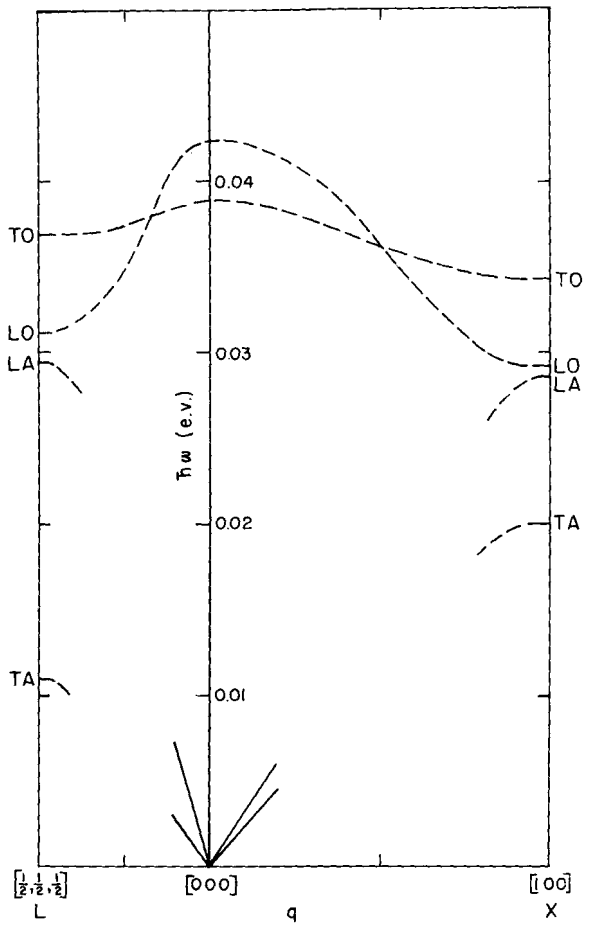


FIG. 12. Schematic diagram of the lattice-mode dispersion curve for InP.

Similar behavior has been observed for other semiconductors and has been attributed to electron-ionized scattering-center interaction.[16] At low temperatures a $\lambda^{3.5}$ behavior is expected, with a decrease to $\lambda^{3.0}$ at temperatures where $\hbar\omega/kT \to 1$, where ω is the frequency of the radiation.

Free-carrier and intervalence-band transitions can be seen in the InAs data of Fig. 3. The light-heavy hole transitions have been reported at 0.17 eV[6] and can be clearly seen at 6.3 microns in Fig. 3.

[16] H. Y. Fan, W. G. Spitzer, and R. J. Collins, *Phys. Rev.* **101**, 566 (1956); H. J. G. Meyer, *ibid.* **112**, 298 (1958).

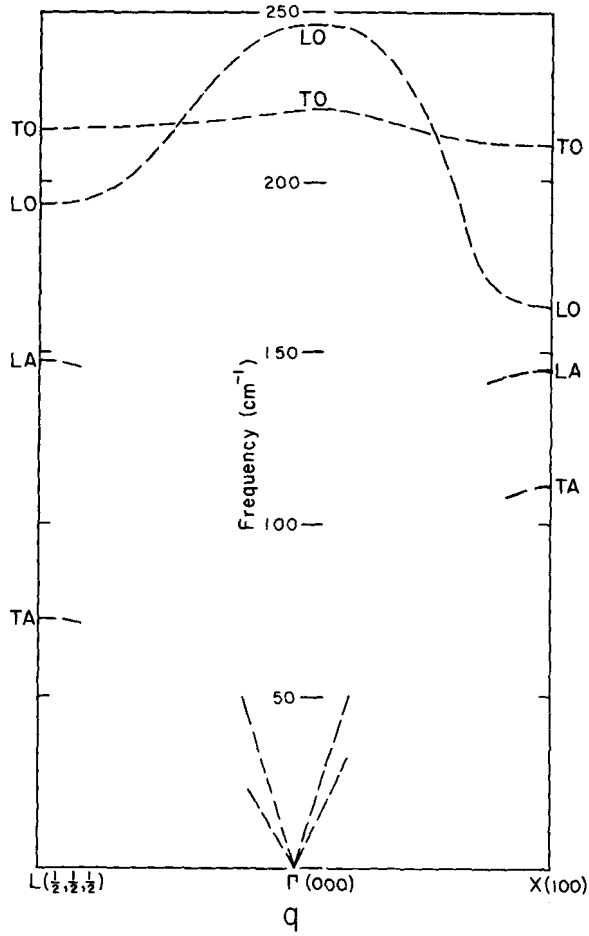


FIG. 13. Schematic diagram of the lattice dispersion curve for InAs (Stierwalt and Potter[5]).

Hole absorption in *p*-type InSb has been reported by Kurnick and Powell[17] using transmittance measurements. The emittance data for the three temperatures shown in Fig. 7A, B, and C have been reduced to the absorption coefficients shown in 7D. These results are in very good agreement with the absorption data reported by Kurnick and Powell for samples having a similar carrier concentration. They reported that longer-wavelength absorption is relatively large for *p*-type material, and at the longer wavelengths the absorption coefficient is larger at 77°K than at 273°K.

[17] S. W. Kurnick and J. M. Powell, *Phys. Rev.* **116**, 597 (1959).

V. Summary

The absorptance-emittance technique has been applied to studies of the III–V compound semiconductors and has been shown to be very useful in studying the various absorption processes that contribute to the optical properties of semiconductors. Although emittance studies cannot displace reflectance and transmittance studies, they do have several advantages, which are well demonstrated in the present collection of data:

(1) The optical properties can be studied in a continuous manner from a quasitransparent region to the totally opaque regions of the spectrum. This permits one to measure to the multiphonon absorption spectrum and the reststrahlen-band spectrum in a continuous manner in a single sample. This is demonstrated for InAs and InP in Figs. 3 and 6.

(2) The technique is excellent for measuring very low absorption coefficients because for $\alpha t \ll 1$, $E_\lambda \approx \alpha t$.

(3) When reducing emittance data, the precise value of the refractive index is not required for values of $\alpha t \leqslant 2.5$ [Eq. (7)].

It is expected that the technique will be extended to lower temperatures (4°K) and to wavelengths longer than 100 microns in the near future. This will open up an interesting area of investigation because in the spectral regions at wavelengths greater than the reststrahlen band many materials become quite transparent at low temperatures. The emittance-absorptance studies will play a role in the study of the difference bands, as it has in the summations bands for photon-phonon interactions. Free-carrier effects and possible effects caused by very-low-energy transitions can be studied profitably in this spectral region.

CHAPTER 4

Ultraviolet Optical Properties

*H. R. Philipp and H. Ehrenreich**

I. Introduction 93
II. Experimental Procedures 95
1. *Instrumentation* 95
2. *Sample Preparation* 97
III. Analysis of Reflectance Data 98
3. *Kramers–Kronig Relations* 98
4. *Procedure and Approximations* 99
IV. Theoretical Framework 101
5. *Complex Dielectric Constant* 101
6. *Sum Rules* 108
V. Discussion of Experimental Results 110
7. *Reflectance Data and Deduced Dielectric Constants* 110
8. *Interband Transitions (Region 1)* 113
9. *Metallic Effects (Region 2)* 114
10. *d-Band Excitations (Region 3)* 121

I. Introduction

The optical properties of solids may be determined by Kramers–Kronig analysis of normal-incidence reflectance data.[1–3] This procedure, which is presented in some detail below, evaluates the real and imaginary parts of the dielectric constant that describe these properties. The curves shown in Fig. 1 for InSb are typical of the results for semiconductors and clearly illustrate the applicability of this technique to an extended energy range, using relatively straightforward experimental procedures.

It is convenient to distinguish three spectral regions in the description of the optical properties of such compounds.[4] The first region, extending to about 8 to 10 eV, is characterized by sharp structure associated with

* Supported in part by Advanced Research Projects Agency.

[1] T. S. Robinson, *Proc. Phys. Soc. (London)* **B65**, 910 (1952).
[2] F. C. Jahoda, *Phys. Rev.* **107**, 1261 (1957).
[3] H. R. Philipp and E. A. Taft, *Phys. Rev.* **113**, 1002 (1959); **120**, 37 (1960).
[4] H. Ehrenreich and H. R. Philipp, *Proc. Intern. Conf. Phys. Semicond., Exeter, 1962* p. 367. Inst. of Phys. and Phys. Soc., London, 1962.

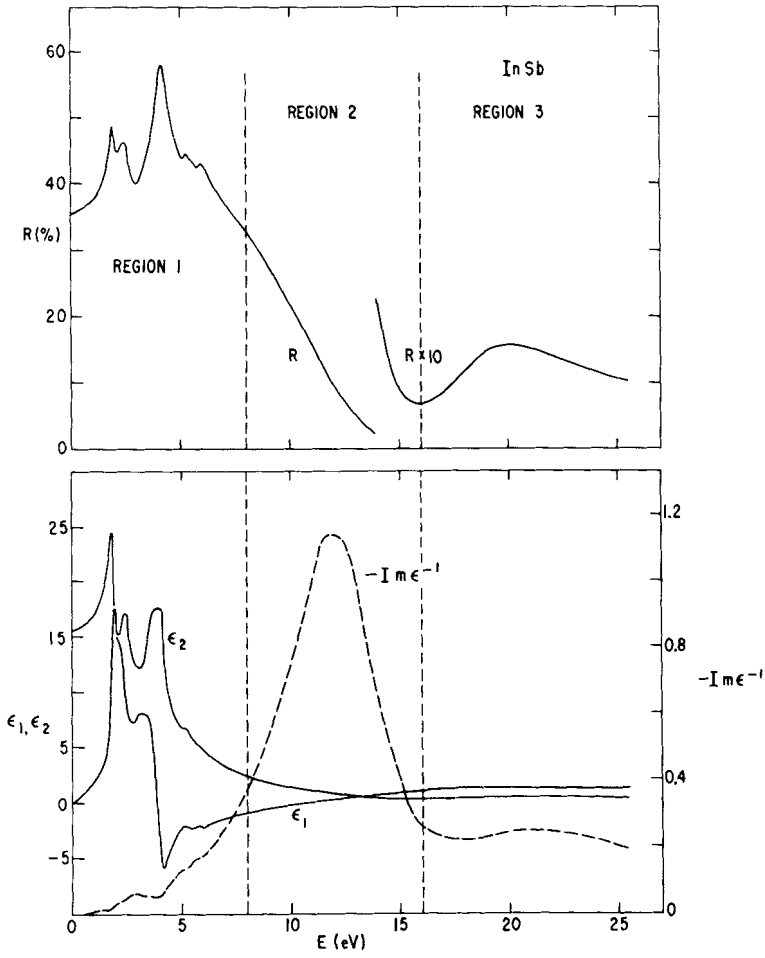


FIG 1. The spectral dependence of the reflectance R, the real and imaginary parts of the dielectric constant, ε_1 and ε_2, and the energy-loss function $-\mathrm{Im}\,\varepsilon^{-1}$ for InSb.

valence- to conduction-band transitions.[5] The second region, which extends to about 16 eV, is marked by a rapid decrease of the reflectance that is reminiscent of the behavior of certain metals in the ultraviolet. Here one may think of the valence electrons as essentially unbound and able to perform collective oscillations. Sharp maxima in the function $-\mathrm{Im}\,\varepsilon^{-1}$, which describes the energy loss of fast electrons traversing the material,[6]

[5] H. Ehrenreich, H. R. Philipp, and J. C. Phillips, *Phys. Rev. Letters* **8**, 59 (1962).
[6] P. Nozieres and D. Pines, *Phys. Rev.* **113**, 1254 (1959).

have been frequently associated with the existence of plasma oscillations.[7] A maximum of this type is seen to occur in the "metallic" region. In the third region, the reflectance again rises, indicating the onset of additional optical absorption. This structure is associated with transitions between filled *d* bands lying below the valence band and empty conduction-band states.[8]

It is the purpose of the following sections to present an account of the physical information to be derived from optical studies on semiconductors and, in particular, the III–V compounds. For completeness, a brief description of the instrumentation involved in such studies is given in Part II, and the techniques used to analyze reflectance data by means of the Kramers–Kronig relations are discussed in Part III. Curves similar to Fig. 1 for GaAs, GaP, and InAs are presented and discussed in Part V, using as guides the theoretical framework outlined in Part IV. For comparison purposes, results for Si and Ge are also given. Since the interpretation of data in the first region has already been discussed by Cardona,[9] these sections are concerned mainly with the remaining two regions.

II. Experimental Procedures

1. Instrumentation

A large variety of apparatus and techniques have been employed in studies of the specular reflectance of crystalline materials, and no attempt will be made here to discuss, evaluate, or even survey this field. Rather, the instrument employed in the present work will be briefly described, since it adequately covers the spectral range of interest and incorporates the essential features necessary for this study.

Measurements of reflectance were performed in the spectral range 1 to 25 eV using a vacuum grating monochromator similar in design to that of Johnson.[10] This instrument is shown schematically in Fig. 2(a). Light from a tungsten bulb or discharge lamp is incident on a concave grating near normal incidence. The grating is rotated about an off-axis pivot, which, in effect, moves the grating-to-slit distance more in accord with a Rowland mount while still retaining the advantages of simplicity, compactness, and constant angle of emergence at the exit slit.[11] The sample chamber is vacuum sealed to the monochromator. Specimens are mounted on each

[7] L. Marton, *Rev. Mod. Phys.* **28**, 172 (1956).
[8] H. R. Philipp and H. Ehrenreich, *Phys. Rev. Letters* **8**, 1 (1962).
[9] M. Cardona, Chapter 5 of this volume.
[10] P. D. Johnson, *J. Opt. Soc. Am.* **42**, 278 (1952).
[11] P. D. Johnson, *Rev. Sci. Instr.* **28**, 833 (1957).

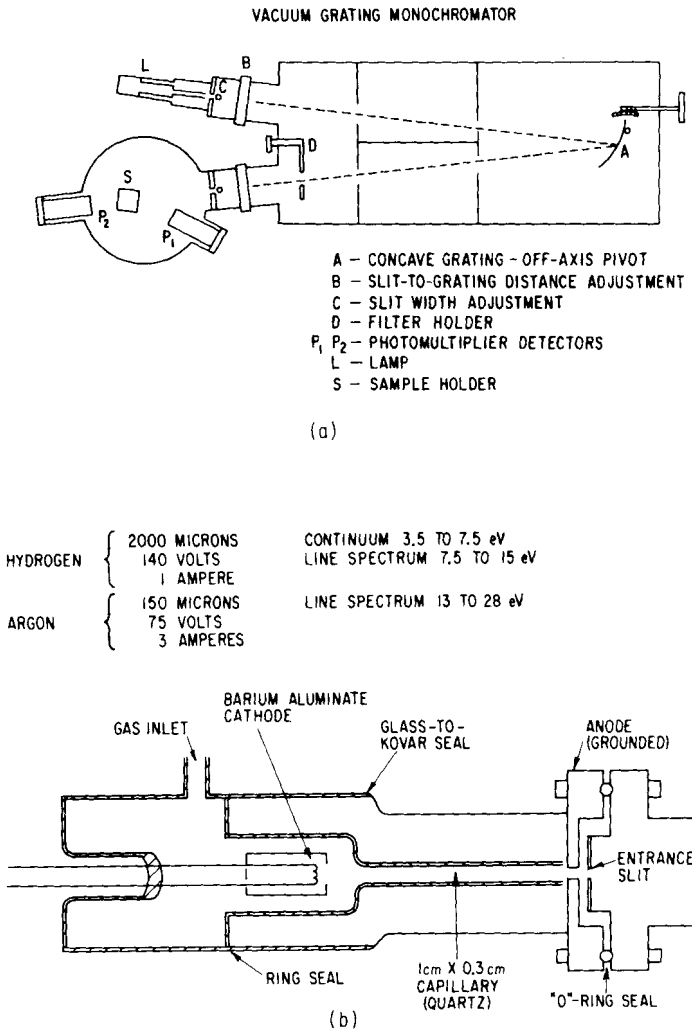


FIG. 2. Schematic drawing of the experimental apparatus: (a) monochromator and sample chamber, (b) light source.

of the four sides of the sample holder, which is rotated into position for measurement of the reflected intensity. The holder is pulled down out of the beam for measurement of incident intensity. For wavelengths in the vacuum ultraviolet, the photomultiplier detectors are coated with sodium salicylate phosphor.

The discharge lamp used for most of the spectral range is shown schematically in Fig. 2(b). The main feature is the use of a quartz capillary to concentrate the arc and to effect an increased voltage drop. Typical operating conditions are given in the figure. The lines in the hydrogen spectrum are relatively dense, and with narrow slits the region between 7.5 and 15 eV can be examined in detail. The lines of the argon spectrum are not so richly populated, and small gaps, perhaps 0.2 and 0.3 eV wide, exist in the spectrum. Above 21 eV the lines are relatively weak, although certainly usable. This situation could be improved by coating the grating with a film of gold, platinum, or other material having high reflectance in this region.[12–14]

2. Sample Preparation

The reflected beam samples a relatively thin layer of material at the crystal surface. Hence, it is important that these surfaces be free of chemical impurities such as oxides and free of the lattice distortions that may result from mechanical polishing.[15–17] Various chemical and electrolytic etches have been developed for the removal of these damaged layers, which leave the surface chemically clean.[18] The use of bulk, single-crystal specimens cleaved just prior to measurement under conditions of ultrahigh vacuum is, perhaps, ideal. However, the application of this procedure in a particular experimental setup may be extremely difficult.

The curves to be presented in Part V were obtained on etched single-crystal samples. After etching, the specimens were exposed to air for the minimum time necessary for mounting in the sample chamber and then, for a longer time, to the poor vacuum of the monochromator during measurement. Although the samples are conceivably subject to atmospheric contamination, the results are considered adequate for the physical interpretation to be discussed later.[18a] Good agreement is found between the

[12] G. Hass and R. Tousey, *J. Opt. Soc. Am.* **49**, 593 (1959).
[13] G. Hass and W. R. Hunter, *J. Quant. Spectr. Radiative Transfer* **2**, 637 (1962).
[14] G. F. Jacobus, R. P. Madden, and L. R. Canfield, *J. Opt. Soc. Am.* **53**, 1084 (1963).
[15] W. C. Dash, *J. Appl. Phys.* **29**, 228 (1958).
[16] T. M. Donovan, E. J. Ashley, and H. E. Bennett, *J. Opt. Soc. Am.* **53**, 1403 (1963).
[17] H. R. Philipp, W. C. Dash, and H. Ehrenreich, *Phys. Rev.* **127**, 762 (1962).
[18] J. W. Faust, *in* "Compound Semiconductors" (R. K. Willardson and H. L. Goering, eds.), Vol. 1, p. 445. Reinhold, New York, 1962.
[18a] Donovan, Ashley, and Bennett[16] present very precise reflectance data for extremely carefully prepared Ge surfaces in the energy range 1 to 5 eV. The curve given in Part V for this crystal agrees substantially with their more sophisticated measurements.

present curves[19] and those in the literature[16,17,20–27] where the spectral ranges overlap.

III. Analysis of Reflectance Data

3. Kramers–Kronig Relations

The Kramers–Kronig relation connecting the modulus and phase of the complex Fresnel equation for normal incidence radiation was first proposed and used by Robinson.[1] His technique for evaluating the optical constants was based on ideas developed extensively for use in electrical network theory,[28] namely, the dispersion relation connecting the resistance to the reactance. Such dispersion relations are known in many fields[29] and are frequently credited to the names of Kramers[30] and Kronig,[31] since they first pointed out the existence of such very general relations.

The Fresnel equation for the reflection of normal-incidence radiation is

$$r = \frac{n - ik - 1}{n - ik + 1} = |r| e^{i\theta} \tag{1}$$

where $n - ik$ is the complex index of refraction. The measured reflectance is the square of the amplitude of r,

$$R = |r|^2 = \frac{(n-1)^2 + k^2}{(n+1)^2 + k^2}, \tag{2}$$

and the phase is

$$\theta = \tan^{-1}[-2k/(n^2 + k^2 - 1)], \tag{3}$$

an angle in the third or fourth quadrant, depending on whether the sum $n^2 + k^2$ is less or greater than unity. Values outside the range $0 \geqq \theta \geqq -\pi$

[19] H. R. Philipp and H. Ehrenreich, *Phys. Rev.* **129**, 1550 (1963).
[20] J. Tauc and E. Antončík, *Phys. Rev. Letters* **5**, 253 (1960).
[21] J. Tauc and A. Abraham, *Proc. Intern. Conf. Semicond. Phys., Prague, 1960* p. 375. Czech. Acad. Sci., Prague, 1961.
[22] M. Cardona, *J. Appl. Phys. Suppl.* **32**, 2151 (1961).
[23] M. Cardona, *J. Appl. Phys.* **32**, 958 (1961).
[24] M. Cardona and H. S. Sommers, Jr., *Phys. Rev.* **122**, 1382 (1961).
[25] R. E. Morrison, *Phys. Rev.* **124**, 1314 (1961).
[26] D. L. Greenaway, *Phys. Rev. Letters* **9**, 97 (1962).
[27] T. Sasaki and K. Ishiguro, *Phys. Rev.* **127**, 1091 (1962).
[28] H. Bode, "Network Analysis and Feedback Amplifier Design," especially Chapter 14. Van Nostrand, Princeton, New Jersey, 1945.
[29] J. S. Toll, *Phys. Rev.* **104**, 1760 (1956).
[30] H. A. Kramers, *Atti Congr. Intern. Fis., Como* **2**, 545 (1927); *Phys. Z.* **30**, 522 (1929).
[31] R. de L. Kronig, *J. Opt. Soc. Am.* **12**, 547 (1926); *Phys. Rev.* **30**, 521 (1929).

have no meaning, since the extinction coefficient k cannot assume negative values. The phase $\theta(\omega_0)$, for any frequency ω_0, can be computed from reflectance data, using the Kramers–Kronig relation between the real and imaginary parts of the complex function

$$\ln r = \ln |r| + i\theta . \tag{4}$$

This relation, which may be written as[32,33]

$$\theta(\omega_0) = \frac{1}{2\pi} \int_0^\infty \frac{d \ln R}{d\omega} \ln \left| \frac{\omega + \omega_0}{\omega - \omega_0} \right| d\omega , \tag{5}$$

can be integrated with the aid of tables[34] or by computer. The equations for R and θ above can be solved simultaneously to obtain n and k at frequency ω_0 and, thus, the dielectric constants and absorption coefficient

$$\begin{aligned} \varepsilon_1 &= n^2 - k^2 \\ \varepsilon_2 &= 2nk \\ \alpha &= 4\pi k/\lambda . \end{aligned} \tag{6}$$

4. Procedure and Approximations

The computation of the exact value of θ requires that the reflectance spectrum be known for all frequencies. However, simple techniques may be used to extrapolate R beyond the range of measurement, so that reasonably accurate values of n and k can be obtained within this range provided the experimental data include the region below the threshold for direct optical transitions and most of the strong structure at higher energies. For many of the III–V compounds significant results can be obtained from measurements in the energy range 1 to 6 eV when careful consideration is given to extrapolation procedures.

The extrapolation to zero frequency is easy, since the reflectance may be assumed to approach the value computed from the high-frequency dielectric constant, which is generally known.[35,36] For certain crystals the variation of the index of refraction in this range is quite accurately known from prism

[32] F. C. Jahoda, *Phys. Rev.* **107**, 1261 (1957).
[33] T. S. Moss, "Optical Properties of Semi-Conductors," Chap. 2. Butterworth, London, 1959.
[34] D. E. Thomas, *Bell System Tech. J.* **26**, 870 (1947).
[35] C. Hilsum and A. C. Rose-Innes, "Semiconducting III–V Compounds." Macmillan (Pergamon), New York, 1961.
[36] M. Hass and B. W. Henvis, *J. Phys. Chem. Solids* **23**, 1099 (1962).

measurements.[37–39] In this connection it should be pointed out that structure in R associated with lattice absorption bands usually can be ignored, since, as one might expect on physical grounds, it does not contribute appreciably to the value of θ at higher energies.

The extrapolation of R above the highest energy datum point does not necessarily follow any simple rule, although its general behavior can be deduced provided this region does not contain strong structure characteristic of interband transitions. The reflectance should remain reasonably high for energies below the plasma frequency and fall rapidly at higher energy.[40] The plasma energy is known for many crystals from characteristic-energy-loss experiments[41–43] or can be estimated using the free-electron formula

$$\omega_p = \left(\frac{4\pi n_v e^2}{m}\right)^{1/2}, \tag{7}$$

where n_v corresponds to four valence electrons per atom in the case of the III–V compounds. At much higher energies we have $n \cong 1$, $k \cong 0$, and $\theta \cong -\pi$. The behavior of R can be deduced from the asymptotic expression for the dielectric constant to be[44,45]

$$R(\omega) = c\omega^{-4}. \tag{8}$$

With these rough guides as to shape, a more quantitative description of R in the extrapolated region above the highest energy datum point can be achieved by evaluating the integral for θ at some frequency ω' near the band gap where the absorption coefficient is either zero or is known accurately from bulk transmission data.[35,46] At this energy the value of $\theta(\omega')$ is fixed (being exactly zero in the region of optical transparency) and must equal the computed value obtained from the integral using the actual values of R in the range of experiment, plus the contribution from the extrapolated region. Hence, not only can the form of the extrapolation be estimated, but its exact contribution can be fixed so as to yield the correct value of θ at one frequency.

[37] D. T. F. Marple, *J. Appl. Phys.* **35**, 1241 (1964).
[38] C. Salzberg and J. Villa, *J. Opt. Soc. Am.* **47**, 244 (1957).
[39] F. Stern, *Phys. Rev.* **133**, A1653 (1964).
[40] H. R. Philipp and H. Ehrenreich, *Phys. Rev.* **131**, 2016 (1963).
[41] C. J. Powell, *Proc. Phys. Soc. (London)* **76**, 593 (1960).
[42] H. Dimigen, *Z. Physik* **165**, 53 (1961).
[43] B. Gauthe, *Phys. Rev.* **114**, 1265 (1959).
[44] H. R. Philipp and H. Ehrenreich, *J. Appl. Phys.* **35**, 1416 (1964).
[45] M. Cardona and D. L. Greenaway, *Phys. Rev.* **133**, A1685 (1964).
[46] W. C. Dash and R. Newman, *Phys. Rev.* **99**, 1151 (1955).

IV. Theoretical Framework

5. Complex Dielectric Constant

An explicit expression for the complex dielectric constant $\varepsilon(\omega)$ of an insulator, valid in the random-phase approximation,[47] and including damping effects qualitatively, may be derived using the approach of Ehrenreich and Cohen.[48]

We consider the response of a solid having cubic symmetry to an external potential $V(\mathbf{x}, t) = V(\mathbf{q}, \omega)e^{i(\mathbf{q}\cdot\mathbf{x} - \omega t)}$ corresponding to the electric field of the light wave. Local field effects[49] will be neglected. Although this approximation has not yet been explicitly tested for semiconductors, it might be expected to have some validity for the group-IV and III–V materials. Indeed, one finds very effective cancellation of the crystal potential by the repulsive "orthogonalization" potential.[50] The resulting energy bands closely resemble those of nearly free electrons.

The Liouville equation describing the response to an external perturbation $V(\mathbf{x}, t)$ is

$$i\hbar\frac{\partial\rho}{\partial t} - [H, \rho] = i\hbar\left(\frac{\partial\rho}{\partial t}\right)_{\text{coll.}} . \tag{9}$$

Here $H = H_0 + V(\mathbf{x}, t)$ is the single particle Hamiltonian and $H_0 = p^2/2m + V_L(\mathbf{x})$ the unperturbed part describing a Bloch electron in a solid characterized by the periodic potential $V_L(\mathbf{x})$. The term $(\partial\rho/\partial t)_{\text{coll.}}$ describes the effect of collisions. Because the external field due to the monochromatic light wave is small, it is sufficient to restrict our attention to a single Fourier component and to linearize the problem. The linearization procedure consists of dividing the density matrix $\rho = \rho_0 + \rho_1$ into an unperturbed part ρ_0 and a perturbed part ρ_1 and neglecting terms involving $\rho_1 V$. The operators H_0 and ρ_0 satisfy the equations

$$\begin{aligned} H_0|\mathbf{k}l\rangle &= E_{l\mathbf{k}}|\mathbf{k}l\rangle , \\ \rho_0|\mathbf{k}l\rangle &= f_{l\mathbf{k}}|\mathbf{k}l\rangle . \end{aligned} \tag{10}$$

Here $|\mathbf{k}l\rangle = \Omega^{-1/2}u_l(\mathbf{k}, \mathbf{x})e^{i\mathbf{k}\cdot\mathbf{x}}$ are the usual Bloch functions describing an electron $\mathbf{k}$ in band l normalized in the volume Ω, and $f_l(\mathbf{k})$ is the unperturbed single-particle (Fermi) distribution.

It then remains to make explicit choices for $(\partial\rho/\partial t)_{\text{coll.}}$ and $V(\mathbf{x}, t)$. The simplest assumption for the collision term, which permits a physically

[47] See, for example, D. Pines, "Elementary Excitations in Solids." Benjamin, New York, 1963.
[48] H. Ehrenreich and M. H. Cohen, *Phys. Rev.* **115**, 786 (1959).
[49] S. L. Adler, *Phys. Rev.* **126**, 413 (1962).
[50] See, for example, F. Bassani and V. Celli, *J. Phys. Chem. Solids* **20**, 64 (1961) and cited references, particularly the work of J. C. Phillips and L. Kleinman.

reasonable, albeit qualitative, incorporation of broadening effects into the theory, is the so-called relaxation-time approximation, which can be made either in the form[51] $(\partial\rho/\partial t)_{\text{coll.}} = \rho_1/\tau$ or $(\partial\rho/\partial t)_{\text{coll.}} = [\rho - \rho_0(H_0 + V)]/\tau$. We may describe the light wave by a vector or scalar potential and compute either the current or charge density that is induced. Unfortunately, even for the same form of the collision term, some of these four ways of arriving at $\varepsilon(\omega)$ lead to different results for nonvanishing τ. The reason behind this lies in the fact that this oversimplified form of $(\partial\rho/\partial t)_{\text{coll.}}$ is not gauge-invariant or, equivalently, corresponds to the introduction of a source term in the continuity equation. Thus, $\nabla\cdot\mathbf{j} + \partial n/\partial t \neq 0$. The extra term in the continuity equation depends on $(\partial\rho/\partial t)_{\text{coll.}}$ and is interpreted in terms of particle creation or annihilation during the collision process. These difficulties, of course, do not arise when collision terms are incorporated properly.

We shall limit our treatment to an outline of a derivation typical of the possible cases that utilize the relaxation-time approximation. We shall calculate the current induced by an external potential (corresponding to the light wave) $V(\mathbf{x}, t) = (e/mc)\mathbf{A}\cdot\mathbf{p}$, described by a vector potential $\mathbf{A}(\mathbf{r}, t) = \mathbf{A}(\mathbf{q}, \omega)e^{i(\mathbf{q}\cdot\mathbf{r} - \omega t)}$. The quantity $\mathbf{p}$ represents the momentum operator. The collision term will be assumed to have the form $(\partial\rho/\partial t)_{\text{coll.}} = -\rho_1/\tau$.

The resulting linearized Liouville equation

$$i\hbar(\partial\rho_1/\partial t) - [H_0, \rho_1] - [V, \rho_0] = -i\hbar\rho_1/\tau \tag{11}$$

is readily solved upon recognizing that $V(\mathbf{x}, t)$ and $\rho_1(\mathbf{x}, t)$ both vary as $e^{i(\mathbf{q}\cdot\mathbf{x} - \omega t)}$ and taking matrix elements with respect to Bloch states $\mathbf{k}l$ and $\mathbf{k}'l'$. Heuristically, it is then also possible to replace τ by $\tau_{\mathbf{k}l,\mathbf{k}'l'}$ to indicate the fact that the relaxation time can depend both on the wave numbers and the band indicies of the initial and final states. We find

$$\rho_{\mathbf{k}+\mathbf{q},l;\mathbf{k},l'} = \frac{f_{\mathbf{k}+\mathbf{q},l} - f_{\mathbf{k},l'}}{\hbar[\omega_{\mathbf{k}+\mathbf{q},l;\mathbf{k},l'} + \omega + i/\tau_{\mathbf{k}+\mathbf{q},l;\mathbf{k},l'}]} V_{\mathbf{k}+\mathbf{q},l;\mathbf{k},l'} \tag{12}$$

where $\hbar\omega_{\mathbf{k}+\mathbf{q},l;\mathbf{k},l'} = E_{\mathbf{k}+\mathbf{q},l} - E_{\mathbf{k},l'}$. Further,

$$V_{\mathbf{k}+\mathbf{q};\mathbf{k},l'} = \frac{e}{mc}\mathbf{A}(\mathbf{q}, \omega)e^{-i\omega t}\cdot\frac{1}{v_a}\int_0 d^3x\, u^*_{\mathbf{k}+\mathbf{q},l}(\mathbf{x})(\mathbf{p} + \hbar\mathbf{k} + \tfrac{1}{2}\hbar\mathbf{q})u_{\mathbf{k},l'}(\mathbf{x})$$

$$\equiv \frac{e}{mc}\mathbf{A}(\mathbf{q}, \omega)\cdot\boldsymbol{\Pi}_{\mathbf{k}+\mathbf{q},l;\mathbf{k},l'}e^{-i\omega t} \tag{13}$$

[51] For a discussion of these assumptions see J. H. Van Vleck and V. Weisskopf, *Rev. Mod. Phys.* **17**, 227 (1945) and R. Karplus and J. Schwinger, *Phys. Rev.* **73**, 1020 (1948).

where the integration extends over the unit cell having volume v_a and the last equality serves as the definition of $\mathbf{\Pi}$. The particle current induced by the light wave is given by

$$\mathbf{j}^{\text{ind}}(\mathbf{x}, t) = \text{Tr}[\mathbf{j}_0\rho_1 + \mathbf{j}_1\rho_0] = \mathbf{j}^{\text{ind}}(\mathbf{q}, \omega)e^{i(\mathbf{q}\cdot\mathbf{x}-\omega t)}$$

where

$$\mathbf{j}_0 = \frac{1}{2m}[\mathbf{p}_e\delta(\mathbf{x} - \mathbf{x}_e) + \delta(\mathbf{x} - \mathbf{x}_e)\mathbf{p}_e]$$

and

$$\mathbf{j}_1 = \frac{e}{mc}\mathbf{A}\delta(\mathbf{x} - \mathbf{x}_e),$$

$\mathbf{p}_e$ and $\mathbf{x}_e$ being, respectively, the momentum and position operators. In matrix representation

$$\mathbf{j}^{\text{ind}}(\mathbf{q}, \omega) = (\Omega m)^{-1}\sum_{\mathbf{k},ll'}\rho_{\mathbf{k}+\mathbf{q},l;\mathbf{k},l'}\mathbf{\Pi}_{\mathbf{k},l';\mathbf{k}+\mathbf{q},l} + \Omega'\frac{e\mathbf{A}}{mc}\sum_{\mathbf{k}l}f_{\mathbf{k}l}$$

$$= \frac{e\mathbf{A}(\mathbf{q}, \omega)}{mc}\left[\frac{1}{\Omega_m}\sum_{\mathbf{k}ll'}\frac{\mathbf{\Pi}_{\mathbf{k}+\mathbf{q},l;\mathbf{k},l'}\cdot\mathbf{\Pi}_{\mathbf{k},l';\mathbf{k}+\mathbf{q},l}(f_{\mathbf{k},l'} - f_{\mathbf{k}+\mathbf{q},l})}{\hbar(\omega_{\mathbf{k}+\mathbf{q},l;\mathbf{k},l'} + \omega + i/\tau_{\mathbf{k}+\mathbf{q},l;\mathbf{k},l'})} + n\right]. \quad (14)$$

The frequency- and wave-number-dependent dielectric constant may be defined by either of the equations

$$\mathbf{j}^{\text{ind}}(\mathbf{q}, \omega) = (i\omega/4\pi e)[\varepsilon(\mathbf{q}, \omega) - 1]\mathscr{E}(\mathbf{q}, \omega)$$
$$= -(\omega^2/4\pi ec)[\varepsilon(\mathbf{q}, \omega) - 1]\mathbf{A}(\mathbf{q}, \omega). \quad (15)$$

The connection between these definitions derives from the relationship $\mathscr{E}(\mathbf{x}, t) = -c^{-1}\,\partial\mathbf{A}(\mathbf{x}, t)/\partial t$. The dielectric constant is now read off by a simple identification of the coefficients of $\mathbf{A}(\mathbf{q}, \omega)$ in Eqs. (14) and (15). Before writing out the explicit result, let us specialize the term in Eq. (14) involving the sum over $\mathbf{k}$, l, and l' to apply to a semiconductor and simplify it. Since the number of thermally excited carriers at room temperature is much smaller than the number filling the valence bands, we may neglect these in discussing the optical properties in the visible and ultraviolet (but not in the infrared). Thus, all bands may be regarded to be either entirely filled or empty; that is, $f_{l\mathbf{k}} = 1$ or 0. It therefore follows from Eq. (14) that all terms involving intraband transitions will vanish. Further, for the wavelength range of interest $\mathbf{q} \ll \mathbf{K}$, a reciprocal lattice vector, which provides a measure of the Brillouin-zone diameter. The interband transitions involved in the sum over $\mathbf{k}$, l, and l' may be regarded therefore as vertical in $\mathbf{k}$-space and $\mathbf{q}$ may be assumed to vanish. Because of these factors, as well as the orthogonality of the $u_{l\mathbf{k}}$ for different l and l', we may

approximate

$$\mathbf{\Pi}_{\mathbf{k}+\mathbf{q},l;\mathbf{k},l'} \approx \mathbf{\Pi}_{\mathbf{k}l,\mathbf{k}l'} = \frac{1}{v_a}\int_0 d^3x\, u^*_{\mathbf{k},l}\mathbf{p}u_{\mathbf{k},l'} \equiv \mathbf{P}_{ll'}(\mathbf{k}).$$

We then find, after some further algebraic rearrangement and replacement of the sum by an integral, that

$$\varepsilon(\mathbf{q},\omega) = 1 - \frac{4\pi ne^2}{m\omega^2} - \left(\frac{4\pi e^2}{\omega^2 m^2 \Omega}\right)\left(\frac{\Omega}{4\pi^3\hbar}\right)$$

$$\times \int d^3k \sum_{ll'}{}' |P_{ll'}|^2 f_l \left[\frac{1}{\omega + \omega_{ll'} + i/\tau_{ll'}} - \frac{1}{\omega - \omega_{ll'} + i/\tau_{ll'}}\right] \quad (16)$$

where we have suppressed the $\mathbf{k}$-dependence of the quantities appearing under the integral sign. It is convenient to introduce the oscillator strength

$$f^{\mu}_{l'l}(\mathbf{k}) = [2/\hbar\omega_{l'l}(\mathbf{k})m]\,|P^{\mu}_{l'l}(\mathbf{k})|^2 \quad (17)$$

corresponding to the μ component of the vector $\mathbf{P}_{l'l}$ which satisfies the f-sum rule

$$\sum_{l'}{}' f^{\mu}_{l'l} = 1 - (m/\hbar^2)\partial^2 E_{l\mathbf{k}}/\partial k_{\mu}{}^2. \quad (18)$$

Substitution of Eq. (17) into (16), together with use of the relationship

$$\frac{\omega^2_{l'l}}{(\omega + i/\tau_{ll'})^2 - \omega^2_{ll'}} = \frac{(\omega + i/\tau_{ll'})^2}{(\omega + i/\tau_{ll'})^2 - \omega^2_{ll'}} - 1, \quad (19)$$

yields the result[19]

$$\varepsilon(\omega) = 1 - \frac{e^2}{\pi^2 m}$$

$$\times \int d^3k \sum_{ll'}{}' f_{l\mathbf{k}} f f^{\mu}_{l'l} B_{ll'} [\omega + \omega_{ll'} + i/\tau_{ll'}]^{-1} [\omega - \omega_{ll'} + i/\tau_{ll'}]^{-1}. \quad (20)$$

It should be noted that the diamagnetic term $4\pi ne^2/m\omega^2$ in Eq. (16) cancels against the term resulting from the -1 in Eq. (19) after use of the f-sum rule:

$$\int d^3k \sum_{ll'}{}' f_{l\mathbf{k}} f^{\mu}_{l'l} = \int d^3k \sum_{l} f_{l\mathbf{k}} = 4\pi^3 n. \quad (21)$$

The term $B_{ll'} = (1 + i/\omega\tau_{ll'})^2$ for this particular calculation. Other typical

and equally valid answers, corresponding to the previously described choices involved in performing the calculation, are $B_{ll'} = 1$ or $(1 + i/\omega\tau_{ll'})$. This term is seen to be relatively unimportant in connection with a heuristic description of broadening effects, which requires only the imaginary term in the resonance denominators, except in the asymptotic frequency range to be discussed in the next section. We shall take $B_{ll'} = 1$ as the simplest choice and that conforming to previous usage.[19]

It should be noted that for insulators the sum in Eq. (20) can be written in any of the following alternate forms.

$$\sum_{ll'}{}' = \sum_{l\leqslant L,l'}{}' = \sum_{l\leqslant L,l'>L}, \tag{22}$$

where L is the uppermost filled valence band. This follows because $f_{l\mathbf{k}}$ takes on only the values 0 and 1, the denominator in Eq. (20) is symmetrical in l and l' if we assume $\tau_{ll'} = \tau_{l'l}$ and $f^{\mu}_{l'l} = f^{\mu}_{ll'}$.

It is of interest to exhibit some special forms of Eq. (20), which are particularly useful in connection with the interpretation of the optical properties of semiconductors in the ultraviolet.

a. Single Group of Valence Bands

For semiconductors like Si, SiC, BN, and AlP having a single group of valence bands (v) that are energetically well isolated from the core states, Eq. (20) reduces to a particularly simple asymptotic form. The asymptotic region here signifies the range of photon frequencies ω for which $\omega > \omega_{fv}$, where ω_{fv} is a typical interband frequency at which the f-sum, Eq. (18), is exhausted. The frequency ω_{fv} corresponds roughly to that separating regions 1 and 2 in Fig. 1 since the exhaustion of the f-sum rule should be marked experimentally by the absence of further sharp structure due to interband transitions originating from the valence bands. The energetic isolation of the valence bands for the semiconductors in question here is due to the fact that the core states are sufficiently far removed ($\sim$80 eV for Si) that they do not contribute to $\varepsilon(\mathbf{q}, \omega)$ for the frequency range of interest here. With the assumption that $\tau_{lv} \equiv \tau_v$ is the same for all valence bands and using Eqs. (20) and (21), we find

$$\varepsilon(\omega) \sim 1 - \frac{e^2}{\pi^2 m}\frac{1}{(\omega + i/\tau_v)^2}\int d^3k \sum_{lv}{}' f_{v\mathbf{k}} f^{\mu}_{lv} = 1 - \frac{\omega_{pv}^2}{(\omega + i/\tau_v)^2}. \tag{23}$$

Here $\omega_{pv}^2 = 4\pi e^2 \Sigma_v n_v/m$ corresponds to the *free*-electron plasma frequency of the valence bands. Equation (23) is seen to be closely related to the Drude formula $\varepsilon(\omega) = 1 - \omega_{pv}^2/\omega(\omega + i/\tau_v)$ for free electrons. The two

differ only in their dependence on τ_v. In fact, the Drude result would have been obtained if in Eq. (20) we had taken $B_{ll'} = (1 + i/\omega\tau)$ instead of 1. The behavior of the valence electrons is seen, therefore, to be that of free particles. Physically, this situation may be visualized in the following way. If we think of the electrons in an insulator according to the classical model of Lorentz, whereby each electron is tied by a spring to the lattice sites, then the asymptotic range just corresponds to applied fields whose frequency is much greater than the natural spring frequencies associated with the electrons. For such frequencies the electrons will behave as though they were unbound.

b. Two Separated Groups of Filled Bands

The semiconductors of interest in this category are those like Ge and InSb, having both valence and d bands and for which the lowest excitation frequency of the d bands into conduction-band states ω_{cd} is greater than ω_{fv} where the f-sum is exhausted. Again the frequency range of interest is $\omega > \omega_{fv}$; that is, the range corresponding to regions 2 and 3. It is clear from the f-sum rule that the d bands can affect the optical properties already in region 2, before real transitions between the d and conduction bands are energetically possible. If there exists an appreciable oscillator-strength coupling f_{dv} between the valence and d bands, then this coupling will make a negative contribution to the f-sum and, therefore, cause an enhancement of the oscillator strengths, f_{cv}, connecting the valence and conduction bands, averaged over the Brillouin zone. To see this explicitly, we introduce

$$g_{ll'} \equiv (\omega - \omega_{ll'} + i/\tau_l)^{-1}(\omega + \omega_{ll'} + i/\tau_l)^{-1} \equiv g^{\mathrm{R}}_{ll'} + ig^{\mathrm{I}}_{ll'} \tag{24}$$

and note that since $\omega > \omega_{fv}$, $g_{lv} \sim (\omega + i/\tau_v)^{-2}$. As in the case of the valence bands, we have assumed here that for the d bands τ_d is independent of the final state involved in the transition. Equation (20) may then be written in the form

$$\varepsilon(\omega) \approx 1 - m^{-1}(e/\pi)^2 \int d^3k\,(\omega + i/\tau_v)^{-2}\Big[\sum_{l>v} f^{\mu}_{lv} + f^{\mu}_{dv}\Big]$$

$$- m^{-1}(e/\pi)^2 \int d^3k\Big[\sum_{l>v} f^{\mu}_{ld} g_{ld} + (\omega + i/\tau_v)^{-2} f^{\mu}_{vd}\Big], \tag{25}$$

where the terms involving f^{μ}_{dv} have been added and subtracted. The second term on the right-hand side of Eq. (25) is now such that the f-sum can be performed. Writing out real and imaginary parts explicitly, we

therefore obtain

$$\begin{aligned}\varepsilon_1(\omega) &= 1 - (\omega^2 - \tau_v^{-2})(\omega^2 + \tau_v^{-2})^{-2}\Big[\omega_{Pv}^2 + m^{-1}(e/\pi)^2 \int d^3k\, f_{vd}^{\mu}\Big] \\ &\quad - m^{-1}(e/\pi)^2 \int d^3k \sum_{l>v} f_{ld}^{\mu} g_{ld}^{R} \\ \varepsilon_2(\omega) &= (2\omega/\tau_v)(\omega^2 + \tau_v^{-2})^2\Big[\omega_{Pv}^2 + m^{-1}(e/\pi)^2 \int d^3k\, f_{vd}\Big] \\ &\quad - m^{-1}(e/\pi)^2 \int d^3k \sum_{l>v} f_{ld}^{\mu} g_{ld}^{I}.\end{aligned} \tag{26}$$

Equation (26) is seen to consist of a linear superposition of terms due to the valence electrons, which behave in this frequency range as though they were free, and others due to the bound d electrons. The term involving g_{ld}^{R} makes a positive contribution to ε_1, since $g_{ld}^{R} < 0$ for $\omega < (\omega_{ld}^2 + \tau_d^{-2})$. It will be shown presently that for $\omega \ll \omega_{ld}$ this term corresponds just to the contribution $\delta\varepsilon_0$ of the d electrons to the optical dielectric constant above the reststrahlen frequency. The term involving g_{ld}^{I} makes a positive contribution to ε_2. It describes real transitions between the d band and empty conduction-band states and will be small until such transitions become energetically allowed. From Eq. (25) it is clear therefore that, for the frequency range $\omega_{fv} < \omega < \omega_{cd}$, the complex dielectric constant may be written approximately in the form

$$\varepsilon(\omega) = (1 + \delta\varepsilon_0)[1 - \Omega_{Pv}^2/(\omega + i/\tau_v)^2], \tag{27}$$

where

$$\Omega_{Pv} = \left[\frac{\omega_{Pv}^2 + m^{-1}(e/\pi)^2 \int d^3k\, f_{vd}^{\mu}}{(1 + \delta\varepsilon_0)}\right]^{1/2} \equiv \frac{\Omega'_{Pv}}{(1 + \delta\varepsilon_0)^{1/2}} \tag{28}$$

is an effective plasma frequency that is enhanced over the free-electron value by a term involving the coupling between the v and d electrons, and diminished by the screening effect due to the d band. Further

$$\delta\varepsilon_0 = -m^{-1}(e/\pi)^2 \int d^3k \sum_{l>v} f_{ld}^{\mu} g_{ld}^{R} \approx m^{-1}(e/\pi)^2 \int d^3k \sum_{n'>v} \frac{f_{ld}^{\mu}}{\omega_{ld}^2 + \tau_{ld}^{-2}} \tag{29}$$

for $\omega \ll \omega_{ld}$. The right-hand side is seen to be just the contribution of the d electrons to the electronic part of the static dielectric constant when the damping is small. Equation (27) closely resembles the Drude-like formula given by Eq. (23). In fact Eq. (23) is recovered if the d bands are sufficiently far removed and uncoupled from the valence bands. When the frequency approaches ω_{cd}, the frequency dependence of the last term in the two Eqs. (26) should really be taken into account. This dependence, however,

will be seen to be weak, and the present treatment, for the sake of simplicity, will assume that $\delta\varepsilon_0$ in Eq. (27) is real and constant.

For much larger frequencies, when the f-sum rule for the d band is also exhausted, Eq. (20) again assumes a simple asymptotic form

$$\varepsilon(\omega) = \varepsilon_0 - \omega_{Pv}^2/(\omega + i/\tau_v)^2 - \omega_{Pd}^2/(\omega + i/\tau_d)^2 . \tag{30}$$

The plasma frequency then is given by $\omega_P{}^2 = \omega_{Pv}^2 + \omega_{Pd}^2$, and it corresponds to the total density $n_v + n_d$ of v and d electrons.

6. Sum Rules

In order to permit comparison of Eq. (27) with the experimental results in region 2, it is desirable to obtain estimates of Ω_{Pv} and $\delta\varepsilon_0$. Several sum rules involving the imaginary part of the dielectric constant are useful in this as well as other connections. The first of these,

$$\varepsilon_0 = 1 + \left(\frac{2}{\pi}\right)\int_0^\infty \omega^{-1}\varepsilon_2(\omega)\, d\omega , \tag{31}$$

is an expression for the static or optical dielectric constant (below or above the Reststrahlen frequency) which is obtained as an elementary consequence of the Kramers–Kronig relations.[6] The static dielectric constant results if the infrared lattice absorption is taken into account in the integration, and the optical dielectric constant is obtained if it is neglected. The sum rules

$$\int_0^\infty \omega\varepsilon_2(\omega)\, d\omega = (\pi/2)\omega_p{}^2 \tag{32}$$

and

$$\int_0^\infty \omega \operatorname{Im} \varepsilon^{-1}(\omega)\, d\omega = -(\pi/2)\omega_p{}^2 , \tag{33}$$

where ω_p is the free-electron plasma frequency corresponding to the *total* electron density of the system, are also completely general and valid for an arbitrary many-electron system.[6]

It will prove to be useful to rewrite Eqs. (31) and (32) for finite intervals of integration and to present explicit expressions for the integrals using the random-phase approximation results for ε_2.

In the absence of d bands and for core states far removed, the result given by Eq. (32) for an infinite range of integration would involve a plasma frequency characteristic simply of four electrons per atom, each having the free-electron mass. It is therefore simplest to express the results of the integration over a finite range 0 to ω_0 in terms of n_{eff}, an effective number of free electrons contributing to the optical properties in this range:

$$(2\pi^2 Ne^2/m)n_{\text{eff}} = \int_0^{\omega_0} \omega\varepsilon_2(\omega)\, d\omega . \tag{34}$$

Here N is the atom density of the crystal. Similarly, the effective dielectric constant $\varepsilon_{0,\text{eff}}$ produced by interband transitions in this range may be written

$$\varepsilon_{0,\text{eff}} = 1 + (2/\pi)\int_0^{\omega_0} \omega^{-1}\varepsilon_2(\omega)\, d\omega . \tag{35}$$

Direct integration, using ε_2 as obtained from Eq. (20), then yields:

$$(2\pi^2 Ne^2/m)n_{\text{eff}} = (2m)^{-1}(e/\pi)^2 \int d^3k \sum f_{l'l}^{\mu} h_{l'l}^{-}(\omega_0) \tag{36}$$

$$\varepsilon_{0,\text{eff}} = 1 + (\pi m)^{-1}(e/\pi)^2 \int d^3k \sum f_{l'l}^{\mu}(\omega_{l'l}^2 + \tau_{l'l}^{-2}) h_{l'l}^{+}(\omega_0), \tag{37}$$

where

$$h_{l'l}^{\pm}(\omega_0) = \tan^{-1}(\omega_0 - \omega_{l'l})\tau_{l'l} + \tan^{-1}(\omega_0 + \omega_{l'l})\tau_{l'l}$$

$$\pm (2\omega_{l'l}\tau_{l'l})^{-1} \ln \frac{(\omega_0 + \omega_{l'l})^2 + \tau_{l'l}^{-2}}{(\omega_0 - \omega_{l'l})^2 + \tau_{l'l}^{-2}} \tag{38}$$

and $\tau_{l'l}$ has been assumed independent of frequency. The summation may be taken in the forms indicated by Eq. (22). This follows from the fact that $h_{l'l}^{\pm}(\omega_0)$ is symmetrical in the indices l and l'. It is seen from Eq. (38) that in the limit $|\omega_{l'l}|\tau_{l'l} \to \infty$, $h_{l'l}^{\pm}$ is a step function: $h_{l'l}^{\pm} = 0$ for $\omega_0 < \omega_{l'l}$ and $h_{l'l}^{\pm} = \pi$ for $\omega_0 > \omega_{l'l}$. As $\tau_{l'l}$ decreases the step is smeared out principally in the direction of higher energies for $h_{l'l}^{-}$ and toward lower energies for $h_{l'l}^{+}$. However, $h_{l'l}(\infty) = \pi$ independently of $\tau_{l'l}$. Thus, for $\omega_0 \to \infty$, our results reduce to the exact ones given by Eqs. (31) and (32).

The step-like character of $h_{l'l}$ results from the fact that ε_2 describes real optical transitions and that ω_0 must be such that they are energetically allowed. Thus, there will be a fairly rapid increase in both n_{eff} and $\varepsilon_{0,\text{eff}}$ as ω_0 passes across a strong absorption edge. From plots of $\varepsilon_{0,\text{eff}}$ vs. $\hbar\omega_0$, for example, it is therefore possible to estimate which transitions make the most important contribution to the static dielectric constant. More important for the present purposes is the fact to be demonstrated in the following section that the quantities Ω_{Pv} and $\delta\varepsilon_0$ may also be estimated from such plots.

In this connection it is useful to examine Eqs. (36) and (37) for the case of two sets of filled bands v and d as treated in the preceding subsection. The frequency range of interest is again $\omega > \omega_{fv}$. We find in this case

$$\int_0^{\omega_0} \omega\varepsilon_2(\omega)\, d\omega = (\pi/2)\Omega'^2_{Pv} + (2m)^{-1}(e/\pi)^2 \int d^3k \sum_{l>v} f_{ld}^{\mu} h_{ld}^{-}(\omega_0), \tag{39}$$

$$\varepsilon_{0,\text{eff}} = \varepsilon_{0,v} + (2m)^{-1}(e/\pi)^2 \int d^3k \sum_{l>v} f_{ld}^{\mu}(\omega_{ld}^2 + \tau_{ld}^{-2})^{-1} h_{ld}^{+}(\omega_0). \tag{40}$$

The first term of Eq. (39) is seen to depend on the same Ω'_{Pv} as that defined by Eq. (28). The last term is zero until real excitations from the d band are allowed. Thus, n_{eff} differs from the number of valence electrons per atom in this case because of (1) the oscillator-strength coupling of the v and d bands, and (2) real transitions taking place between the d and conduction bands. The dielectric constant due to the valence band $\varepsilon_{0,v}$ is similarly modified by a term which vanishes until frequencies ω_0 are obtained at which real d-band excitations are possible. It is seen that the last term of Eq. (40), for sufficiently large ω_0, just corresponds to the quantity involving g^{R}_{ld} in Eq. (24) with $\omega = 0$. This has been written as $\delta\varepsilon_0$ in Eq. (27) and assumed to depart little from its value for $\omega = 0$. As $\omega_0 \to \infty$, Eq. (40) therefore becomes $\varepsilon_0 = \varepsilon_{0,v} + \delta\varepsilon_0$. In this form it is clear that $\delta\varepsilon_0$ just represents the contribution of the d electrons to the low-frequency dielectric constant.

When the oscillator-strength coupling between the v and d bands vanishes, and the f-sum rule for the valence band is exhausted at an energy lower than $\hbar\omega_{cd}$, then it is possible to identify unambiguously the onset of d-band excitations from a plot of n_{eff} vs. $\hbar\omega_0$. Indeed, it is seen from Eq. (39) that such a plot would first saturate at a value of n_{eff} equal to the number of valence electrons per atom, and then increase beyond that value when electrons could be excited out of the d band. The term f_{vd} in Ω_{Pv}, however, can cause n_{eff} to increase beyond that first saturation value when there is oscillator-strength coupling between the v and d bands.

Finally, it should be noted that the same qualitative results are obtained even if the valence band f-sum rule with respect to conduction band states is not quite exhausted. In this case the correction terms in Eqs. (39) and (40) would involve transitions to highly excited states in the conduction bands as well.

V. Discussion of Experimental Results

7. Reflectance Data and Deduced Dielectric Constants

The spectral dependence of the reflectance for Si, Ge, InAs, GaAs, and GaP is shown in Fig. 3. Results for InSb have already been presented in Fig. 1. In the case of the III–V compounds, the data represent measurements on one sample of each material. Good agreement is found between these curves and those in the literature[16,17,20–27] where the spectral ranges overlap. The dielectric constants, as well as the energy-loss function, $-\operatorname{Im}\varepsilon^{-1}$, obtained from Kramers–Kronig analysis are also shown in these figures.

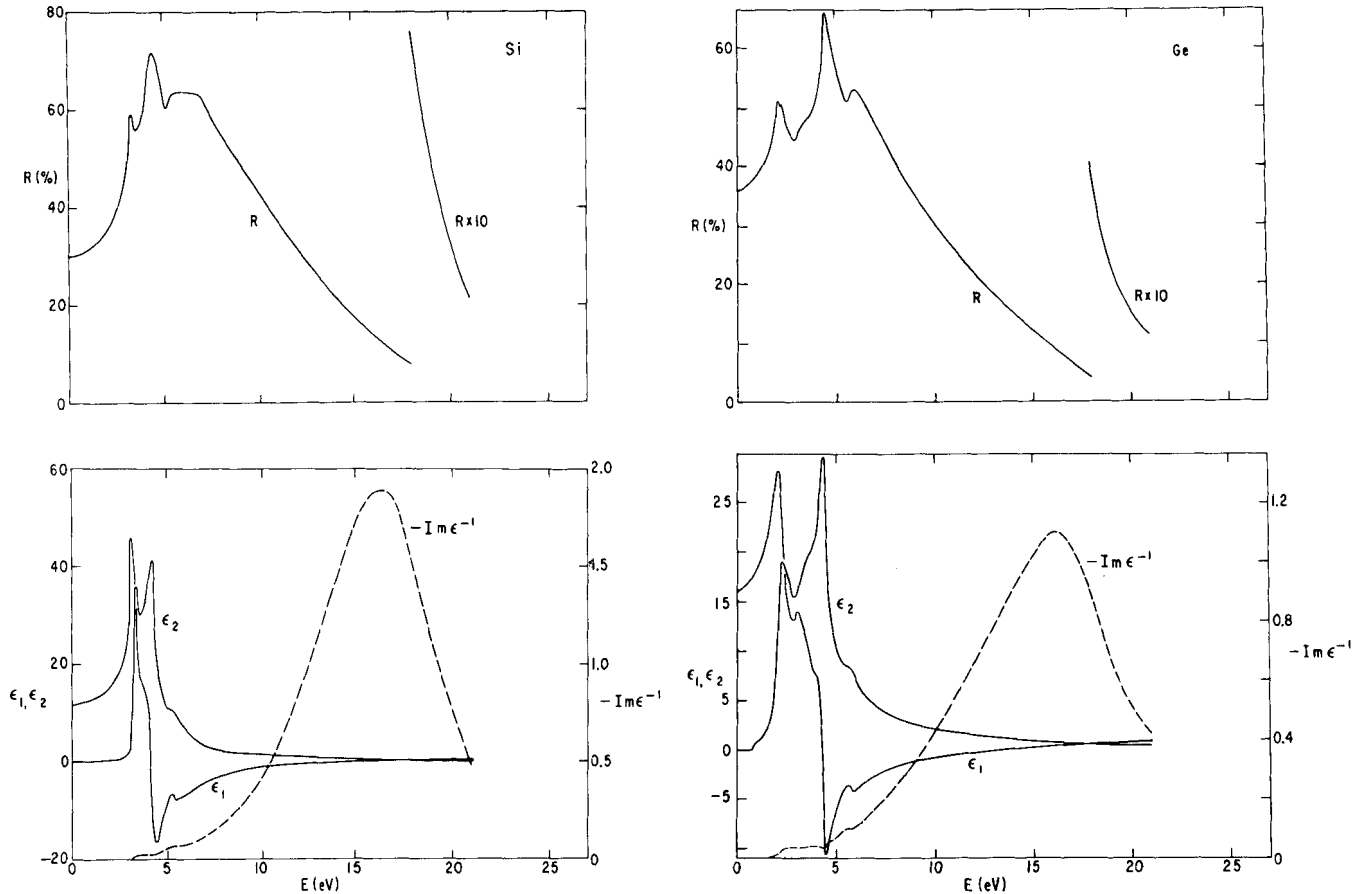


FIG. 3a. The spectral dependence of the reflectance R, the real and imaginary parts of the dielectric constant, ε_1 and ε_2, and the energy-loss function $-\mathrm{Im}\,\varepsilon^{-1}$ for Si and Ge.

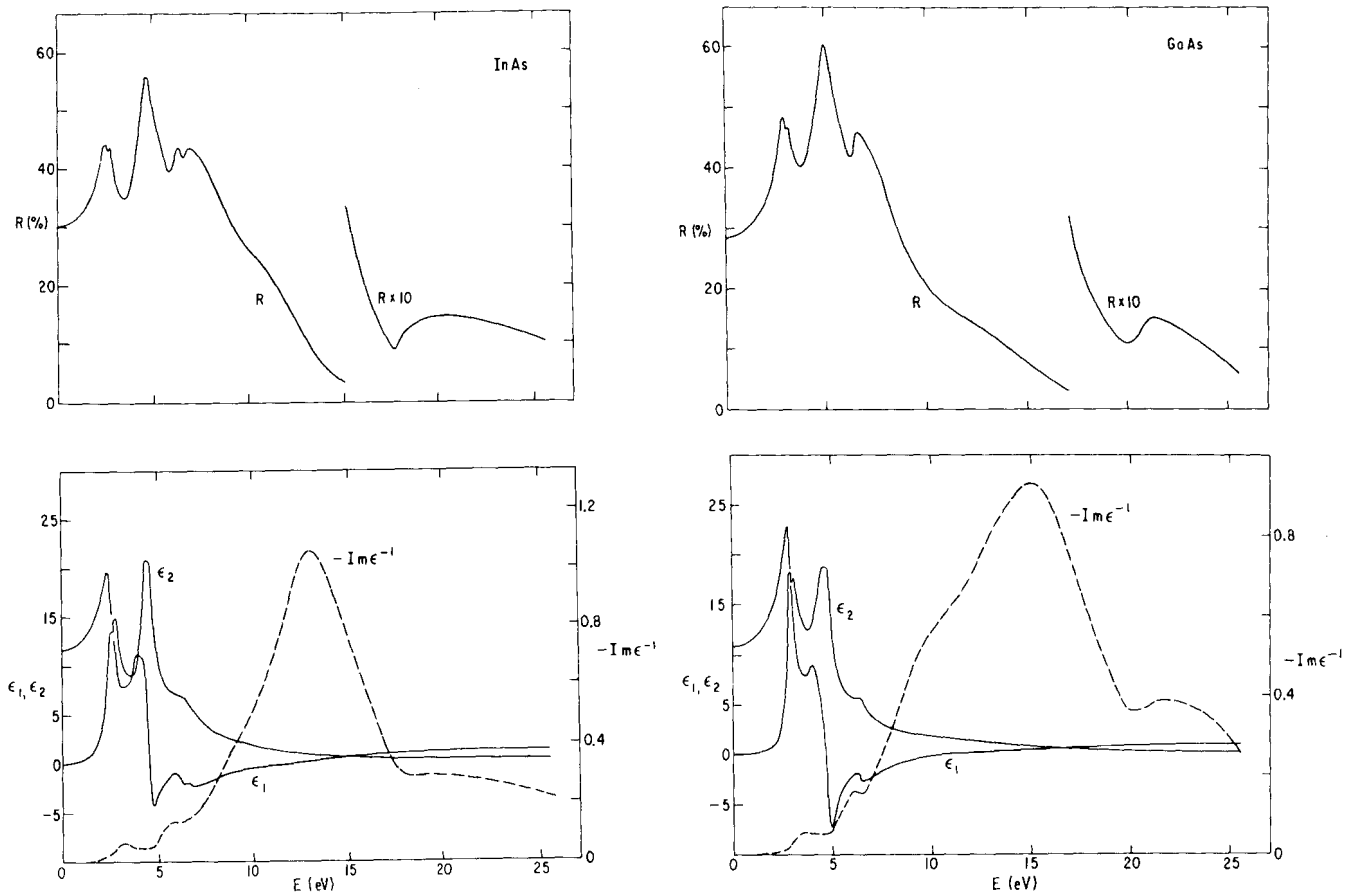


FIG. 3b. The spectral dependence of the reflectance R, the real and imaginary parts of the dielectric constant, ε_1 and ε_2, and the energy-loss function $-\mathrm{Im}\,\varepsilon^{-1}$ for InAs and GaAs.

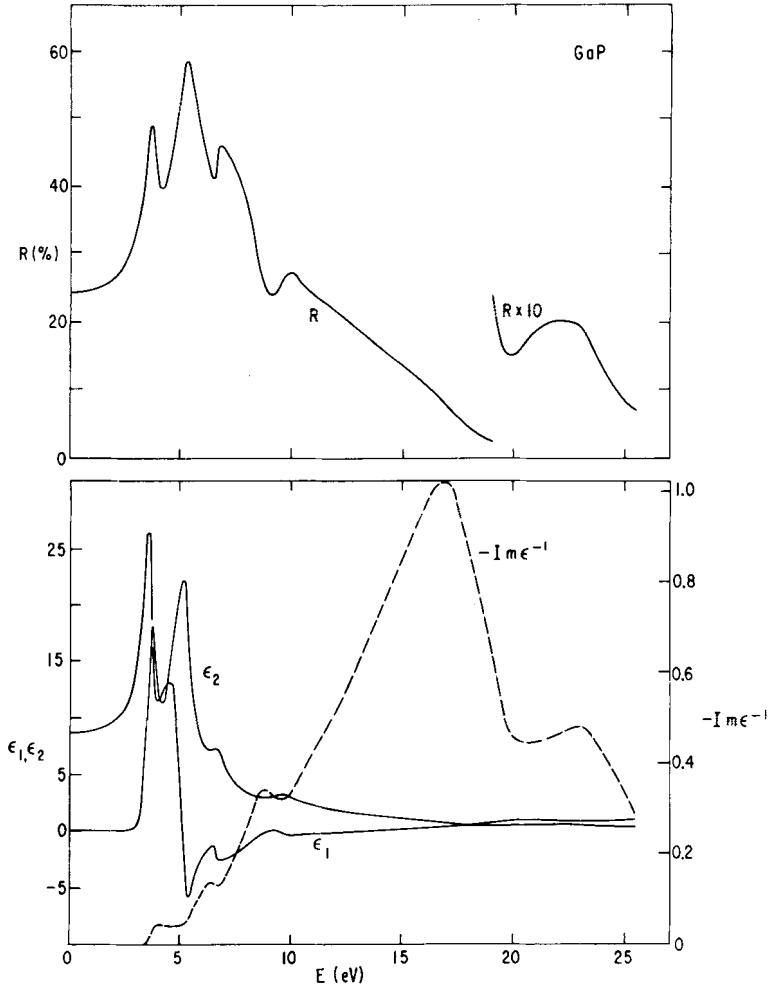


FIG. 3c. The spectral dependence of the reflectance R, the real and imaginary parts of the dielectric constant, ε_1 and ε_2, and the energy-loss function $-\mathrm{Im}\,\varepsilon^{-1}$ for GaP.

8. INTERBAND TRANSITIONS (REGION 1)

The first region, extending to about 8 eV, is characterized by sharp structure that can be associated with valence to conduction band transitions.[5] The detailed interpretation of this structure is presented by Cardona[9] and will not be discussed further here.

9. Metallic Effects (Region 2)

a. Single Group of Valence Bands

Silicon presents an ideal vehicle for the study of region 2, since *d* bands are absent in this material and the next filled band lies about 80 eV below the valence bands.[52] Furthermore, the density of states of the valence band as obtained by Hagstrum[53] appears to be such that most of the electrons lie within 5 eV of the top of the band, although there is a sparsely populated tail extending to about 16 eV. All of these electrons cannot contribute to the optical properties below photon energies of 16 eV; however, the contribution of the remaining electrons to the dielectric constant is small. Because of the absence of structure related to interband transitions in region 2, Eq. (23) should represent a reasonable description of the dielectric constants in this range. Figure 4 compares experimental and theoretical results for this material. The latter were obtained by taking the plasma frequency ω_{P_v} to correspond to that for four free electrons per atom as prescribed by Eq. (23). The relaxation time τ_v, which is assumed constant, was determined by matching the experimental and theoretical values of ε_2 at the plasma frequency. The magnitude will be discussed subsequently. This Drude-like theory is seen to fit quite well, showing that silicon, in this range, indeed behaves essentially like a free-electron metal.

b. Semiconductors Containing d Bands

In order to apply the theory outlined in the preceding section, it is necessary to obtain values for the effective plasma frequency Ω_{P_v} and the contribution $\delta\varepsilon_0$ of the *d* bands to the dielectric constant from the experimental data. This is achieved with the help of the modified sum rules given by Eqs. (34) and (35). The prescription for using these relations consists of performing the indicated integrations numerically, using the experimental data.

The results for the integral given in Eq. (34) are plotted as a function of $E = \hbar\omega_0$ in Fig. 5. It should be noted first that the curve for silicon appears to saturate very nearly at a value of four electrons per atom, as expected. The slight overshoot above four is probably due to a small negative contribution to the *f* sum arising from the core states. By contrast, the curves for germanium and the III–V compounds extend appreciably above four. In the case of germanium, n_{eff} increases smoothly with increasing E. For the III–V compounds, on the other hand, there is a break in the curve which may be associated with the onset of *d*-band excitations. The increase above

[52] J. C. Phillips and L. Kleinman, quoted by L. Liu, *Phys. Rev.* **126**, 1317 (1962).
[53] H. D. Hagstrum, *Phys. Rev.* **122**, 83 (1961).

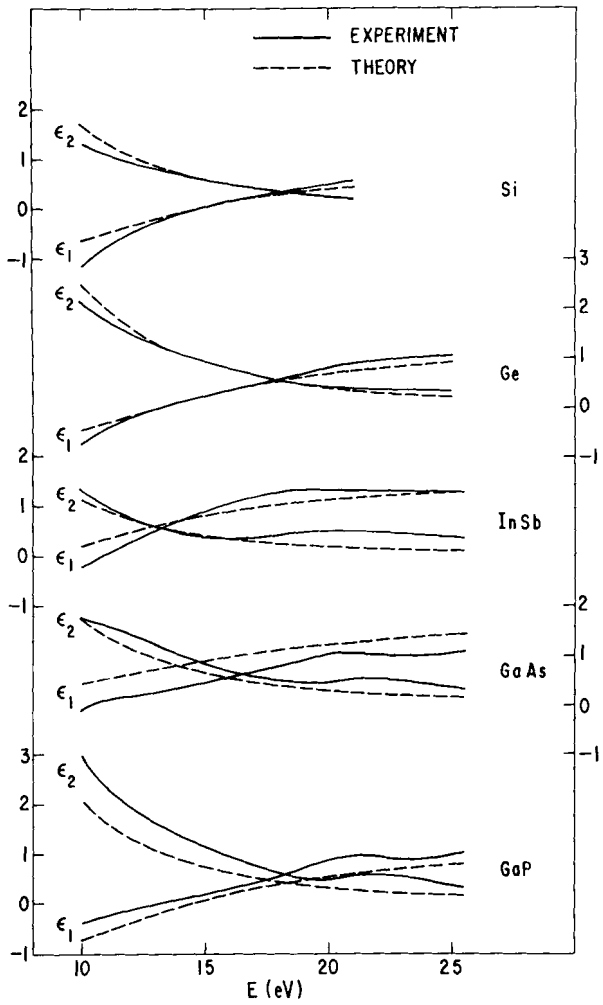


FIG. 4. Experimental and theoretical curves of ε_1 and ε_2 for Si, Ge, InSb, GaAs, and GaP. The theoretically determined parameters Ω_{P_v} and $\delta\varepsilon_0$, which are needed for all materials except Si, are given in Table I and Fig. 6, respectively. The adjustable parameter τ_v was taken to be 1.6, 1.4, and 1.8 $\times 10^{-16}$ sec, respectively, for Si, Ge, and InSb. For GaAs and GaP, τ_v was assumed to have the Ge and Si values, respectively. The curve for InAs is similar to that for InSb.

four at lower energies is then evidently associated with the oscillator-strength coupling between the valence and *d* bands. In germanium the previously mentioned break in the curve is absent because the *d* band lies considerably deeper.[54] From an extrapolation of the smooth part of the

[54] F. Herman and S. Skillman, *Proc. Intern. Conf. Semicond. Phys., Prague, 1960* p. 20. Czech. Acad. Sci., Prague, 1961.

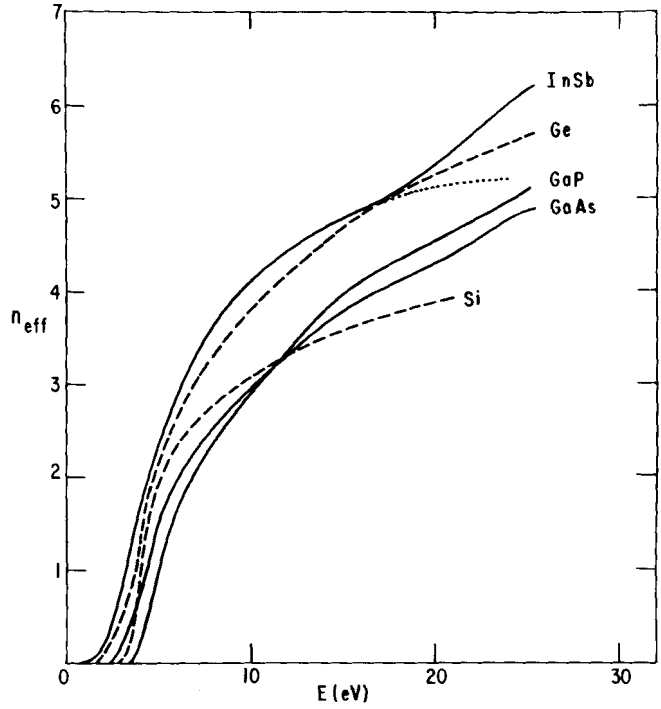


FIG. 5. n_{eff} vs. E for group-IV and III–V semiconductors. The dotted line represents the extrapolation discussed in the text.

curve, such as that indicated by the dotted curve in the InSb graph, it is possible to estimate the first term, depending on Ω'_{P_v} on the right-hand side of Eq. (39). This procedure is admittedly somewhat crude, but will nevertheless be shown to lead to reasonable results.

A plot of the effective dielectric constant $\varepsilon_{0,\text{eff}}$ as a function of $E = \hbar\omega_0$ is shown for several materials in Fig. 6. In addition to providing a good estimate of $\delta\varepsilon_0$, a graph of this type is also interesting in that it permits the identification of interband transitions that contribute most importantly to the low-frequency dielectric constant. From the tendency toward saturation at photon energies below 5 eV, it is clear that strong interband transitions at critical points below this energy are mainly responsible for the value of the low-frequency dielectric constant. Transitions near the band gap do not contribute appreciably. The curve for silicon is seen to saturate at a value corresponding to the independently measured low-frequency dielectric constant.[38,55] As expected, there is no contribution from deeper-lying bands. By contrast, curves for the remaining materials, which all have

[55] W. C. Dunlap, Jr., and R. L. Walters, *Phys. Rev.* **92**, 1396 (1953).

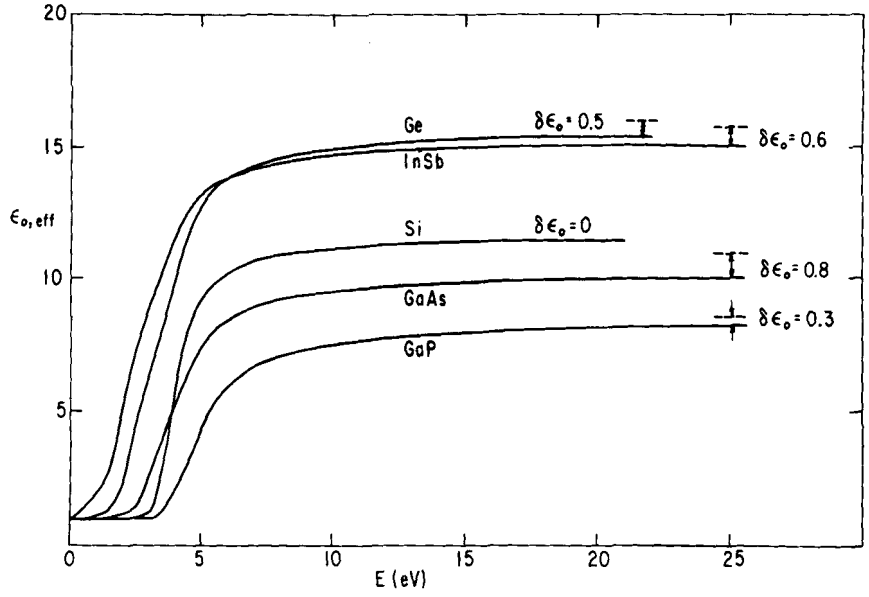


FIG. 6. $\varepsilon_{0,\text{eff}}$ vs. E for group-IV and III–V semiconductors. The low-frequency dielectric constants obtained from Refs. 35 and 36 are indicated by dashed line segments.

d bands, appear to saturate at a value below the independently measured low-frequency dielectric constants,[35,36] shown here by dashed line segments. As indicated by the theory of the preceding section, this difference is due just to the contribution of the d bands. The onset of real d-band excitation does not produce a break in the curves for the III–V compounds as in the case of the n_{eff} plots, since the small increase to the final values is very slow as indicated by Eq. (40) and extends over many volts. This supports our assumption concerning the frequency independence of $\delta\varepsilon_0$.

These results, together with those obtained from Fig. 5, permit the determination of the effective plasma frequency Ω_{P_v} and the contribution of the d bands to the low-frequency dielectric constant. It should be remembered at this point that this type of analysis depends very sensitively on the absolute values of ε_2 and, hence, on the reflectance. Errors in the absolute magnitude of the measured reflectance will produce corresponding errors in the quantities just determined. The preceding cautionary remark may be particularly appropriate for the GaAs results shown in Fig. 5. The difference between these and the Ge results is surprising. If indeed real, this difference would indicate a much weaker oscillator-strength coupling between the valence and d bands in GaAs.

The effective plasma frequency is compared with the free-electron value in Table I. The close correspondence between the two sets of values results

TABLE I

COMPARISON OF PLASMA FREQUENCIES (IN eV) AS GIVEN BY FREE VALENCE ELECTRONS (FOUR PER ATOM), THE CALCULATIONS OF THE PRESENT CHAPTER, THE STANDARD PLASMA-DISPERSION RELATION ($\varepsilon_1 = 0$), AND THE MAXIMUM OF THE ENERGY-LOSS FUNCTION OBTAINED FROM OPTICAL AND ELECTRON-ENERGY-LOSS EXPERIMENTS

	ω_{Pv} (free-electron)	Ω_{Pv} (effective frequency)	$\varepsilon_1(\omega) = 0$	$-\max \operatorname{Im} \varepsilon^{-1}$ (optical)	$-\max \operatorname{Im} \varepsilon^{-1}$ (energy loss)
Si	16.6	16.6	15.0	16.4	16.9[a]
Ge	15.5	16.2	13.8	16.0	16.4[b]
GaP	16.6	16.3	13.3	16.9	—
GaAs	15.5	12.3	9.7	14.7	—
InSb	12.7	11.5	10.9	12.0	13.0[c]

[a] See Ref. 42.
[b] See Ref. 41.
[c] See Ref. 43.

from the fact that the quantity $\frac{1}{4}n_{\text{eff}}/(1 + \delta\varepsilon_0)$ is close to unity for all these materials with the possible exception of GaAs, whose anomalous character was just described. The remaining columns of the table will be discussed subsequently.

With the values of Ω_{Pv} and $\delta\varepsilon_0$ at hand, it is now possible to compare the theoretical expression for the dielectric constant given by Eq. (27) with the experimental values. The only unknown parameter, as before, is the relaxation time. This was assumed constant and determined in the case of Ge and InSb by matching experimental and theoretical values of ε_2 somewhere in the range. The results for silicon have already been discussed. A comparison of the theoretical and experimental results is shown in Fig. 4. Good agreement is obtained for Si, Ge, and InSb. The structure in region 3 arising from the *d*-band excitation, of course, is not included in the present theory and is therefore missing from the theoretical curves. In the case of GaP and GaAs, the relaxation times obtained for Si and Ge, respectively, were used. The GaAs results again are somewhat anomalous, but those for GaP are quite reasonable.

It is remarkable that the relaxation times all appear to lie between 1.4×10^{-16} and 1.8×10^{-16} sec. Since the magnitude of the relaxation time is much less than that ordinarily associated with either lattice or impurity scattering, it seems reasonable to suppose that τ is determined by electron-electron scattering involving Umklapp processes. The similarity

of the actual values of τ may result from the fact that the band structure on a gross scale for all these materials is rather similar.

c. Plasma Effects

Collective oscillations are described in terms of the longitudinal dielectric constant. The condition for the existence of plasma oscillations at frequency ω is just $\varepsilon(\omega) = 0$.[56] This equation, in general, is solved by a complex frequency whose real part corresponds to the plasma frequency and whose imaginary part corresponds to the damping of the plasma resonance. For example, the resonance condition resulting from Eq. (27) is $\omega = \Omega_{P_v} - i/\tau_v$. The relaxation time thus describes the damping of the plasma wave.

Much of the experimental information concerning plasma oscillations has come from characteristic-energy-loss experiments from which one determines the function $-\operatorname{Im}\varepsilon^{-1}$.[7] This function has a maximum at a plasma resonance.[8,56] Because the longitudinal and transverse dielectric constants should be equal at long wavelengths[49] and the energy-loss function $-\operatorname{Im}\varepsilon^{-1}$ can be directly calculated from the optical data, it is of interest to compare directly the results of optical and characteristic-energy-loss experiments. An example of such a comparison for germanium and silicon is shown in Figs. 7(a) and (b), respectively. For Ge the dashed line represents the characteristic-energy-loss data of Powell[41] for 1.5-keV electrons, and for Si that of Dimigen[42] for 47-keV electrons. The energy-loss data were normalized so that the peak value of the curve was equal to the maximum of $-\operatorname{Im}\varepsilon^{-1}$. The agreement in both position and width of the plasma peak in the two cases is very satisfactory. The electron-scattering experiments show, in addition, a low-lying loss that is absent in the optical data. This loss is presumably associated with the specimen boundary[57] and is without analog in optical data. It is also seen that the Ge data exhibit a further rise at higher energies that is absent in Si. The rise is probably associated with the presence of the *d* band in Ge.

The functional form of the dielectric constants in region 2, as given by either Eq. (23) or (27), is such that the real part ω_{P_v} or Ω_{P_v} of the plasma frequency obtained from the relationship $\varepsilon(\omega) = 0$ agrees with the frequency corresponding to the maximum of the energy-loss function to order $1/\omega_P{}^2\tau^2$. By contrast, the frequency corresponding to $\varepsilon_1 = 0$ agrees with the plasma frequency only to lower order. These facts are substantiated by the entries in Table I, from which it is seen that Ω_{P_v} is in good agreement with the results of the maximum of the energy-loss function as obtained from optical and characteristic-energy-loss experiments. On the other

[56] H. Fröhlich and H. Pelzer, *Proc. Phys. Soc.* (*London*) **A68**, 525 (1955).
[57] R. H. Ritchie, *Phys. Rev.* **106**, 874 (1957).

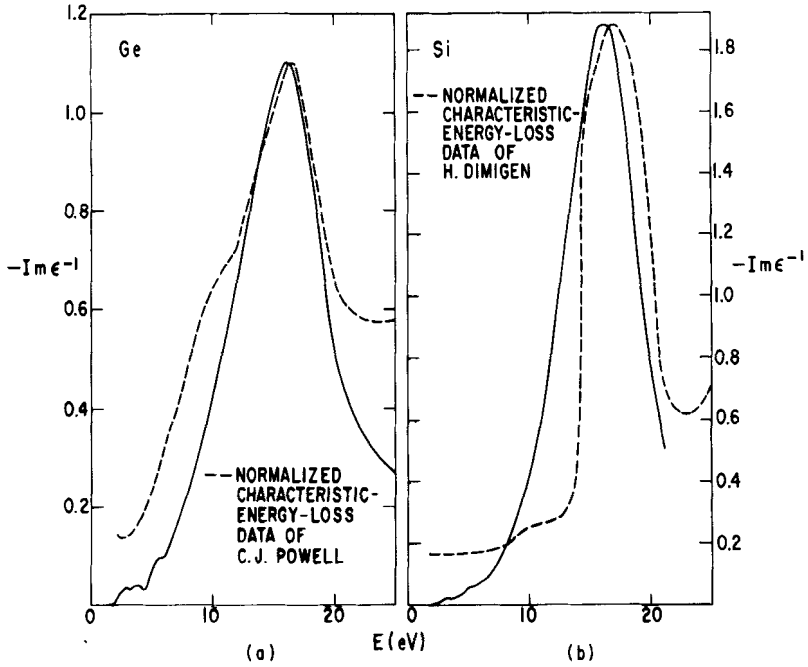


FIG. 7. A comparison of the energy-loss function $-\mathrm{Im}\,\varepsilon^{-1}$ obtained from the results of optical and characteristic-energy-loss experiments for (a) Ge and (b) Si.

hand, the frequency corresponding to $\varepsilon_1 = 0$ is somewhat displaced. This fact is worth noting, since the plasma dispersion relationship applying to a free-electron gas is generally stated as $\varepsilon_1 = 0$, ε_2 being rigorously 0 at 0°K below the plasma cutoff.[58] In an actual solid this idealized situation does not prevail, and it is necessary to use the complete equation describing the existence of a plasma oscillation.

Clearly, peaks in the energy loss function can be associated either with a plasma oscillation or with interband transitions.[59] These two physical phenomena can be distinguished rather unambiguously if the dielectric constants in the vicinity of such a peak are known.[4]

The relaxation time τ appearing in Eqs. (23) and (27), which also describes the lifetime of the plasma oscillations, can be estimated from the total width of the peak of the characteristic-energy-loss function at half maximum. Indeed, one finds that $\Delta\omega/\omega = 2/\omega_{Pv}\tau$. The experimentally observed widths are in good agreement with the values of τ obtained from Fig. 4.

[58] See, for example, R. A. Ferrell, *Phys. Rev.* **107**, 450 (1957).
[59] Y. H. Ichikawa, *Phys. Rev.* **109**, 653 (1958).

10. *d*-Band Excitations (Region 3)

It may be useful to state briefly the reasons for assigning the structure in region 3 to *d*-band excitations. We observe first that the structure in region 3 present in the III–V compounds is absent in Si, which does not have a *d* band, and also does not appear in the energy range of the present measurements in the curve for Ge where the *d* band lies about 30 eV below the top of the valence band.[54] Second, we observe the similarity of structure in curves of reflectance and dielectric constants appearing in Figs. 1 and 3 between GaAs and GaP, and between InAs and InSb, respectively. This similarity also extends to the absorption coefficients, which are shown for the two In compounds in Fig. 8. It is the Ga *d* band that is assigned to the structure observed in GaAs and GaP and the In *d* band to the structure in InAs and InSb. In GaP, indeed, the Ga *d* band is the only one present. In the other III–V compounds considered here the cation *d* bands are more tightly bound, according to atomic data.[60] In this connection the rise in absorption coefficient shown in Fig. 8 agrees closely in energy with the onset of absorption observed in transmission studies on thin In foils.[61,62]

Third, we observe that the curves of n_{eff} in Fig. 5 for the III–V compounds all exhibit a characteristic break near 20 eV and values of n_{eff} that rise above four electrons per atom. Since the valence band contains only four electrons per atom, the additional structure responsible for this behavior must be due to *d* bands. In contrast, the curve for Si appears to saturate at $n_{\text{eff}} = 4$.

Somewhat naively, one might identify the minimum *d*-band–conduction-band separation with the onset of optical absorption, as indicated by the dashed lines in Fig. 8. However, because of broadening effects caused by electron interactions, it is possible for absorption to occur at energies smaller than this minimum separation. This situation would correspond to a partial breakdown of the band approximation and foreshadow the even more serious deviations from the one-electron picture encountered in X-ray spectroscopy.[63] More appropriately, the gap should be assumed to be somewhere between the energies where $\varepsilon_1(\omega)$ and $\varepsilon_2(\omega)$, shown in Fig. 8 for the In compounds, are maximum.[64] This occurs near 21 eV for InSb and InAs, and near 22 eV for GaAs and GaP. Since the Kramers–Kronig analysis

[60] C. E. Moore, "Atomic Energy Levels," Natl. Bur. Std. Circ. 467, Volume 2. U.S. Govt. Printing Office, Washington, D.C., 1952.

[61] O. M. Sorokin, *Opt. i Spektroskopiya* **16**, 139 (1964) [*English Transl.: Opt. Spectry. (USSR)* **16**, 72 (1964)].

[62] W. C. Walker, O. P. Rustgi, and G. L. Weissler, *J. Opt. Soc. Am.* **49**, 471 (1959).

[63] For example, L. G. Parratt, *Rev. Mod. Phys.* **31**, 616 (1959).

[64] D. T. F. Marple and H. Ehrenreich, *Phys. Rev. Letters* **8**, 87 (1962).

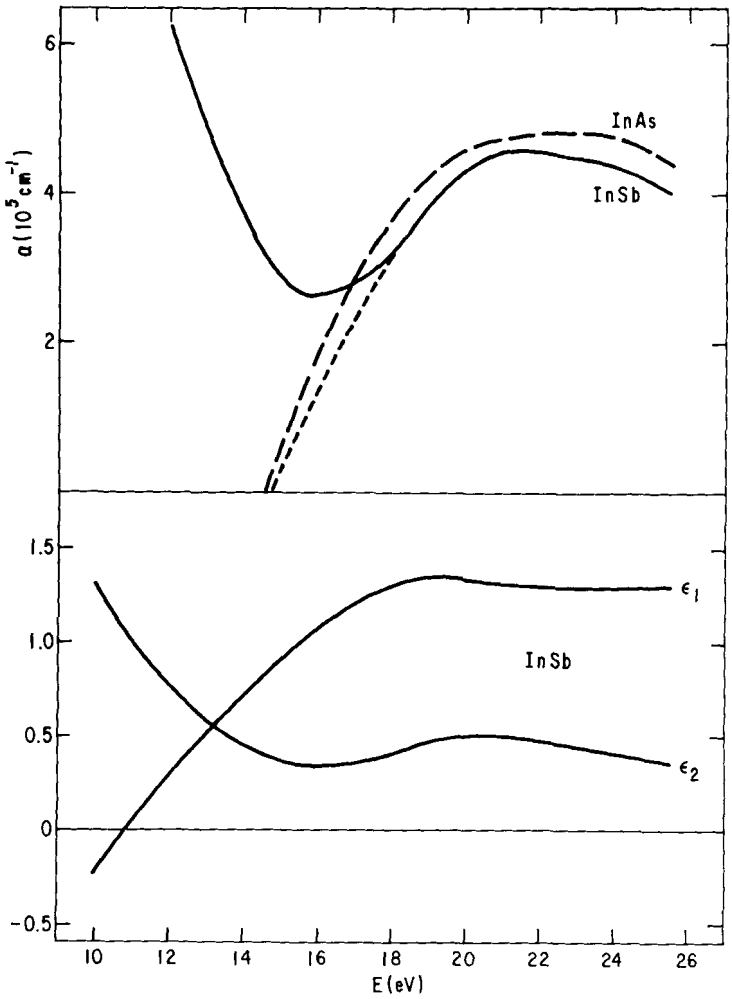


FIG. 8. Dielectric constants ε_1 and ε_2 and absorption coefficient $\alpha = 4\pi k/\lambda$ for InSb (and InAs) vs. E.

may be inaccurate in this energy range for each of these materials because of uncertainties in the extrapolation of the reflectance curve beyond the last experimental point, it is not possible to give these values more precisely.

More detailed structure, similar to that observed in region 1, might be expected in this high-energy region, since the transitions from the d bands terminate at different, energetically close conduction bands. The fact that such fine structure is not observed may be due to experimental difficulties

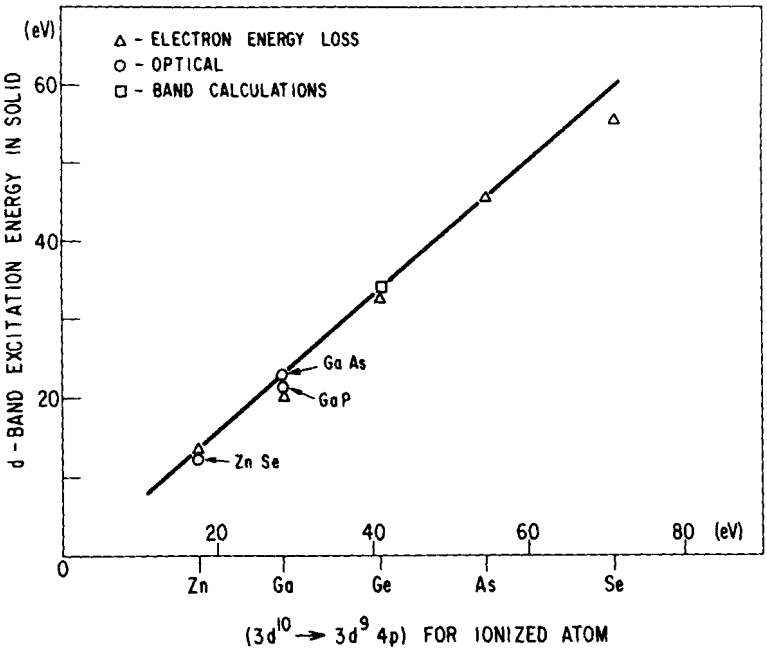


FIG. 9. Energies in various materials attributed to d-band excitations in optical and characteristic-energy-loss experiments and band calculations vs. atomic $3d^{10} \rightarrow 3d^9 4p$ excitation for atoms ionized to the d shell. Unless otherwise indicated, the points refer to the monatomic metals and semiconductors.

in measuring small values of reflectance in this energy range, and also to the broadening effects previously mentioned.

Energetically, the position of the additional optical structure appears to agree very well with the atomic excitations between the d and lowest unfilled p shells, with energy losses assigned to such excitations, and with band calculations where available. Figure 9 summarizes the available information concerning such excitations for a horizontal sequence in the periodic table, which also includes Ge. This figure shows a plot of the energy that has been either experimentally or theoretically attributed to d-band excitation in solids containing the atoms listed on the abscissa, as a function of the d-band excitation energy of the ionized atom stripped to the d shell. This means that we consider the $3d^{10} \rightarrow 3d^9 4p$ transitions in Zn^{III}, Ga^{IV}, Ge^{V}, etc.[60] The figure considers characteristic-energy-loss data for the monatomic metals,[65] optical data for the indicated compounds,

[65] J. L. Robins, *Proc. Phys. Soc. (London)* **79**, 119 (1962).

and the results of Herman's calculations for Ge.[54] The energy for this transition should not be affected seriously on the above energy scale when the ion is embedded in different solids. Thus, one would anticipate a reasonable correlation between the two quantities plotted here if the identification of the *d*-band excitations is correct. Figure 9, indeed, exhibits this correlation. Similar arguments can be made for the indium compounds.[66]

[66] *Footnote added in proof*: References given in this article extend only through early 1964, the date of its completion.

CHAPTER 5

Optical Absorption above the Fundamental Edge

Manuel Cardona

I. Introduction 125
II. Absorption Spectrum of Germanium 128
1. E_0 *Absorption Edge* 128
2. E_1 *Absorption Edge* 129
3. E_0' *Absorption Edge* 130
4. E_2 *Absorption Edge* 132
5. *Structure at Higher Energies* 133
III. Absorption Spectra of the III–V Compounds 134
6. *Experiments* 134
7. *Discussion* 142
IV. Systematics of the Energy Bands of Zinc-Blende Materials . . 146
V. Calculation of Band Parameters 148

I. Introduction

The measurement of the intrinsic absorption of semiconductors is a powerful tool for studying the energy-band structure of solids. The measurement of the fundamental absorption edge (lowest-energy absorption edge) yields the minimum energy separation between the valence and conduction bands and the nature (allowed, forbidden, direct, indirect) of the transitions involved.[1] In the III–V materials, the absorption coefficient rises very rapidly at the fundamental edge to values of the order of $10^4\,\mathrm{cm}^{-1}$ and keeps rising steadily from this value as the photon energy is increased. The absorption coefficient soon becomes too large for a measurement on conventional mechanically polished samples. In order to push the transmission measurements to higher photon energies, one must use extremely thin samples ($\sim 10^3$ Å) prepared by means of "unorthodox" techniques, such as vacuum deposition.[2] Germanium films thin and large enough for the observation of the absorption spectrum up to 5-eV photon energies have been prepared recently from bulk material[3] by grinding,

[1] T. S. Moss, "Optical Properties of Semiconductors." Butterworth, London and Washington, D.C., 1961.
[2] M. Cardona and G. Harbeke, *J. Appl. Phys.* **34**, 813 (1963).
[3] G. Harbeke, *Z. Naturforsch.* **19a**, 548 (1964).

polishing, and chemical etching techniques. The process requires extremely perfect single crystals as starting material and has not yet been successfully applied to the III–V compounds.

The absorption coefficient can be indirectly determined by ellipsometric measurements with polarized light[4] and also by normal-incidence reflection measurements with the help of the Kramers–Kronig dispersion relations.[5] These indirect measurements of reflected light are always subject to some degree of criticism, since their results depend strongly on the surface conditions. However, with the proper precautions, especially concerning the treatment of the surface on which the measurements are performed, they yield results in quantitative agreement with straight transmission measurements.

As one increases the photon energy from the fundamental edge, the first structure to be expected in the fundamental absorption spectrum of the III–V compounds corresponds to transitions from the Γ_7 valence band, split from the top valence bands (Γ_8 and Γ_7) by spin-orbit interaction (see Fig. 1), to the lowest conduction band at $\mathbf{k} = 0$. The observation of these transitions yields the spin-orbit splitting of the top valence band at $\mathbf{k} = 0$. These transitions are rather weak and have not been seen in any III–V compound except GaAs.[6,6a] They are apparently also too weak to be seen by reflection techniques and by transmission in rather imperfect evaporated films. They should be hard to see when the spin-orbit splitting is large (InSb, GaSb, AlSb), due to the large background absorption coefficient at the energy at which they should appear. They should, however, be observable by transmission in mechanically polished InP and InAs films. These transitions have been seen in other materials of the diamond and zinc-blende families such as germanium[7] (by transmission in polished single-crystal films); ZnSe (by transmission in evaporated films[2] and by reflection[8]); ZnTe and CdTe[9] (by reflection); CuI, CuBr, CuCl, and AgI[10] (by transmission in evaporated films).

[4] D. T. F. Marple and H. Ehrenreich, *Phys. Rev. Letters* **8**, 87 (1962).

[5] H. Ehrenreich and H. R. Philipp, Chapter 4 of this volume; F. C. Yahoda, *Phys. Rev.* **107**, 1761 (1957).

[6] M. Sturge, *Phys. Rev.* **127**, 768 (1962).

[6a] *Note added in proof*: Measurements of these transitions for GaP have been recently reported. See W. K. Subashiev and S. A. Abagyan, *in* "Physics of Semiconductors" (Proc. 7th Intern. Conf.), p. 225. Dunod, Paris and Academic Press, New York, 1964.

[7] M. V. Hobden, *J. Phys. Chem. Solids* **23**, 821 (1962).

[8] M. Cardona, *J. Appl. Phys.* **32**, 2151 (1961); M. Cardona, *Z. Physik* **161**, 99 (1961); M. Cardona, *J. Appl. Phys.* **32**, 958 (1961).

[9] M. Cardona and D. L. Greenaway, *Phys. Rev.* **131**, 98 (1963).

[10] M. Cardona, *Phys. Rev.* **129**, 69 (1963).

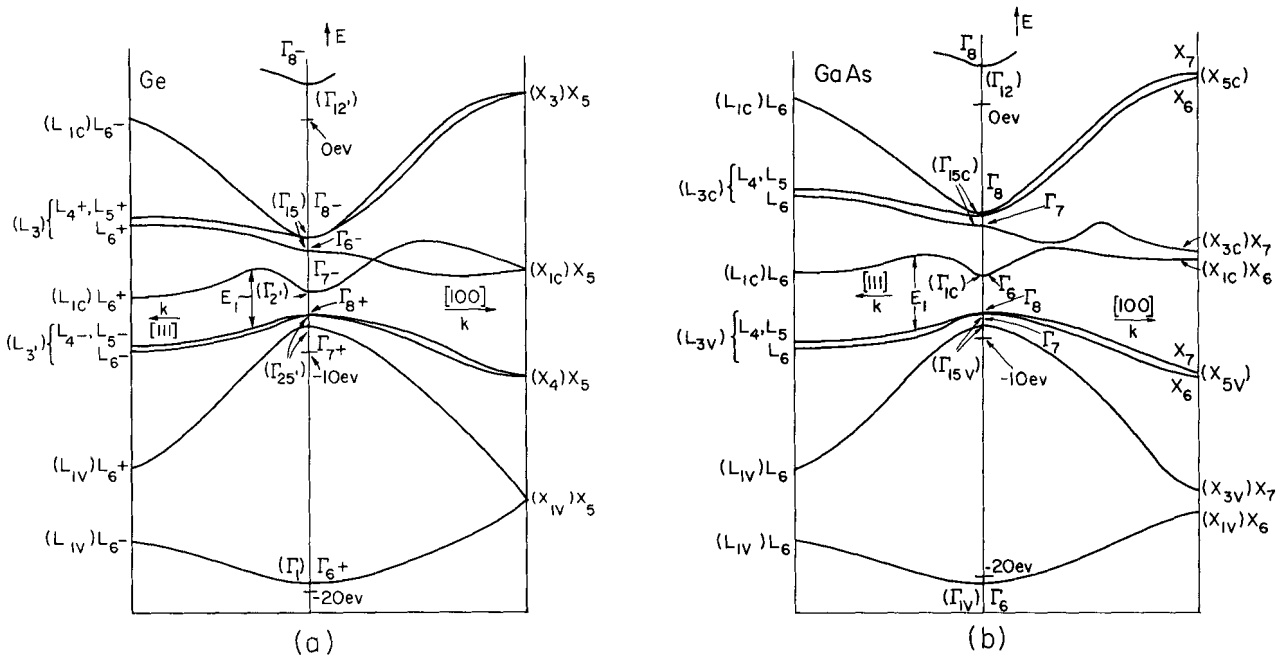


FIG. 1. Band structure of germanium (a) and GaAs (zinc-blende type) (b) with inclusion of the spin-orbit interaction. The irreducible representations corresponding to the various orbital states at Γ, L, and X are given in brackets. The double group representations are given without brackets. v and c have been used as subindices to differentiate between valence and conduction bands when there is more than one state of the same symmetry.

At even higher energies the absorption spectrum of the III–V compounds shows considerable structure. This structure is also very similar to the structure observed in the absorption spectrum of other materials of the diamond and zinc-blende families. We shall first, therefore, describe the absorption spectrum of very thin germanium films, identify the observed structure, and carry over this identification to the III–V compounds by means of several theoretical and semiempirical rules.

II. Absorption Spectrum of Germanium

1. E_0 Absorption Edge

Figure 2 shows the absorption spectra of three germanium thin films (I, II, III) epitaxially deposited[2] on cleaved CaF_2 at 870°K and a film (IV) prepared by Hobden from single-crystal material by mechanical polishing.[7] These films are too thin to exhibit the indirect absorption edge produced by phonon-aided transitions from Γ_{8^+} to L_{1c}. Film IV shows the direct absorption edge ($E_0 \approx 0.806$ eV) due to $\Gamma_{8^+}(\Gamma_{25'}) - \Gamma_{7^-}(\Gamma_{2'})$ transitions

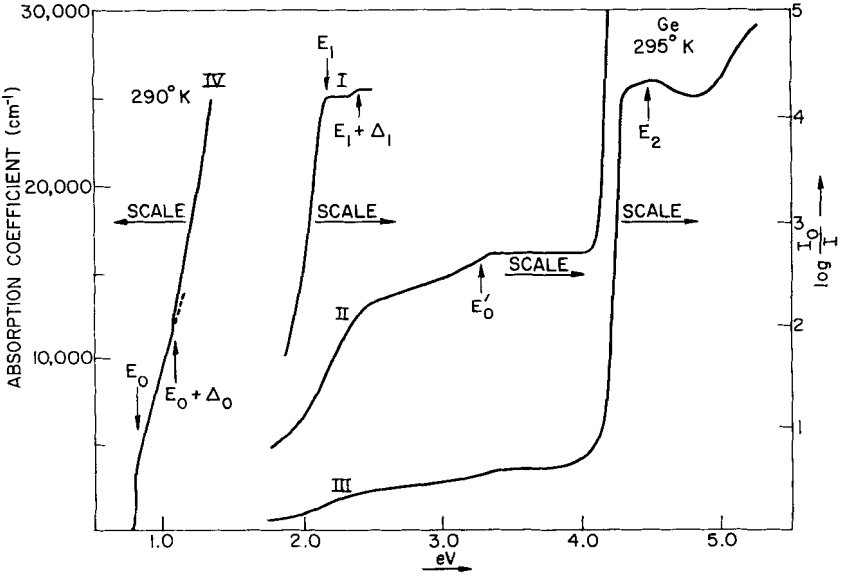


FIG. 2. Absorption of three germanium thin films epitaxially deposited on CaF_2 (film I is 0.3 microns thick; film II, 0.15 microns thick; film III, 0.05 microns thick) and a mechanically ground and polished film (IV, 2 microns thick) at room temperature. The absorption of film IV is given in terms of the absorption coefficient. For films I, II, and III the absorptivity $\log I_0/I$ is given. (After Refs. 2 and 7.)

with the edge split from it by spin-orbit coupling ($E_0 + \Delta_0 \approx 1.10$ eV) due to $\Gamma_{7^+}(\Gamma_{25'}) - \Gamma_{7^-}(\Gamma_{2'})$ transitions. These direct transitions take place at $\mathbf{k} = 0$. The measured value of the $\mathbf{k} = 0$ spin-orbit splitting is 0.29 eV.

2. E_1 Absorption Edge

Film I shows another absorption edge, which levels off at 2.15 eV. This edge has a splitting of 0.2 eV. This edge and its splitting were first observed by normal-incidence reflection techniques,[11,12] and it has also been studied by ellipsometric techniques.[4] This edge was first believed[13] to be due to direct allowed transitions at the L point of the Brillouin zone ([111] direction, edge of the zone) between the top valence band ($L_{3'}$) and the lowest conduction band (L_{1c}). The observations that favor this identification are the following:

(1) The edge had the approximate absorption coefficient that one would expect for such transitions. (The density of states for the $L_{3'}$ to L_{1c} transitions is about fifty times larger than for the $\Gamma_{25'} - \Gamma_{15}$ transitions, due to the fourfold degeneracy of the L state and also to the larger effective masses).

(2) They occur in germanium at about the energy calculated for the $L_{3'}$–L_{1c} gap ($\sim$2 eV). Also the effective mass[14] and the longitudinal g factor[15] at L_{1c} have values consistent with a 2-eV $L_{3'}$–L_{1c} gap.

(3) The spin-orbit splitting expected for the $L_{3'}$ state is about two-thirds of the valence-band splitting at $\mathbf{k} = 0$ ($\Gamma_{25'}$)[14]: the splitting seen for the E_1 edge in film I (0.2 eV) is two-thirds of the splitting shown in film IV (0.29 eV) for the fundamental edge.

Recent band calculations of the combined density of states for direct transitions[16] (approximately proportional to the absorption coefficient) suggest that the edge shown in Fig. 2 at 2.15 eV is due to transitions in the [111] direction but somewhere inside the Brillouin zone (Λ point). The $L_{3'}$–L_{1c} transitions should occur about 0.2 eV lower in energy. This is still consistent with some of the arguments given above for the $L_{3'}$–L_{1c} interpretation: the spin-orbit splitting expected at the L point is the same as at the Λ point, provided one does not get too close to $\mathbf{k} = 0$ and the

[11] J. Tauc and E. Antončík, *Phys. Rev. Letters* **5**, 253 (1960); J. Tauc and A. Abraham, *Proc. Intern. Conf. Semicond. Phys., Prague, 1960* p. 375. Czech. Acad. Sci., Prague, 1961; J. Tauc and A. Abraham, *J. Phys. Chem. Solids* **20**, 190 (1961).

[12] M. Cardona and H. S. Sommers, Jr., *Phys. Rev.* **122**, 1382 (1961).

[13] J. C. Phillips, *J. Phys. Chem. Solids* **12**, 208 (1960).

[14] M. Cardona and D. L. Greenaway, *Phys. Rev.* **125**, 1291 (1961).

[15] L. M. Roth and B. Lax, *Phys. Rev. Letters* **3**, 217 (1959).

[16] D. Brust, J. C. Phillips, and F. Bassani, *Phys. Rev. Letters* **9**, 94 (1962).

$\mathbf{k}\cdot\mathbf{p}$ perturbation of the $\mathbf{k} = 0$ orbital states is larger than the spin-orbit perturbation.[17]

Measurements of the reflection peaks under consideration as a function of doping yield in germanium a decrease in the energy of the peaks of 0.03 eV for the highest donor and acceptor dopings obtainable. The observed shift is the same for donors as for acceptors. If the peaks are due to transitions at L, an increase in the gap would be expected for donor impurities due to the shift in the Fermi level (Burstein shift). Under this assumption, it was concluded[12] that the perturbation of the L absorption edge by donor impurities is much larger than the perturbation produced by the same amount of acceptors. However, if the reflection peaks are due to transitions inside and not at the edge of the Brillouin zone, the Burstein shift for donors disappears, since the electrons occupy a portion of $\mathbf{k}$ space around the L point. The perturbation of the E_1 edge due to donors is the same as the perturbation produced by acceptors, in more reasonable agreement with theoretical considerations.[18]

The interpretation of spin-resonance data in germanium[15] requires an $L_{3'}$–L_{1c} gap smaller than 2 eV at liquid-helium temperature. Hence, our assignment of 2.15 eV (at room temperature) to Λ_1–Λ_3 transitions is in agreement with spin-resonance data: the $L_{3'}$–L_{1c} gap occurs at somewhat lower energy. These considerations have received recent confirmation in several materials with zinc-blende structure. The L_{3v}–L_{1c} gaps (e_1) have been seen below the Λ_3–Λ_1 gaps (E_1) as a small additional structure in ZnTe, CdTe, HgTe,[9] InAs, GaSb, and GaAs.[19] Figure 3 shows the reflection spectrum of ZnTe at 77°K with the e_1 and $e_1 + \Delta_1$ gaps clearly visible as additional structure below the E_1 and $E_1 + \Delta_1$ gaps.

3. E_0' Absorption Edge

Film II in Fig. 2 shows additional structure at 3.2 eV. Comparison with band-structure calculations and calculations of combined density of states as a function of energy suggest that this structure is due to transitions at $\mathbf{k} = 0$ between the top valence band ($\Gamma_{25'}$) and the second-lowest conduction band (Γ_{15}). Due to the spin-orbit splitting of $\Gamma_{25'}$ and Γ_{15}, this peak should show a quadruplet structure (reducing to a triplet if the splittings of $\Gamma_{25'}$ and Γ_{15} are approximately the same). It is obvious from Fig. 2 that the width of the $\Gamma_{25'}$–Γ_{15} peak (called E_0' in the literature) is too large to see structure associated with spin-orbit splitting. Structure

[17] E. O. Kane, *J. Phys. Chem. Solids* **1**, 82 (1956).

[18] E. M. Conwell and B. W. Levinger, *Proc. Intern. Conf. Phys. Semicond., Exeter, 1962* p. 227. Inst. of Phys. and Phys. Soc., London, 1962.

[19] D. L. Greenaway and M. Cardona, *Proc. Intern. Conf. Phys. Semicond., Exeter, 1962* p. 666. Inst. of Phys. and Phys. Soc., London, 1962.

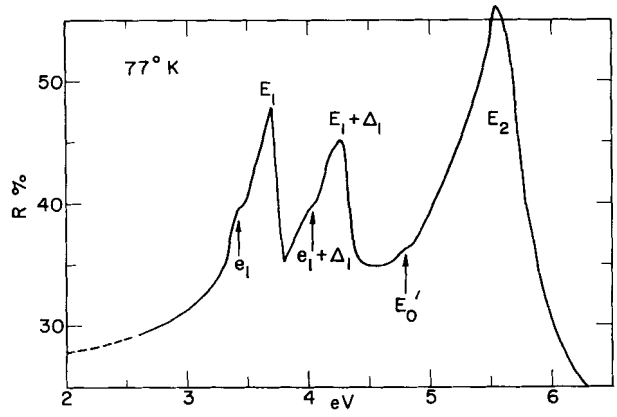


FIG. 3. Reflection spectrum of ZnTe at 77°K, showing the e_1 gap (L_3–L_1) below the E_1 gap (Λ_3–Λ_1). (After Ref. 9.)

observed by reflection, possibly associated with spin-orbit splitting of E_0', has been reported for InSb, GaAs,[19] CuI, and AgI.[10] The energy at which E_0' structure occurs is not very sensitive to the atomic number of the atoms that constitute the semiconductor, since the states involved in these transitions are p-like. The E_1 structure, produced by transitions to an s-like state, is much more sensitive to the atomic number of the constituents.[20] As a result, the E_0' and E_1 gaps occur, in semiconductors whose constituents have low atomic numbers, in reverse order to that described for germanium. E_0' has been seen to occur at about the same or lower energies than E_1 in silicon,[8,11] GaP,[8,21] ZnS,[22] and CuCl.[10]

Two methods have been used to differentiate between the E_0' and the E_1 edges and to determine their crossover. The most conclusive technique consists of the tracking of the energies of these peaks as a function of relative concentration of constituents in binary alloys[10,11]: a definite crossover has been observed for the Ge-Si system (see Fig. 4) and a superposition of the peaks for CuBr-CuCl. This technique has not yet been used for the promising system GaAs-GaP, which also should exhibit a crossover of the E_0' and E_1 peaks. The other technique often used to identify the E_0' and E_2 peaks consists of measuring their temperature dependence[8]: whereas E_1 shifts with temperature at a rate of -5×10^{-4} eV °C^{-1}, E_0' shifts only at about -2×10^{-4} eV °C^{-1}. Correspondingly, the pressure coefficient of E_1 (7.5×10^{-6} eV cm^2 kg^{-1}) is larger than that of E_0' (5.5×10^{-6} eV cm^2 kg^{-1}).[21]

[20] F. Herman and S. Skillman, *Proc. Intern. Conf. Semicond. Phys., Prague, 1960* p. 20. Czech. Acad. Sci., Prague, 1961.

[21] R. Zallen and W. Paul, *Phys. Rev.* **134**, A1628 (1964).

[22] M. Cardona, *Phys. Rev.* **129**, 1068 (1963).

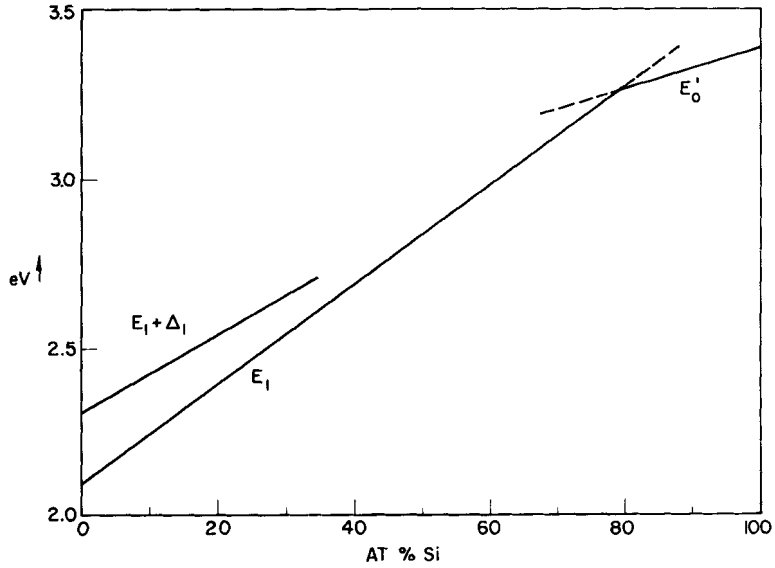


FIG. 4. E_0' and E_1 transmission peaks in germanium–silicon alloys at room temperature. (After Tauc and Abraham, Ref. 11.)

Note added in proof: Recent measurements for the GaAs–GaP alloys[22a–c] indicate that the E_0' peak of GaAs does not cross E_1 when increasing the GaP concentration. The E_0' peak of GaAs tends toward 4.75 eV in GaP. Hence the interpretation above is open to question, and further work is required to interpret the nature of the 3.7-eV peak of GaP.

4. E_2 Absorption Edge

Film III in Fig. 2 shows additional structure at 4.5 eV (E_2). This structure, also seen by reflection,[11,12] has been interpreted as due to transitions at the X point ([100] direction, edge of the Brillouin zone), between the X_4 valence band, the X_1 conduction band,[13,16] and at a Σ point ([110] direction) between the Σ_3 valence band and the Σ_2 conduction band. The X_1 orbital state [see Fig. 1(a)] is doubly degenerate in the germanium structure, but it splits into X_1 and X_3 in the lower-symmetry zinc-blende materials. The splitting of E_2 has been seen by reflection in many materials with zinc-blende structure[9,10,19] and by transmission in HgTe,[2] thus providing a striking confirmation of Phillip's interpretation of the nature of this peak. The splitting of E_2 is larger the larger the polarity of the material.

[22a] T. C. Woolley, A. G. Thompson, and M. Rubinstein, *Phys. Rev. Letters* **15**, 670 (1965).
[22b] T. K. Bergstresser, M. L. Cohen, and E. W. Williams, *Phys. Rev. Letters* **15**, 662 (1965).
[22c] A. G. Thompson, M. Cardona, K. L. Shaklee, and J. C. Woolley, *Phys. Rev.* **141**, 601 (1966).

The X_4 state of the germanium structure (labeled X_5 in zinc blende), splits because of spin-orbit interaction in zinc-blende-type materials. Splittings due to this cause, superimposed on the orbital splittings discussed above, have been observed by reflection for the E_2 peaks of CdTe and HgTe.[9,23]

5. Structure at Higher Energies

Film III in Fig. 2 shows that additional structure must exist in the absorption of germanium above 5.4 eV. This structure has been observed by reflection at 5.7 eV as a doublet with an 0.2-eV splitting.[24] This splitting, equal to the splitting of the E_1 peak, and a comparison with energy-band calculations, suggests the assignment of this doublet to transitions at the L point from the highest $L_{3'}$ valence band to the L_3 conduction band. One may expect that this peak should also show structure associated with the spin-orbit splitting of the L_3 conduction band, but it has been shown by Phillips and Liu[25] that the L_3 spin-orbit splitting is much smaller than the $L_{3'}$ splitting. We shall label the $L_{3'}$–L_3 structure in the optical spectrum E_1'. Neither E_1' nor any structure at shorter wavelengths has been observed by transmission in thin films in any materials of the family under consideration. In order to observe this structure, one must work in the vacuum ultraviolet region. The conventional vacuum ultraviolet spectrometers are single-pass instruments and yield a high amount of scattered light, which makes impossible measurements of high absorption levels. Also the substrates normally used for evaporating films are not transparent at these wavelengths. The use of LiF substrates extends the range of measurements to 1050 Å: transmission measurements have been performed on films of the cuprous halides evaporated on CaF_2 and LiF substrates.[10]

Additional structure in the optical spectra has been predicted for germanium at about 10 eV[26] due to $\Gamma_{25'}$–$\Gamma_{12'}$ transitions. This structure is not seen experimentally. The structure observed by reflection in III–V and II–VI compounds[9,24] around 10 eV has been interpreted as due to L_{3v}–L_{2c} transitions which are forbidden by parity in germanium but become allowed in zinc blende.

By reflection one has also observed transitions to conduction bands from the d core electrons nearest in energy to the valence electrons in the metallic atom of the III–V compounds (at about 21 eV[26]) and the II–VI

[23] W. J. Scouler and G. B. Wright, *Bull. Am. Phys. Soc.* **8**, 246 (1963); *Phys. Rev.* **133**, A736 (1964).

[24] H. Ehrenreich, H. R. Philipp, and J. C. Phillips, *Phys. Rev. Letters* **8**, 59 (1962).

[25] J. C. Phillips and L. Liu, *Phys. Rev. Letters* **8**, 94 (1962).

[26] H. Ehrenreich and H. R. Philipp, *Phys. Rev.* **129**, 1550 (1963).

compounds (at about 13 eV[9]). At even higher energies, transitions from the d levels of the anion to the conduction band should take place. These transitions have not been seen experimentally, since they occur at photon energies beyond the range of conventional vacuum ultraviolet equipment.

Plasma oscillations of the valence electrons, which should occur in these materials at about 15 eV, cannot be excited by transmission under normal incidence, since they are longitudinal oscillations and the electromagnetic field is a transverse disturbance. It should, however, be possible to excite them by transmission under oblique incidence, with the electric-field vector in the plane of incidence.[27] These oscillations are normally excited when one measures transmission of high-energy electron beams through thin films.[28] Information about plasma oscillations can also be obtained from the Kramers–Kronig analysis of the normal-incidence reflection data: at the plasma frequency the function $-\mathrm{Im}(1/\varepsilon)$, which one calculates from Kramers–Kronig analysis of the reflection data, has a strong maximum at the plasma frequency.[5,27]

III. Absorption Spectra of the III–V Compounds

6. Experiments

As mentioned earlier, the spin-orbit splitting of the fundamental absorption edge—$\Gamma_7(\Gamma_{15v}) - \Gamma_6(\Gamma_{1c})$ transitions—has been observed by transmission in GaAs. Figure 5 shows the absorption coefficient α of a

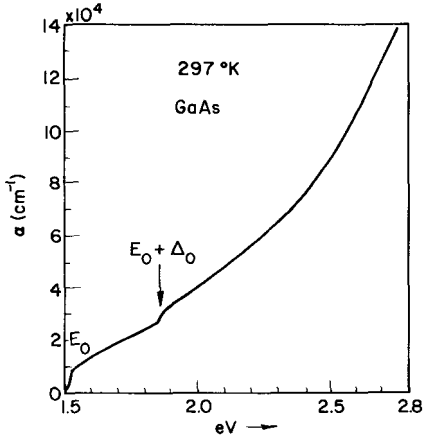


FIG. 5. Absorption of mechanically prepared films of GaAs showing the spin-orbit splitting ($E_0 + \Delta_0$) of the fundamental absorption edge E_0. (After Ref. 6.)

[27] D. W. Berreman, *Phys. Rev.* **130**, 2193 (1963).
[28] L. B. Leder, *Phys. Rev.* **103**, 1721 (1956).

GaAs film prepared by mechanical grinding and polishing techniques.[6] E_0 is the lowest direct absorption edge $[\Gamma_8(\Gamma_{15v})$–$\Gamma_6(\Gamma_{1c})]$ and $E_0 + \Delta_0$ the spin-orbit-split edge $[\Gamma_7(\Gamma_{15v})$–$\Gamma_6(\Gamma_{1c})]$.

Figures 6 and 7 show the absorption spectra of InSb, InAs, GaSb, and GaAs, the only III–V compounds studied by transmission at high energies, at 295° and at 80°K, respectively.[2] The thickness of the films, as measured by the Tolansky multiple-beam interference method, is given in the figure legends. No attempt at deriving exactly the absorption coefficient was made; however, because of the high absorption levels used, it is easy to show that reflection corrections are only significant in the relatively uninteresting low-absorption region, where the fundamental absorption edge occurs. Except in this region, $\log I_0/I$ is proportional to the absorption coefficient.

The samples of Figs. 6 and 7 were all evaporated on fused quartz substrates at temperatures close to 470°K. Some difficulty arises in the evaporation of these materials because of the different volatility of their two components: the vapor pressure of the anions (As, Sb) over the compounds is larger than that of the cations (Ga, In). Unless some precautions are taken, the film is grossly nonstoichiometric or, even worse, contains only one of the components. The evaporation of InSb and GaSb can be carried out from the bulk material by choosing the temperature of the substrate high enough so that only the compound condenses on it. This technique does not work for the evaporation of GaAs and InAs, and it is necessary to evaporate from two boats at different temperatures, one containing the cation (Ga, In) and the other the anion (As) of the semiconductor to be obtained.[2] The vapor pressure of As is kept higher than that of the cation, and its condensation on the substrate is prevented by keeping the temperature high enough. By increasing the temperature of the substrate, one increases the crystallite size, but, at the same time, films with large crystallites have a tendency to have pores and microfissures that make impossible the measurements at the high absorption levels required. Measurements by transmission have not been reported for GaP and InP nor for other less conventional III–V materials, but it is our belief that films of some of these materials could be prepared by the two-boat technique described above.

The measurements of Figs. 6 and 7 have been performed with double-pass spectrometers (Zeiss PMQ II, Cary 14). A double-pass instrument is needed in order to obtain a very low scattered-light level. Low levels of scattered light are required for the measurement of the low transmissivities (one part in 10^5) shown in Figs. 6 and 7. Measurements in the near infrared and visible can be performed with a strong tungsten lamp as source. In the ultraviolet, a conventional hydrogen arc can be used. However, when

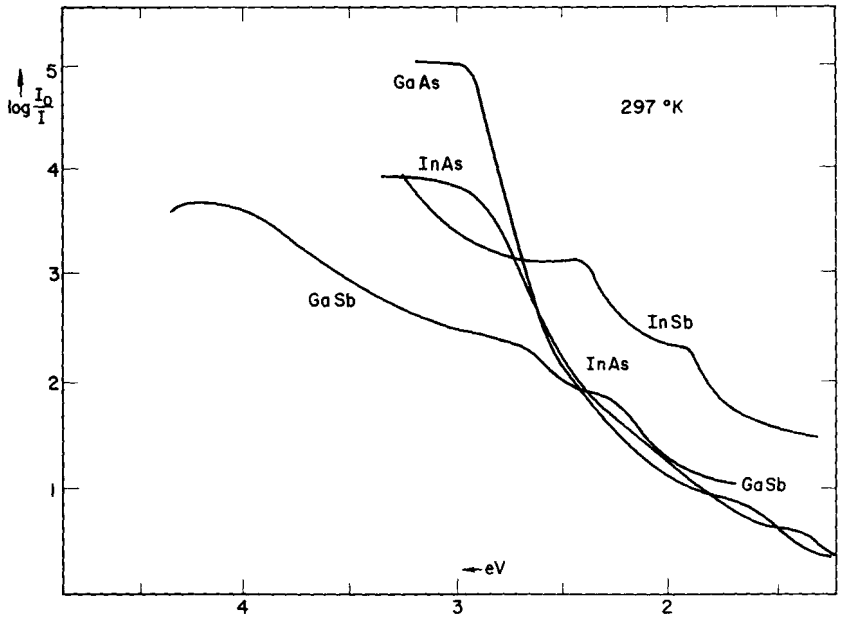


FIG. 6. Room-temperature absorption of evaporated films of some III–V compounds. Thicknesses are 0.25 microns (InSb), 0.08 microns (GaSb), 0.18 microns (InAs), and 0.21 microns (GaAs). (After Ref. 2.)

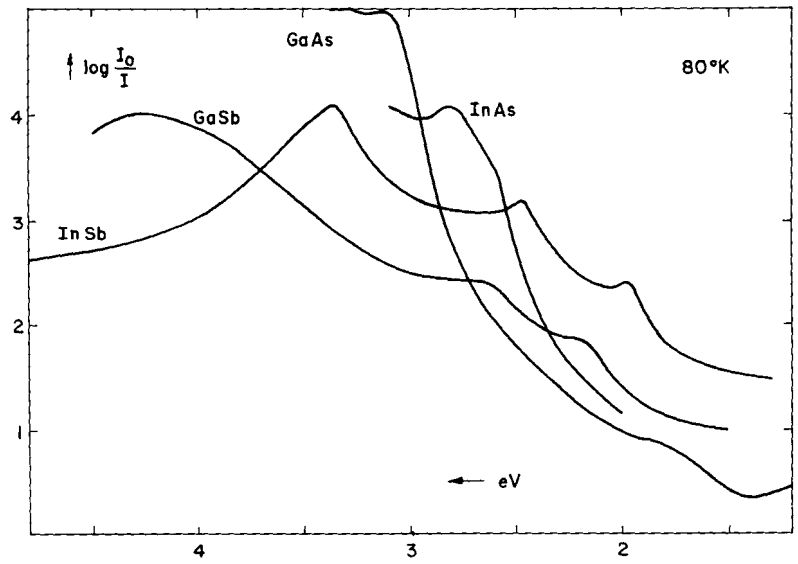


FIG. 7. Absorption of evaporated films of some III–V compounds at 80°K. Thicknesses are the same as in Fig. 6. (After Ref. 2.)

transmission levels of the order of one part in 10^5 around 5-eV photon energy are studied, it is convenient to use a stronger high-pressure xenon arc.

All spectra shown in Figs. 6 and 7 exhibit a strong absorption edge, which occurs at higher energies and is much stronger than the fundamental edge (the fundamental edge can be seen for the GaAs film at about 1.6 eV). That edge has a splitting and thus is similar to the E_1 (Λ_3–Λ_1) edge discussed for germanium. The splitting for GaAs (0.20 eV) and InAs (0.25 eV) is about two-thirds of the spin-orbit splitting at $\mathbf{k} = 0$ (0.35 eV for GaAs, 0.43 eV for InAs[29]). The $\mathbf{k} = 0$ spin-orbit splittings of GaSb and InSb have not been determined directly, but the E_1 splitting shown in Figs. 6 and 7 agrees well with two-thirds of the estimated $\mathbf{k} = 0$ splitting, as we shall show in the next section. We shall therefore assume that these absorption edges are due to Λ_3–Λ_1 transitions. We further assume, in order to tabulate the experimental results, that the E_1 and $E_1 + \Delta_1$ edges occur at the absorption peaks (InSb, GaAs) or at the point of maximum curvature (GaSb, InAs). The position of the E_1 and $E_1 + \Delta_1$ edges, as observed from transmission measurements, is listed in Table I for GaAs, GaSb, InAs,

TABLE I

ENERGIES AND TEMPERATURE COEFFICIENTS OF THE E_1, $E_1 + \Delta_1$, $e_1 + \Delta$ GAPS, AS FOUND BY TRANSMISSION AND REFLECTION

		InP	GaAs	InAs	AlSb	GaSb	InSb
TRANSMISSION (80°K)							
Energy (eV)	E_1	—	3.06[a]	2.60[a]	—	2.16[a]	1.98[a]
	$E_1 + \Delta_1$	—	3.25[a]	2.85[a]	—	2.63[a]	2.48[a]
Temperature coefficient (10^{-4} °C^{-1})	$-(dE_1/dT)$	—	4.2 ± 0.5[a]	—	—	4.0 ± 0.4[a]	4.0 ± 0.2[a]
	$-(d(E_1 + \Delta_1)/dT)$	—	—	—	—	3.6 ± 0.5[a]	3.6 ± 0.2[a]
REFLECTION (80°K)							
Energy (eV)	E_1	3.24[b]	2.99[b]	2.57[b]	2.88[b]	2.08[b]	1.87[b]
	$E_1 + \Delta_1$	3.40[b]	3.23[b]	2.85[b]	3.28[b]	2.55[b]	2.45[b]
Temperature coefficient (10^{-4} °C^{-1})	$-(dE_1/dT)$	4.2	4.6 ± 0.3[c]	5.4 ± 0.3[c]	5 ± 1[b]	4.6 ± 0.3[c]	5.3 ± 0.3[c]
	$-(d(E_1 + \Delta_1)/dT)$	—	6.2 ± 0.3[c]	5.5 ± 0.3[c]	—	5.4 ± 0.3[c]	4.9 ± 0.3[c]
Energy (eV)	e_1	—	1.4[b]	2.2[b]	—	1.4[b]	—
	$e_1 + \Delta_1$	—	1.75[b]	2.45[b]	—	1.9[b]	—

[a] See Ref. 2.
[b] See Refs. 8 and 19.
[c] See Ref. 31.

[29] R. Braunstein and E. O. Kane, *J. Phys. Chem. Solids* **23**, 1423 (1962).

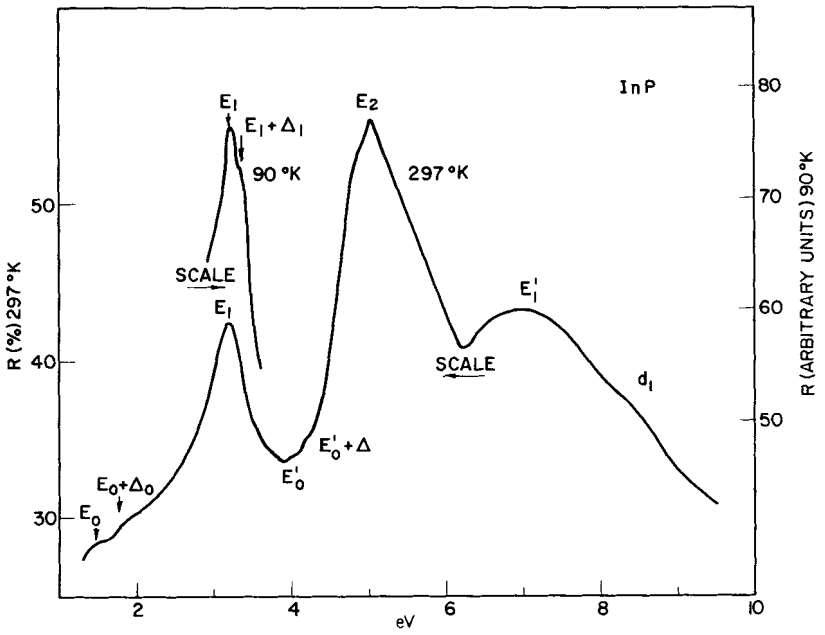


FIG. 8. Room-temperature reflectivity of InP. (After M. Cardona, Ref. 8 and unpublished data.)

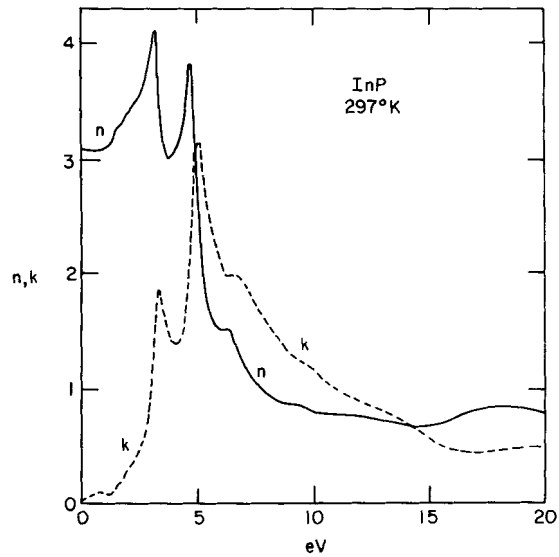


FIG. 9. Real (n) and imaginary (k) part of the refractive index of InP, obtained from the Kramers–Kronig analysis of the room-temperature data shown in Fig. 8.

and InSb. These edges have also been observed in the reflection spectrum of GaSb, GaAs, InSb, InAs, AlSb, and InP.

Figure 8 shows the reflection spectrum of InP at room temperature and a section of the spectrum at 90°K. The real and the imaginary parts of the refractive index, n and k, obtained from the Kramers–Kronig analysis of the room-temperature data of Fig. 8, are shown in Fig. 9. The E_1 peak is seen around 3 eV. Its spin-orbit splitting can be seen only at low temperature. Table I also lists the E_1 and $E_1 + \Delta_1$ reflection peaks observed in the III–V compounds. The absorption edges occur in general at higher energies ($\sim$0.04 eV average) than the corresponding reflection edges. This effect has also been observed in germanium and other zinc-blende-type materials and is believed to be real.[2,10]

The temperature coefficients of the E_1 and $E_1 + \Delta_1$ gaps, observed by transmission and by reflection, are also given in Table I. The agreement between the temperature coefficients of E_1, as measured by reflection and by transmission, is good. The temperature coefficients of $E_1 + \Delta_1$ in InSb and GaSb measured by reflection are larger than measured by transmission. This discrepancy seems due to the arbitrariness in the assignment of the gap energy. Since the reflection spectra change their shape less with temperature than the absorption spectra, the reflection data are believed to be more reliable. An attempt has been made to observe the shift with magnetic field of the E_1 absorption edge in InSb.[30] Up to fields of 200 kG, no shift is observed.

The L_{3v}–L_{1c} transitions discussed for germanium ($L_{3'}$–L_{1c}) have not been observed by transmission. They have been observed by reflection in InAs, GaAs, and GaSb.[19] Their energies are listed under e_1 and $e_1 + \Delta_1$ in Table I.

The absorption spectrum of InSb in Figs. 6 and 7 shows a peak at 3.3 eV. The position in energy of this peak is not very reproducible, and although it may be suggested that it corresponds to Γ_{15v}–Γ_{15c} transitions (the reflection spectrum shows these transitions at 2.8 and 3.4 eV[19]) its irreproducibility casts some doubts on this interpretation. Γ_{15v}–Γ_{15c} transitions have been observed by reflection in a number of III–V compounds. Their energies (E_0') are listed in Table II.

The GaSb transmission spectrum shows a peak at 4.18 eV at room temperature and 4.28 at 80°K. This peak corresponds to the reflection peak seen at room temperature at 4.3 eV[19] and assigned to $X_5 - (X_1, X_3)$ transitions. A broad line due to these transitions also appears in the InSb spectrum above 4 eV. We label this structure E_2. It has been observed in the reflection spectrum of BP, GaAs, GaSb, GaP, InAs, InSb, InP, and AlSb

[30] A. R. Moore, private communication.

TABLE II

EXPERIMENTAL VALUES[a] OF THE E_0', E_1', E_2, AND d_1 GAPS FOR SEVERAL III–V COMPOUNDS

	E_0' (80°K)	E_1' (297°K)	E_2 (297°K)	d_1 (297°K)
BP	5[b]	8[b]	6.9[b]	—
GaP	3.76[c]	7.0[d]	5.3[d]	10.1[d]
InP	4.1[e]	—	5.0[c]	8.4[e]
GaAs	4.2,[f] 4.52[f]	6.6,[d] 6.9[d]	5.1[c]	8.2[d]
InAs	3.9[g]	6.4,[d] 7.0[d]	4.72[f]	11.3[d]
AlSb	3.8[e]	4.85, 5.3[h]	4.22[h]	—
GaSb	3.74[f]	5.7[f]	4.3[c]	—
InSb	2.8,[f] 3.45[f]	5.3,[d] 6.0[d]	4.13[c]	10.8[f]

[a] In eV.
[b] See Ref. 43.
[c] See Ref. 8, see also last paragraph of Sec. 3.
[d] See Ref. 24.
[e] Unpublished.
[f] See Ref. 19.
[g] See Ref. 22.
[h] See Ref. 30a.

Note added in proof: Values of E_0' considerably more reliable than those in this table have been recently obtained by the electroreflectance method.[30b,c]

at room temperature (see Table II) and at 80°K in InAs, InSb, GaAs, and GaSb.[11,19,31] The low-temperature data show a splitting of about 0.5 eV in the E_2 reflection peak. This splitting corresponds to the splitting of the X_1 orbital state of the germanium structure into X_1 and X_3 when the inversion symmetry is lifted. The X_4 state of the germanium structure (X_5 in zinc blende) also splits for zinc-blende materials because of spin-orbit interaction.[32] This splitting is too small to be seen in the III–V compounds, but it can be easily seen by reflection in II–VI materials.[9]

The temperature coefficient of the E_2 peak in the III–V compounds (InSb and GaSb[31]) is -5×10^{-4} eV °C^{-1}, much larger than in Ge (-2×10^{-4} eV °C^{-1}) and Si ($+0.5 \times 10^{-4}$ eV °C^{-1}). This difference has been interpreted[8] as due to the removal of the degeneracy of the X_1 state in zinc-blende materials. The two bands coming to X_1 with equal and opposite slopes [see Fig. 1(a)] give an almost negligible explicit temperature effect (shift due to electron-phonon interaction). In the III–V compounds, since the X degeneracy is lifted, the electron–phonon interaction contributes significantly to the decrease in gap with increasing temperature.

[30a] T. E. Fischer, *Phys. Rev.* **139**, A1228 (1965).
[30b] K. L. Shaklee, M. Cardona, and F. H. Pollak, *Phys. Rev. Letters* **16**, 48 (1966).
[30c] M. Cardona, F. H. Pollak, and K. L. Shaklee, *Phys. Rev. Letters* **16**, 644 (1966).
[31] F. Lukeš and E. Schmidt, *Proc. Intern. Conf. Phys. Semicond., Exeter, 1962*, p. 389. Inst. of Phys. and Phys. Soc., London, 1962.
[32] B. Segall, *Bull. Am. Phys. Soc.* **8**, 51 (1963).

Figure 8 shows a peak in the reflection of InP at 7.2 eV. This peak corresponds to the E_1' structure discussed in Section 5 for germanium and hence seems due to transitions between the L_3 valence band and the L_3 conduction band. In other materials (GaAs, InSb) E_1' shows a splitting (Δ_1'; see Table III) roughly equal to Δ_1, as one would expect since the L_3

TABLE III

EXPERIMENTAL AND CALCULATED VALUES[a] OF THE SPIN-ORBIT SPLITTINGS Δ_0, Δ_1, AND Δ_1' FOR SEVERAL III–V COMPOUNDS[b]

Material	Δ_0 (exp)	Δ_0 (calc.) (*C*)	Δ_0 (calc.) ($B-K$)	Δ_1 (exp.)	Δ_1 (calc.) (*C*)	Δ_1 (calc.) ($B-K$)	Δ_1' (exp.)
InSb	—	0.78	0.89	0.58	0.52	0.59	0.7
InAs	0.43	0.43	0.41	0.28	0.29	0.27	0.6
InP	—	0.21	0.18	0.14	0.14	0.12	—
GaSb	—	0.68	0.81	0.47	0.46	0.54	—
GaAs	0.34	0.35	0.33	0.24	0.24	0.22	0.3
GaP	0.127[c]	0.11	0.10	—	0.08	0.07	—
AlSb	0.75	0.61	0.76	0.40	0.41	0.51	—

[a] In eV.

[b] See Refs. 8, 24, and 29.

[c] J. W. Hodby, *Proc. Phys. Soc.* (*London*) **82**, 324 (1963).

valence-band states are involved in the transition. In InAs one finds for Δ_1' a splitting of 0.6 eV, considerably larger than Δ_1. The splittings of E_1' have been measured only at room temperature. There is the possibility that the peaks will resolve further at low temperatures (as it happens for HgSe and HgTe[23]) because of the spin-orbit splitting of the L_3 conduction band. This could explain the anomalously large E_1' splitting found for InAs at room temperature (the splitting is also anomalously large in CdTe and HgTe[9]).

Additional structure has been seen, only by reflection, in GaP, InP, GaAs, InAs, and InSb.[24] This structure is probably due to transitions at *L* between the L_{3v} and the L_{2c} bands.[33] The position of this structure has been listed in Table II under the label d_1. The reflection spectrum of the III–V compound also shows structure due to transitions from core *d* electrons of the metal to conduction bands. These transitions are discussed by Philipp and Ehrenreich in the previous chapter.[5]

[33] J. C. Phillips, *Phys. Rev.* **133**, A452 (1964).

7. Discussion

We shall first discuss the experimental spin-orbit splittings Δ_0 of the E_0 and Δ_1 of the E_1 edges listed in Table III. The Δ_0 splittings have been obtained from the fundamental absorption edge (GaAs)[6] and from the infrared absorption of p-type material (GaAs, InAs, AlSb).[29] For Δ_1 we have listed what we believe are the most accurate values, obtained from reflection measurements at 80°K. The spin-orbit splitting Δ_0 of the valence band at Γ_{15} is given by[17]

$$\Delta_0 = \left(\frac{3\hbar i}{4mc^2}\right) \left\langle \Gamma_{15}^{(x)} \left| \frac{\partial V}{\partial x} \mathbf{p}_y - \frac{\partial V}{\partial y} \mathbf{p}_x \right| \Gamma_{15}^{(y)} \right\rangle . \tag{1}$$

$\Gamma_{15}^{(x)}$, $\Gamma_{15}^{(y)}$, and $\Gamma_{15}^{(z)}$ are the wave functions, without spin-orbit coupling, which define the Γ_{15} representation; V is the self-consistent crystal potential; and $\mathbf{p}$ the linear momentum operator.

Since V and $\mathbf{p}$ are largest near the atomic cores, it is to be expected that most of the contribution to the matrix element in Eq. (1) is given by the wave functions near the cores; hence we can split Δ_0 into a contribution from the group-III atom and another one from the group-V atom. The crystal wave functions near the cores are very much like atomic (or ionic) wave functions, and hence it is expected that the contribution to Δ_0 from the group-III and -V atoms will be similar to the free-ion (with the proper ionic charge) splittings. It remains to take into account the fact that the square of the wave function of the electrons at Γ_{15} is concentrated a fraction α around the group-III atom and $(1 - \alpha)$ around the group-V atom. Thus we write

$$\Delta_0 = C[\alpha\Delta_{\text{III}} + (1 - \alpha)\Delta_{\text{V}}], \tag{2}$$

where Δ_{III} and Δ_{V} are the one-electron spin-orbit splittings of the corresponding ions. C is a renormalization constant to take into account differences between the matrix element in Eq. (1) for solids and for free ions. Since C is not very different from unity, we assume it is the same for all zinc-blende- and diamond-type materials. The parameter α is related to the ionicity of the compounds in a somewhat obscure way. It should be larger the larger the atomic volume of the components, because of the decrease in ionicity. We find, however, that the agreement between experimental and calculated splittings is not improved by using a different and rather uncertain value of α for each compound,[34] and hence we shall use the same value of α for all III–V compounds under discussion. A certain degree of arbitrariness is also involved in the choice of the values of Δ_{III} and Δ_{V}: the fact that we are dealing with ions and not neutral atoms is difficult to take into account.

[34] H. Ehrenreich, *J. Appl. Phys.* **32**, 2155 (1961).

Braunstein and Kane[29] used for Δ_{III} and Δ_V the one-electron spin-orbit splittings for the neutral atoms, extracted from spectroscopic data under the assumption of $L \cdot S$ coupling. The constant C is then larger than unity, because of the fact that crystal wave functions are normalized over the unit cell whereas atomic wave functions are normalized over all space. From a comparison of the atomic splitting in germanium (0.20 eV) and the crystal splitting Δ_0 (0.29 eV) one derives $C = 29/20$. A good fit to the existing experimental values of Δ_0 in InAs, GaAs, and AlSb is obtained for $\alpha = 0.35$ and listed in Table III as Δ_0 (calc.) $(B - K)$. We used for Δ_{III} and Δ_V the splitting in ions with only one valence electron (doubly ionized group-III, quadruply ionized group-V).[8] The screening of the ionic potential by the discarded valence electrons decreases V in the solid and hence the constant C becomes somewhat smaller than one, approximately 29/40. The values of Δ_0 calculated by this method are given in Table III under Δ_0 (calc.) (C); they agree substantially with the $(B - K)$ estimates.

The spin-orbit splitting Δ_1 at Λ_3 is given by[14]

$$\Delta_1 = \frac{2}{3}\left(\frac{3\hbar i}{4mc^2}\right)\left\langle \Lambda_3^{(x)}\left|\frac{\partial V}{\partial x}\mathbf{p}_y - \frac{\partial V}{\partial y}\mathbf{p}_x\right|\Lambda_3^{(y)}\right\rangle \tag{3}$$

where $|\Lambda_3^{(x)}\rangle$ and $|\Lambda_3^{(y)}\rangle$ are the wave functions that define the Λ_3 representation. Equation (3) assumes that we are far enough from $\mathbf{k} = 0$ along the [111] direction so that the splitting of the orbital degeneracy due to the $\mathbf{k} \cdot \mathbf{p}$ perturbation is larger than the spin-orbit splitting. The factor 2/3 that appears in Eq. (3) but not in Eq. (1) is due to the fact that the spin-orbit perturbation at Γ acts on a triply degenerate orbital state, whereas at Λ the orbital state is only doubly degenerate. For the reasons discussed above, the matrix element in Eq. (3) is roughly the same as in Eq. (1) and also independent of the position of Λ along the [111] direction.

In Table III, we have also listed the values of Δ_1 calculated by the two methods discussed above[35] and also the experimental values of Δ_1 and Δ_1'. The agreement between the C values of Δ_1 and the experiment is somewhat better than for the $B - K$ values (except for InSb); this is probably fortuitous.

We have interpreted the E_1 edge as due to transitions at a Λ point. We have, however, mentioned that transitions at L also should give structure in the absorption, with a splitting equal to Δ_1.[17] The L structure, seen by reflection in InAs, GaAs, and GaSb, does not appear in the transmission

[35] The Δ_1 (C) values in Table III are about 10% higher than in Ref. 8, since we used the somewhat more accurate value of 0.195 eV instead of 0.18 eV for Δ_1 of germanium in the determination of Δ_1 (C) (see Ref. 31).

curves of Figs. 6 and 7, probably because of the broadening produced by the imperfect structure of evaporated films. The reasons for preferring the Λ to the L assignment for E_1 have been discussed in Part III for germanium, and it seems reasonable to assume that they also apply to the III–V compounds. We believe, however, that in order to confirm this assignment combined density-of-states calculations as a function of energy[16] for some III–V compounds are required.

The absence of a shift of the E_1 edge with magnetic field[30] (a Landau shift corresponding to parabolic bands and reduced effective masses of the order of the free-electron mass would have been seen) is easily understood if the transitions occur at points where the individual bands do not have an extremum: Landau levels may not exist at all. The lack of a magnetic-field shift can also be explained for the L assignment if one assumes that the edge is strongly affected by the Coulomb interaction between the excited electron and the hole left behind after an optical transition (exciton effect), since the ground state of the exciton shows only a very small diamagnetic ($\sim H^2$) shift in a magnetic field. Transitions to this state should be dominant in the absorption edge.

Under the assumption of L transitions, one has to invoke either the formation of excitons[36] or strongly nonparabolic bands[4] in order to explain the sharpness of the E_1 peaks shown in Figs. 6 and 7. We have mentioned in Part II that at the Λ point, where the E_1 transitions presumably occur, the energy difference between valence and conduction bands has a saddle point. At this point, the density of states η has a Van Hove singularity.[37] We have plotted in Fig. 10 the density of states η, approximately proportional to the absorption coefficient, in arbitrary units. The absorption above the edge is flat, and hence it becomes difficult to explain the peaks seen in Fig. 7 for InSb, and to a lesser extent, for GaAs and InAs. We have some indication that these peaks would be much sharper in more perfect, single-crystal films.[38] This sharpness is probably due to the Coulomb interaction between electron and hole (exciton). No calculations of exciton effects around a saddle point are available, since it is rather difficult to treat the effective-mass equation with a kinetic energy that is not positive definite. Intuitively it seems reasonable to say that there are no bound exciton states, but that the continuum band-to-band absorption is strongly perturbed. By comparison with the case of a minimum in the

[36] M. Cardona and G. Harbeke, *Phys. Rev. Letters* **8**, 90 (1962).

[37] L. Van Hove, *Phys. Rev.* **89**, 1189 (1953).

[38] Very sharp E_1 and $E_1 + \Delta_1$ peaks have been seen by transmission in single-crystal germanium films produced by grinding, polishing, and etching (G. Harbeke, private communication, also Ref. 3).

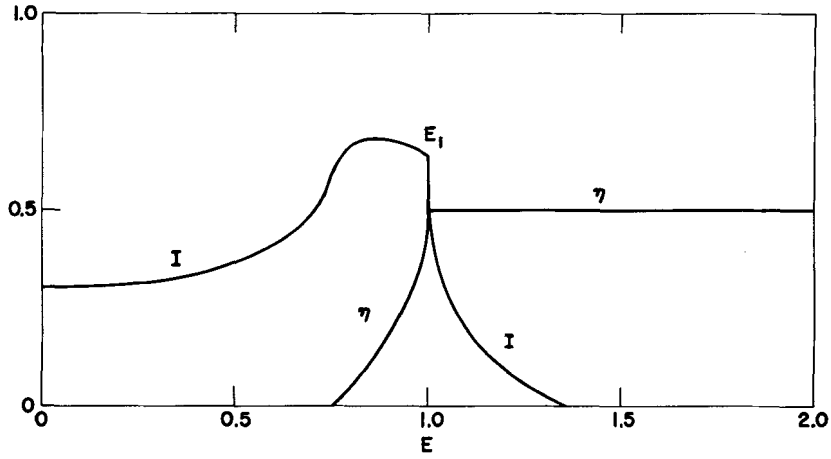


FIG. 10. Density of states η (in arbitrary units) and refractive index I (also in arbitrary units) around an S_1 Van Hove singularity. (After Ref. 10.)

energy separation,[39] it seems reasonable to expect a sharpening of the absorption shown in Fig. 10 around the saddle point.

Figure 10 also shows the refractive index I (in arbitrary units) obtained from η by means of the Kramers–Kronig dispersion relations.[10] The refractive index has its maximum at lower energies than the absorption singularity, and hence the fact mentioned in Section 6, that the absorption singularities occur at slightly higher energies than the reflection peaks, can be easily explained. This can also be explained in terms of a minimum in the band separation: whereas the peak in reflection occurs at the band edge, the peak in absorption occurs at higher energies.

It has been suggested by Phillips[40] that the only transitions that are observed in zinc-blende-type materials are transitions between states that are degenerate for the empty lattice (except for the d-electron bands). In the weak binding limit, only transitions between split degenerate empty lattice states have a large matrix element of **p**. This argument, of course, does not apply to transitions from the d electrons, since they cannot be treated at all by the weak-binding approximation. The matrix elements for these transitions will be close to the corresponding value for atomic transitions.

All the transitions we have discussed occur always either at high-symmetry point (X, L, Γ) or at high-symmetry lines (Σ, Λ). The transitions from d electrons have not been located in **k** space, but their main contribution

[39] R. J. Elliot, *Phys. Rev.* **108**, 1384 (1957).
[40] J. C. Phillips, private communication.

is most likely to take place also at high-symmetry points or lines. At the high-symmetry points, each one of the energy bands involved in the transition has zero gradient with respect to **k**. At the symmetry lines, singularities in the absorption can occur when the difference between the energies in the two bands involved in the transitions has zero gradient.

IV. Systematics of the Energy Bands of Zinc-Blende Materials

A simple method, based on a perturbation approach suggested by Herman,[41] has been devised[9,14] for relating the various gaps of the III–V compounds to the corresponding gaps of other materials with zinc-blende and diamond structure (the method can be extended to wurtzite-type materials[22]). The crystal potential of any group-IV, III–V, II–VI or I–VII semiconductor with diamond or zinc-blende structure is written as

$$V = V^{\mathrm{IV}}_{\mathrm{sym}} + V^{\mathrm{IV}}_{\mathrm{antisym}} + \lambda(V^{\mathrm{polar}}_{\mathrm{sym}} + V^{\mathrm{polar}}_{\mathrm{antisym}}) \tag{4}$$

where $V^{\mathrm{IV}}_{\mathrm{sym}}$ and $V^{\mathrm{IV}}_{\mathrm{antisym}}$ are the symmetrical and antisymmetrical part (with respect to the permutation of the two atoms in the unit cell) of the crystal potential of the corresponding group-IV material, which is obtained by moving the two component atoms horizontally in the periodic table. $V^{\mathrm{polar}}_{\mathrm{sym}}$ and $V^{\mathrm{polar}}_{\mathrm{antisym}}$ are the perturbing terms for obtaining the potential of the polar compound from the unperturbed group-IV potential. $V^{\mathrm{IV}}_{\mathrm{antisym}}$ is zero for horizontal sequences (Sn, InSb, CdTe, AgI; Ge, GaAs, ZnSe, CuBr). We shall assume $V^{\mathrm{IV}}_{\mathrm{antisym}} = 0$ even for skew (nonhorizontal) sequences, since the experimental results do not show any effect due to this term. The coefficient λ represents the strength of the perturbation and, for the sake of simplicity, is taken equal to 1, 2, and 3 for the III–V, II–VI, and I–VII compounds, respectively. The effect of $V^{\mathrm{polar}}_{\mathrm{sym}}$ on the band structure has been shown to be very small for GaAs.[42] We shall assume $V^{\mathrm{polar}}_{\mathrm{sym}} = 0$ in general. The expectation value of $V^{\mathrm{polar}}_{\mathrm{antisym}}$ is zero for all states that give optical structure, except for the X_1 state. At this state $V^{\mathrm{polar}}_{\mathrm{antisym}}$ has a finite expectation value that produces the splitting X_1 in zinc-blende materials into X_1 and X_3. This splitting should be proportional to λ, and a rough indication of this proportionality has been obtained experimentally.[9,10]

When considering spin instead of pure orbital states, and the spin-orbit interaction Hamiltonian, the X_4 (X_5 of zinc blende) states should also have a finite expectation value of the perturbation Hamiltonian, corresponding to the spin-orbit splitting of X_5 in zinc-blende materials. For all other high-symmetry points of interest, the first-order perturbation vanishes and

[41] F. Herman, *J. Electron.* **1**, 103 (1955).
[42] J. Callaway, *J. Electron.* **2**, 230 (1957).

hence the various energy gaps are obtained by second-order perturbation theory:

$$E_p = E + A\lambda^2 \tag{5}$$

with E_p and E the energy gaps of the polar and nonpolar materials, respectively.

We want to apply this analysis to the I–VII compounds whose $A\lambda^2 \approx E$. If the two states forming the gap interact via $V^{\text{polar}}_{\text{antisym}}$, the use of perturbation theory is not justified. If one assumes, however, that the only perturbation produced by $V^{\text{polar}}_{\text{antisym}}$ on the states forming the gap is their mutual repulsion, one obtains by solving the corresponding 2×2 secular equation[10]

$$E_{\text{polar}} = E(1 + 2A\lambda^2/E)^{1/2}. \tag{6}$$

We shall, in accordance with the discussion above, use Eq. (6) for the E_0' and E_1' gaps. For the E_1 and E_2 gaps we shall use Eq. (5) and hope that the intermediate states responsible for the second-order perturbation are far away from the states forming the gap.

Figure 11 shows the various experimental energy gaps of the horizontal sequence α-Sn, InSb, CdTe, and AgI, corrected for the spin-orbit perturbation (unperturbed values), as a function of λ^2. The Λ_3–Λ_1 and X_5–X_1 full curves have been drawn according to Eq. (5). The Γ_{15}–Γ_{15} and L_3–L_3 curves are according to Eq. (6). The discrepancies between the measured

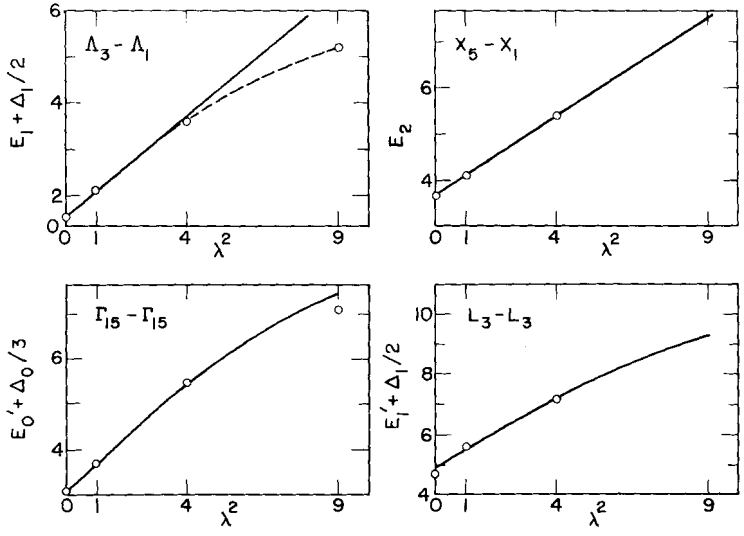


FIG. 11. Energy gaps of the horizontal sequence α-Sn, InSb, CdTe, AgI. (After Ref. 9.)

Λ_3–Λ_1 for AgI and the straight line is to be attributed to some contribution of the d electrons of silver to the valence-band wave function of this material.[10]

Figure 12 shows the same gaps for a skew sequence (Sn–Ge, GaSb, ZnTe, CuI). The gaps of the hypothetical compound Sn–Ge have been assumed to be the average of the gaps of α-Sn and Ge. The good agreement between the experimental points and the curves drawn after Eqs. (5) and (6) justifies our having neglected $V^{IV}_{antisym}$ in Eq. (4).[14] This procedure cannot be generalized to skew sequences having carbon as one of the group-IV constituents,[43] because of the absence of p electrons in the carbon core. For instance, $V^{IV}_{antisym}$ is very large in SiC,[43] and the various gaps of BP can be about the same as, or even smaller than, the corresponding gaps of SiC.

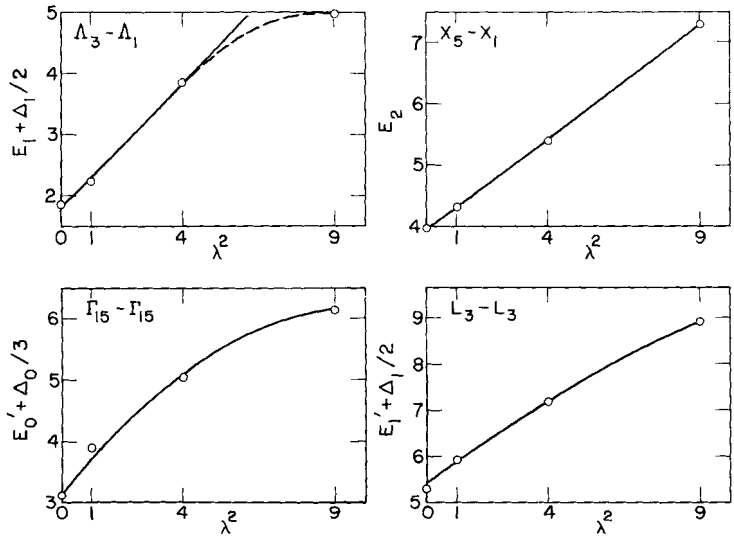


FIG. 12. Energy gaps of the skew sequence α-Sn–Ge, GaSb, ZnTe, CuI. (After Ref. 9.)

V. Calculation of Band Parameters[44]

By applying the method used in deriving Eq. (6) to the interacting states Γ_{15} and $\Gamma_{25'}$ we get the perturbed wave functions of the polar material:

$$\begin{aligned}\psi_p(\Gamma_{15c}) &= a\psi(\Gamma_{15}) - b\psi(\Gamma_{25'})\\ \psi_p(\Gamma_{15v}) &= b\psi(\Gamma_{15}) + a\psi(\Gamma_{25'})\end{aligned} \tag{7}$$

[43] C. C. Wang, M. Cardona, and A. G. Fischer, *RCA Rev.* **25**, 159 (1964).
[44] M. Cardona, *J. Phys. Chem. Solids* **24**, 1543 (1963); **26**, 1351 (1965).

with

$$a = \frac{1}{\sqrt{2}}\left[\frac{E'_{po} + E_0'}{E'_{po}}\right]^{1/2}$$
$$b = \frac{1}{\sqrt{2}}\left[\frac{E'_{po} - E_0'}{E'_{po}}\right]^{1/2} \tag{8}$$

E'_{po} and E_0' are the E_0' gaps of the polar material and its isoelectronic group-IV material, respectively. The effective mass at the Γ_{1c} conduction-band point is given by the $\mathbf{k}\cdot\mathbf{p}$ method[17]:

$$\frac{m}{m^*(\Gamma_{1c})} = 1 + \sum_l \frac{|\langle\Gamma_{1c}|\mathbf{p}|l\rangle|^2}{E(\Gamma_{1c}) - E(\Gamma_l)}\frac{2}{3m}. \tag{9}$$

The only significant terms in the sum of Eq. (9) are for $l = \Gamma_{15c}$ and $l = \Gamma_{15v}$. Substituting the wave functions of Eqs. (7) into Eq. (9) and taking into account the spin-orbit splitting of the Γ_{15v}, which can be of the order of the energy denominator $E_{op} = E(\Gamma_{1c}) - E(\Gamma_{15v})$, we obtain

$$\frac{m}{m^*(\Gamma_{1c})} = 1 + \frac{P^2}{2E'_{op}}\left[\frac{E'_{op} + E_0'}{3}\left(\frac{2}{E_{op}} + \frac{1}{E_{op} + \Delta_0}\right) - \frac{E'_{op} - E_0'}{E'_{op} - E_{op}}\right], \tag{10}$$

where P^2 is a constant proportional to $|\langle\Gamma_{2'}|\mathbf{p}|\Gamma_{25'}\rangle|^2$. In Eq. (10) we have neglected the spin-orbit splitting of the Γ_{15c} state, since it is much smaller than the energy denominator $E'_{op} - E_{op}$.

By a similar method, we obtain the effective g factor at Γ_{1c}:

$$g^*(\Gamma_{1c}) = 2\left\{1 - \frac{P^2\Delta_0}{6E'_{op}}\left[\frac{E'_{op} + E_0'}{E_0(E_0 + \Delta_0)} + \frac{E'_{op} - E_0'}{(E'_{op} - E_{op})^2}\right]\right\} \tag{11}$$

Equation (11) has been derived with the reasonable assumption that the spin-orbit splitting of the Γ_{15c} is approximately equal to Δ_0, the splitting of Γ_{15v}. The quantity P^2 (= 23 eV) can be calculated from the known value of the effective mass at Γ_2' in germanium and Eq. (10) with $E'_{op} = E_0'$. In agreement with considerable experimental and theoretical results we assume that $P^2 = 23$ eV for all group-IV semiconductors.[44]

The same method can be used for estimating the valence-band parameters in the III–V compounds. The shape of the valence band is determined, if linear terms in $\mathbf{k}$ are neglected, by the parameters A, B, and C of Dresselhaus *et al.*[45]:

$$A = \tfrac{1}{3}(F + 2G + 2M) + 1$$
$$B = \tfrac{1}{3}(F + 2G - M) \tag{12}$$
$$C^2 = \tfrac{1}{3}[(F - G + M)^2 - (F + 2G - M)^2].$$

[45] G. Dresselhaus, A. F. Kip, and C. Kittel, *Phys. Rev.* **98**, 368 (1955).

In a group-IV material, F represents the interaction of $\Gamma_{2'}$ with $\Gamma_{25'}$, M that of Γ_{15} with $\Gamma_{25'}$, and G is a small correction term due to the $\Gamma_{12'}$ interaction with $\Gamma_{25'}$, equal to 1.6 eV in germanium. In a III–V compound we must take into account the admixture of $\Gamma_{25'}$ and Γ_{15} into Γ_{15v} and Γ_{15c}. From Eqs. (7) we obtain[44]

$$F = -\frac{P^2[E'_{op} + E_0']}{2E_{op}E'_{op}}, \qquad M = -\frac{Q^2}{E'_{op}}, \qquad G \approx -\frac{1.6(E'_{op} + E_0')}{2E_0'}. \tag{13}$$

Q^2, obtained from the $\Gamma_{25'}$ valence-band parameters of germanium and silicon, is equal to 15.5 eV. The average light and heavy hole masses at $\Gamma_{25'}$, m^*_{lh} and m^*_{hh} and the split-off band mass m^*_{sh} are given by[46]

$$\frac{1}{m^*_{lh}} = -A - B\left(1 + \frac{C^2}{10B^2}\right) \qquad \frac{1}{m^*_{hh}} = -A + B\left(1 + \frac{C^2}{10B^2}\right)$$
$$\frac{1}{m^*_{sh}} = 1 + \frac{1}{3}\left[\frac{E_{op}F}{E_{op} + \Delta_0} + 2G + 2M\right]. \tag{14}$$

We have listed in Table IV the values of $m^*(\Gamma_{1c})$, m^*_{lh}, m^*_{hh}, m^*_{sh}, and $g^*(\Gamma_{1c})$ obtained by the method just discussed from the known values of E_{op} and the values of E'_{op} listed in Table II. The agreement between the calculated and the experimental results, also listed in Table IV, is quite good. The largest discrepancies occur for m^*_{hh}; however, with the exception of InSb, for which cyclotron resonance data are available,[47] the m^*_{hh} masses have all been determined from transport measurements and are subject to large uncertainties. The heavy-hole mass determined by cyclotron resonances for InSb agrees well with the calculated value.

The same method can be used for estimating the transverse effective masses at L_{1c} and L_{3v}. In group-IV materials these masses are determined mainly by the interaction between those two states. The square matrix element for this interaction is approximately 23 eV. In the III–V compounds the L_{3c} gap also interacts with L_{1c}, because of the L_{3c}–L_{3v} mixing, and contributes to the transverse effective mass at L_{1c}. The mass $m_\perp^*(L_{1c})$ can be obtained from Eq. (10) if one replaces E_0' by E_1' and E_0 by the L_{1c}–L_{3v} gap. This gap is known for InAs, GaAs, and GaSb (see Table I).

[46] E. O. Kane, *J. Phys. Chem. Solids* **1**, 249 (1957).
[47] D. M. S. Bagguley, M. L. A. Robinson, and R. A. Stradling, *Phys. Letters* **6**, 143 (1963).

TABLE IV

CALCULATED AND EXPERIMENTAL BAND PARAMETERS AT Γ_{1c} AND Γ_{15v} FOR SOME III–V COMPOUNDS

	$m^*(\Gamma_{1c})$ (calc.)	$m^*(\Gamma_{1c})$ (exp.)	$g^*(\Gamma_{1c})$ (calc.)	$g^*(\Gamma_{1c})$ (exp.)	m^*_{lh} (calc.)	m^*_{lh} (exp.)	m^*_{hh} (calc.)	m^*_{hh} (exp.)	m^*_{sh} (calc.)	m^*_{sh} (exp.)
GaP	0.13	—	1.76	—	0.14	—	0.86	—	0.24	—
InP	0.072	0.073[a]	0.60	—	0.078	—	0.50	0.4[i]	0.15	—
GaAs	0.084	0.07[b]	0.32	0.52[l]	0.09	0.12[f]	0.46	0.68[f]	0.17	0.20[f]
InAs	0.026	0.026[b]	−12	—	0.031	0.025[g]	0.40	0.41[f]	0.96	0.083[f]
AlSb	0.11	—	0.0	—	0.11	—	0.56	0.9[j]	0.22	—
GaSb	0.046	0.047[c]	−6.1	−6.5[m]	0.044	0.06[f]	0.50	0.3[k]	0.14	—
InSb	0.0152	0.0155[d]	−44	−48[e]	0.016	0.021[h]	0.39	0.39[h]	0.11	—

[a] T. S. Moss and A. K. Walton, *Physica* **25**, 1142 (1959).

[b] M. Cardona, *Phys. Rev.* **121**, 752 (1961).

[c] S. Zwerdling, B. Lax, K. J. Button, and L. M. Roth, *J. Phys. Chem. Solids* **9**, 320 (1959).

[d] S. D. Smith, C. R. Pidgeon, and V. Prosser, *Proc. Intern. Conf. Phys. Semicond., Exeter, 1962* p. 301. Inst. of Phys. and Phys. Soc., London, 1962.

[e] S. Zwerdling, W. H. Kleiner, and J. P. Theriault, *J. Appl. Phys.* **32**, 2118 (1961).

[f] H. Ehrenreich, see Ref. 34.

[g] F. Mattossi and F. Stern, *Phys. Rev.* **111**, 472 (1958).

[h] See Ref. 47.

[i] O. Folberth and W. Weiss, *Z. Naturforsch.* **10a**, 615 (1955).

[j] D. N. Nasledov and S. V. Slobodchikov, *Zh. Tekhn. Fiz.* **28**, 715 (1958) [*English Transl.*: *Soviet Phys.–Tech. Phys.* **3**, 669 (1958)].

[k] H. N. Leifer and W. C. Dunlap, Jr., *Phys. Rev.* **95**, 51 (1954).

[l] W. Duncan and E. E. Schneider, *Phys. Letters* **7**, 23 (1963).

[m] E. J. Johnson, I. Filinski, and H. Y. Fan, *Proc. Intern. Conf. Phys. Semicond., Exeter, 1962* p. 375. Inst. of Phys. and Phys. Soc., London, 1962.

The transverse effective mass at X_{1c} can also be estimated from the E_2 gap determined experimentally. X_{1c} seems to be the lowest conduction-band minimum in GaP and AlSb.[44] $m_\perp(X_{1c})$ is obtained from[44]

$$\frac{1}{m_\perp(X_{1c})} = 1 + \frac{19}{E_2} \qquad (E_2 \text{ in eV}). \tag{15}$$

CHAPTER 6

Absorption near the Fundamental Edge*

Earnest J. Johnson

I. INTRODUCTION 154

II. REVIEW OF THE BASIC THEORY 156
1. *Basic Concepts* 156
2. *Band Theory* 158
3. *Optical Absorption* 160
4. *The Kane Band Model* 163

III. THE FUNDAMENTAL ABSORPTION IN THE ABSENCE OF INTERACTIONS 167
5. *Theoretical Background* 167
6. *Experimental Results for Indium Antimonide* 169
7. *Other III–V Compounds* 172
8. *Forbidden Transitions* 175
9. *Population Effects (The Absorption Edge in Degenerate Samples)* 176

IV. EFFECTS DUE TO SCATTERING 183
10. *The Form of the Optical Matrix Element in the Presence of Scattering* 183
11. *The Form of the Scattering Matrix Elements* 186
12. *Absorption Corresponding to an Indirect Gap* 188
13. *Phonon Structure* 191
14. *Phonon Broadening of the Absorption Edge Corresponding to Allowed Transitions* 194

V. EFFECTS OF TEMPERATURE AND PRESSURE ON THE ABSORPTION EDGE 196
15. *Effect on the Energy Gap* 196
16. *Pressure Effects* 198
17. *Temperature Effects* 199

VI. IMPURITY ABSORPTION 201
18. *Theoretical Background* 201
19. *Experimental Results* 205

VII. EXCITON TRANSITIONS 212
20. *General Discussion* 212
21. *Theoretical Background* 213
22. *Experimental Results* 218

* This chapter was prepared at Lincoln Laboratory, a center for research operated by Massachusetts Institute of Technology with the support of the U.S. Air Force.

VIII. The Fundamental Absorption in the Presence of a Magnetic Field 222
23. *General Discussion*. 222
24. *Impurity Absorption* 223
25. *Exciton Absorption* 226

IX. Transitions Involving Impurity–Exciton Complexes 231
26. *General Discussion*. 231
27. *Estimates of Dissociation Energies of Complexes* 232
28. *Experimental Observations in Gallium Antimonide* 237
29. *Experimental Observations in Gallium Phosphide* 242

X. The Fundamental Absorption in the Presence of an Electric Field 243
30. *Theoretical Discussion*. 243
31. *Experimental Results* 247

XI. The Fundamental Absorption in Heavily Doped Material . . 249
32. *General Discussion*. 249

XII. Note Added in Proof. 253

I. Introduction

The fundamental absorption edge of semiconductors and insulators corresponds to the threshold for electron transitions between the highest nearly filled band and the lowest nearly empty band. The absorption is very small for photon energies much less than that corresponding to the energy gap and increases by a factor of $\sim 10^4$ or more at higher photon energies. The study of the fundamental absorption provides information about the electron states near the band extrema. The value of the energy gap for a given specimen can often be estimated to within 20% simply by determining the lowest photon energy at which a sample ~ 0.3 mm thick fails to be opaque—i.e., the transmission becomes greater than 1%. By studying the spectral dependence of the absorption coefficient with reasonable resolution one can often distinguish between direct and indirect transitions, and can estimate the energy gap to within 5%. The variation of the energy gap as deduced from the shift of the absorption edge with hydrostatic pressure can aid in the identification of the band extrema corresponding to the energy gap. By observing the shift of the absorption edge as one populates the levels in the conduction band, as in a degenerate sample, one can deduce an effective mass associated with the density of states.

Various interactions give rise to deviations from the absorption expected on the basis of one-electron energy levels. The study of transitions involving electron–hole, electron–phonon, and electron–impurity interactions can yield considerable information. These interactions usually cause a shift of the absorption edge to lower photon energies. At low temperatures and

under high resolution one can often observe structure due to these effects. The energy gap can be determined with more precision if these interactions are recognized and are taken into account.

Small perturbations such as those introduced by an external magnetic or electric field can introduce further structure whose analysis can yield detailed information about the band states. The use of a magnetic field has been particularly fruitful and is covered as a special topic in Chapter 8 by Lax and Mavroides.

The most direct way of observing the fundamental edge is by determining the absorption from transmission measurements, and this is generally the procedure used. However, other less direct methods can yield supplementary information. The interpretation of the signal obtained in a photoconductivity measurement depends upon the thickness of the sample relative to the penetration depth. In the thin-sample limit the signal is proportional to the part of the absorption that creates free carriers. In this limit one can often distinguish between absorption involving an excited state in which the electron is bound from one in which it is free. Complications occur, however, since the possibility exists that free carriers may be created in the decay of the excited state.

In the thick-sample limit no radiation is transmitted, and the photoconductive signal is independent of the intensity of the absorption, but is proportional to the product of the mobility and the lifetime of the free carriers produced. In this limit, structure due to different absorption processes may be resolved in photoconductivity that is not resolved in transmission.

Spitzer and Mead[1,2] have described a process of evaporating a metal film onto a semiconductor surface for observing the photovoltaic effect. The photovoltaic signal is proportional to the optical absorption if the depletion region and the minority-carrier diffusion length of the resulting junction are both much less than the penetration depth of the light. In this way one avoids the difficulties associated with very thin samples necessary for an absorption measurement.

In photoluminescence one can excite a few carriers to a normally empty band and observe sharp peaks in the photon emission associated with transitions from a few states near the bottom of the band. In this way one can observe structure that is not resolved in transmission because the corresponding absorption would involve all of the states of the band and would be broad. In photoluminescence one can also observe transitions from states normally filled with electrons to lower states.

[1] W. G. Spitzer and C. A. Mead, *J. Appl. Phys.* **34**, 306 (1963).
[2] C. A. Mead and W. G. Spitzer, *Phys. Rev. Letters* **11**, 358 (1963).

An additional method of studying the fundamental edge is by observing reflection as used by Wright and Lax for InSb.[2a] For such measurements one must be careful how one prepares the reflecting surface. Generally, however, the reflectivity induced by the fundamental absorption is small relative to the background reflection and is useful only in observing a resonance as with exciton lines or structure as in magnetoabsorption. On the other hand, reflection can be used where transmission measurements are impossible due to excessive background absorption. In transmission one can relate absorption peaks directly to energy level separations. In reflection the analogous procedure is not valid, and to be precise one must be able to explain the lineshape in the particular case at hand.

In this chapter we wish to review the results of optical studies on the absorption edges of the III–V compounds and to review the implications of these results on the band structure of the compounds concerned. We shall also review the information about excitons, phonons, and impurities obtained by optical studies near the absorption edge.

As has already been mentioned, some specialized studies of the absorption edge are subjects of other chapters of this book and will only be touched on here. McLean[3] has reviewed the work on the fundamental absorption in group-IV semiconductors, and much of his discussion applies to the III–V compounds. General discussions of the fundamental absorption were given earlier by Bardeen *et al.*,[4] Dexter,[5] and Fan.[6] Madelung has given a concise review of the optical properties of III–V compounds in his book.[7] His bibliography and index have proven invaluable in the preparation of this work. Ehrenreich[8] has reviewed the experimental evidence concerning the band structure in the III–V compounds.

II. Review of the Basic Theory

1. Basic Concepts

A good review of the elementary optical properties of solids has been given by Stern.[9] We give here only a brief summary of optical absorption. An

[2a] G. B. Wright and B. Lax, *J. Appl. Phys. Suppl.* **32**, 2113 (1961).

[3] T. P. McLean, *Progr. Semicond.* **5**, 55 (1960).

[4] J. Bardeen, F. Blatt, and L. H. Hall, *in* "Photoconductivity Conference" (Proc. Atlantic City Conf.) (R. G. Breckenridge, B. R. Russell, and E. E. Hahn, eds.), p. 146. Wiley, New York, and Chapman & Hall, London, 1956.

[5] D. L. Dexter, *in* "Photoconductivity Conference" (Proc. Atlantic City Conf.) (R. G. Breckenridge, B. R. Russell, and E. E. Hahn, eds.), p. 155. Wiley, New York, and Chapman & Hall, London, 1956.

[6] H. Y. Fan, *Rept. Progr. Phys.* **19**, 107 (1956).

[7] O. Madelung, "Physics of III–V Compounds." Wiley, New York, 1964.

[8] H. Ehrenreich, *J. Appl. Phys. Suppl.* **32**, 2155 (1961).

[9] F. Stern, *Solid State Phys.* **15**, 299 (1963).

optical plane wave in a solid can be described by the real part of the vector potential

$$\mathbf{A} = A_0 \hat{\mathbf{a}}\, e^{i(\omega t - N\mathbf{q}\cdot\mathbf{r})} \equiv A_0 \mathbf{a}. \tag{1}$$

Here $\hat{\mathbf{a}}$ is a unit vector giving the polarization, and N is the complex index of refraction, which can be written

$$N = n - i\mathscr{k}, \tag{2}$$

where n is the usual index of refraction, which governs the dispersion. The quantity $\mathscr{k}$ is the extinction coefficient, which gives damping. By calculating the intensity associated with Eq. (1) it is seen that $\mathscr{k}$ is related to the absorption coefficient by

$$\alpha = 2\mathscr{k}|q| = \frac{4\pi\mathscr{k}}{\lambda}. \tag{3}$$

Experimentally, one can observe the intensity of the wave reflected from the surface of the sample or the intensity of the wave transmitted through the sample. If the sample thickness is much greater than α^{-1}, the reflectivity at normal incidence is given by

$$R = \frac{I_r}{I_0} = \frac{(n-1)^2 + \mathscr{k}^2}{(n+1)^2 + \mathscr{k}^2}. \tag{4}$$

For experimental conditions such that interference effects due to internal reflections are negligible, the transmission is given by

$$T = \frac{I_t}{I_0} = \frac{(1-R)^2 e^{-\alpha x}}{1 + R^2 e^{-2\alpha x}}. \tag{5}$$

Generally, the reflectivity varies slowly with photon energy, and the spectral variation of the transmission is principally due to the variation of the absorption coefficient. The absorption coefficient characterizes the medium through which the wave is traveling. From the viewpoint of electron band structure we are interested in the probability that, under the influence of the radiation field, an electron will make a transition between two energy levels. This is given by the quantity w, which is also equal to the number of transitions per unit volume per unit time. For one-photon processes this is also equal to the number of photons absorbed per unit volume per unit time. The corresponding energy absorbed is obviously whv. The flow of energy is given by the Poynting vector ($\mathscr{N}$), which can be calculated in the usual way from Eq. (1). The flow of energy and the absorption of energy are related by the conservation condition

$$\nabla \cdot \overline{\mathscr{N}} = -whv, \tag{6a}$$

where the average of $\mathscr{N}$ is taken over a complete cycle. By substituting Eq. (1) in Eq. (6a) we obtain the relation between absorption coefficient

and w:

$$\alpha = 2\pi c\hbar^2 \frac{1}{nhv} \frac{w}{|A_0|^2}. \tag{6b}$$

Note that the absorption coefficient has an inherent inverse dependence on photon energy that is independent of the mechanism of absorption. The effects of the electron band structure enter the problem through w.

2. Band Theory

Consider a system of N electrons with coordinates $\mathbf{r}_i$ in a crystal. In the band approximation[10] the wave function for the ground state of the system can be written in terms of one-electron Bloch functions ψ_j as

$$\Psi_0(\mathbf{r}_1, \mathbf{r}_2 \cdots \mathbf{r}_N) = \frac{1}{\sqrt{N!}} \begin{vmatrix} \psi_1(\mathbf{r}_1) & \psi_2(\mathbf{r}_1) & \cdot & \psi_{v,\mathbf{k}_h}(\mathbf{r}_1) & \cdot & \psi_N(\mathbf{r}_1) \\ \psi_1(\mathbf{r}_2) & \psi_2(\mathbf{r}_2) & \cdot & \psi_{v,\mathbf{k}_h}(\mathbf{r}_2) & \cdot & \psi_N(\mathbf{r}_2) \\ \cdot & \cdot & \cdot & \cdot & \cdot & \cdot \\ \cdot & \cdot & \cdot & \cdot & \cdot & \cdot \\ \cdot & \cdot & \cdot & \cdot & \cdot & \cdot \\ \psi_1(\mathbf{r}_N) & \psi_2(\mathbf{r}_N) & \cdot & \psi_{v,\mathbf{k}_h}(\mathbf{r}_N) & \cdot & \psi_N(\mathbf{r}_N) \end{vmatrix}. \tag{7}$$

In an insulator or an intrinsic semiconductor at low temperatures there are just enough electrons to fill all bands, up to and including the valence band. One can form an excited state by promoting an electron to the conduction band. The corresponding excited-state wave function is obtained from the ground-state wave function by replacing one of the valence-band Bloch functions by a conduction-band Bloch function,

$$\Phi_{\mathbf{k}_e,\mathbf{k}_h}(\mathbf{r}_1, \mathbf{r}_2 \cdots \mathbf{r}_N) = \frac{1}{\sqrt{N!}} \begin{vmatrix} \psi_1(\mathbf{r}_1) & \psi_2(\mathbf{r}_1) & \cdot & \psi_{c,\mathbf{k}_e}(\mathbf{r}_1) & \cdot & \psi_N(\mathbf{r}_1) \\ \psi_1(\mathbf{r}_2) & \psi_2(\mathbf{r}_2) & \cdot & \psi_{c,\mathbf{k}_e}(\mathbf{r}_2) & \cdot & \psi_N(\mathbf{r}_2) \\ \cdot & \cdot & \cdot & \cdot & \cdot & \cdot \\ \cdot & \cdot & \cdot & \cdot & \cdot & \cdot \\ \cdot & \cdot & \cdot & \cdot & \cdot & \cdot \\ \psi_1(\mathbf{r}_N) & \psi_2(\mathbf{r}_N) & \cdot & \psi_{c,\mathbf{k}_e}(\mathbf{r}_N) & \cdot & \psi_N(\mathbf{r}_N) \end{vmatrix}, \tag{8}$$

where $\mathbf{k}_e$ and $\mathbf{k}_h$ are the wave vectors associated with the relevant one-electron wave functions. In this way we create an electron–hole pair. The totality of such excited states can be obtained by permuting $\psi_{v,\mathbf{k}_h}$ and $\psi_{c,\mathbf{k}e}$ among the available one-electron states. The most general excited state can be written as a linear combination of these. Frequently, it is sufficient to consider only the states in one filled and one empty band, and we can write the wave function describing an excited state as

$$\Psi_n(\mathbf{r}_1, \mathbf{r}_2 \cdots \mathbf{r}_N) = \sum_{\mathbf{k}_e,\mathbf{k}_h} c_n(\mathbf{k}_e, \mathbf{k}_h)\, \Phi_{\mathbf{k}_e,\mathbf{k}_h}, \tag{9}$$

where the sum is taken over all possible pairs of $\mathbf{k}_e$ and $\mathbf{k}_h$.

[10] F. Seitz, "The Modern Theory of Solids," pp. 237 and 407. McGraw-Hill, New York, 1940.

The form taken by $c_n(\mathbf{k}_e, \mathbf{k}_h)$ is determined by interactions not taken into account in the one-electron approximation. These include the Coulomb interaction between electron and hole, interaction with impurities, interaction with an applied electric field, etc. The forms of some of the interactions we shall consider are given in Table I. Often the interactions can be treated using effective-mass theory.[11] The function $c_n(\mathbf{k}_e, \mathbf{k}_h)$ is determined using an effective-mass equation. For nondegenerate bands this is obtained from the dispersion relations $E_c(\mathbf{k}_e)$ and $E_v(\mathbf{k}_h)$ by replacing $\hbar\mathbf{k}_e$ and $\hbar\mathbf{k}_h$ by the operators $\mathbf{p}_e$ and $\mathbf{p}_h$ and writing

$$[E_c(\mathbf{p}_e) - E_v(\mathbf{p}_h) + H'(\mathbf{r}_e, \mathbf{r}_h)]\,\psi_n(\mathbf{r}_e, \mathbf{r}_h) = \varepsilon_n\psi_n(\mathbf{r}_e, \mathbf{r}_h), \tag{10}$$

where H' is the perturbation imposed by the interaction. For the case of degenerate bands the reader is referred to Chapter 7 by Dimmock. The function $c_n(\mathbf{k}_e, \mathbf{k}_h)$ is the Fourier transform of the effective-mass eigenfunction $\psi_n(\mathbf{r}_e, \mathbf{r}_h)$. The excited state can be formed by the absorption of the energy given by the eigenvalue, ε_n.

TABLE I

INTERACTIONS RELEVANT TO FUNDAMENTAL ABSORPTION

Type of interaction	H'
Noninteracting pair	0
Screened Coulomb attraction	$\dfrac{e^2}{\kappa\lvert\mathbf{r}_e - \mathbf{r}_h\rvert}\exp(-\lambda\lvert\mathbf{r}_e - \mathbf{r}_h\rvert)$
Uniform electric field	$e\mathbf{E}\cdot(\mathbf{r}_e - \mathbf{r}_h)$
Lattice dilatation	$\sum_{i,j}\varepsilon_{ij}^{e}W_{ij}(\mathbf{r}_e) + \sum_{ij}\varepsilon_{ij}^{h}W_{ij}(\mathbf{r}_h)$
Charged impurity	$-\dfrac{e^2}{\kappa\lvert\mathbf{r}_e\rvert} + \dfrac{e^2}{\kappa\lvert\mathbf{r}_h\rvert}$

There are two types of H' that lead to easy solutions:

(1) $H'(\mathbf{r}_e, \mathbf{r}_h) = H_e'(\mathbf{r}_e) + H_h'(\mathbf{r}_h)$ and (2) $H'(\mathbf{r}_e, \mathbf{r}_h) = H'(\mathbf{r}_e - \mathbf{r}_h)$.

In the first case we can write

$$\psi_n(\mathbf{r}_e, \mathbf{r}_h) = \phi_l(\mathbf{r}_e)\,\phi_m(\mathbf{r}_h), \tag{11}$$

$$\varepsilon_n = \varepsilon_l + \varepsilon_m. \tag{12}$$

Substitution in Eq. (10) gives

$$[E_c(\mathbf{p}_e) + H_e'(\mathbf{r}_e)]\,\phi_l(\mathbf{r}_e) = \varepsilon_l\phi_l(\mathbf{r}_e) \tag{13}$$

$$[E_v(\mathbf{p}_h) + H_h'(\mathbf{r}_h)]\,\phi_m(\mathbf{r}_h) = \varepsilon_m\phi_m(\mathbf{r}_h) \tag{14}$$

$$c_n(\mathbf{k}_e, \mathbf{k}_h) = \int \phi_l(\mathbf{r}_e)\exp(-i\mathbf{k}_e\cdot\mathbf{r}_e)\,d\mathbf{r}_e \int \phi_m(\mathbf{r}_h)\exp(-i\mathbf{k}_h\cdot\mathbf{r}_h)\,d\mathbf{r}_h. \tag{15}$$

[11] J. M. Luttinger and W. Kohn, *Phys. Rev.* **97**, 869 (1955).

If $H'(\mathbf{r}_e, \mathbf{r}_h) = H'(\mathbf{r}_e - \mathbf{r}_h)$ it is convenient to change to the coordinates

$$\mathbf{R} = \tfrac{1}{2}(\mathbf{r}_e + \mathbf{r}_h), \qquad \mathbf{r} = \mathbf{r}_e - \mathbf{r}_h. \tag{16}$$

The momenta conjugate to these are

$$\mathbf{P} = \mathbf{p}_e + \mathbf{p}_h, \qquad \mathbf{p} = \tfrac{1}{2}(\mathbf{p}_e - \mathbf{p}_h). \tag{17}$$

With the transformation, Eq. (10) becomes

$$[E_c(\mathbf{p} + \tfrac{1}{2}\mathbf{P}) + E_v(-\mathbf{p} + \tfrac{1}{2}\mathbf{P}) + H'(\mathbf{r}, \mathbf{R})]\,\psi_n(\mathbf{r}, \mathbf{R}) = \varepsilon_n \psi_n(\mathbf{r}, \mathbf{R}). \tag{18}$$

Since H' does not involve $\mathbf{R}$, $\mathbf{P}$ commutes with the Hamiltonian and the solutions are of the form

$$\psi_n(\mathbf{r}, \mathbf{R}) = \psi_{\mathbf{K},l}(\mathbf{r}, \mathbf{R}) = \exp(i\mathbf{K}_m \cdot \mathbf{R})\,\phi_l(\mathbf{r}), \tag{19}$$

where $\phi_l(\mathbf{r})$ satisfies the equation

$$[E_c(\mathbf{p} + \tfrac{1}{2}\hbar\mathbf{K}_m) + E_v(-\mathbf{p} + \tfrac{1}{2}\hbar\mathbf{K}_m) + H'(\mathbf{r})]\,\phi_l(\mathbf{r}) = \varepsilon_n \phi_l(\mathbf{r}) \tag{20}$$

and

$$c_n = \delta(\mathbf{K} - \mathbf{K}_m) \int \phi_l(\mathbf{r})\, e^{-i\mathbf{r}\cdot\mathbf{k}}\, d\mathbf{r}. \tag{21}$$

For this case the excited-state wave function has the form

$$\Psi_n{}^x(\mathbf{r}_e, \mathbf{r}_h) = \sum_{\mathbf{k}_e, \mathbf{k}_h} \delta(\mathbf{K}_m - \mathbf{k}_e - \mathbf{k}_h)\, c_l(\mathbf{k})\, \Psi^0_{\mathbf{k}_e, \mathbf{k}_h}(\mathbf{r}_e, \mathbf{r}_h). \tag{22}$$

Therefore, in the summation an electron of wave vector $\mathbf{k}_e$ pairs off with a hole of wave vector $\mathbf{K}_m - \mathbf{k}_e$.

3. Optical Absorption

We now consider the optical creation of such excited states.[12,13] The absorption of a photon of energy ε_n is required to form the excited state n. In the presence of a radiation field characterized by the vector potential $\mathbf{A}$, transitions are governed by the matrix element

$$H_{0,n} = \int \Psi_n{}^* \left[\sum_i \frac{e}{mc} \mathbf{A}_i \cdot \mathbf{p}_i\right] \Psi_0\, d\mathbf{r}_1\, d\mathbf{r}_2 \cdots d\mathbf{r}_N. \tag{23}$$

Using Eq. (9) this becomes

$$H_{0,n} = \sum_{\mathbf{k}_e, \mathbf{k}_h} c_n(\mathbf{k}_e, \mathbf{k}_h) \int \Phi^*_{\mathbf{k}_e, \mathbf{k}_h} \left[\sum_i \frac{e}{mc} \mathbf{A}_i \cdot \mathbf{p}_i\right] \Psi_0\, d\mathbf{r}_1\, d\mathbf{r}_2 \cdots d\mathbf{r}_N. \tag{24}$$

By substituting from Eqs. (7) and (8) the integration over the coordinates of

[12] F. Seitz, "The Modern Theory of Solids," p. 326. McGraw-Hill, New York, 1940.
[13] L. I. Shiff, "Quantum Mechanics," p. 240. McGraw-Hill, New York, 1949.

each of the electrons can be reduced to a single integration over the crystal, and Eq. (24) reduces to

$$H_{0,n} = \sum_{\mathbf{k}_e,\mathbf{k}_h} c_n(\mathbf{k}_e, \mathbf{k}_h) \int_{\text{crystal}} \psi^*_{c,\mathbf{k}_e} \left[\frac{e}{mc}\mathbf{A}\cdot\mathbf{p}\right] \psi_{v,\mathbf{k}_h}\, d\mathbf{r}. \tag{25}$$

Equation (25) can be written

$$H_{0,n} = A_0 \sum_{\mathbf{k}_e,\mathbf{k}_h} c_n(\mathbf{k}_e, \mathbf{k}_h)\, H_{c,v}(\mathbf{k}_e, \mathbf{k}_h), \tag{26}$$

where

$$H_{c,v}(\mathbf{k}_e, \mathbf{k}_h) = \int d\mathbf{r}\, \psi_{c,\mathbf{k}_e} \left(\frac{e}{mc}\mathbf{a}\cdot\mathbf{p}\right) \psi_{v,\mathbf{k}_h}. \tag{27}$$

If the wave vector of the radiation is small compared to electron wave vectors, $\mathbf{a}$ can be removed from under the integral sign. It can easily be shown that for Bloch waves ($\psi_{n\mathbf{k}} = u_{n\mathbf{k}}\, e^{i\mathbf{k}\cdot\mathbf{r}}$) the optical matrix element is nonzero only for $n' \neq n$, and for $n' = c$, $n = v$, it is given by

$$H_{c,v}(\mathbf{k}_e, \mathbf{k}_h) = \int d\mathbf{r}\, u^*_{c,\mathbf{k}_e} \left(\frac{e}{mc}\mathbf{a}\cdot\mathbf{p}\right) u_{v,\mathbf{k}_h}\, \delta(\mathbf{k}_e + \mathbf{k}_h) \tag{28}$$

$$\equiv H_{c,v}(\mathbf{k})\, \delta(\mathbf{k}_e + \mathbf{k}_h). \tag{29}$$

If, *a priori*, one has the wave functions $u_{v,\mathbf{k}}$ and $u_{c,\mathbf{k}}$, one can evaluate the matrix element directly. Often, however, it is the nature of these wave functions that one is trying to deduce. At other times one wants to check a proposed band model. Generally, the matrix element varies slowly with $\mathbf{k}$, and one can obtain valuable information by expanding the matrix element in powers of $(\mathbf{k} - \mathbf{k}_0)$, where $\mathbf{k}_0$ corresponds to the minimum band separation. In this manner one obtains

$$H_{c,v}(\mathbf{k}) = H_{c,v}(\mathbf{k}_0) + (\mathbf{k} - \mathbf{k}_0)\cdot\{\nabla_{\mathbf{k}}[H_{c,v}(\mathbf{k})]\}_{\mathbf{k}=\mathbf{k}_0} + \cdots. \tag{30}$$

For transitions allowed at $\mathbf{k} = \mathbf{k}_0$ the terms following the first are negligible near $\mathbf{k} = \mathbf{k}_0$ and one obtains

$$H_{c,v}(\mathbf{k}) \approx H_{c,v}(\mathbf{k}_0) \tag{31}$$

and the matrix element does not contribute to the spectral variation of the absorption near the threshold. However, the matrix element may vanish at $\mathbf{k} = \mathbf{k}_0$ (i.e., the transitions are symmetry forbidden at $\mathbf{k} = \mathbf{k}_0$) and

$$H_{c,v}(\mathbf{k}_e) \approx (\mathbf{k} - \mathbf{k}_0)\cdot\{\nabla_{\mathbf{k}}[H_{c,v}(\mathbf{k}_e)]\}_{\mathbf{k}=\mathbf{k}_0}, \tag{32}$$

giving a variation in matrix element over the band states. The matrix

element then becomes

$$H_{0,n} \approx A_0 H_{c,v}(\mathbf{k}_0) \sum_{\mathbf{k}_e,\mathbf{k}_h} c_n(\mathbf{k}_e, \mathbf{k}_h)\, \delta(\mathbf{k}_e + \mathbf{k}_h) + A_0\{\nabla_{\mathbf{k}}[K_{c,v}(\mathbf{k})]\}_{\mathbf{k}=\mathbf{k}_0} \cdot \sum_{\mathbf{k}_e,\mathbf{k}_h} c_n(\mathbf{k}_e, \mathbf{k}_h)(\mathbf{k} - \mathbf{k}_0)\, \delta(\mathbf{k}_e + \mathbf{k}_h). \quad (33)$$

For the case of H' independent of $\mathbf{R}$ we can substitute from Eq. (22) to obtain

$$H_{0,n} \approx A_0 H_{c,v}(\mathbf{k}_0) \sum_{\mathbf{k}} c_l(\mathbf{k})\, \delta(\mathbf{K} - \mathbf{k}_e - \mathbf{k}_h)\, \delta(\mathbf{k}_e + \mathbf{k}_h) + A_0[\nabla_{\mathbf{k}} H_{c,v}(\mathbf{k})]_{\mathbf{k}=\mathbf{k}_0} \cdot \sum_{\mathbf{k}} c_l(\mathbf{k})(\mathbf{k} - \mathbf{k}_0)\, \delta(\mathbf{K} - \mathbf{k}_e - \mathbf{k}_h)\, \delta(\mathbf{k}_e + \mathbf{k}_h). \quad (34)$$

This is equivalent to

$$H_{0,n} \approx A_0 H_{c,v}(\mathbf{k}_0)\, \delta(\mathbf{K}) \sum_{\mathbf{k}} c_l(\mathbf{k}) + A_0[\nabla_{\mathbf{k}} H_{c,v}(\mathbf{k})]_{\mathbf{k}=\mathbf{k}_0}\, \delta(\mathbf{K}) \sum_{\mathbf{k}} c_l(\mathbf{k})(\mathbf{k} - \mathbf{k}_0). \quad (35)$$

If the first term in Eq. (35) is nonzero, the transitions are said to be "allowed," and to the first approximation the second term can be neglected. In this case, Eq. (35) can be written

$$H_{0,n} \approx A_0 H_{c,v}(\mathbf{k}_0)\, \delta(\mathbf{K}) [\sum_{\mathbf{k}} c_l(\mathbf{k})\, e^{i\mathbf{k}\cdot\mathbf{r}}]_{\mathbf{r}=0} = A_0 H_{c,v}(\mathbf{k}_0)\, \delta(\mathbf{K})\, \phi_l(0). \quad (36)$$

The absolute magnitude squared of the last factor is simply the probability that the hole and electron appear simultaneously at the same point in the crystal. The delta function requires that only excited states be formed where $\mathbf{K}$ is zero.[13a]

If the first term in Eq. (35) is zero, the transitions are said to be "forbidden." We shall call these "symmetry forbidden." In this case

$$H_{0,n} \approx A_0[\nabla_{\mathbf{k}} H_{c,v}(\mathbf{k})]_{\mathbf{k}=\mathbf{k}_0} \cdot [\sum_{\mathbf{k}} c_l(\mathbf{k})(\mathbf{k} - \mathbf{k}_0) \exp(i(\mathbf{k} - \mathbf{k}_0)\cdot \mathbf{r})]_{\mathbf{r}=0}\, \delta(\mathbf{K}) = A_0[\nabla_{\mathbf{k}} H_{c,v}(\mathbf{k})]_{\mathbf{k}=\mathbf{k}_0} \cdot [(1/i)\nabla_{\mathbf{r}} \exp(-i\mathbf{k}_0 \cdot \mathbf{r})\phi_l(\mathbf{r})]_{\mathbf{r}=0}\, \delta(\mathbf{K}). \quad (37)$$

In many cases that we shall consider, the excited state n is part of a continuum of states for which the probability of photon absorption can be given in terms of a density of final states, $\rho_n(k)$ as

$$\frac{w(h\nu)}{|A_0|^2} = \frac{2\pi}{\hbar} \frac{|H_{n0}|^2}{|A_0|^2} \rho_n(k)\, \delta[h\nu - \varepsilon_n(k)], \quad (38)$$

where it is assumed that the Fermi level is many kT from any of the states

[13a] More strictly, $\mathbf{K} = \mathbf{q}$.

involved. There may be several sets of excited states at the same energy above the ground state, and the transition probability will involve a sum of terms of the form of Eq. (38),

$$\frac{w(h\nu)}{|A_0|^2} = \sum_l w_l(h\nu) = \frac{2\pi}{\hbar} \sum_n \left\{ \frac{|H_{n0}|^2}{|A_0|^2} \rho_n(k) \right\} \delta[h\nu - \varepsilon_n(k)]. \tag{39}$$

The absorption coefficient can be written in the convenient form

$$[\alpha h\nu] = \frac{4\pi^2 \hbar c}{n} \sum_n \left\{ \frac{|H_{n,0}|^2}{|A_0|^2} \rho_n(k) \right\} \delta[h\nu - \varepsilon_n(k)]. \tag{40}$$

4. The Kane Band Model

Much information about the band structure can be deduced from the fundamental absorption, even in the absence of a specific model for the band structure. This information can contribute to the creation of such a model, and eventually the absorption can be used to check it. The band model that has been found satisfactory for most of the III–V compounds is due to Kane,[14] and we shall review the model before discussing the experimental results.

The Kane model is based upon $\mathbf{k} \cdot \mathbf{p}$ perturbation theory. For a complete discussion of $\mathbf{k} \cdot \mathbf{p}$ theory the reader should refer to Chapter 3 by E. O. Kane in Volume 1 of this series. The dispersion relations for the energy bands of InSb resulting from Kane's calculations are shown in Fig. 1. For nondegenerate material the Fermi level lies in the energy gap between band E_c and band E_{v1}. The fundamental absorption corresponds to transitions involving bands E_c and E_{v1} or E_{v2}. At higher photon energies transitions involving E_{v3} can occur. With a change of parameters the results can be applied to other III–V compounds. Neglecting certain higher-order corrections, we have found that the dispersion relations for the bands can be given by

$$E_c = \frac{E_g}{2} + \frac{\hbar^2 k^2}{2m} + \frac{E_g}{2} \left[1 + 4 \frac{\hbar^2 k^2}{2m_c} \frac{f_1(E_c)}{E_g} \right]^{1/2}, \tag{41}$$

$$E_{v1} = \frac{\hbar^2 k^2}{2m} - \frac{\hbar^2 k^2}{2m_v} \left(1 - \gamma' \frac{k_x^2 k_y^2 + k_y^2 k_z^2 + k_z^2 k_x^2}{\frac{1}{3} k^4} \right), \tag{42}$$

$$E_{v2} = \frac{E_g}{2} + \frac{\hbar^2 k^2}{2m} - \frac{E_g}{2} \left[1 + 4 \frac{\hbar^2 k^2}{2m_c} \frac{2(E_g + \Delta)}{3E_g + 2\Delta} \frac{f_2(E_{v2})}{E_g} \right]^{1/2}, \tag{43}$$

$$E_{v3} = -\frac{\Delta}{2} + \frac{\hbar^2 k^2}{2m} - \frac{\Delta}{2} \left[1 + 4 \frac{\hbar^2 k^2}{2m_c} \frac{E_g}{3E_g + 2\Delta} \frac{f_3(E_{v3})}{\Delta} \right]^{1/2}, \tag{44}$$

[14] E. O. Kane, *J. Phys. Chem. Solids* **1**, 249 (1957).

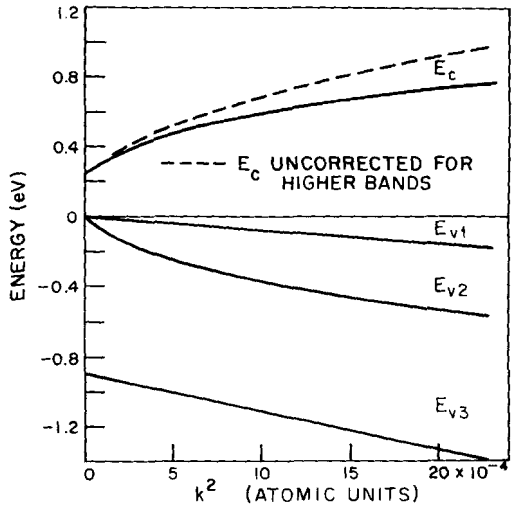


FIG. 1. Valence and conduction band energies versus k^2 for an average direction in indium antimonide. (After E. O. Kane.[14])

The functions f_1, f_2, and f_3 are slowly varying functions of energy that are equal to unity at $k = 0$. They can be treated as correction functions. The coordinate axes are oriented along the $\langle 100 \rangle$ directions. For small $\mathbf{k}$ in the $\langle 100 \rangle$ directions the dispersion relations reduce to

$$E_c \approx E_g + \frac{\hbar^2 k^2}{2m}\left[1 + \frac{m}{m_c}\right], \tag{45}$$

$$E_{v1} = -\frac{\hbar^2 k^2}{2m}\left[\frac{m}{m_v} - 1\right], \tag{46}$$

$$E_{v2} = -\frac{\hbar^2 k^2}{2m}\left[\frac{m}{m_c}\frac{2(E_g + \Delta)}{3E_g + 2\Delta} - 1\right], \tag{47}$$

$$E_{v3} = -\Delta - \frac{\hbar^2 k^2}{2m}\left[\frac{m}{m_c}\frac{E_g}{3E_g + 2\Delta} - 1\right]. \tag{48}$$

It is seen that E_g is the energy gap and Δ is the splitting between valence bands at $k = 0$ (i.e., the spin–orbit splitting). For small k the bands are parabolic, the parameter m_c is related to the electron effective mass (m_e) for small k by

$$\frac{1}{m_e} = \frac{1}{m_c} + \frac{1}{m}, \tag{49}$$

where m is the free-electron mass. The parameter m_v is related to the heavy-hole mass in the $\langle 100 \rangle$ direction (m_{hh}) by

$$\frac{1}{m_{hh}} = \frac{1}{m_v} - \frac{1}{m}. \tag{50}$$

The quantity γ' is a measure of the warping of the energy surfaces of the E_{v1} bands. The dispersion relations are given in Fig. 1 for an average direction. Each of the quantities E_g, Δ, m_c, m_v, and γ', can be determined experimentally, at least in principle. The functions f_1, f_2, and f_3 are given by

$$f_1 = \frac{E_g + \Delta}{E_g + \frac{2}{3}\Delta} \frac{E_c + \frac{2}{3}\Delta}{E_c + \Delta}, \tag{51}$$

$$f_2 = \frac{3}{2} \frac{E_{v2} + \frac{2}{3}\Delta}{E_{v2} + \Delta}, \tag{52}$$

$$f_3 = \frac{3(\Delta + E_g)}{\Delta} \frac{E_{v3} + \frac{2}{3}\Delta}{E_{v3} - E_g}. \tag{53}$$

It should be noted that these are monotonic functions of energy with the limits[14a]

$$1 \leqslant f_1 \leqslant \frac{E_g + \Delta}{E_g + \frac{2}{3}\Delta} \leqslant \frac{3}{2}, \tag{54}$$

$$1 \geqslant f_2 \geqslant 0, \tag{55}$$

$$1 \leqslant f_3 \leqslant 3 + 3\frac{E_g}{\Delta}. \tag{56}$$

The band wave functions can be given as linear combinations of the wave functions S, X, Y, and Z, where S has the symmetry properties of s functions under the operations of the tetrahedral group and X, Y, and Z have the symmetry properties of p functions. In the notation of Dresselhaus[15] the former have Γ_1 symmetry and the latter have Γ_4 symmetry. For $\mathbf{k}$ in the direction of z corresponding to one of the crystal symmetry axes, the wave functions for band E_{v1} depending upon spin are given by

$$u_{v1}(\mathbf{k}) = \begin{cases} b_{v1}(k)\left[(X + iY)\frac{\alpha}{\sqrt{2}}\right] \\ b_{v1}(k)\left[(X - iY)\frac{\beta}{\sqrt{2}}\right] \end{cases}, \tag{57}$$

[14a] Actually, the range of f_2 for unlimited variation of E_{v2} is much greater than that given. However, investigation of Eq. (43) will show that only values of E_{v2} in the range from 0 to $-\frac{2}{3}\Delta$ are relevant.

[15] G. Dresselhaus, *Phys. Rev.* **100**, 580 (1955).

and for the bands E_c, E_{v2}, and E_{v3} the wave functions are given by

$$u_i(\mathbf{k}) = \begin{cases} a_i(k)[iS\beta] + b_i(k)\left[(X - iY)\frac{\alpha}{\sqrt{2}}\right] + c_i(k)[Z\beta] \\ a_i(k)[iS\alpha] + b_i(k)\left[-(X + iY)\frac{\beta}{\sqrt{2}}\right] + c_i(k)[Z\alpha] \end{cases}, \tag{58}$$

where α and β are spin functions. At $\mathbf{k} = 0$ the wave functions reduce to

$$u_c(0) = \begin{cases} [iS\beta] \\ [iS\alpha] \end{cases}, \tag{59}$$

$$u_{v1}(0) = \begin{cases} \left[(X + iY)\frac{\alpha}{\sqrt{2}}\right] \\ \left[(X - iY)\frac{\beta}{\sqrt{2}}\right] \end{cases}, \tag{60}$$

$$u_{v2}(0) = \begin{cases} \left(\frac{1}{3}\right)^{1/2}\left[(X - iY)\frac{\alpha}{\sqrt{2}}\right] + \left(\frac{2}{3}\right)^{1/2}[Z\beta] \\ \left(\frac{1}{3}\right)^{1/2}\left[-(X + iY)\frac{\beta}{\sqrt{2}}\right] + \left(\frac{2}{3}\right)^{1/2}[Z\alpha] \end{cases}, \tag{61}$$

$$u_{v3}(0) = \begin{cases} \left(\frac{2}{3}\right)^{1/2}\left[(X - iY)\frac{\alpha}{\sqrt{2}}\right] - \left(\frac{1}{3}\right)^{1/2}[Z\beta] \\ \left(\frac{2}{3}\right)^{1/2}\left[-(X + iY)\frac{\beta}{\sqrt{2}}\right] - \left(\frac{1}{3}\right)^{1/2}[Z\alpha] \end{cases} \tag{62}$$

For the conduction band, only a_c is nonzero, and the wave functions have s-like symmetry. For the valence bands, only b and c are nonvanishing, and the wave functions have p-like symmetry. The E_{v1} band retains p-like symmetry for $\mathbf{k} \neq 0$, and the symmetry of the remaining bands become mixed. In general, the coefficients are given by

$$a_c = \frac{1}{N_c}, \qquad b_c = \frac{1}{N_c}\frac{\sqrt{2}\Delta}{3(E_g + \varepsilon_c) + 2\Delta}\frac{\varepsilon_c}{kP}, \qquad c_c = \frac{1}{N_c}\frac{\varepsilon_c}{kP}; \tag{63}$$

$$a_{v1} = 0, \qquad b_{v1} = 1, \qquad c_{v1} = 0; \tag{64}$$

$$a_{v2} = \frac{1}{N_{v2}} kP, \qquad b_{v2} = \frac{1}{N_{v2}} \frac{\sqrt{2}\Delta}{3} \frac{\varepsilon_{v2} - E_g}{\varepsilon_{v2} + 2\Delta/3}, \qquad c_{v2} = \frac{1}{N_{v2}} (\varepsilon_{v2} - E_g); \tag{65}$$

$$a_{v3} = \frac{1}{N_{v3}} kP, \quad b_{v3} = \frac{1}{N_{v3}} \frac{\sqrt{2}\Delta}{3} \frac{(\varepsilon_{v3} - \Delta - E_g)}{(\varepsilon_{v3} - \Delta/3)}, \quad c_{v3} = \frac{1}{N_{v3}} (\varepsilon_3 - \Delta - E_g); \tag{66}$$

where[15a]

$$\varepsilon(\mathbf{k}) \equiv E(\mathbf{k}) - E(0) - \frac{\hbar^2 k^2}{2m}. \tag{67}$$

The quantity $N_i^2 = N_i^2(k)$ is a normalizing factor such that $a_i^2 + b_i^2 + c_i^2 = 1$. Theoretically, the band parameters Δ, m_c, m_v, and γ' are related to certain matrix elements. For example,

$$\frac{1}{m_c} = 2\frac{P^2}{\hbar^2} \frac{E_g + \frac{2}{3}\Delta}{E_g(E_g + \Delta)}, \tag{68}$$

where

$$P = -i\frac{\hbar}{m} \langle S|p_z|Z\rangle, \tag{69}$$

$$\Delta = \frac{3\hbar i}{4m^2c^2} \left\langle X \left| \frac{\partial V}{\partial x} p_y - \frac{\partial V}{\partial y} p_x \right| Y \right\rangle, \tag{70}$$

where V is the crystal potential.

III. The Fundamental Absorption in the Absence of Interactions

5. Theoretical Background

We first consider the fundamental absorption in the absence of interactions. Strictly speaking, this situation cannot really exist, since there will always be the Coulomb interaction between the hole and the electron. However, in the presence of screening by carriers and impurities this interaction should be considerably reduced. The neglect of the Coulomb

[15a] Except for this case, we shall use $\varepsilon(\mathbf{k}) \equiv E(\mathbf{k}) - E(0)$.

interaction has been justified by experimental results on samples at high temperatures and on samples that are not so pure. Effects due to the Coulomb interaction are observable in pure samples at low temperatures. These will be discussed in Parts VII, VIII, and IX.

In the absence of interactions the optical selection rule ($\mathbf{K} = 0$) applies, and the relative motion of the corresponding electron–hole pairs is given by

$$[E_c(\mathbf{p}) - E_v(-\mathbf{p})]\,\phi_l(\mathbf{r}) = \varepsilon_l \phi_l(\mathbf{r}). \tag{71}$$

We first consider a simple band structure consisting of two bands given by

$$E_v = -\frac{\hbar^2 k^2}{2m_v}, \qquad E_c = E_g + \frac{\hbar^2 k^2}{2m_c}. \tag{72}$$

For this case Eq. (71) becomes

$$\frac{p^2}{2\mu}\phi_l = (\varepsilon_l - E_g)\phi_l, \tag{73}$$

where μ is the reduced electron–hole mass. Equation (73) has the eigenfunctions

$$\phi_l(\mathbf{r}) = \exp(i\mathbf{k}_l \cdot \mathbf{r}). \tag{74}$$

The Fourier transform of Eq. (74) is a delta function in $\mathbf{k}$; therefore, the excited states are of the form

$$\Psi_n = \Phi_{\mathbf{k}_e = \mathbf{k}_l, \mathbf{k}_h = \mathbf{k}_l}. \tag{75}$$

This is a simple excited state consisting of a noninteracting electron–hole pair.

The optical absorption occurs at the photon energy

$$h\nu = \varepsilon_l = E_g + \frac{\hbar^2 k_l^2}{2\mu}. \tag{76}$$

The density of final states is given by

$$\rho(k_l) = \frac{k_l^2}{\pi^2}\frac{1}{|d\varepsilon_l/dk_l|} = \frac{\mu |k_l|}{\hbar^2 \pi^2}. \tag{77}$$

For allowed transitions the matrix element according to Eq. (36) becomes

$$H_{0,n} \approx A_0 H_{c,v}(0)\,\delta(\mathbf{K}) \tag{78}$$

and the absorption coefficient becomes

$$[\alpha h\nu] = \frac{2c\hbar}{n}\left(\frac{2\mu}{\hbar^2}\right)^{3/2} |H_{cv}(0)|^2 (h\nu - E_g)^{1/2} \equiv A(h\nu - E_g)^{1/2}. \tag{79}$$

The corresponding result for forbidden transitions is

$$[\alpha h\nu] = \frac{2c\hbar}{n}\left(\frac{2\mu}{\hbar^2}\right)^{5/2}\left|\frac{\partial[H_{c,v}(\mathbf{k})]}{\partial k}\right|^2_{\mathbf{k}=0}(h\nu - E_g)^{3/2}$$
$$\equiv A'(h\nu - E_g)^{3/2}. \tag{80}$$

We now consider the implications of the Kane model for the energy bands. According to the Kane model the absorption begins with direct transitions between the conduction band and the valence bands E_{v1} and E_{v2}. Both sets of transitions are allowed at $\mathbf{k} = 0$. The optical matrix element can be calculated for each set using the wave functions of Eqs. (59), (60), and (61) and averaging over all polarizations. The result of this calculation for each set is the same and is given by

$$|H_{c,v}(0)|^2 = \frac{2m^2P^2}{3\hbar^2}, \tag{81}$$

where P is the matrix element given by Eq. (69), and is nonzero. For increasing $\mathbf{k}$ the matrix element for each set decreases slowly according to

$$|H_{c,v}(\mathbf{k})|^2_{c,j} = |H_{c,v}(0)|^2\{(a_cc_j + c_ca_j)^2 + (a_cb_j - b_ca_j)^2\}, \tag{82}$$

where j refers to the valence bands $v1$, $v2$, and $v3$.

The density of states should be proportional to $|\mathbf{k}|$ for small $\mathbf{k}$ and should increase more rapidly at higher $\mathbf{k}$. The density of states for InSb can be calculated using Fig. 1. Because of the effect of the mass difference on the density of states the absorption will be dominated by transitions from the heavy-mass band $v1$, and we need only consider the variation of the matrix element between bands E_c and E_{v1}. This is given by

$$|H_{c,v}(\mathbf{k})|_{c,v1} = |H_{c,v}(0)|^2_{c,v1}a_c^2(k). \tag{83}$$

The variation of $a_c(k)$ is given by Eq. (63) and is shown for InSb in Fig. 2.

6. Experimental Results for Indium Antimonide

The results of absorption edge measurements of Gobeli and Fan[16] on pure InSb are shown in Fig. 3. Additional measurements have been made by Austin and McClymont[17] and Oswald and Schade.[18] The sharp threshold shown in Fig. 3 would tend to confirm the presence of allowed transitions. In Fig. 4 the spectral variation of the experimental data ($T = 5°K$) is compared to various theoretical predictions. The comparison of the

[16] G. W. Gobeli and H. Y. Fan, Semiconductor Research, Second Quarterly Report, Purdue Univ., 1956.

[17] I. G. Austin and D. R. McClymont, *Physica* **20**, 1077 (1954).

[18] F. Oswald and R. Schade, *Z. Naturforsch.* **9a**, 611 (1954).

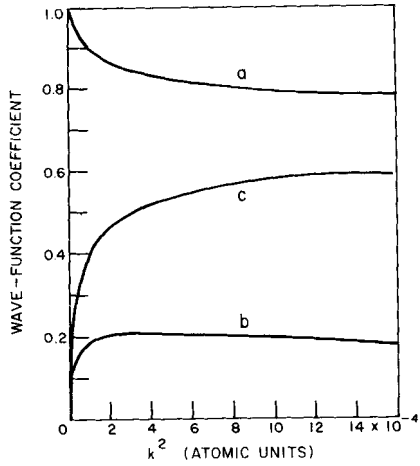


FIG. 2. Wave-function coefficients versus k^2 for the conduction band in indium antimonide. (After E. O. Kane.[14])

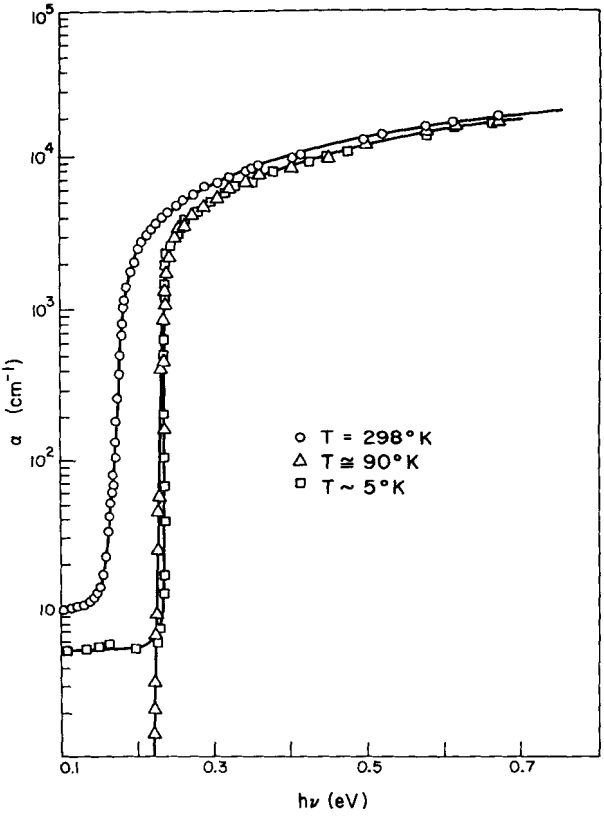


FIG. 3. Absorption edge of pure InSb. (After G. W. Gobeli and H. Y. Fan.[16])

experimental data to the absorption calculated on the basis of simple bands (curves *A* and *B*) clearly favors allowed transitions. However, a deviation from the experimental data occurs at higher photon energies. The Kane theory predicts that the density of states should increase more rapidly than for the case of simple bands. This consideration is taken into account in calculating curve *C* and results in too large a correction to fit the experimental data. The remaining discrepancy is removed by taking into account

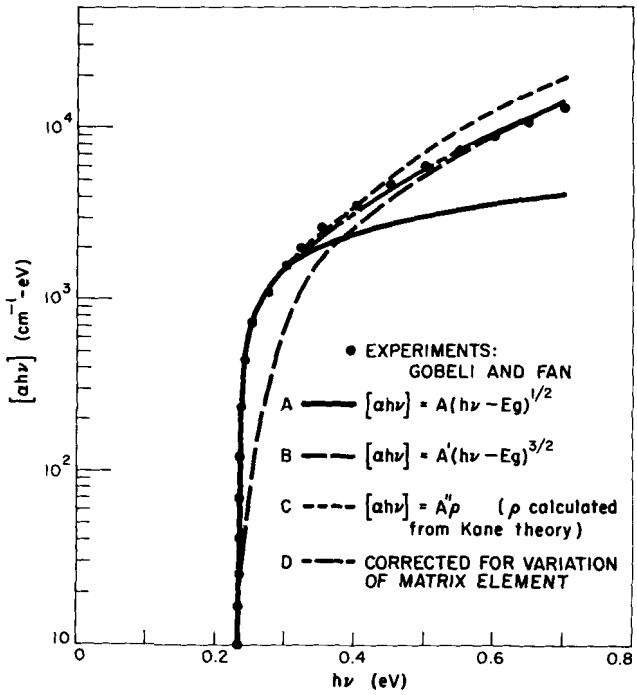


FIG. 4. Theoretical fit to the experimental absorption edge of InSb at ~5°K.

the decrease in the optical matrix element at higher photon energies predicted by Eq. (83). The resulting curve (*D*) fits the experimental data well. In obtaining this fit, however, we employed an arbitrary horizontal shift to the calculated curves. In Fig. 5 the experimental data of Gobeli and Fan are compared to the calculations of Kane[14] that do not include an arbitrary horizontal shift. The calculated absorption is a factor of about 1.5 too low. As will be seen later, this discrepancy is due principally to the neglect of exciton effects.

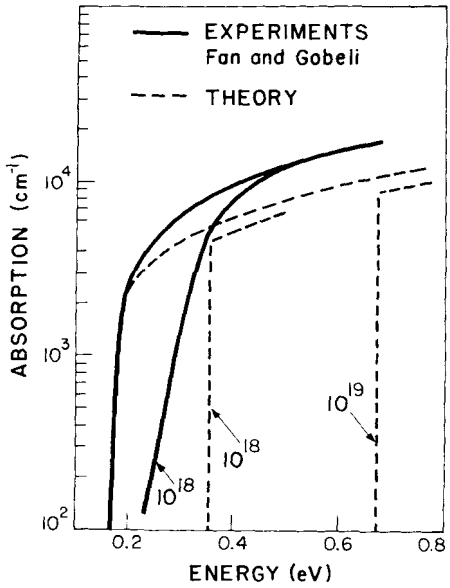


FIG. 5. Fundamental optical absorption in InSb at room temperature. Experimental data are due to Fan and Gobeli. (After E. O. Kane.[14])

7. OTHER III–V COMPOUNDS

Experimentally, Spitzer and Fan[19] and Dixon and Ellis[20] have obtained similar results for the absorption edge of pure InAs. Stern[21] has shown that the absorption is consistent with the Kane theory. From the theoretical fit, the parameters $E_g = 0.35$ and $m_c = 0.024m$ were obtained at room temperature. Measurements on n-type InAs have also been made by Matossi.[21a]

In the case of GaAs the energy gap and effective masses are larger than the corresponding quantities in InSb. The Kane theory would predict [see Eq. (41)] that the nonparabolic effects should be prominent only for much higher values of **k**. For this reason, Kudman and Seidel[22] were able to fit the absorption edge of pure GaAs above $\alpha = 9000\,\text{cm}^{-1}$, assuming parabolic bands as shown in Fig. 6. Moss and Hawkins[23] calculated the absorption for GaAs at room temperature, employing Kane theory and using the

[19] W. G. Spitzer and H. Y. Fan, *Phys. Rev.* **106**, 882 (1957).
[20] J. R. Dixon and J. M. Ellis, *Phys. Rev.* **123**, 1560 (1961).
[21] F. Stern, *Proc. Intern. Conf. Semicond. Phys., Prague, 1960* p. 363. Czech. Acad. Sci., Prague, and Academic Press, New York, 1961.
[21a] F. Matossi, *Z. Naturforsch*, **13a**, 767 (1958).
[22] I. Kudman and T. Seidel, *J. Appl. Phys.* **33**, 771 (1962).
[23] T. S. Moss and T. D. F. Hawkins, *Infrared Phys.* **1**, 111 (1962).

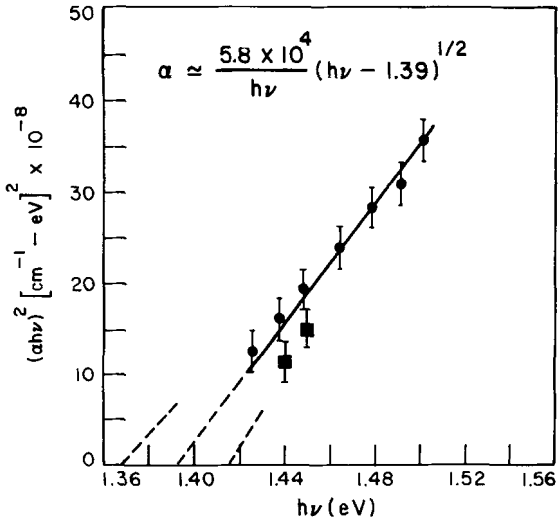


FIG. 6. Direct transition analysis on 10^{17} cm^{-3} p-type GaAs for absorption greater than 9000 cm^{-1}. Threshold energy is 1.39 ± 0.02 eV. Square points are for a second sample. (After I. Kudman and T. Seidel.[22])

parameters $E_g = 1.41$ eV, $\Delta = 0.33$ eV, $m_c = 0.072m$ and an average heavy-hole mass equal to $0.68m$. The results of the calculations are shown in Fig. 7, compared with experimental results. The good fit at high photon energies is surprising, considering that exciton effects were neglected. Below about 10^3 cm^{-1} the absorption decreases much more slowly than that predicted by the theory. The nature of this tail absorption will be discussed later. Sturge[24] has observed a step in the absorption at higher photon energies that corresponds to the onset of transitions between the conduction band and band E_{v3}. The results give $\Delta = 0.35$ eV.

Ramdas and Fan[25] studied the absorption edge in GaSb. Above 100 cm^{-1} the absorption has a spectral variation similar to that for InSb, indicating direct transitions. They obtain $E_g = 0.725$ eV at 300°K, 0.80 eV at ~80°K, and 0.81 eV at ~4.2°K. Below 100 cm^{-1} the absorption edge possesses a tail similar to that observed in GaAs.[25,26] In GaSb the authors found that the tail depends upon temperature and the doping of the sample. Additional measurements have been made by Blunt *et al.*[27] The measurements of Newman[28] on the absorption edge of InP are indicative of direct transitions

[24] M. D. Sturge, *Phys. Rev.* **127**, 768 (1962).
[25] A. K. Ramdas and H. Y. Fan, *Bull. Am. Phys. Soc.* **3**, 121 (1958).
[26] V. Roberts and J. E. Quarrington, *J. Electron.* **1**, 152 (1955).
[27] R. F. Blunt, W. R. Hosler, and H. P. R. Frederikse, *Phys. Rev.* **96**, 576 (1954).
[28] R. Newman, *Phys. Rev.* **111**, 1518 (1958).

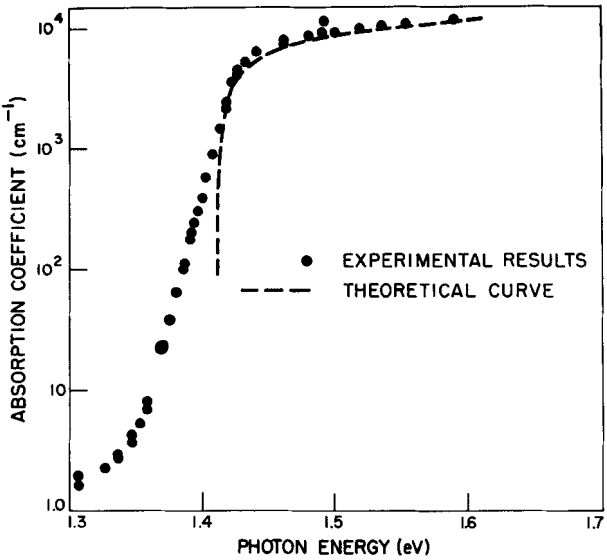


FIG. 7. Absorption edge of GaAs at room temperature. (After T. S. Moss and T. D. F. Hawkins.[23])

with a tail absorption of a nature similar to that in GaAs and GaSb. Other measurements on InP have been made by Oswald.[18,29]

The absorption edge of GaP shows a much different behavior. The results of Spitzer *et al.*[30] are shown in Fig. 8. The average absorption level is somewhat lower than that observed in the previous materials, which would seem to indicate a forbidden transition. The threshold is not sharp, which clearly rules out allowed transitions. In any case, it is obvious that in GaP at least one of the bands involved is different from those in the previous materials. As seen in Fig. 8, the experimental absorption does not appear to fit the theory for symmetry-forbidden transitions. As will be shown later, the spectral variation is closer to that expected for momentum-forbidden (indirect) transitions. Additional measurements of GaP have been made by Folberth and Oswald.[31] Measurements of the absorption in AlSb[2] and AlAs[2] seem to indicate a similar situation in these materials. Measurements on GaN,[32] AlN,[32] and BP[33] have not given any detailed information.

[29] F. Oswald, *Z. Naturforsch.* **9a**, 181 (1954).
[30] W. G. Spitzer, M. Gershenzon, C. J. Frosch, and D. F. Gibbs, *J. Phys. Chem. Solids* **11**, 339 (1959).
[31] O. G. Folberth and F. Oswald, *Z. Naturforsch.* **9a**, 1050 (1954).
[32] E. Kauer and A. Rabenau, *Z. Naturforsch.* **12a**, 942 (1957).
[33] B. Stone and D. Hill, *Phys. Rev. Letters* **4**, 282 (1960).

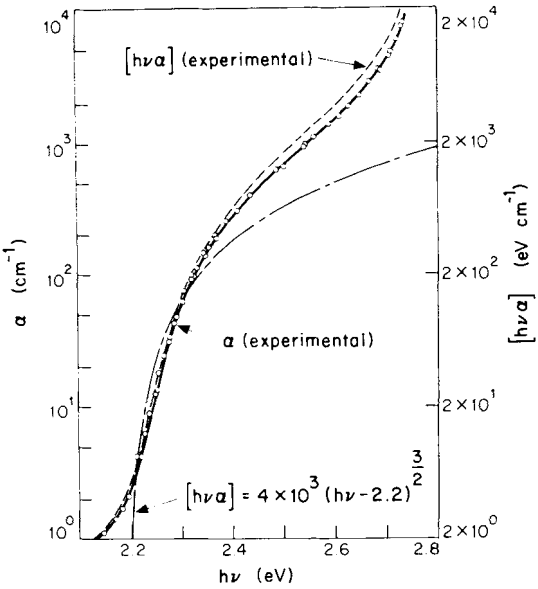


FIG. 8. Absorption edge of GaP at room temperature. The experimental data are due to Spitzer *et al.* (After W. G. Spitzer *et al.*[30])

8. FORBIDDEN TRANSITIONS

Examples of symmetry-forbidden transitions occur in the case of transitions between any two of the three valence bands E_{v1}, E_{v2}, E_{v3}. Calculation of the optical matrix element, using the wave functions given by Eqs. (60), (61), and (62), gives zero for any of the possible transitions. As $\mathbf{k}$ increases from zero, the wave functions corresponding to the bands E_{v2} and E_{v3} receive an admixture of s-like wave functions, giving rise to a nonzero contribution to the optical matrix element that is proportional to $|\mathbf{k}|$. The theory of such transitions has been discussed for Ge by Kahn[34] and by Kane.[35] The absorption requires the presence of holes and therefore is seen only in p-type material. The corresponding absorption has been observed in InSb,[36] InAs,[37,38] GaSb,[25] GaAs,[39,40] and AlSb.[41] An analysis of the effect in InAs utilizing Kane theory has been given by Matossi and Stern.[38]

[34] A. H. Kahn, *Phys. Rev.* **97**, 1647 (1955).
[35] E. O. Kane, *J. Phys. Chem. Solids* **1**, 83 (1956).
[36] W. Kaiser and H. Y. Fan, *Phys. Rev.* **98**, 966 (1955).
[37] F. Stern and R. M. Talley, *Phys. Rev.* **108**, 158 (1957).
[38] F. Matossi and F. Stern, *Phys. Rev.* **111**, 472 (1958).
[39] R. Braunstein and L. Magid, *Phys. Rev.* **111**, 480 (1958).
[40] R. Braunstein, *J. Phys. Chem. Solids* **8**, 280 (1959).
[41] R. Braunstein and E. O. Kane, *J. Phys. Chem. Solids* **23**, 1423 (1962).

9. Population Effects (The Absorption Edge in Degenerate Samples)

In the early studies of the fundamental absorption in InSb it was observed that the position of the edge had a strong variation from sample to sample.[42] This variation was correctly explained by Burstein[43] as being due to differences in the population of the energy bands with carriers. The appropriate density of final states in this case is

$$\rho(k) = \rho_0(k)\,[f_v(E_v - \zeta) - f_c(E_c - \zeta)], \tag{84}$$

where $\rho_0(k)$ is the density of final states without considering their occupation and f_v and f_c are the probabilities that the respective one-electron states are occupied. For degenerate material at $T = 0$ the population factor takes on a simple form for simple bands with spherical energy surfaces

$$(f_v - f_c) = \begin{cases} 0, & k < k_\zeta \\ 1, & k > k_\zeta \end{cases}. \tag{85}$$

In this case either all conduction-band states are filled up to those corresponding to the electron wave vector at the Fermi level, or the corresponding valence-band states are empty. The sum of such states is equal to the carrier concentration in either case, and for spherical energy surfaces is given by

$$n = \frac{2}{(2\pi)^3}\frac{4}{3}\pi k_\zeta^{\,3}. \tag{86}$$

The threshold for the optical formation of electron–hole pairs is

$$(h\nu)_t = E_g + \frac{\hbar^2 k_\zeta^{\,2}}{2\mu} = E_c(k_\zeta) - E_v(k_\zeta). \tag{87}$$

The quantity $(h\nu)_t$ actually corresponds to the case where $f_v - f_c = \frac{1}{2}$. At any finite temperature the absorption will rise to its full value in a range of approximately $4kT$. Consider n-type material. The absorption corresponding to a given value of k will be given by[6]

$$\alpha(k) = \alpha_0(k)\,(f_v - f_c) = \alpha_0(k)\left[1 - \frac{1}{\exp\{[\varepsilon_c(k) - \zeta]/kT\} + 1}\right], \tag{88}$$

where $\alpha_0(k)$ is the absorption in nondegenerate material, and ζ is measured from the bottom of the conduction band. We assume that the energy bands are unchanged by the addition of impurities. The photon energy corresponding to a given transition is

$$h\nu(k) = E_g + \varepsilon_c(k) - \varepsilon_v(k). \tag{89}$$

[42] M. Tanenbaum and H. B. Briggs, *Phys. Rev.* **91**, 1561 (1953).
[43] E. Burstein, *Phys. Rev.* **93**, 632 (1954).

On the other hand, we can treat α/α_0 as the independent variable, and Eq. (89) becomes

$$h\nu\left(\frac{\alpha}{\alpha_0}\right) = E_g + \varepsilon_c\left(\frac{\alpha}{\alpha_0}\right)\left[1 - \frac{\varepsilon_v(k)}{\varepsilon_c(k)}\right]. \tag{90}$$

Equation (88) can be used to determine $\varepsilon_c(\alpha/\alpha_0)$, and substitution in Eq. (90) gives

$$h\nu\left(\frac{\alpha}{\alpha_0}\right) = E_g + \left[\zeta + kT \ln\left(\frac{\alpha/\alpha_0}{1 - \alpha/\alpha_0}\right)\right]\left[1 - \frac{\varepsilon_v(k)}{\varepsilon_c(k)}\right]. \tag{91}$$

By expansion, Eq. (91) becomes

$$h\nu\left(\frac{\alpha}{\alpha_0}\right) \approx E_g + \zeta\left[1 - \frac{\varepsilon_v(k)}{\varepsilon_c(k)}\right] + 2kT\left[\left(2\frac{\alpha}{\alpha_0} - 1\right) + \frac{1}{3}\left(2\frac{\alpha}{\alpha_0} - 1\right)^3\right]. \tag{92}$$

This expansion holds in the range $0 < \alpha/\alpha_0 < 1$. For $\alpha/\alpha_0 = \frac{1}{2}$, Eq. (92) reduces to Eq. (88) and, in the approximation of Eq. (92), α/α_0 goes from 0 to 1 in a range of $16/3\,kT$. For parabolic bands the ratio $\varepsilon_v(k)/\varepsilon_c(k)$ is simply equal to the mass ratio m_c/m_v. Otherwise, it is usually a slowly varying function of k.

The situation becomes slightly more complicated when one considers the multiplicity of valence bands as in the Kane model. In such a case one must resolve the absorption into the components corresponding to each set of bands and apply Eq. (92) to each component. The situation can be visualized with reference to Fig. 9. At $T \approx 0$ the Fermi level separates the filled from the unfilled levels. For n-type material [Fig. 9(a)] interband transitions begin at the photon energy $h\nu_1$. These transitions involve the heavy-mass band, which dominates the absorption. The absorption does not reach its full value, however, until a photon energy $h\nu_2$, corresponding to the onset of transitions to the light-mass band $v2$. In principle, the two steps in absorption can be resolved if $h\nu_2 - h\nu_1 \gg kT$.

The situation in p-type material is just reversed. The absorption begins at a photon energy $h\nu_2$ [Fig. 9(b)] corresponding to the light-mass band. An additional effect occurs in p-type material. As the Fermi level moves deeper into the valence bands, holes appear at greater values of k in the $v1$ band. As a consequence, the maximum photon energy at which $v2$-to-$v1$ transitions can occur [$h\nu_{12}$ in Fig. 9(c)] becomes larger and can become comparable to $h\nu_1$. In this case, absorption associated with 2-to-1 transitions appears near the absorption edge.

a. Indium Antimonide

For a given sample the position of the Fermi level can be determined from the infrared absorption according to Eq. (92). The value of k_ζ can be

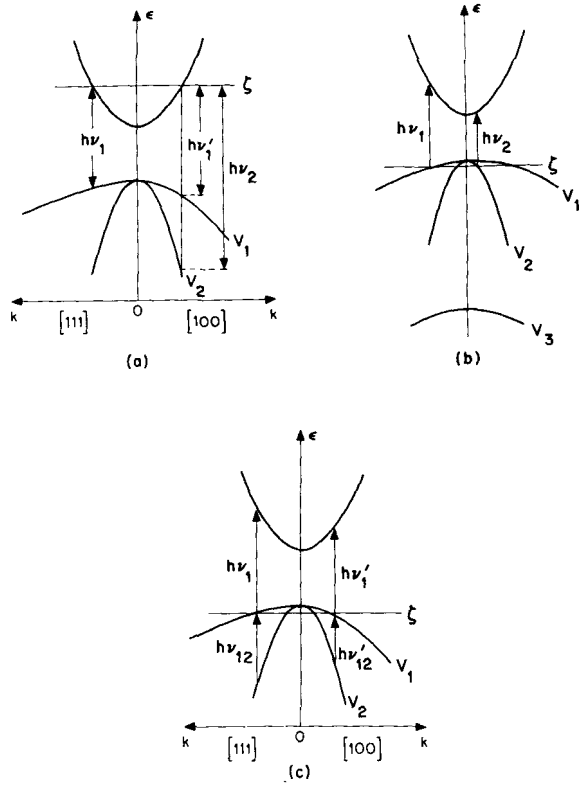


FIG. 9. Schematic diagram of energy bands of indium antimonide: (a) a warped V_1 band and the Fermi level of a degenerate n-type sample; (b) the Fermi level of a degenerate p-type sample; (c) a warped V_1 band and the Fermi level of a degenerate p-type sample. (After G. W. Gobeli and H. Y. Fan.[47])

determined from electrical measurements, using Eq. (86). Using a set of samples of different carrier concentrations one could, in principle, determine the conduction-band dispersion relation. The analyses of the results of Hrostowski *et al.*,[44] of Breckenridge *et al.*,[45] and of Kaiser and Fan[36] were made assuming simple parabolic bands. An electron effective mass of $m_e \approx 0.03m$ was obtained; however, the data were suggestive of an effective mass that increases with k. Cyclotron resonance measurements on purer samples,[46] which measure the effective mass corresponding to lower values of k, gave values in the range 0.013 to 0.015, tending to confirm the presence

[44] H. J. Hrostowski, G. H. Wheatley, and W. F. Flood, *Phys. Rev.* **95**, 1683 (1954).
[45] R. G. Breckenridge, R. F. Blunt, W. R. Hosler, H. P. R. Frederikse, J. H. Becker, and W. Oshinsky, *Phys. Rev.* **96**, 571 (1954).
[46] G. Dresselhaus, A. F. Kip, C. Kittel, and G. Wagoner, *Phys. Rev.* **98**, 556 (1955).

of a nonparabolic conduction band. Measurements of the reflectivity near the plasma edge yield values of the effective mass corresponding to k at the Fermi level. (See Chapter 10 by Palik and Wright.) Spitzer and Fan,[19] using such measurements, were able to establish that the conduction band in InSb is nonparabolic. These authors were able to show that the conduction-band dispersion relation determined by the reflectivity measurements was consistent with the previous results on the shift of the absorption edge. Such a nonparabolic conduction band, as discussed previously, is accounted for by the band model of Kane, and has been confirmed by many other experiments.

Gobeli and Fan[47] observed effects due to the complicated valence band. Their results for a sample with $n = 10^{18}\,\mathrm{cm}^{-3}$ at room temperature are shown in Fig. 5. The shape is in reasonable agreement with Eq. (91). The theoretical curve calculated by Kane that appears in the figure neglects the thermal spread in the electron population. The location of the $\alpha/\alpha_0 = \frac{1}{2}$ point is in reasonable agreement with the theory. The theoretically predicted step corresponding to the onset of transitions to the light-mass band is apparently obscured by the thermal spread in the electron population. Such steps in the absorption in n-type samples have been observed at helium temperature. Analysis of these steps assuming a parabolic $v2$ band yields $m_{v2} = 0.012m$.

The results on degenerate p-type samples are shown in Fig. 10. The absorption at low photon energies corresponds to transitions between the bands $v2$ and $v1'$, and the threshold moves to higher photon energies as the carrier concentration increases, in accordance with the previous discussion. For the purer samples both a threshold for light-hole transitions to the conduction band and a threshold for heavy-hole transitions are observed. For more impure samples the former becomes obscured by the $v2$-to-$v1$ transitions. Because of the difference in effective mass, $h\nu_1$ associated with the heavy-mass band is much more sensitive to a shift in the Fermi level.

A surprising feature of the absorption-edge measurements on degenerate material at low temperatures is that the thresholds are not as sharp as one would expect from Eq. (91). At 77°K the absorption edge of degenerate n-type samples sharpens up, compared to that at 300°K consistent with Eq. (91). For lower temperatures, however, no further sharpening occurs. The effect is much greater in p-type samples, where in some cases the threshold for heavy-hole transitions is spread over a range of ~ 0.3 eV. Gobeli and Fan interpret this as being due to warping of the $v1$ valence band, as predicted by the Kane theory.

[47] G. W. Gobeli and H. Y. Fan, *Phys. Rev.* **119**, 613 (1960).

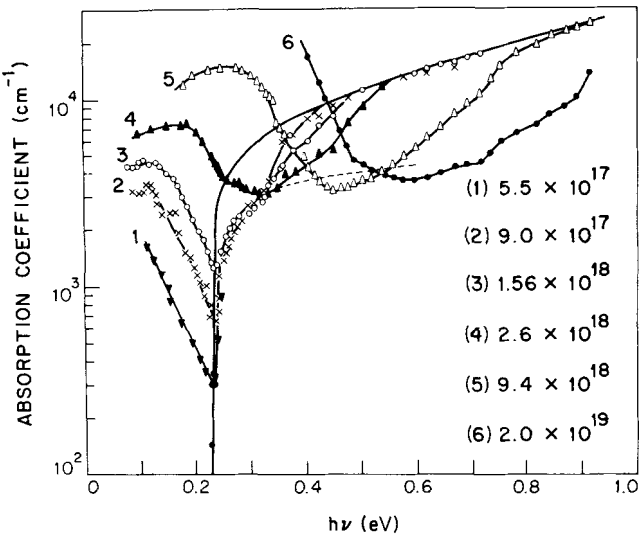


FIG. 10. Absorption coefficient at ~5°K as a function of photon energy for degenerate p-type InSb samples. (After G. W. Gobeli and H. Y. Fan.[47])

For warped energy surfaces there is, in general, no unique value of k_ζ. The values may, however, fall in a limited range ${}_1k_\zeta < k_\zeta < {}_2k_\zeta$. For $T \approx 0$,

$$(f_v - f_c) = \begin{cases} 0, & |\mathbf{k}| < {}_1k_\zeta \\ 1, & |\mathbf{k}| > {}_2k_\zeta \end{cases} \tag{93}$$

and follows a less general behavior for ${}_1k_\zeta < |\mathbf{k}| < {}_2k_\zeta$. The difference between n-type and p-type samples can be visualized with the aid of Fig. 9. In n-type samples, the threshold is spread between $h\nu_1$ and $h\nu_1'$ of Fig. 9(a). The situation for p-type samples is shown in Fig. 9(c), where the threshold is spread between $h\nu_1$ and $h\nu_1'$. Note that the effects of the warping are much greater in p-type samples due to $m_e \ll m_{v2}$.

Gobeli and Fan have analyzed the absorption in p-type material, assuming a $v1$ band given by Eq. (42). The warping is related to the quantity γ' of Eq. (42) since, for a given magnitude of $\mathbf{k}$, ε_{v1} will have a per cent variation given by $100 \times \gamma'$. From the fit to the experimental data they obtain $\gamma = 3\gamma' = 2$. This corresponds to about a 67% variation in the energies of the levels corresponding to a given magnitude of $\mathbf{k}$. This is comparable to the values of $\gamma = 1.2$–1.5 determined by Bagguley *et al.*[48]

[48] D. M. S. Bagguley, M. L. A. Robinson, and R. A. Stradling, *Phys. Letters* **6**, 143 (1963).

using cyclotron resonance and 1.4 determined by Zwerdling *et al.*[49] using interband magnetooptical absorption.

The warping appears to dominate the spread of the threshold, but there may be other factors that contribute. Impurity absorption involving transitions to the conduction band from impurity levels near the valence band may be present. Such absorption will be discussed in Part VI. Indirect (momentum-forbidden) transitions may also occur as discussed in Part IV. In this case the threshold of the absorption corresponds to the energy difference between the Fermi level and the distant band edge:

$$(h\nu)_t = E_g + \zeta. \tag{94}$$

The absorption could be expected to rise to its full value at the photon energy given by Eq. (87), which corresponds to allowed transitions.

There are other effects that could broaden the absorption threshold. The introduction of impurities may perturb the energy bands. In regard to Eq. (88) this amounts to saying that α_0 changes as impurities and carriers are added. A somewhat less interesting effect is that the samples may not be homogeneous and the values of k_ζ may vary throughout each sample. A special case of this would be the case where the energy bands bend up or down at the surface. In *n*-type material, if the bands bend up, the sample may be transparent in the bulk at lower photon energies, but absorb at the surface. This appears to be the case in degenerate *n*-type InAs.[50] As seen in Fig. 11 for absorption coefficients between ~ 1 and 2000 cm^{-1} the absorption coefficients calculated from the transmission assuming a homogeneous sample (curves 1–5) are roughly inversely proportional to the thickness. This would indicate that the absorption in this region occurs at the surface. This can occur if the bands bend up at the surface.

b. Indium Arsenide

A shift in the absorption edge due to the presence of carriers has been observed in InAs in earlier observations by Hrostowski and Tanenbaum,[51] by Stern and Talley,[52] and by Spitzer and Fan.[19] Dixon and Ellis[20] found a shift consistent with a density-of-states mass that varies with Fermi energy as calculated by Stern from Kane theory. The density-of-states mass was found to have the values $0.028m$ ($n = 6.0 \times 10^{17}$ cm^{-3}) and $0.038m$ ($n = 3.8 \times 10^{18}$ cm^{-3}). The authors found that the shape of the edge was given by Eq. (91) for temperatures down to 78°K.

[49] S. Zwerdling, W. H. Kleiner, and J. P. Theriault, *Proc. Intern. Conf. Phys. Semicond., Exeter, 1962* p. 455. Inst. of Phys. and Phys. Soc., London, 1962.

[50] E. J. Johnson, Ph.D. thesis, Purdue University, 1964 (to be published).

[51] H. J. Hrostowski and M. Tanenbaum, *Physica* **20**, 1065 (1954).

[52] F. Stern and R. M. Talley, *Phys. Rev.* **100**, 1638 (1955).

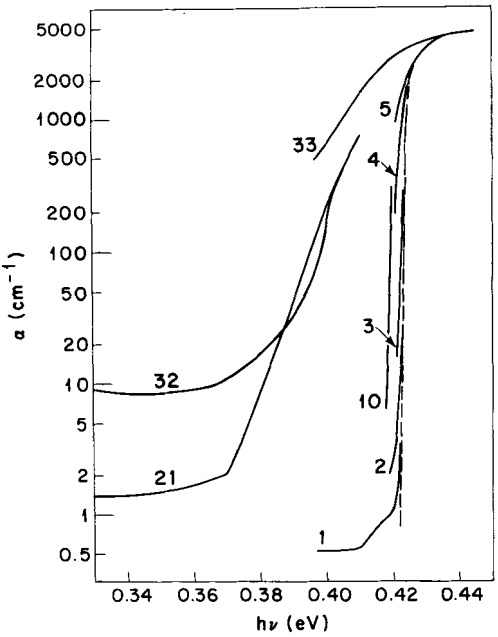


FIG. 11. The absorption edge of InAs showing the effect of surface absorption in degenerate material. Samples 1–5 were obtained from the same *n*-type material. The sample thicknesses are as follows: 1, 12 mm; 2, 1.59 mm; 3, 170 microns; 4, 26 microns; 5, 5.5 microns. Sample 10 is *n*-type with a lower carrier concentration. Samples 21, 32, and 33 are nondegenerate *p*-type material. (After E. J. Johnson.[50])

c. *Gallium Arsenide*

Kudman and Seidel[22] studied the absorption edge in degenerate *p*-type GaAs at room temperature. The absorption involving transitions between valence bands is relatively weak. A shift of the edge to higher photon energies with increased carrier concentration was observed. Structure due to the complicated valence band was not resolved, probably because of the high sample temperature. Kudman and Vieland[53] studied the edge shift in *n*-type GaAs. At room temperature the authors found the edge shift and the edge shape consistent with the calculation of the band parameters by Moss[54] using Kane's theory. Hill[55] extended the results on GaAs to 80°K. In addition to the effects observed by the previous workers, he observed effects of heavy doping which could not be explained on the basis of a

[53] I. Kudman and L. Vieland, *J. Phys. Chem. Solids* **24**, 967 (1963).
[54] T. S. Moss, *J. Appl. Phys. Suppl.* **32**, 2136 (1961).
[55] D. E. Hill, *Phys. Rev.* **133**, A866 (1964).

simple population of the band states. Other measurements have been made by Turner and Reese.[56]

d. Gallium Antimonide

Ramdas and Fan[25] and Becker *et al.*[57] studied the shift of the absorption edge in degenerate *n*-type GaSb. For low carrier concentrations their results are consistent with a conduction-band effective mass of $0.052m$. For higher concentrations they found that with increased doping ζ becomes pinned at a value near 0.08 eV. The authors attribute this effect to the presence of a second conduction-band minimum with a high density of states 0.08 eV above the lower minimum. Further evidence for such a secondary conduction-band minimum has been obtained from magnetoresistance, pressure dependence of resistance, Hall coefficient,[58] and infrared reflectivity,[59] among others.

IV. Effects Due to Scattering

10. The Form of the Optical Matrix Element in the Presence of Scattering

We now consider the effects on the fundamental absorption due to the departures from perfect periodicity that occur in a real crystal at a finite temperature. These departures are due to the existence of thermal lattice vibrations and the presence of lattice imperfections. In a perfect crystal, stationary electronic states exist that can be characterized by a unique wave vector. If departures from periodicity occur, states of different wave vector become mixed. An electron in a given state will be scattered, on the average, after a time equal to its relaxation time, giving a resulting uncertainty in the electron energy. Absorption or emission of thermal energy can occur in the scattering process, and the electronic wave vector in general will be changed after each collision.

It is not convenient to consider the scattering interactions in the manner described in Part II, and we use a different approach. If we consider the system of valence electrons and lattice ions, we can write

$$H = H_e + H_l + H_s, \tag{95}$$

where H_e involves only the electron coordinates and gives rise to the one-electron states discussed previously, H_l gives rise to the vibrational states

[56] W. J. Turner and W. E. Reese, *J. Appl. Phys.* **35**, 350 (1964).
[57] W. M. Becker, A. K. Ramdas, and H. Y. Fan, *J. Appl. Phys. Suppl.* **32**, 2094 (1961).
[58] A. Sagar, *Phys. Rev.* **117**, 93 (1960).
[59] M. Cardona, *J. Phys. Chem. Solids* **17**, 336 (1961).

of the lattice, and H_s gives the electron–lattice interactions. We consider the eigenstates of the unperturbed Hamiltonian $H_e + H_l$ and treat H_s as a perturbation. The eigenvalues of the zero-order Hamiltonian will be

$$\begin{aligned} E_0(l, \mathbf{k}) &= \langle l, \mathbf{k}|H_e + H_l|l, \mathbf{k}\rangle \\ &= E_e(l, \mathbf{k}) + \sum_\theta (n_\theta + \tfrac{1}{2})k\theta, \end{aligned} \tag{96}$$

where the $k\theta$ are the phonon energies and the n_θ are the corresponding phonon concentrations.

The wave functions in the presence of scattering can be obtained from perturbation theory, and can be written

$$|l, \mathbf{k}) = |l, \mathbf{k}\rangle + \sum_{l_\alpha} \sum_{\mathbf{k}_i} \frac{|l_\alpha, \mathbf{k}_i\rangle \langle l_\alpha, \mathbf{k}_i|H_s|l, \mathbf{k}\rangle}{E_0(l, \mathbf{k}) - E_0(l_\alpha, \mathbf{k}_i)}, \tag{97}$$

where $|l, \mathbf{k})$ is the wave function for an electron initially in band l with wave vector $\mathbf{k}$, and $|\rangle$ denote unperturbed wave functions. The matrix element $\langle l_\alpha, \mathbf{k}_i|H_s|l, \mathbf{k}\rangle$ is related to the probability that an electron initially in band l with wave vector $\mathbf{k}$ is scattered to a state in band l_α with wave vector $\mathbf{k}_i$. The denominator is the energy difference between the unperturbed states.

We consider the optical matrix element between a state $|v, \mathbf{k})$ given by Eq. (97) and a similar state $(c, \mathbf{k}'|$. This follows readily:

$$\begin{aligned} &(c, \mathbf{k}'|H_0|v, \mathbf{k}) \\ &= \langle c, \mathbf{k}'|H_0|v, \mathbf{k}\rangle \\ &\quad + \sum_{l_\alpha} \sum_{\mathbf{k}_i} \frac{\langle c, \mathbf{k}'|H_0|l_\alpha, \mathbf{k}_i\rangle \langle l_\alpha, \mathbf{k}_i|H_s|v, \mathbf{k}\rangle}{E_0(v, \mathbf{k}) - E_0(l_\alpha, \mathbf{k}_i)} \\ &\quad + \sum_{l_\beta} \sum_{\mathbf{k}_j} \frac{\langle c, \mathbf{k}'|H_s|l_\beta, \mathbf{k}_j\rangle \langle l_\beta, \mathbf{k}_j|H_0|v, \mathbf{k}\rangle}{E_0(c, \mathbf{k}') - E_0(l_\beta, \mathbf{k}_j)}. \end{aligned} \tag{98}$$

Substituting from Eq. (27), this can be written

$$\begin{aligned} &(c, \mathbf{k}'|H_0|v, \mathbf{k}) \\ &= A_0 H_{c,v}(\mathbf{k})\, \delta(\mathbf{K}) \\ &\quad + A_0 \sum_{l_\alpha} \frac{H_{c,l_\alpha}(\mathbf{k}') \langle l_\alpha, \mathbf{k}'|H_s|v, \mathbf{k}\rangle}{E_0(v, \mathbf{k}) - E_0(l_\alpha, \mathbf{k}')} \\ &\quad + A_0 \sum_{l_\beta} \frac{\langle c, \mathbf{k}'|H_s|l_\beta, \mathbf{k}\rangle\, H_{l_\beta,v}(\mathbf{k})}{E_0(c, \mathbf{k}') - E_0(l_\beta, \mathbf{k})}. \end{aligned} \tag{99}$$

The first term involves no scattering and is unchanged in form from the result of the simple theory. This corresponds to allowed transitions if

$H_{c,v}(0)$ is nonzero. The terms following the first correspond to forbidden transitions, since $\mathbf{K} \neq 0$. The second term involves scattering to an intermediate state $\langle l_\alpha, \mathbf{k}'|$, which is vertically above or below the conduction-band state, followed by an optical excitation to the conduction band. The third term involves an optical excitation to an intermediate state vertically above or below the valence band state, followed by a scattering to the final state in the conduction band. There is no requirement to conserve energy in the intermediate state, but the denominator favors intermediate states that tend to conserve energy in the optical excitation. Generally, it is sufficient to consider only the intermediate states closest in energy to the initial and final states, and it is sufficient to use only one term in the summation over bands. For scattering involving the absorption (H_s^+) and emission (H_s^-) of phonons, Eq. (99) can be written in the form

$$\begin{aligned}
&(l', \mathbf{k}'|H_0|l, \mathbf{k}) \\
&\quad \approx A_0 H_{c,v}(\mathbf{k})\, \delta(\mathbf{K}) \\
&\qquad + A_0 \frac{H_{c,l_\alpha}(\mathbf{k}')\langle l_\alpha, \mathbf{k}'|H_s^+|v, \mathbf{k}\rangle}{E_e(v, \mathbf{k}) - E_e(l_\alpha, \mathbf{k}') - k\theta} + A_0 \frac{H_{c,l_\alpha}(\mathbf{k}')\langle l_\alpha, \mathbf{k}'|H_s^-|v, \mathbf{k}\rangle}{E_e(v, \mathbf{k}) - E_e(l_\alpha, \mathbf{k}') + k\theta} \\
&\qquad + A_0 \frac{\langle c, \mathbf{k}'|H_s^+|l_\beta \mathbf{k}\rangle H_{l_\beta,v}(\mathbf{k})}{E_e(c, \mathbf{k}') - E_e(l_\beta, \mathbf{k}) + k\theta} + A_0 \frac{\langle c, \mathbf{k}'|H_s^-|l_\beta, k\rangle H_{l_\beta,v}(\mathbf{k})}{E_0(c, \mathbf{k}') - E_e(l_\beta, \mathbf{k}) - k\theta}.
\end{aligned} \tag{100}$$

Now we consider the energy of the states as perturbed by the scattering. From Eq. (97) we obtain for the electron energy

$$\begin{aligned}
E_e'(l, \mathbf{k}) &= \langle l, \mathbf{k}|H|l, \mathbf{k}\rangle = \langle l, \mathbf{k}|H_e + H_s|l, \mathbf{k}\rangle \\
&= E_e(l, \mathbf{k}) + \sum_{l_\alpha} \sum_{\mathbf{k}_i} \frac{\langle l, \mathbf{k}|H_s|l_\alpha, \mathbf{k}_i\rangle\langle l_\alpha, \mathbf{k}_i|H_s|l, \mathbf{k}\rangle}{E_0(l, \mathbf{k}) - E_0(l_\alpha, \mathbf{k}_i)}.
\end{aligned} \tag{101}$$

The last term is the so-called electron self-energy, which arises from virtual transitions of the electron to intermediate states. For the case of phonon scattering this is accompanied by the virtual emission and absorption of phonons. The last term can be written

$$E_s(l, \mathbf{k}) \equiv \sum_{l_\alpha} \sum_{\mathbf{k}_i} \frac{|\langle l, \mathbf{k}|H_s|l_\alpha, \mathbf{k}_i\rangle|^2}{E_0(l, \mathbf{k}) - E_0(l_\alpha, \mathbf{k}_i)}. \tag{102}$$

Note that two electron states that are coupled through such an interaction repulse one another. From the form of the denominator one would expect the nearby states to be most effective. Therefore, the states near the bottom of a band would generally be expected to be depressed, whereas those near the top of a band would generally be expected to rise. The photon energy

corresponding to an allowed transition of wave vector $\mathbf{k}$ would be given by

$$h\nu(\mathbf{k}) = E_e'(c, \mathbf{k}) - E_e'(v, \mathbf{k})$$

$$= [E_e(c, \mathbf{k}) - E_e(v, \mathbf{k})] + [E_s(c, \mathbf{k}) - E_s(v, \mathbf{k})]. \tag{103}$$

The terms set off by the first set of brackets correspond to the energy of the electron–hole pair in the absence of scattering. The second term for $\mathbf{k} = 0$ gives the shift of the absorption edge due to the self-energy effect.

The threshold for the fundamental absorption can also be shifted by the presence of transitions forbidden by the selection rule $\mathbf{K} = 0$. This is obviously the case if no transitions are allowed by the selection rule for photon energies corresponding to the energy gap. For the case of a direct gap, the absorption threshold can be broadened by scattering. If the scattering is elastic and the material is not degenerate, the threshold for forbidden transitions is identical to that for allowed transitions. The threshold for forbidden transitions can be shifted to lower photon energies by transitions involving phonon absorption. Generally, the shift will be dominated by transitions involving optical phonon absorption, since the corresponding acoustic phonons will have much lower energies. At higher photon energies the absorption will be dominated by allowed transitions.

An additional shift of the absorption threshold can occur in degenerate material. For simplicity consider elastic scattering. The threshold for allowed transitions occurs at $(h\nu)_t = E_g + \varepsilon_c(k_\zeta) - \varepsilon_v(k_\zeta)$, whereas with impurities to supply the additional crystal momentum the threshold can be shifted to $(h\nu)_t = E_g + \zeta$.

11. The Form of the Scattering Matrix Elements

We now consider the form taken by the scattering matrix elements in specific cases. For detailed discussion of electron scattering in the III–V compounds the reader should refer to the article by Ehrenreich.[60]

a. Ionized-Impurity Scattering

We consider first the case of scattering by an ionized impurity that is screened by free carriers.[61] For this case

$$H_s = \frac{e^2}{\kappa|\mathbf{r}|} e^{-\lambda|\mathbf{r}|}, \tag{104}$$

where λ is the reciprocal of the Debye screening length. The corresponding

[60] H. Ehrenreich, *J. Phys. Chem. Solids* **2**, 131 (1957).

[61] J. M. Ziman, "Principles of the Theory of Solids," p. 131. Cambridge Univ. Press, London and New York, 1964.

matrix element is given by

$$\langle l', \mathbf{k}'|H_s|l, \mathbf{k}\rangle = \frac{4\pi e^2}{\kappa(q^2 + \lambda^2)}\delta(\mathbf{K} + \mathbf{q})$$
$$\approx \frac{4\pi e^2}{\kappa\lambda^2} \qquad q < \lambda$$
$$\approx 0 \qquad q > \lambda, \tag{105}$$

where $\hbar\mathbf{q} = \hbar\mathbf{k} - \hbar\mathbf{k}'$ is the crystal momentum contributed by the impurity center.[61a] The principal effect of impurity scattering is to relax the selection rule $\mathbf{K} = 0$ to $|\mathbf{K}| \lesssim \lambda$. Since the scattering is elastic, no shift of the absorption threshold occurs in nondegenerate samples except that due to the self-energy.

b. Optical-Phonon Scattering

Longitudinal optical phonons[62] scatter principally through the polar interaction as screened by the free carriers. For this case,[60,62a]

$$\langle l', \mathbf{k}'|H_s^{\pm}|l, \mathbf{k}\rangle = \begin{cases} 4\pi eF\dfrac{q}{q^2 + \lambda^2}(n_\mathbf{q} + 1)^{1/2}\,\delta(\mathbf{K} + \mathbf{q}) \\ 4\pi eF\dfrac{q}{q^2 + \lambda^2}(n_\mathbf{q})^{1/2}\,\delta(\mathbf{K} - \mathbf{q}) \end{cases} \tag{106}$$

Here $\mathbf{q}$ is the phonon wave vector and

$$F^2 = \frac{\omega_l}{8\pi}\left[\frac{1}{\kappa_\infty} - \frac{1}{\kappa_0}\right], \tag{107}$$

where the dielectric constant κ_0 includes electronic and ionic polarizabilities, and κ_∞ includes only the electronic contribution. The matrix elements in Eq. (106) correspond respectively to the emission and to the absorption of an optical phonon. Conservation of energy between the initial and final states requires at the threshold

$$h\nu = E_g' \pm k\theta, \tag{108}$$

where E_g' contains the self-energy terms and $k\theta$ is the energy of the phonon absorbed or emitted. Note that optical absorption involving the absorption of a phonon shifts the absorption threshold to lower photon energies. Absorption involving the emission of an optical phonon occurs at higher

[61a] This use of $\mathbf{q}$ is distinct from our previous usage as the photon wave vector.

[62] Transverse optical phonons do not produce the large lattice polarization necessary for coupling to electrons.

[62a] C. Kittel, "Quantum Theory of Solids," p. 140. Wiley, New York, 1963.

photon energies. However, if allowed transitions are present such absorption is overwhelmed by absorption due to allowed transitions. Absorption involving phonons will have a temperature dependence due to the factor $n_{\mathbf{q}}$ in Eq. (106), which is the equilibrium concentration of phonons in mode $\mathbf{q}$ and is given by

$$n_{\mathbf{q}} = \frac{1}{\exp(\theta_{\mathbf{q}}/T) - 1}. \tag{109}$$

c. Acoustic-Phonon Scattering

The long-wavelength acoustic phonons scatter principally through the deformation-potential interaction. The matrix element for scattering by longitudinal acoustic phonons is[63]

$$\langle l', \mathbf{k}'|H_s^{\pm}|l, \mathbf{k}\rangle = \begin{cases} \left[\frac{C_1^2|\mathbf{q}|}{2\rho C_s}\right]^{1/2} (n_{\mathbf{q}} + 1)^{1/2}\, \delta(\mathbf{K} + \mathbf{q}) \\ \left[\frac{C_1^2|\mathbf{q}|}{2\rho C_s}\right]^{1/2} (n_{\mathbf{q}})^{1/2}\, \delta(\mathbf{K} - \mathbf{q}) \end{cases}, \tag{110}$$

where C_1 is the deformation-potential constant and C_s is the longitudinal sound velocity.

12. Absorption Corresponding to an Indirect Gap

In general, the spectral variation of absorption forbidden by the selection rule $\mathbf{K} = 0$ will depend intimately upon the details of the band structure and the details of the scattering processes. However, we shall consider first a case in which such details are not so important. This is the case in which the corresponding allowed transitions occur at much higher photon energies. This situation is illustrated schematically in Fig. 12. The threshold for allowed transitions between the valence-band maximum and the conduction-band minimum at (000) occur at much higher photon energies than the threshold for forbidden transitions between the valence-band maximum at (000) and the conduction-band minimum at (111). We now consider the absorption corresponding to transitions of the latter type, which have been calculated by Cheeseman[64] and by Hall, Bardeen, and Blatt.[4,65]

First consider the optical matrix element for such transitions as given by the last two terms of Eq. (99). For simplicity we consider only the last term. If optical transitions to the intermediate states are allowed at $\mathbf{K} = 0$ we can

[63] C. Kittel, "Quantum Theory of Solids," p. 134. Wiley, New York, 1963.
[64] I. C. Cheeseman, *Proc. Phys. Soc. (London)* **A65**, 25 (1952).
[65] L. H. Hall, J. Bardeen, and F. J. Blatt, *Phys. Rev.* **95**, 559 (1954).

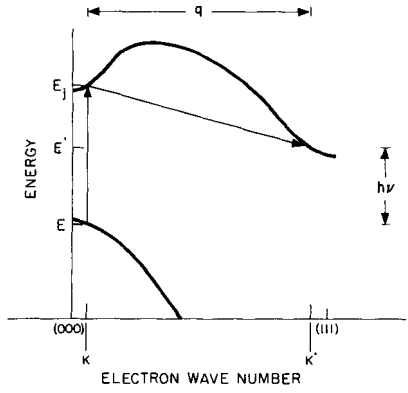


FIG. 12. Schematic diagram of an energy-band structure giving rise to an indirect absorption edge.

set $H_{l,v}(\mathbf{k}) = H_{l,v}(0)$. For transitions near the threshold neither the energy denominator nor the amount of crystal momentum required for the transition varies much. Therefore, each can be replaced by an average. The optical matrix element then becomes

$$(c, \mathbf{k}'|H_0|v, \mathbf{k}) = \frac{\langle c, \mathbf{k}'|H_s|l, \mathbf{k}\rangle_{\text{ave}} H_{l,v}(0)}{[E_0(l', \mathbf{k}') - E_0(l_\beta, \mathbf{k})]_{\text{ave}}} \equiv H'_{c,v} \tag{111}$$

and is approximately constant for all transitions near the threshold.

The probability for the absorption of a photon of energy ($h\nu$) can be written

$$w(h\nu) = \frac{2\pi}{\hbar}|H'_{c,v}|^2 \rho(h\nu), \tag{112}$$

where $\rho(h\nu)$ is the density of states consisting of an electron in the conduction band and a hole in the valence band separated by an energy $h\nu$. This is given by

$$\rho(h\nu) = \int_0^\infty dE_c \int_0^\infty \rho_c \rho_v \, \delta(E_c - E_v - h\nu)\, dE. \tag{113}$$

The first integration gives

$$\rho(h\nu) = \int_0^{h\nu - E_g} \rho_c \rho_v \, dE_c. \tag{114}$$

For parabolic bands,

$$\rho_c = \frac{N}{2\pi^2}\left(\frac{2m_c}{\hbar^2}\right)^{3/2} \varepsilon_c^{1/2}, \qquad \rho_v = \frac{1}{2\pi^2}\left(\frac{2m_v}{\hbar^2}\right)^{3/2} \varepsilon_v^{1/2}, \tag{115}$$

where m_c and m_v are appropriate density-of-states effective masses and N is the number of identical minima corresponding to different crystalline directions. Integration of Eq. (114) gives

$$\rho(h\nu) = \frac{N}{4\pi^4}\left(\frac{2}{\hbar^2}\right)^3 m_c^{3/2} m_v^{3/2} B'(h\nu - E_g)^2, \tag{116}$$

where

$$B' = \int_{-1/2}^{+1/2}\left(\frac{1}{4} - x^2\right)^{1/2} dx = \frac{\pi}{4}. \tag{117}$$

The absorption coefficient is then of the form

$$[\alpha h\nu] = B(h\nu - E_g)^2. \tag{118}$$

If transitions to the intermediate states are forbidden at $\mathbf{k} = 0$, then using the same approach one obtains a cubic dependence.

We have previously noted that the spectral variation of the absorption near the absorption edge of GaP cannot be fitted with allowed transitions. The same data (Spitzer *et al.*)[30] are plotted in Fig. 13, where they are compared to the absorption predicted by Eq. (118). A reasonable fit is obtained, indicating that the transitions are indirect and that the energy gap in GaP corresponds to band extrema that are at different points in the Brillouin zone. The arbitrary horizontal shift needed to fit the data yields a value of 2.21 eV for the energy gap. The quadratic energy dependence also indicates that the transitions corresponding to the band extrema at $\mathbf{k} = 0$ are allowed the same as in InSb.

At higher photon energies the experimental absorption increases somewhat faster than given by Eq. (118). This discrepancy probably results from the assumption of a constant-energy denominator in Eq. (111) as the photon energy approaches the threshold for the allowed transitions.

Mead and Spitzer[2] have observed the fundamental absorption in AlAs and AlSb by utilizing the photovoltaic response of a surface-barrier junction. The response due to the fundamental absorption is superimposed upon a background due to other effects. In AlAs at 300°K they observed a rise of the photovoltaic response above the background that varies as $(h\nu - 2.1)^2$ as shown in Fig. 14. The corresponding absorption apparently involves an indirect gap of 2.1 eV. At higher photon energies the response increases more rapidly, indicating a threshold for direct transitions and a direct gap of $\sim$2.9 eV.

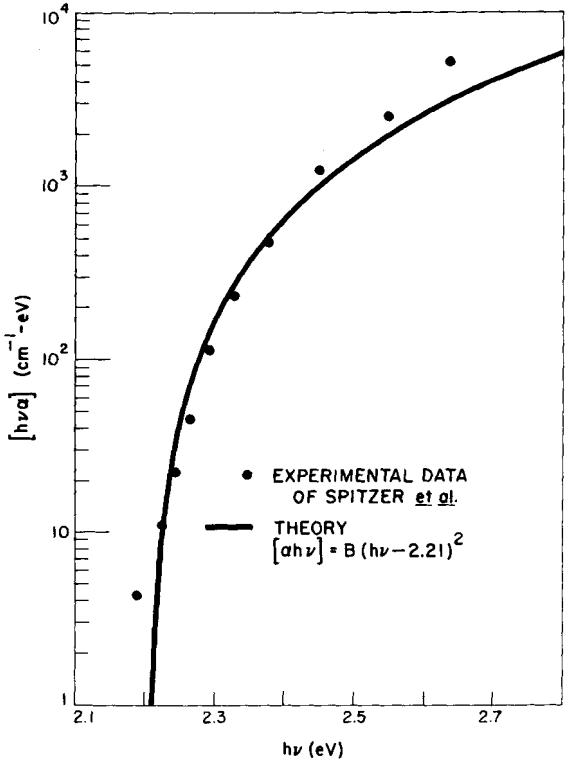


FIG. 13. Comparison of the experimental data for the absorption edge of GaP with the theory for an indirect edge. The experimental data are due to Spitzer *et al.* (After W. G. Spitzer *et al.*[30])

The band gap in AlSb is expected to be indirect. However, the fundamental absorption as observed in transmission[66,67] or as photovoltaic response (Fig. 14) does not show a region of absorption that is strictly quadratic in photon energy. Additional results similar to those on AlAs have been observed by Spitzer and Mead on the system $Ga(As_{1-x}P_x)$ using the photovoltaic response.[68]

13. PHONON STRUCTURE

Absorption involving momentum-forbidden transitions has a set of different thresholds corresponding to different types of scattering. Consider a band structure such as that of GaP, where the change of crystal momentum of the electron is large for transitions near the threshold. For such

[66] R. F. Blunt, H. P. R. Frederikse, J. H. Becker, and W. R. Hosler, *Phys. Rev.* **96**, 578 (1954).
[67] W. J. Turner and W. E. Reese, *Phys. Rev.* **117**, 1003 (1960).
[68] W. G. Spitzer and C. A. Mead, *Phys. Rev.* **133**, A872 (1964).

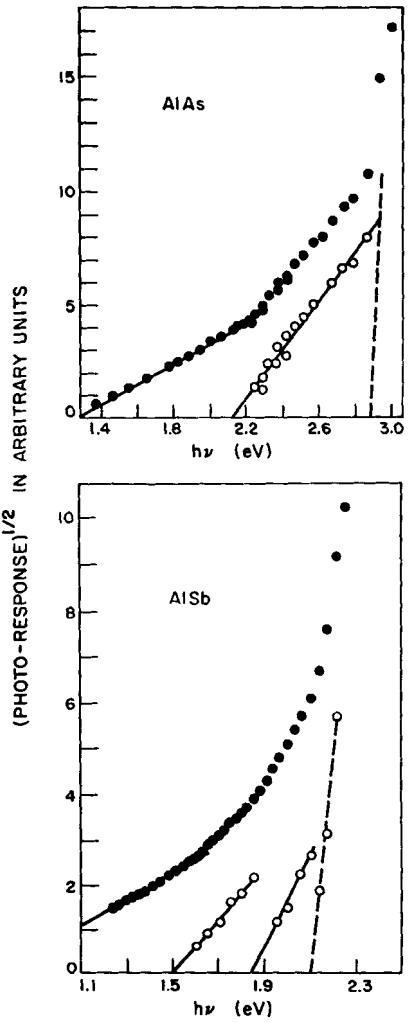


FIG. 14. Photovoltaic response of surface-barrier contacts on AlAs and AlSb. The straight lines are the result of a subtraction procedure based on the assumption of several monotonic components, each varying as the square of the photon energy. (After C. A. Mead and W. G. Spitzer.[2])

transitions the scattering system must supply a certain momentum $\mathbf{q}_0 \approx \mathbf{k}(111)$ (see Fig. 12). Conservation of energy between the initial and final states for the case of phonon scattering gives

$$(h\nu)_t = E_g \pm k\theta_{\mathbf{q}_0}, \tag{119}$$

whereas elastic scattering gives

$$(h\nu)_t = E_g. \tag{120}$$

In general, one can expect two thresholds for each phonon branch and one for elastic scattering. As will be seen later, the thresholds are sharpened by exciton effects.

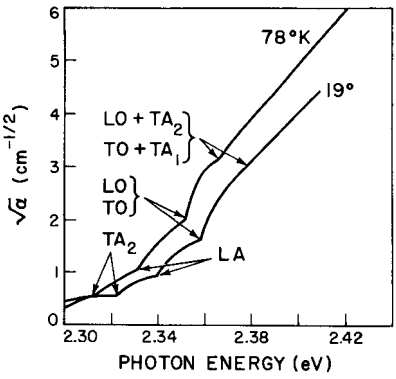


FIG. 15. Absorption spectra at the edge of GaP, showing thresholds associated with the emission of each of several different phonons. (After M. Gershenzon *et al.*[70])

Phonon structure on the absorption edge of GaP was first observed by Gross *et al.*[69] This structure was interpreted by Gershenzon *et al.*[70] in terms of phonon energies previously determined by Kleinman and Spitzer.[71] The absorption threshold labeled TA_2 in Fig. 15 was arbitrarily associated with the emission of the TA_2 phonon. At the low temperatures used, no thresholds due to phonon absorption were observed. The thresholds corresponding to the other phonons were then derived from the TA_2 threshold and the given phonon energies. Reasonable agreement was obtained between the remaining thresholds and the calculated values. These results confirm the analysis of Spitzer *et al.*[30] attributing the absorption to indirect transitions.

[69] E. F. Gross, G. K. Kaluzhnaya, and D. S. Nodzvetskii, *Fiz. Tverd. Tela* **3**, 3543 (1961) [*English Transl.*: *Soviet Phys.-Solid State* **3**, 2573 (1962)].

[70] M. Gershenzon, D. G. Thomas, and R. E. Dietz, *Proc. Intern. Conf. Phys. Semicond., Exeter, 1962* p. 752. Inst. of Phys. and Phys. Soc., London, 1962.

[71] D. A. Kleinman and W. G. Spitzer, *Phys. Rev.* **118**, 110 (1960).

14. Phonon Broadening of the Absorption Edge Corresponding to Allowed Transitions

The absorption edge corresponding to allowed transitions will be shifted due to the electron self-energy resulting from scattering. The discussion of such shifts will be postponed to Part V, and we consider now the shift that results from the absorption of optical phonons, the shift due to acoustic phonons being negligible. Optical phonons have little dispersion, and it is a good approximation to assume that all longitudinal optical phonons in a small range near $\mathbf{q} = 0$ have the same energy. The effect of TO phonons will be slight because of the much lower coupling. Below the threshold for allowed transitions the optical matrix element will be given by

$$|(c, \mathbf{k}'|H_0|v, \mathbf{k})| \approx H_{c,v}(0)\frac{(4\pi eF)\,|\mathbf{k}' - \mathbf{k}|}{|\mathbf{k}' - \mathbf{k}|^2 + \lambda^2}\left[\frac{1}{E_c(\mathbf{k}') - E_v(\mathbf{k}) - h\nu}\right.$$
$$\left. + \frac{1}{h\nu - E_c(\mathbf{k}) - E_v(\mathbf{k})}\right]\frac{1}{(e^{\theta/T} - 1)^{1/2}}. \tag{121}$$

In contrast to the previous situation, the optical matrix element varies strongly among the transitions possible near the threshold.

The probability that a phonon ($h\nu$) will be absorbed is obtained by summing over all pairs of states $\langle l', \mathbf{k}'|$ and $|l, \mathbf{k}\rangle$ giving

$$w(h\nu) = \frac{2\pi}{\hbar}\sum_{c,\mathbf{k}'}\sum_{v,\mathbf{k}}|(c, \mathbf{k}'|H_0|v, \mathbf{k})|^2\,\delta(h\nu + k\theta - E_{c,\mathbf{k}'} + E_{v,\mathbf{k}}). \tag{122}$$

The absorption coefficient is obtained in the usual manner.

We have shown that the bulk of the fundamental absorption in InSb can be attributed to allowed transitions. However, Roberts and Quarrington[26] have observed a tail on the absorption edge at low absorption levels that is not provided for in the theory of allowed transitions (see Fig. 16). Dumke[72] attributed this absorption to transitions involving the absorption of a longitudinal optical phonon, and calculated the absorption along the lines described above. The variation of the intensity of the absorption with temperature follows closely the factor $(e^{\theta/T} - 1)^{-1}$ with $\theta = 290°\text{K}$. The corresponding phonon energy is in good agreement with the reststrahlen reflectivity measurements of Spitzer and Fan.[73] Below 80°K the absorption fails to follow the characteristic temperature dependence. This indicates that other absorption processes dominate the absorption at low temperature.

The agreement of the theory with the spectral shape of the absorption is not as satisfactory. Dumke calculated the absorption along the lines described above but ignoring screening effects. This corresponds to setting

[72] W. P. Dumke, *Phys. Rev.* **108**, 1419 (1957).
[73] W. G. Spitzer and H. Y. Fan, *Phys. Rev.* **99**, 1893 (1955).

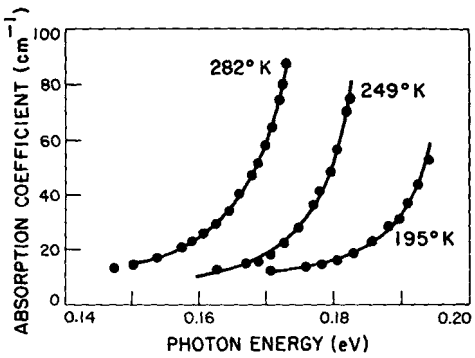


FIG. 16. Comparison of experimental absorption data on InSb, as indicated by circles, with theoretical absorption curves calculated by Dumke. The experimental data are due to Roberts and Quarrington. (After V. Roberts and J. E. Quarrington[26] and W. P. Dumke.[72])

$\lambda = 0$ in Eq. (106). He could not fit the data using such a scattering matrix element. The fit to theory shown in Fig. 16 was obtained assuming a matrix element for scattering that is independent of $\mathbf{k}$ and $\mathbf{k}'$.

Kurnick and Powell[74] extended the measurements to single-crystal specimens and found that if the background is subtracted the fundamental absorption follows the empirical relation

$$\alpha = \alpha_0 \exp \frac{(h\nu - h\nu_0)}{kT}, \tag{123}$$

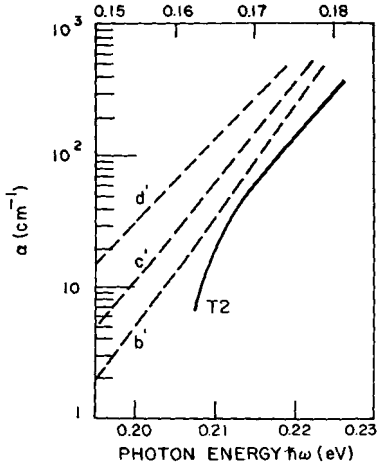


FIG. 17. Comparison of theory, including screening effects, and experiment for the absorption-edge tail in InSb. (After S. W. Kurnick and J. M. Powell.[74])

[74] S. W. Kurnick and J. M. Powell, *Phys. Rev.* **116**, 597 (1959).

where α_0 and $h\nu_0$ are empirical constants. Their results for three specimens are shown in Fig. 17. The shift in the edge between samples is probably not related to the scattering process and will be discussed later. The authors further extended the theory involving polar scattering by taking into account carrier screening. Their theoretical results are given by the solid curve T_2 in Fig. 17. The curve T_2 should be given an arbitrary horizontal displacement to obtain the best fit to the data. The theoretical fit to the data is reasonable and tends to support the interpretation of the tail absorption in InSb at high temperatures, in relatively pure specimens. A similar tail absorption is observed in other III–V compounds (e.g., InAs, GaSb, and GaAs). However, as will be seen later, in these cases the absorption can be attributed to transitions involving impurities. This is also true for InSb at low temperatures.

V. Effects of Temperature and Pressure on the Absorption Edge

15. Effect on the Energy Gap

The principal effect of temperature and pressure on the absorption edge is to shift the threshold because of a change in the energy gap. Changes in the spectral variation of the absorption can occur, particularly in the case of hydrostatic pressure, where different band extrema participate in the fundamental absorption at different pressures.

Both temperature and pressure affect the band structure by varying the lattice spacing. Such a dilation (Δ) can be induced statically either by application of hydrostatic pressure or by changing the sample temperature. In addition, long-wavelength acoustic phonons can be treated as producing a dynamic dilatation. We have already discussed the contribution of phonons to electron scattering and to the electron self-energy.

The variation of the electronic energy levels with lattice spacing is shown qualitatively in Fig. 18. Bardeen and Shockley[75] have shown that for the small strains present in most experiments one can describe the change in a given energy level by the deformation potential tensor E_{ij} such that the change in a given energy level at point $\mathbf{r}$ is given by

$$\delta E(\mathbf{r}) = \sum_{i,j} E_{ij} W_{ij}(\mathbf{r}), \tag{124}$$

where W_{ij} is the strain tensor.

A uniaxial or biaxial strain can produce complicated effects by modifying the symmetry of the crystal. This removes degeneracies in the band extrema

[75] J. Bardeen and W. Shockley, *Phys. Rev.* **80**, 72 (1950).

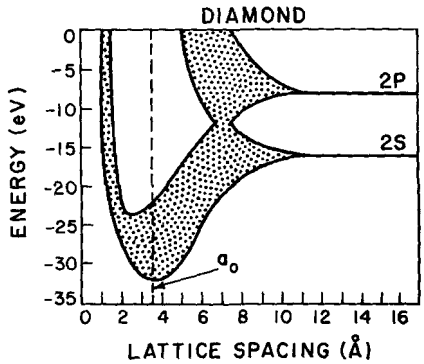


FIG. 18. Schematic diagram showing energy bands versus lattice spacing. (After J. Bardeen and W. Shockley.[75])

and can add fine structure to the absorption edge.[75a] Little work has been done along these lines in the III–V compounds, and we consider only homogeneous dilatations. For a cubic crystal subject to a dilatation Δ the band edge energies E_c or E_v can be expressed in the form

$$E_l(\Delta) = E_l(0) + E_1\Delta. \tag{125}$$

For a given temperature and pressure we can write

$$E_l(T, P) = E_l(T) + E_1\,\Delta(P), \tag{126}$$

where $\Delta(P)$ is the dilatation induced by departure from normal pressure and $E_l(T)$ is the band edge energy at normal pressure given by

$$E_l(T) = E_l(0) + E_{s,l}(T) + E_1\,\Delta(T), \tag{127}$$

where $E_{s,l}$ is the self-energy and $\Delta(T)$ is the dilatation induced by temperature. Therefore,

$$E_l(T, P) = E_l(0) + E_{s,l}(T) + E_1\,\Delta(T, P). \tag{128}$$

The energy gap is then

$$E_g(T, P) = E_g(0) + [E_{s,c}(T) - E_{s,v}(T)] + [E_{1,c} - E_{1,v}]\,\Delta(T, P), \tag{129}$$

[75a]The valence band of the III–V compounds is fourfold degenerate at $\mathbf{k} = 0$. The application of uniaxial strain should result in two valence-band maxima with a small separation in energy. The conduction band of GaP consists of several band minima in different equivalent directions in $\mathbf{k}$ space. A uniaxial strain in a general direction should shift the band minima at different rates. Such investigations would be most fruitful, where one can observe absorption peaks as in the case of excitons or in the case of the interband magnetooptical effect.

where

$$\Delta(T, P) = \int_0^T \left(\frac{\partial \Delta}{\partial T'}\right)_{P_0} dT' + \left(\frac{\partial \Delta}{\partial P}\right)_T (P - P_0), \tag{130}$$

where the partial derivatives are, respectively, the thermal expansion coefficient and the negative of the compressibility. These are macroscopic quantities that can be easily measured. From Eq. (129) we obtain

$$\left(\frac{\partial E_g}{\partial T}\right)_P = \left(\frac{\partial E_{s,c}}{\partial T}\right)_P - \left(\frac{\partial E_{s,v}}{\partial T}\right)_P + [E_{1,c} - E_{1,v}] \left(\frac{\partial \Delta}{\partial T}\right)_P, \tag{131}$$

$$\left(\frac{\partial E_g}{\partial P}\right)_T = [E_{1,c} - E_{1,v}] \left(\frac{\partial \Delta}{\partial P}\right)_T. \tag{132}$$

A common procedure for observing changes in the energy gap is to observe the variation of the photon energy at which the fundamental absorption reaches an arbitrary level. The assumption is that the absorption edge moves without changing shape. In this way one may be able to measure changes in the energy gap to much greater accuracy than one can measure the absolute value of the energy gap. For strictly allowed transitions in the fundamental absorption the procedure is probably justified. However, in general one should be alert for changes in the shape and the intensity of the fundamental absorption. For phonon-assisted transitions the intensity of the absorption is related to the phonon population, and therefore the intensity of the absorption varies with temperature. In the case of an indirect energy gap the optical matrix element may depend upon pressure. Further complications arise from the possibility that exciton or impurity absorption may be present.

16. Pressure Effects

Studies of the effect of pressure on the group-IV elements and the III–V compounds have been performed extensively by Paul and co-workers at Harvard, and Drickamer and co-workers at Illinois, among others. A review of this work has been given by Paul.[76] See also the chapter by Keyes in Volume 4 of this series. Generally, the deduced variation of band gap is linear with pressure, consistent with the linear deformation-potential theory. Frequently there is a switch from one linear region of pressure to another of different slope, indicating a change in the nature of the band extrema that are involved in the absorption.

Theoretically, one expects three types of conduction-band minima: one at the symmetry point Γ of the Brillouin zone, one near the point X, and

[76] W. Paul, *J. Appl. Phys. Suppl.* **32**, 2082 (1961).

one near the point L. The valence-band maximum should occur near the point Γ. The existence of such band extrema has been verified experimentally. A lowest conduction-band minimum at Γ gives rise to allowed transitions in the fundamental absorption. A lowest conduction-band minimum at X or L corresponds to an indirect gap, and the fundamental absorption corresponds to forbidden transitions.

Since each conduction-band minimum moves at its own rate relative to the valence band, different conduction-band minima participate in the fundamental absorption at different pressures. The values of pressure coefficient observed for different materials fall into three general classes. The pressure coefficient at low pressures for those materials where the energy gap has been established as being direct all fall into the same class. It has been postulated that the three classes of pressure coefficients correspond to the three types of conduction-band minima. Zallen and Paul[77] have studied transitions involving higher conduction-band minima at Γ and find differences between pressure coefficients at Γ corresponding to different bands. The nature of the various conduction-band minima in Ge and Si have been established by cyclotron resonance and optical absorption, which provide a means of associating the type of band minimum and the class of pressure coefficient. The observed pressure coefficients are given in Table II, where they are listed according to their tentative classification. The identities of some of the conduction-band minima have been established by independent experiments and generally confirm this classification.

The dilatation coefficients or the relative deformation potentials would seem to be more basic quantities than the pressure coefficients. However, the correlation among the dilatation coefficients is poorer than that among the pressure coefficients. This would seem to indicate that the apparent correlation cannot be explained on a simple basis.

17. Temperature Effects

The change of energy gap with temperature has been observed by several authors. Generally, the variation is found to be approximately linear for temperatures above 80°K. Below 80°K the temperature coefficient decreases rapidly with temperature.

The part of the temperature coefficient associated with static lattice dilatation is related to the pressure coefficient through the relative deformation potential $(E_{1,c} - E_{1,v})$ of Eqs. (131) and (132). With a knowledge of the compressibility and the coefficient of thermal expansion one can calculate the change in energy gap due to static dilatation. For InSb, Ehrenreich[60] has found a value of $(\partial E_g/\partial T)_P = -9.6 \times 10^{-5}$ eV/°K. This is to be

[77] R. Zallen and W. Paul, *Phys. Rev.* **134**, A1628 (1964).

TABLE II

COEFFICIENTS FOR CHANGE OF ENERGY GAP WITH PRESSURE[a]

Material	$(\partial E_g/\partial P)_T \times 10^6$ (eV-cm^2/kg) for conduction-band minima[b] at			Reference
	Γ	X	L	
C	—	<1.0	—	*c*
Si	—	-1.5	5.0	*c, c*
Ge	12.0	0 to -2.0	5.0	*c, c, d*
Sn	—	—	5.0	*e*
AlSb	—	-1.6	—	*f*
GaP	10.7	$-1.1, -1.7, -1.8$	—	*g, g, h, c*
GaAs	9.4, 12.0	-8.7	—	*h, c, h*
InP	4.6, 8.4	-10.0	—	*f, i, f*
GaSb	12.0, 16.0	<0	5.0, 7.3	*f, j, f, c, f*
InAs	4.8, 8.5, 5.5, 10.0	—	3.2	*f, j, k, i, f*
InSb	14.2, 15.5	—	—	*l, m*

[a] Some coefficients have been deduced from electrical measurements as well as optical measurements.

[b] Confirmed or speculated.

[c] See Ref. 76.

[d] See Ref. 7.

[e] F. C. Champion and J. R. Prior, *Nature* **182**, 1079 (1958).

[f] A. L. Edwards and H. G. Drickamer, *Phys. Rev.* **122**, 1149 (1961).

[g] See Ref. 77.

[h] A. L. Edwards, T. E. Slykhouse, and H. G. Drickamer, *J. Phys. Chem. Solids* **11**, 140 (1959).

[i] R. Zallen, Ph.D. thesis, Harvard University (1964).

[j] J. H. Taylor, *Bull. Am. Phys. Soc.* **3**, 121 (1958).

[k] J. H. Taylor, *Phys. Rev.* **100**, 1593 (1958).

[l] D. Long, *Phys. Rev.* **99**, 388 (1955).

[m] R. W. Keyes, *Phys. Rev.* **99**, 490 (1955).

compared to a value of -29×10^{-5} eV/°K observed experimentally by Roberts and Quarrington[26] from optical data. The discrepancy is attributed to the effect of the electron self-energy according to the first two terms of Eq. (131). Fan[78] has calculated the effect of the self-energy terms for germanium due to deformation-potential scattering by acoustic phonons. In the III–V compounds one would expect additional contributions due to polar scattering.

A similar situation has been observed by Dixon and Ellis[20] for the case of InAs. Static thermal dilatation gives $(\partial E_g/\partial T)_P = -7 \times 10^{-5}$ eV/°K, which accounts for only one-fourth of the total shift of energy gap with temperature. Additional measurements of the temperature dependence of the absorption edge have been made by Oswald.[79]

[78] H. Y. Fan, *Phys. Rev.* **82**, 900 (1951).

[79] F. Oswald, *Z. Naturforsch.* **10a**, 927 (1955).

VI. Impurity Absorption

18. Theoretical Background

The simplest absorption involving impurity levels concerns transitions of a carrier between the ground state and the excited states of a neutral impurity. Such absorption usually occurs at photon energies much lower than those at the fundamental absorption edge. We are concerned here with the formation of electron–hole pairs near such an ionized impurity. Consider an electron–hole pair in the neighborhood of a charged donor impurity. The interaction is given by

$$H' = -\frac{e^2}{\kappa|\mathbf{r}_e|} + \frac{e^2}{\kappa|\mathbf{r}_h|} - \frac{e^2}{\kappa|\mathbf{r}_e - \mathbf{r}_h|}, \tag{133}$$

where the origin of coordinates is taken at the impurity site. For $\mathbf{r}_h \gg \mathbf{r}_e$ the last two terms cancel and the hole is screened. For this case Eq. (133) reduces to

$$H' \approx -\frac{e^2}{\kappa|\mathbf{r}_e|}. \tag{134}$$

Absorption involving the scattering of a free-electron–hole pair by such a potential has already been discussed in Part IV. We now consider excited states in which the electron is bound. This problem has been treated theoretically by Eagles,[80] Dumke,[81] Bowlden,[82] and Callaway.[83] The interaction of Eq. (134) is of the form $H'(\mathbf{r}_e, \mathbf{r}_h) = H_1'(\mathbf{r}_e) + H_2'(\mathbf{r}_h)$, and Eqs. (13) and (14) apply, giving

$$\left[E_c(\mathbf{p}_e) - \frac{e^2}{\kappa \mathbf{r}_e}\right]\phi_l(\mathbf{r}_e) = \varepsilon_l \phi_l(\mathbf{r}_e), \tag{135}$$

$$E_v(\mathbf{p}_h)\phi_m(\mathbf{r}_h) = \varepsilon_m \phi_m(\mathbf{r}_h). \tag{136}$$

The solutions are of the form

$$\psi_n = \exp(i\mathbf{k}_m \cdot \mathbf{r}_h)\,\phi_l(\mathbf{r}_e). \tag{137}$$

This effective-mass wave function describes a free hole of wave vector $\mathbf{k}_m$ and an electron that may be trapped on the donor in a localized state l. The latter is just the impurity-level problem that has been reviewed by Kohn.[84] The photon energy corresponding to the optical transition is

$$h\nu = \varepsilon_n = \varepsilon_l + \varepsilon_m = E_g - E_D - E_v(\mathbf{k}_m), \tag{138}$$

where E_D is the ionization energy of a localized level associated with the donor. Equation (15) for the coefficients involved in the electron–hole pair

[80] D. M. Eagles, *J. Phys. Chem. Solids* **16**, 76 (1960).
[81] W. P. Dumke, *Phys. Rev.* **132**, 1998 (1963).
[82] H. J. Bowlden, *Phys. Rev.* **106**, 427 (1957).
[83] J. Callaway, *J. Phys. Chem. Solids* **24**, 1063 (1963).
[84] W. Kohn, *Solid State Phys.* **5**, 257 (1957).

wave function becomes

$$c_n(\mathbf{k}_e, \mathbf{k}_h) = \delta(\mathbf{k}_m - \mathbf{k}_h) \int \phi_l(\mathbf{r}_e) \exp(-\mathbf{k}_e \cdot \mathbf{r}_e)\, d\mathbf{r}_e$$
$$\equiv \delta(\mathbf{k}_m - \mathbf{k}_h)\, c_l(\mathbf{k}_e). \tag{139}$$

The wave function for the excited state becomes

$$\Psi_n = \sum_{\mathbf{k}_e} c_l(\mathbf{k}_e)\, \Phi_{\mathbf{k}_e, \mathbf{k}_m}. \tag{140a}$$

This is equivalent to substituting for the Bloch wave function $\psi_{c,\mathbf{k}_e}$ in the determinant of Eq. (8) the donor wave function[84]

$$\psi_l = \sum_{\mathbf{k}_e} c_l(\mathbf{k}_e)\, \psi_{c,\mathbf{k}_e}. \tag{140b}$$

Therefore, the donor wave function is made up of a linear combination of Bloch wave functions for a range in $\mathbf{k}_e$ given by $c_l(\mathbf{k}_e)$.

Using Eqs. (26) and (29) the optical matrix element corresponding to Eq. (140a) is

$$H_{0,n} = A_0 \sum_{\mathbf{k}_e, \mathbf{k}_h} \delta(\mathbf{k}_m - \mathbf{k}_h)\, c_l(\mathbf{k}_e)\, H_{c,v}(\mathbf{k})\, \delta(\mathbf{k}_e + \mathbf{k}_h)$$
$$= A_0\, c_l(\mathbf{k}_m)\, H_{c,v}(\mathbf{k}_m). \tag{141}$$

In an analogous manner one obtains for the case of an ionized acceptor

$$\psi_n = \exp(i\mathbf{k}_l \cdot \mathbf{r}_e)\, \phi_m(\mathbf{r}_h), \tag{142}$$

$$h\nu = E_g - E_A + E_c(\mathbf{k}_l), \tag{143}$$

$$H_{0,n} = A_0\, c_m(\mathbf{k}_l)\, H_{c,v}(\mathbf{k}_l). \tag{144}$$

According to Eq. (144) the range in photon energy where absorption occurs will be determined by the range of $\mathbf{k}_h$ present in the acceptor wave function. For an s-like ground state we can estimate the range in $\mathbf{k}_h$ from the uncertainty principle. The values of $\mathbf{k}_h$ for which $c_m(\mathbf{k}_l)$ will be significant will be primarily those below some cutoff value given by

$$k_{co} \equiv \frac{1}{a_B}, \tag{145}$$

where a_B is the Bohr radius of the acceptor state. The range of photon energy where appreciable absorption occurs will be

$$E_g - E_A < h\nu < E_g - E_A + E_c(k_{co}). \tag{146}$$

If the conduction band is a simple parabolic band,

$$E_c(k_{co}) = \frac{\hbar^2 k_{co}^2}{2m_e}. \tag{147}$$

For a simple hydrogenic acceptor

$$E_A = \frac{\hbar^2}{2m_h}\left(\frac{1}{a_0}\right)^2 = \frac{\hbar^2 k_{co}^2}{2m_h}. \tag{148}$$

For this case Eq. (146) becomes

$$E_g - E_A < h\nu < E_g - \frac{m_e - m_h}{m_e} E_A. \tag{149}$$

If $m_h \ll m_e$, the two sides of Eq. (149) are nearly equal and the absorption occurs as a sharp peak. On the other hand, if $m_h \gtrsim m_e$, the absorption is very broad and persists into the high-absorption region.

The great difference in absorption-line width between transitions involving donors and those involving acceptors is illustrated in Fig. 19. The impurity level can be represented schematically in an $E(k)$ diagram by a horizontal line at the appropriate energy extending from $k = 0$ to $k = k_{co}$. Equations (141) and (144) are then equivalent to the selection rule requiring only vertical transitions. The electron effective mass in the direct-gap III–V compounds is generally an order of magnitude smaller than the hole mass, giving a relatively large curvature to the conduction band and a relatively small extent in k to the donor state. As seen in Fig. 19, one would expect a broad absorption associated with acceptors and sharp lines associated with donors. In order to observe the corresponding sharp-line spectra one would require finite donor ionization energies, however.

In a real crystal several complications of this simple picture can occur. The impurity wave function may contain contributions from more than one band. This is true in general for deep levels and for acceptors in the III–V

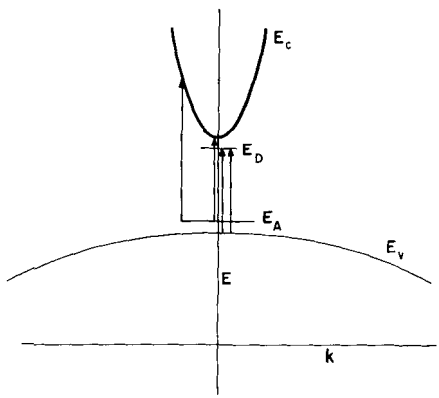


FIG. 19. Schematic energy diagram illustrating spectral spread of impurity absorption due to spread of k of impurity wave functions.

compounds. This complication does not change the qualitative picture much. The transitions at a particular photon energy may involve more than one band. In the case of donors the effect of the light-mass band would show up as a broad background absorption. The excited states of the impurity would give rise to additional absorption, which might not be resolved from that due to the ground state. If the band gap is indirect, allowed transitions cannot occur, and the transitions involve scattering as with the fundamental absorption.

We now consider more quantitatively the case of absorption involving acceptors. The optical density of states is given simply by

$$\rho(k) = N_I \rho_B(k), \tag{150}$$

where $\rho_B(k)$ is the density of states in the relevant band, and N_I is the concentration of impurities. The probability for photon absorption involving the conduction band and a shallow acceptor is then

$$w(k) = \frac{2\pi}{\hbar}|H_{c,v}(k)|^2 |c_m(k)|^2 N_I \rho_c(k)[f(E_A - \zeta) - f(E_c - \zeta)] \times \delta[h\nu - E_c(k) + E_A]. \tag{151}$$

Consider the case of a simple hydrogenic acceptor and a parabolic conduction band. For this case[84]

$$|c_m(k)|^2 = \frac{64\pi^{2/3}}{V}\frac{k_{co}^5}{(k_{co}^2 + k^2)^4} = \frac{64\pi^{2/3}}{V}\left(\frac{\hbar^2}{2m_e}\right)^{3/2}\frac{(bE_A)^{5/2}}{(bE_A + \hbar^2k^2/2m_e)^4}, \tag{152}$$

where $b \equiv m_h/m_e$. Conservation of energy requires

$$h\nu = E_c(k) - E_A = E_g + \frac{\hbar^2k^2}{2m_e} - E_A, \tag{153}$$

and Eq. (152) becomes

$$|c_m(h\nu)|^2 = \frac{64\pi^{2/3}}{V}\left(\frac{\hbar^2}{2m_e}\right)^{3/2}\frac{(bE_A)^{5/2}}{[h\nu - E_g + (1 + b)E_A]}. \tag{154}$$

If $m_h \gg m_e$, Eq. (154) does not vary much between $h\nu = E_g - E_A$ and $h\nu = E_g$, and for allowed transitions the absorption is controlled by the density of states

$$\rho(k) = N_I\frac{2}{(2\pi)^3}4\pi\frac{m_e}{\hbar^2}k = N_I\frac{2}{(2\pi)^3}2\pi\left(\frac{2m_e}{\hbar^2}\right)^{3/2}[E_c(k) - E_g]^{1/2}. \tag{155}$$

With Eq. (153) we obtain

$$\rho(h\nu) = N_I\frac{2}{(2\pi)^3}2\pi\left(\frac{2m_e}{\hbar^2}\right)^{3/2}(h\nu - E_g + E_A)^{1/2}. \tag{156}$$

If the Fermi level is in the neighborhood of the acceptor level,

$$f(E_A - \zeta) - f(E_c - \zeta) = \frac{1}{1 + \exp[(E_A - \zeta)/kT]}. \tag{157}$$

If the associated interband transitions are allowed, Eq. (151) becomes

$$w(h\nu) = \frac{64A_0}{\pi^{1/3}\hbar V}|H_{c,v}(0)|^2 N_I (bE_A)^{5/2} \frac{(h\nu - E_g + E_A)^{1/2}}{[h\nu - E_g + (1+b)E_A]^4} \times \frac{1}{1 + \exp(E_A - \zeta)/kT}. \tag{158}$$

The absorption coefficient is related to $w(h\nu)$ in the usual manner [Eq. (6b)]. For transitions involving acceptors where $b \gg 1$ the denominator does not vary much with $h\nu$ before the band-to-band transitions set in, and Eq. (154) leads to an absorption coefficient of the form

$$[\alpha h\nu] \approx \frac{N_I}{1 + \exp[(E_A - \zeta)/kT]} C(h\nu - E_g + E_A)^{1/2}, \tag{159}$$

where C is a constant that can be obtained from Eqs. (6) and (158) by setting $h\nu - E_g = 0$ in the denominator of Eq. (158). This gives the same spectral variation for the impurity absorption as for the fundamental absorption. In addition, a dependence on impurity concentration and temperature occurs.

19. Experimental Results

Absorption involving zinc or cadmium acceptors in InSb has been observed by Johnson and Fan.[85] As shown in Fig. 20 the spectral shape at helium temperature is close to that given by Eq. (159). Assuming an energy gap of 0.2357,[86] an ionization energy of 7.9 meV is obtained. However, a more accurate value is obtained in the presence of a magnetic field, as discussed in Section 24.

Similar steps are seen in the curves of n-type samples shown in Fig. 21. Since the n-type samples were degenerate at low temperature, the absorption in all cases corresponds to transitions involving an impurity level close to the valence band, probably an acceptor. This is in agreement with the conclusions based upon the spectral shape of the absorption. In fact, there is an approximate correlation between the magnitude of the step and the concentration of ionized acceptors estimated from mobility analysis.

Absorption involving acceptors in GaSb at helium temperature[85] is shown in Fig. 22. There are strong departures from the spectral shape

[85] E. J. Johnson and H. Y. Fan, *Phys. Rev.* **139**, A1991 (1965).

[86] S. Zwerdling, W. H. Kleiner, and J. P. Theriault, *J. Appl. Phys. Suppl.* **32**, 2118 (1961).

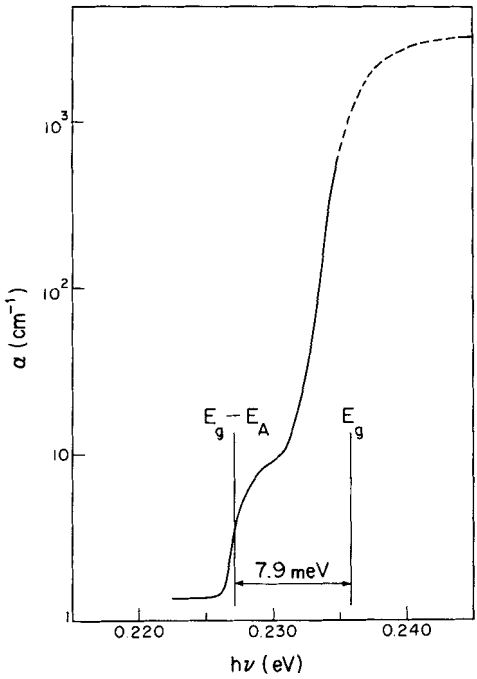


FIG. 20. Impurity absorption in InSb, $T \sim 10°K$. (After E. J. Johnson and H. Y. Fan.[85])

predicted by Eq. (159). This is probably due to broadening effects resulting from the high concentrations of impurities ($\sim 10^{17}$ cm^{-3}) present even in the purest samples. However, one can obtain rough estimates of the ionization energies of the impurities involved and show that the effects of temperature and sample doping can be explained on the basis of absorption involving acceptors and the conduction band.

The results given in Figs. 22 and 23 show that the absorption tail is sensitive to the concentration of impurities and to the sample temperature. Equation (159) predicts that the absorption should increase with the concentration of ionized acceptors. This is confirmed by the experimental results, since electrical measurements indicate that the ionized acceptor concentration increases in the sequence 1, 2, 3 for the samples of Fig. 23. Apparently an additional deeper impurity level has become ionized in sample 3 because of the shift in Fermi level with closer compensation. The increase in ionized-acceptor concentration with temperature would lead to the increases of absorption with temperature shown in Fig. 22.

The results for the undoped samples in Fig. 22 show that the absorption begins at about 0.77 eV at 10°K. The effects of a level at approximately

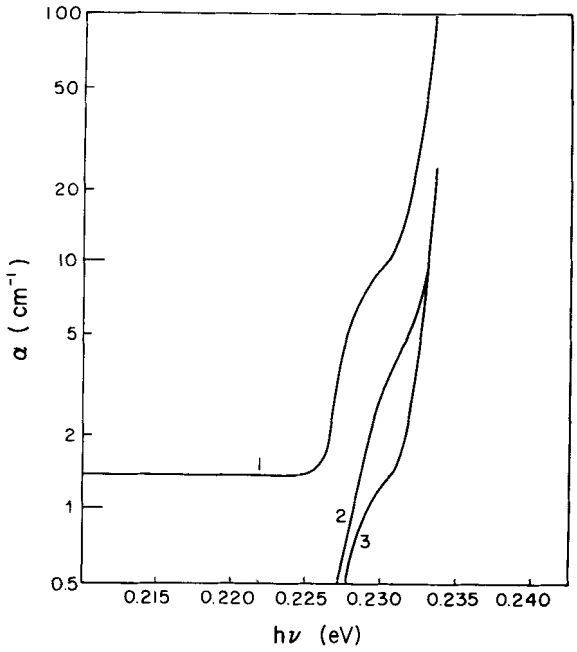


FIG. 21. The effect of impurity concentration on the absorption step for InSb at $\sim 10°K$. (1) p-type: $p = 3.37 \times 10^{15}\,cm^{-3}$, $\mu = 5900\,cm^2/V\text{-}sec$ at 80°K; (2) n-type: $N_A^- = 1.79 \times 10^{15}\,cm^{-3}$; (3) n-type: $N_A^- \lesssim 0.6 \times 10^{15}\,cm^{-3}$. (After E. J. Johnson and H. Y. Fan.[85])

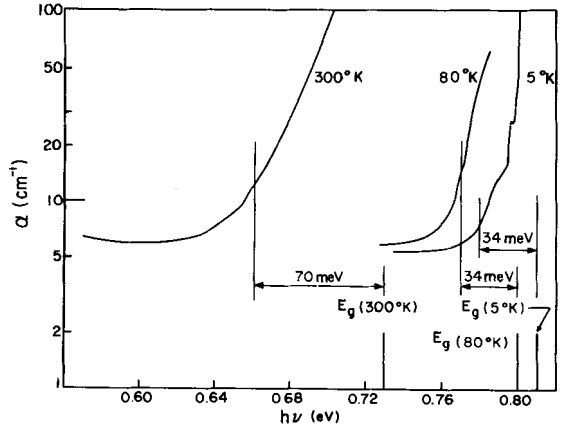


FIG. 22. The effect of temperature on the impurity absorption tail of GaSb: $p = 1.4 \times 10^{17}\,cm^{-3}$ at 300°K; $\mu = 2500$ at 80°K. (After E. J. Johnson and H. Y. Fan.[85])

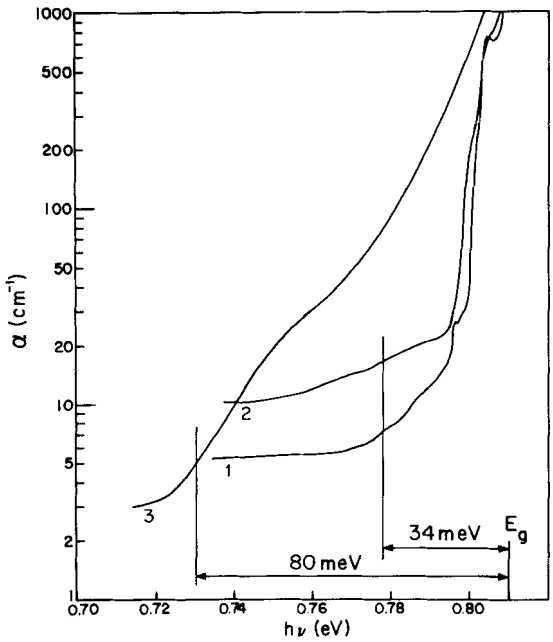


FIG. 23. The effect of impurity concentration on the impurity absorption tail in GaSb. $T \sim 10°K$, (1) Undoped; $p = 1.4 \times 10^{17}\,cm^{-3}$ at 300°K; $\mu = 2800\,cm^2/V\text{-sec}$ at 80°K. (2) Undoped: $p = 2.5 \times 10^{17}$, $\mu = 1520$. (3) Te added: $p = 0.39 \times 10^{17}$, $\mu = 93$. (After E. J. Johnson and H. Y. Fan.[85])

0.034 eV from the valence band have been observed in photoconductivity[87] and recombination emission[88] studies at low temperatures. The absorption tail seen here is very likely due to the same level. This level is apparently also responsible for the tail absorption at 80°K (Fig. 22), which is more intense because of increased concentration of ionized acceptors. At 300°K the absorption indicates the effect of a deeper impurity level ~ 0.07 eV above the valence band. The deeper level gives absorption at 300°K when the Fermi level lies above the impurity level, but not at 80°K or 10°K when the Fermi level falls below it. The measurements of photoconductivity at room temperature show the effect of a level in the range 0.06–0.08 eV from the valence band, which is consistent with the absorption result. Figure 23 shows that in the Te-compensated sample the absorption tail at 10°K rises at ~ 0.08 eV below E_g. It is possible that this is the effect of the same level indicated by the 300°K result for undoped samples, and that the effect of

[87] M. Habegger and H. Y. Fan, *Phys. Rev.* **138**, A598 (1965).

[88] E. J. Johnson, I. Filinski, and H. Y. Fan, *Proc. Intern. Conf. Phys. Semicond., Exeter, 1962* p. 375. Inst. of Phys. and Phys. Soc., London, 1962.

Te compensation is to raise the Fermi level, making the deeper level effective for absorption at low temperature.

When the acceptor levels are occupied, hole transitions to the valence band may give rise to absorption. Such absorption at low photon energies is shown in Figs. 24 and 25. The curves for the compensated samples show clearly an ionization edge at ~ 0.07 eV, corresponding to the deep level deduced from the edge absorption. The 200°K curve for the undoped sample flattens and shows a drop in the vicinity of 0.07–0.08 eV, indicating the presence of the deep level also in undoped material. Measurements on electron-bombarded samples[89] show enhanced absorption due to such a level. This indicates that the level is due to a simple lattice imperfection.

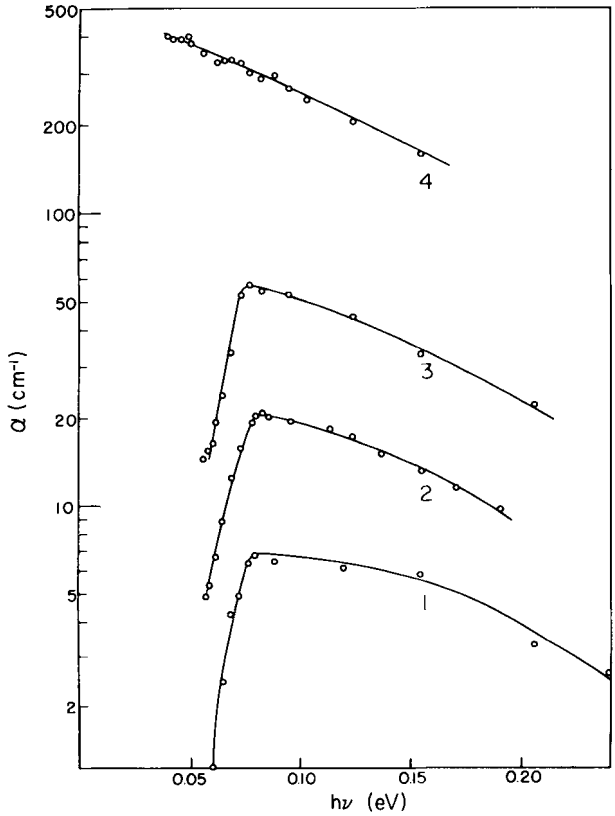


FIG. 24. The impurity absorption at low photon energies for GaSb at 80°K. (1) Te added: p at 300°K unknown. (2) Se added: $p = 4.1 \times 10^{16}$ cm^{-3} at 300°K. (3) Te added: $p = 7.5 \times 10^{16}$. (4) Undoped: $p = 2.4 \times 10^{17}$. (After E. J. Johnson and H. Y. Fan.[85])

[89] R. Kaiser and H. Y. Fan, *Phys. Rev.* **138**, A156 (1965).

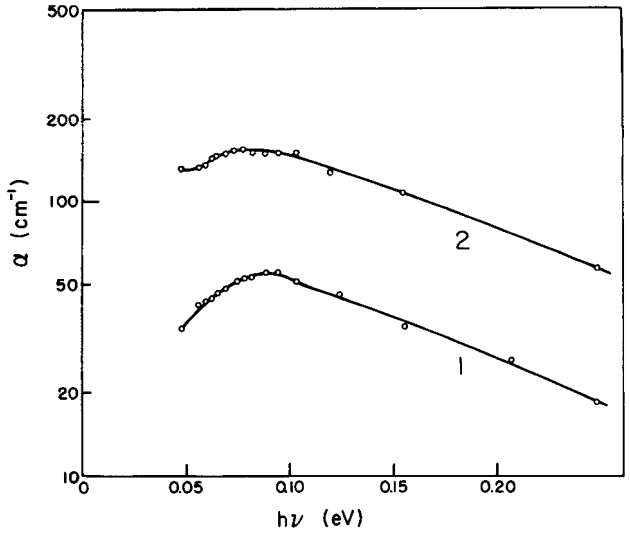


FIG. 25. The impurity absorption at low photon energies for GaSb at 200°K. (1) Te added: $p = 7.5 \times 10^{16}$ cm^{-3} at 300°K. (2) Undoped: $p = 1.5 \times 10^{17}$. (After E. J. Johnson and H. Y. Fan.[85])

A strange behavior in the results of Figs. 24 and 25 is that, in contrast to the absorption in the compensated samples, the drop of absorption in the undoped sample becomes unnoticeable at the lower temperature instead of becoming more pronounced according to increase of level occupation with decreasing temperature. This behavior is an indication that the 0.07-eV level is the level for a second hole bound by the imperfection center.[90] Other work on these impurity levels seems to indicate that they are associated with lattice defect centers.[89,91,92]

Impurity absorption in semi-insulating GaAs has been observed by Sturge.[24] In Fig. 26 a step in absorption on the fundamental edge is shown. The step corresponds in photon energy to a peak observed in emission in Zn-doped GaAs by Nathan and Burns,[93] which was shown to be associated with Zn impurities. The absorption step in semi-insulating GaAs is presumably also associated with a Zn acceptor. The corresponding impurity ionization energy is ~0.04 eV.

[90] R. D. Baxter, R. T. Bate, and F. J. Reid, *J. Phys. Chem. Solids* **26**, 41 (1965).
[91] E. B. Owens and A. J. Strauss, *Proc. Conf. Ultrapurif. Semicond. Mater.* p. 340. Macmillan, New York, and Brett-Macmillan Ltd., Galt, Ontario, 1962.
[92] D. Effer and P. J. Etter, *J. Phys. Chem. Solids* **25**, 451 (1964).
[93] M. I. Nathan and G. Burns, *Appl. Phys. Letters* **1**, 89 (1962).

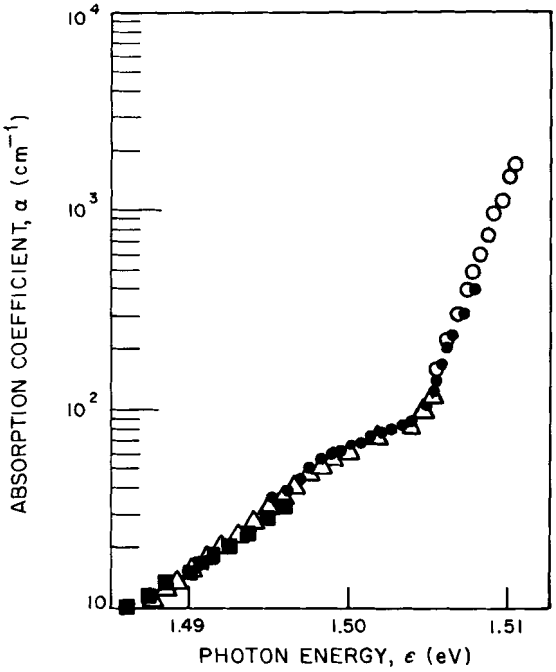


FIG. 26. Absorption edge of GaAs at 21°K. (After M. Sturge.[24])

At lower absorption levels Sturge observed steps in the absorption, which varied significantly from sample to sample as shown in Fig. 27. He resolved three steps in absorption, which he attributed to impurity levels of 0.70, 0.47, and 0.30 eV from the band edges. He found that the thresholds for the impurity absorption vary considerably with temperature, but the position of a threshold at a given temperature relative to the energy gap is independent of temperature. Evidence concerning these impurity levels has also been observed in photoconductivity and related experiments.[94,95] The level at 0.70 eV is probably the deep level responsible for the high resistivity of semi-insulating GaAs.

Impurity absorption has also been observed in InAs[85] and InP.[85] In InAs the absorption apparently involves levels ~0.04 eV and 0.07 eV above the valence band. The absorption in InP is apparently due to levels of 0.02 eV, 0.03 eV, and 0.05 eV from the band edges.

As seen in Fig. 8, the absorption edge of GaP at room temperature[30] shows a tail extending to lower photon energies than the apparent threshold

[94] R. H. Bube, *J. Appl. Phys.* **31**, 315 (1960).

[95] L. R. Weisberg, F. D. Rosi, and P. G. Heckart, "Properties of Elemental and Compound Semiconductors," p. 25. Wiley (Interscience), New York, 1960.

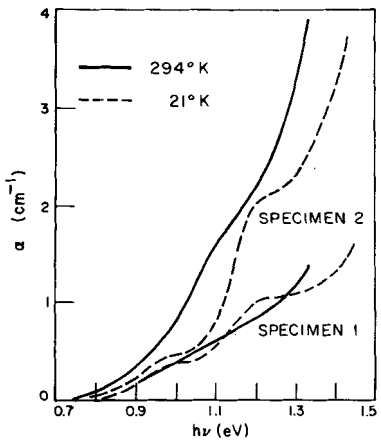


FIG. 27. Absorption due to impurities in GaAs. (After M. Sturge.[24])

for interband transitions. This tail occurs in the spectral region where emission has been observed that has been attributed to transitions involving impurities.[70] The tail absorption in GaP is presumably also due to impurities. It is weak and rises slowly, since the related interband transitions are indirect.

VII. Exciton Transitions

20. General Discussion

We now consider exciton effects on the fundamental absorption. The electron–hole interaction can give rise to very striking features in the fundamental absorption whose analysis can yield considerable information about band structure. The theory of exciton states is discussed extensively in Chapter 7 by Dimmock. References to additional review articles are also given there. We wish here only to place the exciton effects in the context of the fundamental absorption and to discuss the experimental situation in the case of the III–V compounds.

The interaction between the electron and the hole can be described in terms of a simple Coulomb interaction only in special circumstances. We consider two extreme cases. First, consider the interaction in the presence of a background of free carriers. The interaction between the electron and hole will be screened by the additional free carriers and will cease to exist, for all practical purposes, for separations greater than the Debye length. Additional screening results from ionized impurities. If the Debye length is small the exciton effects should be negligible, and the simple theory previously

discussed may apply. Exciton effects are therefore most striking in high-resolution measurements near the threshold for the fundamental absorption in very pure samples at low temperatures.

Second, we consider the case where the separation between electron and hole becomes comparable to a lattice constant. Frenkel[96] proposed the existence of such exciton states in ionic crystals—e.g., NaCl—and the theory has been extended by Overhauser.[97] In this case the concept of an electron–hole pair breaks down, and such excited states are best discussed from an atomic viewpoint. The ground state of the crystal consists of positive and negative ions of the constituent atoms, with the electrons localized on the ions. The lowest excited states are formed by exciting the valence electron on the halogen ion, which increases the electron density near the neighboring halide ions. For tightly bound exciton states, only the influence of the nearest neighbors need be considered, and the problem is tractable.[97] For the case of highly excited states or for the case where the valence electrons are not so tightly bound—e.g., III–V compounds—one must take into account more and more lattice sites, and the problem becomes formidable. For such cases a macroscopic approach first given by Wannier[98] and extended by Dresselhaus[99,100] and by Elliott[101] has proven to be much more successful. In this model the electron and hole are treated as effective-mass particles moving in a medium characterized by the dielectric constant of the material, and they interact through a Coulomb potential. We have already discussed the essentials of this approach.

21. Theoretical Background

To obtain the exciton states we assume an interaction of the form

$$H' = -\frac{e^2}{\kappa|\mathbf{r}_e - \mathbf{r}_h|} = -\frac{e^2}{\kappa|\mathbf{r}|}. \tag{160}$$

Since H' involves only the relative coordinates, the solutions, in general, are of the form

$$\psi_n = \exp(i\mathbf{K}_m \cdot \mathbf{R})\,\phi_l(\mathbf{r}), \tag{161}$$

where $\phi_l(\mathbf{r})$ is given by Eq. (20). Also, the selection rule $\mathbf{K}_m = 0$ applies for optical transitions in the absence of scattering.

[96] J. Frenkel, *Phys. Rev.* **37**, 17 (1931).
[97] A. W. Overhauser, *Phys. Rev.* **101**, 1702 (1956).
[98] G. Wannier, *Phys. Rev.* **52**, 191 (1937).
[99] G. Dresselhaus, *J. Phys. Chem. Solids* **1**, 14 (1956).
[100] G. Dresselhaus, *Phys. Rev.* **106**, 76 (1957).
[101] R. J. Elliott, *Phys. Rev.* **108**, 1384 (1957).

For a thorough discussion of the general case the reader should refer to Chapter 7 by Dimmock. For present purposes we make the simplification that we are dealing with a simple band structure and return to the effective-mass equation

$$\left[\frac{\mathbf{p}_e^2}{2m_e} + \frac{\mathbf{p}_h^2}{2m_h} - \frac{e^2}{\kappa|\mathbf{r}_e - \mathbf{r}_h|}\right]\psi_n(\mathbf{r}_e, \mathbf{r}_h) = (\varepsilon_n - E_g)\,\psi_n(\mathbf{r}_e, \mathbf{r}_h)$$

$$\equiv E_n\psi_n(\mathbf{r}_e, \mathbf{r}_h). \tag{162}$$

This is equivalent to the wave equation for the hydrogen atom, whose solutions are well known. The wave functions can be written

$$\psi_n(\mathbf{r}_e, \mathbf{r}_h) = \exp(i\mathbf{K}\cdot\mathbf{R}_{cm})\,\phi_l(\mathbf{r}), \tag{163}$$

where

$$\left[\frac{\mathbf{p}^2}{2\mu} - \frac{e^2}{\kappa r}\right]\phi_l(\mathbf{r}) = E_l\phi_l(\mathbf{r}) \tag{164}$$

and

$$E_l = E_n - \frac{\hbar^2K^2}{2M}, \tag{165}$$

and μ is the reduced electron–hole mass, M is the total mass, and R_{cm} is the coordinate of the center of mass.

a. Unbound Exciton States

We consider first the solutions of Eq. (164) that correspond to positive E_l. These solutions are associated with the classical comet-like electron orbits, and therefore they correspond closely to the unbound electron–hole pairs considered in Part III. The wave functions for the hydrogen continuum are given in standard textbooks,[102] but a few qualitative observations can be made. Under the Coulomb interaction the wave vectors of the electron and hole are not constants of motion, but the energy of the electron–hole pair is given by

$$\varepsilon_n = \frac{\hbar^2k_\infty^2}{2\mu} + \frac{\hbar^2K^2}{2M} + E_g, \tag{166}$$

where $\mathbf{k}_\infty$ is the wave vector describing the relative motion at a separation greater than a Debye length. This exciton pair corresponds to the free pair with wave vectors $\mathbf{k}_e$ and $\mathbf{k}_h$ given by

$$\frac{\hbar^2k_e^2}{2m_e} + \frac{\hbar^2k_h^2}{2m_h} = \frac{\hbar^2k_\infty^2}{2\mu} + \frac{\hbar^2K^2}{2M}. \tag{167}$$

[102] N. F. Mott and H. S. W. Massey, "Theory of Atomic Collisions," p. 52. Oxford Univ. Press (Clarendon), London and New York, 1949.

If $\mathbf{K} = 0$, then $|\mathbf{k}_\infty| = |\mathbf{k}_e| = |\mathbf{k}_h|$. At closer separations the electron and the hole are accelerated by the Coulomb field, thus mixing in Bloch functions of higher wave vectors. This mixing modifies the absorption due to free electron–hole pairs as given by the simple theory. For wave functions appropriate to the hydrogenic exciton pairs of positive energy Elliott[101] obtains

$$|\phi_l(0)|^2 = \frac{\pi\eta_l \exp(\pi\eta_l)}{\sinh(\pi\eta_l)}, \tag{168}$$

where

$$\eta_l^2 = \frac{R}{\varepsilon_l - E_g} = \frac{1}{\varepsilon_l - E_g}\frac{\mu/mR_0}{\kappa^2} \tag{169}$$

and R_0 is the Rydberg energy. Equation (168) can also be written

$$|\phi_l(0)|^2 = \frac{2\pi\eta_l}{1 - \exp(-2\pi\eta_l)}, \tag{170}$$

and in accordance with Eq. (36) the absorption coefficient is multiplied by a factor

$$|\phi_l(0)|^2 = \frac{2\pi\sqrt{R}}{(h\nu - E_g)^{1/2}} \frac{1}{1 - \exp[-2\pi\sqrt{R}/(h\nu - E_g)]}. \tag{171}$$

The absorption coefficient becomes

$$[\alpha h\nu] = [\alpha h\nu]_0 \frac{2\pi\sqrt{R}}{(h\nu - E_g)^{1/2}} \frac{1}{1 - \exp[-2\pi\sqrt{R}/(h\nu - E_g)]}$$

$$= \frac{2\pi\sqrt{R}\,A}{1 - \exp[-2\pi\sqrt{R}/(h\nu - E_g)]}, \tag{172}$$

where A is a constant defined in Eq. (79). The modification of the fundamental absorption by the excitonic interaction is greatest at the threshold, where $[\alpha h\nu]$ has the nonzero value $2\pi\sqrt{R}A$. The absorption rises beyond the threshold value when the exponential term becomes comparable to unity.

For finite values of $(h\nu - E_g)^{-1}$, Eq. (172) can be written in the form

$$[\alpha h\nu] = A(h\nu - E_g)^{1/2} F\left(\frac{h\nu - E_g}{R}\right), \tag{173}$$

where F has the value $\frac{3}{2}$ for $h\nu - E_g \approx 20R$ and slowly approaches unity for greater values of photon energy, where the exciton effects become

negligible. The factor F may tend to unity also, in the case where screening occurs because of carriers and ionized impurities.

For transitions forbidden at $\mathbf{k} = 0$, Elliott obtains

$$\left|\frac{\partial}{\partial r}\phi_l\right|_0^2 = \pi\eta_l k^2(1 + \eta_l^2)\frac{\exp(\pi\eta_l)}{\sinh \pi\eta_l}. \tag{174}$$

This can also be written

$$\left|\frac{\partial}{\partial r}\phi_l\right|_0^2 = \frac{2\mu}{\hbar^2}\frac{(h\nu - E_g + R)}{(h\nu - E_g)^{1/2}}\frac{2\pi\sqrt{R}}{1 - \exp[-2\pi\sqrt{R}/(h\nu - E_g)]}. \tag{175}$$

Using Eq. (80), the absorption coefficient becomes

$$[\alpha h\nu] = A'\frac{2\pi\sqrt{R}(h\nu - E_g + R)}{1 - \exp[-2\pi\sqrt{R}/(h\nu - E_g)]}. \tag{176}$$

At $h\nu - E_g = 0$ the absorption has the nonzero value $2\pi R^{3/2}A'$. For finite values of $(h\nu - E_g)$, Eq. (176) can be written

$$[\alpha h\nu] \approx A'(h\nu - E_g)^{3/2}F\left(\frac{h\nu - E_g}{R}\right), \tag{177}$$

where F has the value $\frac{3}{2}$ for $h\nu - E_g \approx 20R$ and slowly approaches unity for greater values of photon energy.

b. Bound States

We now consider the eigenfunctions of Eq. (164) that correspond to negative E_n. These correspond to the bound states of the hydrogen atom and give rise to line spectra corresponding to

$$(h\nu)_{0,l} = \varepsilon_{0,l} = E_g - \frac{R}{l^2}. \tag{178}$$

For allowed transitions the intensity of the lines will fall off as

$$|\phi_{0,l}(0)|^2 = \frac{1}{\pi a^3 l^3}, \tag{179}$$

where a is the effective Bohr radius. For high l the lines will overlap, giving a continuous absorption that can be characterized by a density of states

$$\rho(E) = 2\frac{dl}{dE} = \frac{l^3}{R}. \tag{180}$$

Using Eq. (40) the absorption in the quasi-continuum is given by

$$[\alpha h\nu] = 2\pi\sqrt{R}A. \tag{181}$$

Comparison of Eq. (181) with (172) shows that the absorption involving the quasi-continuum is continuous with that due to the true continuum and therefore completely hides the threshold for the creation of ionized pairs.

For symmetry-forbidden transitions only p-states have nonzero matrix elements varying as

$$\left|\frac{\partial\phi_l(0)}{\partial r}\right|_0^2 = \frac{l^2 - 1}{3\pi l^5 a^5}. \tag{182}$$

The $l = 1$ line is absent. In the quasi-continuum the absorption is again continuous with the true continuum.

c. Indirect Transitions

In the case of momentum-forbidden transitions ($\mathbf{K} \neq 0$), the factor $H_{c,v}(0)$ is replaced by the matrix elements calculated in Part V. In the case of a direct energy gap, where line spectra are observed, the absorption involving scattering would occur as a temperature-sensitive weak background to each line, which begins at slightly lower photon energies and increases monotonically with energy.

In the case of an indirect gap the spectral variation of the absorption from each exciton bound state results principally from the variation of the density of states in the exciton band

$$\rho(E) = \frac{1}{2\pi^2}\left(\frac{2M}{\hbar^2}\right)^{3/2}(E)^{1/2}. \tag{183}$$

Therefore, the absorption will occur as steps, where the absorption corresponding to a given bound state and a given phonon will vary as

$$(h\nu - E_g - E_n \pm k\theta)^{1/2}. \tag{184}$$

The absorption involving ionized pairs will be modified in a similar manner.[101] Eventually, the absorption should take on the form obtained in Part V and vary as

$$(h\nu - E_g \pm k\theta)^2. \tag{185}$$

The calculation of exciton energy levels, taking into account the complexities of real band structures and corrections to effective-mass theory, can be accomplished along the same lines as that for impurity levels as reviewed by Kohn.[84] In lieu of such a calculation, one can estimate the binding energy, using a hydrogenic approximation

$$R = R_0\frac{\mu/m}{\kappa^2}, \tag{186}$$

where μ is determined using the heavy-hole mass, and R_0 is the Rydberg

constant (13.6 eV). A closer approximation may be obtained by taking

$$R_0 = R_0' = R' \frac{\kappa^2}{\mu'/m}, \tag{187}$$

where the quantities on the right correspond to a related material where R has been calculated theoretically. The quantities for the direct exciton in germanium[3] give $R_0' = 9.5$ eV.

22. Experimental Results

Exciton effects in the III–V compounds are complicated by the presence of a degenerate valence band and nonparabolic effects. For a discussion of the implications of these complications, the reader should refer to Chapter 7 by Dimmock. Exciton effects have been observed experimentally by Hobden and Sturge in GaAs,[24,103] Johnson and Fan in GaSb,[85] Turner *et al.* in InP,[104] and by Gross *et al.*[69] and Gershenzon *et al.* in GaP.[70]

a. Gallium Antimonide

Absorption showing exciton effects in GaSb is given in Fig. 28. A single peak is observed that apparently corresponds to an allowed transition to the

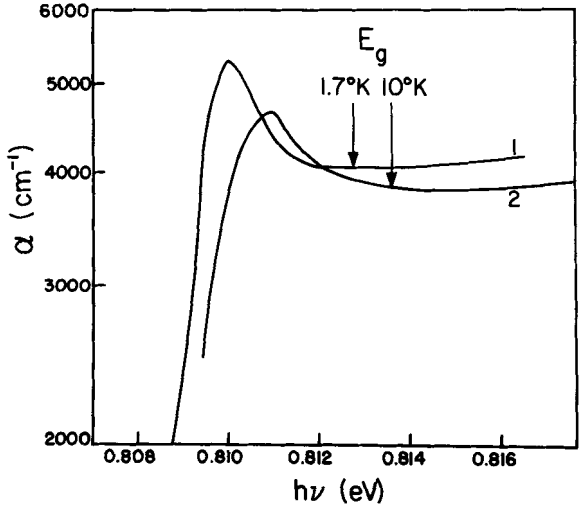


FIG. 28. Effect of temperature on the exciton peak in GaSb. $p = 1.4 \times 10^{17}$ cm^{-3} at 300°K, $\mu = 2800$ at 80°K. (1) $T = 1.7$°K. (2) $T \sim 10$°K. (After E. J. Johnson and H. Y. Fan.[85])

[103] M. V. Hobden and M. D. Sturge, *Proc. Phys. Soc. (London)* **78**, 615 (1961).
[104] W. J. Turner, W. E. Reese, and G. D. Pettit, *Phys. Rev.* **136**, A1467 (1964).

lowest bound state of the exciton. The absorption flattens at higher photon energies, where the transitions probably involve the unresolved higher bound levels and, at still higher photon energies, the ionized pairs.

In lieu of a variational calculation, the exciton binding energy can be approximated by using Eq. (186). For GaSb, a value of $R = 2.8$ meV is obtained. The position of the exciton peaks would indicate $E_g = 0.8137$ eV at 10°K and 0.8128 eV at 1.7°K. The shift of the exciton peak to lower photon energy at 1.7°K is within experimental error, but is unusual because the energy gap is normally expected to increase with decrease in temperature. The exciton peak broadens with a small addition of impurities, as shown in Fig. 29. With a greater impurity concentration no peak is observed.

b. Gallium Arsenide

In GaAs, Sturge[24] observed a single exciton peak, as shown in Fig. 30, similar to that observed in GaSb. Sturge was able to fit the absorption to the high-energy side of the exciton peak with an expression of the form of Eq. (171). In this way he determined R for each temperature. He found R to vary from 2.5 meV to 3.4 meV for temperatures from 10°K to 294°K. These correspond to a theoretical value of 4.4 meV obtained by a variational calculation. The energy gap varies from 1.521 eV to 1.435 eV in the same range of temperature. The value of the absorption in the flat region near $h\nu = E_g$ was calculated from theory to be 8900 cm^{-1}. This corresponds to the observed value 9400 cm^{-1}.

If a thin sample is mounted on glass and subsequently cooled, a strain results. This strain can be considered as a superposition of a uniaxial strain and a uniform dilatation. With the sample under such a strain the exciton

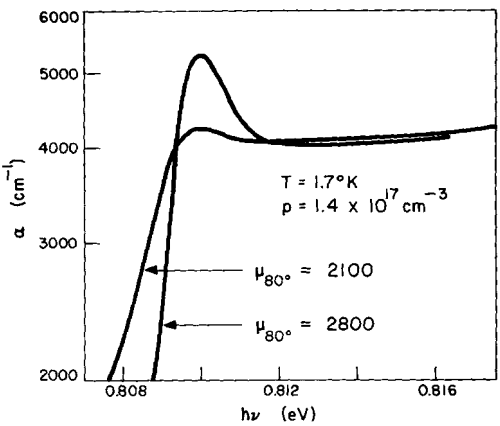


FIG. 29. Impurity broadening of exciton peak in GaSb. (After E. J. Johnson and H. Y. Fan.[85])

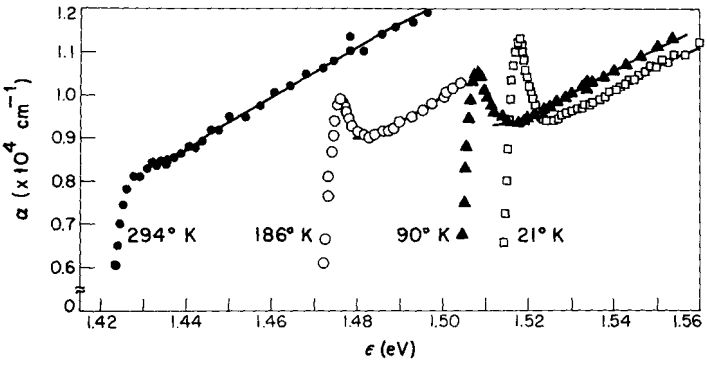


FIG. 30. Exciton peaks in GaAs. (After M. D. Sturge.[24])

peak shifts to higher photon energies and splits into two peaks, as shown in Fig. 31. The splitting apparently corresponds to a splitting of the degeneracy of the valence band.

c. Indium Phosphide

Absorption showing exciton effects in InP is shown in Fig. 32. The data are similar to those observed in GaAs. The exciton binding energy, as

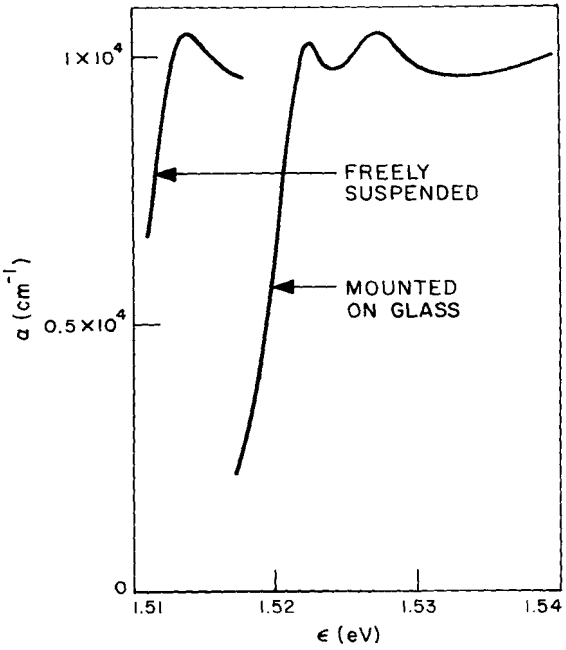


FIG. 31. The effect of strain on the exciton peak in GaAs at 21°K. (After M. D. Sturge.[24])

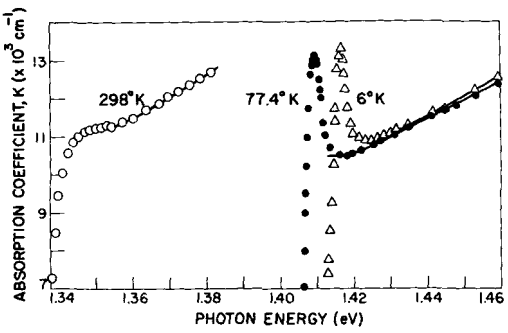


FIG. 32. Absorption of InP showing exciton peaks. The points are representative experimental values for a 4.4-micron-thick sample supported on glass. The low-temperature data have been corrected for strain. The solid line is a theoretical fit to Elliott's theory. (After W. J. Turner *et al.*[104])

determined from the fit to the data, varies from 4.0 meV to 3.6 meV in the range from 60°K to 298°K. The corresponding variation in energy gap is from 1.4205 eV to 1.3511 eV.

d. Gallium Phosphide

In GaP the fundamental absorption begins with indirect transitions. The absorption displaying exciton effects has already been shown in Fig. 15. Several steps are observed having an initial rise in absorption proportional to the square root of the energy difference from the respective thresholds. This behavior is consistent with that predicted by Eq. (184) and is attributed to the creation of excitons in bound states. Apparently, only one exciton state is involved, and the different steps correspond to different phonons. At higher photon energies the absorption approaches a quadratic dependence on photon energy, and this absorption is attributed to the creation of ionized pairs. More recently, an exciton peak associated with direct transitions has been observed by Subashiev and Chalikyan.[105]

e. Ambiguity in the Experimental Results

Absorption involving shallow donors and the valence band (Part VI) has not been identified in the direct-band-gap III–V compounds. Such absorption should have a very close resemblance to the exciton line spectra observed in the III–V compounds. Because $m_e/m_h \ll 1$, the line width of the impurity absorption[105a] should be comparable to that observed in the

[105] V. K. Subashiev and G. A. Chalikyan, *Fiz. Tverd. Tela* 7, 1237 (1965) [*English Transl., Soviet Phys.-Solid State* 7, 992 (1965)].

[105a] The impurity line half-width, assuming a hydrogenic donor ground state, would be $\Delta h\nu \approx \frac{1}{2}(m_e/m_h)E_d$. For GaSb $\Delta h\nu \approx 0.3$ meV.

exciton line absorption. Since the band width is so narrow, the intensity of the absorption would be high for relatively low impurity concentrations. Also because $m_e/m_h \ll 1$, the respective binding energies would be comparable. In the effective-mass approximation,

$$E_d - E_x = R\left[\frac{m_e}{m} - \frac{m_e m_h}{m(m_e + m_h)}\right] \approx \frac{m_e}{m_h} E_d. \tag{188}$$

For GaSb $E_d - E_x \approx 0.5$ meV. This compares to an observed exciton line width of 0.6 meV.

The difficulty in observing the donor absorption in materials where finite ionization energies have been observed (GaAs, InP) would be in resolving the impurity absorption from the exciton absorption. The absorption probably occurs as a broadening of the exciton line that varies with the population of the impurity levels. Since the observed exciton-line widths at low temperatures are probably already significantly broadened by impurities, it should be very difficult to isolate absorption due to shallow donors. On the other hand, the possibility exists that the line spectra observed in GaAs and InP may be absorption due to shallow donors.

VIII. The Fundamental Absorption in the Presence of a Magnetic Field

23. General Discussion

The effective-mass equation for an electron–hole pair in the presence of a magnetic field is given by

$$\left[E_c\left(\mathbf{p}_e + \frac{e}{c}\mathbf{A}_e\right) - E_v\left(\mathbf{p}_h - \frac{e}{c}\mathbf{A}_h\right) + H'(\mathbf{r}_e, \mathbf{r}_h)\right]\psi_n = \varepsilon_n \psi_n, \tag{189}$$

where the vector potentials are related to the magnetic field by

$$\mathbf{A}_e = \tfrac{1}{2}(\mathbf{H} \times \mathbf{r}_e), \qquad \mathbf{A}_h = \tfrac{1}{2}(\mathbf{H} \times \mathbf{r}_h). \tag{190}$$

The term $H'(\mathbf{r}_e, \mathbf{r}_h)$ involves any additional interactions that might be present. To calculate the optical matrix element in the presence of a magnetic field the operator $e/mc\ \mathbf{a} \cdot \mathbf{p}$ of Eq. (27) is replaced by the operator $e/mc\ \mathbf{a} \cdot (\mathbf{p} + e/c\mathbf{A})$, where $\mathbf{A} = \frac{1}{2}(\mathbf{H} \times \mathbf{r})$. For a thorough discussion of the case where $H' \approx 0$, the reader is referred to Chapter 8 by Lax and Mavroides, since only a brief discussion will be given here. For the case of simple parabolic bands and neglecting spin, the effect on the optical absorption is mainly due to the effect on the density of states. Singularities in the density

of states are created by the magnetic field to form "Landau levels" given by[106–108]

$$\varepsilon_n = E_g + (2n + 1)\frac{m}{\mu}\beta H, \tag{191}$$

where n is any integer and β is the Bohr magneton. There are additional Landau levels to those of Eq. (191), which do not give rise to allowed transitions. The corresponding absorption occurs as peaks in the case of direct transitions and steps in the case of indirect transitions. As the magnetic field is decreased, the positions of the absorption peaks converge to a photon energy equal to the energy gap, providing a particularly precise determination. The spacing in photon energy and the variation with magnetic field provide a means of determining the effective mass. Related parameters are determined in the case of a more complicated band structure.

When H' has the form of a Coulomb interaction, as in the case of excitons or impurities, it is convenient to discuss the magnetic-field strength in terms of a dimensionless parameter γ given by

$$\gamma \equiv \frac{\frac{1}{2}\hbar\omega_C}{R} = \left(\frac{m}{m^*}\right)\kappa^2\frac{\beta H}{R_0}, \tag{192}$$

where β is the Bohr magneton and m^* is the appropriate effective mass. For $\gamma < 1$, the exciton (impurity) binding energy is much greater than the spacing between Landau levels, and it is appropriate to talk about the Zeeman effect of the exciton (impurity) levels. For $\gamma > 1$, the qualitative situation corresponds more closely to assuming $H' = 0$.

24. Impurity Absorption

In the III–V compounds a magnetic field will affect the impurity absorption involving shallow acceptors and the conduction band principally through magnetic-field effects on the states of the conduction band. For absorption involving shallow donors and the valence band, a magnetic field would affect principally the impurity levels. Since absorption involving the latter has not been observed, we shall discuss only the former.

Sharp peaks result under a magnetic field because of the formation of Landau levels in the conduction band. Only the peaks corresponding to the lowest Landau levels can be observed, the peaks corresponding to higher Landau levels being covered by the intrinsic absorption. The absorption peaks should occur at photon energies

$$(h\nu)_p = E_g - E_A + \varepsilon_c(H) + \varepsilon_A(H), \tag{193}$$

[106] L. M. Roth, B. Lax, and S. Zwerdling, *Phys. Rev.* **114**, 90 (1959).
[107] R. J. Elliott, T. P. McLean, and G. G. Macfarlane, *Proc. Phys. Soc. (London)* **72**, 553 (1958).
[108] E. Burstein, G. S. Picus, R. F. Wallis, and F. Blatt, *Phys. Rev.* **113**, 15 (1959).

where E_A is the acceptor ionization energy in the absence of a magnetic field, $\varepsilon_A(H)$ is the shift of the impurity level with magnetic field, and $\varepsilon_c(H)$ is the shift of the lowest Landau level of the conduction band. As we have seen, the conduction band in InSb is nonparabolic. However, the nonparabolic effects are not significant at low magnetic fields. Bowers and Yafet[109] have extended the Kane model to the case of an applied magnetic field. We have found that the quantity ε_c can be written in the form

$$\varepsilon_c = -\frac{E_g}{2} + \frac{E_g}{2}\left\{1 + \frac{4f_1(E_c)}{E_g}\left[\frac{m}{m_c}\beta H \pm \frac{1}{2}g_0 f_4(\varepsilon_c)\beta H\right]\right\}^{1/2}, \tag{194}$$

$$g_0 \equiv 2 - \frac{m}{m_c}\frac{2\Delta}{3E_g + 2\Delta}, \tag{195}$$

$$f_4(\varepsilon_c) \equiv \frac{E_g + \frac{2}{3}\Delta}{\varepsilon_c + E_g + \frac{2}{3}\Delta}. \tag{196}$$

The remaining quantities have been defined in Section 4. If $\varepsilon_c \ll E_g$,

$$f_1(E_c) \approx f_4(\varepsilon_c) \approx 1, \tag{197}$$

and Eq. (194) becomes

$$\varepsilon_c = -\frac{E_g}{2} + \frac{E_g}{2}\left\{1 + \frac{4}{E_g}\left[\frac{m}{m_c}\beta H \pm \frac{1}{2}g_0\beta H\right]\right\}^{1/2}. \tag{198}$$

For $E_g \gg |(m/m_c)\beta H \pm \frac{1}{2}g_0\beta H|$, we obtain by expansion

$$\varepsilon_c \approx \left(\frac{m}{m_c}\beta H \pm \frac{1}{2}g_0\beta H\right)\left(1 - \frac{(m/m_c)\beta H \pm \frac{1}{2}g_0\beta H}{E_g}\right). \tag{199}$$

For low H this reduces to the results for a parabolic conduction band,

$$\varepsilon_c \approx \frac{m}{m_c}\beta H \pm \frac{1}{2}g_0\beta H = \frac{1}{2}\hbar\omega_c \pm \frac{1}{2}g_0\beta H. \tag{200}$$

The acceptor ground state may be expected to split under a magnetic field and to display a diamagnetic shift. These effects are included in $\varepsilon_A(H)$ but, as already mentioned, should be much smaller than the conduction-band effects. Thus, we have

$$(h\nu)_p - (E_g - E_A) \approx \left(\frac{m}{m_0} \pm \frac{1}{2}g_0\right)\beta H\left[1 - \left(\frac{m}{m_0} \pm \frac{1}{2}g_0\right)\frac{\beta H}{E_g}\right]. \tag{201}$$

Johnson and Fan[85] have studied the effect of an applied magnetic field on the impurity absorption in InSb. In the presence of a magnetic field

[109] R. Bowers and Y. Yafet, *Phys. Rev.* **115**, 1165 (1959).

the impurity absorption step develops into two peaks shifted to higher photon energies, as shown in Fig. 33. The position of each peak as a function of magnetic field is shown by the data points in Fig. 34. A second sample shows points shifted by ~ 1 meV from those of the first sample, which suggests that a different impurity is involved. Within the range of H used, the second term in brackets in Eq. (201) is small compared to unity. Accordingly, the observed shift is approximately linear with H and amounts to 0.40 meV/kG. This value corresponds to $m_c = 0.015m$, which agrees with the value determined by the interband magnetooptic effect.[86] From the observed splitting of the peak, a value of $|\mathbf{g}_0| = 47 \pm 2$ is obtained, which is in good agreement with the value 48 obtained in the exciton region.[86] The data can be fitted with Eq. (201), as shown by the solid curves in Fig. 34. The fitting gives $E_A = 7.5 \pm 0.5$ meV. Measurements on another sample indicated by the second set of points in Fig. 34 give $E_A = 8.5 \pm 0.5$ meV. These values are probably better than those determined from the absorption at $H = 0$ and compare favorably with the value of 8 meV found by Putley[110] for the acceptor levels of zinc or cadmium, which are indicated as the residual acceptors in InSb by mass-spectrometer studies.[111]

The absorption appears to be closely related to the transitions involved in the InSb diode laser (Phelan *et al.*).[112] The laser results are shown in

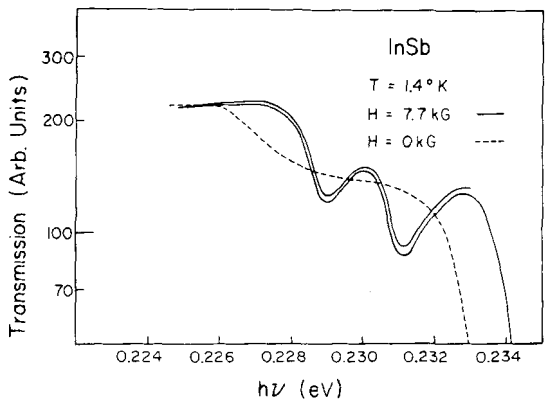


FIG. 33. The effect of a magnetic field on the impurity absorption step for InSb at 1.4°K. The two solid curves are for different polarizations of the radiation. (After E. J. Johnson and H. Y. Fan.[85])

[110] E. H. Putley, *Proc. Phys. Soc. (London)* **73**, 128 (1959).

[111] R. K. Willardson, *Proc. Conf. Ultrapurif. Semicond. Mater., Boston* p. 316. Macmillan, New York, and Brett–Macmillan Ltd., Galt, Ontario, 1962.

[112] R. J. Phelan, A. R. Calawa, R. H. Rediker, R. J. Keyes, and B. Lax, *Appl. Phys. Letters* **3**, 143 (1963).

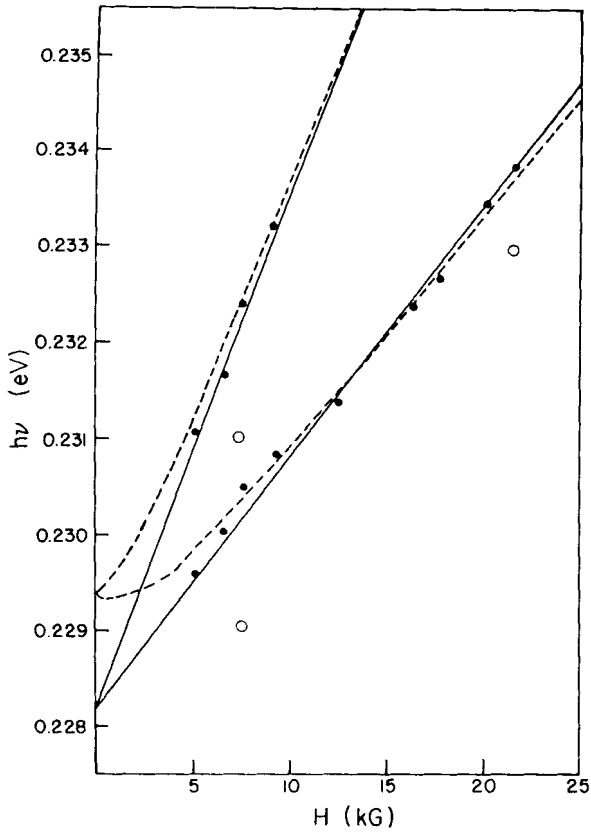


FIG. 34. The shift of the impurity absorption peaks with magnetic field for InSb at 1.7°K. The solid points give the experimental data for sample 1 of Fig. 21; the open points, for sample 3. The solid curves give the theoretical fit. (After E. J. Johnson and H. Y. Fan.[85])

Fig. 35, along with the absorption results. The solid curves extrapolate the theoretical fit to the absorption results of Fig. 34 to higher magnetic fields, using Eq. (201). The data points for the laser emission fit the extrapolation well and indicate that the transitions involved in the laser lines are the same as those involved in the absorption.

25. Exciton Absorption

The behavior of the exciton line spectra in the presence of a magnetic field has been studied by Johnson and Fan in GaSb[85] and by Hobden in GaAs.[113] In InSb no line spectra are observed in the absence of a magnetic field, but in the presence of a small magnetic field Zwerdling *et al.*[86] have

[113] M. V. Hobden, *Phys. Letters* **16**, 107 (1965).

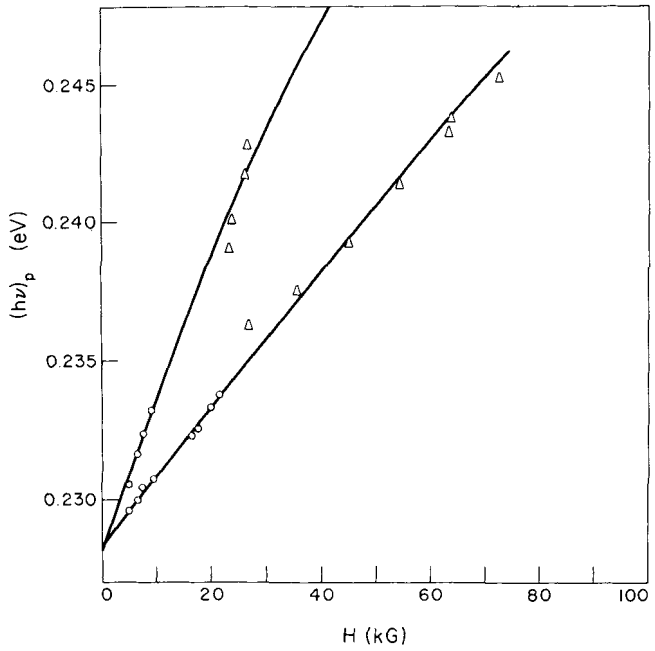


FIG. 35. Comparison of InSb impurity absorption peaks with laser emission. The open points correspond to the absorption, and the triangles correspond to stimulated emission of Phelan *et al.*[112] The solid curve is the theoretical fit to the absorption data. (After E. J. Johnson and H. Y. Fan.[85])

observed line spectra that can be closely associated with the spectra observed in GaSb and GaAs. For a thorough discussion of the theoretical situation the reader is referred to Chapter 7. We restrict the present discussion to effects associated with the lowest Landau levels.

In the III–V compounds, only a single exciton peak is observed in the absence of a magnetic field. This peak is broad relative to the exciton binding energy, and presumably corresponds to the creation of an exciton in a 1*s*-like ground state. The complications of the valence band should not affect the gross features of the optical absorption due to $m_e/m_h \ll 1$. The principal effect of this complication is to introduce degeneracies in some of the energy levels one obtains from a simple hydrogenic model.

If one neglects spin, no splitting occurs in the ground state, but an energy shift occurs because of the diamagnetic effect. For $\gamma \ll 1$, this shift is quadratic and is given by

$$E_0(H) - E_0(0) = \frac{e^2a^2}{4\mu c^2}H^2 = \frac{e^2a_0{}^2}{4mc^2}\left(\frac{m}{\mu}\right)^3\kappa^2H^2, \tag{202}$$

where a is the Bohr radius of the exciton. This expression can be written in the convenient form

$$\frac{E_0(H) - E_0(0)}{R} = \left(\frac{R_0 a_0}{e^2}\right)\gamma^2 = 0.498\gamma^2. \tag{203}$$

For the case $\gamma > 1$, it is more appropriate to consider the exciton levels as bound states associated with each Landau level. Elliott and Loudon[114,115] have obtained numerical results for the bound states associated with the lowest Landau levels.[115a] Their results for the ground state can be given approximately by

$$\frac{E_0(H) - E_0(0)}{R} = \gamma - 1.6\gamma^{1/3}. \tag{204}$$

At high magnetic fields the variation is due principally to the first term, and the shift becomes linear.

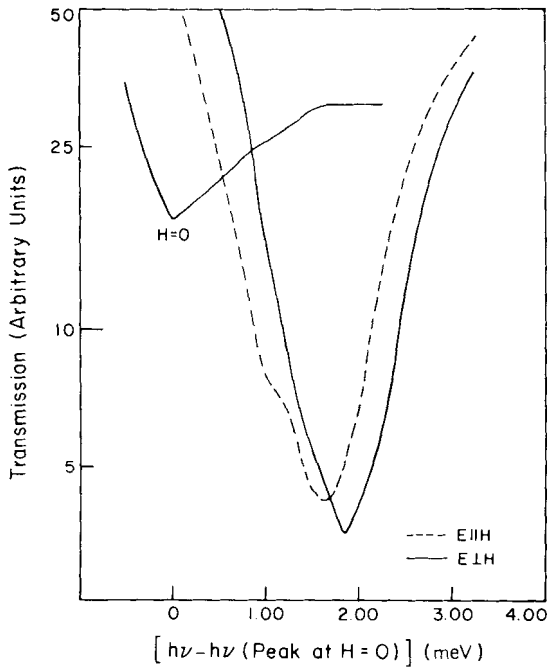


FIG. 36. Zeeman effect of exciton peak in GaSb at 1.5°K and $H = 19.8$ kG. (After E. J. Johnson and H. Y. Fan.[85])

[114] R. J. Elliott and R. Loudon, *J. Phys. Chem. Solids* **8**, 382 (1959).

[115] R. J. Elliott and R. Loudon, *J. Phys. Chem. Solids* **15**, 196 (1960).

[115a] See also R. F. Wallis and H. J. Bowlden, *J. Phys. Chem. Solids* **7**, 78 (1958) and H. Hasegawa and R. E. Howard, *J. Phys. Chem. Solids* **21**, 179 (1961).

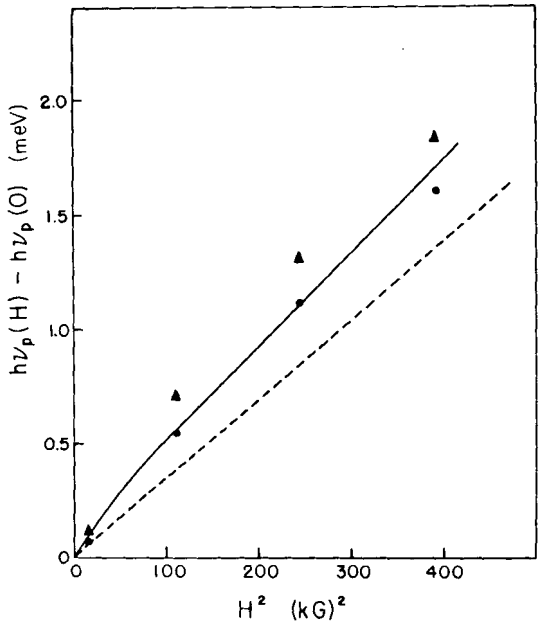


FIG. 37. Shift of exciton peak in GaSb with magnetic field. The circles correspond to data for $\mathbf{E} \parallel \mathbf{H}$, and the triangles correspond to $\mathbf{E} \perp \mathbf{H}$. The dashed curve is the theoretical fit to the diamagnetic shift, and the solid curve incorporates spin splitting. (After E. J. Johnson and H. Y. Fan.[85])

a. Gallium Antimonide

Under a magnetic field the exciton peak in GaSb (Fig. 36) shifts to higher photon energy, increases in intensity, and broadens for both polarizations of the incident radiation. A splitting is nearly resolved with $\mathbf{E} \parallel \mathbf{H}$. These results would indicate that at least two components are present with each polarization. A shift in the energy of the peak with change of polarization gives evidence for additional structure. The energy shift of the exciton peak is due principally to the diamagnetic effect. The dashed curve in Fig. 37 is calculated according to Eq. (203). It should be noted that the perturbation treatment is justifiable only when γ remains small. For excitons in GaSb, $\gamma = 1$ corresponds to a field of ~ 20 kG. Thus, departure from Eq. (203) may be expected near the upper end of the range of measurement.

Consider next the splitting of the exciton state due to electron spin. The g factor of low-energy conduction electrons is relevant, for which Eq. (195) can be used. The spin–orbit splitting of the valence band has been estimated to be $\Delta \sim 0.86$ eV. Using this value we obtain $g = -5.7$. This value of g gives a splitting of $g\beta H = 0.65$ meV for $H = 19.8$ kG. Experimentally, the

exciton peak having a width of about 0.6 meV at $H = 0$ was broadened to a width of ~ 1.2 meV at $H = 19.8$ kG. The broadening is consistent with a splitting of the estimated magnitude, and actually a clear indication of splitting can be seen in the curve for $\mathbf{E} \parallel \mathbf{H}$, as already mentioned. The solid curve in Fig. 37 is obtained by adding one-half of the splitting, $\frac{1}{2}g\beta H$, to the diamagnetic shift. The curve fits reasonably the points representing the positions of the peak, which evidently corresponds to the higher-energy component, the lower-energy component being weaker as indicated by the dashed curve in Fig. 36.

b. Indium Antimonide

In InSb no peaks are present in the absence of a magnetic field. However, because of the low effective mass many of the features that are barely resolved in the case of GaSb are illustrated clearly in the presence of a magnetic field in the case of InSb. The spectra for $\mathbf{E} \perp \mathbf{B}$ are shown in Fig. 38 for $H = 10$ kG and for $H = 39$ kG. The splitting into two peaks due to electron spin is well resolved and corresponds to $|g| = 48$. The additional

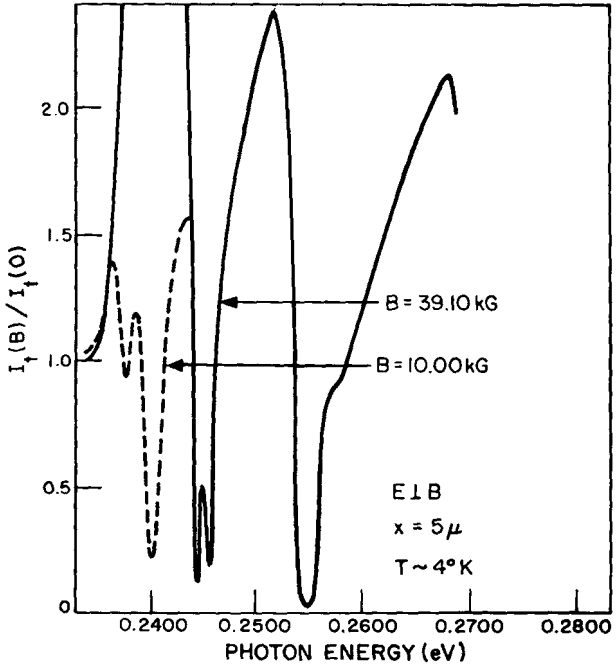


FIG. 38. Exciton absorption corresponding to the lowest Landau levels in InSb. (After S. Zwerdling *et al.*[86])

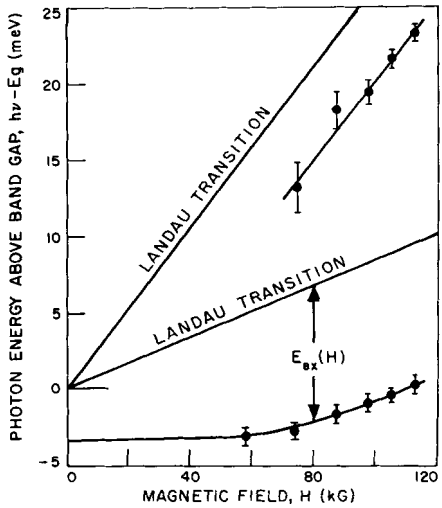


FIG. 39. Shift of exciton peaks in GaAs with magnetic field for $T = 20°K$. (After M. V. Hobden.[113])

splitting in the first peak is due to degeneracies in the valence band and is absent for $\mathbf{E} \parallel \mathbf{H}$.

c. Gallium Arsenide

The exciton peak in GaAs is considerably broader than that in GaSb, and one has to resort to much higher magnetic fields. The magnetic field corresponding to $\gamma = 1$ is approximately 40 kG, and observable effects occur only for $\gamma > \frac{3}{2}$, as shown in Fig. 39. In this case only the diamagnetic shift of the peak is observed, along with a peak associated with the $n = 1$ Landau level.

IX. Transitions Involving Impurity–Exciton Complexes

26. General Discussion

We consider once again the formation of an electron–hole pair in the neighborhood of a charged impurity. The interaction can be written

$$H' = -\frac{e^2}{\kappa|\mathbf{r}_e|} + \frac{e^2}{\kappa|\mathbf{r}_h|} - \frac{e^2}{\kappa|\mathbf{r}_e - \mathbf{r}_h|}. \tag{205}$$

There are two cases where the corresponding effective-mass equation can be easily solved. In one case the first two terms cancel, and the problem reduces to the exciton problem. In the other case the last two terms cancel,

and the problem reduces to the impurity absorption problem of Part VI. We now consider the situation intermediate between these, where the three particles may be expected to form a complex. We refer to such a complex as an ionized impurity–exciton complex. A variation of the problem results by adding either an electron or a hole to produce a neutral complex. We refer to such a complex as a neutral impurity–exciton complex. The corresponding absorption can be expected to occur as lines at photon energies slightly less than the energy gap, even in the case where the energy gap is indirect.

The first experimental evidence for the optical formation of such complexes was the observation of the so-called "Greek peaks" in the I–VII compounds. These have been attributed to the formation of Frenkel excitons near halogen-ion vacancies, which act as charged or neutral donors.[116] Lampert[117] was the first to consider the possibility of the formation of such complexes in materials where the effective-mass approach is applicable. Effective-mass complexes were first observed experimentally by Haynes in Si.[118] He was able to correlate the presence of emission lines in photoluminescence with the presence of neutral impurities for a large variety of group-III and group-V impurities.

The existence of charged impurity–exciton complexes appears to depend critically upon the effective-mass ratio between electron and hole and upon details of the band structure. Such complexes have not been observed in silicon. They have been observed in silicon carbide, but only for certain polytypes.[119]

In the case of III–V compounds absorption peaks that can be attributed to exciton–impurity complexes have been observed in GaSb by Johnson and Fan[85] and in GaP by Gross *et al.*[69] and by Gershenzon *et al.*[70] Such absorption peaks have also been observed in CdS.[120]

27. Estimates of Dissociation Energies of Complexes

It has not been possible to obtain general solutions of the effective-mass equation using the interaction of Eq. (205). Solutions can be obtained for certain limiting values of the mass ratio and if details of the band structure are not taken into account.

The dissociation energy of the complex is of principal interest. This is defined as the minimum energy required to remove an electron–hole pair

[116] F. Seitz, *Rev. Mod. Phys.* **26**, 7 (1954).
[117] M. A. Lampert, *Phys. Rev. Letters* **1**, 450 (1958).
[118] J. R. Haynes, *Phys. Rev. Letters* **4**, 361 (1960).
[119] W. J. Choyke, L. Patrick, and D. R. Hamilton, *in* "Physics of Semiconductors" (Proc. 7th Intern. Conf.), p. 751. Dunod, Paris and Academic Press, New York, 1964.
[120] D. G. Thomas and J. J. Hopfield, *Phys. Rev.* **128**, 2135 (1962).

from the complex. Experimentally, the dissociation energy can be measured in optical absorption or emission as the energy separation between the lowest free-exciton peak and the peak due to the formation of the complex. Theoretically, estimates of E_d can be made from values obtained for limiting values of m_e/m_h. Significant deviations from these simple estimates of E_d can be expected.

In Fig. 40 a schematic energy-level diagram is given, showing possible excited states of a system consisting of an acceptor ion, electrons, and holes. The following discussion applies equally well to a system containing a donor ion, if one inverts the signs of the charges and takes the reciprocal of the mass ratio. Where a set of similar excited states occurs, only the lowest is shown in the diagram. In constructing the diagram it is assumed that the hole mass is larger than the electron mass; however, in the discussion we shall not limit ourselves to this case.

The ground state consists of a single hole bound to an acceptor ion, forming a neutral acceptor complex. The simplest excitation involves the ionization of the acceptor, giving a free hole. Excitations to higher levels each involve the creation of an electron–hole pair and occur near the fundamental absorption edge. Excitation to level 6 results in the creation of an unbound electron–hole pair, and the associated absorption occurs for $h\nu \geqslant E_g$.

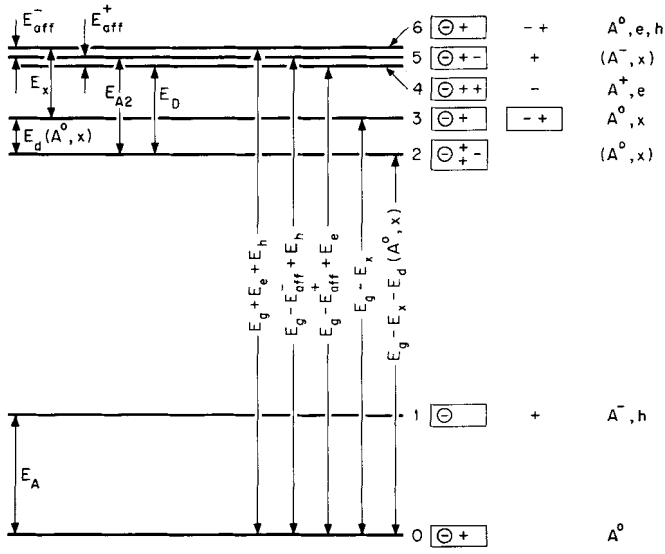


FIG. 40. Schematic energy diagram showing levels for complexes formed from a neutral acceptor.

The neutral acceptor may have an affinity for an electron or a hole and can form complexes corresponding to levels 5 and 4, respectively. The complex formed in level 4 is the analog of the negative hydrogen ion. From the analogy one would expect the neutral acceptor to have an affinity for holes

$$E_{\text{aff}}^{+} = 0.055E_{\text{A}}. \tag{206}$$

The complex formed in level 5 corresponds to the exciton–acceptor complex (A^{-}, x), which will be discussed later in connection with a compensated donor. Absorption involving level 4 or 5 results in the creation of a free carrier, and the corresponding absorption would occur as steps on the absorption edge.

Transitions between the ground state and level 3 result in the formation of a bound exciton, and the corresponding absorption occurs as a peak. At lower photon energies a second absorption peak can occur, associated with the creation of the neutral acceptor–exciton complex (A^{0}, x). The energy difference between this level and level 3 is the dissociation energy. In the limit of $m_{\text{e}}/m_{\text{h}} \to \infty$ this complex is the analog of the hydrogen molecule, whose dissociation energy is well known:

$$E_{\text{d}}(A^{0}, x) = 0.35E_{\text{A}}, \qquad \frac{m_{\text{e}}}{m_{\text{h}}} \to \infty. \tag{207}$$

On the other hand, in the limit of $m_{\text{e}}/m_{\text{h}} \to 0$, we can imagine the complex to be formed from the ground state in the following way. An excitation is first made to level 4, which requires an energy of $E_{\text{g}} - E_{\text{aff}}^{+} + E_{\text{e}}$. To a light electron the complex (E^{-}, h, h) will appear as a single positive charge, and the electron can be captured, giving up an energy approximately equal to the exciton binding energy. This completes the formation of the complex (A^{0}, x) which requires the energy $E_{\text{g}} - E_{\text{aff}}^{+} - E_{x}$.

By subtracting the energy required to form an exciton from the ground state, we obtain

$$E_{\text{d}}(A^{0}, x) = E_{\text{aff}}^{+} = 0.055E_{\text{A}}, \qquad \frac{m_{\text{e}}}{m_{\text{h}}} \to 0. \tag{208}$$

$E_{\text{d}}(A^{0}, x)$ will increase monotonically with $m_{\text{e}}/m_{\text{h}}$, approaching the previous value of $0.35\,E_{\text{A}}$ for large values of $m_{\text{e}}/m_{\text{h}}$.

Next we consider the case of a compensated acceptor. A donor is added to the system at such a distance that its only effect is compensation. We consider only complexes formed with the acceptor. The energy-level diagram is given in Fig. 41. The ground state consists of a bare acceptor ion and a bare donor ion. Excitation to level 2 results in a neutral acceptor and a free electron and corresponds to the impurity absorption of Part VI.

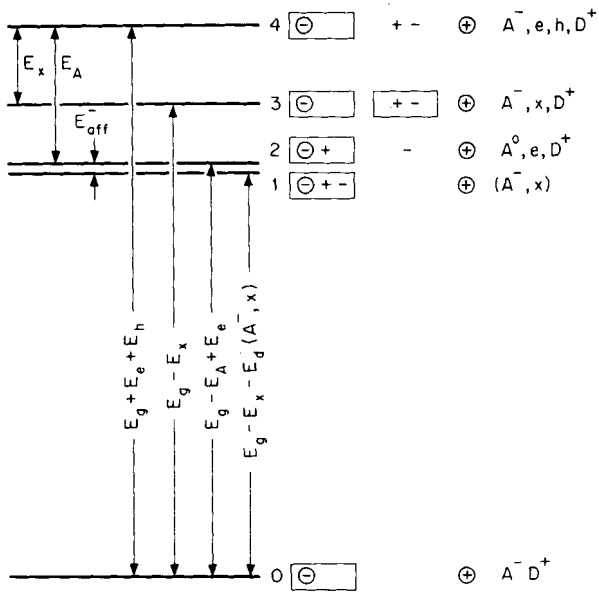


FIG. 41. Schematic energy diagram showing levels for complexes formed from an ionized acceptor.

Excitation from the ground state to level 1 results in the formation of the complex (A^-, x). In the limit of $m_e/m_h \to \infty$, this complex is the analog of the hydrogen-ion molecule. From the analogy we obtain

$$E_d(A^-, x) = 0.21E_A, \qquad \frac{m_e}{m_h} \to \infty. \tag{209}$$

In the limit of $m_e/m_h \to 0$, the situation is not so clear. From the energy difference between level 3 and level 1 it is seen that the dissociation energy in general is

$$E_d(A^-, x) = E_A - E_x + E_{aff}^-. \tag{210}$$

In the limit of $m_e/m_h \to 0$, the affinity of the neutral acceptor for an electron will be small, certainly less than the energy necessary to bind an electron to a charged center—i.e., E_x. In this limit also $E_x \ll E_A$. Therefore, Eq. (210) becomes

$$E_d(A^-, x) \lesssim E_A. \tag{211}$$

This relation locates the corresponding absorption peak in reference to the exciton peak. A more important question, however, involves the quantity E_{aff}^-. That is, can the neutral acceptor bind an electron? The stability of the

complex in a particular case depends upon whether a finite value of E_{aff}^{-} exists. For the limit $m_e/m_h \to \infty$, levels 2 and 3 become indistinguishable, and

$$E_{aff}^{-} = E_d(A^-, x) = 0.21E_A, \qquad \frac{m_e}{m_h} \to \infty. \tag{212}$$

In the other limit, as the separation between the acceptor ion and the hole becomes small relative to the Bohr radius of an electron, it is obvious that the neutral acceptor will have no affinity for the electron, since the kinetic energy required to localize the electron becomes too large:

$$E_{aff}^{-} = 0, \qquad \frac{m_e}{m_h} \to 0. \tag{213}$$

E_{aff}^{-} will be nonzero only for a mass ratio greater than some critical value, which has been estimated by Hopfield[121] to be

$$\left(\frac{m_e}{m_h}\right)_c \approx 1.4. \tag{214}$$

It is clear that details of the band structure will influence this value somewhat. This value applies to the case where the hole is in the ground state of the neutral acceptor. For excited states the critical mass ratio would be correspondingly less, and the possibility exists that in a particular case the neutral acceptor may have a finite affinity for an electron when the hole is in an excited state, but not when it is in the ground state. For such a case, Eq. (211) will be replaced by

$$E_d(A^-, x) \lesssim E_A', \qquad \frac{m_e}{m_h} \to 0, \tag{215}$$

where E_A' is now the energy of an excited state for the hole on the acceptor. The situation for binding is further improved when one considers that in general an excited p state is more easily polarized than a 1s ground state.

An obvious extension of this discussion is to consider the case of a complex consisting of a donor–acceptor pair separated by a distance R (Fig. 42). In the ground state no electrons or holes are present in the complex. By creating an electron–hole pair, the complex (A^-, D^+, x) can be formed. From Fig. 42 the dissociation energy for such a complex is

$$E_d = E_A'(R) + E_D - E_x, \tag{216}$$

where $E_A'(R)$ is the binding energy of a hole to the ion pair. This is reduced from the binding energy of a hole to an isolated acceptor by the average

[121] J. J. Hopfield, *in* "Physics of Semiconductors" (Proc. 7th Intern. Conf.), p. 726. Dunod, Paris, and Academic Press, New York, 1964.

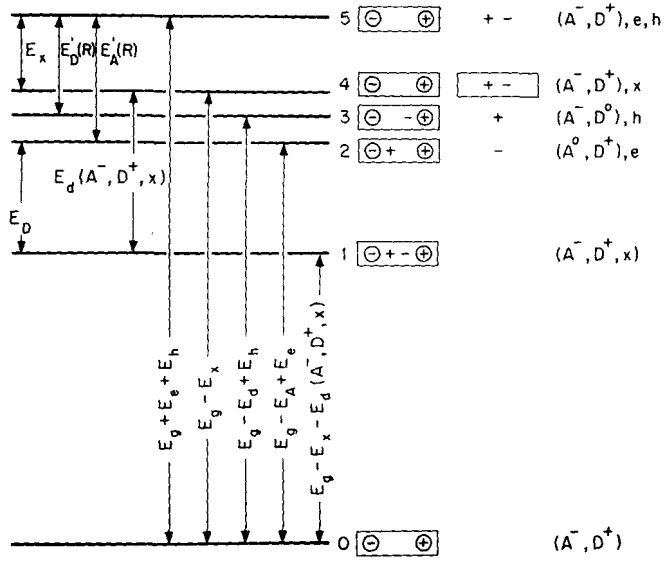


FIG. 42. Schematic energy diagram showing levels for complexes formed from a donor–acceptor pair.

Coulomb repulsion of the donor, giving

$$E_d = E_A + E_D - \frac{e^2}{\kappa R} - E_x. \tag{217}$$

It is not possible to calculate the transition probabilities for the optical creation of such complexes using simple wave functions. In the case where the interband transitions are allowed, one would expect the transition probability[121a] to be proportional to[121]

$$\left| \iint \psi(\mathbf{r}_e, \mathbf{r}_h)\, \delta(\mathbf{r}_e - \mathbf{r}_h)\, d\mathbf{r}_e\, d\mathbf{r}_h \right|^2. \tag{218}$$

In particular, this would indicate that the transition probability should vary strongly with ion separation.

28. Experimental Observations in Gallium Antimonide

The absorption edge of GaSb at 1.7°K is shown in Fig. 43. The peak α is the exciton peak discussed previously. Two additional peaks, β and γ, are observed. The γ peak is also observed in photoluminescence.[88] The peaks β and γ cannot be part of an exciton series with the α peak, since they are

[121a] See also Z. Khás, *Czech. J. Phys.* **15**, 346 (1965).

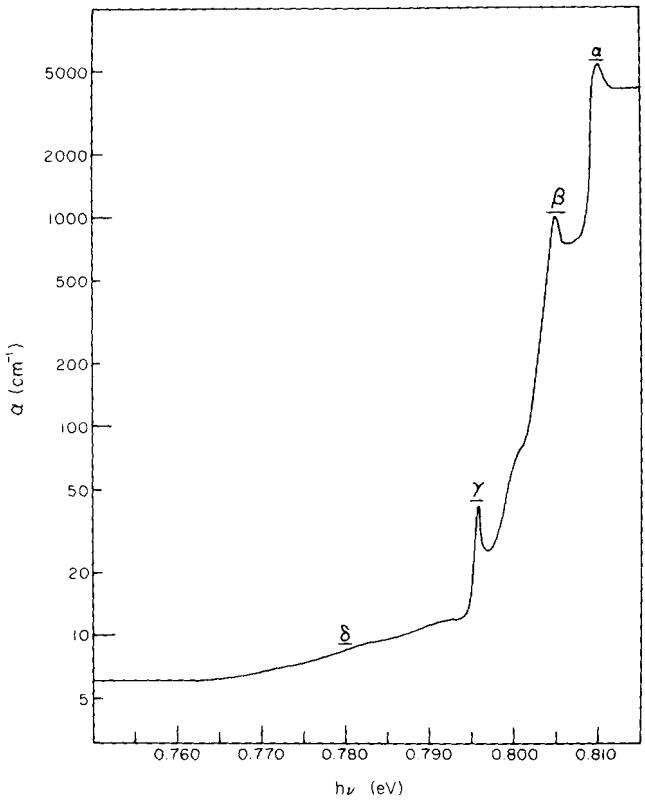


FIG. 43. The absorption edge of undoped GaSb at 1.7°K, showing peaks due to exciton–impurity complexes. (After E. J. Johnson and H. Y. Fan.[85])

separated from α by 5.1 meV and 14.2 meV, respectively, whereas the estimated exciton binding energy is only 2.8 meV. The presence of a second exciton series associated with a different set of bands is very unlikely. The absorption cannot involve optical transitions from the valence band to shallow donor states near the conduction band, since donor states with finite ionization energies have not been observed in GaSb. Furthermore, with an electron effective mass of the order of $\sim 0.05m$, the ionization energy of such donors would be too small to account for the energy differences between these peaks and the α peak.

The β and γ peaks appear to be absorption associated with the creation of exciton—impurity complexes. It has not been possible to correlate the strengths of the observed peaks with the concentration of known impurities because sharp absorption peaks can be observed only in undoped samples (hole concentration $\sim 1.5 \times 10^{17}\,\mathrm{cm}^{-3}$). Measurements made on three

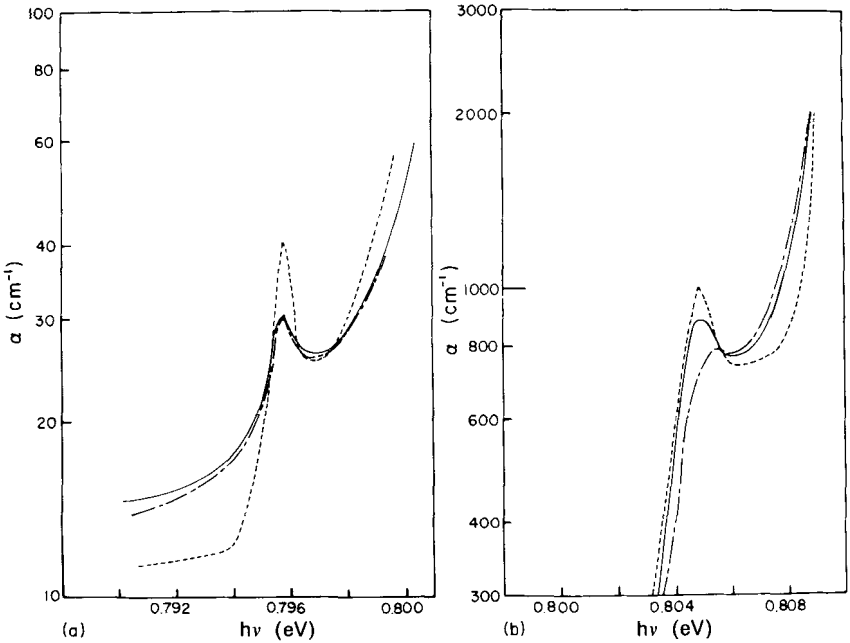


FIG. 44. Variation of impurity-exciton absorption between samples: (a) γ peak; (b) β peak. (After E. J. Johnson and H. Y. Fan.[85])

different samples, shown in Fig. 44, suggest a dependence on the concentrations of unknown impurities. The absorption strength of each peak appears to vary from sample to sample, which is evidence for association with some impurity. It is difficult, however, to rule out the possibility that the apparent differences among the samples were actually produced by varying degrees of broadening.

The behavior of the γ peak under a magnetic field is shown in Fig. 45. The absorption splits into two peaks, with the high-energy peak appreciably stronger. Both peaks shift to higher photon energy with increasing field. The spectra for radiation polarized parallel and perpendicular to the magnetic field differ in the relative intensity of the two peaks, but no significant shift in position occurs with change in polarization. The effect of a magnetic field on the β peak is similar. As the peak becomes broader, the two components are not as well resolved. It is seen that the behavior of the β and γ peaks under a magnetic field is very similar to that of the exciton peak.

The splitting of the γ peak corresponds to $|g| = 9.4$, and that of the β peak corresponds to $|g| = 6.6$. These are on the order of the value of 5.7, estimated for the g factor of the conduction band. It appears that the splitting

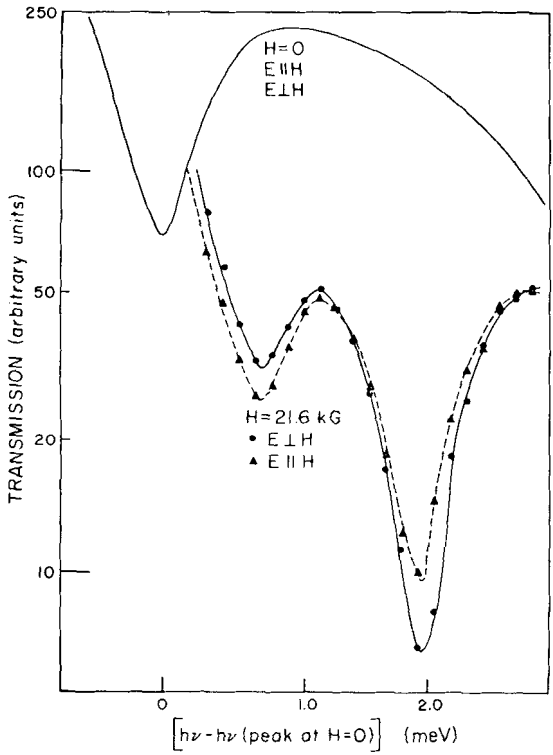


FIG. 45. Zeeman effect of the γ peak at 1.5°K. (After E. J. Johnson and H. Y. Fan.[85])

of the β and γ peaks is principally due to the spin of the electron, as with the exciton peak.

In Fig. 46 the energy of the center between the two split components is plotted as a function of H^2 for the β and γ absorption. The dashed line corresponds to Eq. (203) as in Fig. 37 for the exciton peak. The line fits the data well for either β or γ, except for the deviation near 20 kG that is expected when $\gamma \gtrsim 1$. The quadratic shift lends support to the exciton-complex interpretation. It is interesting that the shift is not noticeably different from that of the exciton, when it is free of the complex.

Consider now the nature of the impurity involved. The dissociation energies, E_d, of the complexes are 5.1 meV for the β complex and 14.2 meV for the γ complex. First, consider donor impurities. With $m_e < m_h$, E_d should be some small fraction of the donor ionization energy E_D, whether the donor involved is neutral or ionized. Since E_D itself should be only $\sim$2.8 meV, donor impurities can be ruled out.

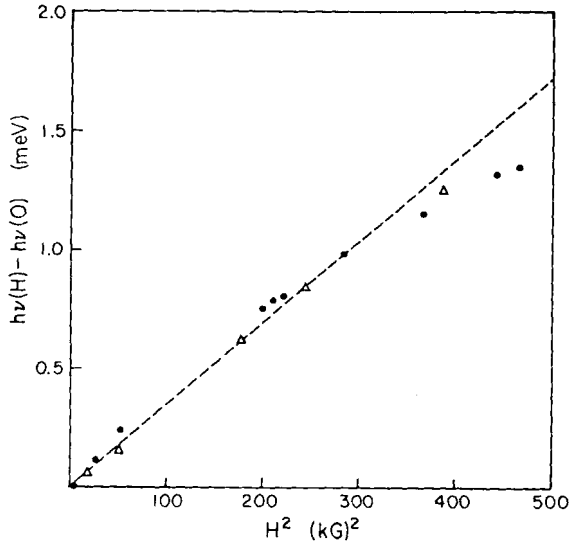


FIG. 46. Quadratic Zeeman effect for impurity–exciton absorption. The solid points correspond to the γ peak, and the triangles correspond to the β peak. The dashed line is the theoretical fit. (After E. J. Johnson and H. Y. Fan.[85])

With a neutral acceptor, E_d should vary monotonically from $0.055\,E_A$ for $m_e \ll m_h$ to $0.35\,E_A$ for $m_e \gg m_h$. Experimentally, Haynes[118] found in silicon $E_d \sim 0.10\,E_A$ for neutral acceptors of group III. The value $E_d = 5.1$ meV for the β complex is 0.14 times 0.034 eV, the energy of one of the acceptor levels in GaSb. The level is attributed to a residual acceptor, which is commonly present in undoped GaSb. It is possible that the β complex is a combination of an exciton with such an acceptor in the neutral state. On the basis of a larger m_h/m_e ratio, we might have expected a smaller ratio of E_d/E_A in GaSb than in silicon (0.10) instead of the observed 0.14. However, the problem is actually very complicated, and such contradictions to the simplified considerations do not seem to be serious.

It is difficult to get a value of E_d as high as that of the γ peak—i.e., 14.2 meV—with a neutral acceptor. On the same basis of $E_d/E_A \sim 0.14$, we would require $E_A \sim 0.1$ eV. There is a level at 0.07 eV, which is the second level of a multilevel center; thus it is likely to be the level of an acceptor in a singly ionized state rather than the level of a neutral acceptor. Baxter and co-workers[90] placed such a level at $\sim$0.1 eV. In any case, the neutral-acceptor model is not concerned with this kind of level. No levels above 0.1 eV have been found. According to the photoconductivity studies,[87] there are possibly two levels in the range 0.06 to 0.08 eV. One of them could be the level of a neutral acceptor needed for γ. However, the ratio E_d/E_A

would be ~ 0.19, which seems to be too large, especially since the ratio should be smaller for a larger ionization energy, E_A, that corresponds to a more tightly bound hole.

A large E_d is to be expected if the complex involves an ionized acceptor. For such a complex $E_d \approx E_A$. In this hypothesis, the acceptor having the 0.034-eV level could be responsible for the γ absorption. The complex may correspond to binding the hole of the exciton in an excited state of the acceptor, thus giving an E_d smaller than the binding energy of the ground state. The difficulty with the model is that there may be no positive values of E_{aff}^-. For a hole bound in a ground state in the case where $m_e/m_h < 1.4$, the electron should not be bound for a simple band structure. The situation is not clear when a degenerate valence band and excited impurity states are involved, as in the present case.

29. Experimental Observations in Gallium Phosphide

In GaP the fundamental absorption begins with indirect transitions, and the absorption corresponding to bound-exciton states occurs as absorption steps. In addition to the absorption steps, Gross *et al.*[69] observed absorption peaks at slightly lower photon energies. Gershenzon *et al.*[70] were able to correlate the presence and location of the peaks with the doping of the sample, and attributed the absorption to transitions involving exciton–impurity complexes. In the complex the states are discrete and the absorption occurs as peaks, in contrast to the indirect exciton absorption. In the complex the cooperation of a phonon is not required to take up the excess crystal momentum as with the excitons. Absorption involving an exciton–neutral-sulphur complex is shown in Fig. 47. The absorption consists principally of one peak that does not involve phonon participation,[121b] followed by weaker ones (not shown in Fig. 47) that involve the emission of one or more phonons. The dissociation energy of the complex is 24 meV. The ionization energy of sulphur donors is 0.14, giving a ratio of 0.17, which is in the range 0.055 to 0.33 expected for such a complex. Gershenzon *et al.* have also observed a splitting of the absorption line due to strain. Further discussion of impurity–exciton complexes and their role in luminescence is given by Thomas *et al.*[122] and in Chapter 13 by Gershenzon in Volume 2 of this series.

Two additional absorption lines are observed at approximately 2.32 eV at 1.6°K. The two lines are apparently associated with the same impurity center, and have been attributed to a complex involving an exciton associ-

[121b] In the original reference the strong peak was attributed to a transition involving a TA_2 phonon. The authors now believe that it is a zero phonon line.[123]

[122] D. G. Thomas, M. Gershenzon, and J. J. Hopfield, *Phys. Rev.* **131**, 2397 (1963).

[123] M. Gershenzon, private communication.

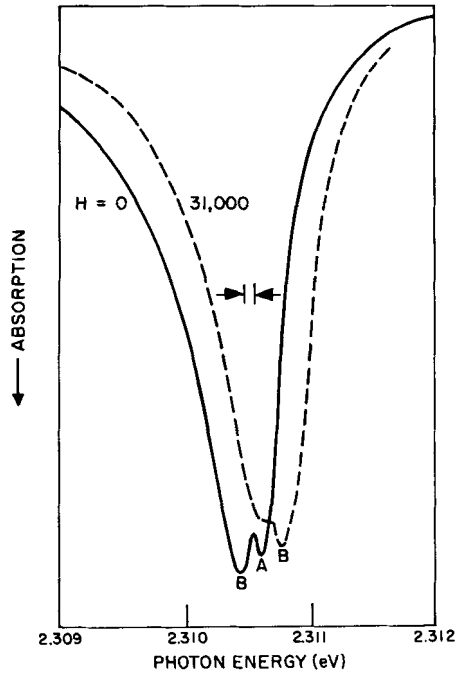


FIG. 47. Splitting of impurity–exciton peak due to sulphur in GaP at 1.6°K and its behavior in a magnetic field. Component *B* shifts and becomes strongly polarized in the field. (After M. Gershenzon *et al.*[70])

ated with a higher-lying conduction-band minimum at $k = 0$ and an ionized donor of binding energy ~ 0.4 eV.

Experimental evidence for the existence of complexes involving donor–acceptor pairs in GaP have been seen mostly in luminescence. The reader is referred to the chapter by Gershenzon for a complete discussion.

X. The Fundamental Absorption in the Presence of an Electric Field

30. Theoretical Discussion

The effect of an applied homogeneous electric field on the fundamental absorption has been treated theoretically by Franz[124] and Keldysh,[125] among others.[126–128] For a discussion of the striking effects of crossed

[124] W. Franz, *Z. Naturforsch.* **13a**, 484 (1958).

[125] L. V. Keldysh, *Zh. Eksperim. i Teor. Phys.* **34**, 1138 (1958) [*English Transl.*: *Soviet Phys. JETP* **7**, 788 (1958)].

[126] J. Callaway, *Phys. Rev.* **130**, 549 (1963).

[127] K. Tharmalingam, *Phys. Rev.* **130**, 2204 (1963).

[128] D. S. Bulyanitsa, *Zh. Eksperim. i Teor. Phys.* **38**, 1201 (1960) [*English Transl.*: *Soviet Phys. JETP* **11**, 868 (1960)].

electric and magnetic fields the reader is referred to Chapter 8 by Lax and Mavroides. We shall restrict the present discussion to the case where no magnetic field is present. The interaction of an electron–hole pair with a homogeneous electric field (**F**) is given by

$$H' = e\mathbf{F}\cdot(\mathbf{r}_e - \mathbf{r}_h) - \frac{e^2}{\kappa|\mathbf{r}_e - \mathbf{r}_h|}. \tag{219}$$

Since Eq. (219) involves only the relative coordinates, the solutions are of the general form

$$\psi_n = \exp(i\mathbf{K}_m\cdot\mathbf{R})\phi_l(\mathbf{r}), \tag{220}$$

and for optical transitions the selection rule $\mathbf{K}_m = 0$ applies in the absence of scattering. In the following discussion we consider only the case of simple parabolic bands and use the center-of-mass transformation. In addition, we neglect the term giving the exciton interaction. In this case, the effective-mass equation becomes

$$\left[\frac{\mathbf{P}^2}{2M} + \frac{\mathbf{p}^2}{2\mu} + e\mathbf{F}\cdot\mathbf{r}\right]\psi_n = E_n\psi_n. \tag{221}$$

The wave equation describing the internal motion of the pair is given by

$$\left[\frac{\mathbf{p}^2}{2\mu} + e\mathbf{F}\cdot\mathbf{r}\right]\phi_l(\mathbf{r}) = E_l\phi_l(\mathbf{r}). \tag{222}$$

The solutions to such an equation have been discussed by Landau and Lifshitz.[129] The solutions have been applied to the present problem by Tharmalingam.[127] The equation can be separated in cylindrical coordinates (ρ, ϕ, z) with the electric field in the positive z direction. The eigenvalues are of the form

$$E_l = E_z + \frac{\hbar^2 k_\rho{}^2}{2\mu} + E_g, \tag{223}$$

where E_z is the part of the energy that is directly affected by the electric field. The eigenfunctions are given by

$$\phi_l(\mathbf{r}) = B\frac{\exp(ik_\rho\rho)}{2\pi\hbar}Ai\left(-\frac{E_z - eFz}{E_0}\right), \tag{224}$$

where

$$E_0 = \left(\frac{\hbar^2}{2\mu}\right)^{1/3}(eF)^{2/3}. \tag{225}$$

[129] L. D. Landau and E. M. Lifshitz, "Quantum Mechanics," p. 70. Macmillan (Pergamon), New York, 1959.

The normalization factor B is given by

$$B = \frac{(2\mu)^{1/3}}{\pi^{1/2}(eF)^{1/6}\hbar^{2/3}}, \tag{226}$$

and $Ai(\beta)$ is the Airy function defined by[130]

$$Ai(\beta) \equiv \frac{1}{\pi^{1/2}} \int_0^\infty \cos\left(\frac{1}{3}u^3 + u\beta\right) du. \tag{227}$$

Since the functional behavior of Eq. (224) is not obvious, we consider the asymptotic forms. As z tends to $+\infty$, ϕ_l tends to zero exponentially for a given value of k_ρ, as

$$\phi_l(\mathbf{r}) \sim \left(\frac{E_0}{eFz - E_z}\right)^{1/4} \exp\left[-\frac{2}{3}\left(\frac{eFz - E_z}{E_0}\right)^{3/2}\right]. \tag{228}$$

For positive z, ϕ_l becomes oscillatory, and as $z \to -\infty$, the amplitude tends to zero. The behavior for large z is given by

$$\phi_l(\mathbf{r}) \sim \left(\frac{E_0}{E_z - eFz}\right)^{1/4} \sin\left[\frac{2}{3}\left(\frac{E_z - eFz}{E_0}\right)^{3/2} + \frac{\pi}{4}\right]. \tag{229}$$

There are satisfactory solutions to Eq. (222) for all values of E_z, either positive or negative. The eigenfunctions are well-behaved for $\pm\infty$, and therefore the usual periodic boundary conditions do not apply. The density of states for motion in a plane is independent of energy ($\hbar^2 k_\rho{}^2/2\mu$), so the energy levels corresponding to Eq. (222) are evenly spaced.

To determine the optical absorption in the case of allowed transitions we need the value of $\phi_l(0)$:

$$\phi_l(0) = \frac{B}{2\pi\hbar} Ai\left(-\frac{E_z}{E_0}\right). \tag{230}$$

Conservation of energy in the optical transition requires

$$h\nu = E_g + E_z + \frac{\hbar^2 k_\rho{}^2}{2\mu}. \tag{231}$$

Equation (230) becomes

$$\phi_l(0) = \frac{B}{2\pi\hbar} Ai\left(\frac{E_g + \hbar^2 k_\rho{}^2/2\mu - h\nu}{E_0}\right). \tag{232}$$

An electron–hole pair can be created with the absorption of a photon of

[130] H. Jeffreys and B. S. Jeffreys, "Methods of Mathematical Physics," p. 508. Cambridge Univ. Press, London and New York, 1946.

arbitrarily small energy. For a given photon energy the values of E_z involved vary from $h\nu - E_g$ to $-\infty$. This corresponds to a variation of $\hbar^2 k_\rho^2/2\mu$ from zero to $+\infty$.

The absorption coefficient obtained by integrating Eq. (232) and substituting in Eq. (40) is given by

$$[\alpha h\nu] = AE_0^{1/2} \int_{(E_g - h\nu)/E_0}^{\infty} |Ai(t)|^2 \, dt, \tag{233}$$

where A is given by Eq. (79).

The integral in Eq. (233) can be evaluated analytically[127]; however, the asymptotic forms are more revealing. As anticipated above, absorption occurs for $h\nu < E_g$ and has the asymptotic form

$$[\alpha h\nu] \approx \frac{AE_0^{3/2}}{(E_g - h\nu)} \exp\left[-\frac{4}{3}\left(\frac{E_g - h\nu}{E_0}\right)^{3/2}\right]. \tag{234}$$

Therefore, the absorption decreases exponentially for photon energies less than the energy gap.

For $h\nu \gg E_g$,[130a]

$$[\alpha h\nu] \approx A(h\nu - E_g)^{1/2}\left\{1 - \frac{1}{4}\frac{E_0^{3/2}}{(h\nu - E_g)^{3/2}} \cos\left[\frac{4}{3}\frac{(h\nu - E_g)^{3/2}}{E_0^{3/2}}\right]\right\}. \tag{235}$$

For vanishingly small fields E_0 tends to zero and the absorption correctly approaches the value obtained in the absence of an electric field.

Callaway[126,131] has discussed the oscillatory behavior of the absorption with photon energy that can arise in an electric field. From Eq. (235) it is seen that an oscillatory component is present with a period

$$\Delta(h\nu) \approx \pi \frac{E_0^{3/2}}{(h\nu - E_g)^{1/2}}. \tag{236}$$

Additional oscillations arise because of the formation of discrete "stark levels."[126,132]

The experimentally observed absorption edge for III–V compounds is frequently found to be exponential over two or more orders of magnitude in absorption coefficient—e.g., GaAs, Fig. 7. This observation has led to suggestions that the presence of internal electric fields might explain the exponential behavior.[133] Indeed, the author has observed that the absorp-

[130a] In certain approximate calculations a term involving the electric field but independent of photon energy would appear in Eq. (235). This term appears to be spurious. The version given is due to D. E. Aspnes, University of Illinois (private communication).

[131] J. Callaway, *Phys. Rev.* **134**, A998 (1964).

[132] G. Wannier, *Phys. Rev.* **117**, 432 (1960).

[133] D. Redfield, *Phys. Rev.* **130**, 916 (1963).

tion near the edge for GaAs is quite sensitive to surface treatment, which might indicate the presence of a field at the surface. On the other hand, Franz[124] has attributed the exponential behavior to the variation of the density of states near the band extrema and has found that in such a case the effect of an applied electric field is to shift the absorption edge by

$$\Delta(h\nu) = \frac{\hbar^2\lambda^2 e^2 F^2}{12\mu}, \tag{237}$$

where the absorption in the absence of an electric field is given by

$$\alpha = \alpha_0 \exp[\lambda(h\nu - E_g)]. \tag{238}$$

31. Experimental Results

Experimentally, it is difficult to observe the effect of high electric fields on the fundamental absorption under ideal conditions. To avoid heating from large currents one must resort to samples of very high resistivity or to the use of *p-n* junctions.[134,135] In GaAs one can obtain high resistivity by introducing deep impurity levels with chemical doping. In the case of silicon one can introduce the deep levels by bombardment.

Moss has observed the effect of an electric field on the fundamental absorption in semi-insulating GaAs.[54] The signal proportional to the transmitted radiation intensity in the absence of an electric field is shown in Fig. 48 for photon energies at the absorption edge. This signal is obtained

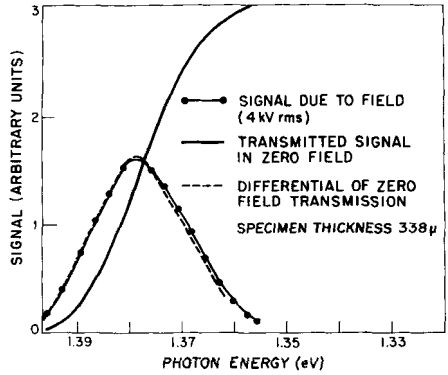


FIG. 48. Spectral dependence of the change in transmission in GaAs due to an electric field. (After T. S. Moss.[54])

[134] P. Handler, *Phys. Rev.* **137**, A1862 (1965).
[135] A. Frova and P. Handler, *Phys. Rev.* **137**, A1857 (1965).

in the usual manner by chopping the radiation, and observing the ac component of the intensity. Also shown is the signal obtained by employing unchopped radiation and applying an ac electric field to the sample. The latter signal was found to be proportional to the differential of the transmitted intensity. This result would occur if the effect of the electric field were to simply shift the absorption edge. Such a shift had been predicted previously by Franz. The magnitude of the shift varies quadratically with electric field in agreement with Eq. (237), and agrees within 10% with the calculated value [9.3×10^{-16} eV/(V/cm)^2]. These results support the theory and would seem to indicate that the assumption of an exponentially varying density of states has some merit. Similar good agreement has been obtained in CdS and CdSe.[136] However, the role of excitons and the role of impurities in the edge absorption should be considered carefully before such a measurement is used to determine effective masses. On the other hand, recent results of Kireev *et al.*[137] on GaAs films indicate that the shift of the absorption edge may not be as simple as observed by Moss.

The experimental requirements have severely limited observations in the other III–V compounds. Effects of an electric field have been observed in Si,[138–140] Ge,[141] CdS,[142–144] PbI_2,[145] and HgI_2.[145] Results similar to those in GaAs were observed in CdS. In Si, structure is observed associated with the different phonons that can participate in the absorption.[146,147] The theory of such absorption has been discussed recently by Penchina,[148] and by Chester and Fritsche.[149]

Frova and Penchina[150] have recently pointed out that the spectral variation of the absorption for $h\nu < E_g$ is sensitive to the precise choice

[136] E. Gutsche and H. Lange, *in* "Physics of Semiconductors" (Proc. 7th Intern. Conf.), p. 129. Dunod, Paris, and Academic Press, New York, 1964.

[137] P. S. Kireev, N. N. Orlova, V. N. Saurin, and L. N. Strel'tsov, *Fiz. Tverd. Tela* **7**, 1271 (1965) [*English Transl.*: *Soviet Phys.-Solid State* **7**, 1029 (1965)].

[138] V. S. Vavilov and K. I. Britsyn, *Fiz. Tverd. Tela* **2**, 1937 (1960) [*English Transl.*: *Soviet Phys.-Solid State* **2**, 1746 (1961)].

[139] L. V. Keldysh, V. S. Vavilov, and K. I. Britsyn, *Proc. Intern. Conf. Semicond. Phys., Prague, 1960* p. 824. Czech. Acad. Sci., Prague, and Academic Press, New York, 1961.

[140] K. I. Britsyn and V. S. Vavilov, *Fiz. Tverd. Tela* **3**, 2497 (1961) [*English Transl.*: *Soviet Phys.-Solid State* **3**, 1816 (1962)].

[141] A. Frova and P. Handler, *Appl. Phys. Letters* **5**, 11 (1964).

[142] K. W. Böer, H. J. Hänsch, and U. Kümmel, *Z. Physik* **155**, 170 (1959).

[143] R. Williams, *Phys. Rev.* **117**, 1487 (1960).

[144] E. Gutshe and H. Lange, *Phys. Status Solidi* **4**, K21 (1964).

[145] R. Williams, *Phys. Rev.* **126**, 442 (1962).

[146] M. Chester and P. H. Wendland, *Phys. Rev. Letters* **13**, 193 (1964).

[147] A. Frova and P. Handler, *Phys. Rev. Letters* **14**, 178 (1965).

[148] C. M. Penchina, *Phys. Rev.* **138**, A924 (1965).

[149] M. Chester and L. Fritsche, *Phys. Rev.* **139**, A518 (1965).

[150] A. Frova and C. M. Penchina, *Phys. Status Solidi* **9**, 767 (1965).

of the value for the energy gap. [See Eq. (234).] The value of E_g of 0.8807 eV determined from measurements on germanium *p-n* junctions at 89°K compares well with a value of 0.8805 eV determined by Macfarlane *et al.*[151] from exciton measurements.

XI. The Fundamental Absorption in Heavily Doped Material

32. General Discussion

The fundamental absorption in highly doped materials is experimentally rather simple, but it is rather difficult to analyze theoretically. We first consider the simple case where we ignore all complications and then consider each complication separately. The simplest case would be that where the doping is high enough so that the exciton and impurity interactions are highly screened and no localized states occur. In such a case we are dealing with a degenerate electron gas subjected to a random distribution of charged scattering centers. The effects of impurity scattering have been considered in Part IV. The electron energy levels are shifted as given formally by Eq. (101), and indirect transitions are enhanced according to Eq. (99). Electron–electron scattering would further enhance these effects. One might even conceive of a situation where the scattering is sufficiently frequent to make the assignment of a wave vector to the electron meaningless. This would have the effect of making the matrix element for scattering independent of the change of electron wave vector required for the optical transition—i.e., the selection rule $\mathbf{K} = 0$ would be completely broken down. In such a situation, it would be reasonable to assume a constant optical matrix element connecting any state in the valence band with any state in the conduction band, particularly if the corresponding transitions are allowed in the pure material. The spectral variation of the absorption would then simply reflect the variation in the number of electron–hole pairs separated by an energy equal to the photon energy or

$$[\alpha h\nu] \sim \iint \frac{\rho_c(E_c)\,\rho_v(E_v)\,\delta(h\nu - E_c + E_v)\,dE_c\,dE_v}{\left\{\left[1 - f\left(\frac{E_c - \zeta}{kT}\right)\right] f\left(\frac{E_v - \zeta}{kT}\right)\right\}^{-1}}, \tag{239}$$

where the integration is over all the states in the respective bands. To keep things simple, assume that with increased doping the conduction-band states shift uniformly downward and the valence-band states shift uniformly

[151] G. G. Macfarlane, T. P. McLean, J. E. Quarrington, and V. Roberts, *Proc. Phys. Soc. (London)* **71**, 863 (1958).

upward. Further, assume that kT is much less than the resolution. For p-type material Eq. (239) then becomes

$$[\alpha h\nu] \sim \int_{-h\nu+E_g}^{-\zeta} (E_v + h\nu - E_g)^{1/2}(-E_v)^{1/2}\, dE_v. \tag{240}$$

Equation (240) can be written

$$[\alpha h\nu] \sim \frac{1}{4}(h\nu - E_g)^2 \int_{-1}^{1-2\zeta/(h\nu-E_g)} (1 - x^2)^{1/2}\, dx$$

$$= \frac{1}{8}(h\nu - E_g)^2 F\left(\frac{h\nu - E_g}{\zeta}\right). \tag{241}$$

The function $F(h\nu - E_g/\zeta)$ in Eq. (241) can be written in analytic form.[151a] It serves to cut off gradually the absorption for $h\nu - E_g > \zeta$. For $h\nu - E_g \gg \zeta$, F approaches unity and the spectral variation of the absorption is the same as in the case of indirect transitions involving band extrema at different points of the Brillouin zone.

It is unlikely that any case observed is as simple as this. The effects of doping should be particularly serious in InSb, where the effective masses are quite low. However, the absorption appears to be dominated by direct transitions for $h\nu > E_g + \varepsilon_c(k_\zeta) - \varepsilon_v(k_\zeta)$, even in samples with impurity concentrations as high as 10^{19} cm^{-3}.[147] The indirect transitions are likely to result in the presence of a tail absorption in the range $E_g + \zeta < h\nu < E_g + \varepsilon_c(k_\zeta) - \varepsilon_v(k_\zeta)$. However, tails on the absorption edge are commonplace and can result from a variety of causes. In a particular case there is the problem of isolating the cause or causes responsible for a given tail. We have previously discussed such tails and how they might be recognized. However, with heavy doping the structure present at low doping levels is absent, and the problem of analysis is difficult. We shall summarize these complications and comment relative to the case of heavy doping.

a. Change in Band Structure

The change in band structure with doping is at the center of interest in the study of the fundamental absorption in heavily doped material. Theoretically, it is rather clear that the impurity levels might shift and become broadened as a result of the intense electron–impurity and electron–electron scattering. The effects could be described in terms of a change in energy gap and a change in the density of states. However, it is not clear just

[151a] $F(x) = (\pi/2) - \sin^{-1}\{(2/x) - 1\} - (2/x^2)(2 - x)(x - 1)^{1/2}$.

what form these changes take. Theoretically, several authors[152–160] have considered the effects of high impurity concentrations on the energy bands. This subject is reviewed in the chapter by Bonch-Bruevich in Volume 1 of this series. Parmenter[154] considered the effect of impurity scattering. He found that for lower impurity concentrations the energy gap decreases in a manner similar to that due to the lattice vibrations. At higher impurity concentration, in addition to states given by the usual square-root dependence, a tail of states extends to lower energies. Other workers have extended the calculations to include electron–electron interaction. Wolff[158,159] found that the states near the band edge shift so as to decrease the energy gap with increased doping, but he did not find a band tailing. Bonch-Bruevich[160] found that the density of states is finite everywhere in the forbidden gap. However, the number of states in the tail is small relative to the total number of occupied states. Kane,[155–157] using the Thomas–Fermi approximation, found that the density of states approaches a Gaussian distribution near the band extrema.

Experimentally, the steep portion of the absorption edge tends to be exponential.[54,55,104,161] (See, for example, GaAs in Fig. 7.) This would tend to support an exponential or a Gaussian tail. In InAs Johnson and Fan[50] have observed a shift with increased doping of the absorption peaks seen in the interband magnetooptic effect. This observation might be interpreted as due to a general shift of the conduction-band levels just above the Fermi level.

b. Optical Matrix Element

It is not clear what role the optical matrix element will play in the region of the tail absorption. It is not likely to be independent of **K**.

c. Impurity–Band Absorption

Impurity absorption near the edge was discussed in Part VI. For sharp impurity levels it is easy to separate the impurity absorption from

[152] P. Aigrain, *Physica* **XX**, 978 (1954).
[153] P. Aigrain and J. des Cloizeaux, *Compt. Rend.* **241**, 859 (1955).
[154] R. H. Parmenter, *Phys. Rev.* **100**, 573 (1955).
[155] E. O. Kane, *Phys. Rev.* **125**, 1094 (1962).
[156] E. O. Kane, *Phys. Rev.* **131**, 79 (1963).
[157] E. O. Kane, *Phys. Rev.* **131**, 1532 (1963).
[158] P. A. Wolff, *Proc. Intern. Conf. Phys. Semicond., Exeter, 1962* p. 220. Inst. of Phys. and Phys. Soc., London, 1962.
[159] P. A. Wolff, *Phys. Rev.* **126**, 405 (1962).
[160] V. L. Bonch-Bruevich, *Proc. Intern. Conf. Phys. Semicond., Exeter, 1962* p. 216. Inst. of Phys. and Phys. Soc., London, 1962.
[161] R. Braunstein, J. I. Pankove, and H. Nelson, *Appl. Phys. Letters* **3**, 31 (1963).

absorption involving interband transitions. With increased doping the impurity levels broaden, and it is not easy to resolve the absorption associated with bound states of the impurity from the absorption associated with band levels. Morgan[162] has treated theoretically the problem of the broadening of impurity levels due to fluctuations in the local potential resulting from a random distribution of ions. He finds the localized impurity bands are approximately Gaussian in shape. Morgan has applied this approach to the analysis of emission bands in GaAs. Turner has applied the approach to the absorption in GaAs, but his paper has not appeared.[162]

d. Impurity–Impurity Absorption

Sharp lines in photoluminescence have been seen in GaP,[163] which have been attributed to the recombination involving donor–acceptor pairs.[121] With heavy doping individual lines cannot be resolved, and one must resort to an analysis along the lines described for impurity–band absorption.

At low doping levels a step in absorption at about 1.5 eV has been observed in GaAs.[24] At higher doping levels the step is not resolved. Lucovsky[164] has found that the absorption shifts and changes slope with degree of compensation. He attributes the absorption to transitions involving zinc–tellurium pairs.[165] The shift of the absorption results from the motion of the Fermi level through the impurity levels with compensation. He was able to fit the data satisfactorily, using a Gaussian distribution for the impurity levels,[166–168] as suggested by Callaway.[83]

e. Internal Strains

The presence of local strain resulting from inhomogeneities can shift the absorption edge in one neighborhood of a crystal relative to that in other neighborhoods of the crystal.

f. Exciton Effects

Exciton effects should play a minor role in highly doped material because of screening.

[162] T. N. Morgan, *Phys. Rev.* **139**, A343 (1965).
[163] A. T. Vink and C. Z. Van Doorn, *Phys. Letters* **1**, 332 (1962).
[164] G. Lucovsky, *Appl. Phys. Letters* **5**, 37 (1964).
[165] G. Lucovsky, A. J. Varga, and R. F. Schwartz, *Solid State Commun.* **3**, 9 (1965).
[166] G. Lucovsky, *Bull. Am. Phys. Soc.* **10**, 302 (1965).
[167] G. Lucovsky, *Solid State Commun.* **3**, 105 (1965).
[168] G. Lucovsky, *in* "Physics of Quantum Electronics" (Proc. Conf. San Juan, Puerto Rico, 1965) p. 467. McGraw-Hill, New York, 1966.

XII. Note Added in Proof

The fundamental absorption edge was the object of some of the earliest investigations of the optical properties of semiconductors. In spite of the large amount of activity that has taken place since the early work of Becker and Fan,[169–171] the study of the fundamental absorption edge is still quite lively. Three recent developments worthy of note are (1) the experimental observation of polaron effects on the fundamental absorption, (2) the continued development of modulation techniques, and (3) theoretical calculations demonstrating that exciton-ionized acceptor complexes can be stable for the case $m_h > m_e$.

Polaron Effects. Some of the effects of the electron–lattice interaction on the fundamental absorption have been discussed in Parts IV and V. For the case of phonon scattering the electron–lattice interaction results in the mixing of the no phonon state $|\mathbf{k}, 0>$ with all states $|\mathbf{k}', \mathbf{q}>$ such that the sum of $\mathbf{q}$ (the phonon wave vector) and $\mathbf{k}'$ is equal to $\mathbf{k}$. Such a mixed state is called a polaron state.[171a] The presence of scattering permits transitions that violate the selection rule ($\mathbf{K} = 0$). On the other hand, one might take the viewpoint that $\mathbf{K}$ is no longer a constant of the motion. We did not give a detailed discussion of the self energy of the polaron state except to note that it gives rise to a change in the energy gap.

The detailed effects on the electron self-energy have been the subject of much theoretical attention.[172] The effects are particularly strong when they involve the longitudinal optical phonon in a polar crystal. The chief results of the theoretical effort concerning such polaron effects are a variety of different formulas for the effect on electron mobility and various expressions for the ground-state energy and effective mass of the polaron as a function of the coupling constant α.

The energy of a conduction electron in the presence of weak coupling to the longitudinal optical phonons and in the limit of small k is given by simple perturbation theory as[173]

$$E = \frac{\hbar^2 k^2}{2m_e}\left(1 - \frac{\alpha}{6}\right) - \alpha\hbar\omega_0, \tag{242}$$

[169] M. Becker and H. Y. Fan, *Phys. Rev.* **76**, 1530 (1949).

[170] M. Becker and H. Y. Fan, *Phys. Rev.* **76**, 1531 (1949).

[171] H. Y. Fan and M. Becker, *Semi-cond. Mater., Proc. Conf. Univ., Reading*, 1950 pp. 132–147. Butterworths, London and Washington, D.C., 1951.

[171a] We assume weak coupling and neglect higher order terms involving multiphonon states.

[172] See, for example, "Polarons and Excitons" (C. G. Kuper and G. D. Whitfield, eds.). Plenum Press, New York, 1963.

[173] H. Fröhlich, see Ref. 172, p. 1.

where m_e is the electron effective mass, $\hbar\omega_0$ is the LO phonon energy, and α is the coupling constant:

$$\alpha = \frac{e^2}{\hbar}\left(\frac{1}{\varepsilon_\infty} - \frac{1}{\varepsilon}\right)\sqrt{\frac{m_e}{2\hbar\omega_0}} \quad . \tag{243}$$

where ε and ε_∞ are the dielectric constant and the high frequency dielectric constant, respectively.

The polaron effects would show up as an increase in effective mass by the factor $(1 + \frac{1}{6}\alpha)$ and a downward shift of the energy levels of $\alpha\hbar\omega_0$. For InSb, the former effect would be quite small (on the order of 1 %) whereas the latter should be $\alpha\hbar\omega_0 \approx 0.02 \times 25 \approx 0.5$ meV. Both of these effects are difficult to observe, and unfortunately the electron energy, as given, displays no qualitative features that are experimentally distinguishable from those in the absence of the electron–lattice interaction. One way to obtain distinguishing qualitative features is to apply a magnetic field sufficiently strong that the electron in moving in its cyclotron orbit is in near resonance with the lattice (i.e., $\hbar\omega_c \approx \hbar\omega_0$).

Consider first the polaron effects at very low magnetic fields in the case of weak coupling. For this case, simple Rayleigh–Schrödinger perturbation theory is applicable giving for the $n = 1$ Landau level[174]:

$$E_{n=1} \approx \tfrac{3}{2}\hbar\omega_c\left(1 - \frac{\alpha}{6}\right) - \alpha\hbar\omega_0 \qquad (\hbar\omega \ll \hbar\omega_0), \tag{244}$$

where $\hbar\omega_c$ would be the cyclotron energy in the absence of polaron effects. This differs from the case of no electron–phonon interaction (i.e., $\alpha \to 0$) only in that the band mass is replaced by the polaron mass and the energy is shifted.

To study the polaron effects for conditions near resonance, one must use more sophisticated theory. For a detailed discussion, the reader should consult the literature.[174–176] A theory for weak-coupled polarons in a magnetic field correct to order α is given by Larsen and Johnson.[175] The energy of the $n = 1$ Landau level is given by the implicit relation

$$E_{n=1} = \tfrac{3}{2}\hbar\omega_c - \frac{\alpha\hbar\omega_0}{2\pi^2}\rho\int d^3k \sum_n \frac{|H'_{n,1}(k)|^2}{E_{n=0} + n\hbar\omega_c + \hbar\omega_0 + (\hbar^2 k_z^2/2m_e) - E_{n=1}}, \tag{245}$$

[174] D. M. Larsen, *Phys. Rev.* **135**, A419 (1964).

[175] D. M. Larsen and E. J. Johnson, *Proc. Intern. Conf. Phys. Semicond., Kyoto, 1966* (*J. Phys. Soc. Japan* **21**, Suppl.), p. 443. Phys. Soc. Japan, Tokyo, 1966.

[176] D. M. Larsen, *Phys. Rev.* **144**, 697 (1966).

where $H'_{n,1}(k)$ is a matrix element given by

$$H'_{n,1}(k) = \frac{r_0}{(n!)^{\frac{1}{2}}} \frac{n - a^2k_\rho{}^2}{(ak_\rho)^{1-n}} \frac{\exp(-\frac{1}{2}a^2k_\rho{}^2)}{k} \quad , \tag{246}$$

and

$$a = \left(\frac{\hbar^2}{2m_e}/\hbar\omega_c\right)^{\frac{1}{2}}; \qquad r_0 = \left(\frac{\hbar^2}{2m_e}/\hbar\omega_0\right)^{\frac{1}{2}}. \tag{247}$$

The quantity a is the cyclotron radius for an electron in the $n = 0$ Landau level, and r_0 corresponds to the polaron radius. The magnetic field is in the z direction. Evaluation of Eq. (245) shows that $E_{n=1}$ becomes double valued for $\hbar\omega_c \approx \hbar\omega_0$, with the lower branch bending off and approaching $E_{n=0} + \hbar\omega_0$ for $\hbar\omega_c > \hbar\omega_0$. The upper branch follows closely the unperturbed value of $E_{n=1}$. By studying the relevant wave functions, one can make predictions concerning the fundamental absorption involving the energy level $E_{n=1}$. These considerations would indicate that one should see absorption lines in the interband absorption associated with $E_{n=1}$ that occur as doublets for $\hbar\omega_c \approx \hbar\omega_0$. For increasing magnetic field, the low energy member of a doublet should rapidly decrease in intensity and, neglecting contributions from the valence band, should follow a magnetic field dependence close to that of the $n = 0$ level. The upper member of the doublet should rapidly increase in intensity and follow a magnetic field dependence close to that of the $n = 1$ level (again neglecting the relevant valence band level). Such polaron doublets for InSb at helium temperature have been observed experimentally, and their predicted effects verified.[175,177] They represent the first unambiguous demonstration of the existence of polarons. These experiments appear to contain complications due to excitons and to forbidden transitions involving close-lying valence band levels. *Intraband* magnetoabsorption (cyclotron resonance) provides a cleaner experiment. *Intraband* measurements confirming and supplementing the *interband* results have been made.[178] Unfortunately, the *intraband* experiments are limited by the large reflection losses for photon frequencies in the interval including ω_0 and ω_T, the TO phonon frequency. In the case of the highly polar materials, where very striking polaron effects should occur, the effective masses are generally too large to obtain the resonant condition with accessible magnetic fields.

Modulation Techniques. A modulation technique is a natural one for the study of electroabsorption and has been discussed in Part X. Consideration

[177] E. J. Johnson and D. M. Larsen, *Phys. Rev. Letters* **16**, 655 (1966).

[178] D. H. Dickey, E. J. Johnson, and D. M. Larsen, *Bull. Am. Phys. Soc.* **11**, 828 (1966); and to be published.

of the reflection measurements[179] and the study of indirect transitions in absorption[180] show the need for such techniques. In the former case, one looks for small variations superimposed upon a large background; in the latter, one looks principally for changes of slope of a gradually increasing absorption. The purpose of each of the modulation techniques is to minimize the effect of the background.

The general approach is to apply some cyclic perturbation to the sample which changes the absorption (reflection). This results in a partial modulation of the transmitted (reflected) intensity. The associated detector electronics discriminates in favor of the ac component of the intensity, giving an output that is proportional to the derivative of the absorption (reflection) in respect to the applied perturbation.

As mentioned in Part I, reflection techniques possess the uncertainty of interpreting the position of reflection peaks in terms of the separation of energy levels. This uncertainty is compounded when reflection is used in combination with modulation techniques. However, the increased sensitivity makes it possible to observe effects that cannot be seen otherwise.

In Part X, on the effect of an electric field on the fundamental absorption, the author neglected to discuss the work of Seraphin and co-workers on electroreflection. This work has been extended considerably in the time since the original manuscript was completed. Seraphin *et al.*[181] applied an ac electric field along with a dc bias to the surface using a transparent electrode and observed the modulation of the intensity of the light reflected through the electrode. The electric field was monitored by observing the surface conductance. Results have been reported for germanium,[181] silicon,[182] and GaAs.[183] Cardona and co-workers[184] have utilized a variation of this arrangement employing an electrolyte in place of a transparent electrode and have used the technique to measure a large variety of semiconducting materials. Feinleib[185] found that the electrolytic method could be applied to metals. This is surprising since the penetration of the low frequency electric field in metals should be insufficient to affect the reflectivity. This indicates that the role of the electrolyte in the electroreflectance cannot be ignored. Groves *et al.*[186] have extended the electrolytic technique into the infrared by using a thin film of electrolyte and have observed magnetoreflectance in Ge, GaSb, and InSb.

[179] See discussion in Part I.

[180] See Section 12.

[181] B. O. Seraphin, R. B. Hess, and N. Bottka, *J. Appl. Phys.* **36**, 2242 (1965).

[182] B. O. Seraphin and N. Bottka, *Phys. Rev. Letters* **15**, 104 (1965).

[183] B. O. Seraphin, *Proc. Phys. Soc. (London)* **87**, 239 (1966).

[184] K. L. Shaklee, F. H. Pollak, and M. Cardona, *Phys. Rev. Letters* **15**, 883 (1965).

[185] J. Feinleib, *Phys. Rev. Letters* **16**, 1200 (1966).

[186] S. H. Groves, C. R. Pidgeon, and J. Feinleib, *Phys. Rev. Letters* **17**, 643 (1966).

Engeler *et al.*[187] have modulated the stress using a transducer to study the piezoreflectivity of metals and semiconductors and to study indirect transitions in the piezoabsorption of germanium.[188] Similar studies of the piezoreflectivity of silicon have been made by Gobeli and Kane.[189] Mavroides *et al.*[190] and Aggarwal *et al.*[191] have applied acoustical modulation of sample stress to the study of the fundamental absorption under a magnetic field in InSb and Ge. Considerable improvement in sensitivity over the previous results was obtained. In particular, it has been possible to observe transitions involving the split-off valence band giving an estimate of the spin orbit splitting. A modulation technique employing a heating pulse of electric current[192] and one employing wavelength modulation[193] have also been successful.

Ionized Acceptor–Exciton Complexes. In Section 27 we discussed the possibility of the formation of an ionized acceptor–exciton complex in the usual situation where $m_e < m_h$. It was pointed out that the dissociation energy of such a complex would be approximately E_A, the ionization energy of the acceptor. However, whether such a complex can exist hinges upon the question of whether the neutral acceptor in the ground state, or in an excited state, has an affinity for an electron (i.e., whether an electron localized near a neutral acceptor lowers the energy of the system from that when the electron is removed to infinity). According to a simple model, Hopfield[121] concluded that the neutral acceptor has no electron affinity for the case $m_e < 1.4m_h$. However, he did not consider excited states of the acceptor nor details of the band structure. Experimental results on GaSb by Johnson and Fan[85] can be simply interpreted if one assumes the existence of an ionized acceptor–exciton complex. This would indicate that the neutral acceptor has an electron affinity for $m_e = 0.23m_h$, contrary to the considerations of Hopfield. Sharma and Rodriguez[194] have recently performed variational calculations on the system consisting of an exciton and an ionized impurity to obtain the ground state energy. Their criterion for the existence of the complex is that the energy obtained in this manner be lower than the ground state energy of a hole bound to the acceptor. They conclude that an ionized

[187] W. E. Engeler, H. Fritzsche, M. Garfinkel, and J. J. Tiemann, *Phys. Rev. Letters* **14**, 1069 (1965); M. Garfinkel, J. J. Tiemann, and W. E. Engeler, *Phys. Rev.* **148**, 695 (1966).

[188] W. E. Engeler, M. Garfinkel, and J. J. Tiemann, *Phys. Rev. Letters* **16**, 239 (1966).

[189] G. W. Gobeli and E. O. Kane, *Phys. Rev. Letters* **15**, 142 (1965).

[190] J. G. Mavroides, M. S. Dresselhaus, R. L. Aggarwal, and G. F. Dresselhaus, *Proc. Intern. Conf. Phys. Semicond., Kyoto, 1966* (*J. Phys. Soc. Japan* **21**, Suppl.) p. 184. Phys. Soc. Japan, Tokyo, 1966.

[191] R. L. Aggarwal, L. Rubin, and B. Lax, *Phys. Rev. Letters* **17**, 8 (1966).

[192] B. Batz, *Solid State Commun.* **4**, 241 (1966); C. N. Berglund, *J. Appl. Phys.* **37**, 3019 (1966).

[193] I. Balslev, *Phys. Rev.* **143**, 636 (1966).

[194] R. R. Sharma and S. Rodriguez, *Phys. Rev.* **153**, 823 (1967).

acceptor–exciton complex can exist if $m_e < 0.25m_h$, in addition to the case where $m_e > 1.4m_h$. This would tend to support the interpretation of the experimental results in GaSb, where they would predict a dissociation energy of $1.17E_A = 18$ meV. This agrees well with the value of 14 meV observed experimentally for the γ-peak in GaSb. However, it is not clear what value should be taken for E_A in applying the theory to experimental results in GaSb. The value used by Sharma and Rodriguez is the value calculated from the simple effective-mass hydrogen model of the acceptor using the heavy-hole mass. Experimentally there is no evidence for the existence of acceptors in GaSb with such low ionization energies. One might argue that the central cell correction is, somehow, much reduced in the case of the complex from that in the neutral acceptor ion and that the effective mass value of E_A is the proper one to use. But if one accepts the high experimental values of acceptor ionization energy ($\geqslant 35$ meV), the criterion of Sharma and Rodriguez for binding in the complex is violated. It would appear that excited states of the ionized acceptor–exciton complex can exist with lifetimes sufficiently long for the observation of optical absorption peaks, but the precise conditions for their existence are not clear. It should be noted that Sharma and Rodriguez do not regard their theory as a means of calculating accurate experimental binding energies.[195]

ACKNOWLEDGMENTS

The author would like to express his appreciation to Drs. J. O. Dimmock, P. N. Argyres, and G. B. Wright for many helpful discussions concerning this work. The work was started at Purdue University, where the author benefited from conversations with Professor H. Y. Fan. The author would like to thank Dr. G. Lucovsky for supplying material before publication. He would also like to thank Mrs. S. F. Simon for typing the manuscript.

[195] S. Rodriguez, private communication.

CHAPTER 7

Introduction to the Theory of Exciton States in Semiconductors*

John O. Dimmock

I. INTRODUCTION 259
1. *Basic Concepts* 260
2. *Qualitative Considerations on a Simplified Model* 263

II. EFFECTIVE-MASS THEORY FOR EXCITON STATES 267
3. *Hartree–Fock Approximation* 267
4. *Interaction Potential* 269
5. *Development of the Exciton Effective-Mass Equation* 270
6. *Reduction of the Exciton Effective-Mass Equation* 283

III. OPTICAL ABSORPTION BY EXCITONS. 287
7. *Direct Transitions*. 288
8. *Selection Rules for Direct Exciton Transitions*. 293
9. *Indirect Transitions* 294

IV. THE EFFECTS OF AN EXTERNAL MAGNETIC FIELD 299
10. *g-Factors for Electrons and Holes* 299
11. *Exciton States in a Magnetic Field and Landau Levels* 301

V. APPLICATION TO GROUP III–V COMPOUNDS 310
12. *Structure of the Valence and Conduction Bands* 311

VI. SUMMARY 317

I. Introduction

In this chapter an attempt is made to introduce the theory of exciton states in semiconductors on two levels. On one level we develop, discuss, and use the general effective-mass equations for exciton states in semiconductors with arbitrary degenerate bands. Since the formalism involved in this is often extensive, we have fallen back on a simple model from time to time in hope of providing additional physical insight into the situation. No attempt has been made to discuss all aspects of the exciton problem. The topics chosen to be discussed are, in the view of the author, those most useful to understanding the phenomena associated with exciton states

* This chapter was prepared at Lincoln Laboratory, a center for research operated by Massachusetts Institute of Technology with the support of the U. S. Air Force.

specifically in group-IV and group III–V semiconductors. What we do attempt is to develop the theory and concepts necessary to the understanding of exciton states in these materials in a deductive manner and in sufficient detail that the reader may obtain an understanding of the basic concepts involved as well as a working knowledge of the formal aspects of the problem.

1. Basic Concepts

In the ground state of ideal, impurity-free, semiconducting and insulating crystals there exists a set of fully occupied electronic energy levels, separated from a set of unoccupied levels by a finite energy gap. Electronic excitation in these crystals occurs when a single electron is transferred from one of the occupied levels to one of the unoccupied levels. The electronic state resulting from such an excitation is referred to as an exciton. Since the energy gaps are typically of the order of a few electron volts, the excitation processes usually take place through the absorption of an optical photon. The theoretical description of exciton states in a solid is a many-body problem and cannot be solved without making many simplifying assumptions. Depending on the material involved, one of two basic approximations is normally applied. If the atoms in the solid interact weakly, as in molecular, rare gas and some ionic crystals, the electronic excitation can be thought of as being essentially that of a single atom or molecule, perturbed, perhaps, by its surrounding neighbors. This approach to the theory of excitons was first considered by Frenkel in 1931.[1–3] The excitation is more or less localized in space, spreading out over, at most, a few atomic sites. It may nevertheless propagate through the crystal and provide a means of transferring energy from one point to another.[4] Such a localized excitation is referred to as a Frenkel exciton.

In semiconducting crystals, however, the interactions between individual atoms in the solid are quite strong, and any elementary excitation cannot be localized in space but will spread out over a large number of atomic sites. In this case, the localized model of Frenkel is completely inadequate. The electronic properties of semiconducting crystals are usually described in terms of an energy-band model in which the single-particle eigenstates are Bloch waves with energies that form quasicontinuous bands in momentum or **k** space. An elementary excitation in this system occurs when an electron is transferred from one of the fully occupied (valence) bands into an unoccupied (conduction) band. This process leaves an unoccupied state in the

[1] J. Frenkel, *Phys. Rev.* **37**, 17, 1276 (1931).
[2] R. E. Peierls, *Ann. Physik* [5] **13**, 905 (1932).
[3] J. Frenkel, *Physik. Z. Sowjetunion* **9**, 158 (1936).
[4] W. R. Heller and A. Marcus, *Phys. Rev.* **84**, 809 (1951).

valence band. Many aspects of this situation can be described by representing the unoccupied electronic state by a particle with a positive charge, referred to as a "hole." The excited state of the crystal therefore consists of an electron in an otherwise unoccupied conduction band and a hole in an otherwise occupied valence band. This description of excited states in semiconducting crystals was first discussed by Wannier[5] and later by Slater.[6] These states are known as Wannier excitons. Again, this excitation process occurs through the absorption of an optical photon, accompanied, perhaps, by the creation or destruction of a lattice phonon.

Ideal semiconducting and insulating crystals are transparent to light of energy less than the energy gap separating the occupied from the unoccupied energy bands. The energy at which the crystal starts to absorb radiation is referred to as the fundamental absorption edge. The optical properties of crystals in the vicinity of the absorption edge are strongly influenced by the fact that the electron and hole created in the excitation process interact with each other. In many crystals this absorption edge exhibits a structure that is due to this interaction, or in other words, to the formation of exciton states in the crystal, and the most direct information on exciton states is obtained by studying the optical properties of the crystal in the vicinity of the absorption edge. From the definition of excitons as being the elementary electronic excitations in semiconductors and insulators, we should consider all of the optical properties of an ideal crystal in the vicinity of the absorption edge to be due to the creation of exciton states. Although this is fundamentally correct, it is necessary here to restrict our attention to those effects that are due specifically to the interaction between the electron and the hole. We can refer to these as exciton effects, keeping in mind the fact that all of the optical properties actually involve the creation of exciton states.

The principal qualitative difference between the situation described by Wannier and that described by Frenkel lies in the spatial extent of the exciton state, which depends in turn on the strength of interaction between neighboring atoms in the crystal. In the present treatment we are concerned with excitations in group-IV elements and in group-III–V compounds. These excitons have a rather large spatial extent and are described more adequately by the Wannier model. In this model, the exciton state is described by an "effective-mass" equation, which involves various properties of the band states occupied by the electron and the hole. A discussion of this equation and some of the approximations involved in its derivation are given in Sections 3–6. Since the properties of the band states are of wide general interest in the study of semiconductors, we are concerned here

[5] G. H. Wannier, *Phys. Rev.* **52**, 191 (1937).

[6] J. C. Slater, *Phys. Rev.* **76**, 1592 (1949).

largely in how the study of exciton states can yield information about the properties of the relevant energy bands. This comes about most directly through the investigation of the effects of external magnetic fields on the optical properties of the absorption edge. Consequently, in Section 7, 8, and 9, we consider the influence of exciton states on the optical properties of the absorption edge. In Sections 10 and 11 we examine in a little more detail the properties of exciton states in the presence of an external magnetic field for the simple band case, and in Section 12 we discuss briefly the specific properties of exciton states in group-IV and group-III–V semiconductors.

There is considerable literature of both theoretical and experimental work pertaining to the properties of exciton states in crystals. We shall not discuss all of this work here by any means, partly because of space limitations and partly because we are primarily interested in excitons in group-III–V semiconductors. For completeness, however, we cite here some of the literature pertaining to excitons in molecular and ionic crystals. The properties of exciton states in molecular crystals have been reviewed by McClure[7] and Wolf,[8] and the interested reader is referred to these papers for further references in this field. Nikitine has recently reviewed many aspects of the theory of excitons in semiconductors and ionic compounds[9] and also much of the experimental work.[10,11] He has, however, been mostly concerned with ionic materials, rather than with the more traditional semiconductors. There has been much work done on the exciton spectra in cuprous oxide, which we shall not discuss in any detail here. The reader is referred instead to the review articles by Nikitine cited above and by Gross.[12,13] Also a number of review papers on exciton states in molecular and ionic crystals are contained in Supplement 12 of the *Progress of Theoretical Physics* (1959).[13a]

The theory of exciton states in semiconductors appropriate to a study of group-III–V compounds has recently been discussed in some detail by Knox[14] and by Elliott.[15] I am greatly indebted to both of these treatments for much of the material contained in this chapter, both in substance and in

[7] D. S. McClure, *Solid State Phys.* **8**, 1 (1959).
[8] H. C. Wolf, *Solid State Phys.* **9**, 1 (1959).
[9] S. Nikitine, *Progr. Semicond.* **6**, 233 (1962).
[10] S. Nikitine, *Progr. Semicond.* **6**, 269 (1962).
[11] S. Nikitine, *Phil. Mag.* **4**, 1 (1959).
[12] E. F. Gross, *Izvest. Akad. Nauk. S.S.S.R. Ser. Fiz.* **20**, 89 (1956) [*English Transl.: Bull. Acad. Sci. USSR, Phys. Ser.* **20**, 78 (1956)].
[13] E. F. Gross, *Nuovo Cimento* **3**, 672 (1956).
[13a] *Progr. Theor. Phys. (Kyoto), Suppl.* No. 12 (1959).
[14] R. S. Knox, *Solid State Phys., Suppl.* No. 5 (1963).
[15] R. J. Elliott, Theory of Excitons I *in* "Polarons and Excitons" (C. G. Kuper and G. D. Whitfield, eds.), p. 269. Plenum Press, New York, 1963.

concept, and the reader is enthusiastically referred to both of these works for further information. Much of the recent literature on excitons in semiconductors is contained in the proceedings of the recent conferences on semiconducting compounds.[16–20]

2. Qualitative Considerations on a Simplified Model

Before developing the general effective-mass theory for Wannier excitons, it is useful as an introduction to investigate the predictions of a simple model in order to discuss some of the qualitative aspects of the problem. Let us consider a semiconducting or insulating crystal with the electronic band structure shown schematically in Fig. 1. In the ground state of the crystal the lower (valence) band states are completely occupied while the upper (conduction) band is empty. Low-energy single-electron excitations are indicated in the figure by the two processes *A* and *B*. Process *A* represents the transfer of an electron from a state near the valence-band maximum to a state with approximately the same wave vector **k** near the conduction-band minimum, in this case at the center of the Brillouin zone. This process

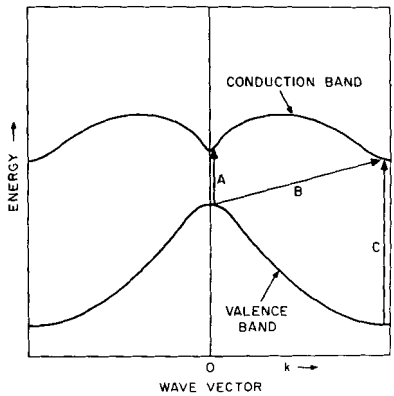


FIG. 1. Schematic representation of a simple band structure, illustrating three types of elementary electronic excitations. Type *A* represents a low-energy direct transition, type *B*, a low-energy indirect transition, and type *C*, a higher-energy direct transition.

[16] *J. Phys. Chem. Solids* **8** (1959) [*Proc. Intern. Conf. Semicond., Rochester, New York, 1958*].

[17] *Proc. Intern. Conf. Semicond. Phys., Prague, 1960.* Czech. Acad. Sci., Prague, and Academic Press, New York, 1961.

[18] *J. Appl. Phys.* **32** Suppl. No. 10 (1961) [*Proc. Conf. Semicond. Compds., Schenectady, New York, 1961*].

[19] *Proc. Intern. Conf. Phys. Semicond., Exeter, 1962.* Inst. of Phys. and Phys. Soc., London, 1962.

[20] "Physics of Semiconductors" (*Proc. 7th Intern. Conf.*). Dunod, Paris, and Academic Press, New York, 1964.

can occur through the absorption of an optical photon, and is referred to as a direct transition. The resultant excited (exciton) state is consequently referred to as a direct exciton. Process *B* represents the transfer of an electron from a state near the valence-band maximum to a state with a different wave vector near a conduction-band minimum, in this case at the zone edge. In this process the absorption of an optical photon must be accompanied by the creation or annihilation of a lattice phonon. This process is referred to as an indirect transition, and the resultant excited state as an indirect exciton. In all cases, the important low-energy processes involve the transfer of an electron from a state near a valence-band maximum to a state near a conduction-band minimum.

It is clear that the interaction between the electron and the hole is greatest when the relative velocity of the two particles is smallest. Since the velocity of a particle in a band state of wave vector $\mathbf{k}$ is proportional to the gradient of the band energy with respect to $\mathbf{k}$, we should consider transitions between all valence- and conduction-band states that have approximately the same gradient. However, all such transitions that take place at larger photon energies—for example, process *C* in Fig. 1—are, for the most part, obscured and are difficult to observe.[20a] Consequently, we shall be interested here only in processes *A* and *B*, referred to as direct and indirect transitions, respectively. Note that these processes need not involve states at the center of the Brillouin zone but that the important considerations are as follows:

(1) The processes involve relatively-low-energy photons.
(2) The velocities of the two states involved are approximately the same.
(3) Process *A* does not involve a phonon, whereas process *B* does.

Consider a simple model in which the band energies for the conduction and valence bands in the vicinity of $\mathbf{k} = 0$ are given respectively by

$$E_c(\mathbf{k}) = E_g + \frac{\hbar^2 k^2}{2m_e^*} \tag{1}$$

and

$$E_v(\mathbf{k}) = -\frac{\hbar^2 k^2}{2m_h^*} \tag{2}$$

for simple spherical bands. It can be shown then[5] that the relative motion of the electron in the conduction band and the hole in the valence band,

[20a] However, exciton effects due to transitions of type *C* have been observed in the absorption spectra of thin films of InSb and CdTe by Cardona and Harbeke.[21]

[21] M. Cardona and G. Harbeke, *Phys. Rev. Letters* **8**, 90 (1962).

in process A, is obtained from a hydrogen-like wave equation

$$\left\{-\frac{\hbar^2}{2m_e^*}\nabla^2 - \frac{\hbar^2}{2m_h^*}\nabla^2 - \frac{e^2}{\kappa_0 r}\right\}\psi(\mathbf{r}) = \varepsilon\psi(\mathbf{r}) \tag{3}$$

in which the electron and hole behave as though they possessed the "effective masses" of the conduction and valence band extrema, m_e^* and m_h^*, respectively, and interact with each other via a Coulomb force modified by the static dielectric constant of the crystal, κ_0. The solutions of Eq. (3) form a hydrogenic series of discrete levels with energies given by

$$\varepsilon_n = -R/n^2, \tag{4}$$

where

$$R = \frac{\mu e^4}{2\hbar^2 \kappa_0^2}, \tag{5}$$

and μ is referred to as the reduced mass of the exciton and is given by

$$\frac{1}{\mu} = \frac{1}{m_e^*} + \frac{1}{m_h^*}. \tag{6}$$

The energy ε_n is related to the energy of the corresponding state of a hydrogen atom by

$$\varepsilon_n = \frac{\mu}{m\kappa_0^2} E_n^{\mathrm{H}}, \tag{7}$$

where m is the free-electron mass. Typically, $\mu/m \approx 0.05$ and $\kappa_0 \approx 13$, so that $\varepsilon_n \approx 3 \times 10^{-4} E_n^{\mathrm{H}}$. This gives a binding energy for the ground-state exciton of about 4 meV. The total energy of the exciton state above the ground state of the crystal is $E_n = E_g + \varepsilon_n$. Therefore, the absorption spectrum for photons of energy a few meV less than the gap energy E_g will, in this simplified example, consist of a series of discrete absorption lines. Such an ideal spectrum has actually been observed in Cu_2O. A typical absorption spectrum for Cu_2O is shown in Fig. 2. In addition to this set of discrete energy levels Eq. (3) possesses a *continuous* set of solutions with ε_n positive. Optical absorption involving transitions to these states forms the actual absorption edge of the crystal. These states are strongly affected by the electron–hole Coulomb interaction, which leads, then, not only to a series of discrete energy levels below the absorption edge but also to a modification of the edge itself. Both of these effects will be discussed in more detail later.

The distinction between Wannier and Frenkel excitons has been made above on the basis of the spatial extent of the exciton. We stated that a Frenkel exciton should extend over at most a few atomic sites—say, 3–7 Å.

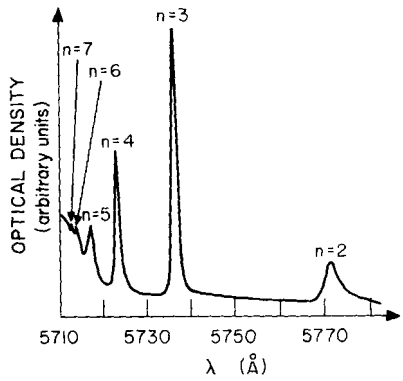


FIG. 2. Densitometer trace of the absorption spectra of the yellow series of exciton lines in Cu_2O. (After S. Nikitine *et al.*[22])

The spatial extent of the Wannier exciton state in the simple model considered here is given by the modified Bohr radius of the state. This is given by

$$\left\langle \frac{1}{r} \right\rangle^{-1} = n^2 a_0 , \tag{8}$$

where

$$a_0 = \frac{\hbar^2 \kappa_0}{\mu e^2} = \frac{m}{\mu} \kappa_0 a_0^{\mathrm{H}} \tag{9}$$

and a_0^{H} is the Bohr orbit radius for the hydrogen atom. The value of a_0 is typically about 150 Å, or about thirty times the radius of a Frenkel exciton. Nevertheless, we should note that the effective-mass approach breaks down at small distances (less than about 50 Å), partly because the effective-mass method essentially treats the Coulomb interaction between the electron and the hole as a perturbation and at small distances this interaction becomes large. Also, the interaction itself is not given correctly at small distances in Eq. (3). These effects are discussed briefly in Sections 3 and 5.

In general, exciton states are observed only in relatively pure semiconducting crystals. This occurs for a number of reasons. First, the electron–hole interaction is strongly shielded by the presence of other free carriers in the system. Casella[23] has indicated, in fact, that for concentrations greater

[22] S. Nikitine, J. Biellmann, J. L. Deiss, M. Grosmann, J. B. Grun, J. Ringeissen, C. Schwab, M. Sieskind, and L. Wursteisen, *Proc. Intern. Conf. Phys. Semicond., Exeter, 1962* p. 431. Inst. of Phys. and Phys. Soc., London, 1962.

[23] R. C. Casella, *J. Appl. Phys.* **34**, 1703 (1963).

than about $N_0 = 5 \times 10^{-2} a_0^{-3}$ no bound exciton states can exist. For $a_0 = 160$ Å, as found in GaAs,[24] the upper carrier-concentration limit is $2 \times 10^{16}\,\mathrm{cm}^{-3}$. This indicates that bound excitons probably do not exist in heavily doped semiconductors and definitely do not exist as such in semimetals and metals. Exciton effects will therefore not be as important in these materials as in materials with lower carrier concentrations.

However, if only the free-carrier effects were important, one might expect to observe discrete exciton absorption in heavily doped but compensated material. This is, in fact, not the case. In addition to the free-carrier effects, the presence of a high concentration of impurity atoms results in a broadening of the exciton absorption lines such that above a certain impurity concentration the discrete spectra are wiped out.

II. Effective-Mass Theory for Exciton States

In the effective-mass theory for exciton states the eigenfunctions and eigenenergies are obtained, in general, as solutions of a set of coupled differential equations. These equations involve terms of two different types: kinetic-energy terms, which involve various properties of the band states occupied by the electron and hole; and a potential-energy term, which arises because of the interaction between the electron and hole. In a sense, we can say that all the exciton effects which we shall be discussing below arise because of this interaction. Although our concern will be primarily with the kinetic-energy terms, let us start by briefly indicating the origin of the potential term.

3. Hartree–Fock Approximation

In this section we show that an effective Coulomb interaction occurs between the electron and the hole when the exciton problem is treated in the framework of the Hartree–Fock theory (see, for example, Refs. 25 and 26). The interaction is, however, not calculated correctly by this approach, since it is inherently a many-body effect and the Hartree–Fock theory is a single-particle approximation. In the absence of external fields, the electronic wave function of the crystal is an eigenfunction of the Hamiltonian

$$\mathscr{H} = \sum_i U(\mathbf{r}_i) + \sum_{i<j} V(\mathbf{r}_i - \mathbf{r}_j), \tag{10}$$

[24] M. D. Sturge, *Phys. Rev.* **127**, 768 (1962).

[25] D. J. Thouless, "The Quantum Mechanics of Many Body Systems," p. 15. Academic Press, New York, 1961.

[26] R. S. Knox, *Solid State Phys. Suppl.* No. 5, Section 2 (1963).

where

$$U(\mathbf{r}_i) = -\frac{\hbar^2}{2m}\nabla_i^2 - \sum_\alpha \frac{Z_\alpha e^2}{|\mathbf{R}_\alpha - \mathbf{r}_i|} \tag{11}$$

and

$$V(\mathbf{r}_i - \mathbf{r}_j) = \frac{e^2}{|\mathbf{r}_i - \mathbf{r}_j|}. \tag{12}$$

$\mathbf{R}_\alpha$ is the position of the αth nucleus of the charge Z_α and $\mathbf{r}_i$ is the position of the ith electron. Let us digress a moment to point out that Eq. (10) already involves the assumption that the nuclear and electronic motions can be separated—that is, it depends on the Born-Oppenheimer approximation.[27] To lowest order, the total wave function for the crystal is written as a product of a nuclear wave function, which depends only on the nuclear coordinates, and an electronic wave function, which is an eigenstate of Eq. (10) and which depends only parametrically on the nuclear coordinates. Normally, the nuclei are assumed to be fixed in their equilibrium positions. Electron–phonon scattering occurs when the nuclei are allowed to move. As long as this scattering provides only a small perturbation to the electron states, the separation of nuclear and electronic wave functions is justified. If the interaction between the electron and the lattice is not small, one must consider the coupled electron–lattice (polaron) problem (see, for example, Ref. 28). In semiconducting crystals this interaction leads to a large modification in the effective electron–hole interaction.

In the Hartree–Fock approximation, the electronic wave function is written as a determinant of single electron functions. The ground-state function can be written as

$$\Psi_0 = \frac{1}{\sqrt{N!}} A\, \psi_{v_1\mathbf{k}_1}(\mathbf{r}_1) \cdots \psi_{v_1\mathbf{k}_n}(\mathbf{r}_n)\, \psi_{v_2\mathbf{k}_1}(\mathbf{r}_{n+1}) \cdots \psi_{v_m\mathbf{k}_n}(\mathbf{r}_N) \tag{13}$$

for an N-electron system, where v_i runs over all occupied valence bands and $\mathbf{k}_i$ runs over the first Brillouin zone. The symbol A denotes the antisymmetrizing operator, and the coordinate $\mathbf{r}_i$ should be taken to include the spin coordinate. Consider an excited state of the system,

$$\Psi' = \frac{1}{\sqrt{N!}} A\, \psi_{v_1\mathbf{k}_1}(\mathbf{r}_1) \cdots \psi_{c_i\mathbf{k}'}(\mathbf{r}_j) \cdots \psi_{v_m\mathbf{k}_n}(\mathbf{r}_N), \tag{14}$$

[27] M. Born and K. Huang, "Dynamical Theory of Crystal Lattices," Chap. 4. Oxford Univ. Press, London and New York, 1956.

[28] "Polarons and Excitons" (C. G. Kuper and G. D. Whitfield, eds.). Plenum Press, New York, 1963.

in which a single electron has been transferred from the valence-band state $\psi_{v_j\mathbf{k}}$ to a conduction-band state $\psi_{c_i\mathbf{k}'}$. The excitation energy of this state above the ground state is given by

$$E(c_i\mathbf{k}';v_j\mathbf{k}) - E_0 = E(c_i\mathbf{k}') - E(v_j\mathbf{k}) + V(c_i\mathbf{k}';v_j\mathbf{k}), \tag{15}$$

where $E(c_i\mathbf{k}')$ and $E(v_j\mathbf{k})$ are the single-electron conduction- and valence-band energies and are given by

$$E(c_i\mathbf{k}') = \langle c_i\mathbf{k}'|U(\mathbf{r})|c_i\mathbf{k}'\rangle + \sum_{v,\mathbf{k}''}\{\langle c_i\mathbf{k}';v\mathbf{k}''|V(\mathbf{r}_1-\mathbf{r}_2)|c_i\mathbf{k}';v\mathbf{k}''\rangle - \langle c_i\mathbf{k}';v\mathbf{k}''|V(\mathbf{r}_1-\mathbf{r}_2)|v\mathbf{k}'';c_i\mathbf{k}'\rangle\} \tag{16a}$$

and

$$E(v_j\mathbf{k}) = \langle v_j\mathbf{k}|U(\mathbf{r})|v_j\mathbf{k}\rangle + \sum_{v,\mathbf{k}''}\{\langle v_j\mathbf{k};v\mathbf{k}''|V(\mathbf{r}_1-\mathbf{r}_2)|v_j\mathbf{k};v\mathbf{k}''\rangle - \langle v_j\mathbf{k};v\mathbf{k}''|V(\mathbf{r}_1-\mathbf{r}_2)|v\mathbf{k}'';v_j\mathbf{k}\rangle\}, \tag{16b}$$

where the sum goes over *all* valence-band states that are occupied in the ground state of the crystal. The effective interaction $V(c_i\mathbf{k}';v_j\mathbf{k})$ is given by

$$V(c_i\mathbf{k}';v_j\mathbf{k}) = -\{\langle c_i\mathbf{k}';v_j\mathbf{k}|V(\mathbf{r}_1-\mathbf{r}_2)|c_i\mathbf{k}';v_j\mathbf{k}\rangle - \langle c_i\mathbf{k}';v_j\mathbf{k}|V(\mathbf{r}_1-\mathbf{r}_2)|v_j\mathbf{k};c_i\mathbf{k}'\rangle\}. \tag{17}$$

Note that all matrix elements in Eqs. (16) and (17) involve a summation over spin coordinates. The second term in Eq. (17) is of an exchange nature and is generally small and short ranged.[29,15] If this term is neglected, we see that an effective interaction arises between the electron and the hole with a potential given by $-V(\mathbf{r}_1-\mathbf{r}_2) = -e^2/|\mathbf{r}_1-\mathbf{r}_2|$, which is Coulombic and attractive. This substantiates our intuitive picture of the situation. However, as mentioned above, many important aspects of this problem are neglected by the Hartree–Fock approach, and must be included to obtain the correct value of the effective electron–hole interaction potential. Some of these are considered below.

4. Interaction Potential

The calculation of the correct value of the effective electron–hole interaction potential is reasonably complicated, and consequently only a brief qualitative discussion is attempted here.[30–32] For a more detailed treatment of this problem, the reader is referred to a recent discussion by Haken,[33]

[29] E. O. Kane, *J. Phys. Chem. Solids* **6**, 236 (1958); **8**, 38 (1959).
[30] W. Kohn, *Phys. Rev.* **105**, 509 (1957); **110**, 857 (1958); *J. Phys. Chem. Solids* **8**, 45 (1959).
[31] L. Roth and G. Pratt, *J. Phys. Chem. Solids* **8**, 47 (1959).
[32] H. Haken, *J. Phys. Chem. Solids* **8**, 166 (1959).
[33] H. Haken, Theory of Excitons II *in* "Polarons and Excitons" (C. G. Kuper and G. D. Whitfield, eds.), p. 295. Plenum Press, New York, 1963.

which is to some extent followed here. When the electron and hole are widely separated and moving relatively slowly with respect to one another, the Coulomb interaction between them is screened by the static dielectric constant κ_0. The effective potential is given by

$$V(\mathbf{r}) = -\frac{e^2}{\kappa_0 r}. \tag{18}$$

This screening is due to the combined effects of electronic and lattice polarization. As the electron and hole approach one another, their relative velocity increases until their motion is so rapid that the lattice polarization cannot follow it. This occurs when the frequency of motion is greater than the reststrahlen frequency of the crystal. In this region the interaction is given by Eq. (18) with κ_0 replaced by the high-frequency dielectric constant κ_∞. For the simple system considered in the introduction, the frequency of motion for the ground-state exciton is given by $\omega = \hbar/2\mu a_0^2$. The effective interaction therefore deviates from Eq. (18) in the region $r^2 < \hbar/2\mu\omega_0$, where ω_0 is the reststrahlen frequency of the crystal. Typical reststrahlen frequencies in III–V compound semiconductors[34] are of the order of $5 \times 10^{13}\,\text{sec}^{-1}$, yielding the result that Eq. (18) is invalid for r less than about 50 Å, in that in this region κ_0 should be replaced by κ_∞.

As the electron and hole continue to approach one another, the situation becomes increasingly complicated as various effects become important. As the relative motion becomes more rapid, the electrons cease to be able to follow and the effective dielectric constant is further reduced. Also, in this region, the effects of the exchange term in Eq. (17) begin to be important, and finally the entire effective-mass formalism—to be developed below—breaks down. Fortunately, these effects are not particularly important for excitons in most semiconducting crystals, since a_0 is usually somewhat greater than the limiting value of about 50 Å, so that it is generally sufficient to consider the effective interaction to be given Eq. (18).

5. Development of the Exciton Effective-Mass Equation

In the previous sections we have considered an exciton to be an excited electronic state of the crystal that differs from the ground state by having an electron in a conduction-band state $\psi_{c_i,\mathbf{k}'}$ and an electron missing from the valence-band state $\psi_{v_j,\mathbf{k}}$. Starting from the ground state of the crystal

$$\psi'_{ij}(\mathbf{r}_e\mathbf{r}_h)^\dagger = \psi_{c_i,\mathbf{k}'}(\mathbf{r}_e)^\dagger \psi_{v_j,\mathbf{k}}(\mathbf{r}_h) \tag{19}$$

can be interpreted[35] as an exciton-creation operator, which removes an

[34] G. S. Picus, E. Burstein, B. W. Henvis, and M. Hass, *J. Phys. Chem. Solids* **8**, 282 (1959).
[35] J. J. Hopfield, *J. Phys. Chem. Solids* **15**, 97 (1960).

electron from the valence-band state $\psi_{v_j,\mathbf{k}}$ and places it in the conduction-band state $\psi_{c_i,\mathbf{k}'}$. The properties of a crystal with an electron missing from a valence-band state $\psi_{v_j,\mathbf{k}}$ can be described by considering that a single particle of positive charge is placed in the state $\psi_{v_{j'},\mathbf{k}_h} = \psi^*_{v_j,\mathbf{k}}$. We can thus represent the exciton state by the two-particle wave function

$$\psi'_{ij}(\mathbf{r}_e, \mathbf{r}_h) = \psi_{c_i,\mathbf{k}_e}(\mathbf{r}_e)\,\psi_{v_{j'},\mathbf{k}_h}(\mathbf{r}_h), \tag{20}$$

where $\psi_{c_i,\mathbf{k}_e}(\mathbf{r}_e) = \psi_{c_i,\mathbf{k}'}(\mathbf{r}_e)$ is the occupied conduction-band wave function and $\psi_{v_{j'},\mathbf{k}_h}(\mathbf{r}_h) = \psi_{v_j,\mathbf{k}}(\mathbf{r}_h)^*$ is the hole wave function. If one wishes to include spin, this last relation becomes $\psi_{v_{j'},\mathbf{k}_h}(\mathbf{r}_h) = \theta\psi_{v_j,\mathbf{k}}(\mathbf{r}_h)$, where θ is the time-reversal operator. In the absence of external magnetic fields the velocity and momentum properties of the two states are reversed while their energies and charge densities are the same. The total wave vector of the excited state is $\mathbf{K} = \mathbf{k}' - \mathbf{k} = \mathbf{k}_e + \mathbf{k}_h$.

Because of the Coulomb interaction between the electron and the hole, Eq. (20) does not represent an eigenstate of the system. Let us, however, construct an approximate eigenstate from a linear combination of electron and hole states.

$$\Psi^{n,\mathbf{K}}(\mathbf{r}_e, \mathbf{r}_h) = \sum_{c,\mathbf{k}_e} \sum_{v,\mathbf{k}_h} A^{n,\mathbf{K}}_{c,v}(\mathbf{k}_e, \mathbf{k}_h)\,\psi_{c,\mathbf{k}_e}(\mathbf{r}_e)\,\psi_{v,\mathbf{k}_h}(\mathbf{r}_h), \tag{21}$$

where n and $\mathbf{K}$ are used to label the exciton state. The energy difference E between this excited state and the ground state of the crystal can be found as the solution of a set of simultaneous equations,

$$\{E_c(\mathbf{k}_e) - E_v(\mathbf{k}_h) - E\}A^{n,\mathbf{K}}_{c,v}(\mathbf{k}_e, \mathbf{k}_h) + \sum_{c',\mathbf{k}_e'} \sum_{v',\mathbf{k}_h'} \langle c\mathbf{k}_e\,; v\mathbf{k}_h|V(\mathbf{r}_e - \mathbf{r}_h)|c'\mathbf{k}_e'\,; v'\mathbf{k}_h'\rangle A^{n,\mathbf{K}}_{c',v'}(\mathbf{k}_e', \mathbf{k}_h') = 0, \tag{22}$$

where $E_c(\mathbf{k}_e)$ and $E_v(\mathbf{k}_h)$ are given by Eq. (16) and $V(\mathbf{r}_e - \mathbf{r}_h)$ is the effective electron–hole interaction potential, which we shall take to be given by Eq. (18). In Eq. (22) we have neglected the exchange term [see Eq. (17)]. Equation (22) is similar to the equation that is obtained for impurity states. The development given below, in fact, parallels, for the exciton case, Kohn's treatment[36] of shallow impurity states. The electron and hole states are Bloch functions and may be written in the form

$$\psi_{\mathbf{k}}(\mathbf{r}) = \frac{1}{N^{1/2}} e^{i\mathbf{k}\cdot\mathbf{r}}\,u_{\mathbf{k}}(\mathbf{r}), \tag{23}$$

where $u_{\mathbf{k}}$ is a periodic function with the period of the crystal lattice and is normalized to unity in a unit cell of volume Ω. $\psi_{\mathbf{k}}$ is normalized in a large volume V if $N = V/\Omega$.

[36] W. Kohn, *Solid State Phys.* **5**, 257 (1957).

The crux of the following development is the assumption that $u_{\mathbf{k}}$ varies slowly with $\mathbf{k}$ over the range of interest—that is, over the range of $\mathbf{k}_e$ and $\mathbf{k}_h$ for which $A_{c,v}^{n,\mathbf{K}}(\mathbf{k}_e, \mathbf{k}_h)$ is appreciable—and that this range is small compared to the dimensions of the Brillouin zone. These assumptions will be justified below for our simple model. Since the $u_{\mathbf{k}}$ are periodic we can write

$$u_{c\mathbf{k}_e}^*(\mathbf{r}_e)\, u_{c'\mathbf{k}_e'}(\mathbf{r}_e) = \frac{1}{\Omega}\sum_{\nu} C^{\nu}(c\mathbf{k}_e\,;\, c'\mathbf{k}_e')e^{i\mathbf{K}_\nu\cdot\mathbf{r}_e} \tag{24a}$$

and

$$u_{v,\mathbf{k}_h}^*(\mathbf{r}_h)\, u_{v',\mathbf{k}_h'}(\mathbf{r}_h) = \frac{1}{\Omega}\sum_{\mu} C^{\mu}(v\mathbf{k}_h\,;\, v'\mathbf{k}_h')e^{i\mathbf{K}_\mu\cdot\mathbf{r}_h}, \tag{24b}$$

where $\mathbf{K}_\nu$ and $\mathbf{K}_\mu$ are reciprocal lattice vectors. Making these substitutions, we obtain

$$\langle c\mathbf{k}_e\,;\, v\mathbf{k}_h|V(\mathbf{r}_e - \mathbf{r}_h)|c'\mathbf{k}_e'\,;\, v'\mathbf{k}_h'\rangle$$
$$= \frac{1}{V}\sum_{\mu}\sum_{\nu} C^{\nu}(c\mathbf{k}_e\,;\, c'\mathbf{k}_e')\, C^{\mu}(v\mathbf{k}_h\,;\, v'\mathbf{k}_h')\, U\{\tfrac{1}{2}(\mathbf{K}_\nu - \mathbf{K}_\mu - \boldsymbol{\kappa}_e + \boldsymbol{\kappa}_h)\}, \tag{25}$$

where

$$U(\mathbf{q}) = \int d\mathbf{r}\, e^{i\mathbf{q}\cdot\mathbf{r}}\, V(\mathbf{r}) \tag{26}$$

is the Fourier transform of the electron–hole interaction potential. [If $V(\mathbf{r})$ is given by Eq. (18), then $U(\mathbf{q}) = -4\pi e^2/\kappa_0 q^2$.] In Eq. (25) we have substituted

$$\boldsymbol{\kappa}_e = \mathbf{k}_e - \mathbf{k}_e' \tag{27a}$$

and

$$\boldsymbol{\kappa}_h = \mathbf{k}_h - \mathbf{k}_h' \tag{27b}$$

and have the additional result that

$$\boldsymbol{\kappa}_e + \boldsymbol{\kappa}_h = \mathbf{K}_\mu + \mathbf{K}_\nu. \tag{28}$$

The total exciton wave vectors $\mathbf{K} = \mathbf{k}_e + \mathbf{k}_h$ and $\mathbf{K}' = \mathbf{k}_e' = \mathbf{k}_h'$ can be restricted such that they both be within the first Brillouin zone. With this restriction the only possible solution of Eq. (28) is

$$\mathbf{K}_\mu + \mathbf{K}_\nu = 0. \tag{29}$$

We therefore have the result that the total wave vector of the exciton state is conserved—that is,

$$\mathbf{K} = \mathbf{k}_e + \mathbf{k}_h = \mathbf{k}_e' + \mathbf{k}_h' \tag{30}$$

—and we can identify this with the exciton-state label in Eq. (21). Equation (25) can then be rewritten as

$$\langle c\mathbf{k}_e\,; v\mathbf{k}_h|V(\mathbf{r}_e - \mathbf{r}_h)|c'\mathbf{k}_e'\,; v'\mathbf{k}_h'\rangle$$

$$= \frac{1}{V}\sum_{\nu} C^{\nu}(c\mathbf{k}_e\,; c'\mathbf{k}_e')\, C^{-\nu}(v\mathbf{k}_h\,; v'\mathbf{k}_h')\, U(\boldsymbol{\kappa} + \mathbf{K}_\nu), \tag{31}$$

where $\boldsymbol{\kappa} = \boldsymbol{\kappa}_e = -\boldsymbol{\kappa}_h$. If $V(\mathbf{r})$ is approximately given by a Coulomb potential and $\boldsymbol{\kappa}$ is small, the largest contribution to Eq. (31) is for $\mathbf{K}_\nu = 0$, and we can obtain an approximation to Eq. (31) by retaining only this term. This is equivalent to assuming that the interaction potential does not vary greatly over a unit cell. This breaks down, of course, as $\mathbf{r} \to 0$; but if the exciton radius is large compared to the dimensions of a unit cell as discussed above, these approximations will be valid. A possible exception to this occurs for s-state excitons for which the envelope wave functions are finite at $\mathbf{r} = 0$.

So far, we have considered only that the range of $\mathbf{k}_e$ and $\mathbf{k}_h$ over which $A_{c,v}^{n,\mathbf{K}}(\mathbf{k}_e, \mathbf{k}_h)$ is appreciable is small compared to the dimensions of the Brillouin zone. Next we consider that the periodic functions $u_{\mathbf{k}}$ do not vary strongly with $\mathbf{k}$ over this range, so that we can write

$$u_{c',\mathbf{k}_e'}(\mathbf{r}_e) = u_{c',\mathbf{k}_e}(\mathbf{r}_e) + (\mathbf{k}_e' - \mathbf{k}_e)\nabla_{\mathbf{k}_e} u_{c',\mathbf{k}_e}(\mathbf{r}_e) + \cdots \tag{32a}$$

and

$$u_{v',\mathbf{k}_h'}(\mathbf{r}_h) = u_{v',\mathbf{k}_h}(\mathbf{r}_h) + (\mathbf{k}_h' - \mathbf{k}_h)\nabla_{\mathbf{k}_h} u_{v',\mathbf{k}_h}(\mathbf{r}_h) + \cdots. \tag{32b}$$

Substituting these expressions into Eq. (24) and integrating over a unit cell, we obtain

$$C^0(c\mathbf{k}_e\,; c'\mathbf{k}_e') = \delta_{c,c'} - \boldsymbol{\kappa}\cdot\mathbf{X}_{c,c'}(\mathbf{k}_e) \tag{33a}$$

and

$$C^0(v\mathbf{k}_h\,; v'\mathbf{k}_h') = \delta_{v,v'} + \boldsymbol{\kappa}\cdot\mathbf{X}_{v,v'}(\mathbf{k}_h), \tag{33b}$$

where

$$\mathbf{X}_{n,n'}(\mathbf{k}) = \langle u_{n,\mathbf{k}}|\nabla_{\mathbf{k}} u_{n',\mathbf{k}}\rangle_\Omega = \frac{m}{\hbar}[E_{n'}(\mathbf{k}) - E_n(\mathbf{k})]^{-1}\langle\psi_{n,\mathbf{k}}|\pi|\psi_{n',\mathbf{k}}\rangle \tag{34}$$

and π is the pseudomomentum operator given by Eq. (65). Retaining only the $\mathbf{K}_\nu = 0$ term in Eq. (31) and using Eq. (33), we obtain

$$\langle c\mathbf{k}_e\,; v\mathbf{k}_h|V(\mathbf{r}_e - \mathbf{r}_h)|c'\mathbf{k}_e'\,; v'\mathbf{k}_h'\rangle$$

$$= \frac{1}{V}U(\boldsymbol{\kappa})\{\delta_{c,c'}\cdot\delta_{v,v'} - \boldsymbol{\kappa}\cdot(\delta_{v,v'}\mathbf{X}_{c,c'} - \delta_{c,c'}\mathbf{X}_{v,v'}) + \cdots\} \tag{35}$$

to first order in κ. Retaining only the first term in Eq. (35) for the time being, Eq. (22) becomes

$$[E_c(\mathbf{k}_e) - E_v(\mathbf{k}_h) - E]\, A_{c,v}^{n,\mathbf{K}}(\mathbf{k}_e, \mathbf{k}_h) + \frac{1}{V}\sum_{\kappa} U(\kappa)\, A_{c,v}^{n,\mathbf{K}}(\mathbf{k}_e - \kappa, \mathbf{k}_h + \kappa) = 0. \tag{36}$$

The effective-mass equation is obtained by introducing the Fourier transform of $A_{c,v}^{n,\mathbf{K}}(\mathbf{k}_e, \mathbf{k}_h)$:

$$\Phi_{c,v}^{n,\mathbf{K}}(\mathbf{r}_e, \mathbf{r}_h) = \frac{1}{V}\sum_{\mathbf{k}_e}\sum_{\mathbf{k}_h} e^{i\mathbf{k}_e\cdot\mathbf{r}_e} e^{i\mathbf{k}_h\cdot\mathbf{r}_h} A_{c,v}^{n,\mathbf{K}}(\mathbf{k}_e, \mathbf{k}_h). \tag{37}$$

Taking the Fourier transform of Eq. (36), one can show that the functions $\Phi_{c,v}^{n,\mathbf{K}}$ satisfy the differential equation

$$[E_c(-i\nabla_e) - E_v(-i\nabla_h) + V(\mathbf{r}_e - \mathbf{r}_h) - E]\, \Phi_{c,v}^{n,\mathbf{K}}(\mathbf{r}_e, \mathbf{r}_h) = 0, \tag{38}$$

where $E_c(-i\nabla_e)$ is the expression obtained by replacing $\mathbf{k}_e$ in the power-series expansion of $E_c(\mathbf{k}_e)$ by $-i\nabla_e$, where ∇_e is the gradient with respect to $\mathbf{r}_e$, and analogously for $E_v(-i\nabla_h)$. In obtaining Eq. (38) use was made of the fact[5] that if a function $f(\mathbf{k})$ is expandable in powers of the components of $\mathbf{k}$, then

$$\frac{1}{V}\sum_{\mathbf{k}} e^{i\mathbf{k}\cdot\mathbf{r}} f(\mathbf{k})\, G(\mathbf{k}) = f(-i\nabla)\, g(\mathbf{r}), \tag{39}$$

where

$$g(\mathbf{r}) = \frac{1}{V}\sum_{\mathbf{k}} e^{i\mathbf{k}\cdot\mathbf{r}}\, G(\mathbf{k}). \tag{40}$$

Equation (38) is a special case of the effective-mass equation that is valid provided $E_c(\mathbf{k}_e)$ and $E_v(\mathbf{k}_h)$ are analytic and can be expanded in powers of $\mathbf{k}$. At points of high symmetry a degeneracy often occurs and $E_c(\mathbf{k}_e)$ and/or $E_v(\mathbf{k}_h)$ may not be analytic, so that Eq. (38) is not valid. In such cases one must use instead the more general form of the effective-mass equation, Eq. (61).

The approximations that lead to the effective-mass equation [Eq. (38)] have resulted in a separation of the exciton problem so that, in the simple case, exciton states formed from different valence and conduction bands are not mixed with one another. To this order we can therefore consider an exciton formed from a hole in a given valence band and an electron in a given conduction band. This separation was obtained by neglecting the variation of $u_{c,\mathbf{k}_e}(\mathbf{r}_e)$ and $u_{v,\mathbf{k}_h}(\mathbf{r}_h)$ with $\mathbf{k}_e$ and $\mathbf{k}_h$. To first order, this variation

is represented by the additional terms in Eq. (32). If these terms are included, we obtain instead of Eq. (38),

$$[E_{c_i}(-i\nabla_e) - E_{v_i}(-i\nabla_h) + V(\mathbf{r}_e - \mathbf{r}_h) - E]\,\Phi^{n,\mathbf{K}}_{c_i v_i}(\mathbf{r}_e, \mathbf{r}_h) + i\nabla V(\mathbf{r}_e - \mathbf{r}_h)\cdot\{\sum_{c_j} \mathbf{X}_{c_i c_j}\,\Phi^{n,\mathbf{K}}_{c_j v_i}(\mathbf{r}_e, \mathbf{r}_h) - \sum_{v_j} \mathbf{X}_{v_i v_j}\,\Phi^{n,\mathbf{K}}_{c_i v_j}(\mathbf{r}_e, \mathbf{r}_h)\} = 0, \quad (41)$$

where c_j runs over all unoccupied (conduction) bands and v_j runs over all occupied (valence) bands. As seen from Eq. (41), the exciton states formed from different bands are mixed when one includes the linear terms in the variation of $u_{c,\mathbf{k}_e}(\mathbf{r}_e)$ and $u_{v,\mathbf{k}_h}(\mathbf{r}_h)$ with $\mathbf{k}_e$ and $\mathbf{k}_h$, respectively. We shall not concern ourselves further with this mixing except to point out that it exists but is probably not important in most cases.

The wave functions for the exciton states are given by

$$\Psi^{n,\mathbf{K}}(\mathbf{r}_e, \mathbf{r}_h) = \sum_{\mathbf{k}_e}\sum_{\mathbf{k}_h} A^{n,\mathbf{K}}(\mathbf{k}_e, \mathbf{k}_h)\,\psi_{c,\mathbf{k}_e}(\mathbf{r}_e)\,\psi_{v,\mathbf{k}_h}(\mathbf{r}_h), \quad (42)$$

where $\psi_{c,\mathbf{k}_e}(\mathbf{r}_e)$ and $\psi_{v,\mathbf{k}_h}(\mathbf{r}_h)$ are the conduction and valence band wave functions, respectively, and $A^{n,\mathbf{K}}(\mathbf{k}_e, \mathbf{k}_h)$ is the Fourier transform of $\Phi^{n,\mathbf{K}}(\mathbf{r}_e, \mathbf{r}_h)$. The approximations that resulted in Eq. (38), the effective-mass equation for simple bands, allow us to write the conduction- and valence-band wave functions in our simple example as

$$\psi_{c,\mathbf{k}_e}(\mathbf{r}_e) = \frac{1}{N^{1/2}} e^{i\mathbf{k}_e\cdot\mathbf{r}_e}\,u_c(\mathbf{r}_e) \quad (43a)$$

and

$$\psi_{v,\mathbf{k}_h}(\mathbf{r}_h) = \frac{1}{N^{1/2}} e^{i\mathbf{k}_h\cdot\mathbf{r}_h}\,u_v(\mathbf{r}_h), \quad (43b)$$

where $u_c(\mathbf{r}_e)$ and $u_v(\mathbf{r}_h)$ are independent of $\mathbf{k}_e$ and $\mathbf{k}_h$. Substituting these equations into Eq. (42), we obtain from Eq. (37)

$$\Psi^{n,\mathbf{K}}(\mathbf{r}_e, \mathbf{r}_h) = \Omega\Phi^{n,\mathbf{K}}(\mathbf{r}_e, \mathbf{r}_h)u_c(\mathbf{r}_e)u_v(\mathbf{r}_h). \quad (44)$$

The exciton wave function is therefore made up of a product of the electron and hole band functions times a modulating function $\Phi^{n,\mathbf{K}}$. Consider the state for $\mathbf{K} = 0$. Then,

$$\Psi^{n}(\mathbf{r}_e, \mathbf{r}_h) = V\Phi^{n}(\mathbf{r}_e, \mathbf{r}_h)\psi_c(\mathbf{r}_e)\psi_v(\mathbf{r}_h). \quad (45)$$

Since ψ_c and ψ_v are rapidly varying functions and Φ^n is comparatively long ranged, we can consider $\Phi^n(\mathbf{r}_e, \mathbf{r}_h)$ as a sort of modulating function. This situation is again exactly analogous to the impurity problem.

As mentioned above, Eq. (38) is a special case of the general effective-mass equation. Before investigating the form of the general equation, however, let us consider the solution of Eq. (38) in the case of our simple model discussed above. This will also lead to a justification of the various assumptions that have been made.

The band energies for the conduction and valence bands in the vicinity of $\mathbf{k} = 0$ in our simple model are again

$$E_c = E_g + \frac{\hbar^2 k^2}{2m_e^*}$$

and

$$E_v = -\frac{\hbar^2 k^2}{2m_h^*},$$

and the interaction potential is

$$V(\mathbf{r}_e - \mathbf{r}_h) = -\frac{e^2}{\kappa_0 |\mathbf{r}_e - \mathbf{r}_h|}.$$

Substituting these expressions into Eq. (38), we obtain

$$\left\{-\frac{\hbar^2}{2m_e^*}\nabla_e^2 - \frac{\hbar^2}{2m_h^*}\nabla_h^2 - \frac{e^2}{\kappa_0|\mathbf{r}_e - \mathbf{r}_h|}\right\}\Phi^{n,\mathbf{K}}(\mathbf{r}_e, \mathbf{r}_h) = \varepsilon\Phi^{n,\mathbf{K}}(\mathbf{r}_e, \mathbf{r}_h), \tag{46}$$

where $\varepsilon = E - E_g$. Making the center-of-mass transformation

$$\begin{aligned} \mathbf{r} &= \mathbf{r}_e - \mathbf{r}_h, \\ \mathbf{R} &= \frac{m_e^* \mathbf{r}_e + m_h^* \mathbf{r}_h}{m_e^* + m_h^*}, \end{aligned} \tag{47}$$

Eq. (46) becomes

$$\left\{-\frac{\hbar^2}{2\mu}\nabla_{\mathbf{r}}^2 - \frac{\hbar^2}{2M}\nabla_{\mathbf{R}}^2 - \frac{e^2}{\kappa_0 r}\right\}\Phi^{n,\mathbf{K}}(\mathbf{r}; \mathbf{R}) = \varepsilon\Phi^{n,\mathbf{K}}(\mathbf{r}; \mathbf{R}), \tag{48}$$

where μ is again the reduced mass of the exciton given by Eq. (6) and M is the total exciton mass

$$M = m_e^* + m_h^*. \tag{49}$$

Since $\nabla_{\mathbf{R}}$ commutes with the effective-mass Hamiltonian

$$H = -\frac{\hbar^2}{2\mu}\nabla_{\mathbf{r}}^2 - \frac{\hbar^2}{2M}\nabla_{\mathbf{R}}^2 - \frac{e^2}{\kappa_0 r}, \tag{50}$$

the eigenfunctions may be taken to be of the form

$$\Phi^{n,\mathbf{K}}(\mathbf{r}, \mathbf{R}) = \frac{1}{V^{1/2}} e^{i\mathbf{K}\cdot\mathbf{R}} \psi^n(\mathbf{r}). \tag{51}$$

The wave functions $\psi^n(\mathbf{r})$ satisfy

$$\left\{ -\frac{\hbar^2}{2\mu} \nabla_{\mathbf{r}}^2 - \frac{e^2}{\kappa_0 r} \right\} \psi^n(\mathbf{r}) = \varepsilon_n \psi^n(\mathbf{r}), \tag{52}$$

where

$$\varepsilon = \varepsilon_n + \frac{\hbar^2 K^2}{2M}. \tag{53}$$

Equation (52) is identical to Eq. (3). The solutions of this equation are simply the hydrogenic states for a reduced mass μ and electronic charge $e/\kappa_0^{1/2}$. The ground-state wave function for $n = 1$ is

$$\psi(\mathbf{r}) = \frac{1}{(\pi a_0^3)^{1/2}} e^{-r/a_0}, \tag{54}$$

where again a_0 is the Bohr radius of the ground state and is given by Eq. (9). We can now Fourier invert Eq. (37) to obtain $A^{n,\mathbf{K}}(\mathbf{k}_e, \mathbf{k}_h)$:

$$A_{c,v}^{n,\mathbf{K}}(\mathbf{k}_e, \mathbf{k}_h) = \frac{1}{V} \int d\mathbf{r}_e \, d\mathbf{r}_h \, e^{-i\mathbf{k}_e\cdot\mathbf{r}_e} \, e^{-i\mathbf{k}_h\cdot\mathbf{r}_h} \, \Phi_{c,v}^{n,\mathbf{K}}(\mathbf{r}_e, \mathbf{r}_h). \tag{55}$$

Substituting Eqs. (51) and (54) into Eq. (55), we obtain

$$A^{\mathbf{K}}(\mathbf{k}_e, \mathbf{k}_h) = \frac{1}{V^{1/2}} \left[\frac{64\pi}{a_0^5} \right]^{1/2} \frac{1}{[k^2 + (1/a_0)^2]^2} \delta_{\mathbf{K},\mathbf{k}_e+\mathbf{k}_h}, \tag{56}$$

where

$$\mathbf{k} = \frac{m_h^*}{M} \mathbf{k}_e - \frac{m_e^*}{M} \mathbf{k}_h. \tag{57}$$

From Eq. (56) it is seen that $\mathbf{K}$ in Eq. (51) is equal to $\mathbf{k}_e + \mathbf{k}_h$ and represents the total wave vector for the exciton, as one might expect. Equation (56) is equivalent to the equation obtained by Kohn[36] in the case of shallow impurity states in semiconductors.

In most cases, we are interested in those exciton states that are created by the absorption of an optical photon. For these states, $\mathbf{K}$ is equal to the wave vector of the photon in the crystal and is quite small (see Section 7). Let us therefore investigate the case where $\mathbf{K} = 0$. For this case we have $\mathbf{k} = \mathbf{k}_e = -\mathbf{k}_h$. We see that $A(\mathbf{k}_e, \mathbf{k}_h)$ is appreciable only for values of k_e

and k_h less than or equal to

$$\bar{k} = \frac{1}{a_0}. \tag{58}$$

One of the approximations made was that the range of $\mathbf{k}_e$ and $\mathbf{k}_h$ is small compared to the dimensions of the Brillouin zone. This will be satisfied if a_0 is much greater than a unit-cell dimension. In all semiconductors studied thus far, this has been true, so that in fact the range of $\mathbf{k}_e$ and $\mathbf{k}_h$ is small.

The other approximation made was that over the range of $\mathbf{k}_e$ and $\mathbf{k}_h$ for which $A^{n,\mathbf{K}}(\mathbf{k}_e, \mathbf{k}_h)$ is appreciable, the periodic part of the conduction- and valence-band wave functions can be taken to be independent of $\mathbf{k}$. The additional terms that arise from including this variation to first order in $\mathbf{k}$ are given in Eq. (41). The interband mixing that arises because of the inclusion of these terms can be estimated[36] to be proportional to

$$\frac{R}{\Delta E}\frac{a}{a_0},$$

where R is the ground-state exciton energy, ΔE is the energy separation between the interacting bands, and a is the lattice spacing. In most cases, this mixing is of the order of 10^{-2} to 10^{-3} and is negligible. This is true for group-IV and group-III–V semiconductors. However, in the group-II–VI compounds CdS and ZnS, exciton states originating from two spin–orbit-split valence bands overlap in energy, and here the mixing may be appreciable. In these, Eq. (41) should be evaluated explicitly for the system involved.

Before proceeding with the general theoretical development, it is interesting to mention some simple relationships that may yield some insight into the situation. Consider first the energy range in which the band states contribute appreciably to the formation of the lowest exciton state at $\mathbf{K} = 0$. This is given by

$$\bar{\varepsilon} = E_c(\bar{k}) - E_v(\bar{k}) - E_g = \frac{\hbar^2\bar{k}^2}{2\mu} = \frac{\hbar^2}{2\mu a_0^2} = R. \tag{59}$$

That is, the range in energy over which band states contribute to the formation of the lowest exciton state, in our simple model, is just equal to the binding energy of that state. The situation is shown in Fig. 3. The shaded regions indicate the band states that contribute to the $\mathbf{K} = 0$ exciton ground state.

Recall that in the introduction we mentioned that the presence of free carriers strongly shielded the electron–hole interaction, so that for concentrations greater than $N_0 = 5 \times 10^{-2}\, a_0^{-3}$ no discrete exciton states could exist. The Fermi wave vector corresponding to such a concentration, $k_F{}^0$,

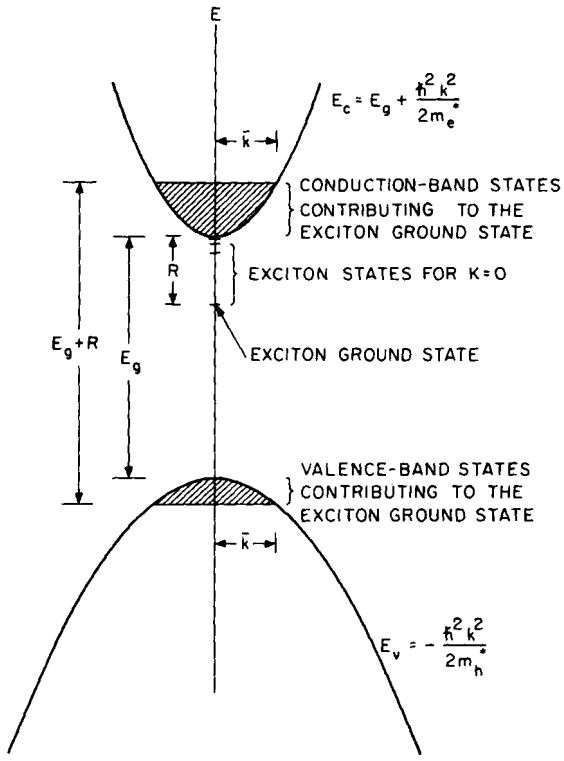


FIG. 3. Schematic representation of direct exciton states at $\mathbf{K} = 0$ for the simple band model, indicating the conduction- and valence-band states that contribute to the formation of the exciton ground-state wave function.

may be obtained from

$$N_0 = \frac{2}{(2\pi)^3} \cdot \frac{4}{3}\pi(k_F{}^0)^3 = 5 \times 10^{-2}\, a_0^{-3} = 5 \times 10^{-2}\, \bar{k}^3,$$

which yields

$$k_F{}^0 \approx \bar{k}. \tag{60}$$

In Fig. 4 we show an energy-level diagram for the electronic energies $E(\mathbf{K})$ for the exciton states that are solutions of Eq. (38). The ground state of the crystal is at the origin, having $E = 0$ and $\mathbf{K} = 0$. The excited states represent excited states of the entire crystal and are the two-particle exciton states $\Psi_{c,v}^{n,\mathbf{K}}(\mathbf{r}_e, \mathbf{r}_h)$ of Eq. (21). The exciton levels which we have referred to as discrete are shown split off from the cross-hatched continuum. Direct transitions are indicated by vertical arrows, while the diagonal arrows

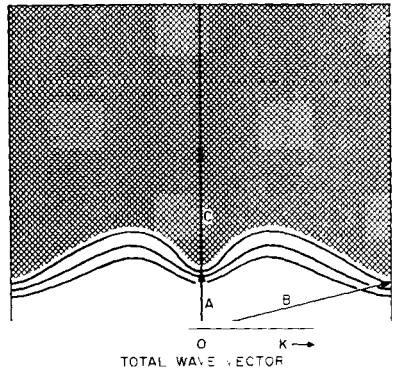


FIG. 4. Schematic representation of the exciton energy levels as a function of the total wave vector $\mathbf{K} = \mathbf{k}_e + \mathbf{k}_h$. The cross-hatched region represents a true continuum of states. The three types of transitions, *A*, *B*, and *C* shown in Fig. 1, are indicated again in this figure to illustrate the differences between the two representations.

indicate indirect transitions. Notice that the cross-hatched region represents a true continuum of states, since a transition can occur to any point in this region. This is not the case in Fig. 3. The energy-level diagram represented by Fig. 4 should be contrasted with those of Figs. 1 and 3, which are plots of the energies $E(\mathbf{k})$ for one-particle electron states $\psi_{\mathbf{k}}(\mathbf{r})$. The exciton states of Fig. 4 are related to these through Eq. (21), where $\mathbf{K} = \mathbf{k}_e + \mathbf{k}_h$. In Fig. 3 we have indicated the relative positions of the $\mathbf{K} = 0$ exciton levels compared to the band energies. It would, however, be inappropriate to include the exciton bands in either this figure or in Fig. 1, since the plots have an essentially different interpretation.

Let us now return to the development of the general effective-mass equation. In the above discussion the valence and conduction bands have been considered to be nondegenerate. In the situations of interest the bands are, in fact, degenerate and we must consider the appropriate modification of the effective-mass equation. In the general case where $E_c(-i\nabla_e)$ and $E_v(-i\nabla_h)$ are expanded about points of conduction and valence band degeneracy, one can show[37,38] that the effective-mass equation can be written as

$$\sum_{i'=1}^{r}\sum_{j'=1}^{s}\{H^c_{ii'}(-i\nabla_e)\,\delta_{jj'} - H^v_{jj'}(-i\nabla_h)\delta_{ii'} + V(\mathbf{r}_e - \mathbf{r}_h)\,\delta_{ii'}\,\delta_{jj'}\}\,\Phi^{n,\mathbf{K}}_{c_{i'}v_{j'}}(\mathbf{r}_e, \mathbf{r}_h) = E\,\Phi^{n,\mathbf{K}}_{c_i,v_j}(\mathbf{r}_e, \mathbf{r}_h), \tag{61}$$

[37] C. Kittel and A. H. Mitchell, *Phys. Rev.* **96**, 1488 (1954)
[38] J. M. Luttinger and W. Kohn, *Phys. Rev.* **97**, 869 (1955)

where i and i' run over the r-degenerate conduction bands and j and j' run over the s-degenerate valence bands. Equation (61) represents a set of r times s simultaneous differential equations that must be solved to obtain the exciton eigenstates and energies. If the conduction-band energy is expanded about the degenerate point $\mathbf{k}_e^0$, then it can be shown in a straightforward manner, following the treatment of Luttinger and Kohn,[38] that to second order in $\mathbf{k}_e' = \mathbf{k}_e - \mathbf{k}_e^0$,

$$H^c_{ii'}(\mathbf{k}_e) = E_{c_i}(\mathbf{k}_e^0)\,\delta_{ii'} + \frac{\hbar^2}{2m}k_e'^2\,\delta_{ii'} + \frac{\hbar}{m}k_e'^\alpha\,\pi^\alpha_{ii'} + \frac{\hbar^2}{m^2}k_e'^\alpha\,k_e'^\beta\sum_n{}'\frac{\pi^\alpha_{in}\pi^\beta_{ni'}}{E_{c_i}(\mathbf{k}_e^0) - E_n(\mathbf{k}_e^0)}, \tag{62}$$

where α and β run over the directions x, y, and z, and π^α_{in} is the αth component of the pseudo-momentum matrix element between the band states i and n at $\mathbf{k}_e^0$. The sum runs over both valence- and conduction-band states. The prime on the sum, however, indicates that the set of r degenerate states is excluded. The expression for $H^c_{ii'}(-i\nabla_e)$ is obtained by replacing $\mathbf{k}_e' = \mathbf{k}_e - \mathbf{k}_e^0$ by $-i\nabla_e - \mathbf{k}_e^0$ in Eq. (62). Similar expressions hold for $H^v_{jj'}(\mathbf{k}_h)$ and $H^v_{jj'}(-i\nabla_h)$—that is,

$$H^v_{jj'}(\mathbf{k}_h) = E_{v_j}(\mathbf{k}_h^0)\,\delta_{jj'} + \frac{\hbar^2}{2m}k_h'^2\,\delta_{jj'} + \frac{\hbar}{m}k_h'^\alpha\,\pi^\alpha_{jj'} + \frac{\hbar^2}{m^2}k_j'^\alpha\,k_j'^\beta\sum_n{}'\frac{\pi^\alpha_{jn}\pi^\beta_{nj'}}{E_{v_j}(\mathbf{k}_h^0) - E_n(\mathbf{k}_h^0)}, \tag{63}$$

where $\mathbf{k}_h' = \mathbf{k}_h - \mathbf{k}_h^0$, etc. The quasi-momentum operator $\boldsymbol{\pi}$ is defined in terms of the single-electron Hamiltonian H_0, where

$$H_0\psi_{\mathbf{k}}(\mathbf{r}) = E(\mathbf{k})\,\psi_{\mathbf{k}}(\mathbf{r}) \tag{64}$$

gives the band energies $E(\mathbf{k})$ as[38]

$$\boldsymbol{\pi} \equiv m\mathbf{v} = -\frac{m}{i\hbar}[H_0, \mathbf{r}], \tag{65}$$

where $\mathbf{v}$ is the velocity operator. The one-electron crystal Hamiltonian with spin–orbit and other relativistic terms included is given by[39]

$$H_0 = -\frac{\hbar^2}{2m}\nabla^2 + V - \frac{1}{2mc^2}(E - V)^2 + \frac{i\hbar^2}{4m^2c^2}(\nabla V \times \boldsymbol{\sigma})\cdot\nabla - \frac{\hbar^2}{4m^2c^2}\nabla V\cdot\nabla, \tag{66}$$

[39] H. A. Bethe and E. E. Salpeter, "Quantum Mechanics of One- and Two-Electron Atoms," Sec. 12. Springer, Berlin, 1957.

where V is the crystal potential and $\boldsymbol{\sigma}$ is the Pauli spin operator. For this Hamiltonian, Eq. (65) gives

$$\boldsymbol{\pi} = -i\hbar\nabla - \frac{\hbar}{4mc^2}(\nabla V \times \boldsymbol{\sigma} + i\nabla V). \tag{67}$$

The relativistic contributions to Eq. (67) are usually small and neglected.[40] In the absence of these terms, $\boldsymbol{\pi}$ is given by the usual momentum operator $\mathbf{p} = -i\hbar\nabla$. Actually, in the presence of an external magnetic field Eqs. (66) and (67) contain additional terms.[39] The contribution of these additional terms to Eq. (67) is proportional to the spin splitting of the band states compared to the band gaps present and is usually completely negligible. It is convenient to use $\boldsymbol{\pi}$, as defined by Eq. (65), rather than $\mathbf{p}$, since the equations then remain valid when these effects are present. Equations (62) and (63) can be given a simple intuitive meaning in the case of nondegenerate bands. From the f-sum rule[38] we have

$$\frac{\partial^2 E_{c_i}(\mathbf{k}_e{}^0)}{\partial k_e{}^\alpha \partial k_e{}^\beta} = \frac{\hbar^2}{m^2}\sum_n{}' \frac{\{\pi_{in}^\alpha \pi_{ni}^\beta + \pi_{in}^\beta \pi_{ni}^\alpha\}}{E_{c_i}(\mathbf{k}_e{}^0) - E_n(\mathbf{k}_e{}^0)} + \frac{\hbar^2}{m}\delta_{\alpha\beta}. \tag{68}$$

Using Eq. (68) and the fact that

$$\frac{\partial E_{c_i}(\mathbf{k}_e{}^0)}{\partial k_e{}^\alpha} = \frac{\hbar}{m}\pi_{ii}^\alpha, \tag{69}$$

we see that

$$H_{ii}^c(\mathbf{k}_e) = E_{c_i}(\mathbf{k}_e{}^0) + k_e'{}^\alpha \frac{\partial E_{c_i}(\mathbf{k}_e{}^0)}{\partial k_e{}^\alpha} + \frac{1}{2}k_e'{}^\alpha k_e'{}^\beta \frac{\partial^2 E_{c_i}(\mathbf{k}_e{}^0)}{\partial k_e{}^\alpha \partial k_e{}^\beta} = E_{c_i}(\mathbf{k}_e), \tag{70}$$

which is just a Taylor series expansion of $E_{c_i}(\mathbf{k}_e)$ about $\mathbf{k}_e{}^0$. Similarly, $H_{jj}^v(\mathbf{k}_h) = E_{v_j}(\mathbf{k}_h)$ is a Taylor series expansion of $E_{v_j}(\mathbf{k}_h)$ about $\mathbf{k}_h{}^0$. Equations (62), (63), and (61) therefore reduce to those obtained previously in the case of nondegenerate bands.

The same is true for $H_{ii}^c(-i\nabla_e)$ and $H_{jj}^v(-i\nabla_h)$, which are obtained from Eqs. (62) and (63) respectively by replacing $\mathbf{k}_e$ with $-i\nabla_e$ and $\mathbf{k}_h$ with $-i\nabla_h$. This replacement, however, is correct only in the absence of an external magnetic field. In the presence of a magnetic field, $\mathbf{H}$, $\mathbf{k}_e$ is replaced by[38]

$$\frac{1}{\hbar}\mathbf{P}_e = -i\nabla_e + \frac{e}{2\hbar c}(\mathbf{H} \times \mathbf{r}_e) \tag{71}$$

and $\mathbf{k}_h$ is replaced by

$$\frac{1}{\hbar}\mathbf{P}_h = -i\nabla_h - \frac{e}{2\hbar c}(\mathbf{H} \times \mathbf{r}_h). \tag{72}$$

[40] E. O. Kane, *J. Phys. Chem. Solids* **1**, 249 (1957).

The various components of these operators do not commute with each other, and this results in additional terms[41] in Eqs. (62) and (63) that are associated with the orbital contribution to the band splitting in the presence of a magnetic field. We can obtain an expression for this contribution directly from Eq. (62). The last term of this equation can be separated into a symmetric and an antisymmetric part (see, for example, Yafet[42]),

$$k_e^{\prime\alpha} k_e^{\prime\beta} \sum_n{}' \frac{\pi_{in}^{\alpha} \pi_{ni'}^{\beta}}{E_{c_i}(\mathbf{k}_e^0) - E_n(\mathbf{k}_e^0)}$$

$$= \frac{1}{2}(k_e^{\prime\alpha} k_e^{\prime\beta} + k_e^{\prime\beta} k_e^{\prime\alpha}) \cdot \frac{1}{2} \sum_n{}' \frac{\pi_{in}^{\alpha} \pi_{ni'}^{\beta} + \pi_{in}^{\beta} \pi_{ni'}^{\alpha}}{E_{c_i}(\mathbf{k}_e^0) - E_n(\mathbf{k}_e^0)}$$

$$+ \frac{1}{2}(k_e^{\prime\alpha} k_e^{\prime\beta} - k_e^{\prime\beta} k_e^{\prime\alpha}) \cdot \frac{1}{2} \sum_n{}' \frac{\pi_{in}^{\alpha} \pi_{ni'}^{\beta} - \pi_{in}^{\beta} \pi_{ni'}^{\alpha}}{E_{c_i}(\mathbf{k}_e^0) - E_n(\mathbf{k}_e^0)}, \tag{73}$$

with an understood summation of α and β over the directions x, y, and z. The first term in Eq. (73), which involves $k_e^{\prime\alpha}$ and $k_e^{\prime\beta}$ in a symmetric combination, also involves the interband matrix elements π_{in}^{α} and π_{in}^{β} in a symmetric combination. This then, from Eq. (68), represents the effective-mass part of the Hamiltonian. The second term in Eq. (73) involves $k_e^{\prime\alpha}$ and $k_e^{\prime\beta}$, and π_{in}^{α} and π_{in}^{β} in an antisymmetric combination. This term represents a purely magnetic contribution to the energy. In the effective-mass equation $(k_e^{\prime x} k_e^{\prime y} - k_e^{\prime y} k_e^{\prime x}) = (k_e{}^x k_e{}^y - k_e{}^y k_e{}^x)$ is replaced by $(P_e{}^x P_e{}^y - P_e{}^y P_e{}^x)/\hbar^2 = -ieH_z/\hbar c$ and cyclic permutations. Written in vector form this becomes

$$\mathbf{P}_e \times \mathbf{P}_e = -i\frac{e\hbar}{c}\mathbf{H} \tag{74a}$$

and

$$\mathbf{P}_h \times \mathbf{P}_h = +i\frac{e\hbar}{c}\mathbf{H}. \tag{74b}$$

Actually, Eqs. (71) and (72) contain terms of relativistic origin similar to those in Eq. (67). These correspond to spin–orbit and other relativistic corrections to the exciton states themselves. These terms, however, are proportional to $(a_0{}^{\mathrm{H}})^3/\kappa_0 a_0'^3$ times the relativistic corrections for the hydrogen atom and are completely negligible.

6. Reduction of the Exciton Effective-Mass Equation

In this section we obtain a partial reduction of the exciton effective-mass equation, following the treatment of Dresselhaus[43] but with the inclusion of

[41] J. M. Luttinger, *Phys. Rev.* **102**, 1030 (1956).
[42] Y. Yafet, *Solid State Phys.* **14**, 1 (1963).
[43] G. Dresselhaus, *J. Phys. Chem. Solids* **1**, 14 (1956).

an external magnetic field. It is convenient to write the exciton effective mass equation as

$$\left\{\sum_{i'=1}^{r}\sum_{j'=1}^{s} H^{e}_{ii'}(-i\nabla_e - \mathbf{k}_e{}^0)\,\delta_{jj'} - H^{h}_{jj'}(-i\nabla_h - \mathbf{k}_h{}^0)\,\delta_{ii'} + V(\mathbf{r}_e - \mathbf{r}_h)\,\delta_{ii'}\,\delta_{jj'}\right\}\Phi^{n,\mathbf{K}}_{c_i'v_j'}(\mathbf{r}_e, \mathbf{r}_h) = \varepsilon\Phi^{n,\mathbf{K}}_{c_i'v_j'}(\mathbf{r}_e, \mathbf{r}_h), \tag{75}$$

where

$$H^{e}_{ii'}(-i\nabla_e - \mathbf{k}_e{}^0) = H^{c}_{ii'}(-i\nabla_e) - E_{c_i}(\mathbf{k}_e{}^0)\,\delta_{ii'},$$
$$H^{h}_{jj'}(-i\nabla_h - \mathbf{k}_h{}^0) = H^{v}_{jj'}(-i\nabla_h) - E_{v_j}(\mathbf{k}_h{}^0)\,\delta_{jj'},$$

and

$$\varepsilon = E - E_{c_i}(\mathbf{k}_e{}^0) + E_{v_j}(\mathbf{k}_h{}^0).$$

We can write Eq. (75) in matrix form as

$$\mathscr{H}\Phi^{n,\mathbf{K}} = \varepsilon\Phi^{n,\mathbf{K}}, \tag{76}$$

where

$$\mathscr{H} = \mathscr{H}^{e}(-i\nabla_e - \mathbf{k}_e{}^0) - \mathscr{H}^{h}(-i\nabla_h - \mathbf{k}_h{}^0) + \mathscr{V}(\mathbf{r}_e - \mathbf{r}_h). \tag{77}$$

In the presence of an external magnetic field $\mathbf{H}$, the Hamiltonian operator in Eqs. (76) and (77) becomes[44]

$$\mathscr{H} = \mathscr{H}^{e}\left(-i\nabla_e + \frac{e}{\hbar c}\mathbf{A}_e - \mathbf{k}_e{}^0\right) - \mathscr{H}^{h}\left(-i\nabla_h - \frac{e}{\hbar c}\mathbf{A}_h - \mathbf{k}_h{}^0\right) + \mathscr{V}(\mathbf{r}_e - \mathbf{r}_h) + 2\beta(\mathbf{s}_e + \mathbf{s}_h)\cdot\mathbf{H}, \tag{78}$$

where

$$\mathbf{A}_e = \tfrac{1}{2}(\mathbf{H}\times\mathbf{r}_e),$$
$$\mathbf{A}_h = \tfrac{1}{2}(\mathbf{H}\times\mathbf{r}_h).$$

The last term in Eq. (78) arises because of the electron and hole spin. The symbol $\mathbf{s}_e$ represents the electron spin operator and $\mathbf{s}_h$ the hole spin operator. The magnetic field contribution to the hole energy terms in Eq. (78) is opposite in sign to the magnetic contribution to the electron energy terms. One can say simply that this is due to the fact that the hole behaves like a particle of positive charge. Perhaps a more precise way of viewing this is to recall that the hole state involved is generated from the unoccupied valence-band electron state through the time-reversal operator. It was remarked above that in the absence of external magnetic fields these states have the

[44] W. E. Lamb, *Phys. Rev.* **85**, 259 (1952).

same energy. However, in the presence of a magnetic field, the two states have the same energy only in magnetic fields of opposite sign.

Making the coordinate transformation,[43]

$$\begin{aligned} \mathbf{R} &= \tfrac{1}{2}(\mathbf{r}_e + \mathbf{r}_h), \\ \mathbf{r} &= \mathbf{r}_e - \mathbf{r}_h, \end{aligned} \tag{79}$$

Eq. (78) becomes

$$\begin{aligned} \mathscr{H} = {} & \mathscr{H}^e\left(-i\nabla_\mathbf{r} - \frac{1}{2}i\nabla_\mathbf{R} + \frac{e}{2\hbar c}\mathbf{A}_\mathbf{r} + \frac{e}{\hbar c}\mathbf{A}_\mathbf{R} - \mathbf{k}_e{}^0\right) \\ & - \mathscr{H}^h\left(+i\nabla_\mathbf{r} - \frac{1}{2}i\nabla_\mathbf{R} + \frac{e}{2\hbar c}\mathbf{A}_\mathbf{r} - \frac{e}{\hbar c}\mathbf{A}_\mathbf{R} - \mathbf{k}_h{}^0\right) \\ & + \mathscr{V}(\mathbf{r}) + 2\beta(\mathbf{s}_e + \mathbf{s}_h)\cdot\mathbf{H}, \end{aligned} \tag{80}$$

where

$$\mathbf{A}_\mathbf{r} = \tfrac{1}{2}(\mathbf{H} \times \mathbf{r})$$

and

$$\mathbf{A}_\mathbf{R} = \tfrac{1}{2}(\mathbf{H} \times \mathbf{R}).$$

If we substitute[44]

$$\Phi^{n,\mathbf{K}}(\mathbf{r}, \mathbf{R}) = F^{n,\mathbf{K}}(\mathbf{r}, \mathbf{R}) \exp\left(\frac{ie}{\hbar c}\mathbf{A}_\mathbf{r}\cdot\mathbf{R}\right), \tag{81}$$

then $F^{n,\mathbf{K}}(\mathbf{r}, \mathbf{R})$ satisfies

$$\mathscr{H}' F^{n,\mathbf{K}}(\mathbf{r}, \mathbf{R}) = \varepsilon F^{n,\mathbf{K}}(\mathbf{r}, \mathbf{R}), \tag{82}$$

where

$$\begin{aligned} \mathscr{H}' = {} & \mathscr{H}^e\left(-i\nabla_\mathbf{r} - \frac{1}{2}i\nabla_\mathbf{R} + \frac{e}{\hbar c}\mathbf{A}_\mathbf{r} - \mathbf{k}_e{}^0\right) \\ & - \mathscr{H}^h\left(+i\nabla_\mathbf{r} - \frac{1}{2}i\nabla_\mathbf{R} + \frac{e}{\hbar c}\mathbf{A}_\mathbf{r} - \mathbf{k}_h{}^0\right) \\ & + \mathscr{V}(\mathbf{r}) + 2\beta(\mathbf{s}_e + \mathbf{s}_h)\cdot\mathbf{H}. \end{aligned} \tag{83}$$

Since $\nabla_\mathbf{R}$ commutes with $\mathscr{H}'$, we can write

$$F^{n,\mathbf{K}}(\mathbf{r}, \mathbf{R}) = \frac{1}{V^{1/2}} e^{i\mathbf{K}\cdot\mathbf{R}} \psi^{n,\mathbf{K}}(\mathbf{r}). \tag{84}$$

Then $\psi^{n,\mathbf{K}}(\mathbf{r})$ satisfies

$$\mathscr{H}'' \psi^{n,\mathbf{K}}(\mathbf{r}) = \varepsilon \psi^{n,\mathbf{K}}(\mathbf{r}), \tag{85}$$

where

$$\mathscr{H}'' = \mathscr{H}^{e}\left(-i\nabla_{r} + \frac{1}{2}\mathbf{K} + \frac{e}{\hbar c}\mathbf{A}_{r} - \mathbf{k}_{e}^{0}\right) - \mathscr{H}^{h}\left(+i\nabla_{r} + \frac{1}{2}\mathbf{K} + \frac{e}{\hbar c}\mathbf{A}_{r} - \mathbf{k}_{h}^{0}\right) + \mathscr{V}(\mathbf{r}) + 2\beta(\mathbf{s}_{e} + \mathbf{s}_{h})\cdot\mathbf{H}. \tag{86}$$

This result could have been obtained directly by observing that the operator $\mathbf{V}_{\mathbf{R}} - (ie/\hbar c)\,\mathbf{A}_{r}$ commutes with $\mathscr{H}$ in Eq. (80). Finally, we can substitute

$$\psi^{n,\mathbf{K}}(\mathbf{r}) = \exp\left\{\frac{i}{2}(\mathbf{k}_{e}^{0} - \mathbf{k}_{h}^{0})\cdot\mathbf{r}\right\}\bar{\psi}^{n,\mathbf{K}}(\mathbf{r}). \tag{87}$$

Then $\bar{\psi}^{n,\mathbf{K}}(\mathbf{r})$ satisfies

$$\bar{\mathscr{H}}\bar{\psi}^{n,\mathbf{K}}(\mathbf{r}) = \varepsilon\bar{\psi}^{n,\mathbf{K}}(\mathbf{r}), \tag{88}$$

where

$$\bar{\mathscr{H}} = \mathscr{H}^{e}\left(-i\nabla_{r} + \frac{e}{\hbar c}\mathbf{A}_{r} + \frac{1}{2}\boldsymbol{\kappa}\right) - \mathscr{H}^{h}\left(+i\nabla_{r} + \frac{e}{\hbar c}\mathbf{A}_{r} + \frac{1}{2}\boldsymbol{\kappa}\right) + \mathscr{V}(\mathbf{r}) + 2\beta(\mathbf{s}_{e} + \mathbf{s}_{h})\cdot\mathbf{H} \tag{89}$$

and

$$\mathbf{K} = \mathbf{k}_{e}^{0} + \mathbf{k}_{h}^{0} + \boldsymbol{\kappa}. \tag{90}$$

This essentially completes our development of the general effective-mass equation for excitons in the presence of external electric and magnetic fields, which is Eq. (88) above. This equation represents a set of r times s simultaneous differential equations, as does Eq. (61) from which Eq. (88) was derived. The wave function for the exciton state is given by

$$\Psi^{n,\mathbf{K}}(\mathbf{r}_{e}, \mathbf{r}_{h}) = \sum_{i=1}^{r}\sum_{j=1}^{s}\sum_{\mathbf{k}_{e}}\sum_{\mathbf{k}_{h}} A_{c_i v_j}^{n,\mathbf{K}}(\mathbf{k}_{e}, \mathbf{k}_{h})\,\psi_{c_i\mathbf{k}_{e}}(\mathbf{r}_{e})\,\psi_{v_j\mathbf{k}_{h}}(\mathbf{r}_{h}), \tag{91}$$

where $\psi_{c_i\mathbf{k}_{e}}$ and $\psi_{v_j\mathbf{k}_{h}}$ are the conduction- and valence-band wave functions respectively and $A_{c_i v_j}^{n,\mathbf{K}}(\mathbf{k}_{e}, \mathbf{k}_{h})$ is the Fourier transform of the solutions of Eq. (75). The expansions are about $\mathbf{k}_{e}^{0}$ and $\mathbf{k}_{h}^{0}$ such that we can write

$$\psi_{c_i\mathbf{k}_{e}}(\mathbf{r}_{e}) = \exp\{i(\mathbf{k}_{e} - \mathbf{k}_{e}^{0})\cdot\mathbf{r}_{e}\}\,\psi_{c_i\mathbf{k}_{e}^{0}}(\mathbf{r}_{e}) \tag{92a}$$

and

$$\psi_{v_j\mathbf{k}_{h}}(\mathbf{r}_{h}) = \exp\{i(\mathbf{k}_{h} - \mathbf{k}_{h}^{0})\cdot\mathbf{r}_{h}\}\,\psi_{v_j\mathbf{k}_{h}^{0}}(\mathbf{r}_{h}). \tag{92b}$$

The exciton wave function thus becomes

$$\Psi^{n,\mathbf{K}}(\mathbf{r}_e, \mathbf{r}_h) = V^{1/2} \exp\{\tfrac{1}{2}i\boldsymbol{\kappa} \cdot (\mathbf{r}_e + \mathbf{r}_h)\} \exp\left\{\frac{ie}{2\hbar c}\mathbf{H} \cdot (\mathbf{r}_e \times \mathbf{r}_h)\right\} \times \sum_{i=1}^{r} \sum_{j=1}^{s} \bar{\psi}_{ij}^{n,\mathbf{K}}(\mathbf{r}_e - \mathbf{r}_h)\, \psi_{c_i \mathbf{k}_e{}^0}(\mathbf{r}_e)\, \psi_{v_j \mathbf{k}_h{}^0}(\mathbf{r}_h). \tag{93}$$

Again, for excitons of large radius $\bar{\psi}_{i,j}^{n,\mathbf{K}}$ is a slowly varying function compared to $\psi_{c_i \mathbf{k}_e{}^0}$ and $\psi_{v_j \mathbf{k}_h{}^0}$ and can be thought of as an envelope function for the exciton state. The factor $\exp\{\frac{1}{2}i\boldsymbol{\kappa} \cdot (\mathbf{r}_e + \mathbf{r}_h)\}$ can be incorporated into the band functions via Eq. (92). The result is given in Eq. (94):

$$\Psi^{n,\mathbf{K}}(\mathbf{r}_e, \mathbf{r}_h) = V^{1/2} \exp\left\{\frac{ie}{2\hbar c}\mathbf{H} \cdot (\mathbf{r}_e \times \mathbf{r}_h)\right\} \times \sum_{i=1}^{r} \sum_{j=1}^{s} \bar{\psi}_{ij}^{n,\mathbf{K}}(\mathbf{r}_e - \mathbf{r}_h)\, \psi_{c_i \mathbf{k}_e}(\mathbf{r}_e)\, \psi_{v_j \mathbf{k}_h}(\mathbf{r}_h), \tag{94}$$

where $\mathbf{k}_e = \mathbf{k}_e{}^0 + \frac{1}{2}\boldsymbol{\kappa}$ and $\mathbf{k}_h = \mathbf{k}_h{}^0 + \frac{1}{2}\boldsymbol{\kappa}$. The magnetic-field factor in Eqs. (93) and (94) can be thought of as being due to the effect of a magnetic field on a moving dipole. If the exciton is at rest in the crystal we can choose the origin such that $\mathbf{R} = \frac{1}{2}(\mathbf{r}_e + \mathbf{r}_h) = 0$, in which case the exponent vanishes.

III. Optical Absorption by Excitons

The effects of the formation of exciton states are most directly observed in the optical properties of the crystal in the vicinity of its various absorption edges. In the following three sections we consider the simple theory of optical absorption by excitons. Hopfield[45] has pointed out that this simple approach needs justification, since the exciton is, in a sense, the quantum of electronic polarization of the crystal and should not be considered independent of the radiation field. For a discussion of these problems the reader is referred to papers by Hopfield[45] and Pekar[46–49] and the discussion by Knox.[50]

[45] J. J. Hopfield, *Phys. Rev.* **112**, 1555 (1958).

[46] S. I. Pekar, *Zh. Eksperim. i Teor. Fiz.* **33**, 1022 (1957) [*English Transl.: Soviet Phys. JETP* **6**, 785 (1958)].

[47] S. I. Pekar, *Zh. Eksperim. i Teor. Fiz.* **34**, 1176 (1958) [*English Transl.: Soviet Phys. JETP* **7**, 813 (1958)].

[48] S. I. Pekar, *Fiz. Tverd. Tela* **4**, 1301 (1962) [*English Transl.: Soviet Phys.-Solid State* **4**, 953 (1962)].

[49] S. I. Pekar, *Proc. Intern. Conf. Phys. Semicond., Exeter, 1962* p. 419. Inst. of Phys. and Phys. Soc., London, 1962.

[50] R. S. Knox, *Solid State Phys., Suppl.* No. 5, Sec. 11 (1963).

Two basically different absorption processes can occur involving either direct or indirect transitions. These are illustrated schematically in Fig. 1. We refer to the exciton states created in these two processes as direct and indirect excitons respectively and will consider the optical properties of the two processes separately.

7. Direct Transitions

The probability per unit time that the crystal makes an electronic transition from the ground state Ψ^0 to an excited (exciton) state $\Psi^{n,\mathbf{K}}$ is given by[51,52] (see also Schiff[53] and Pauling and Wilson[54])

$$W = \frac{4\pi^2 e^2}{\eta m^2 c\hbar^2 \omega^2} |\langle \Psi^{n,\mathbf{K}} | \sum_i e^{i\mathbf{q}\cdot\mathbf{r}_i} \boldsymbol{\xi} \cdot \boldsymbol{\pi}_i | \Psi_0 \rangle|^2 I(\omega), \tag{95}$$

where $\mathbf{q}$ and $\boldsymbol{\xi}$ are respectively the wave vector and polarization vector of the photon of frequency ω; $\boldsymbol{\pi}_i$ is the pseudomomentum operator for the ith electron at the position $\mathbf{r}_i$ and is given by Eq. (65). The index of refraction of the crystal is η, and $I(\omega)$ is the radiation intensity measured at the frequency ω, which corresponds to the energy separation between the ground state Ψ^0 and the exciton state $\Psi^{n,\mathbf{K}}$. In order to evaluate Eq. (95) we must calculate the matrix element $\langle \Psi^{n,\mathbf{K}} | \Sigma_i e^{i\mathbf{q}\cdot\mathbf{r}_i} \boldsymbol{\xi} \cdot \boldsymbol{\pi}_i | \Psi_0 \rangle$. From Eqs. (13), (14), and (91) we obtain

$$\langle \Psi^{n,\mathbf{K}} | \sum_i e^{i\mathbf{q}\cdot\mathbf{r}_i} \boldsymbol{\xi} \cdot \boldsymbol{\pi}_i | \Psi_0 \rangle = \sum_{i=1}^{r} \sum_{j=1}^{s} \sum_{\mathbf{k}_e} \sum_{\mathbf{k}_h} A^{n,\mathbf{K}}_{c_i v_j}(\mathbf{k}_e, \mathbf{k}_h) \langle \psi_{c_i \mathbf{k}_e} | e^{i\mathbf{q}\cdot\mathbf{r}} \boldsymbol{\xi} \cdot \boldsymbol{\pi} | \theta\psi_{v_j \mathbf{k}_h} \rangle, \tag{96}$$

where θ is the time-reversal operator and $\theta\psi_{v_j \mathbf{k}_h}$ is the unoccupied valence-band state out of which the electron was excited. Let us write $\theta\psi_{v_j \mathbf{k}_h} \equiv \psi_{v_{j'} - \mathbf{k}_h}$. Substituting Eq. (92) and making use of the fact that for direct transitions $\mathbf{k}_e{}^0 = -\mathbf{k}_h{}^0 \equiv \mathbf{k}^0$, one can show that Eq. (96) reduces to

$$\langle \psi^{n,\mathbf{K}} | \sum_i e^{i\mathbf{q}\cdot\mathbf{r}_i} \boldsymbol{\xi} \cdot \boldsymbol{\pi}_i | \Psi_0 \rangle = \sum_{i=1}^{r} \sum_{j=1}^{s} \sum_{\mathbf{k}_e} A^{n,\mathbf{K}}_{c_i v_j}(\tfrac{1}{2}\mathbf{q} + \mathbf{k}_e, \tfrac{1}{2}\mathbf{q} - \mathbf{k}_e) \langle \psi_{c_i \mathbf{k}^0} | \boldsymbol{\xi} \cdot \boldsymbol{\pi} | \psi_{v_{j'} \mathbf{k}^0} \rangle \delta_{\mathbf{K},\mathbf{q}}, \tag{97}$$

where the matrix element is evaluated between the conduction- and valence-band functions at $\mathbf{k}^0$. We can substitute in Eq. (97) for $A^{n,\mathbf{K}}_{c_i v_j}$ the Fourier

[51] R. J. Elliott, *Phys. Rev.* **108**, 1384 (1957).

[52] G. Dresselhaus, *Phys. Rev.* **106**, 76 (1957).

[53] L. I. Schiff, "Quantum Mechanics," Sec. 35. McGraw-Hill, New York, 1955.

[54] L. Pauling and E. B. Wilson, "Introduction to Quantum Mechanics," Sec. 40. McGraw-Hill, New York, 1935.

transform of the solution of Eq. (61) in the absence of an external magnetic field to obtain

$$\langle \Psi^{n,\mathbf{q}} | \sum_i e^{i\mathbf{q}\cdot\mathbf{r}_i} \boldsymbol{\xi}\cdot\boldsymbol{\pi}_i | \Psi_0 \rangle = V^{1/2} \sum_{i=1}^{r} \sum_{j=1}^{s} \bar{\psi}^{n,\mathbf{q}}_{c_i v_j}(0) \langle \psi_{c_i \mathbf{k}_0} | \boldsymbol{\xi}\cdot\boldsymbol{\pi} | \psi_{v_{j'}\mathbf{k}_0} \rangle, \quad (98)$$

where $\bar{\psi}^{n,\mathbf{q}}_{c_i v_j}(0)$ is the solution of Eq. (88) evaluated at $\mathbf{r} = 0$. We have also the additional result that $\mathbf{K} = \mathbf{q}$—that is, the wave vector for the exciton state formed is the same as that of the photon. The transition probability per unit time is therefore

$$W = \frac{4\pi^2 e^2 V}{\eta m^2 c\hbar^2 \omega^2} \left| \sum_{i=1}^{r} \sum_{j=1}^{s} \bar{\psi}^{n,\mathbf{q}}_{c_i v_j}(0) \langle \psi_{c_i \mathbf{k}_0} | \boldsymbol{\xi}\cdot\boldsymbol{\pi} | \psi_{v_{j'}\mathbf{k}_0} \rangle \right|^2 I(\omega). \quad (99)$$

For the simple model considered above we have only a single conduction-band function and a single valence-band function such that for this model Eq. (99) reduces to

$$W = \frac{4\pi^2 e^2 V}{\eta m^2 c\hbar^2 \omega^2} |\bar{\psi}^{n}_{cv}(0)|^2 \cdot |\langle \psi_{c\mathbf{k}_0} | \boldsymbol{\xi}\cdot\boldsymbol{\pi} | \psi_{v\mathbf{k}_0} \rangle|^2 I(\omega), \quad (100)$$

where we have taken $\mathbf{q} = 0$ for simplicity. Consider $|\bar{\psi}^{n}_{cv}(0)|^2$ for the exciton states of our simple model. Recall that the solutions of the simple model were just hydrogenic wave functions for a reduced mass μ and electronic charge $e/\kappa_0^{1/2}$. These eigenstates form a discrete hydrogenic series for $E < E_g$ and a continuous band for $E > E_g$. It was remarked above that this continuous band forms the absorption edge of the crystal. In the discrete series, $\bar{\psi}^{n}_{cv}(0)$ is nonzero only for S states, for which

$$|\bar{\psi}^{n}_{cv}(0)|^2 = (\pi a_0{}^3 n^3)^{-1}, \quad (101)$$

where n is the principal quantum number of the state. The discrete spectra therefore consist of a series of lines at energy

$$E = E_g - \frac{R}{n^2} \quad (102)$$

with intensity proportional to n^{-3}.[51] This series of lines converges to the absorption edge, and as this edge is approached the lines overlap so that they may be considered as a continuum. The absorption coefficient for a continuum of states is given by[51,15]

$$\alpha(\omega) = \frac{1}{V} \cdot \frac{4\pi^2 e^2}{\eta m^2 c\omega} |\langle \psi' | \sum_i e^{i\mathbf{q}\cdot\mathbf{r}_i} \boldsymbol{\xi}\cdot\boldsymbol{\pi}_i | \Psi_0 \rangle|^2 S(\hbar\omega), \quad (103)$$

where $S(\hbar\omega)$ is the density of states per unit energy. In our simple model this reduces to

$$\alpha(\omega) = \frac{4\pi^2 e^2}{\eta m^3 c\omega} |\bar{\psi}^n_{cv}(0)|^2 \cdot |\langle \psi_c | \xi \cdot \pi | \psi_v \rangle|^2 \, S(\hbar\omega). \tag{104}$$

The density of states $S(\hbar\omega)$ is given for the discrete states by

$$S(E) = 2\left(\frac{dE}{dn}\right)^{-1} = \frac{n^3}{R}. \tag{105}$$

The factor of 2 is introduced in Eq. (105) to take account of a simple twofold degeneracy due to spin. From Eqs. (101), (104), and (105) we obtain for the quasicontinuum of discrete exciton states that

$$\alpha_0(\omega) = \frac{4\pi e^2}{\eta m^2 c\omega}\left(\frac{2\mu}{\hbar^2}\right)^{3/2} R^{1/2} |\langle \psi_c | \xi \cdot \pi | \psi_v \rangle|^2. \tag{106}$$

The absorption coefficient for the true continuum is given by[15]

$$\alpha(\omega) = \alpha_a(\omega)\, \pi\gamma \frac{e^{\pi\gamma}}{\sinh(\pi\gamma)}, \tag{107}$$

where $\gamma = [R/(\hbar\omega - E_g)]^{1/2}$ and $\alpha_a(\omega)$ is the absorption coefficient for direct band-to-band transitions in the absence of exciton effects, which is given by[15]

$$\alpha_a(\omega) = \frac{2e^2}{\eta m^2 c\omega}\left(\frac{2\mu}{\hbar^2}\right)^{3/2} (\hbar\omega - E_g)^{1/2} |\langle \psi_c | \xi \cdot \pi | \psi_v \rangle|^2. \tag{108}$$

For large $\hbar\omega$ or low exciton binding energy, $\gamma \to 0$ and $\alpha(\omega) \to \alpha_a(\omega) + \frac{1}{2}\alpha_0(\omega)$. For photon energies just above the direct gap energy E_g, $\gamma \to \infty$ and $\alpha(\omega)$ goes continuously to the value given by Eq. (106) for the quasicontinuum of discrete states. Consequently, at the band edge for $\hbar\omega = E_g$ there is no abrupt change in absorption coefficient. The situation is depicted schematically in Fig. 5. The electron–hole interaction results not only in a series of discrete levels but also in a strong modification of the absorption edge, to the extent that the absorption edge itself does not appear but blends with the quasicontinuum of discrete exciton states.

Optical absorption due to direct transitions to exciton states has been observed in germanium by Macfarlane *et al.*,[55] by Zwerdling *et al.*,[56–58]

[55] G. G. Macfarlane, T. P. McLean, J. E. Quarrington, and V. Roberts, *Proc. Phys. Soc. (London)* **71**, 863 (1958).
[56] S. Zwerdling, L. M. Roth, and B. Lax, *Phys. Rev.* **109**, 2207 (1958).
[57] S. Zwerdling, L. Roth, and B. Lax, *J. Phys. Chem. Solids* **8**, 397 (1959).
[58] S. Zwerdling, B. Lax, L. M. Roth, and K. J. Button, *Phys. Rev.* **114**, 80 (1959).

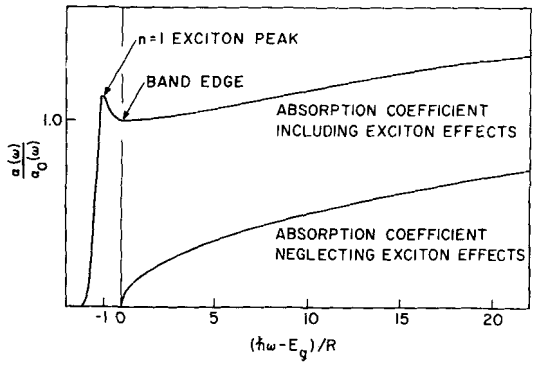


FIG. 5. Theoretical predictions of the optical absorption coefficient for direct transitions in the simple band model. The expected $n = 1$ exciton peak below the band edge is indicated schematically.

and by Edwards and Lazazzera.[59] In group-III–V compounds direct excitons have been observed in GaSb by Johnson *et al.*,[60] in GaAs by Sturge[24] and in InP by Turner *et al.*[61] The experimental absorption coefficient for GaAs in the vicinity of the direct gap obtained by Sturge is shown in Fig. 6. As can be seen from the figure, the spectrum is highly temperature dependent with the $n = 1$ exciton peak being wiped out at high temperatures. There is good agreement between the observed low-temperature curve and the theoretical absorption coefficient, including exciton effects shown in Fig. 5. The exciton binding energy at 21°K obtained from Fig. 6 is 0.0034 eV.[24] For further information and references to experimental

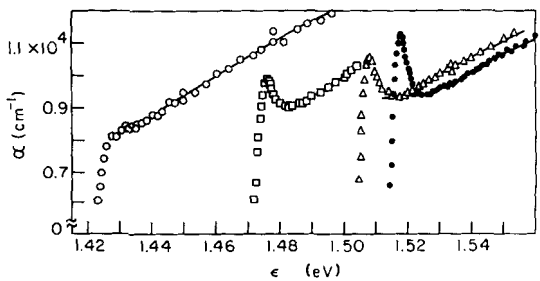


FIG. 6. Exciton absorption spectra in GaAs: ○ 294°K, □ 186°K, △ 90°K, ● 21°K. (After M. D. Sturge.[24])

[59] D. F. Edwards and V. J. Lazazzera, *Phys. Rev.* **120**, 420 (1960).
[60] E. J. Johnson, I. Filinski, and H. Y. Fan, *Proc. Intern. Conf. Phys. Semicond., Exeter, 1962* p. 375. Inst. of Phys. and Phys. Soc., London, 1962.
[61] W. J. Turner, W. E. Reese, and G. D. Pettit, *Phys. Rev.* **136**, A1467 (1964).

work the reader is referred to articles by McLean[62,63] and Chapter 6 by E. J. Johnson in this volume.

In obtaining Eq. (99) we made the assumption that the interband matrix element $\langle \psi_{ck}|e^{i\mathbf{q}\cdot\mathbf{r}}\,\boldsymbol{\xi}\cdot\boldsymbol{\pi}|\psi_{vk'}\rangle$ is independent of $\mathbf{k}$. This follows directly from the assumption that the periodic part of the conduction- and valence-band wave functions is independent of $\mathbf{k}$. If we drop these assumptions and allow the interband matrix element to vary with $\mathbf{k}$, additional contributions to the absorption coefficient arise. These additional contributions can be obtained by starting with Eq. (95) and inserting Eq. (96), which is still valid. When this is done, one finds

$$\left\langle \Psi^{n,\mathbf{K}} \middle| \sum_i e^{i\mathbf{q}\cdot\mathbf{r}_i}\,\boldsymbol{\xi}\cdot\boldsymbol{\pi}_i \middle| \Psi_0 \right\rangle = \sum_{i=1}^{r}\sum_{j=1}^{s}\sum_{\mathbf{k}_e} A^{n,\mathbf{K}}_{c_i,v_j}(\tfrac{1}{2}\mathbf{q}+\mathbf{k}_e,\tfrac{1}{2}\mathbf{q}-\mathbf{k}_e) \times \langle \psi_{c_i,\mathbf{k}_e+\frac{1}{2}\mathbf{q}}|e^{i\mathbf{q}\cdot\mathbf{r}}\,\boldsymbol{\xi}\cdot\boldsymbol{\pi}|\psi_{v_j',\mathbf{k}_e-\frac{1}{2}\mathbf{q}}\rangle. \tag{109}$$

Let us expand the matrix element in Eq. (109) about $\mathbf{k}_e = \mathbf{k}^0$ in a Taylor series:

$$\langle \psi_{c_i,\mathbf{k}_e+\frac{1}{2}\mathbf{q}}|e^{i\mathbf{q}\cdot\mathbf{r}}\,\boldsymbol{\xi}\cdot\boldsymbol{\pi}|\psi_{v_j',\mathbf{k}_e-\frac{1}{2}\mathbf{q}}\rangle = \{1 + (k_e - k^0)^\alpha \nabla_{\mathbf{k}}{}^\alpha + \tfrac{1}{2}(k_e-k^0)^\alpha(k_e-k^0)^\beta \nabla_{\mathbf{k}}{}^\alpha \nabla_{\mathbf{k}}{}^\beta + \cdots\} \langle \psi_{c_i,\mathbf{k}+\frac{1}{2}\mathbf{q}}|e^{i\mathbf{q}\cdot\mathbf{r}}\,\boldsymbol{\xi}\cdot\boldsymbol{\pi}|\psi_{v_j',\mathbf{k}-\frac{1}{2}\mathbf{q}}\rangle_{\mathbf{k}=\mathbf{k}^0}, \tag{110}$$

where α and β run over the directions x, y, and z and the operators $\nabla_{\mathbf{k}}$ yield the derivatives of the band-to-band matrix element with respect to $\mathbf{k}$. Substituting for $A^{n,\mathbf{K}}_{c_i,v_j}$ the Fourier transform of $\Phi^{n,\mathbf{K}}_{c_i,v_j}$, the solutions of Eq. (75), and using Eq. (110) it can be shown that

$$\langle \Psi^{n,\mathbf{K}}|\sum_i e^{i\mathbf{q}\cdot\mathbf{r}_i}\,\boldsymbol{\xi}\cdot\boldsymbol{\pi}_i|\Psi_0\rangle = V^{1/2}\sum_{i=1}^{r}\sum_{j=1}^{s}\{\bar{\psi}^{n,\mathbf{K}}_{c_i,v_j}(\mathbf{r})\Big|_{\substack{\mathbf{r}=0\\ \mathbf{K}=\mathbf{q}}} + D^\alpha \bar{\psi}^{n,\mathbf{K}}_{c_i,v_j}(\mathbf{r})\Big|_{\substack{\mathbf{r}=0\\ \mathbf{K}=\mathbf{q}}} \nabla_{\mathbf{k}}{}^\alpha + \tfrac{1}{2}D^\alpha D^\beta \bar{\psi}^{n,\mathbf{K}}_{c_i,v_j}(\mathbf{r})\Big|_{\substack{\mathbf{r}=0\\ \mathbf{K}=\mathbf{q}}} \nabla_{\mathbf{k}}{}^\alpha \nabla_{\mathbf{k}}{}^\beta + \cdots\} \langle \psi_{c_i,\mathbf{k}+\frac{1}{2}\mathbf{q}}|e^{i\mathbf{q}\cdot\mathbf{r}}\,\boldsymbol{\xi}\cdot\boldsymbol{\pi}|\psi_{v_j,\mathbf{k}-\frac{1}{2}\mathbf{q}}\rangle_{\mathbf{k}=\mathbf{k}^0}\delta_{\mathbf{K},\mathbf{q}}, \tag{111}$$

where $\mathbf{D}$ operates on $\bar{\psi}^{n,\mathbf{K}}_{c_i,v_j}$ [see Eqs. (88) and (89)], which is then evaluated at $\mathbf{r} = 0$ and $\mathbf{K} = \mathbf{q}$. In the presence of an external magnetic field,

$$\mathbf{D} = -i\nabla_{\mathbf{r}} - \frac{ie}{2\hbar c}\mathbf{H}\times\nabla_{\mathbf{K}}, \tag{112}$$

[62] T. P. McLean, *Progr. Semicond.* **5**, 53 (1960).

[63] T. P. McLean, Excitons in Germanium *in* "Polarons and Excitons" (C. G. Kuper and G. D. Whitfield, eds.), p. 367. Plenum Press, New York, 1963.

where $\nabla_{\mathbf{K}}$ takes the derivative of $\bar{\psi}^{n,\mathbf{K}}_{c_i v_j}$ with respect to $\mathbf{K}$. Note that $\bar{\psi}^{n,\mathbf{K}}_{c_i v_j}$ is an implicit function of $\mathbf{K}$, since the Hamiltonian $\mathscr{H}$, Eq. (89), of which $\bar{\psi}^{n,\mathbf{K}}_{c_i,v_j}$ is an eigenfunction, depends on $\mathbf{K}$. Again, the transition probability vanishes except for states with $\mathbf{K} = \mathbf{q}$.

If in the expansion Eq. (111) we let $\mathbf{q} = 0$, we are left with the transitions that Hopfield[35] has referred to as "allowed." The additional terms, which are linear in $\mathbf{q}$, result in transitions that are referred to[64] as "first forbidden," etc. Elliott,[51] on the other hand, has considered only the terms that remain for $\mathbf{q} = 0$. Recall that the functions $\bar{\psi}^{n,\mathbf{K}}_{c_i v_j}$ are solutions of a hydrogen-like effective-mass equation. Consequently, these states can be classified as S, P, D, etc., at least for our simple model. $\bar{\psi}^{n,\mathbf{K}}_{c_i v_j}(\mathbf{r})|_{\mathbf{r}=0}$ is nonvanishing only for S states; $\nabla_{\mathbf{r}}\psi^{n,\mathbf{K}}_{c_i v_j}(\mathbf{r})|_{\mathbf{r}=0}$ is nonvanishing only for P states, and so on. In the nomenclature of Hopfield, we have allowed and forbidden transitions for all exciton symmetries. In Elliott's terminology, the transition is allowed if $\langle \psi_{c_i \mathbf{k}^0} | \boldsymbol{\xi} \cdot \boldsymbol{\pi} | \psi_{v_{j'} \mathbf{k}^0} \rangle$ is nonvanishing—that is, if the direct band-to-band transition is allowed—and is forbidden if this matrix element vanishes. In this terminology, S-state transitions are referred to as allowed and P- and D-state exciton transitions, etc., are referred to as forbidden.

In summary, we find the transition probability depends not only on the polarization of the light but also on its wave vector $\mathbf{q}$ and on the presence and direction of external magnetic fields. All three of these effects have been observed in CdS by Hopfield and Thomas[64] and in CdSe by Wheeler and Dimmock.[65]

8. Selection Rules for Direct Exciton Transitions

If one is interested only in what exciton transitions are allowed and not necessarily in calculating their intensities, one can obtain by the use of symmetry arguments the general selection rules for optical absorption to direct exciton states.[35] Since the ground state of the crystal Ψ_0 is invariant under all crystallographic transformations, direct transitions are allowed only to those exciton states that transform in the same way as does the operator $e^{i\mathbf{q}\cdot\mathbf{r}}\,\boldsymbol{\xi}\cdot\boldsymbol{\pi}$. The exciton function must transform, therefore, as a basis of some irreducible representation of the group of the wave vector for the point $\mathbf{q}$ in the Brillouin zone. This was obtained explicitly above where we found that the transition probability vanished except to states $\Psi^{n,\mathbf{K}}$ for which $\mathbf{K} = \mathbf{q}$. In accord with the previous discussion, let us consider first the situation that prevails if we assume $\mathbf{q} = 0$. In the absence of an external magnetic field, the exciton wave function is given by

$$\Psi^{n}_{c_i v_j}(\mathbf{r}_e, \mathbf{r}_h) = V^{1/2}\,\bar{\psi}^{n}_{c_i v_j}(\mathbf{r}_e - \mathbf{r}_h)\,\psi_{c_i \mathbf{k}^0}(\mathbf{r}_e)\,\psi_{v_{j'} - \mathbf{k}^0}(\mathbf{r}_h)$$

[64] J. J. Hopfield and D. G. Thomas, *Phys. Rev.* **122**, 35 (1961).
[65] R. G. Wheeler and J. O. Dimmock, *Phys. Rev.* **125**, 1805 (1962).

[see Eq. (93)]. We need consider only one of a set of r times s such functions, since for a set of degenerate states they must all transform according to the same irreducible representation. Consider that $\psi_{c_i\mathbf{k}^0}$ transforms as a basis function of the irreducible representation $\mathbf{D}_c(\mathbf{k}^0)$ of the group of the wave vector $\mathbf{k}^0$. Recall also that the hole-band function $\psi_{v_{j'}-\mathbf{k}^0}$ is given by the time-reversed conjugate of the valence-band state $\psi_{v_j\mathbf{k}^0}$. Therefore, $\psi_{v_{j'}-\mathbf{k}^0}$ transforms as a basis function of the irreducible representation $\mathbf{D}_v{}^*(\mathbf{k}^0)$, which is the complex conjugate of the representation for which $\psi_{v_j\mathbf{k}^0}$ is a basis function. Further, we can consider that the function $\overline{\psi}^n_{c_iv_j}$ transforms as a basis function for the irreducible representation $\mathbf{D}_n$ of the group of the wave vector $\mathbf{k} = 0$ at the center of the Brillouin zone. Likewise, the operator $\boldsymbol{\xi}\cdot\boldsymbol{\pi}$ transforms as a basis function for an irreducible representation $\mathbf{D}_\xi$ at the center of the zone. The requirement for an allowed transition is then that the decomposition of the direct product of the representations $\mathbf{D}_c(\mathbf{k}^0)$, $\mathbf{D}_v{}^*(\mathbf{k}^0)$, and $\mathbf{D}_n$ contain the representation $\mathbf{D}_\xi$. This is equivalent to saying that transitions to exciton states whose representations $\mathbf{D}_n$ are contained in the decomposition of the direct product $\mathbf{D}_c{}^*(\mathbf{k}^0) \times \mathbf{D}_\xi \times \mathbf{D}_v(\mathbf{k}^0)$ are allowed in the terminology of Hopfield.

Let us now consider the additional transitions that are allowed theoretically if we drop the assumption that $\mathbf{q} = 0$. Since the wave vector $\mathbf{q}$ of the light is small, we can consider an expansion of the operator $e^{i\mathbf{q}\cdot\mathbf{r}}$ in powers of $(\mathbf{q}\cdot\mathbf{r})$. The term linear in $\mathbf{q}$ produces transitions that Hopfield has referred to as first forbidden. These transitions will occur to exciton states whose representations $\mathbf{D}_n$ are contained in the decomposition of the direct product $\mathbf{D}_c{}^*(\mathbf{k}^0) \times \mathbf{D}_{\xi,\mathbf{q}} \times \mathbf{D}_v(\mathbf{k}^0)$, where $\mathbf{D}_{\xi,\mathbf{q}}$ is the representation for which $(\mathbf{q}\cdot\mathbf{r})(\boldsymbol{\xi}\cdot\boldsymbol{\pi})$ is a basis function. For second forbidden transitions, the operator becomes $(\mathbf{q}\cdot\mathbf{r})^2(\boldsymbol{\xi}\cdot\boldsymbol{\pi})$, and so on.

9. Indirect Transitions

In addition to the direct transitions that occur between conduction- and valence-band extrema at the same point in the Brillouin zone via the absorption of an optical photon and in which the wave vector of the electrons is approximately conserved, transitions may also occur between conduction- and valence-band extrema that are not at the same point in the Brillouin zone.[66–68] These transitions are indirect and do not conserve the wave

[66] I. C. Cheeseman, *Proc. Phys. Soc.* (*London*) **A65**, 25 (1952).

[67] L. H. Hall, J. Bardeen, and F. J. Blatt, *Phys. Rev.* **95**, 559 (1954).

[68] J. Bardeen, F. J. Blatt, and L. H. Hall *in* "Photoconductivity Conference" (Proc. Atlantic City Conf.) (R. G. Breckenridge, B. R. Russell, and E. E. Hahn, eds.), p. 146. Wiley, New York, and Chapman & Hall, London, 1956.

vector of the electrons. It is obvious that these indirect transitions can occur only if there is a breakdown in the selection rule that conserves the wave vector $\mathbf{k}$ of the electrons. This in fact occurs because the crystal is never, in reality, perfectly periodic. The periodicity is destroyed because of the presence of impurities, defects, and lattice vibrations or phonons. These perturbing forces mix the single-electron band functions at different points in the Brillouin zone and make it possible for indirect transitions to occur through the absorption of an optical photon with essentially zero wave vector.

Consider the indirect transition between a set of valence-band states near a valence-band maximum at $\mathbf{k}_v{}^0$ and a set of conduction-band states near a conduction-band minimum at $\mathbf{k}_c{}^0$ (see Fig. 1, process *B*). Because of the perturbation, the valence-band states near $\mathbf{k}_v{}^0$ are mixed with states of wave vector near $\mathbf{k}_c{}^0$, and similarly the conduction-band states near $\mathbf{k}_c{}^0$ are mixed with states of wave vector near $\mathbf{k}_v{}^0$. Optical transitions between these mixed states are therefore allowed. For simplicity we shall consider here that the perturbation of band states in the indirect absorption processes occurs because of lattice vibrations or phonons, since this adequately illustrates the essential aspects of the theory.

In the perturbation process, the strongest effect occurs when one phonon is either created or destroyed.[15,68] The total wave vector for the system, including that of the phonon, is conserved. The calculation of the absorption coefficient for indirect transitions differs in three essential ways from that for direct transitions.

(1) The matrix element between band states includes the perturbation by the phonon field as well as the interaction with the light wave.
(2) Since in the perturbation process a phonon is created or destroyed, account must be taken of the phonon energy.
(3) Since the phonon field can provide a large range of momentum to the electronic system, we no longer have the conservation rule that the wave vector $\mathbf{K}$ of the exciton state formed must be equal to the wave vector of the light. Instead, a continuum of states in $\mathbf{K}$ may be excited such that there is no discrete spectrum per se for indirect excitons.

The wave vector $\mathbf{Q}$ of the phonon that is created or destroyed in the perturbation process is approximately equal to $\pm(\mathbf{k}_c{}^0 - \mathbf{k}_v{}^0)$. In addition to the possibility of either creating or annihilating a particular phonon, there may be several phonons or branches in the phonon spectrum with wave vector $\mathbf{Q}$. Each of these branches may contribute to the indirect absorption process. The matrix element for an indirect transition from the valence-band state $\psi_{v,\mathbf{k}}$ to the conduction-band state $\psi_{c,\mathbf{k}'}$ accompanied by the creation or annihilation of a phonon of wave vector $\mathbf{Q}$ belonging to the lth phonon

branch of energy $\hbar\omega_l(\mathbf{Q})$ is given by[15,51]

$$\sum_i \left[\frac{\langle \psi_{c,\mathbf{k}'} | \boldsymbol{\xi} \cdot \boldsymbol{\pi} | \psi_{i,\mathbf{k}'} \rangle \langle \psi_{i,\mathbf{k}'} | \mathscr{H}_l^{\pm}(\mathbf{Q}) | \psi_{v,\mathbf{k}} \rangle}{E_v(\mathbf{k}) - E_i(\mathbf{k}') \mp \hbar\omega_l(\mathbf{Q})} + \frac{\langle \psi_{c,\mathbf{k}'} | \mathscr{H}_l^{\pm}(\mathbf{Q}) | \psi_{i,\mathbf{k}} \rangle \langle \psi_{i,\mathbf{k}} | \boldsymbol{\xi} \cdot \boldsymbol{\pi} | \psi_{v,\mathbf{k}} \rangle}{E_c(\mathbf{k}') - E_i(\mathbf{k}) \pm \hbar\omega_l(\mathbf{Q})} \right], \tag{113}$$

where we have neglected the wave vector of the light. The quantity $\mathscr{H}_l^{\pm}(\mathbf{Q})$ is the effective electronic perturbation due to the creation or destruction of a phonon of wave vector $\mathbf{Q}$. The situation is indicated schematically in Fig. 7. The relative strength of these two interactions depends on the number of phonons $n_l(\mathbf{Q})$ present at a given temperature, the creation process being proportional to $[n_l(\mathbf{Q}) + 1]^{1/2}$ and the destruction process being proportional to $n_l(\mathbf{Q})^{1/2}$, where

$$n_l(\mathbf{Q}) = \left\{ \exp\left[\frac{\hbar\omega_l(\mathbf{Q})}{kT} \right] - 1 \right\}^{-1}. \tag{114}$$

At very low temperatures, $n_l(\mathbf{Q}) \approx 0$, so that only the creation process is important. In Eq. (113), ψ_i is a set of so-called intermediate states, which, when mixed with the valence- and conduction-band states, allow the indirect process to occur. The matrix element, Eq. (113), is approximately independent of $\mathbf{k}$ and $\mathbf{k}'$ for $\mathbf{Q} = \pm(\mathbf{k} - \mathbf{k}')$ over the range of interest and may be written as $C^{\pm}(c_i, v_j; l)$. The absorption coefficient thus becomes

$$\alpha(\omega) = \frac{1}{V} \frac{4\pi^2 e^2}{\eta m^2 c\omega} \sum_l \sum_{\pm} \sum_{n,\mathbf{K}} \left| \sum_{i=1}^{r} \sum_{j=1}^{s} C^{\pm}(c_i, v_j'; l) \sum_{\mathbf{k}_e, \mathbf{k}_h} A_{c_i,v_j}^{n,\mathbf{K}}(\mathbf{k}_e, \mathbf{k}_h) \right|^2 \times \delta[\hbar\nu - E \mp \hbar\omega_l(\mathbf{Q})], \tag{115}$$

where $\mathbf{K} = \mathbf{k}_e + \mathbf{k}_h = \mathbf{Q}$. In addition, the phonon energy $\hbar\omega_l(\mathbf{Q})$ is usually nearly constant over the range of interest, so that we can perform the sums over $\mathbf{k}_e$ and $\mathbf{k}_h$ to obtain

$$\alpha(\omega) = \frac{4\pi^2 e^2}{\eta m^2 c\omega} \sum_l \sum_{\pm} \sum_{n,\mathbf{K}} \left| \sum_{i=1}^{r} \sum_{j=1}^{s} C^{\pm}(c_i, v_j'; l) \bar{\psi}_{c_i,v_j}^{n,\mathbf{K}}(0) \right|^2 \times \delta[\hbar\omega - E \mp \hbar\omega_l(\mathbf{Q})].$$

Consider the simple model for which

$$E_c(\mathbf{k}) = E_g + \frac{\hbar^2}{2m_e^*}(\mathbf{k} - \mathbf{k}_c^0)^2 \tag{116a}$$

and

$$E_v(\mathbf{k}) = -\frac{\hbar^2}{2m_h^*}(\mathbf{k} - \mathbf{k}_v^0)^2, \tag{116b}$$

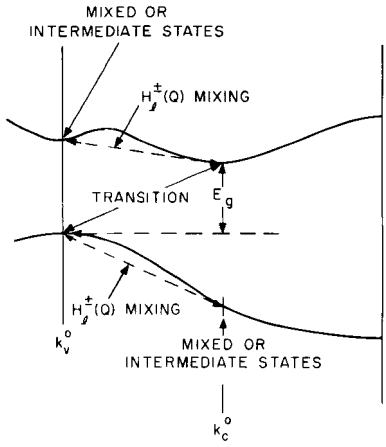


FIG. 7. Schematic diagram for indirect transitions, indicating the band state mixing that occurs because of the perturbation of the phonon field. The phonon energy is not represented in the figure.

where both band extrema are spherical. The effective-mass equation for this situation has the solution

$$E = E_g - \frac{R}{n^2} + \frac{\hbar^2}{2M}\kappa^2, \tag{117}$$

where $\mathbf{K} = \mathbf{k}_e^0 + \mathbf{k}_h^0 + \boldsymbol{\kappa}$, $\mathbf{M} = m_e^* + m_h^*$, and $\bar{\psi}^n(\mathbf{r})$ satisfies Eq. (52). The absorption coefficient for this simple model is given by[15]

$$\alpha(\omega) = V\frac{e^2}{\eta m^2 c\omega}\left(\frac{2M}{\hbar^2}\right)^{3/2}\sum_l\sum_{\pm}|C^{\pm}(c,v;l)|^2\sum_n\left[\hbar\omega - E_g + \frac{R}{n^2} \mp \hbar\omega_l(\mathbf{Q})\right]^{1/2} \times |\bar{\psi}^n_{c,v}(0)|^2. \tag{118}$$

This appears at first glance to be proportional to the crystal volume V. This is actually not the case, since the electron–phonon matrix element $|\langle\psi_{\mathbf{k}}|\mathscr{H}_l^{\pm}(\mathbf{Q})|\psi_{v,\mathbf{k}}\rangle|^2$ is inversely proportional to the crystal volume.[69]

As in the case of direct transitions, the selection rules governing indirect transitions can be obtained group theoretically. In addition to the conduction- and valence-band symmetries one must, of course, include the symmetry of the phonon or phonons involved. Selection rules for indirect

[69] J. M. Ziman, "Electrons and Phonons," Chap. 5. Oxford Univ. Press, London and New York, 1960.

transitions have been considered by Elliott and Loudon,[70] Lax and Hopfield,[71] Birman,[72] and Lax.[73,74] The situation here is somewhat more complicated than in the case of direct transitions, and the reader is referred to the above papers for further information.

The indirect absorption spectrum, therefore, consists of a series of steps, one for each exciton state, n, and two for each phonon branch, l, corresponding to either the creation or destruction of that particular phonon. Optical absorption due to indirect transitions to exciton states has been observed in germanium and silicon by Macfarlane *et al.*,[75–77] in germanium by Zwerdling *et al.*,[57,58] and in GaP by Gershenzon *et al.*[78] The spectrum obtained by these last authors is shown in Fig. 8. Again, for further information on the experimental situation, the reader is referred to the review article by McLean[63] and Chapter 6 by E. J. Johnson in this volume.

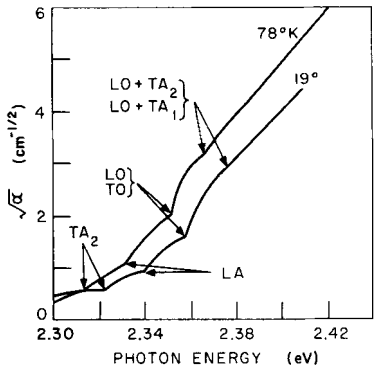


FIG. 8. Indirect absorption spectra at the absorption edge in GaP, showing the thresholds for the formation of free excitons with the emission of several different phonons. (After M. Gershenzon *et al.*[78])

[70] R. J. Elliott and R. Loudon, *J. Phys. Chem. Solids* **15**, 146 (1960).
[71] M. Lax and J. J. Hopfield, *Phys. Rev.* **124**, 115 (1961).
[72] J. L. Birman, *Phys. Rev.* **127**, 1093 (1962); **131**, 1489 (1963).
[73] M. Lax, *Proc. Intern. Conf. Phys. Semicond., Exeter, 1962* p. 395. Inst. of Phys. and Phys. Soc., London, 1962.
[74] M. Lax, *Phys. Rev.* **138**, A793 (1965).
[75] G. G. Macfarlane, T. P. McLean, J. E. Quarrington, and V. Roberts, *Phys. Rev.* **108**, 1377 (1957).
[76] G. G. Macfarlane, T. P. McLean, J. E. Quarrington, and V. Roberts, *Phys. Rev.* **111**, 1245 (1958).
[77] G. G. Macfarlane, T. P. McLean, J. E. Quarrington, and V. Roberts, *J. Phys. Chem. Solids* **8**, 388 (1959).
[78] M. Gershenzon, D. G. Thomas, and R. E. Dietz, *Proc. Intern. Conf. Phys. Semicond., Exeter, 1962* p. 752. Inst. of Phys. and Phys. Soc., London, 1962.

In practice, the indirect absorption edge observed experimentally is not particularly rich in structure, at least in the absence of an external magnetic field, so that detailed information is difficult to obtain. In order to investigate the indirect absorption process in more detail and to obtain information about the conduction- and valence-band extrema, it is necessary to apply an external magnetic field. When this is done, the absorption edge develops a more detailed structure, which reflects the presence of so-called Landau levels in the conduction and valence bands. This is even more apparent in the spectra due to direct absorption processes. In the next section we consider the effect of a magnetic field on the absorption edge and the connection between exciton states and Landau levels.

IV. The Effects of an External Magnetic Field

10. g-Factors for Electrons and Holes

The principal problem remaining in our theoretical consideration of excitons in crystals is the solution of the reduced effective-mass equation, Eq. (88). This, of course, depends on the form of the electron and hole effective-mass tensors $\mathscr{H}^{e}$ and $\mathscr{H}^{h}$. In the case of group-IV elements and group-III–V semiconductors, these tensors are quite complex. It is nevertheless of interest to investigate the properties of a somewhat simpler model, as we have been doing from time to time throughout the course of this development. Consider the situation in which the conduction- and valence-band extrema are each twofold degenerate because of spin and occur at the same point in the Brillouin zone. Consider further that the crystal possesses a center of symmetry such that there are no terms linear in $\mathbf{k}$. In this case $H^{e}_{ii'}(\mathbf{k}_e')$ and $H^{h}_{jj'}(\mathbf{k}_h')$ become

$$H^{e}_{ii'}(\mathbf{k}_e') = \frac{\hbar^2}{2m} k_e'^2\, \delta_{ii'} + \frac{\hbar^2}{m^2} k_e'^{\alpha}\, k_e'^{\beta} \sum_n \frac{\pi^{\alpha}_{in}\, \pi^{\beta}_{ni'}}{E_c(\mathbf{k}_e{}^0) - E_n(\mathbf{k}_e{}^0)}, \tag{119a}$$

and

$$H^{h}_{jj'}(\mathbf{k}_h') = \frac{\hbar^2}{2m} k_h'^2\, \delta_{jj'} + \frac{\hbar^2}{m^2} k_h'^{\alpha}\, k_h'^{\beta} \sum_n{}' \frac{\pi^{\alpha}_{jn}\, \pi^{\beta}_{nj'}}{E_v(\mathbf{k}_h{}^0) - E_n(\mathbf{k}_h{}^0)}, \tag{119b}$$

respectively. In the effective-mass equation for excitons, $\mathbf{k}_e'$ is replaced by

$$\frac{1}{\hbar}\mathbf{P}_e = -i\nabla_r + \frac{e}{\hbar c}\mathbf{A}_r + \frac{1}{2}\boldsymbol{\kappa} \tag{120a}$$

and $\mathbf{k}_h'$ is replaced by

$$\frac{1}{\hbar}\mathbf{P}_h = +i\nabla_r + \frac{e}{\hbar c}\mathbf{A}_r + \frac{1}{2}\boldsymbol{\kappa}. \tag{120b}$$

In our model, the conduction band has a minimum at $\mathbf{k}_e^0$ and the valence band has a maximum at $\mathbf{k}_h^0 = \mathbf{k}_e^0$. Substituting Eqs. (119) into Eq. (75) and using Eqs. (73) and (74), the effective-mass Hamiltonian may be written in the form[79]

$$\bar{H}_{ii'jj'} = \frac{1}{2}P_e^{\alpha}\left(\frac{1}{m_e^*}\right)^{\alpha\beta}P_e^{\beta}\,\delta_{ii'}\,\delta_{jj'} + \frac{1}{2}P_h^{\alpha}\left(\frac{1}{m_h^*}\right)^{\alpha\beta}P_h^{\beta}\,\delta_{ii'}\,\delta_{jj'}$$
$$+ \frac{1}{2}\beta_0\,\sigma_{ii'}^{\alpha}\,g_e^{\alpha\beta}\,H^{\beta}\,\delta_{jj'} + \frac{1}{2}\beta_0\,\sigma_{jj'}^{\alpha}\,g_h^{\alpha\beta}\,H^{\beta}\,\delta_{ii'}$$
$$+ V(\mathbf{r})\,\delta_{ii'}\,\delta_{jj'} \tag{121}$$

where

$$\left(\frac{1}{m_e^*}\right)^{\alpha\beta} = \frac{1}{\hbar^2}\frac{\partial^2 E_c(\mathbf{k}_e)}{\partial k_e^{\alpha}\,\partial k_e^{\beta}}\bigg|_{\mathbf{k}_e=\mathbf{k}_e^0} \tag{122a}$$

is the completely symmetric effective-mass tensor for the conduction band, which may be obtained from the sum rule Eq. (68), and

$$\left(\frac{1}{m_h^*}\right)^{\alpha\beta} = -\frac{1}{\hbar^2}\frac{\partial^2 E_v(\mathbf{k}_h)}{\partial k_h^{\alpha}\,\partial k_h^{\beta}}\bigg|_{\mathbf{k}_h=\mathbf{k}_h^0} \tag{122b}$$

is the completely symmetric effective-mass tensor for the valence band. Note that both quantities are positive. The third and fourth terms in Eq. (121) arise, as mentioned above, because the components of $\mathbf{P}$ do not commute in the presence of a magnetic field. In tensor notation,[79]

$$\boldsymbol{\sigma}_{ii'}\cdot\mathbf{g}_e = 4(\mathbf{s}_e)_{ii'} + \frac{2}{im}\sum_n{}' \frac{\boldsymbol{\pi}_{in}\times\boldsymbol{\pi}_{ni'}}{E_c(\mathbf{k}_e^0) - E_n(\mathbf{k}_e^0)} \tag{123a}$$

and

$$\boldsymbol{\sigma}_{jj'}\cdot\mathbf{g}_h = 4(\mathbf{s}_h)_{jj'} + \frac{2}{im}\sum_n{}' \frac{\boldsymbol{\pi}_{jn}\times\boldsymbol{\pi}_{nj'}}{E_v(\mathbf{k}_h^0) - E_n(\mathbf{k}_h^0)}. \tag{123b}$$

In Eq. (123) $(\mathbf{s}_e)_{ii'}$ and $(\mathbf{s}_h)_{jj'}$ are the matrix elements of the electron spin operator between the conduction-band edge wave functions, and between the valence-band edge wave functions respectively. The appropriate Pauli spin vectors $\boldsymbol{\sigma}_{ii'}$ and $\boldsymbol{\sigma}_{jj'}$ can be obtained from the transformation properties of the conduction- and valence-band states and are equal to $2(\mathbf{s}_e)_{ii'}$ and $2(\mathbf{s}_h)_{jj'}$ respectively in the absence of spin–orbit effects. In this case $\boldsymbol{\pi}\times\boldsymbol{\pi} = 0$ so that $\mathbf{g}_e$ and $\mathbf{g}_h$ both equal 2. Also, $\boldsymbol{\sigma}_{jj'}$, $\mathbf{s}_{jj'}$, and $\boldsymbol{\pi}_{jn}\times\boldsymbol{\pi}_{nj'}$ for the hole states are all opposite in sign to their values for the corresponding unoccupied electronic valence-band states, since the former are generated

[79] L. M. Roth, *Phys. Rev.* **118**, 1534 (1960).

from the latter by time reversal. Consequently, $\mathbf{g}_e$ and $\mathbf{g}_h$ are the electronic conduction- and valence-band $\mathbf{g}$ factors with the correct sign. The third and fourth terms in Eq. (121) represent the splitting of the conduction- and valence-band states in the presence of a magnetic field. Equation (121) indicates, for the simple band case, how the splitting of the valence- and conduction-band states in the presence of a magnetic field contributes to the exciton effective-mass Hamiltonian and thus to the energies of the exciton states.

11. Exciton States in a Magnetic Field and Landau Levels

Let us now examine in more detail the individual terms arising in Eq. (121). If the spin terms are neglected, the set of simultaneous effective-mass equations separate such that we can consider a single equation with a Hamiltonian that consists of a sum of terms,[65]

$$H = H_1 + H_2 + H_3 + H_4 + H_5 + H_6, \tag{124}$$

where

$$H_1 = \frac{1}{2} p^\alpha \left(\frac{1}{\mu}\right)^{\alpha\beta} p^\beta + V(\mathbf{r}), \tag{125a}$$

$$H_2 = \frac{e}{c} A^\alpha \left(\frac{1}{\Delta}\right)^{\alpha\beta} p^\beta, \tag{125b}$$

$$H_3 = \frac{e^2}{2c^2} A^\alpha \left(\frac{1}{\mu}\right)^{\alpha\beta} A^\beta, \tag{125c}$$

$$H_4 = \frac{1}{2} \hbar \kappa^\alpha \left(\frac{1}{\Delta}\right)^{\alpha\beta} p^\beta, \tag{125d}$$

$$H_5 = \frac{e\hbar}{2c} \kappa^\alpha \left(\frac{1}{\mu}\right)^{\alpha\beta} A^\beta, \tag{125e}$$

$$H_6 = \frac{1}{8} \hbar^2 \kappa^\alpha \left(\frac{1}{\mu}\right)^{\alpha\beta} \kappa^\beta, \tag{125f}$$

in which $\mathbf{p} = -i\hbar \mathbf{V}_\mathbf{r}$,

$$\left(\frac{1}{\mu}\right)^{\alpha\beta} = \left(\frac{1}{m_e^*}\right)^{\alpha\beta} + \left(\frac{1}{m_h^*}\right)^{\alpha\beta} \tag{126}$$

is the reduced exciton effective-mass tensor, and

$$\left(\frac{1}{\Delta}\right)^{\alpha\beta} = \left(\frac{1}{m_e^*}\right)^{\alpha\beta} - \left(\frac{1}{m_h^*}\right)^{\alpha\beta}. \tag{127}$$

The first term, H_1, represents a hydrogen-like Hamiltonian with an anisotropic effective-mass tensor. The second term, H_2, represents an $\mathbf{L}\cdot\mathbf{H}$ orbital contribution to the magnetic energy, and the third term, H_3, represents the H^2 diamagnetic contribution. The remaining terms all involve the motion of the exciton in the crystal through the wave vector $\boldsymbol{\kappa}$. The inversion operator commutes with all components of the exciton Hamiltonian, Eq. (124), except the terms H_4 and H_5. Consequently, if these terms are considered small and treated in perturbation theory, their diagonal contributions must vanish. The resultant exciton energy then contains no terms linear in $\boldsymbol{\kappa}$. The exciton band in $\boldsymbol{\kappa}$ space therefore has a minimum, in this case, at $\boldsymbol{\kappa} = 0$. It is usually possible, in the simple-band case, to choose a coordinate system in which the electron and hole effective-mass tensors are both diagonal.[79a] If this is true, we can then write

$$\left(\frac{1}{m_e^*}\right)^{\alpha\beta} = \frac{1}{m_e^{\alpha}}\delta_{\alpha\beta}, \tag{128a}$$

$$\left(\frac{1}{m_h^*}\right)^{\alpha\beta} = \frac{1}{m_h^{\alpha}}\delta_{\alpha\beta}, \tag{128b}$$

and

$$\left(\frac{1}{\mu}\right)^{\alpha\beta} = \frac{1}{\mu^{\alpha}}\delta_{\alpha\beta}, \tag{128c}$$

$$\left(\frac{1}{\Delta}\right)^{\alpha\beta} = \frac{1}{\Delta^{\alpha}}\delta_{\alpha\beta}. \tag{128d}$$

Considering H_4 as a perturbation on the Hamiltonian H_1, in the absence of a magnetic field, the contribution of H_4 to the exciton energy can be summed exactly in second-order perturbation theory using the sum rule,[43]

$$\sum_n{}' (E_i^0 - E_n^0)^{-1}\{\langle i|p^{\alpha}|n\rangle\langle n|p^{\beta}|i\rangle + \langle i|p^{\beta}|n\rangle\langle n|p^{\alpha}|i\rangle\} = -\mu^{\alpha}\delta_{\alpha\beta}, \tag{129}$$

where i and n label exciton energy levels. This yields the contribution

$$E_4 = -\frac{1}{8}\hbar^2 \sum_{\alpha} \mu^{\alpha}\left(\frac{1}{\Delta^{\alpha}}\right)^2 (\kappa^{\alpha})^2. \tag{130}$$

Adding this to the H_6 term gives the $\boldsymbol{\kappa}$ dependence of the exciton energy in the absence of a magnetic field to order κ^2,

$$E_{\kappa} = \frac{1}{2}\hbar^2 \sum_{\alpha} \frac{1}{M^{\alpha}}(\kappa^{\alpha})^2, \tag{131}$$

[79a] The diagonalization is always possible in cubic crystals for direct-transition excitons in the simple-band case.

where $M^\alpha = m_e{}^\alpha + m_h{}^\alpha$ is the total exciton mass. In the presence of a magnetic field we must consider a perturbation on the Hamiltonian $H_0 = H_1 + H_2 + H_3$. In this case, since

$$[H_0, r^\alpha] = -i\hbar\left(\frac{1}{\mu^\alpha}\right)\left[p^\alpha + \frac{e}{c}A^\alpha\left(\frac{\mu^\alpha}{\Delta^\alpha}\right)\right] \equiv -i\hbar\left(\frac{1}{\mu^\alpha}\right)\mathscr{P}^\alpha \tag{132}$$

and

$$[\mathscr{P}^\alpha, r^\beta] = -i\hbar\,\delta_{\alpha\beta}, \tag{133}$$

the sum rule, Eq. (129), remains valid provided $\mathbf{p}$ is replaced by $\mathscr{P}$, and $E_i{}^0$ and $E_n{}^0$ are eigenenergies of H_0. Replacing H_4 by

$$H_4' = \frac{1}{2}\hbar\kappa^\alpha\left(\frac{1}{\Delta^\alpha}\right)\mathscr{P}^\alpha \tag{134}$$

such that H_5 becomes

$$H_5' = \frac{e\hbar}{2c}\kappa^\alpha\left[\left(\frac{1}{\mu^\alpha}\right) - \left(\frac{1}{\Delta^\alpha}\right)\left(\frac{\mu^\alpha}{\Delta^\alpha}\right)\right]A^\alpha = 2\frac{e\hbar}{c}\sum_\alpha \frac{\kappa^\alpha}{M^\alpha}A^\alpha \tag{135}$$

to maintain $H_4 + H_5 = H_4' + H_5'$, the contribution of H_4' to the exciton energy can be summed exactly in second-order perturbation theory to yield Eq. (130) and Eq. (131), leaving Eq. (135) as the only $\boldsymbol{\kappa}$-dependent perturbation.

This intuitive result could have been obtained directly by separating the exciton effective-mass equation in the center-of-mass coordinates

$$R^\alpha = \frac{m_e{}^\alpha r_e{}^\alpha + m_h{}^\alpha r_h{}^\alpha}{m_e{}^\alpha + m_h{}^\alpha}$$

$$r^\alpha = r_e{}^\alpha - r_h{}^\alpha,$$

which is possible if the electron and hole effective-mass tensors are both diagonal in a given coordinate system. If this separation is made initially, the first three terms, H_1, H_2, and H_3, are the same, the H_4 term is eliminated, and the H_6 term is given instead by Eq. (131). The H_5 term becomes H_5', given by Eq. (135). Writing the exciton velocity as

$$v^\alpha = \frac{1}{\hbar}\frac{\partial}{\partial\kappa^\alpha}E_\kappa = \hbar\frac{\kappa^\alpha}{M^\alpha},$$

this becomes

$$H_5' = 2\frac{e}{c}\mathbf{v}\cdot\mathbf{A} = \frac{e}{c}\mathbf{r}\cdot(\mathbf{v}\times\mathbf{H}). \tag{136}$$

This term has the same effect as that of an electric field of strength $\mathbf{E} = (1/c)\mathbf{v} \times \mathbf{H}$. Recall that exciton states are created with wave vector $\boldsymbol{\kappa}$ equal to $\mathbf{q}$, the vector in the crystal of the light that creates the exciton state. The effects of this term on the exciton spectra of CdS have been directly measured by Thomas and Hopfield.[80,81] These measurements yield the combined electron and hole mass M^{α} and directly demonstrate effects due to the exciton motion in the crystal.

Let us turn our attention now to the first three terms in Eq. (124), considering the case where $\boldsymbol{\kappa} = 0$. For simplicity we return to the case of isotropic masses, for which

$$H = -\frac{\hbar^2}{2\mu}\nabla^2 + \frac{e\hbar}{2c}\left(\frac{1}{\Delta}\right)\mathbf{H}\cdot[\mathbf{r} \times (-i\nabla)] + \frac{e^2}{8\mu c^2}(\mathbf{H} \times \mathbf{r})^2 - \frac{e^2}{\kappa_0 r}. \quad (137)$$

It has not been possible to find solutions of the eigenvalue problem

$$H\psi = \varepsilon\psi \quad (138)$$

with H given by Eq. (137) for arbitrary values of $\mathbf{H}$. The solutions for $\mathbf{H} = 0$ are of course just the hydrogenic wave functions for an effective mass μ and charge $e/\kappa_0^{1/2}$, as discussed above. In the limit of very large magnetic fields or very large magnetic-field energies, we can obtain an approximate solution if we neglect the Coulomb term $-e^2/\kappa_0 r$. The eigenstates of the remaining Hamiltonian are well known and were first obtained by Page[82] in cylindrical coordinates and by Landau[83] in Cartesian coordinates. Since then, these solutions have been studied by many people.[84–86] In cylindrical coordinates (ρ, ϕ, z) where the magnetic field is along z, the solution can be conveniently written as[85]

$$\bar{\psi}(\mathbf{r}) = \frac{1}{(2\pi L_z)^{1/2}} e^{ik_z z} e^{im\phi} R^m_{n+m}(\sigma), \quad (139)$$

where L_z is the length of the crystal in the z direction and

$$R^m_{n+m}(\sigma) = \left\{\frac{2\lambda n!}{[(n+m)!]^3}\right\}^{1/2} e^{-\sigma^2/2}\,\sigma^m\, L^m_{n+m}(\sigma^2) \quad (140)$$

[80] D. G. Thomas and J. J. Hopfield, *Phys. Rev. Letters* **5**, 505 (1960).
[81] D. G. Thomas and J. J. Hopfield, *Phys. Rev.* **124**, 657 (1961).
[82] L. Page, *Phys. Rev.* **36**, 444 (1930).
[83] L. D. Landau, *Z. Physik* **64**, 629 (1930).
[84] L. I. Schiff and H. Snyder, *Phys. Rev.* **55**, 59 (1939).
[85] M. H. Johnson and B. A. Lippman, *Phys. Rev.* **76**, 828 (1949).
[86] R. B. Dingle, *Proc. Roy. Soc. (London)* **211**, 500, 517 (1952).

and $\sigma = \lambda^{1/2}\rho$, where $\lambda = eH/2\hbar c$. L^m_{n+m} is a Laguerre polynomial.[87] The functions $\bar{\psi}(\mathbf{r})$ have the advantage that they are eigenfunctions of the translation operator along the field axis and of the angular-momentum operator about the field axis. In Eq. (139) k_z specifies the motion along the field and m is the quantum number of orbital motion about the field axis. The energy of these states is given by[88]

$$E = \frac{e\hbar}{2c}H\left\{\frac{1}{\mu}(2n + m + 1) - \frac{1}{\Delta}m\right\} + \frac{\hbar^2 k_z^2}{2\mu}. \tag{141}$$

This may be put into a more familiar form by introducing two new quantum numbers,

$$n_e = n$$

and

$$n_h = n + m,$$

which independently take on all nonnegative integer values. With these substitutions and Eqs. (126) and (127), Eq. (141) becomes

$$E = \hbar\omega_e(n_e + \tfrac{1}{2}) + \hbar\omega_h(n_h + \tfrac{1}{2}) + \frac{\hbar^2 k_z^2}{2m_e^*} + \frac{\hbar^2 k_z^2}{2m_h^*}, \tag{142}$$

where

$$\omega_e = \frac{eH}{m_e^* c}$$

and

$$\omega_h = \frac{eH}{m_h^* c}.$$

The approach taken here is useful because it shows how the energy and eigenfunctions depend on the quantum number m, which is the only quantum number preserved when the Coulomb interaction is introduced.

It is also easy to obtain the absorption coefficient[88,89] in the presence of a strong magnetic field, using Eqs. (139), (140), and (104). The density of states is given by

$$S(h\nu) = \frac{L_z}{4\pi}\left(\frac{2\mu}{\hbar^2}\right)^{1/2} \sum_{n,m}\left\{\hbar\omega - E_g - \frac{e\hbar}{2c}H\left[\frac{1}{\mu}(2n + m + 1) - \frac{1}{\Delta}m\right]\right\}^{1/2}. \tag{143}$$

[87] E. U. Condon and G. H. Shortley, "The Theory of Atomic Spectra," p. 115. Cambridge Univ. Press, London and New York, 1959.

[88] R. J. Elliott and R. Loudon, *J. Phys. Chem. Solids* **8**, 382 (1959).

[89] R. J. Elliott, T. P. McLean, and G. G. Macfarlane, *Proc. Phys. Soc. (London)* **73**, 553 (1958).

$\bar{\psi}(0)$ is nonvanishing only for $m = 0$, in which case

$$|\bar{\psi}(0)|^2 = \frac{2\lambda}{2\pi L_z} = \frac{1}{2\pi L_z}\frac{eH}{\hbar c}. \tag{144}$$

The absorption coefficient is then

$$\alpha(\omega) = \frac{e^2}{\eta m^2 c\omega}\cdot\frac{eH}{2\hbar c}\left(\frac{2\mu}{\hbar^2}\right)^{1/2} |\langle\psi_{c,\mathbf{k}_0}|\boldsymbol{\xi}\cdot\boldsymbol{\pi}|\psi_{v,\mathbf{k}_0}\rangle|^2 \times\sum_n \{\hbar\omega - E_g - \hbar\omega_0(n+\tfrac{1}{2})\}^{-1/2}, \tag{145}$$

where $\omega_0 = \omega_e + \omega_h = eH/\mu c$. This is the familiar result obtained for direct band-to-band transitions in a magnetic field. The absorption spectrum shows a sharp peaking at the energies

$$\hbar\omega = E_g + \hbar\omega_0(n+\tfrac{1}{2}), \tag{146}$$

which depend only on the reduced effective mass μ.

Other transitions become allowed if we consider the variation of the band matrix element with $\mathbf{k}$.[88,89] Specifically, transitions occur for which $\mathbf{D}\bar{\psi}(\mathbf{r})|_{\mathbf{r}=0} \neq 0$, where $\mathbf{D}$ is given by Eq. (112),

$$D^z = -i\frac{\partial}{\partial z}, \tag{147}$$

$$\begin{aligned} D^+ = D^x + iD^y &= -i\left(\frac{\partial}{\partial x} + i\frac{\partial}{\partial y}\right) + \lambda\left(\frac{\partial}{\partial\kappa_x} + i\frac{\partial}{\partial\kappa_y}\right), \\ D^- = D^x - iD^y &= -i\left(\frac{\partial}{\partial x} - i\frac{\partial}{\partial y}\right) - \lambda\left(\frac{\partial}{\partial\kappa_x} - i\frac{\partial}{\partial\kappa_y}\right). \end{aligned} \tag{148}$$

From Eqs. (139) and (140) we have

$$D^z\bar{\psi}_{n,m,k_z}\Big|_{\mathbf{r}=0} = \left(\frac{2\lambda}{2\pi L_z}\right)^{1/2} k_z \tag{149}$$

nonzero only for $m = 0$ again. The contributions from the terms involving D^+ and D^- may be obtained in a straightforward manner. The eigenfunctions given in Eq. (140) and (141) are independent of $\boldsymbol{\kappa}$, and hence the second terms would be thought to give no contribution. However, these functions are not eigenfunctions of the total exciton effective-mass equation even for the simple band case. The complete Hamiltonian in the center-of-mass system is

$$H = H_0 + 2\frac{e\hbar}{Mc}\boldsymbol{\kappa}\cdot\mathbf{A} + \frac{\hbar^2\kappa^2}{2M}, \tag{150}$$

where H_0 is given by Eq. (137), with now the Coulomb term neglected. The functions given in Eqs. (139) and (140) are eigenfunctions of H_0. If we treat the second term in Eq. (150) as a perturbation, the resultant wave functions depend on $\boldsymbol{\kappa}$. (The third term, of course, does nothing, since it is just a constant.) From this $\boldsymbol{\kappa}$ dependence we can obtain the contributions from the second terms in Eq. (148) by writing

$$\psi'_{n,m,k_z} = \psi_{n,m,k_z} + \sum_{n',m',k_z'} \frac{\langle \psi_{n',m',k_z'} | H' | \psi_{n,m,k_z} \rangle}{\varepsilon_{n,m,k_z} - \varepsilon_{n',m',k_z'}} \psi_{n',m',k_z'}, \tag{151}$$

where ψ_{n,m,k_z} is an eigenfunction of H_0 and

$$H' = \frac{e\hbar}{Mc} \boldsymbol{\kappa} \cdot (\mathbf{H} \times \mathbf{r}). \tag{152}$$

Making these substitutions we obtain, at $\boldsymbol{\kappa} = 0$,

$$\mathbf{D}\psi'_{n,m,k_z} = -i\nabla\psi_{n,m,k_z} + i\frac{e^2H^2}{2Mc^2} \sum_{n',m',k_z'} \frac{\langle \psi_{n',m',k_z'} | \boldsymbol{\rho} | \psi_{n,m,k_z} \rangle}{\varepsilon_{n,m,k_z} - \varepsilon_{n',m',k_z'}} \psi_{n',m',k_z'}, \tag{153}$$

where $\boldsymbol{\rho} = x\hat{\mathbf{i}} + y\hat{\mathbf{j}}$. If $\boldsymbol{\rho}$ can be written as the commutator of some operator with H_0, all diagonal elements of $\boldsymbol{\rho}$ vanish and we can evaluate Eq. (153) by use of a sum rule. In fact, one can show that

$$\left[H_0, -i\nabla - \frac{\mu}{\Delta}\frac{e}{\hbar c}\mathbf{A} \right] = i\frac{e^2H^2}{Mc^2}\boldsymbol{\rho}, \tag{154}$$

so that we obtain

$$\mathbf{D}\psi'_{n,m,k_z} = -\frac{1}{2} i\nabla\psi_{n,m,k_z} + \frac{\mu}{\Delta}\frac{e}{2\hbar c}\mathbf{A}\psi_{n,m,k_z}. \tag{155}$$

The second term in Eq. (155) vanishes at $\mathbf{r} = 0$. The contributions of D^+ and D^- can be obtained from Eqs. (139), (140), and (155). The only non-vanishing results are

$$D^+\bar{\psi}_{n,m,k_z}\Big|_{\mathbf{r}=0} = -i\left(\frac{2\lambda^2}{2\pi L_z}\right)^{1/2} n^{1/2} \tag{156}$$

for $m = -1$, and

$$D^-\bar{\psi}_{n,m,k_z}\Big|_{\mathbf{r}=0} = +i\left(\frac{2\lambda^2}{2\pi L_z}\right)^{1/2} (n+1)^{1/2} \tag{157}$$

for $m = +1$.

If the direct band-to-band transition is forbidden, Eq. (145) vanishes and the absorption coefficient consists of two terms: $\alpha(\nu) = \alpha_1(\nu) + \alpha_2(\nu)$, where, from the D^z term,[88,89]

$$\alpha_1(\omega) = \frac{e^2}{\eta m^2 c\omega}\left(\frac{eH}{2\hbar c}\right)\left(\frac{2\mu}{\hbar^2}\right)^{3/2}\left|\frac{d}{dk_z}\langle\psi_{c,\mathbf{k}}|\xi\cdot\pi|\psi_{v,\mathbf{k}}\rangle_{\mathbf{k}=\mathbf{k}^0}\right|^2 \times \sum_n [\hbar\omega - E_g - \hbar\omega_0(n+\tfrac{1}{2})]^{1/2}, \tag{158}$$

which consists of a series of steps as in the indirect transition. The second term is given by[88,89]

$$\alpha_2(\omega) = \frac{e^2}{\eta m^2 c\omega}\cdot\left(\frac{eH}{2\hbar c}\right)^2\left(\frac{2\mu}{\hbar^2}\right)^{1/2}\left|\frac{d}{dk_\perp}\langle\psi_{c,\mathbf{k}}|\xi\cdot\pi|\psi_{v,\mathbf{k}}\rangle_{\mathbf{k}=\mathbf{k}^0}\right|^2$$

$$\times \sum_n (n+1)\{[\hbar\omega - E_g - \hbar\omega_0(n+\tfrac{1}{2}) - \hbar\omega_e]^{-1/2}$$

$$+ [\hbar\omega - E_g - \hbar\omega_0(n+\tfrac{1}{2}) - \hbar\omega_h]^{-1/2}\}. \tag{159}$$

The absorption spectrum shows a sharp peaking at the energies

$$\hbar\omega = E_g + \hbar\omega_0(n+\tfrac{1}{2}) + \hbar\omega_e$$

and

$$\hbar\omega = E_g + \hbar\omega_0(n+\tfrac{1}{2}) + \hbar\omega_h. \tag{160}$$

The positions of the peaks depend not only on the reduced effective mass μ but also directly on the individual electron and hole effective masses such that these quantities may be obtained separately.

We have examined the solutions of Eq. (138) in two limiting cases: (1) zero external magnetic field, in which the solutions are hydrogenic wave functions, and (2) vanishing Coulomb interaction, in which the solutions are the so-called Landau levels or Landau sublevels given by Eqs. (139) and (140). A rough criterion to determine which limit, if either, is applicable in a given situation is a comparison between the magnetic energy $\frac{1}{2}\hbar\omega_0 = e\hbar H/2\mu c$ and the ground-state exciton energy $R = \mu e^4/2\hbar^2\kappa_0{}^2$. For small magnetic fields, $\frac{1}{2}\hbar\omega_0 \ll R$, the magnetic-field terms in Eq. (137) are treated as a perturbation.[64,65] The effect of a magnetic field on the discrete levels is similar to an atomic Zeeman effect. The second term in Eq. (137) gives the linear Zeeman splitting, while the third term gives a quadratic diamagnetic shift. At higher fields the second term contributes appreciably in second-order perturbation theory. The effect of this is in opposition to the diamagnetic term, causing the energy to become linear in field as H is increased. No satisfactory theory has been given for the continuum states in the presence of both the Coulomb interaction and a small or moderate field.

For large magnetic fields, $\frac{1}{2}\hbar\omega_0 \gg R$, however, approximate theories have been developed by Elliott and Loudon[90] and by others.[91–94] For sufficiently high fields the Coulomb interaction does not greatly perturb the motion in the plane perpendicular to **H** but strongly affects the motion along **H**, so that n and m in Eqs. (139) and (140) are still good quantum numbers but the continuous quantum number k_z is not. For a given n and m the Coulomb interaction breaks up the continuum of states in k_z into a series of discrete levels. Elliott and Loudon[90] have shown that discrete exciton states are formed from each Landau sub-band with energies slightly less than that of the bottom of the band. The main absorption for each sub-band takes place at the lowest discrete exciton state associated with that sub-band. Consequently, the peaks observed in magnetooptical absorption are actually due to transitions to discrete exciton states and occur at energies that are slightly less than predicted by Eqs. (146) and (160). This situation has been discussed by Edwards and Lazazzera[59] in connection with their observed direct allowed magnetooptical absorption in germanium. Their data and interpretation are shown in Fig. 9.

Approximate theories of the behavior of exciton states are therefore available in both the low- and high-field limits. It is clear that there is no fundamental distinction between a peak in the magnetooptical absorption spectrum caused by a Landau level and that caused by an exciton. Only a quantitative difference exists, which depends on the ratio $\frac{1}{2}\hbar\omega_0/R$. However, at a given field it is possible for some higher quantum-number states to be in the high-field limit while some of the lower states still have a quadratic field dependence and are in the low-field limit. The values of H for which $\frac{1}{2}\hbar\omega_0/R = 1$ vary from well over 100 kG for Si and AlSb to about 2 kG for InSb. Representative approximate values are given in Table I.

TABLE I

REPRESENTATIVE VALUES OF MAGNETIC FIELD FOR WHICH $\frac{1}{2}\hbar\omega_0 = R$

Si	300 kG	Ge	15 kG
AlSb	200 kG	GaSb	20 kG
InP	100 kG	InAs	10 kG
GaAs	60 kG	InSb	2 kG

[90] R. J. Elliott and R. Loudon, *J. Phys. Chem. Solids* **15**, 196 (1960).
[91] Y. Yafet, R. W. Keyes, and E. N. Adams, *J. Phys. Chem. Solids* **1**, 137 (1956).
[92] R. F. Wallis and H. J. Bowlden, *J. Phys. Chem. Solids* **7**, 78 (1958).
[93] W. S. Boyle and R. E. Howard, *J. Phys. Chem. Solids* **19**, 181 (1961).
[94] H. Hasegawa and R. E. Howard, *J. Phys. Chem. Solids* **21**, 179 (1961).

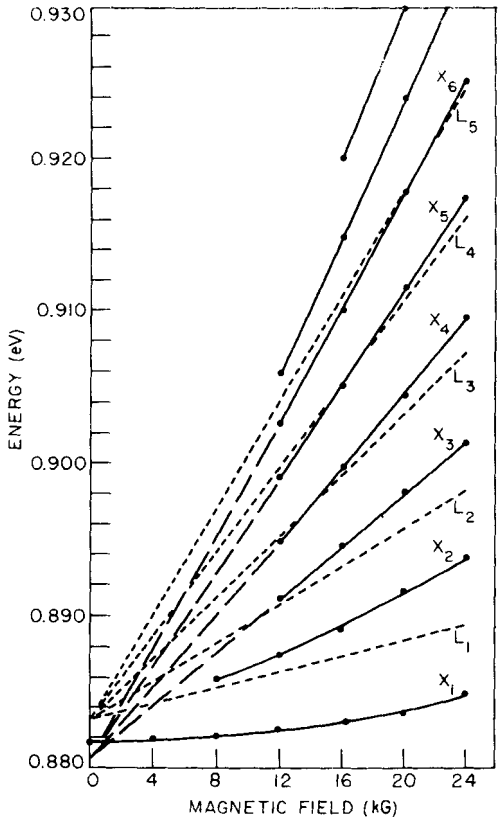


FIG. 9. Interband magnetooptical absorption spectrum for germanium. The levels labeled X_i mark the absorption maxima and correspond to exciton transitions. The levels labeled L_i correspond to the associated Landau transitions in the absence of the electron–hole interaction. (After D. F. Edwards and V. J. Lazazzera.[59])

V. Application to Group III–V Compounds

In this section we consider in more detail the properties of exciton states in group-III–V compounds. These materials possess rather large dielectric constants and have relatively small effective masses associated with their valence- and conduction-band extrema. Consequently, excitons in these compounds have a large spatial extent and are well described by the effective-mass approximation developed above. Also, as a result, the energy of the lowest exciton state is not very different from that of the absorption edge itself, and so-called, "exciton effects" due to the interaction between the electron and hole are not as marked as in, say, II–VI semiconductors.

In group-III–V compounds exciton effects appear more as a modification of the absorption edge and of the magnetooptical spectrum. Rather than discuss in detail the experimental situation in III–V compounds—which, as noted above, is being covered by E. J. Johnson in another chapter—we shall concern ourselves instead with the details of the effective-mass theory for excitons as applied to group-III–V semiconductors.

12. Structure of the Valence and Conduction Bands

The form of the effective-mass equation, or set of simultaneous equations, that must be solved to obtain the exciton states in a given crystal depends on the structure of the valence- and conduction-band extrema. The approximate energy-band structure of group-III–V semiconductors is shown in Fig. 10.[95] The valence-band extremum occurs at or near the center of the Brillouin zone and consists of a complicated set of degenerate or nearly degenerate bands. The absolute minimum of the conduction band appears to be also at the center of the zone in most of these compounds, with subsidiary minima probably occurring along the [111] and [100] axes. Consequently, low-lying exciton states of both the direct and indirect types can contribute to the absorption spectra in these compounds.

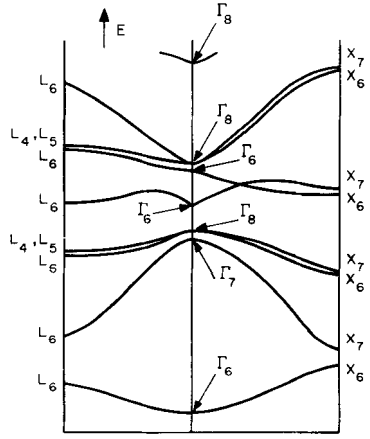


FIG. 10. Band structure of GaAs, including spin–orbit effects. The double group representations are indicated for the various bands at the symmetry points in the Brillouin zone. The linear splitting of the Γ_8 states with wave vector is too small to appear in the figure. (After M. Cardona.[95])

[95] M. Cardona, *in* "Physics of Semiconductors" (Proc. 7th Intern. Conf.), p. 181. Dunod, Paris, and Academic Press, New York, 1964.

The uppermost valence-band state at $\mathbf{k} = 0$ is a fourfold degenerate state (including spin) that is usually labeled Γ_8. The next lower state, Γ_7, is a doubly degenerate state (including spin) that is removed from the Γ_8 state by spin–orbit splitting. These states are made up mostly from anion atomic p-states in the crystal. The separation between the Γ_7 and Γ_8 states can therefore be expected to increase with increasing anion atomic number. For most of the group-III–V compounds this separation is large compared to the exciton binding energy, so that only the Γ_8 states need be considered. For the lighter materials, however, both sets of levels should be included.

In all instances the conduction minima are simply twofold degenerate with spin. The exciton states in these crystals are therefore described by a set of coupled differential equations of the form developed by Dresselhaus[43] and discussed in Section 6. The forms of the electron and hole contributions to the exciton Hamiltonian can be obtained by symmetry arguments and use of the $\mathbf{k} \cdot \mathbf{p}$ theory. This has been done for crystals with diamond and zinc-blende symmetry by Elliott,[96] Luttinger and Kohn,[38] Dresselhaus *et al.*[97] Dresselhaus,[98] Luttinger,[41] and Kane.[40,99] The situation has been reviewed recently by Cardona[100] and by Kane in Volume 1 of this series, to which the reader is referred for further information. For a crystal with the zinc-blende structure, the conduction-band minimum at $\mathbf{k} = 0$ has the symmetry of a cation s-state and is labeled Γ_6. The conduction-band effective-mass Hamiltonian $H^{e}_{ii'}(\mathbf{k})$ can be shown to be of the form

$$\mathscr{H}^{e} = \begin{pmatrix} ak^2 + 2bH_z & -ib(H_x + iH_y) \\ ib(H_x - iH_y) & ak^2 - 2bH_z \end{pmatrix}. \tag{161}$$

In the case where spin–orbit splitting is small compared to the band gap, the valence-band effective-mass Hamiltonian $H^{h}_{jj'}(\mathbf{k})$ for the coupled set of Γ_8 and Γ_7 states can be shown to have the form[96,97,38]

$$\mathscr{H}^{h} = \begin{pmatrix} P - \frac{1}{2}Q + 3R/2 & L + N & M & 0 & i(L + N)/\sqrt{2} & -i\sqrt{2}M \\ L^* + N^* & P + \frac{1}{2}Q + \frac{1}{2}R & 2N/\sqrt{3} & M & i(Q - R)/\sqrt{2} & i(3L - N)/\sqrt{6} \\ M^* & 2N^*/\sqrt{3} & P + \frac{1}{2}Q - \frac{1}{2}R & -L + N & -i(3L^* + N^*)/\sqrt{6} & i(Q + R)/\sqrt{2} \\ 0 & M^* & -L^* + N^* & P - \frac{1}{2}Q - 3R/2 & -i\sqrt{2}M^* & -i(L^* - N^*)/\sqrt{2} \\ -i(L^* + N^*)/\sqrt{2} & -i(Q - R)/\sqrt{2} & i(3L + N)/\sqrt{6} & i\sqrt{2}M & P + R - \Delta & -2N/\sqrt{3} \\ i\sqrt{2}M^* & -i(3L^* - N^*)/\sqrt{6} & -i(Q + R)/\sqrt{2} & i(L - N)/\sqrt{2} & -2N^*/\sqrt{3} & P - R - \Delta \end{pmatrix}. \tag{162}$$

[96] R. J. Elliott, *Phys. Rev.* **96**, 266 (1954).
[97] G. Dresselhaus, A. F. Kip, and C. Kittel, *Phys. Rev.* **98**, 368 (1955).
[98] G. Dresselhaus, *Phys. Rev.* **100**, 580 (1955).
[99] E. O. Kane, *J. Phys. Chem. Solids* **1**, 82 (1956).
[100] M. Cardona, *J. Phys. Chem. Solids* **24**, 1543 (1963).

where

$$P = \tfrac{1}{3}(3\alpha_1 + 2\alpha_2)k^2,$$

$$Q = -\tfrac{1}{3}\alpha_2(2k_z^2 - k_x^2 - k_y^2),$$

$$L = \alpha_3\{k_y k_z + ik_z k_x\}/\sqrt{3},$$

$$M = [-\alpha_2(k_x^2 - k_y^2) + 2i\alpha_3\{k_x k_y\}]/\sqrt{12},$$

$$N = i\alpha_4(H_x - iH_y)/\sqrt{3},$$

$$R = 2\alpha_4 H_z/3,$$

Δ = Spin–orbit splitting,

$$\alpha_1 = A\ ;\ \alpha_2 = B - A\ ;\ \alpha_3 = -C\ ;\ \alpha_4 = (e\hbar/2mc)(mK + 1)$$

and A, B, C, and K are constants that can be determined by cyclotron resonance or interband magnetooptical absorption. For a review of the cyclotron resonance work the reader is referred to the article by Lax and Mavroides[101] and Chapter 10 in this volume by E. D. Palik and G. B. Wright. For a review of the interband magnetooptical absorption work, the reader is referred to the articles by Lax and Zwerdling[102] and Lax[103,104] and Chapter 8 in this volume by B. Lax and J. G. Mavroides.

Equations (161) and (162) are exactly the same as the corresponding equations for the diamond lattice. The absence of inversion symmetry in the zinc-blende compounds affects the valence- and conduction-band symmetries at Γ only in the presence of large spin–orbit splitting. Substituting Eq. (161) and (162) into the effective-mass equation for excitons [Eq. (75)], we find that the eigenstates are solutions of a set of twelve simultaneous differential equations. The solution of such a problem is a very formidable task. In the absence of an external magnetic field, the conduction-band Hamiltonian becomes diagonal and two independent sets of solutions can be obtained from two identical sets of six simultaneous differential equations of the form

$$\left[H_{jj'}(+i\nabla_{\mathbf{r}}) - \frac{e^2}{\kappa_0 r}\delta_{jj'}\right]\bar{\psi}^n_{ij'}(\mathbf{r}) = \varepsilon\bar{\psi}^n_{ij}(\mathbf{r}), \tag{163}$$

[101] B. Lax and J. G. Mavroides, *Solid State Phys.* **11**, 261 (1960).

[102] B. Lax and S. Zwerdling, *Progr. Semicond.* **5**, 223 (1960).

[103] B. Lax, *Proc. Intern. Conf. Semicond. Phys., Prague, 1960* p. 321. Czech. Acad. Sci., Prague, and Academic Press, New York, 1961.

[104] B. Lax, *in* "Physics of Semiconductors" (Proc. 7th Intern. Conf.), p. 253. Dunod, Paris, and Academic Press, New York, 1964.

TABLE II

VALUES OF THE DIRECT ENERGY GAP, VALENCE-BAND SPIN–ORBIT SPLITTING AND DIRECT EXCITON BINDING ENERGY FOR SOME GROUP IV AND GROUP III–V SEMICONDUCTORS

Compound	E_g(eV)	Δ(eV)	R(eV)
Si	3.6[a]	0.044[a]	0.0084*
Ge	0.89[b]	0.29[j]	0.0014[o]
GaP	2.2[c]	0.12[k]	
AlSb	1.6[d]	0.78[l]	0.0075*
GaAs	1.41[e]	0.33[m]	0.0051*
InP	1.29[f]	0.28[k]	0.0065*
GaSb	0.813[g]	0.86[k]	0.0018*
InAs	0.360[h]	0.43[n]	0.0018*
InSb	0.2357[i]	0.90[k]	0.0005*

[a] M. Cardona, *J. Phys. Chem. Solids* **24**, 1543 (1963).
[b] B. Lax, L. M. Roth, and S. Zwerdling, *J. Phys. Chem. Solids* **8**, 311 (1959).
[c] W. G. Spitzer and J. M. Whelan, *Phys. Rev.* **114**, 59 (1959); W. G. Spitzer, M. Gershenzon, C. J. Frosch, and D. F. Gibbs, *J. Phys. Chem. Solids* **11**, 339 (1959).
[d] R. F. Blunt, H. P. R. Fredrikse, J. H. Becker, and W. R. Hosler, *Phys. Rev.* **96**, 578 (1954).
[e] T. S. Moss, *J. Appl. Phys. Suppl.* **32**, 2136 (1961).
[f] R. Newman, *Phys. Rev.* **111**, 1518 (1958).
[g] S. Zwerdling, B. Lax, K. J. Button, and L. M. Roth, *J. Phys. Chem. Solids* **9**, 320 (1959).
[h] S. Zwerdling, B. Lax, and L. M. Roth, *Phys. Rev.* **108**, 1402 (1957).
[i] S. Zwerdling, W. H. Kleiner, and J. P. Theriault, *J. Appl. Phys. Suppl.* **32**, 2118 (1961).
[j] M. V. Hobden, *J. Phys. Chem. Solids* **23**, 821 (1962).
[k] H. Ehrenreich, *J. Appl. Phys. Suppl.* **32**, 2155 (1961).
[l] W. J. Turner and W. E. Reese, *Bull. Am. Phys. Soc.* **4**, 408 (1959).
[m] R. Braunstein, *J. Phys. Chem. Solids* **8**, 280 (1959).
[n] F. Matossi and F. Stern, *Phys. Rev.* **111**, 472 (1958).
[o] T. P. McLean and R. Loudon, *J. Phys. Chem. Solids* **13**, 1 (1960).
* These values were estimated by scaling the calculated value for Ge obtained by McLean and Loudon, using the conduction-band masses quoted by Cardona (Ref. *a*), the static dielectric constants given by H. P. R. Frederikse, "American Institute of Physics Handbook," p. 9 (Second Edition, McGraw-Hill, New York, 1963) and the simple band formula Eq. (5).

where $H_{jj'}$ is equal to $H^{h}_{jj'}$ with α_1 replaced by $\alpha_1 + a$, where a is the constant appearing in Eq. (161). The solutions of Eq. (163) with a Hamiltonian of the form of Eq. (162) have been investigated by Kohn and Schechter[105,106] and by Mendelson and James[107] in connection with the shallow acceptor state problem in germanium and silicon. The exciton problem is identical except for the change in α_1. McLean and Loudon[108] have applied the same

[105] W. Kohn and D. Schechter, *Phys. Rev.* **99**, 1903 (1955).
[106] D. Schechter, *J. Phys. Chem. Solids* **23**, 237 (1962).
[107] K. S. Mendelson and H. M. James, *J. Phys. Chem. Solids* **25**, 729 (1964).
[108] T. P. McLean and R. Loudon, *J. Phys. Chem. Solids* **13**, 1 (1960).

theory to a calculation of the direct exciton energy levels in Ge and Si.

When the spin–orbit splitting is small compared to the band gap, Eq. (162) also applies to the III–V compounds, and a calculation similar to that performed by McLean and Loudon could be applied to them. Note that with the possible exception of Si, the spin–orbit splitting of the valence band, Δ, is large compared to the exciton binding energy, so that we need include only the upper left-hand 4×4 section of Eq. (162) in the solution of the exciton problem. Values of the direct band gap E_g, the spin–orbit splitting of the valence band Δ, and of the estimated lowest-lying exciton binding energy R are given in Table II. The lower-lying exciton states obtained may be associated with hydrogenic $1S$, $2S$, $2P$, and $3P$ states, but with a fair amount of mixing from higher states because of the fact that the valence band is not spherically symmetric. If the spin–orbit splitting is not small compared to the band gap, we consider only the uppermost Γ_8 valence-band state, but Eq. (162) is no longer valid. The effective-mass Hamiltonian $H^{h}_{jj'}(\mathbf{k})$ can, in this case, be shown to have the form[40,41]

$$\mathcal{H}^h = \begin{pmatrix} P - \frac{1}{2}Q + 3R/2 + 27S & L + N + U + 7T/4 & M - V & \sqrt{3}(U^* + T^*/2) \\ L^* + N^* + U^* + 7T^*/4 & P + \frac{1}{2}Q + \frac{1}{2}R + S & (2N - 3U + 5T)/\sqrt{3} & M + V \\ M^* - V & (2N^* - 3U^* + 5T^*)/\sqrt{3} & P + \frac{1}{2}Q - \frac{1}{2}R - S & -L + N + U + 7T/4 \\ \sqrt{3}(U + T/2) & M^* + V & -L^* + N^* + U^* + 7T^*/4 & P - \frac{1}{2}Q - 3R/2 - 27S \end{pmatrix}, \tag{164}$$

where

$$P = (\beta_1 + 5\beta_2/4)k^2,$$

$$Q = -\beta_2(2k_z^2 - k_x^2 - k_y^2),$$

$$L = \sqrt{3}\beta_3\{k_y k_z + ik_z k_x\}/2,$$

$$M = \sqrt{3}[-\beta_2(k_x^2 - k_y^2) + i\beta_3\{k_x k_y\}]/2,$$

$$N = i\sqrt{3}\beta_4(H_x - iH_y)/2,$$

$$R = \beta_4 H_z,$$

$$S = \beta_5 H_z/8,$$

$$T = i\sqrt{3}\beta_5(H_x - iH_y)/2,$$

$$U = -\sqrt{3}i\beta_6(k_x + ik_y)/4,$$

$$V = \sqrt{3}\beta_6 k_z/2.$$

A correspondence can be made between the parameters β_1 through β_4 and the parameters α_1 through α_4 in the case of small spin–orbit splitting,[41] namely,

$$\beta_1 = (3A + B)/4 = \alpha_1 + \alpha_2/4,$$

$$\beta_2 = -(A - B)/3 = \alpha_2/3,$$

$$\beta_3 = -2C/3 = 2\alpha_3/3,$$

$$\beta_4 = (e/3mc)(mK + 1) = 2\alpha_4/3.$$

In this limit the parameters β_5 and β_6 vanish. The terms involving β_5 represent an additional contribution to the magnetic-field splitting due to spin–orbit coupling. The terms involving β_6 are linear in $\mathbf{k}$ and arise from the combined effects of spin–orbit splitting and the lack of inversion symmetry in zinc-blende compounds. Because of these terms, the valence-band maximum does not occur exactly at $\mathbf{k} = 0$ but is split from it by a small amount.[98]

With $H^{\mathrm{h}}_{jj'}$ given by Eq. (164), the exciton energy levels are obtained as solutions of a set of eight simultaneous differential equations. These can be reduced to two identical sets of four equations as above in the absence of external magnetic fields. Again, Kohn and Schechter[105,106] and Mendelson and James[107] have investigated the solutions of the analogous equations for acceptor states in Ge, which do not possess any terms linear in $\mathbf{k}$, and McLean and Loudon[108] have applied the theory to the exciton problem.

No attempt has been made to solve the exciton effective-mass equations including the linear terms. The reason for this is that experimentally, in the absence of an external magnetic field, one observes, at best, only a single broad absorption peak in the III–V compounds, due, most likely, to transitions to the lowest exciton level. The absorption spectrum does not show any other structure, but blends in smoothly with the absorption edge as shown in Figs. 5 and 6. In view of the lack of structural detail in the experimental spectra, a detailed theoretical calculation using Eq. (164) is not warranted.

In addition to the minimum at $\mathbf{k} = 0$, the conduction bands in III–V compounds have additional minima along the [111] and [001] axes. In the absence of an external magnetic field, the two spin-degenerate conduction-band states are decoupled, and the electron contribution to the exciton effective-mass equation can be written as either

(a) [111]

$$H_{ii}^{e}(\mathbf{k}) = \frac{\hbar^2}{2m_{\perp}^*} \cdot \frac{3}{2}[k^2 - (k_y k_z + k_z k_x + k_x k_y)] + \frac{\hbar^2}{2m_{\parallel}^*} \cdot \frac{1}{3}[k^2 + 2(k_y k_z + k_z k_x + k_x k_y)] \tag{165}$$

or

(b) [001]

$$H_{ii}^{e}(\mathbf{k}) = \frac{\hbar^2}{2m_{\perp}^*}(k_x^2 + k_y^2) + \frac{\hbar^2}{2m_{\parallel}^*}k_z^2. \tag{166}$$

McLean and Loudon[108] have used a variational procedure to obtain approximate solutions to the exciton effective-mass equation, using Eq. (75) with H^h given by Eq. (162) and H^e given by Eq. (165) for Ge and by Eq. (166) for Si. Their calculations yielded a ground-state exciton binding energy of about 0.003 eV for Ge and 0.013 eV for Si. No similar calculations have been done for any of the III–V compounds.

VI. Summary

In this chapter we have discussed the properties of exciton states in semiconducting crystals largely from a theoretical point of view. In doing this we have considered, on the one hand, the general effective-mass theory for excitons, which involves the solution of a complicated set of simultaneous differential equations, and, on the other hand, a simple hydrogenic model, in which the exciton states and energies are obtained simply from a hydrogenic Schrödinger equation. The general theory was discussed because the valence-band maximum in III–V compounds is complex and the simple theory is not strictly applicable. Although this is the case, most considerations of excitons in III–V compounds can be carried out using the simple model. This is true because the exciton binding energies in these compounds are small, and consequently exciton effects are not as pronounced as in other materials. In general, only one exciton peak is observed associated with a given absorption edge, which corresponds to transitions to the lowest exciton state.

As is appropriate in any discussion of exciton states, we have emphasized the associated optical properties of the crystal. Exciton states are best studied through their effects on the optical properties of the crystal in the vicinity of its absorption edges. In this connection, we have discussed the effects of excitons on the optical properties of semiconductors in the vicinity

of both the direct and indirect absorption edges. Again, our discussion has been primarily theoretical, since the experimental absorption spectra of III–V compounds are being discussed by E. J. Johnson in this volume.

The emphasis in this chapter has been largely on the "kinetic energy" terms $H^{e}_{ii'}(\mathbf{k})$ and $H^{h}_{jj'}(\mathbf{k})$ in the exciton effective-mass equation. These terms reflect the properties of the conduction and valence bands involved in a given exciton state. One of the primary motivations to study the properties of exciton states is that of hopefully obtaining thereby information about the parameters of the conduction and valence bands involved. This information is obtained by studying the optical properties of crystals near the absorption edge in the presence of an external magnetic field. Again, since the exciton binding energy in these compounds is small, the interband magnetooptical phenomena are best discussed in terms of magnetic Landau levels, perturbed, perhaps, by the electron–hole interaction as in the theory of Elliott and Loudon. This perturbation is most noticeable in the lower-lying transitions, which have consequently been often labeled as "exciton" states with the higher transitions labeled as Landau transitions. It is well to emphasize here again that, technically, all transitions observed are to exciton states, in that the electron–hole binding energy is involved. Each absorption maximum is associated with transitions to the lowest bound-exciton state associated with a given Landau level. The apparent distinction between the lower and upper levels arises only because in the higher transitions the exciton binding energy is small compared to the Landau or magnetic-field energy.

Finally, we wish to reemphasize the fact that the term exciton should be taken in general to refer to any elementary electronic excitation in an ideal semiconducting or insulating crystal. In semiconductors this elementary excitation is described as a transfer of a single electron from a completely filled valence band to a completely empty conduction band. In general, this occurs through the absorption of an optical photon and may be accompanied by the absorption or emission of a lattice phonon. Excitons in this general sense are involved in all optical phenomena associated with the absorption edges of ideal semiconductors. However, it has been prudent and, in fact, necessary to emphasize those effects that are due to the electron–hole interaction, and we have referred to these as specific "exciton effects." In general, the electron–hole interaction gives rise to a series of discrete states below the absorption edge of a semiconductor. These have been referred to as "bound exciton states" and yield a series of discrete lines or edges in the absorption spectra. The interaction also gives rise to a continuum of unbound exciton states, which then form the absorption edge of the crystal. These unbound states are Coulomb-scattering states and differ markedly from plane-wave states. Consequently, the electron–hole

interaction produces not only a series of discrete absorption lines below the absorption edge but also a major modification in the edge itself. In III–V compound semiconductors, because of the small exciton binding energy, the only discrete transition that is usually observed in the absence of a magnetic field is to the lowest bound-exciton state. The absorption due to this transition blends in continuously with that of the higher bound states and with the absorption edge itself. Consequently, exciton effects in III–V compounds do not yield truly discrete spectra but act at zero magnetic field to strongly modify the shape of the absorption edge and in the presence of a magnetic field to shift the Landau absorption peaks to lower energy and to greatly modify their shape.

ACKNOWLEDGMENTS

I should like to thank several of my colleagues for their assistance in the preparation of this manuscript. I have benefited from conversations with Drs. P. N. Argyres, G. F. Dresselhaus, W. H. Kleiner, and L. L. Van Zant on theoretical points and with Drs. E. J. Johnson, G. B. Wright, A. J. Strauss, and J. G. Mavroides on the experimental situation. I should also like to thank Mrs. S. F. Simon for her very careful job of typing the manuscript.

CHAPTER 8

Interband Magnetooptical Effects*

B. Lax and J. G. Mavroides

I. INTRODUCTION 321
1. *History* . . . 321
2. *Basic Concepts* . . . 326
II. THEORY . . . 345
3. *Semiclassical Theory* . . . 345
4. *Quantum Theory* . . . 347
III. EXPERIMENTS . . . 368
5. *Germanium* . . . 368
6. *Indium Antimonide* . . . 379
7. *Indium Arsenide* . . . 387
8. *Gallium Antimonide* . . . 388
9. *Gallium Arsenide* . . . 391
10. *Aluminum Antimonide and Gallium Phosphide* . . . 394
IV. DISCUSSION . . . 394
V. NOTE ADDED IN PROOF . . . 399

I. Introduction

1. HISTORY

Magnetooptical phenomena had their beginnings with Michael Faraday,[1] who in 1845 discovered that when plane-polarized light is sent through a block of glass that is subjected to a strong magnetic field, the plane of vibration of the light is rotated. Somewhat later, in 1896, Zeeman[2] discovered that the two yellow lines of a sodium flame were broadened considerably when the flame was placed in a magnetic field. This effect was explained by Lorentz[3] shortly thereafter on the basis of the electron theory of matter. Another important magnetooptical effect, in which a vapor became doubly

* This work was performed at Lincoln Laboratory, M.I.T., which is operated with support from the U. S. Air Force, and at the Physics Department and the National Magnet Laboratory of M.I.T. The National Magnet Laboratory is supported by the Air Force Office of Scientific Research.

[1] M. Faraday, *Phil. Trans. Roy. Soc.* p. 1 (1846).

[2] P. Zeeman, "Researches in Magneto-Optics." Macmillan, New York, 1913.

[3] H. A. Lorentz, "Theory of Electrons." Teubner, Leipzig, 1906.

refracting to light passing transverse to the magnetic field, was discovered by Voigt[4] in 1902. An effect similar to the Voigt effect was discovered in liquids by Cotton and Mouton[5] in 1907.

Some of these phenomena have played an important role in the development of the theory of atomic spectra. In particular, the Zeeman effect led to the introduction of the electron-spin hypothesis and was treated quantum mechanically to account for complexities of the phenomena observed.[6] The Faraday effect at optical wavelengths was studied both in atoms and molecules. A complete quantum-mechanical treatment in the case of monatomic molecules was given by Rosenfeld[7] and the beginning of a theory for diatomic molecules was made by Kronig[8] in the late 1920's. However, the field of magnetooptics in solids remained relatively unexciting until seven or eight years ago, when the availability of single crystals of high purity, combined with low temperatures and high magnetic fields were used to investigate a new class of magnetooptical phenomena. Coupled with the development of a sophisticated treatment of the related electronic band structure of these solids, new and quantitative information about the complex energy bands of these crystals evolved.

Although in this article we shall treat only the interband magnetooptical phenomena, it should be mentioned that the impetus for these new investigations was the early intraband cyclotron-resonance experiment, first carried out at microwave frequencies[9,10] and later, at infrared wavelengths.[11,12] Actually, the first definitive interband experiments involved the transmission of light through thin single crystals of InSb[13] and germanium[14,15] at energies just above the energy gap. Under these conditions an oscillatory variation with a magnetic field of the transmission of light was observed. This phenomenon was immediately interpreted in terms of transitions between the quantized magnetic levels in the valence and conduction bands of the crystals. Extensive investigations in germanium and InSb yielded new and quantitative information on the effective masses, effective spectroscopic

[4] W. Voigt, *Göttinger Nachr.* **5** (1902).
[5] R. W. Wood, "Physical Optics," p. 718. Macmillan, New York, 1934.
[6] See, for example, H. E. White, "Introduction to Atomic Spectra." McGraw-Hill, New York, 1934.
[7] L. Rosenfeld, *Z. Physik* **57**, 835 (1930).
[8] R. de L. Kronig, *Z. Physik* **45**, 508 (1927).
[9] G. Dresselhaus, A. F. Kip, and C. Kittel, *Phys. Rev.* **92**, 827 (1953).
[10] B. Lax, H. J. Zeiger, R. N. Dexter, and E. S. Rosenblum, *Phys. Rev.* **93**, 1418 (1954).
[11] E. Burstein, G. S. Picus, and H. A. Gebbie, *Phys. Rev.* **103**, 825 (1956).
[12] R. J. Keyes, S. Zwerdling, S. Foner, H. H. Kolm, and B. Lax, *Phys. Rev.* **104**, 1804 (1956).
[13] E. Burstein and G. S. Picus, *Phys. Rev.* **105**, 1123 (1957).
[14] S. Zwerdling and B. Lax, *Phys. Rev.* **106**, 51 (1957).
[15] S. Zwerdling, B. Lax, and L. M. Roth, *Phys. Rev.* **108**, 1402 (1957).

spin factors, and energy gaps. It was also possible to study the two types of bound hole–electron pairs, known as excitons, and the associated complex structure in a magnetic field. The theoretical foundations for the quantitative interpretation of these phenomena were established in papers by Elliott *et al.*,[16] Roth *et al.*,[17] and Burstein *et al.*[18] Subsequently, experimental results have been reported in InAs,[15,19] GaSb,[19,20] CuO by Gross and Zacharcenja,[21] Cu_2O by Gross *et al.*[22] and also by Nikitine and coworkers,[23] CdS,[24,25] and, more recently, in PbS,[26,27] PbSe[27] and PbTe.[27,28] The oscillatory magnetoabsorption has now been observed in GaAs using the crossfield magnetoabsorption technique.[29] Finally, oscillations in the absorption with magnetic field have been observed in GaSe by Sugano and Misu[29a] and also by Halpern.[29b]

Interestingly, the first interband magnetoabsorption experiments were actually carried out in the semimetal bismuth in 1956[12]; at that time, the observations were interpreted as cyclotron resonance. It was not until 1960 that Lax *et al.*[30] reanalyzed the data and deduced that an interband phenomenon had been observed. Consequently, Brown *et al.*[31,32] carried out

[16] R. J. Elliott, T. P. McLean, and G. G. Macfarlane, *Proc. Phys. Soc. (London)* **72**, 553 (1958).
[17] L. M. Roth, B. Lax, and S. Zwerdling, *Phys. Rev.* **114**, 90 (1959); B. Lax, L. M. Roth, and S. Zwerdling, *J. Phys. Chem. Solids* **8**, 311 (1959).
[18] E. Burstein, G. S. Picus, R. F. Wallis, and F. J. Blatt, *Phys. Rev.* **113**, 15 (1959); *J. Phys. Chem. Solids* **8**, 305 (1959).
[19] E. J. Johnson, I. Filinski, and H. Y. Fan, *Proc. Intern. Conf. Phys. Semicond., Exeter, 1962* p. 375. Inst. of Phys. and Phys. Soc., London, 1962.
[20] S. Zwerdling, B. Lax, K. J. Button, and L. M. Roth, *J. Phys. Chem. Solids* **9**, 320 (1959).
[21] E. F. Gross and B. P. Zacharcenja, *J. Phys. Radium* **1**, 68 (1957).
[22] E. F. Gross, B. P. Zacharcenja, and A. A. Kaplyansky, *Proc. Intern. Conf. Phys. Semicond., Exeter, 1962* p. 409. Inst. of Phys. and Phys. Soc., London, 1962.
[23] S. Nikitine, J. B. Grun, M. Certier, J. L. Deiss, and M. Grosmann, *Proc. Intern. Conf. Phys. Semicond., Exeter, 1962* p. 411. Inst. of Phys. and Phys. Soc., London, 1962.
[24] R. G. Wheeler and J. O. Dimmock, *Phys. Rev. Letters* **3**, 372 (1959); J. J. Hopfield and D. G. Thomas, *ibid* **4**, 357 (1960).
[25] A. Misu, K. Aoyagi, G. Kuwabara, and S. Sugano, *in* "Physics of Semiconductors" (Proc. 7th Intern. Conf.), p. 317. Dunod, Paris, and Academic Press, New York, 1964.
[26] D. L. Mitchell, E. D. Palik, J. D. Jensen, R. B. Schoolar, and J. N. Zemel, *Phys. Letters* **4**, 262 (1963).
[27] D. L. Mitchell, E. D. Palik, and J. N. Zemel, *in* "Physics of Semiconductors" (Proc. 7th Intern. Conf.), p. 325. Dunod, Paris, and Academic Press, New York, 1964.
[28] D. L. Mitchell, E. D. Palik, J. D. Jensen, R. B. Schoolar, and J. N. Zemel, *Bull. Am. Phys. Soc.* **9**, 292 (1964).
[29] Q. H. F. Vrehen, *Bull. Am. Phys. Soc.* **10**, 534 (1965).
[29a] H. Hasegawa and E. Hanamura, *Phys. Letters* **19**, 378 (1965).
[29b] J. Halpern, *Bull. Am. Phys. Soc.* **11**, 206 (1966).
[30] B. Lax, J. G. Mavroides, H. J. Zeiger, and R. J. Keyes, *Phys. Rev. Letters* **5**, 505 (1960).
[31] R. N. Brown, J. G. Mavroides, M. S. Dresselhaus, and B. Lax, *Phys. Rev. Letters* **5**, 506 (1960).
[32] R. N. Brown, J. G. Mavroides, and B. Lax, *Phys. Rev.* **129**, 2055 (1963).

definitive magnetoreflection experiments in bismuth and demonstrated that such phenomena can be observed in semimetals. These observations were later extended to alloys of bismuth and antimony.[33,34] Oscillations in the magnetoabsorption of bismuth were also observed by Boyle and Rodgers,[35] but were incorrectly identified as arising from de Haas–van Alphen type oscillations of the Fermi level. Later, more detailed magnetoabsorption experiments by Engeler[36] established that these oscillations were actually due to interband transitions.

The magnetoreflection technique has also been applied to InSb[37] and $Hg_{0.85}Cd_{0.15}Te$.[38] However, the most elegant applications have been made by Dresselhaus and Mavroides in graphite,[39] where the technique was utilized to obtain quantitative values for the electron-band parameters of this semimetal and also in antimony, where, in addition to the interband effects,[40] the optical analog of the Shubnikov–de Haas effect was observed for the first time.[41] We shall not discuss the details of the results in semimetals, since this chapter is concerned with semiconducting compounds; however, the technique involved is worth mentioning, since it will be applicable at high magnetic fields to semiconductors as well, particularly if they are degenerate or exhibit large absorption coefficients.

Dispersion effects, such as the Faraday rotation, due to interband transitions were considered by Darwin and Watson[42] in 1927 and later by Stephen and Lidiard[42a]; they both represented band-to-band transitions by a simple model of bound electrons with a resonant frequency corresponding to the energy gap. The experimental observations by Brown and Lax[43] in InSb, Smith *et al.*[44] (also in InSb) and Hartmann and Kleman[45] in germanium gave qualitative confirmation to this hypothesis. However, Lax[46] suggested

[33] R. N. Brown, private communication.
[34] L. Hebel and G. E. Smith, *Phys. Letters* **10**, 273 (1964).
[35] W. S. Boyle and K. F. Rodgers, *Phys. Rev. Letters* **2**, 338 (1959).
[36] W. E. Engeler, *Phys. Rev.* **129**, 1509 (1963).
[37] G. B. Wright and B. Lax, *J. Appl. Phys. Suppl.* **32**, 2113 (1961).
[38] T. C. Harman, A. J. Strauss, D. H. Dickey, M. S. Dresselhaus, G. B. Wright, and J. G. Mavroides, *Phys. Rev. Letters* **7**, 403 (1961).
[39] M. S. Dresselhaus and J. G. Mavroides, *IBM J. Res. Develop.* **8**, 262 (1964).
[40] M. S. Dresselhaus and J. G. Mavroides, *Phys. Rev. Letters* **14**, 259 (1965).
[41] M. S. Dresselhaus and J. G. Mavroides, *Solid State Commun.* **2**, 297 (1964).
[42] C. G. Darwin and W. H. Watson, *Proc. Roy. Soc.* (*London*) **A114**, 474 (1927).
[42a] M. J. Stephen and A. B. Lidiard, *J. Phys. Chem. Solids* **9**, 43 (1959).
[43] R. N. Brown and B. Lax, *Bull. Am. Phys. Soc.* **4**, 133 (1959); R. N. Brown, Masters Thesis, M.I.T. (1958).
[44] S. D. Smith, T. S. Moss, and K. W. Taylor, *J. Phys. Chem. Solids* **11**, 131 (1959).
[45] B. Hartmann and B. Kleman, *Arkiv. Fysik* **18**, 75 (1960).
[46] B. Lax, *Proc. Intern. Conf. Semicond. Phys., Prague, 1960* p. 321. Czech. Acad. Sci., Prague, and Academic Press, New York, 1961.

that the actual band properties should be taken into account in order to obtain a quantitative understanding of the phenomenon, and he derived a simple expression for the dominant term in the Faraday rotation near the energy gap. Lax and Nishina[47] obtained a more general expression for the Faraday rotation and Voigt effect, using the Kramers–Kronig relations. However, their results gave an incorrect low-frequency behavior that was inconsistent with experimental observations, such as those of Smith *et al.*[48] in InSb, Piller and Potter[49] in silicon, and Moss *et al.*[50] in GaP. Subsequently, this expression was corrected by Kolodziejczak, Lax, and Nishina (KLN),[51] who developed a semiclassical theory, and also by Boswarva, Howard, and Lidiard (BHL)[52] who used a quantum-mechanical Kramers–Heisenberg approach to the problem. These two explicit results are both different approximations to the more exact problem, as was indicated by a more general treatment by Bennett and Stern[53] and Roth,[54] in which the matrix elements were expanded as a function of the magnetic field.

Oscillatory effects associated with the Faraday rotation and Voigt effect were reported by Nishina *et al.*[55] and have been recently analyzed by Korovin and Kharitonov.[56] Similar results were also obtained by Mitchell and Wallis[57] who found evidence for the possible influence of exciton transitions on the rotation.

The first quantitative calculation of the magnitude of the interband Faraday rotation was made by Suffczynski[58] in germanium. Later, more detailed treatments were carried out by Roth,[54] and also Boswarva and Lidiard,[59] using a modified Bloch representation to calculate the conductivity tensor. In both of these treatments the Faraday rotation was analyzed in terms of the Luttinger–Kohn Landau ladders to estimate quantitatively the rotation in various semiconductors. A similar calculation of the Faraday rotation in

[47] B. Lax and Y. Nishina, *Phys. Rev. Letters* **6**, 464 (1961).

[48] S. D. Smith, C. R. Pidgeon, and V. Prosser, *Proc. Intern. Conf. Phys. Semicond., Exeter, 1962* p. 301. Inst. of Phys. and Phys. Soc., London, 1962.

[49] H. Piller and R. F. Potter, *Phys. Rev. Letters* **9**, 203 (1962).

[50] T. S. Moss, A. K. Walton, and B. Ellis, *Proc. Intern. Conf. Phys. Semicond., Exeter, 1962* p. 295. Inst. of Phys. and Phys. Soc., London, 1962.

[51] J. Kolodziejczak, B. Lax, and Y. Nishina, *Phys. Rev.* **128**, 2655 (1962).

[52] I. M. Boswarva, R. E. Howard, and A. B. Lidiard, *Proc. Roy. Soc. (London)* **A269**, 125 (1962).

[53] H. S. Bennett and E. A. Stern, *Phys. Rev.* **137**, A448 (1965); H. S. Bennett, Masters Thesis, University of Maryland (1960).

[54] L. M. Roth, *Phys. Rev.* **133**, A542 (1964).

[55] Y. Nishina, J. Kolodziejczak, and B. Lax, *Phys. Rev. Letters* **9**, 55 (1962).

[56] K. I. Korovin and E. V. Kharitonov, *Fiz. Tverd. Tela* **4**, 2813 (1962) [*English Transl.: Soviet Phys.-Solid State* **4**, 2061 (1963)].

[57] D. L. Mitchell and R. F. Wallis, *Phys. Rev.* **131**, 1965 (1963).

[58] M. Suffczynski, *Proc. Phys. Soc. (London)* **77**, 1042 (1961).

[59] I. M. Boswarva and A. B. Lidiard, *Proc. Roy. Soc. (London)* **A278**, 588 (1964).

InSb was carried out by Boswarva.[60] Halpern, Lax, and Nishina (HLN)[61] have modified and extended the BHL treatment[52] and obtained expressions for the Faraday rotation that are the same as the semiclassical KLN[51] results.

Other observations of the interband Faraday rotation include the work of Austin[62] in Bi_2Te_3; Cardona[63] in GaAs and InAs; Walton and Moss[64] in germanium; Piller and Patton[65] in AlSb, germanium, and GaSb; Piller[66] in GaSb and GaAs; Halpern on oscillatory effects in GaSb,[66a] Pidgeon and Smith[67] in InSb at room temperature and below; Ukhanov and Mal'tsev[68] in InSb at room temperature and above; Moss and Ellis[69] in GaP; and Pidgeon *et al.*[70] on the effect of uniaxial strain on the rotation in germanium and InSb.

2. Basic Concepts

a. Magnetoabsorption

In its simplest form, the interband magnetooptical phenomenon can be understood by considering Schrödinger's equation in the effective-mass approximation. Including a term for the magnetic field **H**, we obtain the following wave equation for an electron of effective mass m_c:

$$\frac{1}{2m_c}\left(\mathbf{p} + \frac{e}{c}\mathbf{A}\right)^2 \psi = \mathscr{E}\psi, \tag{1}$$

where **p** is the momentum operator and $\mathbf{A} = \frac{1}{2}(\mathbf{H} \times \mathbf{r})$ is the vector potential. The solution of Eq. (1) for the eigenvalues $\mathscr{E}_n$, in the case where **H** lies in the z direction and spin is neglected, is given by

$$\mathscr{E}_n = (n + \tfrac{1}{2})\hbar\omega_c + \frac{\hbar^2 k_z^2}{2m_c}. \tag{2}$$

[60] I. M. Boswarva, *Proc. Phys. Soc. (London)* **84**, 389 (1964).
[61] J. Halpern, B. Lax, and Y. Nishina, *Phys. Rev.* **134**, A140 (1964).
[62] I. G. Austin, *Proc. Phys. Soc. (London)* **76**, 169 (1960).
[63] M. Cardona, *Phys. Rev.* **121**, 752 (1961).
[64] A. K. Walton and T. S. Moss, *J. Appl. Phys.* **30**, 951 (1959).
[65] H. Piller and V. A. Patton, *Phys. Rev.* **129**, 1169 (1963).
[66] H. Piller, *in* "Physics of Semiconductors" (Proc. 7th Intern. Conf.), p. 297. Dunod, Paris, and Academic Press, New York, 1964.
[66a] J. Halpern, *Bull. Am. Phys. Soc.* **10**, 594 (1965).
[67] C. R. Pidgeon and S. D. Smith, *Infrared Phys.* **4**, 13 (1964).
[68] Yu. I. Ukhanov and Yu. V. Mal'tsev, *Fiz. Tverd. Tela* **4**, 3215 (1962) [*English Transl.: Soviet Phys.-Solid State* **4**, 2354 (1963)].
[69] T. S. Moss and B. Ellis, *Proc. Phys. Soc. (London)* **83**, 217 (1964).
[70] C. R. Pidgeon, C. J. Summers, T. Arai, and S. D. Smith, *in* "Physics of Semiconductors" (Proc. 7th Intern. Conf.), p. 289. Dunod, Paris, and Academic Press, New York, 1964.

Here n (≥ 0) is the magnetic quantum number, $\omega_c = eH/m_c c$ is the cyclotron frequency, and the other quantities have their usual meanings. This solution, first obtained by Landau,[71] can be represented by a series of two-dimensional harmonic oscillator-like levels, known as Landau levels, with a spacing between levels equal to the cyclotron energy $\hbar\omega_c$. By solving an equation similar to Eq. (1) for the holes in the valence band, one obtains for the hole energy $\mathscr{E}_{n'}$

$$\mathscr{E}_{n'} = -\mathscr{E}_g - (n' + \tfrac{1}{2})\hbar\omega_v - \frac{\hbar^2 k_z^2}{2m_v}, \tag{3}$$

where $\mathscr{E}_g$ is the energy gap and the remaining symbols refer to the valence band. The energy levels for two simple spherical energy bands such as represented by Eq. (2) and (3) are illustrated in Fig. 1. The calculation of the

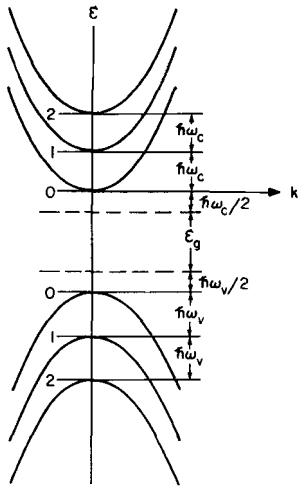


FIG. 1. Energy levels for simple bands as quantized by a magnetic field. Here the energy gap is denoted by $\mathscr{E}_g$ and ω_c and ω_v are the cyclotron frequencies for the conduction and valence bands respectively.

absorption coefficient α for transitions between the valence and conduction bands has been carried out using the "golden rule" by a number of workers including Hall *et al.*[72] as

$$\alpha(0) = \frac{A}{\omega}(\omega - \omega_g)^{1/2}, \tag{4}$$

[71] L. D. Landau, *Z. Physik* **64**, 629 (1930).

[72] L. H. Hall, J. Bardeen, and F. J. Blatt, *Phys. Rev.* **95**, 559 (1954); "Photoconductivity Conference" (Proc. Atlantic City Conf.) (R. G. Breckenridge, B. R. Russell, and E. E. Hahn, eds.), p. 146. Wiley, New York, and Chapman & Hall, London, 1965.

where for allowed direct transitions $A = \kappa e^2(2\mu)^{3/2}|\mathbf{P}_{cv}|^2/16\pi c\varepsilon m^2\hbar^{5/2}$ in MKS units, $\mu = m_c m_v/(m_c + m_v)$ is the reduced mass, $\mathbf{P}_{cv}$ is the momentum matrix, κ is the dielectric constant and ε is the permittivity. The extension of this treatment to include the effect of a magnetic field gives an absorption edge corresponding to each pair of Landau levels. Summing over pairs of initial and final states, the absorption coefficient becomes[17]

$$\alpha(H) = \frac{A\omega_c^*}{2\omega} \sum_n \frac{1}{(\omega - \omega_n)^{1/2}}. \tag{5}$$

Here $\omega_c^* = eH/\mu c$ and $\omega_n = \omega_g + (n + \frac{1}{2})\omega_c^*$, since we are neglecting spin. From Eq. (5) it is apparent that the absorption coefficient will exhibit singularities or peaks for transitions between magnetic levels. These transitions are subject to the selection rules $\Delta n = 0$, $\Delta k_z = 0$, and have the appearance shown in the theoretical curve of Fig. 2. This phenomenon, which has been observed in transmission experiments in germanium[14,15] and indium antimonide,[13] exhibits the general features shown in Fig. 2; however, the amplitude of the oscillations does not increase exactly linearly with magnetic field, as suggested by Eq. (5).

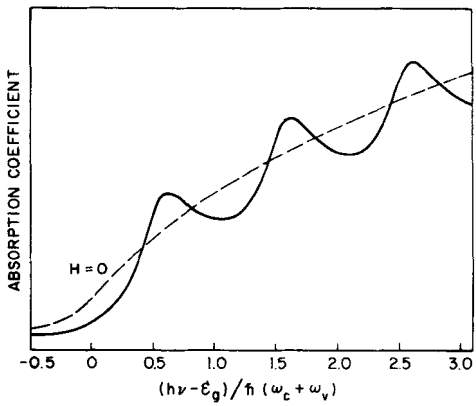


FIG. 2. Absorption coefficient as a function of energy for direct transitions between simple bands, such as shown in Fig. 1. The solid curve shows the oscillatory magnetoabsorption with $(\omega_c + \omega_v)\tau = 5$. (After L. M. Roth *et al.*[17])

So far, we have considered direct allowed transitions in which only a photon is involved. There are however, two other types of transitions that can occur. One of these, the indirect transition, involves the emission or

absorption of a phonon of energy $\hbar\omega_{ph}$. The absorption coefficient in this case is given by[73,74]

$$\alpha_{\pm}(0) = C_{\pm}(\omega - \omega_g \mp \omega_{ph})^2, \tag{6}$$

where $C_{\pm} = \pm(D/\omega)\,[\exp(\pm\hbar\omega_{ph}/kT) - 1]$, T is the absolute temperature, D is a coefficient involving fundamental parameters, such as phonon matrix elements, density of states, etc., and the plus-or-minus sign refers to absorption or emission of a phonon of energy $\hbar\omega_{ph}$. The application of a magnetic field modifies this expression to[17]

$$\alpha(H) = 2C_{\pm}\omega_c\omega_v \sum_{n,n'} S(\omega - \omega_{nn'}), \tag{7}$$

where $\omega_{nn'} = \omega_g + (n + \frac{1}{2})\omega_c + (n' + \frac{1}{2})\omega_v \pm \omega_{ph}$ and $S(\omega - \omega_{nn'})$ is a step function. Again, for simplicity, the spin splitting is omitted. Because of the phonon transitions, there are now no selection rules for n and n'. A theoretical curve of the absorption coefficient for indirect transitions between two simple bands in a magnetic field is shown in Fig. 3. Experimental step function spectra of this type have been observed by the Lincoln group[74] and will be discussed later.

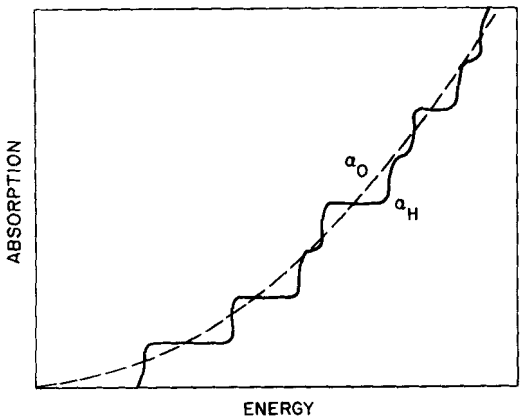


FIG. 3. Absorption coefficient as a function of energy for indirect transitions between two simple bands. This curve was constructed for $\omega_c/\omega_v = \frac{4}{7}$. (After L. M. Roth *et al.*[17])

The other type of transition that is of interest is the direct forbidden transition. This case corresponds to the situation where direct transitions are not allowed at $k = 0$ because the two bands involved have the same

[73] G. G. Macfarlane and V. Roberts, *Phys. Rev.* **97**, 1714 (1955); **98**, 1865 (1955).
[74] S. Zwerdling, B. Lax, L. M. Roth, and K. J. Button, *Phys. Rev.* **114**, 80 (1959).

symmetry. Such is the case, for example, between valence bands in germanium and other similar semiconductors such as InSb. The theory for this situation at zero magnetic field, which has been developed by Kahn,[75] gives

$$\alpha(0) = \frac{B}{\omega}(\omega - \omega_g)^{3/2}, \tag{8}$$

where $B = \kappa e^2(2\mu)^{5/2}|\mathbf{P}_{cv}|^2/48\pi c\varepsilon m^2\hbar^{7/2}$ and $\mathbf{P}_{cv}$ is the momentum matrix element between the two bands. In a magnetic field, the absorption coefficient can be shown to have two components depending on the polarization of the electric vector relative to the magnetic field. Again neglecting spin, for the polarization with the electric field parallel to the static magnetic field,

$$\alpha_{\parallel}(H) = \frac{3\omega_c^* B}{2}\sum_n (\omega - \omega_n)^{1/2}, \tag{9}$$

where $\omega_n = \omega_g + (n + \frac{1}{2})\omega_c^*$,[76] and the selection rule for this transition is $\Delta n = 0$. For the electric field perpendicular to the magnetic field the magnetoabsorption between bands 1 and 2 becomes

$$\alpha_{\perp}(H) = \frac{3}{2}\left(\frac{\omega_c^*}{2}\right)^2 B\sum_n (n+1)[(\omega - \omega_{n_1})^{-1/2} + (\omega - \omega_{n_2})^{-1/2}]. \tag{10}$$

Here $\omega_{n_{1,2}} = \omega_g + (n + \frac{1}{2})\omega_c^* + \omega_{c_{1,2}}$ and the selection rule is $\Delta n = \pm 1$. The curve for the direct forbidden transition, given in Fig. 4, is more complex than the others, since it is a combination of two terms—one with a simple behavior, Eq. (9), and the other with singularities, Eq. (10). This transition has not yet been observed in a magnetic field, probably for two reasons. One is that ω_c^* involves the difference between two reciprocal masses, so that the Landau-level spacings are very close; the other is that the heavy doping required to observe the effect results in increased scattering and therefore smaller magnetooptical effects.

b. Faraday Rotation

When a linearly polarized light wave propagates through certain materials along the direction of the magnetic field, the plane of polarization is rotated per unit length of material through an angle, θ, that is given by

$$\theta = \frac{\beta_+ - \beta_-}{2} = \frac{\omega}{2c}(\eta_+ - \eta_-), \tag{11}$$

[75] A. H. Kahn, *Phys. Rev.* **97**, 1647 (1955).

[76] Since the sign of the curvature in germanium is the same for both valence bands, $\omega_c^* = (eH/c)(1/m_1 - 1/m_2)$.

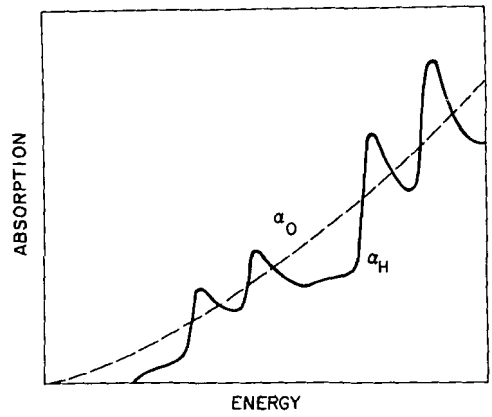


FIG. 4. Absorption coefficient as a function of energy for two simple bands when the transition at $\mathbf{k} = 0$ is forbidden. This curve was constructed for the case $\omega_c/\omega_c = 3$. (After L. M. Roth *et al.*[17])

where $\beta_\pm$ and $\eta_\pm$ are the phase shift and index of refraction, respectively, and the $\pm$ refers to the two senses of circular polarization. In semiconductors this phenomenon becomes particularly interesting at energies just below the energy gap. In this range it can be shown by use of the Kramers–Kronig relations that, analogous to the singularities in the absorption, one obtains singularities (as well as other terms) also in the dispersion, which in general has the form

$$\beta_\pm \approx \frac{A\omega_c^*}{2\omega^2} \sum_n \frac{1}{[\omega_n - (\omega \mp \gamma H)]^{1/2}}, \tag{12}$$

where A and ω_n are defined previously in Eqs. (4) and (5), $\gamma = (\mu_B/2\hbar)(g_v + g_c)$, μ_B is the Bohr magneton and the $g_{v,c}$ are the g factors for the valence and conduction bands, respectively. This is essentially the expression given earlier by Lax[46] to account for the singularity in the Faraday rotation near the energy gap. From this expression, it is easily shown that near the gap the Faraday rotation θ is dominated by a term of the form

$$\theta \approx \frac{A\omega_c^*}{8\omega c} \sum_n \frac{\gamma H}{(\omega_n - \omega)^{3/2}} \qquad (\omega \approx \omega_g). \tag{13}$$

The above predicts oscillatory effects above the energy gap, and these have been observed experimentally.[55] The expression in Eq. (13) is incomplete; for the above expression to be valid in the frequency domain, the appropriate use of the Kramers–Kronig or the Kramers–Heisenberg dispersion relations

in a tensor magnetooptical medium, as we shall show, gives the low-frequency expression

$$\theta \approx \frac{A\gamma H}{8\omega c}\left\{(\omega_g + \omega)^{-1/2} - (\omega_g - \omega)^{-1/2} + \frac{4}{\omega}[2\omega_g^{1/2} - (\omega_g + \omega)^{1/2} - (\omega_g - \omega)^{1/2}]\right\} \qquad (\omega < \omega_g). \tag{14}$$

Equation (14) also predicts a singularity just below the energy gap. In the low-frequency limit, well below the gap, this expression reduces to

$$\theta \approx \frac{5A\gamma H\omega^2}{64c\omega_g^{7/2}} \qquad (\omega \to 0). \tag{15}$$

This simple expression indicates that the interband Faraday rotation varies as ω^2 in the low-frequency limit. This holds true not only for the case of the direct transitions but also for direct forbidden and for indirect transitions, as has been verified experimentally by the work of Piller and Potter.[49] The complete expressions for the various cases will be presented later; however, the contribution to the rotation near the energy gap from the indirect transition, which is of interest, is of the form

$$\theta_i = \frac{F\gamma H}{2c}\left[\frac{\omega_g^2}{2}\ln\frac{\omega_g^2}{\omega_g^2 - \omega^2} + \frac{\omega_g}{\omega}\ln\frac{\omega_g - \omega}{\omega_g + \omega} + 1\right] \qquad (\omega < \omega_g \pm \omega_{ph}),$$
$$\theta_i = -\frac{F\gamma H}{c}\frac{\omega_v\omega_c}{\omega^2}\sum_{nn'}\left(\ln\frac{\omega_{nn'}^2 - \omega^2}{\omega_{nn'}^2} + \frac{\omega^2}{\omega_{nn'}^2 - \omega^2}\right) \qquad (\omega > \omega_g \pm \omega_{ph}), \tag{16}$$

where $F = e^2(m_v m_c)^{3/2}|\mathbf{P}_{kk'}|^2\kappa^{1/2}/16\pi^3 m^2\hbar^4\varepsilon$, $\omega_{c,v} = eH/m_{c,v}$, ω_{ph} is the phonon frequency, and $\omega_{nn'} = \omega_g + (n + \frac{1}{2})\omega_c + (n' + \frac{1}{2})\omega_v \pm \omega_{ph}$.

c. *Voigt Effect*

In a manner analogous to the results for the Faraday rotation it can be shown that a polarized wave that is propagated perpendicular to a static magnetic field will exhibit birefringence in media, since the component of electric field parallel to the magnetic field will have a propagation velocity different for the component that has the electric field perpendicular to the magnetic field. It can be shown that the phase shift δ in the oscillatory region is dominated by the term of the form

$$\delta = \frac{\omega}{c}(\eta_\perp - \eta_\parallel) \sim \frac{A(\gamma H)^2\omega_c^*}{\omega}\sum_n \frac{1}{(\omega_n - \omega)^{5/2}} \qquad (\omega > \omega_g). \tag{17}$$

This result predicts a singularity and also an oscillatory component for the Voigt effect near the energy gap. This has now been observed by Nishina *et al.*[55] In the low-frequency limit it can be shown that

$$\delta \sim \frac{B(\gamma H)^2 \omega^3}{512 c \omega_g^{11/2}}; \tag{18}$$

thus

$$\frac{\delta}{\theta} \approx \frac{1}{40} \frac{\omega \gamma H}{\omega_g^2}. \tag{19}$$

From Eq. (19) it is evident that the Voigt effect is very small in the low-frequency limit, since $\gamma H, \omega \ll \omega_g$. Consequently, only the oscillatory Voigt effect is of interest.

d. Cross-Field Magnetoabsorption

It was shown theoretically by Aronov[77] that the interband magnetoabsorption in semiconductors would be substantially modified when crossed electric and magnetic fields were applied simultaneously. This can be readily seen by considering the matrix element P for the allowed direct transition between two energy bands, which is given by

$$P = \int \phi_i^* \left[\left(\mathbf{p} + \frac{e\mathbf{A}}{c}\right) \cdot \boldsymbol{\alpha}\right] \phi_j \, d\tau, \tag{20}$$

where $\boldsymbol{\alpha}$ is a unit vector in the direction of the electric field, and the wave function ϕ_i can be written as

$$\phi_n(\mathbf{r}) = u_{nk}(\mathbf{r}) f_n(\mathbf{r}). \tag{21}$$

Here $u_{nk}(\mathbf{r})$ is the periodic part of the Bloch function, repeating in each cell, and $f(\mathbf{r})$ is the envelope function, which gives the spatial distribution in the crystal. Expanding the matrix element in terms of the $\phi_n(\mathbf{r})$, it is easily shown that for the interband term

$$P = \int_{\substack{\text{entire} \\ \text{crystal}}} f_i^*(\mathbf{r}) \left[\left(\mathbf{p} + \frac{e\mathbf{A}}{c}\right) \cdot \boldsymbol{\alpha}\right] f_j(\mathbf{r}) \, d\tau \int_{\substack{\text{unit} \\ \text{cell}}} u_{il}^*(\mathbf{r}) \, u_{jl}(\mathbf{r}) \, d\tau$$
$$+ \int_{\substack{\text{entire} \\ \text{crystal}}} f_i^*(\mathbf{r}) \, f_j(\mathbf{r}) \, d\tau \int_{\substack{\text{unit} \\ \text{cell}}} u_{il}^*(\mathbf{r}) \, (\mathbf{p} \cdot \boldsymbol{\alpha}) \, u_{jl}(\mathbf{r}) \, d\tau. \tag{22}$$

In the usual case, when there is no applied electric field, the envelope functions are solutions of an effective-mass Hamiltonian that is the same as that given by Landau for the free electron in terms of the well-known

[77] A. G. Aronov, *Fiz. Tverd. Tela* **5**, 552 (1963) [*English Transl.*: *Soviet Phys.-Solid State* **5**, 402 (1963)].

simple-harmonic oscillator-like functions. The argument of these functions for both the conduction and valence bands—i.e., the appropriate gauge—is given by $(x + \hbar k_y c/eH)$. The introduction of an electric field modifies the Hamiltonian in such a way that the arguments for the valence and conduction bands are different, so that in evaluating the integral $\int f_i^*(\mathbf{r}) f_2(\mathbf{r})\, d\tau$, one of the $f_i(\mathbf{r})$ functions is expanded in a Taylor series about the other, thus leading to the following expression for the absorption coefficient α:

$$\alpha = G \exp\left(-\frac{a^2}{2}\right) \sum_{n,n'} \left| \sum_{m=0}^{n'+1} b_m(n', n)\, a^{n+n'-2m} \right|^2 (\omega - \omega_{nn'})^{-1/2}, \qquad (23)$$

where $G = 4\pi^2 e^3 H (2/\mu)^{1/2} P^2/\hbar^{5/2} \eta c^2 m^2 \omega$, μ is the reduced effective mass of holes and electrons, $a = eEL_M/\hbar\omega_{cv}$; $\omega_{cv} = eH/c(m_c + m_v)$; $L_M = (\hbar c/eH)^{1/2}$; $\mathscr{E}_{nn'} = \hbar\omega_{nn'} = \mathscr{E}_g + (n + \frac{1}{2})\hbar\omega_c + (n' + \frac{1}{2})\hbar\omega_v - (m_c + m_v)c^2E^2/2H^2$; η is the index of refraction, and $b_m(n', n) = (-1)^{n-m} n!n'!2^m/m!(n' - m)!(n - m)!$ The significance of this result is that the matrix element is now a function of the electric field. The amplitude of the matrix element for the allowed transition $\Delta n = 0$ decreases with electric field and, for high quantum numbers, becomes an oscillatory function of the electric field, as shown in Fig. 5(a).

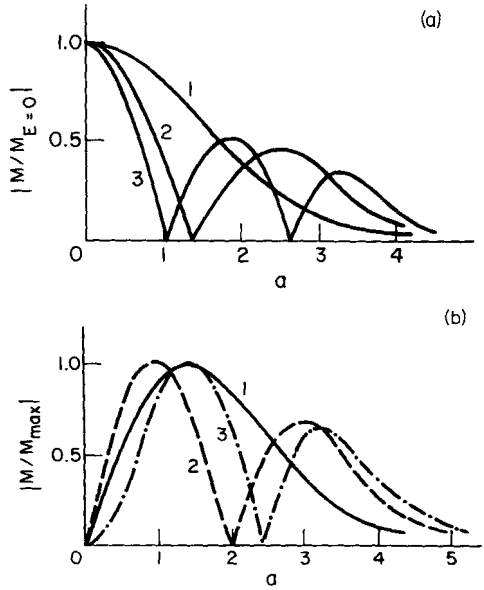


FIG. 5. Variation of the intensity of the magnetoabsorption maxima as a function of the reduced electric field a. (a) For transitions that are allowed when $E = 0$—i.e., (1) $n' = 0, n = 0$; (2) $n' = 1, n = 1$; (3) $n' = 2, n = 2$. (b) For transitions that are forbidden when $E = 0$—i.e., (1) $n' = 1, n = 0$; (2) $n' = 1, n = 2$; (3) $n' = 1, n = 3$. (After A. G. Aronov.[77])

In addition to the transition $\Delta n = 0$, there is now no selection rule for n, so that now the transitions $\Delta n = \pm 1, \pm 2 \ldots$, normally forbidden in magnetoabsorption, can also occur, with an amplitude that increases with electric field in the manner shown in Fig. 5(b).

In practice, it is difficult to perform this experiment with a d-c electric field because of heating and ionization effects. However, Vrehen and Lax[78] have used an r-f electric-field modulation technique in which both the $\Delta n = 0$ and the normally forbidden $\Delta n = \pm 1$ transitions are observed at twice the modulation frequency, even at room temperature. The differential absorption $\Delta\alpha$ of the latter transitions are given by

$$\Delta\alpha = G \sum_n 2^{2m-1}(m+1)!\,(m+1)!\,(\omega - \omega_{nn'})^{-1/2} E_0^{\,2} c^3 \frac{(m_c + m_v)^2}{\hbar e H^3}, \tag{24}$$

where $m = n$ for $\Delta n = +1$ and $m = n - 1$ for $\Delta n = -1$. By allowing the electric field to be a sinusoidal function, the second harmonic alone can be detected, with additional lines due to the forbidden transition. It was also observed that the amplitude of this cross-field magnetoabsorption as a function of the magnetic field exhibited a maximum at 25 kG and a $1/H^2$ dependence at high magnetic fields; this is in accordance with the present theory. More recently, the simultaneous application of d-c and r-f electric fields has provided a bias, thus allowing the observation of the first harmonic and the study of its behavior as a function of both electric and magnetic fields.

One of the consequences of the Aronov theory is that in the limit of high magnetic field the energy gap for simple parabolic bands is given by the simple expression

$$\mathscr{E}_{(n=0)} = \mathscr{E}_g + \tfrac{1}{2}\hbar\omega_c + \tfrac{1}{2}\hbar\omega_v - \frac{c^2E^2}{2H^2}(m_v + m_c), \tag{25}$$

since $\mathscr{E}_c = (n + \frac{1}{2})\hbar\omega_c + cEp_y/H - (c^2E^2/2H^2)m_c$, and $\mathscr{E}_v = -(n' + \frac{1}{2})\hbar\omega_v + cEp_y/H + (c^2E^2/2H^2)m_v$. This expression appears to hold in germanium. Consequently, the absorption due to interband transitions between the lowest Landau levels, as represented by the above expression, should show an absorption peak for the appropriate values of E and H in the region where the quadratic term in E would dominate, and a plot of the position of the absorption line as a function of E^2/H^2 should yield a straight line with an intercept that gives the energy gap $\mathscr{E}_g$. Indeed, these effects have been observed by Vrehen[79] and are shown in Figs. 6 and 7, respectively.

[78] Q. H. F. Vrehen and B. Lax, *Phys. Rev. Letters* **12**, 471 (1964).
[79] Q. H. F. Vrehen, *Phys. Rev. Letters* **14**, 558 (1965).

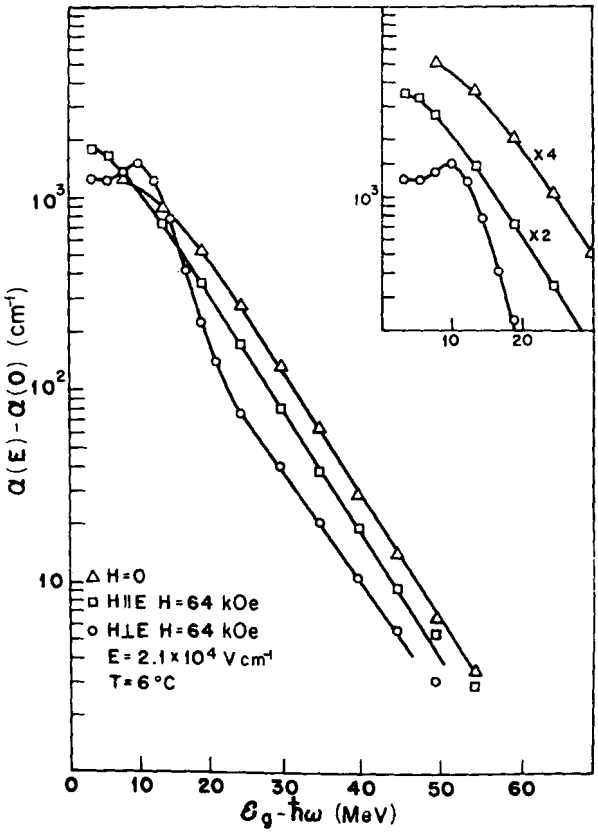


FIG. 6. Electric field induced optical absorption below the direct gap in germanium at 6°C, in both the longitudinal and transverse configuration. In cross-fields a resonance shows up approximately 10 MeV below the energy gap. In the inset the absorption curves are given on an expanded scale in order to indicate the resonance more clearly. (After Q. H. F. Vrehen.[79])

It is possible by use of perturbation theory to derive the principal results of the Aronov treatment merely by treating the electric field E as a perturbation on the magnetic levels of the holes and electrons.[80] It can be shown that in first order the eigenvalues are shifted linearly with electric field, since the argument of the wave functions is shifted by $\hbar ck_y/eH$. Thus

$$\mathscr{E}_n = \int \psi_n\left(x - \frac{\hbar c}{eH}k_y\right) eEx\psi_n\left(x - \frac{\hbar c}{eH}k_y\right) d\tau = \frac{\hbar cE}{H}k_y. \tag{26}$$

[80] Q. H. F. Vrehen, *Phys. Rev.* **145**, 675 (1966).

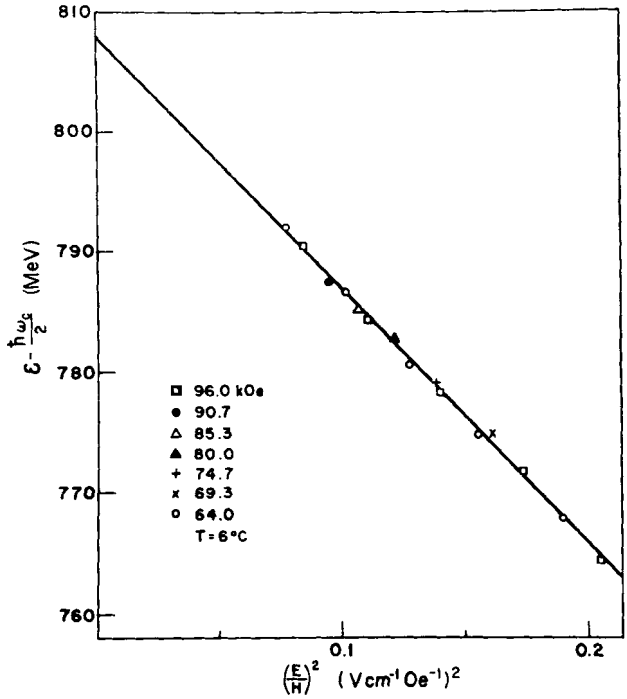


FIG. 7. Plot of $\mathscr{E} - \hbar\omega_c^*/2$ as a function of $(E/H)^2$. The intercept yields the energy gap. (After Q. H. F. Vrehen.[79])

Since the selection rule for the transition is $\Delta\mathbf{k} = 0$, there is no shift to first order. In a similar manner we can show that to second order the shift for electrons is given by

$$\Delta\mathscr{E}_{n'} = \frac{e^2E^2}{\hbar\omega_c}(\bar{x}^2_{n,n+1} - \bar{x}^2_{n,n-1}) = -\frac{c^2E^2}{2H^2}m_c, \tag{27}$$

since $\bar{x}_{n,n+1} \equiv \int \psi_n x \psi_{n+1}\, d\tau = [(\hbar c/2eH)(n+1)]^{1/2}$. The net shift is $(\Delta\mathscr{E}_{n'})_{\text{electrons}} - (\Delta\mathscr{E}_{n'})_{\text{holes}} = -(c^2E^2/2H^2)(m_c + m_v)$. Furthermore, we can also show, by using the first-order wave functions and calculating the matrix elements, that the transition probability for the observable transition $(\Delta n = \pm 1)$ is exactly that obtained by Aronov in Eq. (23). This perturbation treatment indicates explicitly that the transitions subject to the selection rule $\Delta n = \pm 2$ are allowed, but to a higher order so that they should be much weaker. Thus it is not unreasonable that they have been difficult to observe at high electric fields and low magnetic fields, where presumably they should have been strongest.

The more generalized result for the energy levels in crossed fields of the complicated valence band of germanium or silicon has been treated by Hensel[80a] in connection with cyclotron resonance, by Shindo,[80b] and most recently by Vrehen.[80] Each has used the perturbation theory outlined above, but applied to the matrix operator in a magnetic field. Vrehen[80] has compared his calculations with interband optical experiments in crossed fields in which both the transmission in the absence of an electric field and modulation of this transmission by an r-f electric field are measured. Strain-free as well as thin strained germanium samples were used in magnetic fields up to 96 kG and electric fields up to 1000 V/cm. Both the allowed transitions ($\Delta n = 0, \ -2$ for germanium) and electric-field-induced transitions ($\Delta n = -3, \pm 1$) were observed, and good agreement was found between theory and experiment as is shown in Fig. 8.

The significance of the cross-field technique is that interband transitions between Landau levels can be observed with relatively modest magnetic fields. In principle, the detection of the usually forbidden transitions permits the measurement in simple bands of the effective mass of holes and electrons separately, rather than combined in the reduced effective mass as is the case in the conventional magnetoabsorption experiment.

e. Photon-Assisted Magnetotunneling

The solution to the cross-field magnetoabsorption problem developed by Aronov[77] is really valid in the limit of high magnetic fields, where the simple effective-mass Schrödinger equation for the eigenvalues in the cross-field is applicable. In the limit of low magnetic field and high electric field, however, this solution to the wave equation is no longer appropriate. We can consider this problem from the following viewpoint. When the electron is in a very high electric field and a low magnetic field, then it can no longer maintain a classical cycloidal or localized orbit. The electron actually drifts along the electric field, gaining energy as it goes; in quantum-mechanical terms, the wave function is no longer localized in the direction of the magnetic field. Under these conditions the Landau wave functions are no longer the appropriate solutions to the problem. This situation can be readily understood by solving the eigenvalue problem by use of the Dirac or Klein–Gordon equation[81] for the free electrons. One can obtain an analogous result for the Bloch electron by taking the Kane nonparabolic-band

[80a] J. C. Hensel, *Proc. Intern. Conf. Phys. Semicond., Exeter*, 1962 p. 281. Inst. of Phys. and Phys. Soc., London, 1962.

[80b] T. Shindo, *in* "Physics of Semiconductors" (Proc. 7th Intern. Conf.), p. 91. Dunod, Paris, and Academic Press, New York, 1964.

[81] See, for example, H. A. Bethe, "Intermediate Quantum Mechanics," p. 181. Benjamin, New York, 1964.

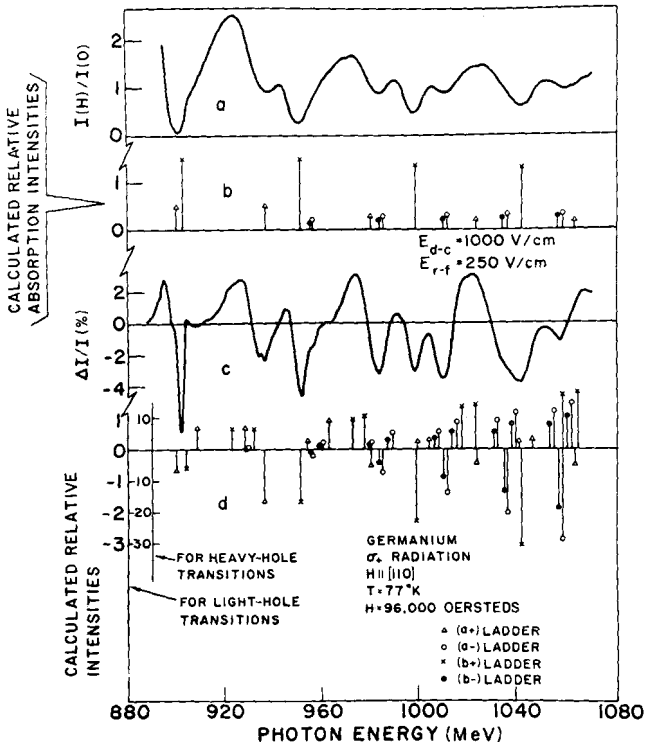


FIG. 8. Magnetoabsorption and cross-field differential absorption in "strain-free" germanium at 77°K and 96 kG for $\mathbf{H} \parallel [110]$ and σ_+ polarization: (a) magnetoabsorption spectrum; (b) calculated absorption spectrum; (c) cross-field differential spectrum, measured with $E_{d-c} = 1000$ V/cm and $E_{r-f} = 250$ V/cm (rms); and (d) calculated differential spectrum. The positive lines correspond to forbidden transitions; negative lines, to allowed transitions. For clarity of presentation the strengths of the heavy-hole transitions are shown on a $10\times$ smaller scale than those of light-hole transitions in the calculated spectrum (d). Note that heavy-hole transitions are relatively stronger in the differential spectrum than in the magnetoabsorption spectrum. (After Q. H. F. Vrehen.[80])

Hamiltonian $\mathscr{H}$ as in InSb, which, neglecting spin, can be given in the form[82]

$$\mathscr{H} = \begin{pmatrix} \frac{\mathscr{E}_g}{2} + \frac{\hbar^2 k^2}{2m} & \mathbf{k}\cdot\mathbf{p} \\ \mathbf{k}\cdot\mathbf{p} & -\frac{\mathscr{E}_g}{2} + \frac{\hbar^2 k^2}{2m} \end{pmatrix}, \tag{28}$$

[82] P. A. Wolff, *J. Phys. Chem. Solids* **25**, 1057 (1964).

or the equivalent energy–momentum equation of the form

$$\mathscr{E}^2 = \frac{\mathscr{E}_g^2}{4} + \mathscr{E}_g \frac{\hbar^2 k^2}{2m_0^*}, \tag{29}$$

where, for mathematical simplicity, we have assumed that the effective mass m_0^* at the bottom of the band is relatively small and, therefore, have neglected the term containing the free-electron mass m. This form is equivalent to the Klein–Gordon equation; its solution in the presence of a magnetic field is[82a]

$$(\mathscr{E} - eEx)^2 = \frac{\mathscr{E}_g}{2m_0^*}\left[\left(\hbar k_y - \frac{eH}{c}x\right)^2 + \hbar^2 k_z^2\right] \tag{30}$$

or

$$\mathscr{E}^2 = e^2x^2\left(\frac{\mathscr{E}_g H^2}{2m_0^* c^2} - e^2E^2\right) - 2ex\left(\frac{\hbar k_y \mathscr{E}_g H}{2m_0^* c} - \mathscr{E}E\right) + \frac{\mathscr{E}_g}{2m_0^*}(\hbar^2 k_y^2 + \hbar^2 k_z^2), \tag{31}$$

where the spin has been neglected. This particular solution corresponds to the harmonic oscillator only when $H > E(2m_0^* c^2/\mathscr{E}_g)^{1/2}$.[82b] The corresponding condition for a relativistic free electron is $H > E$. For example, in the case of InSb for a field of 10^4 gauss, the electric field must be less than 10^4 V/cm for this condition to be satisfied. At much lower magnetic fields this condition is not satisfied, as, for example, in the depletion layer of a junction or tunnel diode. In this case, the wave function is no longer localized, so that it is more appropriate to consider photon-assisted tunnelling theoretically in the manner of Franz[83] and Keldysh.[84] To do this, the magnetic field is considered as a perturbation of the electric field. In a large electric field it has been shown that it is possible to obtain absorption below the energy gap, with an absorption coefficient for parabolic energy bands given by [84a]

$$\alpha_0 = I(\omega_g - \omega)^{-1} \exp[-\beta(\omega_g - \omega)^{3/2}], \tag{32}$$

[82a] This equation neglects an additional term due to the noncommuting operators which in the effective-mass approximation is equivalent to an effective spin orbit term as shown by W. Zawadzki and B. Lax, *Phys. Rev. Letters* **16**, 1001 (1966).

[82b] This criterion for the validity of the effective-mass treatment in cross-fields has been established by Zak and Zawadzki by considering the Bloch electron in a periodic field of a crystal. (J. Zak and W. Zawadzki, to be published.)

[83] W. Franz, *Z. Naturforsch.* **13a**, 484 (1958).

[84] L. V. Keldysh, *Zh. Eksperim. i Teor. Fiz.* **34**, 1138 (1958) [*English Transl.: Soviet Phys. JETP* **34**, 788 (1958)].

[84a] K. Tharmalingam, *Phys. Rev.* **130**, 2204 (1963).

where

$$I = \frac{e^3 E\mu}{2\hbar^3 \omega c n m^2} |\mathbf{P}_{cv}|^2$$

and

$$\beta = \frac{4}{3eE}\sqrt{2\mu\hbar}.$$

Thus the effect of the electric field is to change the frequency dependence of the absorption coefficient near the threshold and to shift the absorption edge to lower energies by an amount of the order of

$$\Delta\omega_E \approx \left[\frac{(eE)^2}{\hbar\mu}\right]^{1/3}. \tag{33}$$

For an electric field of the order of 10^5 V/cm and a free-electron mass, Eq. (33) gives a shift of an absorption edge at 1 eV of about 0.02 eV. This shift is further modified by the application of a longitudinal magnetic field. The electroabsorption in the presence of a magnetic field is given by[84b]

$$\alpha_l = I\omega_c \sum_n [(\omega_n - \omega)^{-2} + \tfrac{3}{2}\beta(\omega_n - \omega)^{-1/2}] \exp[-\beta(\omega_n - \omega)^{3/2}]. \tag{34}$$

An examination of this expression indicates that the effect of the magnetic field on the electroabsorption is to decrease it, so that the absorption edge is now shifted back toward higher frequencies. This is shown in Fig. 7. However, for the particular situation considered above ($m^* \sim m$ and $E \sim 10^5$ V/cm), it can easily be shown by use of Eq. (34) that a magnetic field of the order of 1 MG is required to counteract the shift due to the electric field. By selecting a material with a small effective mass, it is possible to achieve these conditions with magnetic fields that are available in the laboratory.

Since in electroabsorption we are operating at energies below the energy gap, in principle one must sum up the contributions from all the bands; in the limit of zero magnetic field, the absorption in the longitudinal case should reduce to the same answer as before. However, in the presence of the magnetic field the contribution of the lowest level is most important, since each term is weighted by an exponential factor. Thus, retaining only this lowest level, one can obtain

[84b]This expression is an approximate one, valid to the approximation corresponding to Eq. (32), in which the zero-field absorption coefficient is expanded only to one term in the manner of Tharmalingam.[84a] However, the coefficient of the first term of Eq. (34) is modified when Eq. (32) is expanded to higher order, and also extended to include a magnetic field. This higher-order result has been worked out by M. Reine, Q. H. F. Vrehen, and B. Lax, *Phys. Rev. Letters* **16**, 1001 (1966).

$$\frac{\alpha_l}{\alpha_0} \approx \omega_c \frac{(\omega_g - \omega)\exp[\beta(\omega_g - \omega)^{3/2}]}{(\omega_g' - \omega)^2 \exp[\beta(\omega_g' - \omega)^{3/2}]}$$

$$\approx \omega_c \frac{(\omega_g - \omega)}{(\omega_g' - \omega)^2} \exp[-\tfrac{3}{4}\omega_c\beta(\omega_g - \omega)^{1/2}], \tag{35}$$

where $\omega_g' = \omega_g + \frac{1}{2}\omega_c$; thus

$$\ln \alpha_l - \ln \alpha_0 \approx \ln \omega_c \frac{(\omega_g - \omega)}{(\omega_g' - \omega)^2} - \frac{3}{4}\omega_c\beta(\omega_g - \omega)^{1/2}. \tag{36}$$

Equation (36), in agreement with the experimental results of Fig. 6, indicates that the plots for $\ln \alpha_l$ and $\ln \alpha_0$ versus $(\omega_g - \omega)$ are nearly parallel, since $(\omega_g - \omega)$ is a slowly varying function. Furthermore, this equation predicts quantitatively the experimentally observed change in the absorption coefficient of Fig. 6. On the other hand, for the transverse-magnetic-field case it can be shown by use of Eq. (31) that for nonparabolic bands the transmission T is given by the expression

$$T \sim \exp(-(2m_0^*/\mathscr{E}_g)^{1/2}(1/\hbar e E_{\text{eff}}^3)\{-\hbar\omega E + [\mathscr{E}_g^2 E^2 - (\mathscr{E}_g^2 - \hbar^2\omega^2)H_{\text{eff}}^2]^{1/2}\}(\mathscr{E}_g^2 - \hbar^2\omega^2)^{1/2}) \tag{37}$$

and

$$\frac{\alpha_t}{\alpha_0} \approx \exp\left\{-\frac{(\mathscr{E}_g - \hbar\omega)^{5/2}}{2\hbar e\mathscr{E}_g}(m_0^*)^{1/2}\frac{H_{\text{eff}}^2}{E_{\text{eff}}^3}\right\} \tag{38}$$

where $E_{\text{eff}} = (E^2 - H^2\mathscr{E}_g/2m_0^*c^2)^{1/2}$ and $H_{\text{eff}} = H(\mathscr{E}_g/2m_0^*c^2)^{1/2}$. This expression can also be used to obtain the current for a tunnel diode in transverse electric and magnetic fields. The above theoretical result for transverse tunneling was obtained for nonparabolic bands, and appears to be a good approximation for InSb. The theory in this form predicts a cutoff for a given electric field at high enough magnetic fields for the photon-assisted tunneling. As before, the condition for cutoff is that the electric field $E < H(\mathscr{E}_g/2m_0^*c^2)^{1/2}$. Again, this cutoff seems to agree semiquantitatively with the cutoff for photon-assisted tunneling, as well as for magnetotunneling at $\hbar\omega = 0$, in the transverse case for InSb.

An alternative result for photon-assisted tunneling may be obtained from the theoretical work of Haering and Adams,[85] who considered the magnetotunneling current for both transverse and longitudinal magnetic fields. The situations in these two cases are somewhat different. In the longitudinal case, for high enough magnetic fields, they assumed that the dominant transition is between the lowest quantum levels. For the transverse case,

[85] R. R. Haering and E. N. Adams, *J. Phys. Chem. Solids* **19**, 8 (1964).

on the other hand, since the quantized energy of motion provides the kinetic energy for tunneling, it is transitions between the highest quantum levels that are principally involved. With these assumptions, expressions for both the longitudinal and transverse currents have been obtained; when the ratio of these two currents is taken, it is found that the spin moment cancels out. By analogy to their final result, it is possible to obtain a similar expression for the optical absorption, namely,

$$\frac{\alpha_t}{\alpha_l} \approx \exp\left[-C\left(\frac{H^2}{E^2}\right)(\omega_g - \omega)^{5/2}\right]. \tag{39}$$

In this expression, which holds only for parabolic bands, we have merely substituted $\hbar(\omega_g - \omega)$ for the energy gap, since the assumption is made that the electron has merely to tunnel through a certain distance corresponding to the junction and then be raised up to the conduction band by a photon. Implicit in this result is the reasonable assumption that the electric field is very large. The approximate expression of Eq. (39) obtained here is very similar to Eq. (38) in this limit. The above expression is probably quite suitable for analyzing the data in germanium, where the parabolic-band model is more appropriate. However, for InSb one would expect the previous expression, Eq. (37), for nonparabolic bands to be more suitable.

f. Magnetodispersion

In studying the dielectric properties of semiconductors and in measuring the index of refraction, a number of investigators have found that the index exhibits a noticeable increase with photon energy as the energy gap for a direct transition is approached. Such measurements have been made directly and also indirectly by means of interference fringes in thin samples. In this context, a most unusual experiment exhibiting this anomalous dispersion involved a GaAs diode operated just below laser threshold so that the spontaneous emission was amplified; within the broad spontaneous envelope many Fabry–Perot interference modes were dominantly displayed.[86] By the use of a high-resolution spectrometer, the spacing between adjacent modes $\Delta\lambda$ was measured, and from this the dispersion as a function of wavelength was obtained. In this case, it can be shown that the important quantity is

$$\eta - \lambda\frac{d\eta}{d\lambda} = \frac{\lambda^2}{2L\,\Delta\lambda}, \tag{40}$$

where L is the parallel-plate spacing. Since all quantities can be accurately measured, the dispersion is readily calculated from the above equation. In the case of GaAs diode, the radiation energy corresponds closely to the

[86] M. I. Nathan, A. B. Fowler, and G. Burns, *Phys. Rev. Letters* **11**, 152 (1963).

gap energy and the dispersion is reasonably approximated by the simple-band expression[87]

$$\left(\eta - \lambda \frac{d\eta}{d\lambda}\right) \approx \eta_0 + \frac{A}{32\pi\omega}(\omega_g - \omega)^{-1/2}, \tag{41}$$

where A has been previously defined—e.g., in connection with Eq. (4). This expression follows from the fact that below the energy gap the index η is given by

$$\eta \approx \eta_0 + \frac{A}{16\pi\omega^2}[2(\omega_g)^{1/2} - (\omega_g + \omega)^{1/2} - (\omega_g - \omega)^{1/2}], \tag{42}$$

where the last term in the brackets is the significant one, in the derivative, close to the energy gap. This result suggests a number of interesting magnetodispersion phenomena that can be observed in high magnetic fields, particularly in low energy-gap, low effective-mass materials, which exhibit large magnetooptical effects. One conceivable experiment involves the transmission of polarized light through a thin sample. Placing the magnetic field perpendicular to the sample surface, the radiation can be resolved into left and right circularly polarized waves with an index given by

$$\eta_\pm \approx \eta_0 - \frac{A\omega_c^*}{32\pi\omega^2}\sum_n \left[\frac{2}{[\omega_n \pm \gamma H]^{1/2}} - \frac{1}{[\omega_n + (\omega \pm \gamma H)]^{1/2}} - \frac{1}{[\omega_n - (\omega \pm \gamma H)]^{1/2}}\right], \tag{43}$$

so that the dispersion becomes

$$\eta_\pm - \lambda\frac{d\eta_\pm}{d\lambda} \approx \eta_0 + \frac{A\omega_c^*}{32\pi\omega}\left\{\frac{2}{\omega}\sum_n \left[\frac{1}{[\omega_n - (\omega \pm \gamma H)]^{1/2}} + \frac{1}{2[\omega_n - (\omega \pm \gamma H)]^{3/2}}\right]\right\}, \tag{44}$$

where again $\omega_n = \omega_g + (n + \frac{1}{2})\hbar\omega_c^*$. Similarly, when we consider propagation transverse to the magnetic field with **E** perpendicular to **H**, then

$$\eta_\perp \approx \eta_0 - \frac{A\omega_c^*}{32\pi\omega^2}\sum_n \left[\frac{2}{\omega_n^{1/2}} - \frac{1}{(\omega_n + \omega)^{1/2}} - \frac{1}{(\omega_n - \omega)^{1/2}}\right]. \tag{45}$$

If the wavelength is fixed, as the magnetic field is increased the index of refraction should decrease according to the expression[87]

[87] B. Lax, *in* "Physics of Semiconductors" (Proc. 7th Intern. Conf.), p. 253. Dunod, Paris, and Academic Press, New York, 1964.

$$\frac{\Delta\lambda}{\lambda} = \frac{1}{\eta}\frac{d\eta}{d\omega_c}\Delta\omega_c = -\frac{A}{\eta}\frac{\Delta\omega_c}{(\omega_g - \omega)^{1/2}}. \tag{46}$$

Thus, presently available magnetic fields will linearly shift the modes in absolute wavelength by $\Delta\lambda$, which is significantly observable in low-energy-gap materials such as indium arsenide and indium antimonide. This phenomenon has now been observed by Butler and Calawa.[87a]

II. Theory

3. Semiclassical Theory

Since the original theoretical work on the magnetooptical phenomena was carried out in connection with magnetoabsorption experiments, it would appear natural that the extension of the theory to dispersion phenomena be carried out by use of the Kramers–Kronig relations. Indeed, this was the approach that was first considered.[46] However, it is pedagogically more appealing to develop the theory through a classical approach and then to relate it to the quantum-mechanical treatment through the Kramers–Heisenberg relations. The interband magnetooptic phenomena can be approached classically by considering two simple bands as a collection of complementary bound states with energy states distributed over the bands according to the usual energy momentum relations

$$\begin{aligned} \mathscr{E}_c &= \frac{\hbar^2 k^2}{2m_c}, \\ \mathscr{E}_v &= -\mathscr{E}_g - \frac{\hbar^2 k^2}{2m_v} \end{aligned} \tag{47}$$

for the conduction and valence bands respectively. With this model, an electron in the valence band, under the influence of a d-c magnetic field, $\mathbf{H}$, and an electromagnetic field, can be described in terms of a classical oscillator by the equation of motion[51]

$$\frac{d^2\mathbf{r}_k}{dt^2} + \omega_k{}^2\mathbf{r}_k + \frac{1}{\tau_k}\frac{d\mathbf{r}_k}{dt} + \frac{d\mathbf{r}_k}{dt} \times \boldsymbol{\omega}_c = \frac{e\mathbf{E}}{m}e^{i\omega t}. \tag{48}$$

Here ω_k is the oscillator frequency, which corresponds to the energy associated with a particular interband transition; $\mathbf{r}_k$ is the displacement vector; $\boldsymbol{\omega}_c = e\mathbf{H}/mc$ is the cyclotron frequency; $\mathbf{E}$ is the electric vector of the incident radiation, and τ_k is the collision time. Solving Eq. (48) for the case where the d-c magnetic field is in the z direction, one obtains for cubic materials the complex conductivity tensor $\boldsymbol{\sigma}$ given by

[87a] J. F. Butler and A. R. Calawa, *Proc. Quantum Elect. Conf. San Juan, 1965*, p. 458. McGraw Hill, New York, 1966.

$$\boldsymbol{\sigma} = \begin{vmatrix} \sigma_{xx} & \sigma_{xy} & 0 \\ \sigma_{yx} & \sigma_{yy} & 0 \\ 0 & 0 & \sigma_{zz} \end{vmatrix}. \tag{49}$$

Here $\sigma_{xx} = \sigma_{yy} = \frac{1}{2}(\sigma_+ + \sigma_-)$, $\sigma_{xy} = -\sigma_{yx} = \frac{1}{2}(\sigma_+ - \sigma_-)$, and $\sigma_{zz} = \sigma_0$, the conductivity at zero magnetic field. The conductivities $\sigma_\pm$ are obtained by considering circularly polarized waves that follow from Maxwell's equations. Furthermore, from the relation above,

$$\sigma_\pm = \sigma_{xx} \mp i\sigma_{xy}. \tag{50}$$

The solution of Eq. (48) then yields

$$\sigma_\pm = \frac{e^2}{m} \sum_{\mathbf{k}} \frac{i\omega N_{\mathbf{k}}}{\omega_{\mathbf{k}}^2 - \omega^2 \mp \omega\omega_c + i\omega/\tau_{\mathbf{k}}}, \tag{51}$$

where $N_{\mathbf{k}}$ represents the number of transitions corresponding to the wave vector $\mathbf{k}$ and depends on the product of the oscillator strength $f_{\mathbf{kk}'}$ and the combined density of states. Equation (51) can be used to calculate the absorption coefficient $\alpha \equiv 2nk\omega/c$. This gives

$$\alpha = \frac{2nk\omega}{c} = \frac{\kappa}{\varepsilon c} \mathscr{R}\sigma_\pm, \tag{52}$$

where $\mathscr{R}$ refers to the real part, κ is the dielectric constant, and ε is the permittivity. For the dispersive effects, however, we can, as a first approximation, ignore the losses, since losses are mainly important only in investigating line shapes. Under these conditions, $(1/\tau_{\mathbf{k}}) = 0$ and Eq. (51) can be written in terms of the sum of transitions between any two states $\mathbf{k}$ and $\mathbf{k}'$ with oscillator strength $f_{\mathbf{kk}'}$ as

$$\sigma_\pm = \frac{ie^2\omega}{m} \sum_{\mathbf{k}} \sum_{\mathbf{k}'} \frac{f_{\mathbf{kk}'}}{(\omega_{\mathbf{kk}'}^2 - \omega^2 \mp 2\omega\gamma_{\mathbf{kk}'}H)}, \tag{53}$$

where, for a direct transition, $f_{\mathbf{kk}'} = (1/m\hbar)|P_{\mathbf{kk}'}|^2/\omega_{\mathbf{kk}'}$, $P_{\mathbf{kk}'} = \langle \mathbf{k}|\mathbf{p}\cdot\boldsymbol{\alpha}|\mathbf{k}'\rangle$, is the momentum matrix element, $\omega_{\mathbf{kk}'} = \omega_g + k^2/2\mu\hbar$, μ is the reduced effective mass of the two bands involved in the transition, and $2\gamma_{\mathbf{kk}'}H = \omega_c$. The substitution of $2\gamma_{\mathbf{kk}'}H$ for ω_c essentially takes into account the actual properties of the energy bands in the effective-mass model; here the levels involved in the transition are not split by the free-electron cyclotron frequency but by an amount that depends on the electron effective mass and the spin–orbit coupling. We represent this splitting phenomenologically by the parameter $\gamma_{\mathbf{kk}'}$. This phenomenological approach will be justified later by the more rigorous quantum treatment. In the physical situation involved

in experiments, $\omega \gg \gamma_{\mathbf{kk}'}H$; therefore, Eq. (53) can be expanded as

$$\sigma_{\pm} = \frac{ie^2\omega}{m^2\hbar}\sum_{\mathbf{k}}\sum_{\mathbf{k}'}\frac{|P_{\mathbf{kk}'}|^2}{\omega_{\mathbf{kk}'}(\omega_{\mathbf{kk}'}^2 - \omega^2)}\left[1 \mp \frac{2\omega\gamma_{\mathbf{kk}'}H}{\omega_{\mathbf{kk}'}^2 - \omega^2} + \cdots\right]. \tag{54}$$

From the relation for the index of refraction $\eta_{\pm}$

$$(\eta - ik)_{\pm}^2 = \kappa\left(1 + \frac{\sigma_{\pm}}{i\omega\varepsilon}\right) \tag{55}$$

the Faraday rotation per unit length θ, defined in Eq. (11), is given in the low-field limit by

$$\theta = \frac{\kappa^{1/2}e^2}{c\hbar m^2}\sum_{\mathbf{k}}\sum_{\mathbf{k}'}\frac{|P_{\mathbf{kk}'}|^2\gamma_{\mathbf{kk}'}H\omega^2}{\omega_{\mathbf{kk}'}(\omega_{\mathbf{kk}'}^2 - \omega^2)^2}. \tag{56}$$

The Voigt phase shift, defined in Eq. (17), is obtained by calculating $\eta_{\perp}$ and $\eta_{\parallel}$ from the appropriate conductivities in a manner similar to that of Eq. (54). The result, given in the low-field limit by an expansion like that of Eq. (53), is

$$\delta = -\frac{2\kappa^{1/2}e^2}{c\hbar m^2}\sum_{\mathbf{k}}\sum_{\mathbf{k}'}\frac{|P_{\mathbf{kk}'}|^2\gamma_{\mathbf{kk}'}^2H^2\omega^3}{\omega_{\mathbf{kk}'}(\omega_{\mathbf{kk}'}^2 - \omega^2)^3}. \tag{57}$$

The phenomenological $\gamma_{\mathbf{kk}'}$ used above can be expressed in terms of the band parameters for each set of magnetic levels, by a proper quantum treatment, even in materials with complex bands, such as Ge, GaAs, GaSb, InAs, and InSb. This problem has been considered by Roth[54] and also Boswarva and Lidiard.[59]

4. Quantum Theory

The results given in Eqs. (56) and (57) can be obtained quantum mechanically by using the Kramers–Heisenberg relations and time-dependent perturbation theory. In this manner, the diagonal and off-diagonal components, respectively, of the conductivity tensor can be shown to be[61]

$$\sigma_{ii} = -\frac{ie^2}{m^2\hbar}\sum_{\mathbf{k}}\sum_{\mathbf{k}'}\frac{1}{\omega_{\mathbf{kk}'}}\left\{\frac{P_{\mathbf{kk}'}^i P_{\mathbf{k}'\mathbf{k}}^i}{\omega + \omega_{\mathbf{kk}'}} + \frac{P_{\mathbf{kk}'}^i P_{\mathbf{k}'\mathbf{k}}^i}{\omega - \omega_{\mathbf{kk}'}}\right\}, \tag{58}$$

$$\sigma_{ij} = \frac{ie^2}{m^2\hbar\omega}\sum_{\mathbf{k}}\sum_{\mathbf{k}'}\left\{\frac{P_{\mathbf{kk}'}^i P_{\mathbf{k}'\mathbf{k}}^j}{\omega + \omega_{\mathbf{kk}'}} - \frac{P_{\mathbf{kk}'}^j P_{\mathbf{k}'\mathbf{k}}^i}{\omega - \omega_{\mathbf{kk}'}}\right\}. \tag{59}$$

Here the momentum matrix for transitions between states $\mathbf{k}$ and $\mathbf{k}'$, $P_{\mathbf{kk}'}$, includes both the magnetic field and the spin–orbit coupling—i.e.,

$$\mathbf{P} = \mathbf{p} + \frac{e\mathbf{A}}{c} + \frac{1}{2m^2c^2}(\mathbf{S} \times \nabla V). \tag{60}$$

From Eq. (59) and the definition of the Faraday rotation, Eq. (11), it can be shown that for propagation in the z direction

$$\theta = \frac{i\kappa^{1/2}e^2}{m^2\hbar\varepsilon c}\sum_{\mathbf{k}}\sum_{\mathbf{k}'}\frac{P^x_{\mathbf{k}\mathbf{k}'}P^y_{\mathbf{k}'\mathbf{k}}}{\omega^2_{\mathbf{k}\mathbf{k}'} - \omega^2}. \tag{61}$$

It is useful to transform Eq. (61) to a rotation frame of reference by introducing momentum operators corresponding to polarization vectors of two circularly polarized fields rotating in clockwise and counterclockwise directions—i.e., $P^{\pm} = P^x \pm iP^y$. Under these conditions it can be shown that

$$|P^+_{\mathbf{k}\mathbf{k}'}|^2 - |P^-_{\mathbf{k}\mathbf{k}'}|^2 = 2i(P^y_{\mathbf{k}\mathbf{k}'}P^x_{\mathbf{k}'\mathbf{k}} - P^x_{\mathbf{k}\mathbf{k}'}P^y_{\mathbf{k}'\mathbf{k}}). \tag{62}$$

Substituting Eq. (62) into Eq. (61) we then obtain

$$\theta = -\frac{\kappa^{1/2}e^2}{4m^2\hbar ec}\sum_{\mathbf{k}}\sum_{\mathbf{k}'}\left\{\frac{|P^+_{\mathbf{k}\mathbf{k}'}|^2}{(\omega^+_{\mathbf{k}\mathbf{k}'})^2 - \omega^2} - \frac{|P^-_{\mathbf{k}\mathbf{k}'}|^2}{(\omega^-_{\mathbf{k}\mathbf{k}'})^2 - \omega^2}\right\}. \tag{63}$$

In order to obtain more tractable expressions so as to be able to deal with a specific model for the energy bands, certain assumptions must be made. BHL[52] assumed that $P^+_{\mathbf{k}\mathbf{k}'} = P^-_{\mathbf{k}\mathbf{k}'}$ and then used the sum rule to obtain a correction term $-|P_{\mathbf{k}\mathbf{k}'}|^2[1/(\omega^+_{\mathbf{k}\mathbf{k}'})^2 - 1/(\omega^-_{\mathbf{k}\mathbf{k}'})^2]$ to derive

$$\theta_{\mathrm{BHL}} \sim \sum_{\mathbf{k}}\sum_{\mathbf{k}'}\omega^2|P_{\mathbf{k}\mathbf{k}'}|^2\left\{\frac{1}{(\omega^+_{\mathbf{k}\mathbf{k}'})^2[(\omega^+_{\mathbf{k}\mathbf{k}'})^2 - \omega^2]} - \frac{1}{(\omega^-_{\mathbf{k}\mathbf{k}'})^2[(\omega^-_{\mathbf{k}\mathbf{k}'})^2 - \omega^2]}\right\}. \tag{64}$$

HLN,[61] on the other hand, assumed $|P^+_{\mathbf{k}\mathbf{k}'}|/\omega^+_{\mathbf{k}\mathbf{k}'} = |P^-_{\mathbf{k}\mathbf{k}'}|/\omega^-_{\mathbf{k}\mathbf{k}} \equiv |P_{\mathbf{k}\mathbf{k}'}|/\omega_{\mathbf{k}\mathbf{k}'}$, where $\omega^{\pm}_{\mathbf{k}\mathbf{k}'} = \omega_{\mathbf{k}\mathbf{k}'} \pm \gamma H$. Under these conditions, Eq. (63) becomes

$$\theta_{\mathrm{HLN}} = -\frac{\kappa^{1/2}e^2}{4m^2\hbar\varepsilon c}\sum_{\mathbf{k}}\sum_{\mathbf{k}'}\left\{|P_{\mathbf{k}\mathbf{k}'}|^2\frac{\omega^2}{\omega^2_{\mathbf{k}\mathbf{k}'}}\left(\frac{1}{(\omega^+_{\mathbf{k}\mathbf{k}'})^2 - \omega^2} - \frac{1}{(\omega^-_{\mathbf{k}\mathbf{k}'})^2 - \omega^2}\right)\right\}. \tag{65}$$

In the limit of small $\mathbf{H}$, Eq. (65) of HLN reduces to the semiclassical result, Eq. (56) of KLN.[51] In an analogous manner, HLN develop an Ansatz for the Voigt effect that also leads to the classical result. In this case, the Voigt

phase shift δ is given by

$$\delta = \frac{\kappa^{1/2}e^2}{2m^2\hbar\varepsilon c}\sum_{\mathbf{k}}\sum_{\mathbf{k}'}\frac{1}{\omega_{\mathbf{kk}'}}\left\{\left(\frac{P^x_{\mathbf{kk}'}P^x_{\mathbf{k}'\mathbf{k}}}{\omega_{\mathbf{kk}'}+\omega}-\frac{P^x_{\mathbf{kk}'}P^x_{\mathbf{k}'\mathbf{k}}}{\omega_{\mathbf{kk}'}-\omega}\right)-\left(\frac{P^z_{\mathbf{kk}'}P^z_{\mathbf{k}'\mathbf{k}}}{\omega_{\mathbf{kk}'}+\omega}-\frac{P^z_{\mathbf{kk}'}P^z_{\mathbf{k}'\mathbf{k}}}{\omega_{\mathbf{kk}'}-\omega}\right)\right\}. \tag{66}$$

Again making transformations to a rotating coordinate system, as was previously done for θ, we obtain, after some manipulation,

$$\delta = \frac{\kappa^{1/2}e^2\omega}{4m^2\varepsilon c\hbar}\sum_{\mathbf{k}}\sum_{\mathbf{k}'}\left\{\frac{4|P^z_{\mathbf{kk}'}|^2}{\omega^z_{\mathbf{kk}'}[(\omega^z_{\mathbf{kk}'})^2-\omega^2]}-\frac{|P^+_{\mathbf{kk}'}|^2}{\omega^+_{\mathbf{kk}'}[(\omega^+_{\mathbf{kk}'})^2-\omega^2]}-\frac{|P^-_{\mathbf{kk}'}|^2}{\omega^-_{\mathbf{kk}'}[(\omega^-_{\mathbf{kk}'})^2-\omega^2]}\right\}. \tag{67}$$

Further simplification is obtained by assuming that

$$|P_{\mathbf{kk}'}|2/\omega_{\mathbf{kk}'} = 2|P^z_{\mathbf{kk}'}|2/\omega^z_{\mathbf{kk}'},$$

i.e., that the oscillator strength for z transitions equals that of an average of $\pm$ transitions, and $\omega^z_{\mathbf{kk}'} = \omega^2_{\mathbf{kk}'} - (\gamma H)^2$. This assumption, together with the relation $|P^z_{\mathbf{kk}'}|^2 = (\frac{1}{2})|P_{\mathbf{kk}'}|^2 \times [1 - (\frac{1}{2})(\gamma H/\omega_{\mathbf{kk}'})^2]$, obtained by making the expression with the braces of Eq. (67) go to zero for $\omega = 0$, allows considerable simplifications. In the low-frequency limit it is easily seen that Eq. (67) reduces to Eq. (57).

In order to calculate expressions for the observed phenomena, it is necessary to sum the contributions from all the electrons—i.e., to carry out all the summations from states $\mathbf{k}$ to $\mathbf{k}'$ in expressions such as Eqs. (53), (65), and (67). The procedure for these calculations is given in the following section.

a. Direct Transitions

(1) *Magnetoabsorption.* As is evident from Eq. (52), the calculation of the magnetoabsorption reduces essentially to the problem of calculating the conductivity $\sigma_\pm$ of Eq. (53). For low magnetic fields, where $\omega \gg \gamma H$, this expression can be rewritten in terms of the momentum matrix element, $P_{\mathbf{kk}'}$, as

$$\sigma_\pm = \frac{ie^2\omega}{m^2\hbar}\sum_{\mathbf{k}}\sum_{\mathbf{k}'}\frac{|P_{\mathbf{kk}'}|^2}{\omega_{\mathbf{kk}'}}\left\{\frac{1}{\omega^2_{\mathbf{kk}'}-(\omega\pm\gamma H)^2}\right\}. \tag{68}$$

Assuming a two simple-band model, we now replace one of the summations by an integral over p_z to obtain the contribution to the conductivity for a transition between a pair of Landau levels. Thus, using the transformation

$$\sum_{\mathbf{k}} \rightarrow \frac{1}{h^3}\int d^3p \rightarrow \sum_n \frac{\mu\omega_c^*}{4\pi^2\hbar^2}\int dp_z, \tag{69}$$

the conductivity becomes

$$\sigma_{\pm} = \frac{A\varepsilon c\omega_c^*}{2\kappa\omega}\sum_n \left\{\frac{2}{\omega_n^{1/2}} - \frac{1}{[\omega_n - (\omega \pm \gamma H)]^{1/2}} - \frac{1}{[\omega_n + (\omega \pm \gamma H)]^{1/2}}\right\}, \tag{70}$$

where $\omega_n = \omega_g + (n + \frac{1}{2})\omega_c^*$ and $\omega_c^* = eH/\mu c$. Equation (70) is useful in describing both absorption and dispersion phenomena. For example, it is obvious that in the frequency domain $\omega > \omega_n$ the middle term in the brackets becomes imaginary, which indicates that the medium is absorptive. From the above expression it is evident that the absorption is an oscillatory function of both the magnetic field and the frequency of the radiation. Neglecting γH, the spin splitting of the Landau levels, the absorption coefficient obtained by substituting Eq. (70) into Eq. (52) is

$$\alpha = \frac{A\omega_c^*}{2\omega}\sum_n \frac{1}{(\omega - \omega_n)^{1/2}}. \tag{71}$$

This expression, of course, gives a singularity at $\omega = \omega_n$, since the relaxation frequency $1/\tau_{\mathbf{k}}$ of Eq. (51) was set equal to zero. One can rederive Eq. (71) from Eq. (51) by retaining the scattering term, or alternately, one can modify Eq. (71) to include losses by letting $\omega \rightarrow (\omega - i/\tau)$. Using the latter technique, the real part of Eq. (71) becomes

$$\alpha = \frac{A\omega_c^*}{2\omega}\sqrt{\tau}\sum_n \left[\frac{(X_n^2 + 1)^{1/2} + X_n}{2(X_n^2 + 1)}\right]^{1/2}, \tag{72}$$

where $X_n = (\omega - \omega_n)\tau$. Using this expression, it is possible to obtain the variation of the transmission in a thin sample as a function of photon energy. Such a plot is shown in Fig. 2. This phenomenon has been observed in a number of semiconductors; experimental results will be discussed later.

(2) *Faraday Rotation.* Before integrating Eq. (65) to obtain the contribution to the Faraday rotation from a transition between two magnetic levels, it is mathematically convenient to expand this expression in partial fractions. The result is

$$\theta = \frac{\kappa^{1/2}e^2\omega}{8m^2\hbar c\varepsilon}\sum_{\mathbf{k}}\sum_{\mathbf{k}'}|P_{\mathbf{kk}'}|^2\left\{\frac{8\gamma H\omega}{[\omega^2-(\gamma H)^2]^2\omega_{\mathbf{kk}'}}\right.$$
$$-\frac{1}{(\omega-\gamma H)^2(\omega_{\mathbf{kk}'}-\omega+\gamma H)}+\frac{1}{(\omega+\gamma H)^2(\omega_{\mathbf{kk}'}+\omega+\gamma H)}$$
$$\left.+\frac{1}{(\omega+\gamma H)^2(\omega_{\mathbf{kk}'}-\omega-\gamma H)}-\frac{1}{(\omega-\gamma H)^2(\omega_{\mathbf{kk}'}+\omega-\gamma H)}\right\}. \tag{73}$$

This expression can now be integrated over p_z, using the transformation of Eq. (69), to obtain the rotation due to a single transition as

$$\theta = \frac{\kappa^{1/2}e^2\omega\omega_c^*(2\mu)^{3/2}}{128\pi m^2c\varepsilon\hbar^{5/2}}|P_{\mathbf{kk}}|^2\left\{\frac{8\gamma H\omega}{[\omega^2-(\gamma H)^2]^2\omega_n^{1/2}}\right.$$
$$-\frac{1}{(\omega-\gamma H)^2(\omega_n-\omega+\gamma H)^{1/2}}+\frac{1}{(\omega+\gamma H)^2(\omega_n+\omega+\gamma H)^{1/2}}$$
$$\left.+\frac{1}{(\omega+\gamma H)^2(\omega_n-\omega-\gamma H)^{1/2}}-\frac{1}{(\omega-\gamma H)^2(\omega_n+\omega-\gamma H)^{1/2}}\right\}, \tag{74}$$

where again $\omega_n = \omega_g + (n+\frac{1}{2})\omega_c^*$. This expression is useful in predicting the oscillatory behavior of the rotation; however, to obtain line shapes in the vicinity of a transition it is necessary to modify the terms with singularities by introducing damping. It is these terms with the singularities that will make the significant contributions near a Landau level. Letting $\omega \to (\omega - i/\tau)$ as before, making use of the fact that $\omega \gg \gamma H$ and keeping only the significant terms, we obtain, after some manipulation,

$$\theta = K\left\{\frac{1}{[(X-Y)^2+1]^{1/2}}\{[(X-Y)^2+1]^{1/2}+(X-Y)\}^{1/2}\right.$$
$$\left.-\frac{1}{[(X+Y)^2+1]^{1/2}}\{[(X+Y)^2+1]^{1/2}+(X+Y)\}^{1/2}\right\}, \tag{75}$$

where

$$K = \frac{\kappa^{1/2}e^2\omega_c^*\mu^{3/2}\tau^{1/2}}{64\pi m^2c\varepsilon\hbar^{5/2}\omega}|P_{\mathbf{kk}}|^2$$

$$X = (\omega_n - \omega)\tau,$$

and

$$Y = \gamma H\tau.$$

The line shapes predicted by Eq. (75) are given in Fig. 9. It is observed that the shape is considerably altered in going from low $\gamma H\tau$ to high $\gamma H\tau$. Also evident is the change in the sign of the rotation near the transition frequency. Equation (75) may be summed or integrated over all the Landau levels to obtain the background rotation. Since for most experimental arrangements this contribution is small relative to the single Landau singularities, the result is not given here.

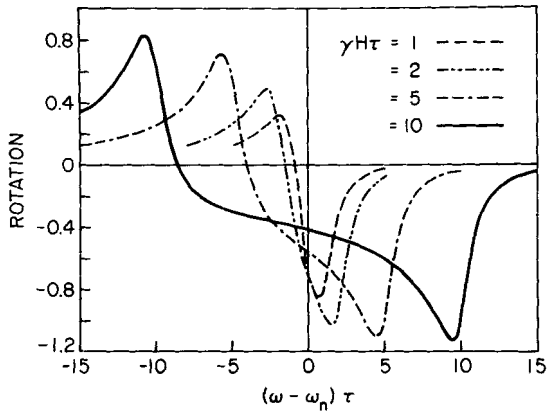


FIG. 9. Plot of the line shapes for the Faraday-rotation direct transition between a given pair of Landau levels as a function of frequency for different values of $\gamma H\tau$. The constant K of Eq. (75) has been normalized to unity. (After J. Halpern *et al.*[61])

(3) *Voigt Effect.* We can obtain an expression for the contribution to the Voigt shift of a direct transition between a pair of Landau levels by working with Eq. (67). In a manner analogous to the case of the Faraday rotation, Eq. (67) can be expanded in partial fractions and then integrated over p_z. The result is

$$\delta = -\frac{\kappa^{1/2}e^2(2\mu)^{3/2}\omega\omega_c^*}{128\pi m^2\hbar^{5/2}\varepsilon c}|P_{\mathbf{kk}}|^2\left\{\frac{-16\omega^2(\gamma H)^2}{[\omega^2-(\gamma H)^2][\omega^4-(\gamma H)^4]\omega_n^{1/2}}\right.$$
$$+\frac{1}{(\omega+\gamma H)^2(\omega_n+\omega+\gamma H)^{1/2}}+\frac{1}{(\omega+\gamma H)^2(\omega_n-\omega-\gamma H)^{1/2}}$$
$$+\frac{1}{(\omega-\gamma H)^2(\omega_n+\omega-\gamma H)^{1/2}}+\frac{1}{(\omega-\gamma H)^2(\omega_n-\omega+\gamma H)^{1/2}}$$
$$\left.-\frac{2}{\Omega^2(\omega_n+\Omega)^{1/2}}-\frac{2}{\Omega^2(\omega_n-\Omega)^{1/2}}\right\}. \tag{76}$$

Here $\Omega^2 \equiv \omega^2 + (\gamma H)^2$, and again the assumption has been made that $|P^+_{\mathbf{kk}'}|/\omega^+_{\mathbf{kk}'} = |P^-_{\mathbf{kk}'}|/\omega^-_{\mathbf{kk}'} \equiv |P_{\mathbf{kk}'}|/\omega_{\mathbf{kk}'}$ and $|P_{\mathbf{kk}'}|^2/\omega_{\mathbf{kk}'} = 2|P^z_{\mathbf{kk}'}|^2/\omega^z_{\mathbf{kk}'}$. Again, an expression can be developed for the line shape near a transition by taking $\omega \gg \gamma H$, considering only the singular terms and setting $\omega \to (\omega - i/\tau)$. The final expression is

$$\delta = K\left[\frac{2}{(X^2+1)^{1/2}}[(X^2+1)^{1/2}+X]^{1/2} - \frac{1}{[(X+Y)^2+1]^{1/2}}\{[(X+Y)^2+1]^{1/2}+(X+Y)\}^{1/2} - \frac{1}{[(X-Y)^2+1]^{1/2}}\{[(X-Y)^2+1]^{1/2}+(X-Y)\}^{1/2}\right], \quad (77)$$

where again $X = (\omega_n - \omega)\tau$ and $Y = \gamma H\tau$. The line shapes given in Eq. (77) for the Voigt phase shift arising from a direct transition between two Landau levels are plotted as a function of frequency for different values of $\gamma H\tau$ in Fig. 10. The background phase shift, obtained by summing Eq. (77) over n, is small at high magnetic fields or at low temperatures—i.e., large $\gamma H\tau$—compared to the individual Landau-level transitions, and it will therefore not be given in this chapter.

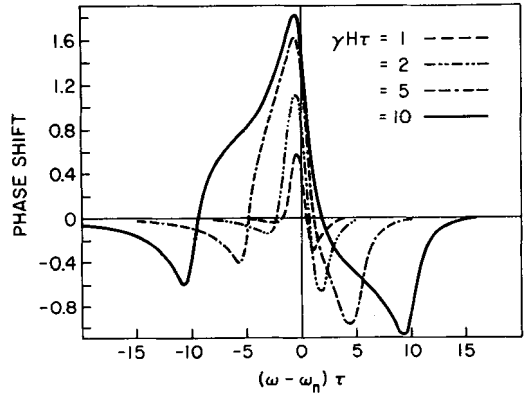


FIG. 10. Plot of the line shapes for the Voigt phase shift, direct transition, between a given pair of Landau levels as a function of frequency for different values of $\gamma H\tau$. The constant K of Eq. (77) has been normalized to unity. (After J. Halpern *et al.*[61])

b. Indirect Transitions

Until recently, the indirect transition had been observed most extensively in absorption studies at the band edge involving exciton and Landau

transitions. Recently, however, oscillatory effects have also been observed in the Faraday rotation in germanium. To date, the only solid that has exhibited any oscillatory effects in the indirect transition is germanium.[74,88,88a] Nevertheless, it is likely that in the future, as purer materials and higher magnetic fields become available, other solids, such as GaP and AgCl, may exhibit the same type of oscillatory behavior. Since the expressions for the complex index of refraction are rather complicated, we shall restrict ourselves to studying the absorption and dispersion separately. The complete derivations are given by HLN.[61]

(1) *Magnetoabsorption.* The original theory for absorption in the case of indirect transitions, which is due to Hall *et al.*,[72] involved second-order perturbation theory. The derivation presented here, however, will be based on the Kramers–Heisenberg formulation. The procedure in this calculation is basically the same as that given for the case of direct transitions. The conductivity $\sigma_{\pm}$ given in Eq. (68) is again expanded in partial fractions in order to expedite the summation of the contributions to the absorption from the various Landau transitions. For indirect transitions,

$$\omega_{\mathbf{k}\mathbf{k}'} = \omega_g + (n + \tfrac{1}{2})\omega_c + (n' + \tfrac{1}{2})\omega_v + \frac{p_{cz}^2}{2m_c\hbar} + \frac{p_{vz}^2}{2m_v\hbar} \pm \omega_{ph} \tag{78}$$

and

$$\sum_{\mathbf{k}}\sum_{\mathbf{k}'} \to \sum_{n}\sum_{n'}\iint \frac{m_c m_v \omega_c \omega_v}{16\pi^2\hbar^4}\, dp_{cz}\, dp_{vz},$$

so that the conductivity becomes

$$\sigma = \frac{\pi e^2(m_c m_v)}{h^5 m^2 \omega}\sum_{n}\sum_{n'}\iint |P_{\mathbf{k}\mathbf{k}'}|^2 \omega_c \omega_v\, dp_{cz}\, dp_{vz}$$

$$\times\left\{-\frac{2}{\left[\omega_g + (n+\tfrac{1}{2})\omega_c + (n'+\tfrac{1}{2})\omega_v + \dfrac{p_{cz}^2}{2m_c\hbar} + \dfrac{p_{vz}^2}{2m_v\hbar} \pm \omega_{ph}\right]}\right.$$

$$+\frac{1}{\left[\omega_g + \omega + (n+\tfrac{1}{2})\omega_c + (n'+\tfrac{1}{2})\omega_v + \dfrac{p_{cz}^2}{2m_c\hbar} + \dfrac{p_{vz}^2}{2m_v\hbar} \pm \omega_{ph}\right]}$$

$$\left.+\frac{1}{\left[\omega_g - \omega + (n+\tfrac{1}{2})\omega_c + (n'+\tfrac{1}{2})\omega_v + \dfrac{p_{cz}^2}{2m_c\hbar} + \dfrac{p_{vz}^2}{2m_v\hbar} \pm \omega_{ph}\right]}\right\}, \tag{79}$$

[88] J. Halpern, *Bull. Am. Phys. Soc.* **10**, 545 (1965).

[88a] J. Halpern and B. Lax, *J. Phys. Chem. Solids* **26**, 911 (1965).

where $\pm\omega_{ph}$ is the energy of the absorbed or emitted phonon. With these transformations the absorption, Eq. (52), can be derived from the $\sigma_{\pm}$ expression. Again, the principal contribution arises from the term with a singularity. Keeping only this term, the absorption α becomes

$$\alpha = D_{\pm} \sum_{n} \sum_{n'} \iint \frac{\omega_c \omega_v \, dp_{cz} \, dp_{vz}}{\omega_g - \omega + (n + \frac{1}{2})\omega_c + (n' + \frac{1}{2})\omega_v + \dfrac{p_{cz}^2}{2m_c\hbar} + \dfrac{p_{vz}^2}{2m_v\hbar} \pm \omega_{ph}}. \tag{80}$$

Here $D_{\pm}$ includes the density of states associated with the valence and conduction bands as well as the matrix element $P_{\mathbf{kk}'}$, which in this case is a product of a matrix element for allowed transitions to the intermediate state and a phonon matrix element from the intermediate to the final state. After one integration, Eq. (80) becomes

$$\alpha = D_{\pm} \sum_{n} \sum_{n'} \omega_c \omega_v \int_0^{p_{vz\,max}} \frac{dp_{vz}}{(\omega - \omega_{nn'} - p_{vz}^2/2m_v\hbar)^{1/2}}, \tag{81}$$

where $p_{vz\,max} = [2m_v\hbar(\omega - \omega_g)]^{1/2}$ and $\omega_{nn'} = \omega_g + (n + \frac{1}{2})\omega_c + (n' + \frac{1}{2})\omega_v \pm \omega_{ph}$. Integrating over p_{vz}, the z component of the valence band, the final result

$$\alpha = \text{const} \frac{\omega_c \omega_v}{2} \sum_{n} \sum_{n'} S(\omega - \omega_{nn'}) \tag{82}$$

is obtained, where $S(\omega - \omega_{nn'})$ is a unit step function. When losses are included by introducing a phenomenological relaxation time—i.e., $\omega \to (\omega - i/\tau)$—it can be shown that

$$a \sim \arctan(\omega - \omega_{nn'})\tau. \tag{83}$$

The experiments carried out in germanium at low temperatures did indeed exhibit such steps in the magnetoabsorption;[74] these experiments will be discussed in a later section.

(2) *Faraday Rotation.* The Faraday effect due to the indirect transition can be calculated in a similar manner as the absorption. Again, the terms of interest to us are those with the singularities. We can carry out the calculation by adding up the contributions to the rotation from a given Landau level in the valence band to one in the conduction. The final result including losses is

$$\theta = M\left\{\frac{-16Y}{Z}(\ln Z + \tfrac{1}{8}) - \ln[(X + Y)^2 + 1] + \ln[(X - Y)^2 + 1]\right\}, \tag{84}$$

where

$$X = (\omega_{nn'} - \omega)\tau, \qquad Y = \gamma H\tau, \qquad Z = \omega\tau,$$

and

$$M = \frac{\kappa^{1/2}e^2(m_c m_v)^{3/2}\omega_c\omega_v}{512\pi^3 m^2 c\varepsilon\hbar^4\omega}|P_{\mathbf{kk}'}|^2.$$

This expression gives line shapes such as shown in Fig. 11, which have been observed experimentally by Halpern.[88] As for the case of rotation due to the direct transition, the contributions to the background due to the indirect transition can be obtained by integrating θ over the Landau levels of the valence and conduction bands. Since the background is small compared to the rotation of a single Landau level, it will not be considered here.

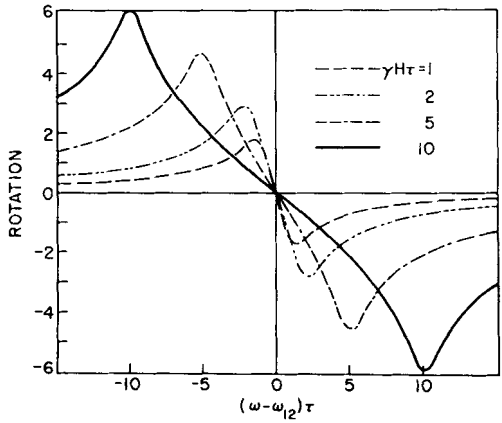


FIG. 11. Plot of the line shapes obtained for the Faraday rotation, indirect transition, between a given pair of Landau levels as a function of frequency for different values of $\gamma H\tau$. The constant M of Eq. (84) has been normalized to unity. (After J. Halpern *et al.*[61])

(3) *Voigt Effect.* Using the technique just described for magneto-absorption and the Faraday rotation, it can be shown that the contribution to the Voigt phase shift of the indirect transition, neglecting background, is

$$\delta = M\left\{-\left(\frac{Y^2}{2Z^2}\right)(1 + 64\ln Z) + \ln[(X + Y)^2 + 1] + \ln[(X - Y)^2 + 1] - 2\ln[X^2 + 1]\right\}, \tag{85}$$

where X, Y, Z, and M are as defined above; the theory indicates that the maximum value of the ratio of the Voigt effect to Faraday rotation occurs

when $\gamma H \sim 10$. At these high fields the Voigt phase shift is about twice the Faraday rotation and consequently should be observable. It has not been observed, however, chiefly because of the more complex experimental techniques required to make the former measurement.

c. Detailed Band Structure Treatment

In attempting to interpret the fine structure of the interband magnetoabsorption spectra or the related dispersion effects, such as the oscillatory Faraday rotation, it is important to consider the detailed properties of the degenerate valence bands. For germanium and silicon, the energy–momentum relations for the valence bands were derived by Dresselhaus *et al.*[89] and followed from the work of Shockley[90] and Herman.[91] This development led to the relations

$$\mathscr{E}(k) = -\frac{\hbar^2}{2m}\{Ak^2 \pm [B^2k^4 + C^2(k_x^2k_y^2 + k_y^2k_z^2 + k_x^2k_z^2)]^{1/2}\},$$
$$\mathscr{E}(k) = -\Delta - \frac{\hbar^2}{2m}Ak^2, \tag{86}$$

where the plus sign is associated with the light holes, the minus sign, with the heavy holes, and the second equation corresponds to the split-off band. Here the **k** coordinate system is coincident with the cubic axes, and Δ is the spin–orbit splitting; the constants A, B, and C were determined from the cyclotron-resonance experiments.

The quantized energy levels obtained when these complex bands are subjected to a magnetic field were developed by Luttinger and Kohn.[92] In general, their theory applies not only to germanium and silicon but also to most of the intermetallic compounds, such as InSb, as well. As an initial approach, the higher-order effects that give rise to nonparabolic bands as developed by Kane[93] for the valence bands of these materials are neglected. Luttinger and Kohn derived a general Hamiltonian for the degenerate bands in a magnetic field, which consisted of a system of coupled differential equations. This system of equations was subsequently treated in more detail by Luttinger,[94] who was able to obtain the most general Hamiltonian for the spin–orbit case with cubic symmetry. However, because of its complexity, it was not possible to solve this Hamiltonian and obtain a general solution to the problem. Consequently, approximate methods were

[89] G. Dresselhaus, A. Kip, and C. Kittel, *Phys. Rev.* **98**, 368 (1955).
[90] W. Shockley, *Phys. Rev.* **78**, 173 (1950).
[91] F. Herman, *Phys. Rev.* **88**, 1210 (1952).
[92] J. M. Luttinger and W. Kohn, *Phys. Rev.* **97**, 869 (1955).
[93] E. O. Kane, *J. Phys. Chem. Solids* **1**, 82 (1956).
[94] J. M. Luttinger, *Phys. Rev.* **102**, 1030 (1956).

developed that, although not completely general, were applicable to the actual physical situation in germanium and silicon, where a sixfold degenerate p-like valence band is split by spin–orbit interaction into a fourfold ($p_{3/2}$) and a twofold ($p_{1/2}$) degenerate band. Furthermore, since cyclotron resonance experiments have established that the fourfold degenerate level lies above the twofold one, the pertinent valence bands for the energies near the band edge can be described by a 4×4 effective-mass Hamiltonian. For this situation, Luttinger showed that the wave functions in the presence of a magnetic field can be represented by the linear combinations

$$\begin{aligned} \psi_{n,1} &= a_1 F_{n-2,l+2,0} u_{3/2} + a_2 F_{n,l,0} u_{-1/2}, \\ \psi_{n,2} &= b_1 F_{n-2,l+2,0} u_{1/2} + b_2 F_{n,l,0} u_{-3/2}, \end{aligned} \tag{87}$$

where the F's are wave functions for free electrons in a magnetic field, which have been given by Dingle,[95] and the u's are the four degenerate Bloch functions at $\mathbf{k} = 0$ belonging to the $J = \frac{3}{2}$ multiplet. These basis functions may be represented as

$$\begin{aligned} u_{3/2} &= \left(\frac{1}{\sqrt{2}}\right)[X + iY]\alpha, \\ u_{1/2} &= \left(\frac{1}{\sqrt{6}}\right)[(X + iY)\beta - 2Z\alpha], \\ u_{-1/2} &= \left(\frac{1}{\sqrt{6}}\right)[(X - iY)\alpha + 2Z\beta], \\ u_{-3/2} &= \left(\frac{1}{\sqrt{2}}\right)[X - iY]\beta, \end{aligned} \tag{88}$$

where the X, Y, and Z functions have the symmetry properties of the atomic p functions X, Y, Z under the operations of the tetrahedral group.

Luttinger obtained first-order explicit solutions for the energy bands for the configuration of pertinence in experimental investigations—i.e. the magnetic field in the (110) plane—by reducing the eigenvalue problem to the following set of linear equations for the a and b coefficients:

$$\begin{aligned} [(\gamma_1 + \gamma')(n - \tfrac{3}{2}) + \tfrac{3}{2}\kappa]a_1 - \sqrt{3}\gamma''[n(n-1)]^{1/2}a_2 &= \mathscr{E}_1 a_1 \\ n &= 2, 3, \ldots \\ -\sqrt{3}\gamma''[n(n-1)]^{1/2}a_1 + [(\gamma_1 - \gamma')(n + \tfrac{1}{2}) - \tfrac{1}{2}\kappa]a_2 &= \mathscr{E}_1 a_2 \\ n &= 0, 1, 2, \ldots \end{aligned} \tag{89}$$

[95] R. B. Dingle, *Proc. Roy. Soc.* (*London*) **A211**, 500 (1952).

and

$$\begin{gathered}[(\gamma_1 - \gamma')(n - \tfrac{3}{2}) + \tfrac{1}{2}\kappa]b_1 - \sqrt{3}\gamma''[n(n-1)]^{1/2}b_2 = \mathscr{E}_2 b_1 \\ n = 2, 3, \ldots \\ -\sqrt{3}\gamma''[n(n-1)]^{1/2}b_1 + [(\gamma_1 + \gamma')(n + \tfrac{1}{2}) - \tfrac{3}{2}\kappa]b_2 = \mathscr{E}_2 b_2 \\ n = 0, 1, 2, \ldots .\end{gathered} \tag{90}$$

The solutions of the above equations yield the characteristic energy values, in units of $\hbar eH/mc$,

$$\begin{aligned}\mathscr{E}(n, 1^{\pm}) = \gamma_1 n - (\tfrac{1}{2}\gamma_1 + \gamma' - \tfrac{1}{2}\kappa) \pm \{[\gamma' n - (\tfrac{1}{2}\gamma' + \gamma_1 - \kappa)]^2 \\ + 3\gamma''^2 n(n-1)\}^{1/2}\end{aligned} \tag{91}$$

and

$$\begin{aligned}\mathscr{E}(n, 2^{\pm}) = \gamma_1 n - (\tfrac{1}{2}\gamma_1 - \gamma' + \tfrac{1}{2}\kappa) \pm \{[\gamma' n + (-\tfrac{1}{2}\gamma' + \gamma_1 - \kappa)]^2 \\ + 3\gamma'' n(n-1)\}^{1/2},\end{aligned} \tag{92}$$

where θ is the angle between the magnetic field and the cubic axis,

$$s \equiv \sin\theta,\ c \equiv \cos\theta,\ \gamma' = \tfrac{1}{4}[(3c^2 - 1)^2\gamma_2 + 3s^2(3c^2 + 1)\gamma_3],$$

and

$$\gamma'' = \tfrac{1}{8}[(3 - 2c^2 + 3c^4)\gamma_2 + (5 + 2c^2 - 3c^4)\gamma_3],$$

κ is a constant that arises from the noncommutivity of the effective-mass operator, and the γ's are dimensionless parameters defined in terms of the energy surfaces of Eq. (86)—i.e.,

$$\gamma_1 = A, \qquad \gamma_2 = -\tfrac{1}{2}B, \qquad \gamma_3 = -\tfrac{1}{2}[B^2 + (C^2/3)]^{1/2}. \tag{93}$$

For the plus sign, which represents the light holes, $n = 0, 1, 2, \ldots$, and for the minus sign, which represents the heavy holes, $n = 2, 3, 4, \ldots$. These solutions, which are more general than those sometimes quoted in the literature,[16,59] take into account the anisotropy of the energy bands, which is rather important in determining the band parameters from magneto-optical data. The solutions, however, ignore a small correction term due to spin–orbit splitting, which in such materials as InSb with very small energy gaps introduces higher order terms. Nevertheless, in a semi-quantitative way, the above eigenvalues provide a good approximation for determining the band parameters of many of these semiconductors and in accounting approximately for the dominant features of the magneto-optical spectrum, namely, the position of the lines and the identification of the strong transitions by the appropriate calculation of the corresponding

matrix elements in terms of the a and b coefficients. This type of analysis has been carried out by various workers in an effort to identify spectra with transitions in magnetoabsorption and Faraday-rotation experiments. In this connection, Goodman[96] has evaluated the valence-band ladders for the three principal crystallographic directions in germanium, and his results are shown in Figs. 12, 13, and 14. Although the particular parameters in these figures are those of germanium, these also represent a good approximation for GaSb, but not for other intermetallic materials such as InSb, InAs, and GaAs. However, of the latter materials, enough experimental data to justify such a calculation exist only in InSb.

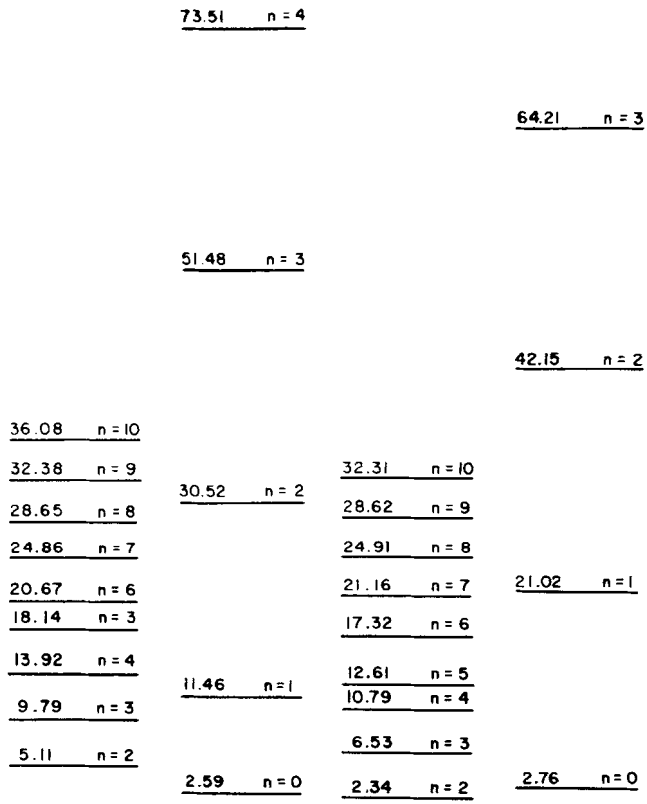


FIG. 12. Energy-level diagram for the valence bands of germanium for **H** in the (100) direction (in units of eH/mc). (After R. R. Goodman.[96])

[96] R. R. Goodman, Ph.D. Thesis, University of Michigan (1958).

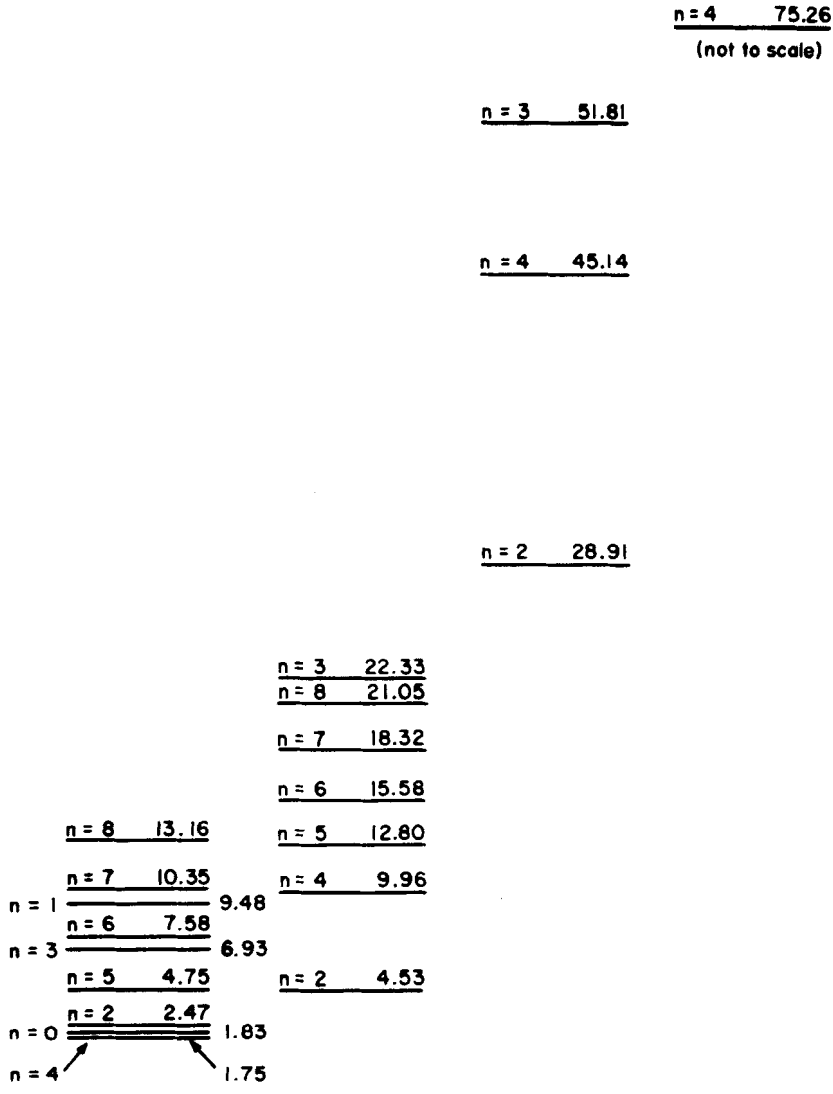


FIG. 13. Energy-level diagram for the valence bands of germanium for **H** in the (111) direction (in units of eH/mc). (After R. R. Goodman.[96])

The Faraday rotation spectrum in semiconductors due to interband transitions has been analyzed by Boswarva and Lidiard[59] by neglecting the warping of the valence bands. They obtain the selection rules by evaluating the matrix elements of the momentum P between the Bloch conduction band at $k = 0$, with wave functions $u_{c,m_j}(\mathbf{r})\, F_{n,l,k_z}(\mathbf{r})$, where u_c includes

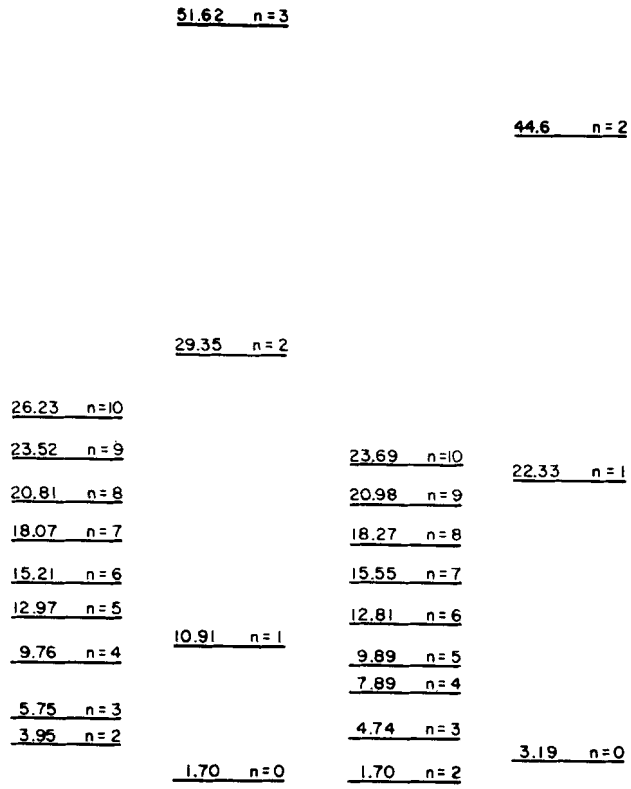


FIG. 14. Energy-level diagram for the valence bands of germanium for **H** in the (110) direction (in units of eH/mc). (After R. R. Goodman.[96])

spin, which may be up ($m_j = +\frac{1}{2}$) or down ($m_j = -\frac{1}{2}$), and F is again the wave function for a free electron in a magnetic field located in the z direction, and the degenerate valence band with wave functions $\psi_{n,1}$ and $\psi_{n,2}$, which are given in Eqs. (87) and (88). The only nonzero elements are

$$\begin{aligned}
\langle u_{c,\pm 1/2}|P_z|u_{\pm 1/2}\rangle &\equiv \pm P_{cv}, \\
\langle u_{c,\pm 1/2}|P_x|u_{\pm 3/2}\rangle &= -\tfrac{1}{2}\sqrt{3}P_{cv}, \\
\langle u_{c,\pm 1/2}|iP_y|u_{\pm 3/2}\rangle &= \pm\tfrac{1}{2}\sqrt{3}P_{cv}, \\
\langle u_{c,\pm 1/2}|P_x|u_{\mp 1/2}\rangle &= -\tfrac{1}{2}P_{cv}, \\
\langle u_{c,\pm 1/2}|iP_y|u_{\mp 1/2}\rangle &= \mp\tfrac{1}{2}P_{cv}.
\end{aligned} \tag{94}$$

Thus the only nonzero matrix elements of $P(\pm) \equiv P_x \pm iP_y$ are

$$\text{and} \qquad \begin{aligned} \langle u_{c,\pm 1/2}|P(\mp)|u_{\pm 3/2}\rangle &= -\sqrt{3}P_{cv} \\ \langle u_{c,\pm 1/2}|P(\pm)|u_{\mp 1/2}\rangle &= -P_{cv}, \end{aligned} \tag{95}$$

confirming that the selection rule is $\Delta M = \pm 1$. Furthermore, the orthogonality of the F functions of differing quantum numbers, n, l, and k_z results in $\Delta k_z = 0$, while the mixing of the two F functions $\psi_{n,1}$ and $\psi_{n,2}$ in the degenerate valence band allows the transitions $\Delta n = 0$ or -2 and $\Delta l = 0$ or $+2$. The allowed transitions and corresponding matrix elements summarized in Table I were worked out by Roth.[17] A study of Table I indicates that for $\mathbf{E} \perp \mathbf{H}$ the light-hole $\Delta n = -2$ transition is most intense, whereas for the heavy hole the $\Delta n = 0$ and -2 transitions are of equal intensity. In addition, if the density-of-states factor is taken into account, the heavy hole is favored by an additional factor of 1.4. Consequently, when these factors are all considered, the dominant light- and heavy-hole transitions should be of comparable strength. The transitions for $\mathbf{E} \perp \mathbf{H}$ are also those of importance in Faraday rotation. We have two sets of transitions, depending on sense of polarization. Indeed, the analysis of Boswarva and Lidiard is consistent with these results.

TABLE I

STATISTICAL WEIGHTS FOR VARIOUS ALLOWED DIRECT TRANSITIONS IN GERMANIUM[a]

Transition	$\mathbf{E} \parallel \mathbf{H}$	$\mathbf{E} \perp \mathbf{H}$		
		Plane polarization	+ Circular polarization	− Circular polarization
$\bar{a}_{\pm}\alpha n'$	0	$\frac{3}{4}a_1^2$	$\frac{3}{2}a_1^2$	0
$a_{\pm}\alpha n'$	0	$\frac{1}{4}a_2^2$	0	$\frac{1}{2}a_2^2$
$a_{\pm}\beta n'$	a_2^2	0	0	0
$a_{\pm}\alpha n'$	b_1^2	0	0	0
$b_{\pm}\beta n'$	0	$\frac{1}{4}b_1^2$	$\frac{1}{2}b_1^2$	0
$b_{\pm}\beta n'$	0	$\frac{3}{4}b_2^2$	0	$\frac{3}{2}b_2^2$

[a] The transitions are labeled by the valence-band set $a_{\pm}$, $b_{\pm}$, where + and − refer to light and heavy holes, by the spin for the conduction band α or β, and by the quantum number n' for the conduction band. $\Delta n = -2$ transitions have bars over a or b; $\Delta n = 0$ transitions do not. Thus $\bar{a}_{+}\alpha n'$ represents the transition from the $n' + 2$ light-hole level of set a to the n' level of the spin-up conduction band. To give orders of magnitude for high quantum numbers, from Eqs. (89) and (90), we have $a_1^2 \approx 3a_2^2$ and $b_2^2 \approx 3b_1^2$ for the light hole, with the opposite relations holding for the heavy hole. The density-of-states factor $[m_c m_v/(m_c + m_v)]^{1/2}$ is not included in the above statistical weights. [L. M. Roth, B. Lax, and S. Zwerdling, *Phys. Rev.* **114**, 90 (1959)].

Boswarva[60] has extended his theoretical treatment of interband Faraday rotation to the region of the absorption edge by introducing a phenomenological relaxation time. He has calculated the shape of the Faraday-rotation peaks as well as the relative intensities of the transitions and the positions in the energy spectrum. Using the parameters from cyclotron resonance[97] as well as from magnetoabsorption,[98] he finds that the numerical values of the relative intensities in InSb are close to those in germanium, although the relative positions in energy of the lines are quite different.

One of the important problems in the theory for Faraday rotation in semiconductors has been the question of predicting the sign of the rotation due to the direct interband transition below the energy gap. Two such calculations, one by Roth[54] and the other by Boswarva and Lidiard,[59] have taken the detailed band structure of the valence band into account. The calculation by Roth was based on the problem of Bloch electrons in a magnetic field, in which the conductivity tensor is expanded to first order in the magnetic field. Her final result for rotation between two parabolic bands is an expression of the form

$$\theta = \frac{e^3 H}{8\eta c^2 (2m\mathscr{E}_g)^{1/2}} \left(\frac{\mu}{m}\right)^{3/2} (g_c g_c' - g_v g_v') F_1\left(\frac{\omega}{\mathscr{E}_g}\right), \tag{96}$$

where

$$F_1(x) \equiv \frac{1}{x}\left[\frac{1}{(1-x)^{1/2}} - \frac{1}{(1+x)^{1/2}}\right] - \frac{4}{x^2}[2 - (1-x)^{1/2} - (1+x)^{1/2}]. \tag{97}$$

Here the primed and unprimed g_c and g_v refer to the g factors of the conduction and valence bands, respectively, and ω is in energy units. The function $F_1(x)$ is the same as that derived by KLN[51] from semiclassical arguments. In general, the above function could be replaced by one in which the integrals are not carried out to the limit of infinite energies for the band but truncated at a suitable value. The equivalent of this approximation has been carried out by Roth for a model of two simple interacting bands, an s-like conduction band and a p-like valence band, in which the spin contribution to the g factor was neglected. The function thus obtained gave an expression for the Faraday rotation of the form

$$\theta = -\frac{(\sqrt{2}-1)e^3 H}{6\eta c^2} \frac{P}{m\mathscr{E}_g} F\left(\frac{\omega}{\mathscr{E}_g}\right), \tag{98}$$

[97] D. M. S. Bagguley and R. A. Stradling, *Phys. Letters* **6**, 143 (1963).

[98] S. Zwerdling, W. H. Kleiner, and J. P. Theriault, *Proc. Intern. Conf. Phys. Semicond., Exeter, 1962* p. 455. Inst. of Phys. and Phys. Soc., London, 1962.

where P is the matrix element between the two bands and

$$F(x) = \frac{2}{\pi}\frac{1}{(\sqrt{2}-1)}\left\{\frac{2}{x(1-x^2)^{1/2}}\tan^{-1}\frac{x}{(1-x^2)^{1/2}} - \frac{1}{[x(1-x)]^{1/2}}\tan^{-1}\left(\frac{x}{1-x}\right)^{1/2} - \frac{1}{[x(1+x)]^{1/2}}\ln[(1+x)^{1/2}+x^{1/2}]\right\}. \tag{99}$$

The theoretical functions $F(x)$ and $F_1(x)$, along with the corresponding function $F_2(x)$ of Boswarva *et al.*,[52] are shown in Fig. 15. In essence, the difference between these various functions is not substantial, so that any of these expansions is quite useful.

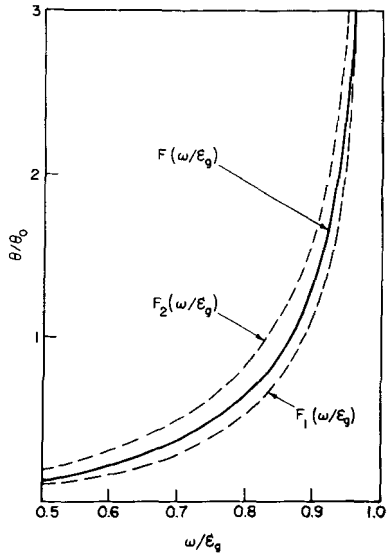


FIG. 15. Comparison of functions F_1, F_2, and F. (After L. M. Roth.[54])

Perhaps the principal criticism of all three treatments is that the calculations have been based on the assumption that the transitions involved are between free Landau states. That the above simple approximation is so useful is surprising, in view of the established fact that bound or exciton transitions do contribute to the rotation.

Roth has also evaluated the g factor for the various semiconductors by considering a model that is applicable to germanium and III–V inter-

metallic compounds, namely a spin–orbit valence band. She arrives at an expression for the Faraday rotation given by

$$\theta = \theta_0 H F_1\left(\frac{\omega}{\mathscr{E}_g}\right) = \frac{e^3 H P^2}{48c^2\eta m^3}\left(\frac{2}{\mathscr{E}_g}\right)^{3/2}(\mu_h^{3/2} + \mu_l^{3/2})g_{eff}F_1\left(\frac{\omega}{\mathscr{E}_g}\right). \quad (100)$$

Here g_{eff} takes on a form that is associated with band parameters of the specific energy bands involved in the transitions, namely,

$$g_{eff} = \frac{-(g_c + 10\kappa) + 10\bar{\gamma}(r^3 - 1)}{(r^3 + 1)} - \frac{4(\gamma_1 - \bar{\gamma} - \kappa)(r^3 - 1)(r - 1)}{(r^3 + 1)(r + 1)}, \quad (101)$$

where $r \equiv (\mu_h/\mu_l)^{1/2} > 1$, μ_h and μ_l being the reduced masses involving the conduction band and the heavy- and light-hole bands, respectively. The parameter $\bar{\gamma}$, a particular average of γ_2 and γ_3, equals $\bar{\gamma} = (2\gamma_2 + 3\gamma_3)/5$; and

$$\begin{aligned} \gamma_1 &= (f + 2g + 2h_1 - 3)/3, \\ \bar{\gamma} &= (5f + g + h_1)/30, \\ \kappa &= (f - g - h_1 - 2)/6, \\ P^2 &= m\mathscr{E}_g(f/2), \\ \alpha_c &= 1 + f[(3\mathscr{E}_g + 2\Delta)/3(\mathscr{E}_g + \Delta)], \end{aligned} \quad (102)$$

and

$$g_c = 2 - f[2\Delta/3(\mathscr{E}_g + \Delta)].$$

Here α_c and $(\gamma_1 \pm 2\bar{\gamma})$ are the reciprocal effective masses of the conduction and valence bands, respectively; $f, g, h_1 > 0$ are the magnitudes of F, G, and H_1 of Dresselhaus *et al.*[89] in units of $(\frac{1}{2})m$ and $H_2 = 0$. The effective mass and g factor of the conduction band, $1/\alpha_c$ and g_c, respectively, were calculated on the assumption that this band interacts only with the two degenerate valence bands and the split-off valence.

Substituting the appropriate numerical values obtained from the literature into the above expressions, one obtains

$$\theta_0 = \left(5.17\frac{f}{\eta}\sqrt{\mathscr{E}_g}\right)\left[\left(\frac{\mu_h}{m}\right)^{3/2} + \left(\frac{\mu_l}{m}\right)^{3/2}\right]g_{eff} \quad (103)$$

in deg/cm kG, when $\mathscr{E}_g$ is expressed in eV. This expression yielded values in reasonable agreement with experiment. The fit of the function $F_1(\omega/\mathscr{E}_g)$ to the experimental data is shown in Fig. 16.

Boswarva and Lidiard[59] also obtained expressions for the Faraday rotation in terms of the parameters of the valence bands; however, in their treatment the individual transitions are considered explicitly with no

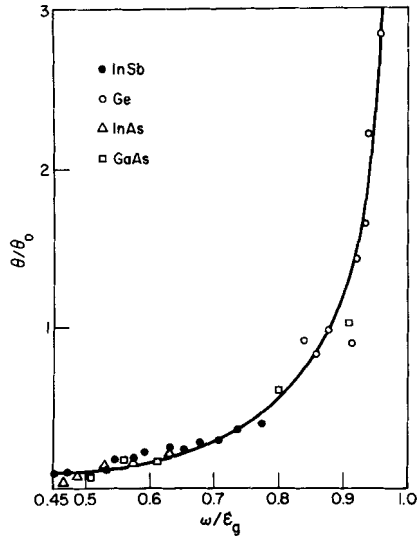


FIG. 16. Room-temperature experimental data fit to the function $F_1(\omega/\mathscr{E}_g)$. (After L. M. Roth.[54])

adjustable parameters. In contrast to the simplified models, they obtain contributions from light and heavy holes that are linear in magnetic field, in terms of the Dingle[95] wave functions for free electrons in a magnetic field, with the appropriate expressions for the matrix elements associated with the four possible transitions assigned to a given magnetic quantum number n. In addition, they take into account the field-dependent terms in the matrix elements to first order in magnetic field. Essentially, it was this term that had been ignored in their original calculation.[52]

Boswarva and Lidiard have used this theory to calculate the rotations in germanium, GaAs, GaSb, InAs, and InSb. They find that the interband Faraday rotation is determined principally by a competing process between virtual transitions from the heavy valence states, which give a positive contribution, and transitions from the light valence states, which give a negative contribution. For the above compounds, the contribution of the split-off valence band can be ignored. A small energy gap and light valence-band mass favor the light–valence-state negative contribution, whereas large energy gaps and heavy hole masses emphasize the heavy-hole positive rotation. For example, in InSb which has a small energy gap, $|\theta^+| > \theta^-$, whereas in GaAs, with a relatively large gap, $|\theta^+| < \theta^-$. In germanium, these two quantities are nearly equal, so that there should be a relatively small interband contribution. At long wavelengths the heavy hole dominates

and the net rotation is positive; however, as the band edge is approached, the singularities associated with the light-hole transition, which lie at lower energies than the heavy-hole states, cancel out the heavy-hole contribution, so that the sign of the rotation is determined by the electron g factor, g_c. The quantitative agreement between theory and experiment is not too good, as shown in Fig. 17 for germanium. In GaAs, in disagreement with observation for intrinsic material,[98a] the positive contribution apparently is more dominant and remains positive close to the band edge, since g_c is positive. InSb, on the other hand, has a large negative g_c, and near the band edge it dominates the rotation.

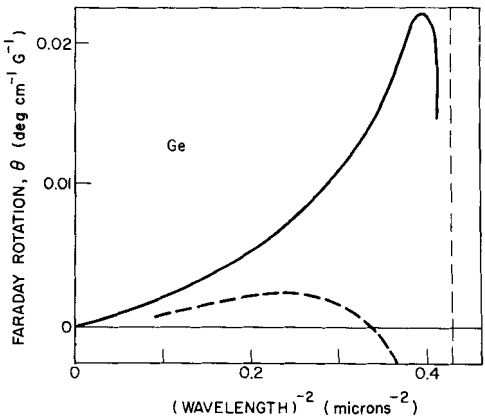


FIG. 17. The Faraday rotation of Ge as a function of the inverse square of the wavelength (room temperature). The solid line is the calculated curve and the dashed line represents the experimental results of Ref. 64. The vertical dashed line is drawn at the wavelength corresponding to the energy gap at the zone center. (After I. M. Boswarva and A. B. Lidiard.[59])

III. Experiments

5. GERMANIUM

a. Magnetoabsorption

(1) *Direct Transitions.* Although germanium is not an intermetallic compound, it is felt that a discussion of this semiconductor is appropriate at this time, since historically germanium has served as a model for our understanding of the physics of semiconductors. The initial interband magnetooptical experiments[15] were performed at room temperature on thin single crystal germanium samples, of the order of 10 microns or less, using

[98a]H. Piller, *in* "Physics of Semiconductors" (Proc. 7th Intern. Conf.), p. 297. Dunod, Paris, and Academic Press, New York, 1964.

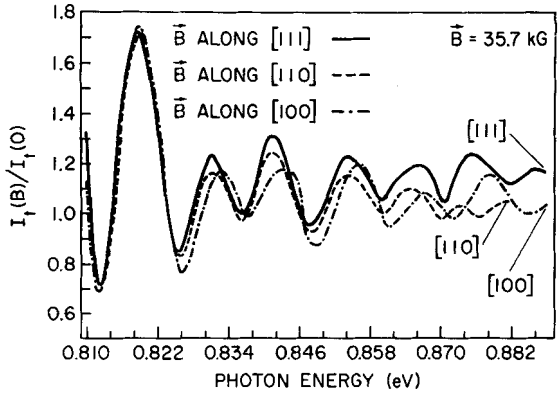


FIG. 18. Anisotropy of the oscillatory magnetoabsorption of the direct transition in germanium at room temperature (B = 35.7 kG, along the directions indicated). (After S. Zwerdling *et al.*[15])

prism spectrometers; they exhibited oscillatory effects such as shown in Fig. 18. These experiments, which were observed using an electromagnet and unpolarized light, with the direction of the Poynting vector perpendicular to the magnetic field, indicated anisotropy in the absorption when the (110) face of the sample was rotated relative to the magnetic field. This anisotropy was attributed to the properties of the valence band, since it was known that the direct transition in germanium involved excitation of electrons from the Γ_{25}^{+} valence band to the spherical Γ_2^{-} conduction band. By plotting the position of absorption maxima or transmission minima as a function of magnetic field at a fixed temperature, straight lines such as shown in Fig. 19 were obtained. When extrapolated to zero field, these lines converged to a point yielding an energy gap $\mathscr{E}_g$ = 0.803 eV. Furthermore, from the slope of the lowest line or from the difference at a value of fixed magnetic field of the energies between two adjacent lines, the effective mass of the higher conduction band was determined for the first time. This experimental determination, $m_c = 0.036m$, was in good agreement with theoretical predictions of Dresselhaus *et al.*[89] and Dumke.[99] The theoretical interpretation of these experiments was made in terms of the Kohn–Luttinger ladder for the magnetic levels of the valence bands. A simple evaluation of the allowed transitions between this ladder and the levels of the conduction band predicted a multiplicity of lines, which could not be observed at room temperature or with a prism spectrometer. Consequently, these experiments were repeated at low temperatures with a high-resolution grating instrument. The experimental results are compared with the predicted fine

[99] W. P. Dumke, *Phys. Rev.* **105**, 139 (1957).

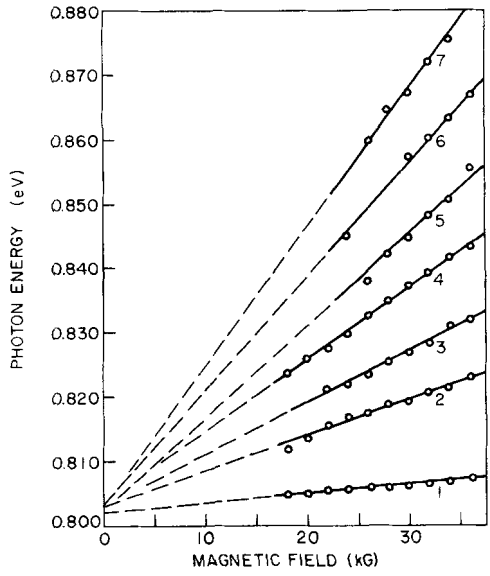


FIG. 19. Energy values of transmission minima versus magnetic field for successive transitions of electrons between Landau levels of valence and conduction bands in germanium. Convergence of lines yields energy-gap value $\mathscr{E}_g = 0.803 \pm 0.001$ eV at room temperature. (After S. Zwerdling and B. Lax.[14])

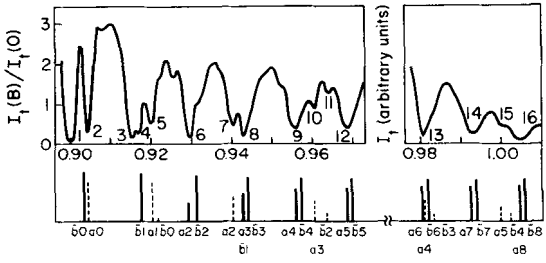


FIG. 20. Comparison of theoretical spectrum with experimental data for germanium at 4.2°K with high-resolution grating spectrometer and a field of 38.9 kG (**E** ∥ **H**). (After L. M. Roth *et al.*[17])

structure in Fig. 20, for a magnetic field of 38.9 kG, where a rough correlation is observed between the predicted and observed intensities for all lines except the two lowest, which persisted down to zero field and were therefore attributed to the direct exciton.[17] The two-component nature of the exciton

was subsequently recognized as due to the strain, resulting from the mounting of the sample on a glass substrate, which split the valence bands. In studying the exciton by means of magnetoabsorption, as the magnetic field increases, the lowest exciton line broadens and the structure of the splitting due to the magnetic field is not observed; the magnetic field merely produces broadening, as shown in Fig. 21. Similar experiments were also carried out by Edwards and Lazazzera,[100] using unstrained samples. They demonstrated that at high magnetic fields the observed Landau transitions were essentially those to higher bound exciton states, which behaved linearly with magnetic field in accordance with the theory of Elliott and Loudon.[101] The Coulomb attraction associated with the excitons essentially depresses the Landau ladder, so that the lines converge at a point below the exciton-series limit or the true energy gap. Consequently, the best value of the energy gap is obtained by taking the zero-field exciton level and adding to it the exciton binding energy, which was calculated by means of the variation technique by Roth and Lax,[74] and independently by McLean,[103] as $\mathscr{E}_{ex} = 0.0015$ eV. In this manner one obtains an energy gap at 77°K, $\mathscr{E}_g = 0.8833$ eV.

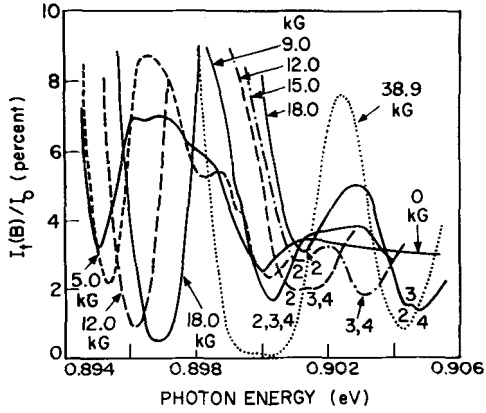


FIG. 21. The Zeeman effect of the direct exciton in germanium at 1.5°K for different values of magnetic field. The first exciton line exhibits the onset of twofold splitting at 38.9 kG. (After S. Zwerdling *et al.*[74])

[100] D. F. Edwards and V. J. Lazazzera, *Proc. Intern. Conf. Semicond. Phys., Prague, 1960* p. 355. Czech. Acad. Sci., Prague, and Academic Press, New York, 1961.
[101] R. J. Elliott and R. Loudon, *J. Phys. Chem. Solids* **8**, 382 (1959).
[102] L. M. Roth and B. Lax, *Phys. Rev. Letters* **3**, 217 (1959).
[103] T. P. McLean, *Progr. Semicond.* **5**, 55 (1960).

In spite of the interpretation of the lines at high magnetic fields as due to bound excitons, however, in the linear region the spacings of the magnetic levels for the higher quantum states are essentially those of the free electron Landau levels. Consequently, the quantitative interpretation of Roth, Lax, and Zwerdling, which gave a value for the 4°K effective mass at the bottom of the conduction band $m_c = 0.036m$, was substantially correct. A small nonparabolic correction at high energies and large magnetic fields was found for this band.

(2) *Indirect Transitions.* As has already been discussed, the energy dependence of the absorption at a fixed value of magnetic field for the indirect, or phonon-assisted interband transition was predicted theoretically to be a series of steps rather than oscillations. Experiments to observe this effect were carried out by Zwerdling *et al.*[74] on samples 0.5 to 1 cm thick in a transverse magnetic field; the line shapes were found to be in agreement with the theoretical predictions as shown in Fig. 22, where the first strong indirect edge is due to the exciton. A study of these transitions as a function of magnetic field gave a value for the energy at zero field of 0.771 eV at liquid-helium temperatures, which corresponds to the indirect energy gap plus the energy of the emitted phonon. After subtracting the energy of the longitudinal acoustical phonon, the indirect energy gap was found to be $\mathscr{E}_g = 0.744$ eV. In addition, a mean energy of the exciton line extrapolated to a value well below that of the free Landau levels. In this case, the interpretation of the exciton transition as distinct from the free Landau levels is justified, since such a second-order transition does not necessarily favor a bound state, except for the lowest energy.

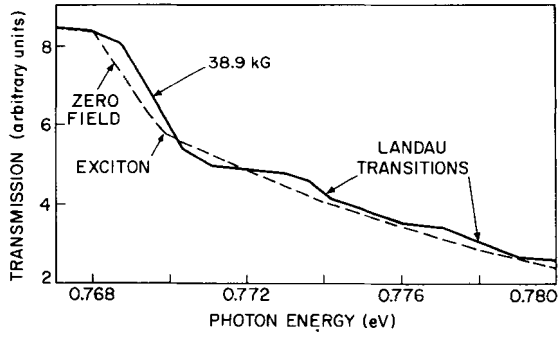


FIG. 22. The magnetoabsorption spectrum of the indirect transition in germanium at 1.5°K, showing the exciton absorption edge at zero field and the development of the "staircase" absorption edges for the Landau transitions at higher energies at 38.9 kG. (After S. Zwerdling *et al.*[74])

Upon further examination of the exciton line with a high-resolution grating instrument, a zero-field splitting of 1.1×10^{-3} eV was found, which was in good agreement with the theoretical results of Roth and Lax[74] and also McLean.[103] The exciton lines were also studied as a function of magnetic field. The observed fine structure due to the Zeeman splitting of the lines, shown in Fig. 23, was analyzed by Button *et al.*[104] in terms of the

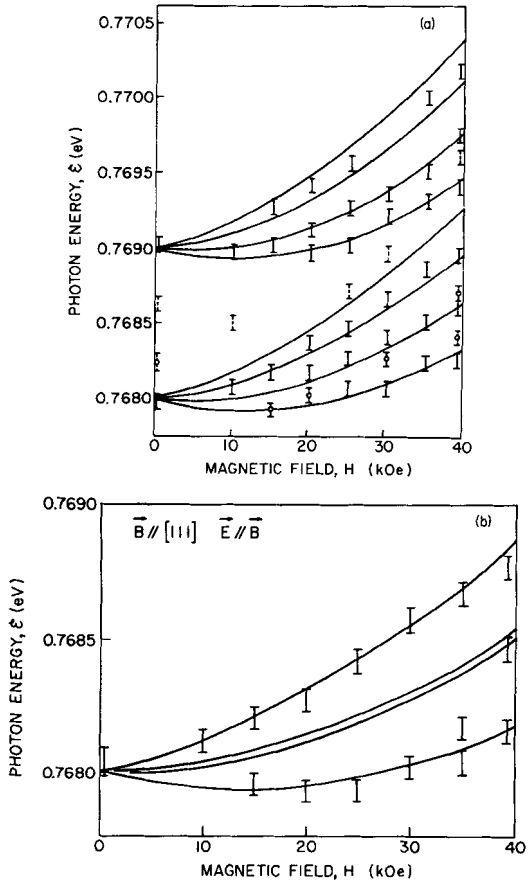


FIG. 23. (a) Zeeman spectrum of the indirect exciton in germanium for $\mathbf{H} \parallel [100]$, $\mathbf{E} \parallel \mathbf{H}$ at 1.5°K. The "bars" represent experimental points. The solid lines are the theoretical curves obtained from the spin Hamiltonian. (b) The Zeeman spectrum for $\mathbf{H} \parallel [111]$, $\mathbf{E} \parallel \mathbf{H}$. The theoretical curves using the above parameters demonstrate agreement with experimental data. (After K. J. Button *et al.*[104])

[104] K. J. Button, L. M. Roth, W. H. Kleiner, S. Zwerdling, and B. Lax, *Phys. Rev. Letters* **2**, 161 (1959).

Roth and Kleiner spin Hamiltonian $\mathscr{H}$

$$\mathscr{H} = D\left(J_z^2 - \frac{J^2}{3}\right) - \mu_B[\mathbf{J}\cdot\mathbf{g}_v + \mathbf{S}\cdot\mathbf{g}_c]\cdot\mathbf{H} + \mathrm{CH}^2, \tag{104}$$

in which the first term gives the zero-field splitting with the total angular momentum of the hole $J = \frac{3}{2}$, the second term, the linear Zeeman effect due to holes, the third term, the linear Zeeman effect due to electron with spin $S(=\frac{1}{2})$, and the final term, an isotropic quadratic effect. The above expression was fitted to the experimental data in the [100] and [111] directions as shown in Fig. 23; from this fit the first experimental values of the g factors of holes g_v and electrons g_c in germanium were determined. For the [100] direction, $g_v \approx g_c \approx 1.6$. Following these results, Roth[102] developed the following expressions for the g factors, using $\mathbf{k}\cdot\mathbf{p}$ second-order perturbation theory:

$$g_{\|} - 2 = -\frac{\delta}{\Delta\mathscr{E}_{13'}}\left(\frac{m}{m_t} - 1\right),$$

and

$$g_{\perp} - 2 = -\frac{\delta}{\Delta\mathscr{E}_{13'}}\left(\frac{m}{m_t} - 1\right) + \Delta g_{\perp'}. \tag{105}$$

Here the spin–orbit splitting of the $L_{3'}$ valence band at the [111] edge of the Brillouin zone $\delta \approx 2\Delta/3$, where $\Delta(\approx 0.3\,\mathrm{eV})$ is the spin–orbit splitting of the $\mathbf{k} = 0$ valence band. $\Delta\mathscr{E}_{13'}$ is the energy difference between the L_3' band edge and the L_1 [111] conduction-band minimum, and $\Delta g_{\perp'}$ is a small term only the absolute value of which can be estimated. With the energy difference $\Delta\mathscr{E}_{13'} \approx 2.0\,\mathrm{eV}$, as determined from the experimental data of Philipp and Taft,[105] and $\delta \approx 0.2\,\mathrm{eV}$, $g_{\|} \approx 0.9$ and $g_{\perp} \approx 2$. These predictions were subsequently more accurately determined by Feher *et al.*[106] from microwave spin-resonance experiments.

The study of the indirect transition was extended by Halpern and Lax[88a] to higher magnetic fields, and in the Faraday configuration, in which the electromagnetic energy is propagated along the direction of the magnetic field, and to lower temperatures, since the samples were immersed in a helium bath. From traces such as shown in Fig. 24, an extrapolated value of the energy gap was found that was in agreement with that of previous workers. In quantitatively interpreting the experiment, plots were made of

[105] H. R. Philipp and E. A. Taft, *Phys. Rev.* **113**, 1002 (1959).
[106] G. Feher, D. K. Wilson, and E. A. Gere, *Phys. Rev. Letters* **3**, 25 (1959).

the ratio of intensities; curves of the form shown in Fig. 25 were obtained for the three principal directions. From these curves, strong transitions were observed in addition to the fine structure. These strong transitions were interpreted as taking place from the top of the valence band to the successive Landau levels in the conduction band. Such transitions would be expected, since the selection rules on the magnetic quantum number break down for the indirect transition. With this interpretation, it was possible to determine the electron effective-mass values as a function of orientation by using the spacing between the dominant lines and the cyclotron-resonance formula for ellipsoidal energy surfaces,[107] namely,

$$\omega = \frac{eH}{c} \frac{(m_1\alpha^2 + m_2\beta^2 + m_3\gamma^2)^{1/2}}{m_1 m_2 m_3}, \tag{106}$$

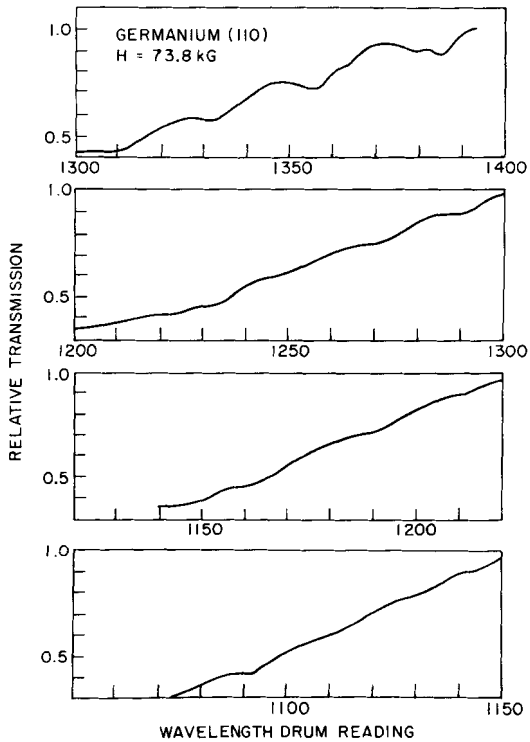


FIG. 24. Indirect-transition transmission trace for the (110) orientation at 73.8 kG. (After J. Halpern.[88a])

[107] B. Lax and J. G. Mavroides, *Solid State Phys.* **11**, 365 (1960).

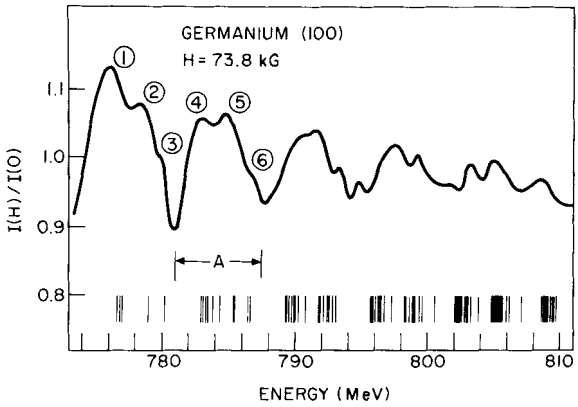


FIG. 25. Plot of $I(H)/I(0)$ as a function of energy for the (100) orientation. The periodic spacing denoted by A corresponds to indirect transitions from the top of the valence band to the electronic ladders in the conduction band. The superposed fine structure, denoted by 1–6, arises principally from the valence-band ladders, given in Fig. 12 for this configuration. (After J. Halpern.[88a])

where the m_i are the three components of the effective-mass tensor and α, β, and γ are the directional cosines of the magnetic field relative to the principal axes of the ellipsoid. In this manner, the effective-mass values given in Table II were determined. These data are in good agreement with those obtained from microwave cyclotron-resonance experiments.[107]

In addition, for both the [100] and [110] orientations, a splitting was observed in the first step of the transmission traces at the highest fields used (74 kG). This was interpreted as spin splitting in the conduction band, since no other energy difference could fit it. These splittings correspond to electronic g factors of (1.8 ± 0.3) and (1.5 ± 0.3), respectively, which are in agreement with the theoretical work of Roth and Lax.[102]

TABLE II

EFFECTIVE ELECTRON RESONANCE MASSES IN GERMANIUM, AS DETERMINED FROM INDIRECT-TRANSITION MAGNETOABSORPTION EXPERIMENTS[a]

Magnetic-field direction	[100]	[111]	[110]
m^*/m	—	0.197 ± 0.005	0.340 ± 0.014
	0.131 ± 0.003	—	—
	—	0.079 ± 0.002	0.101 ± 0.002

[a] J. Halpern and B. Lax, *J. Phys. Chem. Solids* **26**, 911 (1965).

b. Faraday Rotation

(1) *Direct Transitions.* It is not surprising that the interband Faraday-rotation experiments in the oscillatory region were first studied experimentally in the semiconductor germanium. The initial observations, which were made by NKL[55] at room temperature, exhibited the oscillatory character very distinctly. These observations were repeated in greater detail and confirmed by Mitchell and Wallis.[57] They analyzed the detailed structure of the Verdet constant as well as line shapes at room temperature in terms of Landau transitions between free hole and electron states, following the theory of KLN,[51] which has already been presented in this chapter. The theoretical curves were in quantitative agreement with the experimental data, although Mitchell and Wallis contended that vestiges of exciton transitions were present both at weak and high magnetic fields. The experimental evidence, however, does not fully resolve this question, although, in principle, a good case exists for their theoretical arguments.

More recently, NKL[108] have extended their earlier measurements to low temperatures, where the exciton transitions were definitely expected to dominate. The crystals used in these experiments were those that had been used earlier by Zwerdling,[74] who had mounted these thin samples on a glass substrate, thereby providing a strain and removing the degeneracy of the lowest exciton state. The data at high magnetic fields are shown in Fig. 26. The interesting result of the NKL experiment was that the exciton line, which appeared broad in magnetoabsorption and therefore did not allow the resolution of structure, was now fully resolved by the Faraday-rotation technique. Thus the identification of the individual transitions in terms of Landau quantum numbers was possible. The interpretation in this context is that the Coulomb force of the excitons merely perturbs the quantized magnetic Landau levels, so that the dependence of the energy as a function of magnetic field can still be analyzed in terms of the Landau states.

At low magnetic fields, Hanamura *et al.*[109] identified the direct exciton lines in terms of the Luttinger–Kohn ladder. The lines that were split by the applied strain crossed again as a magnetic field was increased. At still higher fields there was a splitting of the lines again, but this time with a reversal in relative position. This was evident in the experiment by a reversal as a function of magnetic field in the sign of rotation, as indicated in Fig. 27. The details of the exciton behavior with strain in a magnetic field were analyzed in a manner analogous to the zero-magnetic-field deformation-potential analysis of Kleiner and Roth.[110] For weak magnetic fields, the

[108] Y. Nishina, J. Kolodziejczak, and B. Lax, *in* "Physics of Semiconductors" (Proc. 7th Intern. Conf.), p. 867. Dunod, Paris, and Academic Press, New York, 1964.

[109] E. Hanamura, M. Okazaki, K. Suzuki, and H. Hasegawa, to be published.

[110] W. H. Kleiner and L. M. Roth, *Phys. Rev. Letters* **2**, 334 (1959).

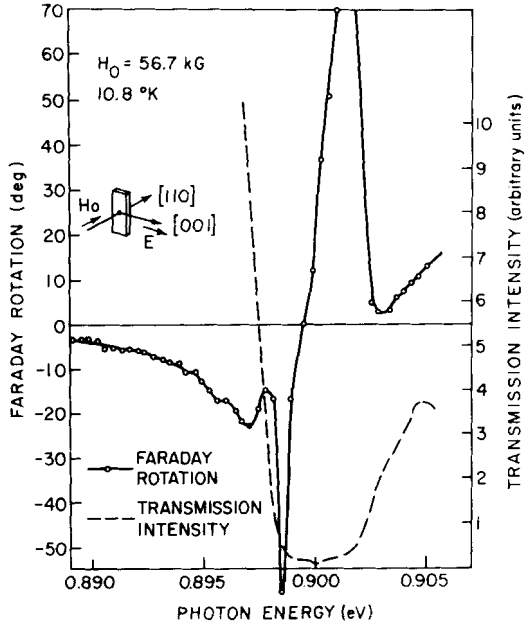


FIG. 26. Faraday rotation in germanium (direct transition) at a magnetic field of 56.7 kG. The dashed line indicates the relative intensity of the transmitted radiation. (After Y. Nishina *et al.*[108])

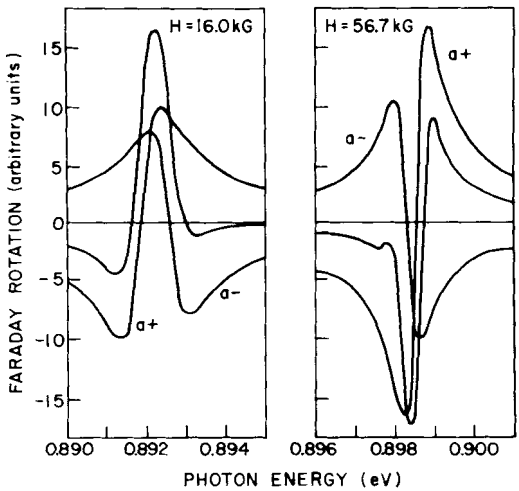


FIG. 27. Theoretical oscillatory dispersion of the rotation angle $\theta(\omega)$ in germanium for the direct transitions involving two bound exciton states, (a^+) and (a^-): (a) $H = 16.0$ kG, $\tau = 1.3 \times 10^{-12}$ sec; (b) $H = 56.7$ kG, $\tau = 2.2 \times 10^{-12}$ sec. (After E. Hanamura *et al.*[109])

transition energy $\mathscr{E}$ equals

$$\mathscr{E} = \mathscr{E}_g + \frac{\hbar eH}{2\mu c} + \frac{\hbar e}{4mc}(g_c + g_v)H, \tag{107}$$

and for fields high enough so that $\hbar eH/m_1{}^*c \gg$ strain splitting, $\mathscr{E}$ equals

$$\mathscr{E} = \mathscr{E}_g + \frac{\hbar eH}{2m_1{}^*c} + \frac{\hbar e}{4mc}g_v H, \tag{108}$$

where $m_1{}^* \neq \mu$, $m_1{}^*$ being a complicated function of the band parameters. The latter expression differs from the common one, Eq. (107), because both the reduced cyclotron mass μ and the g factor of the hole are modified by the high magnetic field from their band edge values because of mixing of the $n = 0$ and $n = 2$ cyclotron motions.

(2) *Indirect Transitions.* Halpern[111] has observed the oscillatory Faraday rotation of the indirect transition in intrinsic germanium by transmission experiments at liquid-helium temperatures and high magnetic fields up to 103 kG. Both the Faraday rotation and relative transmission were studied as a function of energy, as shown in Fig. 28. It was found by comparing these two effects that the oscillatory behavior of the rotation corresponds to both the exciton absorption and to the Landau steps. The rotation due to the indirect transition is superimposed on the dispersive background, which probably arises from the direct transition. The oscillatory effects were found to be of the order of 2% of the total rotation.

6. Indium Antimonide

a. Magnetoabsorption

Next to germanium, the material in which interband effects have been studied most extensively is the intermetallic compound InSb. These effects were first observed by Burstein *et al.*[11] and further studied by Zwerdling *et al.*[15] at room temperature. Low-temperature measurements were carried out on transmission by Zwerdling *et al.*[98,112] and subsequently on reflection by Wright and Lax,[37] and most recently on both reflection and transmission by Pidgeon and Brown,[113] with high magnetic fields. These experiments, combined with the Faraday-rotation experiments of Smith *et al.*[48] and Pidgeon and Smith[67] and the corresponding analysis of Boswarva,[60] are now beginning to yield a more consistent picture of the transitions involved, in terms of spectral identification and line intensities. Each of these papers in succession has made a contribution to our knowledge of this material,

[111] J. Halpern, *J. Phys. Chem. Solids* **27**, 1505 (1966).
[112] S. Zwerdling, W. H. Kleiner, and J. P. Theriault, *J. Appl. Phys. Suppl.* **32**, 2118 (1961).
[113] C. R. Pidgeon and R. N. Brown, *Phys. Rev.* **146**, 575 (1966).

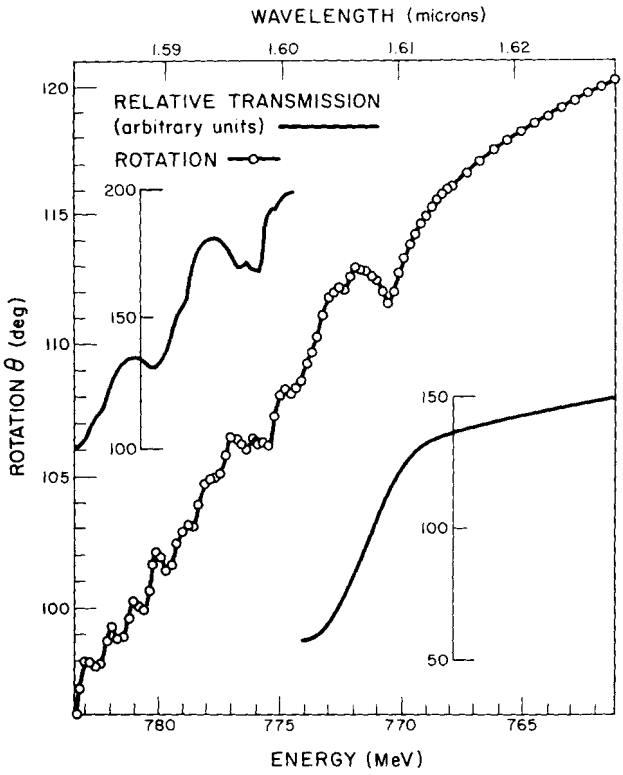
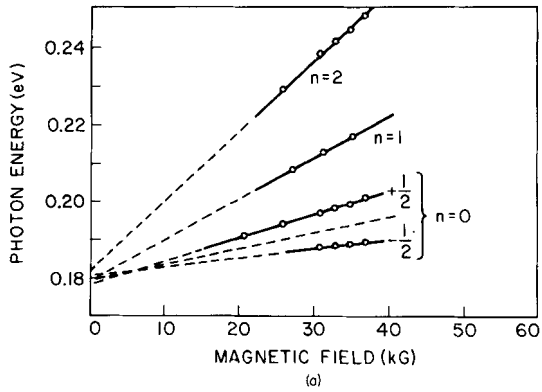


FIG. 28. Faraday rotation and relative transmission in germanium (indirect transition), for a (110) face, at a magnetic field of 103.3 kG and $T = 8°K$. (After J. Halpern.[111])

which has been correlated with the early work from cyclotron resonance by Dresselhaus *et al.*,[114] Lax *et al.*,[115] and most recently by Bagguley and Stradling,[97] as well as the key theoretical work of Kane.[116] The latter has provided a good model for the conduction band; however, the valence band, particularly in the limit of low quantum number, is still best analyzed in terms of the Luttinger–Kohn theory.[92,94] Most recently, Pidgeon and Brown[113] have actually incorporated both warping and nonparabolic effects to analyze their InSb data by using an 8×8 matrix to obtain the corrected energy levels for both holes and electrons.

The magnetoabsorption phenomenon first observed at room temperature is shown in Fig. 29(a). These lines were initially interpreted as arising from transitions from the magnetic levels near the top of the valence band, which

[114] G. Dresselhaus, A. F. Kip, C. Kittel, and G. Wagoner, *Phys. Rev.* **98**, 556 (1955).
[115] B. Lax, J. G. Mavroides, H. J. Zeiger, and R. J. Keyes, *Phys. Rev.* **122**, 31 (1961).
[116] E. O. Kane, *J. Phys. Chem. Solids* **1**, 249 (1957).



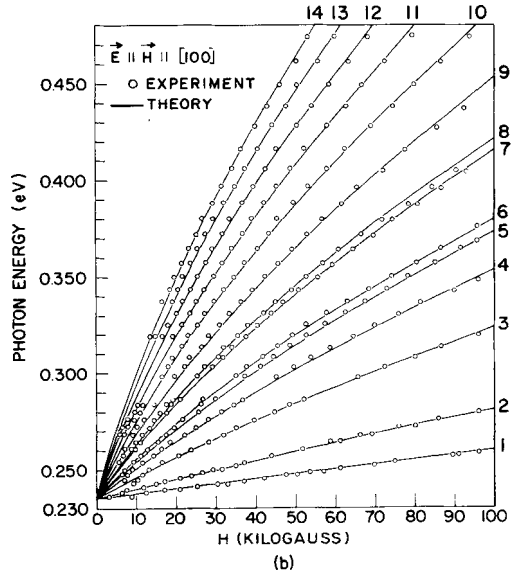


FIG. 29. (a) Energy values of transmission minima versus magnetic field for electron transitions between Landau levels of valence and conduction bands in indium antimonide. The first level ($n = 0$) is split by spin–orbit interaction, yielding an anomalous g value for the conduction electron of $g \simeq 54$. The energy gap at zero field and room temperature obtained from the convergence of the lines is $\mathscr{E}_g = 0.180 \pm 0.002$ eV. (After S. Zwerdling *et al.*[15]) (b) Plot of the photon energy of the principal transmission minima as a function of magnetic field for $\mathbf{E} \parallel \mathbf{H} \parallel [100]$. The solid lines represent the best theoretical fit to the experimental data. The numeral next to each line identifies the quantum assignment. (After C. R. Pidgeon and R. N. Brown.[113])

were unresolved, to the Landau ladder of the conduction band. The first two lines were identified as due to the spin splitting of the $n = 0$ conduction band, and the next two higher lines were interpreted as transitions to the $n = 1$ and 2 quantum states in the conduction band. In essence, this early interpretation, which neglected the details of the valence band, was confirmed by subsequent analysis. The spin splitting calculated from this type of experiment at 4°K on the basis of this interpretation gave a g factor of -48, which is in very good agreement with the value $g^* = -47$ calculated from the following expression, derived by Roth[17] using $\mathbf{k} \cdot \mathbf{p}$ theory:

$$g^* = 2\left[1 + \left(1 - \frac{m}{m^*}\right)\left(\frac{\Delta}{3\mathscr{E}_g + 2\Delta}\right)\right], \tag{109}$$

with the band parameters that are tabulated in Table III and $\Delta = 0.9$ eV. The room-temperature g^* has not been accurately measured yet.

TABLE III

BAND PARAMETERS USED IN CALCULATING g^* IN InSb[a]

T	$\mathscr{E}_g$	m^*/m	Δ	g^*
4°	0.24 eV	0.0145[b]	0.9 eV	−47
300°	0.18 eV	0.0116	0.9 eV	−64

[a] B. Lax, J. G. Mavroides, H. J. Zeiger, and R. J. Keyes, *Phys. Rev.* **122**, 31 (1961).

[b] S. Zwerdling, W. H. Kleiner, and J. P. Theriault, *Proc. Intern. Conf. Phys. Semicond., Exeter, 1962* p. 455. Inst. of Phys. and Phys. Soc., London, 1962.

The low-temperature, high-magnetic-field magnetooptical experiments of Pidgeon and Brown[113] indicate the nonparabolic effects that are predicted by the Kane theory,[116] as shown in Fig. 29(b). In addition to the nonparabolic character, the other feature of interest indicated by these measurements is that the spacings between the levels of high quantum numbers correspond to those for the electron, with a variation in curvature as predicted by the Kane theory—i.e., with the conduction band levels given by

$$\mathscr{E}_n\left(1 + \frac{\mathscr{E}_n}{\mathscr{E}_g}\right) = (n + \tfrac{1}{2})\hbar\omega_{c0} \pm \frac{\beta}{2} g_0^* H, \tag{110}$$

where ω_{c0} and g_0^* are the cyclotron frequency and effective g factor, respectively, at the bottom of the energy band. The interpretation of these experiments is that the dominant transitions occur from the valence band to successive levels in the conduction band with selection rules $\Delta n = 0$,

$\Delta n = -2$. The fine structure observed for low quantum numbers by Zwerdling, Kleiner, and Theriault and also by Pidgeon and Brown can be explained in terms of the valence-band structure and transitions between the light- and heavy-hole levels and the electron levels; for warped induced transitions $\Delta n = 2, \pm 4, -6$. The band parameters obtained from magnetoabsorption by Zwerdling *et al.*[98] and Pidgeon and Brown[113] are in closer agreement with one another than those obtained from cyclotron resonance by Bagguley and Stradling.[97] The comparison of the band parameters and mass values determined by the two techniques is shown in Table IV. The discrepancy in the mass values for the heavy hole is of the order of 5%. The major disagreement is in the mass value of the light hole.

TABLE IV

COMPARISON BETWEEN BAND PARAMETERS IN InSb OBTAINED FROM MAGNETOABSORPTION AND FROM CYCLOTRON RESONANCE

Band parameter	Technique		
	Magnetoabsorption		Cyclotron resonance
A	36[a]	32.5[b]	25[c]
B	29	28.6	21
C	25	20.2	16
m_e/m	0.0145	0.0145	—
m_l/m	—	0.0160	0.021
$m_h[100]/m$	—	0.32	0.34
$m_h[110]/m$	—	0.42	0.42
$m_h[111]/m$	—	0.44	0.45
γ_1	36	—	25
$\bar{\gamma}$	15.35	—	11
κ	13.87	—	10.13

[a] S. Zwerdling, W. H. Kleiner and J. P. Theriault, *Proc. Intern. Conf. Phys. Semicond., Exeter, 1962* p. 455. Inst. of Phys. and Phys. Soc., London, 1962.
[b] C. R. Pidgeon and R. N. Brown, *Phys. Rev.* **146**, 575 (1966).
[c] D. M. S. Bagguley and R. A. Stradling, *Phys. Rev. Letters* **6**, 143 (1963).

b. Faraday Rotation

The InSb Faraday experiments at low magnetic fields in the absorption-edge region carried out by Smith *et al.*[48] exhibited oscillatory structure analogous to that in germanium. The assignment of transitions and intensities as carried out by Boswarva[60] is indicated in the diagram of Fig. 30,

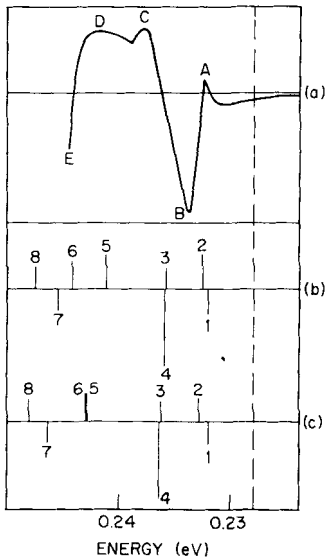


FIG. 30. (a) Faraday rotation through the absorption-edge region in InSb at 77°K, using $H = 14$ kG. (After S. D. Smith *et al.*[48]) (b) Energies and strengths of allowed transitions, at $\mathbf{k} = 0$, computed from the Kohn–Luttinger model, using the band parameters of Bagguley and Stradling. (c) As (b), using band parameters of Zwerdling *et al.*[98] (After I. M. Boswarva.[60])

using the band parameters of both Zwerdling *et al.*[98] and Bagguley and Stradling.[97] These two sets of parameters produce quite different spectra and do not correlate well with experiment, except for the lowest levels indicated by numbers 1, 2, 3, and 4; the Bagguley–Stradling parameters give the better agreement. In addition, it is shown that the weaker transitions, particularly those lying close to a strong transition, have a distinct influence on the observed shapes. In studying these line shapes, Boswarva concludes that the analysis in terms of transitions between free Landau states satisfactorily accounts for the observed spectra, without the necessity of invoking the bound exciton states suggested by Mitchell and Wallis.[57] Qualitatively, this interpretation seems to be in agreement with that given by Nishina *et al.*[55] in connection with studies in germanium.

Another Faraday-rotation experiment attempted in InSb by Nishina and Lax[117] involved the study of reflection of the 2-eV transition at the L point in the Brillouin zone. They observed small but well-defined rotations in which the spin–orbit splitting was clearly defined. As shown in Fig. 31, no fine structure was observed.

[117] Y. Nishina and B. Lax, *J. Appl. Phys. Suppl.* **32**, 2128 (1961).

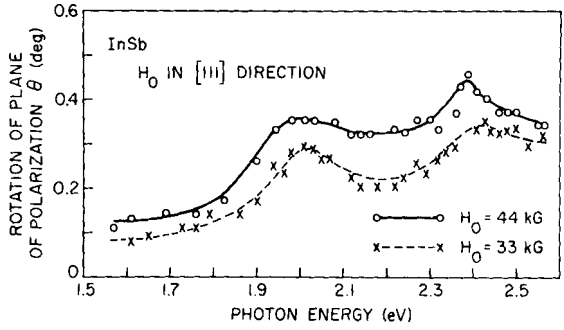


FIG. 31. Interband Faraday rotation in intrinsic InSb, observed by reflection measurements. (After Y. Nishina and B. Lax.[117])

c. *Emission Phenomena*

In connection with magnetooptical laser action in a junction diode, another interesting interband phenomenon was observed and studied in InSb. This effect was based on the well-known phenomenon that in a magnetic field there is a coalescence of the energy states into Landau levels and consequently an increase in the density of states, which results in strong absorption maxima and therefore an enhancement of the emission characteristics of the interband transition. Indeed, the magnetooptical laser action observed in InSb junction diodes[118] did exhibit the characteristics expected from these considerations, as shown in Fig. 32. The threshold current necessary for laser action decreased with increasing magnetic field H, approximately as $1/H$, except at very high magnetic fields, where a saturation effect was observed. The diode used in this particular experiment would not operate as a laser below ~ 20 kG. Furthermore, the frequency of emission of the laser, as well as that of the incoherent diode, changed with magnetic field because of the motion of the Landau levels. At low values of magnetic field, the diode exhibited a quadratic Zeeman effect, thus suggesting that either a donor or an exciton, rather than a simple free-electron state, was involved in the transition. At high magnetic fields the Coulomb field can be neglected, and the levels involved are then those of the free electron. This mechanism observed in the laser, where initially a line of a higher-energy state begins to emit coherently, and then at higher fields a lower one takes over and provides the important transition. This action is consistent with the interpretation of the spectral properties of interband transitions as suggested by Boswarva[60] in explaining the experimental magnetoabsorption

[118] R. J. Phelan, A. R. Calawa, R. H. Rediker, R. J. Keyes, and B. Lax, *Appl. Phys. Letters* **3**, 143 (1963); R. H. Rediker and R. J. Phelan, *Proc. IEEE* **52**, 91 (1964).

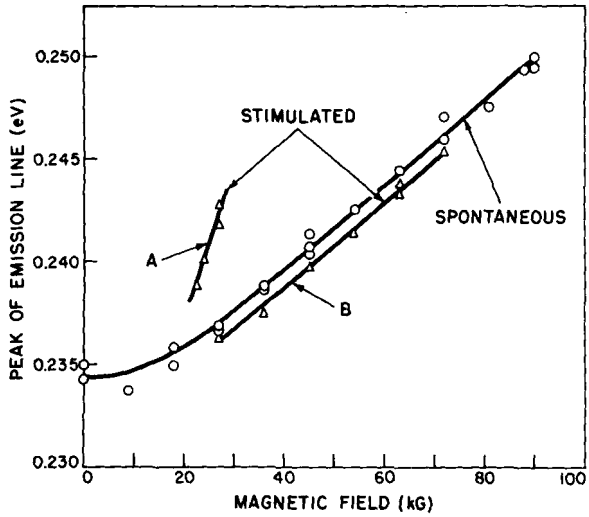


FIG. 32. The energy of the peaks of the photon spectra vs. magnetic field in an InSb laser diode for a temperature of 1.7°K. (After R. J. Phelan *et al.*[118])

observations. The theory, in agreement with the experiment, shows that the lowest transition, and the next succeeding one, which is separated to a good approximation by the electron-spin splitting, have relative intensities of approximately 3 to 1. At modest fields both these levels are populated by the injection of electrons into the *p* side of the diode; consequently, the upper level, with the stronger transitions, begins to emit first. However, as the magnetic field increases, the spacings of the energy levels increase until the population of the lower level is raised enough to overcome the lower transition probability of this state and ultimately to take over. Similar results were obtained in InSb by optically pumping a single crystal with a GaAs laser.[119]

In studying the operation of the Fabry–Perot laser modes in InSb, two effects were observed as the magnetic field was varied. The first of these involved the discontinuity in frequency, which occurred as the successive modes of the Fabry–Perot interferometer were excited by increasing the magnetic field. This phenomenon could readily be observed, since well above threshold more than one mode was excited simultaneously. The second effect involved the alteration by the magnetic field of the spacing of each of these modes, as well as the shifting of their absolute position on the frequency scale. The source of these effects is readily understood in terms of the variation of the index of refraction with magnetic field, which was discussed

[119] R. J. Phelan, and R. H. Rediker, *Appl. Phys. Letters* **6**, 70 (1965).

in the Introduction. The contribution to the polarizability due to interband transitions near the energy gap is estimated to be $\sim 20\%$ of the total dielectric constant; thus the magnetic effects should be large.

7. Indium Arsenide

a. Magnetoabsorption

Oscillatory interband effects were studied in InAs at room temperature by Zwerdling *et al.*[15] Only two peaks were observed in the magnetoabsorption, the second only at higher fields (~ 36.8 kG). From these data, an energy gap $\mathscr{E}_g = 0.36$ eV and an electron effective mass $m^* \approx 0.03m$ were obtained. More recently, this work has been extended to 80°K and 1.5°K by Johnson and Fan,[120] using polarized light and magnetic fields up to 21 kG. Johnson found considerable nonparabolicity for the conduction band; his data of the variation of electron effective mass with magnetic field joined in a smooth curve with the earlier high-magnetic-field cyclotron resonance data of Keyes[107] for the same carrier concentration.

b. Faraday Rotation

The rotation due to interband transitions was measured by Cardona[63] at 100°K and 300°K for two samples of quite different doping. The rotation in the purer sample was measured by transmission, whereas that for the more heavily doped sample ($N = 5.7 \times 10^{18}/\text{cm}^3$) was measured using the reflectivity technique. The rotation due to the interband effects was found to be opposite to that due to free electrons and yielded effective masses that again indicated nonparabolic bands.

c. Emission Phenomena

Magnetic effects in the interband emission from diodes and lasers have also been observed in InAs.[121] Results analogous to those in InSb were observed. At high magnetic fields the diode emission exhibited a linear variation with field; this behavior would be expected for a small effective mass in either a bound or a free state. However, a most interesting and as yet unexplained effect was found for heavily doped material, where the linear variation was characteristic not of the known effective mass but rather of a higher mass. A tentative explanation is that at the high doping levels, the conduction band is altered significantly by the impurities. However, no quantitative theory is yet available.

The magnetic-field effects on the cavity modes already mentioned in the

[120] E. J. Johnson and H. Y. Fan, *Phys. Rev.* **139**, A1991 (1965).

[121] I. Melngailis and R. H. Rediker, *Appl. Phys. Letters* **2**, 202 (1963); F. L. Galeener, I. Melngailis, G. B. Wright, and R. H. Rediker, *J. Appl. Phys.* **36**, 1574 (1965).

discussion of InSb were actually first observed in InAs. Figure 33 indicates the shift in operation with magnetic field from one mode to the next, as well as the absolute motion to higher frequencies. InAs single crystals have been excited as a laser by optical pumping with a GaAs laser. A lowering of the threshold with magnetic field was observed.[122]

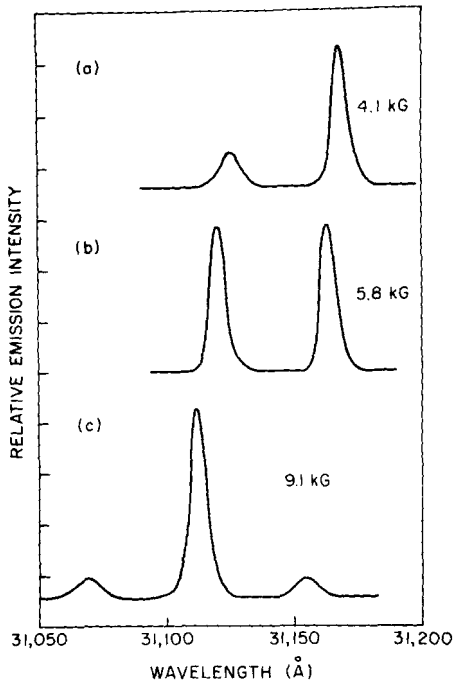


FIG. 33. Spectra of CW emission from cleaved surface of InAs diode at 4.2°K, for three different values of magnetic field. The diode forward current was 220 mA d-c. (After I. Melngailis and R. H. Rediker.[121])

8. GALLIUM ANTIMONIDE

a. Magnetoabsorption

Interband effects have been studied less extensively in GaSb than in the other materials discussed so far. The oscillatory magnetoabsorption[20] definitely established that the lowest-energy transition is a direct transition and indicated a spectrum similar to that of germanium. As a matter of fact, the identifications were so close that it was possible to estimate the effective mass of the electrons from the higher-quantum-number transitions by assuming that the observed transitions took place from the heavy holes to

[122] I. Melngailis, *Bull. Am. Phys. Soc.* **8**, 202 (1963).

the conduction band. The effective mass thus determined was $m^* = (0.047 \pm 0.003)m$, which was in good agreement with the subsequent determination from free-carrier Faraday-rotation measurements[65,66] in n-type GaSb. Recent cyclotron measurements by Stradling[122a] in p-type GaSb indicate effective masses of $0.052m$ and $\sim 0.35m$ for the light and heavy holes, respectively. If this is correlated with the Kane model and the recent optical data of Halpern,[66a] an effective mass of $0.041m$ is deduced for the electron. Using the spin–orbit splitting obtained recently by Kosicki and Paul,[122b] it is then possible to calculate the valence-band parameters and the energy gap.

The magnetoabsorption spectra observed at low temperatures in thin samples exhibited polarization effects such as shown in Fig. 34 and yielded an energy gap $\mathscr{E}_g = 0.81$ eV. At these low temperatures some fine structure was observed in the first absorption peak at the highest magnetic field available (38.9 kG), and this structure was associated with the exciton. However, since the thin 8-micron sample was mounted on glass, a good possibility exists that the apparent splitting may have been due to the strain, which can remove degeneracies. Halpern's extension[66a] of these measurements to high magnetic fields up to 100 kG, lower temperatures, and circularly polarized light yields $m^* = 0.041m$ and has provided better resolution of the fine structure, including exciton effects, in the magnetoabsorption

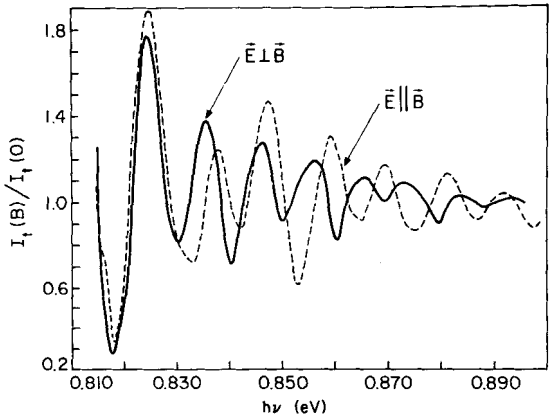


FIG. 34. Oscillatory magnetoabsorption in GaSb at photon energies slightly greater than the direct absorption edge. The plot shows the ratio of the transmission of infrared radiation at 38.9 kG to that at zero field versus photon energy. The magnetic field was applied along the [111] crystal direction. The crystal was about 4 microns thick, the temperature was 1.5°K, and the incident radiation was polarized as indicated. (After S. Zwerdling *et al.*[20])

[122a]R. A. Stradling, *Phys. Letters* **20**, 217 (1966).

[122b]B. B. Kosicki and W. Paul, *Bull. Am. Phys. Soc.* **3**, 52 (1966).

and Faraday rotation. Nonparabolic behavior has been observed at high magnetic fields, and a more quantitative analysis of the band structure should now be possible.

Johnson *et al.*[19] have also studied the magnetoabsorption in GaSb. They observed three sharp peaks superimposed on the intrinsic absorption edge, as shown in Fig. 35, which they attributed to excitons and exciton impurity complexes. By investigating the magnetic behavior of these peaks with polarized light, it was found that they shifted to higher photon energies with increasing magnetic field, the shift being quadratic for low fields and linear at the higher fields, as summarized in Fig. 36. The splittings of the γ and β peaks into two well-resolved components exhibited qualitatively similar polarization effects. The α peak, on the other hand, was broader than the other two peaks and broadened even further with magnetic field, but indicated no resolvable splitting. However, if the splitting of this peak had been of the same order of magnitude as that of the γ and β levels, it would have been masked by the magnetic broadening. By interpreting the splitting of the γ and β levels as arising from the spin splitting of the $n = 0$ conduction-band Landau level, Johnson *et al.* estimated a value of $|g^*| \sim 9.5$ from the γ peak and $|g^*| \sim 6.5$ from the β peak. These values are in qualitative agreement with the value of $g^* = -5.9$ they calculated by the use of Eq. (109), assuming $\Delta = 0.86$ eV.[123]

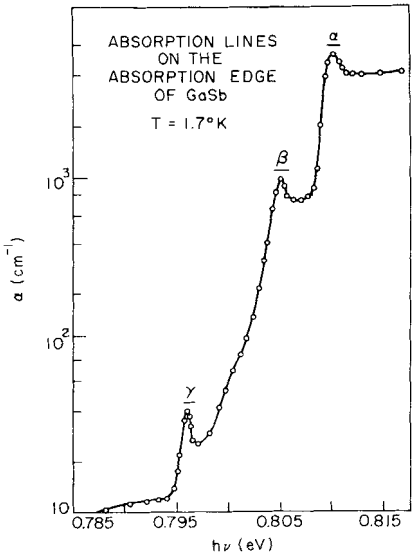


FIG. 35. Absorption edge of *p*-type, undoped GaSb. (After E. J. Johnson *et al.*[19])

[123] H. Ehrenreich, *J. Appl. Phys. Suppl.* **32**, 2158 (1961).

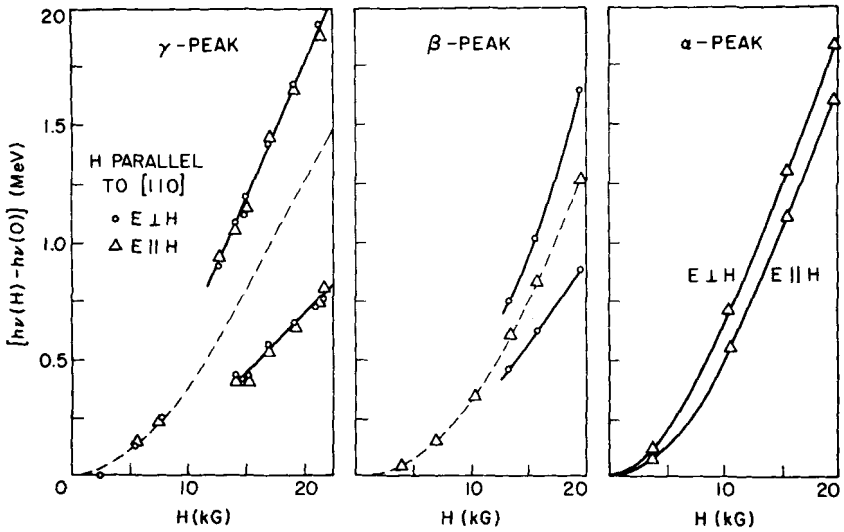


FIG. 36. Photon energy of absorption peaks plotted against applied magnetic field. Diagram on the left shows the shift and splitting of the γ band measured with polarized radiation. Center diagram shows the result for the β band obtained with unpolarized radiation. Diagram on the right gives the results for the α band obtained with polarized radiation. (After E. J. Johnson *et al.*[19])

b. Faraday Rotation

The behavior of the interband Faraday rotation observed in GaSb[65] is similar to that reported in germanium, with a singularity below the energy gap. It is of interest that at low temperatures, as in germanium, the rotation exhibits a peak before becoming negative (Fig. 37). This would suggest that the interpretation of a competitive behavior between the direct and indirect transition is not appropriate, since the indirect energy gap is much higher than the direct gap, so that the contribution of the former is negligible near the direct gap. Therefore, the interpretation here is that the residual plus the interband rotation must be due to direct transition at higher bands, at Brillouin-zone points such as L and X, which are assumed to contribute a positive rotation, which is of opposite sign to the contribution from the direct energy gap at Γ (the center of the zone).

9. GALLIUM ARSENIDE

a. Magnetoabsorption and Faraday Rotation

Attempts to observe oscillatory interband effects in GaAs have not been too successful until very recently, when such effects were observed by

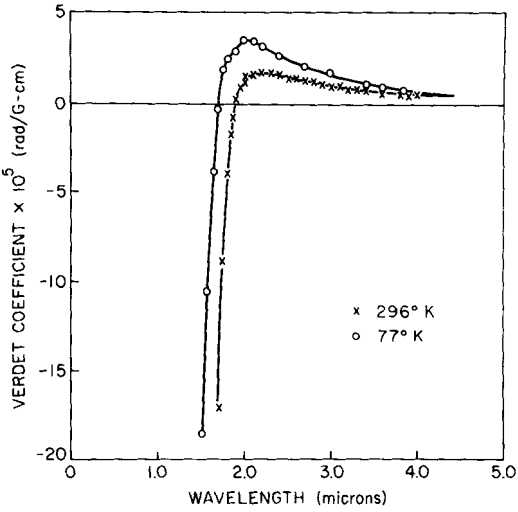


FIG. 37. Verdet coefficient for gallium antimonide. (After H. Piller and V. A. Patton.[65])

Vrehen,[29] using the crossed-field technique, and Hobden,[123a] using conventional techniques. The difficulty initially encountered was surprising, since cyclotron resonance in the far infrared[124] and also the exciton[125] had already been observed. Nevertheless, there are a few interband magneto-optical effects worth recording, namely, the interband Faraday rotation observed by Cardona,[63] and magnetic effects in diodes and lasers.[126] The interband Faraday rotation of intrinsic material[98a] indicates the same sign as InSb, which is opposite to that of the free-electron rotation, the sign in germanium, Si, InAs, GaP, and InP. This measured rotation in GaAs has been explained theoretically by Roth;[54] Boswarva and Lidiard[59] calculate a rotation of the wrong sign.

b. Emission Phenomena

The other interband effects are associated with diodes and lasers. In attempting to identify the transitions involved in these devices, they were subjected to a high magnetic field and their properties were studied while operating either in spontaneous or stimulated emission. It was found that the energy of the radiation exhibited a quadratic dependence on magnetic field, as shown in Fig. 38, thus suggesting that either a donor or an exciton, rather than a simple free conduction electron, was involved in the transition.

[123a] M. V. Hobden, *Phys. Letters* **16**, 107 (1965).
[124] E. D. Palik, J. R. Stevenson, and R. F. Wallis, *Phys. Rev.* **124**, 701 (1961).
[125] M. V. Hobden and M. D. Sturge, *Proc. Phys. Soc. (London)* **78**, 615 (1961).
[126] F. L. Galeener, G. B. Wright, W. E. Krag, T. M. Quist, and H. J. Zeiger, *Phys. Rev. Letters* **10**, 472 (1963).

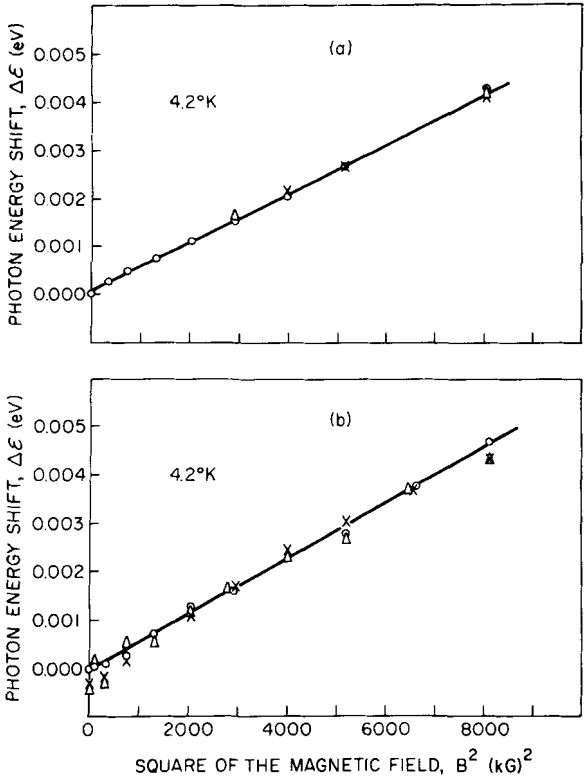


FIG. 38. Shift of emission energy of GaAs diodes with magnetic field: (a) laser diode (△, ×, ○ identify different series); (b) incoherent diodes. (After F. L. Galeener *et al.*[126])

The terminal state was identified as an acceptor state, which, according to some investigators, may be an impurity state, or the top of the valence band distorted by a heavy impurity concentration. In any event, the fact that the radiation occurs at an energy of 1.47 eV, or 0.04 eV below the energy gap, militates against the interpretation of a simple interband transition.

In addition to these measurements, Galeener and Wright[127] have studied the magnetic-field dependence of the photoluminescence of GaAs. They observe in *n*-type material additional lines besides those reported at zero field by Nathan and Burns.[128] The exciton lines, as well as several transitions proceeding through holes trapped at acceptors, all exhibited the same variation of photon energy with magnetic field. The energy shift, which was

[127] G. B. Wright and F. L. Galeener, *Bull. Am. Phys. Soc.* **10**, 369 (1965); F. L. Galeener and G. B. Wright, to be published.

[128] M. I. Nathan and G. Burns, *Phys. Rev.* **129**, 125 (1963).

quadratic at low fields and linear at high fields, could be described by a simple effective-mass hydrogenic model with an electron effective mass $m^* = 0.06m$ and a binding energy ~ 5 meV. Attempts to observe a spin splitting due to holes were unsuccessful. Unlike the n-type material, in which the intensity of the lines was practically unaffected by the magnetic field, large magnetic effects on line intensity were observed in p-type GaAs. An additional line was observed, which shrank as the magnetic field increased while the other lines grew with magnetic field, sometimes by as much as a factor of ten. Evidently, the magnetic field was changing the relative electron capture cross-section.

10. Aluminum Antimonide and Gallium Phosphide

Two other compounds that have exhibited interband effects are AlSb and GaP, investigated by Moss and Ellis.[69] The former of these two materials, which has also been studied by Piller and Patton,[65] seems to be the more interesting. In the first place, the sign of the Faraday rotation due to interband transitions is positive, contrary to the result expected for pure samples; however, this behavior may be expected for heavily doped n- or p-type material on the basis of the Boswarva and Lidiard[59] analysis, since at modest magnetic fields the contributions of the lower quantum states in the valence band, particularly those of the light holes, is negligible. Secondly, the experimental data below the energy gap exhibit structure as a function of wavelength of an oscillatory character. However, no correlation between these two effects has yet been established. It appears that a reexamination of the interband Faraday rotation in AlSb at high magnetic fields would be of considerable interest.

In GaP, no oscillatory effects have been observed, and the interband Faraday rotation at energies below the gap indicates a normal behavior with a negative sign, which suggests a strong direct transition. In heavily doped n-type material, some structure has been observed below the energy gap, but the origin of this structure is not yet known. In relatively pure materials, exciton complexes have been observed and studied;[129] this work will not be discussed in the present article. However, the Zeeman effect of such complexes should prove to be interesting and helpful in evaluating the band parameters.

IV. Discussion

In this review, emphasis has been placed on the theoretical and experimental developments and particularly on the correlation between the two.

[129] J. J. Hopfield, D. G. Thomas, and M. Gershenzon, *Phys. Rev. Letters* **10**, 162 (1963).

A number of outstanding problems have been indicated. In general, it appears that the basic interband phenomena are fairly well understood, quantitatively in most cases. However, there are some problems—for example, the interband Faraday rotation below the energy gap as estimated by Boswarva and Lidiard[59]—where good quantitative agreement between theory and experiment does not exist. Another such case is the unsatisfactory analysis of the line shape of these dispersive effects in the oscillatory region in terms of either free Landau-level transitions or the bound-oscillator model for the exciton. Thus it appears that a theory for the exciton levels in a magnetic field similar to that considered by Elliott and Loudon[101] for absorption phenomena may be required to understand this aspect of the dispersive effects. In principle, one would expect that the application of the Kramers–Kronig relations to the work of Elliott and Loudon would be in order to accomplish this. However, this appears to be a formidable analytical problem, although the possibility of a numerical calculation exists. As yet, this has not been attempted. In any event, the task will be difficult, and more than one approach will be desirable.

So far, one of the apparent theoretical successes has been the identification of the energy spectra in terms of interband transitions by means of the Kohn–Luttinger model for the valence band. In germanium, which has been studied most extensively, quite satisfactory agreement has been obtained between theory and experiment, although at low temperatures complex spectra are observed because of the Coulomb term. The general effect of the Coulomb term at high magnetic fields is to lower the entire Landau-level spectrum as a whole and not to affect the energy separations appreciably.

The status of the theory for the line shape of the indirect transition appears to be in some doubt, even in germanium, for the following reason: At low magnetic fields, where the earlier data were taken, the observed line shape for the magnetoabsorption appeared as a step function, which was consistent with the theory for transitions between free Landau states. At high magnetic fields, however, for both the exciton and the "Landau" transitions one finds a line shape that deviates considerably from this model—possibly suggesting that Coulomb effects are important or that the theory needs to be modified in some other manner. As a matter of fact, no satisfactory theory exists for the indirect-exciton line shape with or without a magnetic field.

In InSb such detailed comparisons as in germanium have recently been made possible by the high-field expressions of Pidgeon and Brown. This reexamination is significant, and comparison with the parameters for the valence band indicates good agreement with those determined from cyclotron-resonance measurements.[97] In InSb the complex structure of the

valence band due to warping, considered by Dresselhaus,[130] was combined in the theoretical treatment with the nonparabolic nature, such as considered by Kane,[116] for the conduction band. Kane has solved this problem without magnetic field; however, the combination of warped energy surfaces and nonparabolic effects in the presence of a magnetic field was developed for the valence band. Also, it appears that this procedure was necessary for a proper evaluation of the energy levels in InSb and comparison with the data as shown in Fig. 29(b). Furthermore, the nonparabolic form of the bands has a significant effect on the theory of the dispersion and line shape, as has been shown in this chapter. However, as yet no comparison has been made between theory and experiment for these line shapes. Nevertheless, it is anticipated that at high magnetic fields for materials with small energy gaps such as InSb, this nonparabolicity would be a more significant factor than the Coulomb interaction; the latter interaction is more significant in high-energy-gap materials.

So far, in both theoretical and experimental programs for magneto-optical effects, the emphasis has been on the phenomenon of the transition itself and on the identification of the spectra, which in turn has permitted a quantitative evaluation of the energy bands. Not much effort has been given to the examination of relaxation phenomena in a magnetic field, either for intra- or interband processes. Some theoretical work by Argyres and Roth,[131] Adams and Holstein,[132] and Meyer[133] has indicated that the scattering time is definitely dependent on magnetic field. In this case, only interband acoustical-phonon scattering and impurity scattering have been considered. In general, it has been shown that in the quantum limit for $\omega_c\tau > 1$, the scattering time varies inversely as the magnetic field for the acoustical-phonon scattering. Obviously, the intraband scattering itself would have a profound effect on the line width of an interband phenomenon, since the lifetime in the final state will be influenced by intraband processes. At high magnetic fields the scattering becomes more complex, since there are a number of scattering mechanisms that can take place. For example, an electron can be scattered within a given subband of magnetic index n, or it can be scattered to other magnetic subbands by impurities or lattice vibrations. Finally, as the Landau-level spacings increase so that electrons are excited between states with an energy difference comparable to that of the optical phonon, the scattering due to optical phonons becomes significant. One would expect that maximum scattering would occur at values of

[130] G. Dresselhaus, *Phys. Rev.* **100**, 580 (1955).

[131] P. N. Argyres and L. M. Roth, *J. Phys. Chem. Solids* **12**, 89 (1959); P. N. Argyres, *Phys. Rev.* **132**, 1527 (1963).

[132] E. N. Adams and T. D. Holstein, *J. Phys. Chem. Solids* **10**, 254 (1959).

[133] H. J. G. Meyer, *Phys. Letters* **2**, 259 (1962).

magnetic field for which the energy difference between two magnetic levels is exactly equal to the energy of the optical phonon. Such an effect has been predicted theoretically and also observed in the magnetoresistance, where an optical phonon assists transitions to higher energy states.[134] However, at low temperatures in the analogous magnetooptical situation where the electron is excited to a higher state, an optical phonon is emitted rather than absorbed and quantum phenomena would, in principle, be even more apparent. Thus the study of photoconduction in a magnetic field using interband radiation in materials such as InSb offers very promising possibilities.

It also appears conceivable that the magnetic field could have an effect on the interband recombination between the conduction and valence bands. It has been shown theoretically that the recombination depends on the momentum matrix element, which is a product of the momentum matrix elements of Bloch functions, unaffected by magnetic field, and overlap integrals of the envelope functions, which in some materials are seriously affected by magnetic field, both for the free-carrier case and for excitons. Consequently, the direct allowed interband recombination would be unaffected by magnetic field, whereas the direct forbidden transition will be affected, since in the latter case the matrix elements of the envelope function enter into the calculation. It may be expected that the magnetic field would reduce the lifetime. In this context the measurement of relaxation times, particularly in small–energy-gap materials where magnetic effects are large, would be of interest. For example, the PEM effect would exhibit interesting results at high magnetic fields. The effect should be magnetic-field dependent, and although it basically involves an intraband phenomenon, nevertheless it should be an interesting tool for studying magnetooptical effects.

On the experimental side, perhaps the greatest limitation in extending magnetooptical phenomena to new materials has been the inability to make high-quality pure crystals. This appears to be the case even in such common compounds as GaAs, InAs, and GaP. For example, no oscillatory effects have been observed in some of these materials, such as GaP, InP, and AlSb; and even where they are observed, the structure is not resolved because of the inferior quality of the crystals. Oscillatory magnetoreflection effects have so far been reported in only one semiconductor, namely, InSb;[37] in principle, if proper surfaces are available, magnetoreflection effects should be observed in other compounds as well. Furthermore, in materials with large energy gaps and heavy effective masses, the interband oscillatory effects have not been observed. For example, in silicon, where the material

[134] V. L. Gurevich and Yu. A. Firsov, *Zh. Eksperim. i Teor. Fiz.* **40**, 199 (1961) [*English Transl.*: *Soviet Phys. JETP* **13**, 137 (1961)].

is presumably very pure, the experiments even at fairly high magnetic fields do not reveal any oscillatory effect at the indirect edge either for absorption or Faraday rotation. Both of these oscillatory effects are observed in germanium, which has a smaller energy gap. Again, in AgCl, the indirect edge has been found, but magnetooptical effects have not been observed even at high magnetic fields.

A new development, the piezoreflection in a magnetic field, which promises to be extremely useful in extending magnetoreflection measurements, has now been observed in germanium and InSb.[134a] The oscillatory effect with this derivative technique at room temperature is quite distinct and is more sensitive than the conventional magnetoreflection technique. It is possible that this differential technique can be extended to the study of higher bands and also semimetals and other semiconductors.

Although the direct forbidden transition between the valence bands of materials such as germanium,[135] GaAs,[136] InAs,[137] and AlSb[138] have been observed at zero magnetic field, no magnetic effects have been found for the following two reasons. First of all, the high doping required to empty states in the valence band to allow the possibility that this effect be observed at low temperatures would require a degenerate sample; this would result in rather strong scattering. Second, the reduced effective mass involved in this case is the reciprocal mass difference rather than the sum, so that the spacing between the Landau levels would be small. Even at high magnetic fields this would militate against the observation of the phenomenon unless the scattering were anomalous, as in the lead salts. However, in the lead compounds the spin–orbit splitting is so large that this effect would be masked by the absorption due to the direct transition, which takes place at a lower photon energy.

The cross-field experiment appears to be a very sensitive technique for studying interband phenomena. This method has already made possible the observation of interband magnetoabsorption effects in GaAs,[29] where other techniques had failed. Furthermore, in recent experiments in zero magnetic field, the reflectivity from germanium due to direct transitions to higher bands was readily observed by applying an electric field to the crystal surface. As a matter of fact, the transition between the split-off valence band and the conduction band was observed by this method.[139]

[134a] R. L. Aggarwal, L. Rubin, and B. Lax, *Phys. Rev. Letters* **17**, 8 (1966); J. G. Mavroides, M. S. Dresselhaus, R. L. Aggarwal, and G. F. Dresselhaus, *Proc. Intern. Conf. Phys. Semicond., Kyoto, 1966* (*J. Phys. Soc. Japan* **21**, Suppl.) p. 184. Phys. Soc. Japan, Tokyo, 1966.

[135] H. B. Briggs and R. C. Fletcher, *Phys. Rev.* **91**, 1342 (1953).

[136] R. Braunstein, *J. Phys. Chem. Solids* **8**, 280 (1959).

[137] F. Stern and R. M. Talley, *Phys. Rev.* **108**, 158 (1957).

[138] R. Braunstein and E. O. Kane, *J. Phys. Chem. Solids* **23**, 1423 (1962).

[139] B. O. Seraphin and R. B. Hess, *Phys. Rev. Letters* **14**, 138 (1956).

Thus it appears that the cross-field technique on magnetoreflection should allow the study of these higher bands and possibly provide information on the band parameters, provided that structure is detected with magnetic field.

It is anticipated that new techniques, such as electron bombardment[140] and optical excitation by lasers,[119] will allow transitions involving both interband and exciton phenomena to be observed in emission. Exciton transitions in GaAs lasers have already been studied in high magnetic fields by Galeener and Wright;[127] however, no interband effects, particularly due to higher transitions, have been observed. In the lowest bands where laser action by electron excitation has been observed, as in InSb for example, interband emission of coherent radiation in a magnetic field should be observable in both pure and doped materials. The principal advantage of this technique arises from the high intensity and narrow line widths, which should permit accurate measurements of even the small magnetic effects that would be expected from high-energy-gap materials.

V. Note Added in Proof

Since the initial writing of this chapter, a number of important developments have taken place which we now include in order to bring this report up to date.

Using the traditional magneto-absorption techniques and high magnetic fields, Pidgeon *et al.* have investigated InAs[141] and obtained the energy band parameters with an accuracy comparable to that previously reported for InSb. The theory developed for these two compounds, modified to include the possibility of a negative energy gap of the *s*-band as in gray tin,[142] was then used by Groves and Pidgeon[143] to analyze the magnetoreflection data in HgTe and to obtain the band parameters for this material; they observed both allowed and direct forbidden transitions. This is the second instance where such a forbidden transition has been observed, the other case being in tellurium by Rigaux and Drilhon.[144]

[140] N. G. Basov, O. V. Bogdankevich, and A. G. Devyatkov, *in* "Radiative Recombination in Semiconductors" (7th Intern. Conf.), p. 225. Dunod, Paris, and Academic Press, New York, 1965; C. Benoit a la Guillaume and T. M. DeBever, *in* "Radiative Recombination in Semiconductors" (7th Intern. Conf.), p. 255, Dunod, Paris, and Academic Press, New York, 1965; C. E. Hurwitz and R. J. Keyes, *Appl. Phys. Letters* **5**, 139 (1964).

[141] C. R. Pidgeon, D. L. Mitchell, and R. N. Brown, *Phys. Rev.* to be published.

[142] S. H. Groves and W. Paul, *Phys. Rev. Letters* **11**, 194 (1963).

[143] S. H. Groves and C. R. Pidgeon, to be published; R. N. Brown and S. H. Groves, *Bull. Am. Phys. Soc.* **11**, 206 (1966).

[144] C. Rigaux and G. Drilhon, *Proc. Intern. Conf. Phys. Semicond., Kyoto, 1966* (*J. Phys. Soc. Japan* **21**, Suppl.) p. 193. Phys. Soc. Japan, Tokyo, 1966.

The room temperature piezoreflection measurements[134a] have made possible the observation of magnetooscillations deep into the bands. Transitions from the $p_{1/2}$ spin orbit split-off valence band, which is 0.28 eV below the $p_{3/2}$ band, to the $\mathbf{k} = 0$ conduction band were studied. Similar results were also obtained at this temperature by the electroreflectance and thermoreflectance techniques.[145] However, by extending the piezoreflectance method to low temperatures, magnetooscillations could be observed in InSb to photon energies in excess of 1 eV, so that transitions from the spin orbit split-off band could be studied and thereby an accurate measurement of the spin orbit splitting of the $p_{3/2}$ band ($= 0.80$ eV) be obtained.[146] In addition, structure due to the reduced effective mass and g-factor was observed. But more significantly, this experiment allows the observation of magnetooscillations to very large energies, making it possible to trace quantitatively the curvature of the energy bands over a relatively large range of energy, which should provide data for improved band calculations or for testing the accuracy of existing calculations. Furthermore, a study of the linewidths and intensities of these oscillations should test theories of relaxation phenomena for electrons at high energies both for intra- and interband transitions, since these differential optical techniques allow the observation of oscillatory components over a dynamic range of about four orders of magnitude. Thus, in addition to extending the range of observation, the possibility of finding additional structure in many of the semiconductors is very likely.

For example, by a more careful examination of the magnetooptical spectrum of InSb, Johnson and Larsen[147] have been able to observe the perturbation of the conduction band Landau level structure due to coupling of the electrons to the longitudinal optical phonons in the presence of a magnetic field. This strong interaction between the electrons and phonons, when the cyclotron energy is close to that of the optical phonon, had been predicted by Larsen[148] and was observed for low quantum numbers. The piezoreflection technique should allow a quantitative study of this phenomenon at large quantum numbers as well.

Another new important development in magnetooptical effects has been the observation of multiphoton absorption in the semiconducting compounds InSb and PbTe.[149] One interesting aspect of this phenomenon is that, in the presence of a magnetic field, the multiphoton absorption effect, obtained by using either a focused or collimated CO_2 laser, can be observed

[145] S. H. Groves, C. R. Pidgeon, and J. Feinleib, *Phys. Rev. Letters* **17**, 643 (1966); J. Feinleib, C. R. Pidgeon, and S. H. Groves, A.P.S. Meeting, Nashville, Tenn., December, 1966.

[146] R. L. Aggarwal, to be published.

[147] E. J. Johnson and D. M. Larsen, *Phys. Rev. Letters* **16**, 655 (1966).

[148] D. M. Larsen, *Phys. Rev.* **135**, A419 (1964).

[149] C. K. N. Patel, P. A. Fleury, R. E. Slusher, and H. L. Frisch, *Phys. Rev. Letters* **16**, 971 (1966).

as well-defined peaks in the photoconductivity.[150] Apparently the selection rules are altered in the presence of a magnetic field so that two or three photon absorptions are observed. In PbTe, the two-photon absorption appears strongest with selection rule $\Delta n = \pm 1$, as seen experimentally and interpreted in terms of higher order perturbation theory[151] in which the magnetic levels play a role as intermediate states. This technique should permit the study of higher bands, the mechanisms of multiphoton processes, and other nonlinear interband and intraband magnetooptical phenomena in semiconductors.

ACKNOWLEDGMENTS

We should like to thank Professor L. M. Roth for reading the manuscript and for constructive criticisms and suggestions; Dr. Q. H. F. Vrehen and Dr. C. R. Pidgeon for helpful discussions of their work prior to publication—the former for his experimental and theoretical results on cross-field magnetoabsorption, and the latter for his InSb data. We are also indebted to Dr. John Halpern for suggestions and discussions in connection with his work on GaSb and results on the indirect transition in germanium, and Dr. W. Zawadzki for discussions on cross-field phenomena. Finally, we should like to thank Mrs. S. F. Simon for typing the manuscript.

[150] K. J. Button, B. Lax, M. Weber, and M. Reine, *Phys. Rev. Letters* **17**, 1005 (1966).
[151] W. Zawadzki and E. Hanamura, to be published.

CHAPTER 9

Effects of Free Carriers on the Optical Properties

H. Y. Fan

I. Absorption Due to Free Carriers 406
1. *Free-Carrier Absorption* 406
2. *Interband Absorption* 410
II. Carrier Susceptibility and Infrared Reflection 414
3. *Free-Carrier Susceptibility* 415
4. *Hole Susceptibility* 418

In semiconductors, the effect of free carriers on the optical properties becomes important at wavelengths longer than the intrinsic absorption edge. Free carriers produce absorption and affect also the dispersion at sufficiently long wavelengths. The refractive index n and the extinction coefficient k that characterize the optical properties are related to the conductivity σ and electric susceptibility χ of the material in the well-known way:

$$\begin{aligned} n^2 &= \tfrac{1}{2}[K + (K^2 + 4\sigma^2/\nu^2)^{1/2}], \\ k^2 &= \tfrac{1}{2}[-K + (K^2 + 4\sigma^2/\nu^2)^{1/2}], \end{aligned} \tag{1}$$

where K is the dielectric constant, defined as

$$K = 1 + 4\pi\chi. \tag{2}$$

Alternately, these relations can be written

$$\begin{aligned} n^2 - k^2 &= K, \\ nk\nu &= \sigma. \end{aligned} \tag{3}$$

In a radiation field, the current of the carriers has a component in phase and a component out of phase with the electric field. The in-phase current contributes to the conductivity, and the out-of-phase component contributes to the susceptibility.

In terms of the electronic energy bands of the crystal, the effects of the carriers may be intraband or interband in nature. The intraband effects

involve only the energy band that contains the carriers, and will be simply referred to as free-carrier effects. The interband effects involve another energy band.

I. Absorption Due to Free Carriers

The absorption coefficient α is related to n and k by

$$\alpha = \frac{4\pi\nu}{c}k = \frac{4\pi\sigma}{cn}. \tag{4}$$

In the infrared region, the condition

$$4\sigma^2/\nu^2 \ll K \tag{5}$$

usually holds. We then have

$$n \sim K^{1/2}. \tag{6}$$

Furthermore, provided the carrier concentration is not too high, the carrier contribution χ_c to the susceptibility may be negligible—i.e.,

$$K \sim K_0 \gg 4\pi\chi_c, \tag{7}$$

where K_0 is the dielectric constant of the crystal in the absence of free carriers. Under conditions (5) and (7), the free carriers affect the optical properties only through their contribution to conductivity, influencing α or k but not n. These conditions usually apply in the studies on absorption.

1. Free-Carrier Absorption

a. Theory

With $n \sim K_0^{1/2}$, the carriers contribute an absorption coefficient that is additive to the absorption coefficient in the absence of carriers. Also we can consider separately free-carrier and interband-carrier absorption coefficients. It is convenient to express the free-carrier absorption in terms of the ratio α/N, where N is the carrier concentration. The ratio is often referred to as the photon capture cross section of carriers.

Perfectly free carriers do not produce absorption. Absorption arises from the fact that there is scattering of carriers in motion. The treatment of the effect of acoustic-mode scattering by the method of second-order perturbation, due originally to Fröhlich, was reported by Fan.[1-3] The treat-

[1] H. Y. Fan and M. Becker, *in* "Semi-conducting Materials" (H. K. Henisch, ed.), p. 132. Butterworth, London and Washington, D.C., 1951.
[2] H. Y. Fan, W. Spitzer, and R. J. Collins, *Phys. Rev.* **101**, 566 (1956).
[3] H. Y. Fan, *Rept. Progr. Phys.* **19**, 107 (1956).

ment has since been extended with refinement to many-valley energy bands having ellipsoidal energy surfaces.[4,5] For a classical distribution of carriers, the results may be written in the form[2,4]

$$\frac{\alpha}{N} = \frac{4\pi}{cn}\frac{e^2(2m^*)^{1/2}}{3\pi\hbar^2}\frac{E^2}{\rho C_l^2}\frac{kT}{(h\nu)^{3/2}}\left[\left(\frac{2}{\pi}\right)^{1/2} X^{1/2}e^X(1 - e^{-2X})\,K_2(X)\right], \quad (8)$$

where $X = h\nu/2kT$, $K_2(X)$ is the modified Bessel function of order 2, ρ is the density of the crystal, n is the refractive index, C_l is the sound velocity, and E is the deformation potential. In the case of a many-valley band with ellipsoidal energy surfaces, m^* is a combination of the effective-mass parameters and E is a combination of the deformation-potential parameters. For $X \gg 1$, the quantity in the square brackets reduces to unity. For spherical energy bands, expression (8) can be written[3]

$$\frac{\alpha}{N} = \frac{4\pi}{cn}\frac{1}{9\pi^{3/2}}\frac{e^3}{m^{*2}}\frac{1}{\nu^2}\left(\frac{h\nu}{kT}\right)^{1/2}\frac{1}{\mu_a}, \quad (8a)$$

where μ_a is the mobility corresponding to acoustic-mode scattering.[5a]

The effect of scattering by energetic modes such as optical phonon scattering and intervalley scattering in the case of a many-valley band can be expressed in the following form, according to Rosenberg and Lax[4]:

$$\frac{\alpha}{\alpha_a} \propto \frac{Z}{\sinh Z}\frac{1}{X^2K_2(X)}[(X + Z)^2K_2(X + Z) + (X - Z)^2K_2(X - Z)], \quad (9)$$

where α_a is the α for acoustic modes given by (8), $Z = \hbar\omega_0/2kT$, and ω_0 is some mean frequency for the relevant modes. The constant of proportionality depends on the optical phonon coupling and intervalley scattering parameters. For sufficiently high temperatures, $kT > \hbar\omega_0$, and sufficiently short wavelengths, $h\nu > \hbar\omega_0$, the absorption becomes nearly constant. In germanium, the contribution of energetic-mode scattering is estimated to be comparable to the effect of acoustic-mode scattering at room temperature and above, in the wavelength region around 10 microns.

The effect of ionized-impurity scattering can also be treated by the second-order perturbation method, using the Born approximation for the electron interaction with a Coulomb or screened Coulomb center.[2,4]

[4] R. Rosenberg and M. Lax, *Phys. Rev.* **112**, 843 (1958).

[5] H. J. G. Meyer, *Phys. Rev.* **112**, 298 (1958).

[5a] The practice, which is quite consistently followed throughout the literature, of using the lower-case k to denote the extinction coefficient, the Boltzmann constant, and the magnitude of the wave vector is followed here. It should be apparent from the text which quantity is meant.

A preferable approach is to treat the absorption as the inverse process of bremsstrahlung, giving the result[2]

$$\frac{\alpha}{N} = \frac{4\pi}{cn} N_i \frac{8\pi}{3} \left(\frac{Ze^2}{K}\right)^2 \frac{e^2\hbar^2}{m^*} \frac{1}{(2\pi m^* kT)^{1/2}} \frac{1}{(h\nu)^3} (1 - e^{-2X}) e^X K_0(X), \quad (10)$$

in the case of classical distribution of carriers, where K_0 is the modified Bessel function of order zero, N_i is the impurity concentration, and Ze is the charge of an impurity center. The expression is an approximation valid when

$$\varepsilon_0 \gg E_i, \quad (11)$$

where ε_0 is the thermal energy of the carriers and E_i is the impurity ionization energy. Approximations for other conditions of limited applicability have been considered.[5,6] Numerical calculations can always be made, using the matrix elements known from bremsstrahlung. For high carrier concentrations, the screening of the impurity charge should be taken into account. An expression in the form of an integral has been given by Wolfe.[7]

The effect of polar-mode scattering has been treated by Visvanathan.[8] For classical distribution of carriers, the expression obtained in the form of an integral can be written

$$\frac{\alpha}{N} = \frac{4\pi}{cn} \frac{\sqrt{2}}{3} \frac{e^4(K_\infty^{-1} - K_0^{-1})}{m^*} \frac{\hbar\omega_l}{(h\nu)^{2.5}} \frac{e^{2Z} + 1}{e^{2Z} - 1} \times \left(1 + \frac{11}{8X} - \frac{4}{(2\pi X)^{1/2}} \cdots\right), \quad (12)$$

under the limiting condition

$$2(X - Z) = (h\nu - \hbar\omega_l)/kT \gg 1. \quad (13)$$

b. Experimental Results

Free-carrier absorption has been observed in most of the III–V compounds. Table I summarizes some of the experimental observations, with representative data for germanium given for comparison. Figure 1 shows the measurements of Dixon for InAs.[8a]

[6] S. Visvanathan, *Phys. Rev.* **120**, 379 (1960).
[7] R. Wolfe, *Proc. Phys. Soc. (London)* **A67**, 74 (1954).
[8] S. Visvanathan, *Phys. Rev.* **120**, 376 (1960).
[8a] J. R. Dixon, *Proc. Intern. Conf. Semicond. Phys., Prague, 1960* p. 366. Czech. Acad. Sci., Prague, and Academic Press, New York, 1961.

TABLE I

FREE-CARRIER ABSORPTION IN *n*-TYPE COMPOUNDS[a]

	Carrier concentration (10^{17} cm^{-3})	α/N (10^{-17} cm^{-3})	p	Reference
GaAs	1–5	3	3	*b*
InAs	0.3–8	4.7	3	*c*
GaSb	0.5	6	3.5	*d*
InSb	1–3	2.3	2	*e*
InP	0.4–4	4	2.5	*f*
GaP	10	(32)	(1.8)	*g*
AlSb	0.4–4	15	2	*h*
Ge	0.5–5	~4	~2	*i*

[a] The ratio α/N of absorption coefficient to carrier concentration is given for the wavelength of 9 microns. The parameter p expresses the wavelength dependence of absorption in the approximation $\alpha \propto \lambda^p$.

[b] See Ref. 18.

[c] See Ref. 8a.

[d] See Ref. 26.

[e] S. W. Kurnick and J. M. Powell, *Phys. Rev.* **116**, 597 (1959); see also Ref. 22.

[f] See Ref. 25.

[g] See Ref. 13.

[h] See Ref. 17.

[i] See Ref. 2.

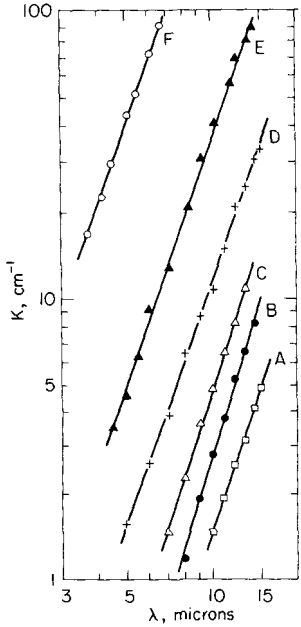


FIG. 1. Free-carrier absorption in *n*-type InAs at room temperature. The electron concentrations in units of 10^{17} cm^{-3} are: (*A*) 0.28, (*B*) 0.85, (*C*) 1.4, (*D*) 2.5, (*E*) 7.8, (*F*) 39. (After Dixon.[8a])

It has been shown for a number of III–V compounds that for mobility, polar-mode scattering is the dominant mechanism of lattice scattering.[9] Visvanathan[8] made estimates for GaAs and InP by using expression (12) and obtained results of the order of magnitude of the observed absorptions. Acoustic-mode deformation-potential scattering is estimated to give high mobilities—e.g., $\mu_a \sim 10^5$ cm^2/V-sec for GaAs[10] and 2×10^6 cm^2/V-sec for InSb.[11] According to (8*a*), α/N would be an order of magnitude lower than the observed values. The effect of scattering by ionized impurities is proportional to $(m^*)^{-3/2}$, and it may be expected to be an important absorption mechanism for the compounds. If the carrier concentration is a measure of the amount of ionized impurities, then an indication for the effect of ionized impurities is an increase of α/N with increasing carrier concentration. Such behavior can be seen in the GaAs and InAs data for $N \gtrsim 10^{18}$ cm^{-3}.

Careful study of the absorption should be very useful for the understanding of the scattering mechanisms. In order to obtain reliable results, however, extensive measurements in conjunction with the electrical measurements have to be made, and the results must be carefully analyzed. Haga and Kimura[12] made analyses of the available absorption and electrical data for InSb and InAs. They concluded that acoustic-mode scattering is most important for the absorption in InSb, corresponding to a rather high deformation potential. For InAs, their analysis does show the optical-mode scattering to be dominant in absorption. In the analyses, the carrier distribution was calculated instead of being approximated by Maxwellian distribution. An attempt was also made to treat the conduction band more accurately, according to Kane's calculation.

2. Interband Absorption

a. n-Type Compounds

In *n*-type GaP, an absorption band in the region 1–4 microns with a peak at ~3 microns was observed by Spitzer *et al.*[13] as shown in Fig. 2. The band increased with carrier concentration and shifted to somewhat higher energy when the carriers froze out at low temperature. The lowest minima of the conduction band in GaP are believed to be in the $\langle 100 \rangle$ directions. It was suggested that the 3-micron band arose from electron transitions from the $\langle 100 \rangle$ minima to the minimum at $\mathbf{k} = 0$. Measurements

[9] H. Ehrenreich, *J. Appl. Phys.* **32**, 2155 (1961).
[10] H. Ehrenreich, *Phys. Rev.* **120**, 1951 (1960).
[11] H. Ehrenreich, *J. Phys. Chem. Solids* **2**, 131 (1957).
[12] E. Haga and H. Kimura, *J. Phys. Soc. Japan* **18**, 777 (1963); **19**, 471 (1964).
[13] W. G. Spitzer, M. Gershenzon, C. J. Frosch, and D. F. Gibbs, *J. Phys. Chem. Solids* **11**, 339 (1959).

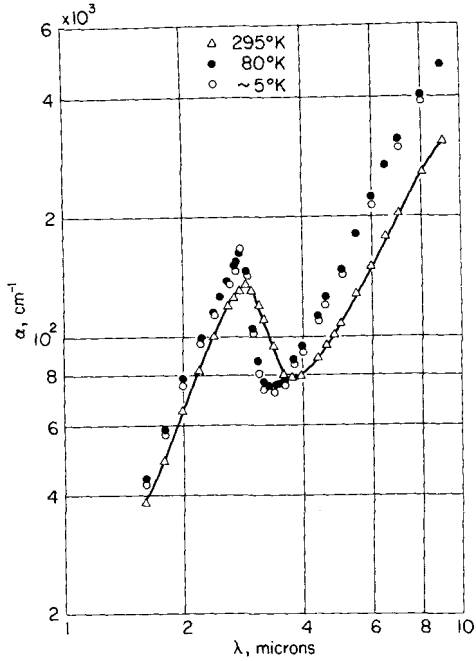


FIG. 2. Absorption coefficient versus wavelength for an n-type GaP specimen of $N = 1 \times 10^{18}\,\text{cm}^{-3}$. (After Spitzer *et al.*[13])

by Zallen[14] showed that the absorption band did not shift with pressure as might be expected from the pressure shift of the energy difference between the $\mathbf{k} = 0$ and the $\langle 100 \rangle$ minima. Paul[14] suggested that the absorption may correspond to vertical transitions between two sets of $\langle 100 \rangle$ minima, Δ_1 and Δ_2, split from each other. Recent measurements of Allen and Hodby on GaP_xAs_{1-x} alloys[15] support this hypothesis. The 3-micron band, the threshold of which shifted but slightly with composition, became unobservable when the $\mathbf{k} = 0$ minimum became lowest at high concentrations of As. At low temperatures, the absorption corresponds to transitions from the impurity levels to the higher (Δ_2) minima; interband transitions $\Delta_1 \rightarrow \Delta_2$ come in at higher temperatures. From the results on the 3-micron band, the splitting of the $\langle 100 \rangle$ minima is estimated to be 0.27 eV for GaAs, as compared to the value 0.43 eV indicated by optical reflection spectrum.[16]

[14] W. Paul, *J. Appl. Phys.* **32**, 2082 (1961).
[15] J. W. Allen and J. W. Hodby, *Proc. Phys. Soc. (London)* **82**, 315 (1963).
[16] D. L. Greenaway, *Phys. Rev. Letters* **9**, 97 (1962).

Turner and Reese[17] observed in AlSb an absorption band with a peak at 4.3 microns (0.29 eV) that was proportional to the carrier concentration. The absorption was interpreted as carrier transition to a higher minimum of the conduction band at $\mathbf{k} = 0$. With freeze-out of carriers at low temperature, the absorption band diminished and two other bands appeared at approximately 2.5 microns and 7 microns. The observation indicated that the two bands correspond to transitions from the impurity level to the lowest and the next higher minima of the conduction band, respectively. The edge of the conduction band in AlSb is believed to be given by $\langle 100 \rangle$ minima. Paul[14] suggested that the 4.3-micron absorption also corresponds to transitions between split $\langle 100 \rangle$ minima, as in GaP. It is likely that the absorption bands in the two compounds correspond to similar transitions. The observed α/N has nearly the same value for both materials, and it is unlikely that the absorption corresponds to vertical transitions in one compound and indirect transitions in the other.

The measurements of Spitzer and Whelan[18] on gallium arsenide showed absorption in excess of free-carrier absorption in the region 1–5 microns. The absorption was found to be proportional to the carrier concentration and independent of the doping impurity. It was attributed to transitions from the $\mathbf{k} = 0$ minimum, Γ_1, to higher-lying $\langle 111 \rangle$ minima, and the energy separation between the minima was estimated to be ~ 0.25 eV. Vertical transitions from Γ_1 to a higher minimum, Γ_{15}, at $\mathbf{k} = 0$ have also been suggested; however, 0.25 eV seems to be too small for Γ_1–Γ_{15} separation. The origin of the excess absorption has not been established definitely. It is interesting to note that the absorption corresponds to an $\alpha/N \sim 4 \times 10^{-18}\,\mathrm{cm}^{-2}$, which is much lower than the value $\alpha/N \sim 10^{-16}\,\mathrm{cm}^{-2}$ we estimate for the absorption bands of AlSb and GaP.

b. p-Type Compounds

The absorption due to free holes is dominated by transitions between valence bands. There are a heavy-hole band v_1, a light-hole band v_2, and a split-off band v_3, which lies lower by Δ. In the more detailed picture, each of the doubly degenerate bands, v_1 and v_2, is split for $\mathbf{k} \neq 0$.[19,20] The spectrum of the interband absorption and its dependences on temperature and carrier concentration can be used to verify the detailed structure of the valence bands, although it is difficult to determine the band structure in detail from the absorption alone.

[17] W. J. Turner and W. E. Reese, *Phys. Rev.* **117**, 1003 (1960).
[18] W. G. Spitzer and J. M. Whelan, *Phys. Rev.* **114**, 59 (1959).
[19] G. Dresselhaus, *Phys. Rev.* **100**, 580 (1955); R. H. Parmenter, *ibid.* **100**, 573 (1955).
[20] E. O. Kane, *J. Phys. Chem. Solids* **1**, 249 (1957).

Absorption due to $v_2 \rightarrow v_1$ transitions has been observed in all the compounds studied: AlSb, GaSb, InAs, and InSb. Transitions $v_3 \rightarrow v_1$ and $v_3 \rightarrow v_2$ have been seen in the spectra of AlSb and GaAs. Figure 3 shows the results for GaAs. For the other compounds, Δ is larger than the energy gap, and absorption due to transitions involving v_3 should fall within the region of strong intrinsic absorption.[21] Hodby studied GaP and GaP_xAs_{1-x} alloys. All three types of transitions were seen in the spectra of alloys with

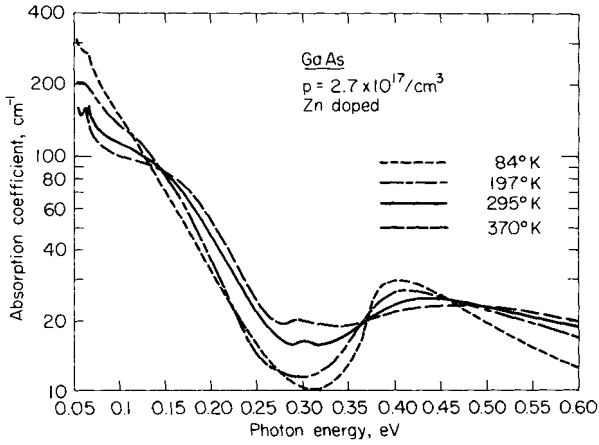


FIG. 3. Absorption due to free holes in p-type GaAs. The peaks at 0.42 eV and 0.31 eV are due to $v_3 \rightarrow v_1$ and $v_3 \rightarrow v_2$ transitions, respectively. The band at 0.15 eV is attributed to $v_2 \rightarrow v_1$ transitions. (After Braunstein and Kane.[21])

$x < 0.87$; strong free-hole absorption prevented the study of interband transition for larger x.

The information derived from the studies is summarized in Table II. In the cases of AlSb, GaAs, and GaP_xAs_{1-x}, each valence band was approximated by an effective mass in the interpretations of the absorption spectra. In the work on InSb, v_2 is approximated by a spherical and v_1 by a warped band; information on the v_1 band was obtained separately from studies of intrinsic absorption in degenerate p-type samples. For GaSb, it was found only that the absorption spectra due to $v_2 \rightarrow v_1$ transitions could not be fitted by representing each of the two bands with an effective mass. In the study of InAs, the spectra measured at different temperatures were fitted by using many parameters that are relevant to the details of the conduction and valence bands according to Kane's theory.[20] Such fitting indicated, among other things, that the maximum energy of the valence band may be slightly higher than the energy at $\mathbf{k} = 0$.

[21] R. Braunstein and E. O. Kane, *J. Phys. Chem. Solids* **23**, 1423 (1962).

TABLE II

INTERBAND ABSORPTION DUE TO FREE HOLES

	Transitions observed	Information derived	Reference
AlSb	all 3	$\Delta \sim 0.75$ eV	*a*
GaAs	all 3	$m_1/m_3 = 3.38$; $m_2/m_3 = 1.70$ $\Delta \sim 0.33$ eV	*b*
GaP_xAs_{1-x}	all 3	$\Delta(x)$ extrapolates to $\Delta(1) \sim 0.127$ eV $m_1/m_2 \sim 6.2$ for $x = 0.87$	*c*
InSb	$v_2 \rightarrow v_1$	$m_2 \sim 0.014\, m$	*d*
GaSb	$v_2 \rightarrow v_1$	At least one of v_1 and v_2 nonspherical	*e*
InAs	$v_2 \rightarrow v_1$	$m_c = 0.021\, m$ (near the bottom) $m_1 = 0.41\, m$ (far from the top) $m_2 = 0.025\, m$ (near the top) $m_3 = 0.083\, m$ (near the top) $\Delta = 0.43$ eV	*f*

[a] See Ref. 21.
[b] R. Braunstein, *J. Phys. Chem. Solids* **8**, 280 (1959); see also Ref. 21.
[c] J. W. Hodby, *Proc. Phys. Soc. (London)* **82**, 324 (1963).
[d] G. W. Gobeli and H. Y. Fan, *Phys. Rev.* **119**, 613 (1960).
[e] See Ref. 26.
[f] F. Matossi and F. Stern, *Phys. Rev.* **111**, 472 (1958)

II. Carrier Susceptibility and Infrared Reflection

At sufficiently high carrier concentrations, condition (7) may not be valid, and the dielectric constant of the material may be strongly affected by the susceptibility of carriers. Under such conditions, both n and k are influenced by the effect of carriers, and two independent optical measurements are necessary in order to determine n and k and to obtain the susceptibility and conductivity of carriers. The effect of carrier susceptibility was first noticed in the reflectivity of germanium in the far infrared.[1] The reflectivity given by

$$R = \frac{(n-1)^2 + k^2}{(n+1)^2 + k^2} \tag{14}$$

is suitable for the study of the carrier susceptibility. If carrier scattering is not too strong, the carrier susceptibility may significantly affect K while the carrier conductivity is still sufficiently low for condition (5) to apply. In this case, it can be seen from (1) that k is small and R depends on n,

which is essentially determined by K. The departure of reflectivity from that of specimens with very low carrier concentrations shows the effect of carrier susceptibility on K.

3. Free-Carrier Susceptibility

a. Theory

Unlike the conductivity, the susceptibility does not depend on carrier scattering as an essential process. For infrared radiation, the condition

$$\omega\tau \gg 1 \tag{15}$$

is usually satisfied, where ω is the angular frequency of radiation and τ is the relaxation time for scattering. The scattering then has negligible effect, and the susceptibility is determined entirely by the structure of carrier energy band.

A theoretical expression for the susceptibility has been given by Spitzer and Fan,[22] which becomes

$$\chi_c = \left(\frac{e}{\hbar\omega}\right)^2 \int \frac{\partial^2 \varepsilon}{\partial k_x{}^2} f(\mathbf{k}) \frac{2}{(2\pi)^3} d\Omega_k \tag{16}$$

under condition (15), where $f(\mathbf{k})$ is the carrier-distribution function and x is an arbitrary direction in the crystal assumed to be of cubic symmetry. An effective mass m_s for susceptibility is defined by the equation

$$\chi_c \equiv -Ne^2/\omega^2 m_s. \tag{17}$$

The susceptibility of free carriers is negative in sign because free charged particles give current lagging in phase. Given $\varepsilon(\mathbf{k})$ of the carrier energy band, the susceptibility can be evaluated readily from (16). Simple expressions for m_s can be written for several cases of interest:

(1) $\varepsilon = \hbar^2 k^2/2m^*$:

$$m_s = m^*. \tag{18a}$$

(2) Multivalley ellipsoidal band, $\varepsilon = (\hbar^2/2)(k_1{}^2/m_1 + k_2{}^2/m_2 + k_3{}^2/m_3)$:

$$\frac{1}{m_s} = \frac{1}{3}\left(\frac{1}{m_1} + \frac{1}{m_2} + \frac{1}{m_3}\right). \tag{18b}$$

(3) Two degenerate bands, $\varepsilon_1 = \hbar^2 k^2/2m_1$ and $\varepsilon_2 = \hbar^2 k^2/2m_2$:

$$\frac{1}{m_s} = \frac{m_1^{1/2} + m_2^{1/2}}{m_1^{3/2} + m_2^{3/2}}. \tag{18c}$$

[22] W. G. Spitzer and H. Y. Fan, *Phys. Rev.* **106**, 882 (1957).

If ε is not simply a quadratic function of $\mathbf{k}$, m_s will depend on temperature on account of the distribution function in the integrand of (16). Also, m_s will depend on the carrier concentration unless the distribution function is nearly classical. In general, m_s is not the same as the effective mass defined usually by

$$1/m^* \equiv (1/\hbar^2)\nabla_{\mathbf{k}}\nabla_{\mathbf{k}}\varepsilon. \tag{18d}$$

For degenerate carriers at sufficiently low temperatures, (16) may be written

$$\chi_c \sim -\frac{2}{(2\pi)^3}\frac{e^2}{\omega^2}\frac{1}{3\hbar}\langle v\rangle S, \tag{19}$$

where S is the area of Fermi surface and $\langle v\rangle$ is the carrier velocity averaged over the Fermi surface. In case the constant-energy surfaces are spherical, we get

$$\frac{1}{m_s} = \frac{1}{\hbar^2 k_\zeta}\left|\frac{\partial\varepsilon}{\partial k}\right|_\zeta. \tag{20}$$

If ε is not simply a parabolic function of $\mathbf{k}$, m_s will depend on the Fermi energy or carrier concentration.

b. Experimental Results for n-Type Compounds

Spitzer and Fan[22] studied InSb using degenerate samples of various concentrations ranging from 3.5×10^{17} to $4.0 \times 10^{18}\,\mathrm{cm}^{-3}$. Figure 4 shows the reflectivity spectra. Absorption measurements showed that $k^2 \ll 1$ on the short-wavelength side of the minima. The reduction of K to $K = 1$ by the negative-carrier susceptibility was responsible for $n = 1$ and $R \sim 0$ near the minimum. The susceptibility χ_c obtained showed the $1/\omega^2$ dependence according to (16). The value of m_s obtained for the samples showed a dependence on carrier concentration, varying from $0.023m$ to $0.041m$. By using (20), $\varepsilon(\mathbf{k})$ was calculated for ε up to 0.3 eV. The procedure of deducing $\varepsilon(\mathbf{k})$ from m_s for different carrier concentrations involves, of course, the assumption that the conduction band is not affected by the doping impurity.

Several samples of GaAs were measured by Spitzer and Whelan.[18] The carrier concentrations were 5.4, 1.12, 1.09, and 0.49 in units of $10^{18}\,\mathrm{cm}^{-3}$. The corresponding values of m_s obtained were $0.089m$, $0.079m$, $0.079m$, and $0.078m$. Cardona[23] used an expression

$$\varepsilon \sim -E_g/2 + [(E_g/2)^2 + \beta^2 k^2]^{1/2} \tag{21}$$

[23] M. Cardona, *Phys. Rev.* **121**, 752 (1961).

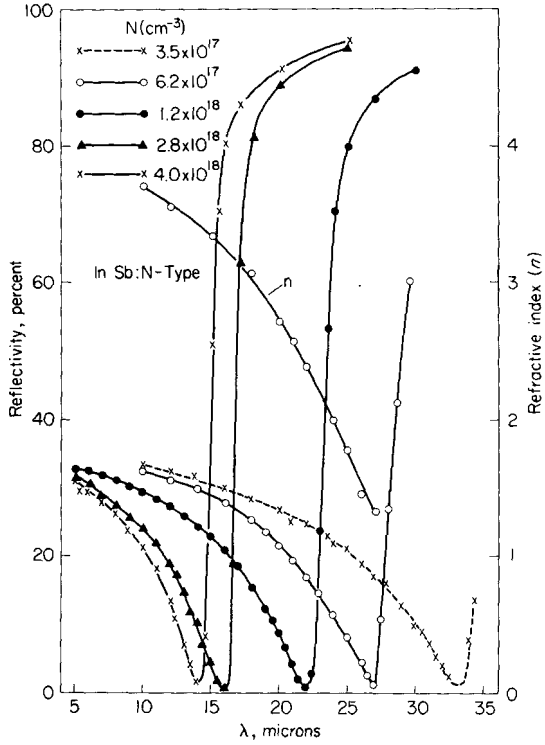


FIG. 4. Reflectivity spectra for five n-type InSb samples. The refractive index curve labeled n is for the sample of $N = 6.2 \times 10^{17}\,\text{cm}^{-3}$. (After Spitzer and Fan.[22])

for the $\mathbf{k} = 0$ valley of the conduction band. The constant β is the momentum matrix element between the conduction and valence bands at $\mathbf{k} = 0$, and E_g is the energy gap. According to this approximation, the effective mass deduced from Faraday rotation is the same as m_s. Cardona made Faraday-rotation measurements on GaAs and interpreted the effective-mass variation given by his data and that of Spitzer and Whelan on the basis of (21). As mentioned above, a temperature dependence of m_s is expected when ε is not simply a quadratic function of $\mathbf{k}$. Experimentally, no more than a few percent change in m_s was found for GaAs,[23] InAs,[23] and InP[24] between 100° and 296°K. The smallness of the temperature effect was explained by Cardona by considering temperature variation of effective mass due to lattice dilatation, which compensates the variation of m_s due to carrier distribution.

[24] M. Cardona, *Proc. Intern. Conf. Semicond. Phys., Prague, 1960* p. 388. Czech. Acad. Sci., Prague, and Academic Press, New York, 1961.

For InAs, Spitzer and Fan[22] obtained $m_s = 0.030m$ for a sample of $N = 2.4 \times 10^{17}\,\mathrm{cm}^{-3}$ and $m_s = 0.033m$ for $N = 1.4 \times 10^{18}\,\mathrm{cm}^{-3}$. Cardona[23] obtained $m_s = 0.052m$ for $N = 5.2 \times 10^{18}\,\mathrm{cm}^{-3}$ and deduced from Faraday-rotation measurement an effective mass of $0.027m$ for a sample of $N = 4.9 \times 10^{16}\,\mathrm{cm}^{-3}$. The variation of m_s indicated by the combined data was interpreted by Cardona on the basis of (21).

Reflectivity measurements have been made on an InP sample[24,25] with $N \sim 5 \times 10^{18}\,\mathrm{cm}^{-3}$, giving $m_s = 0.26m$ which is considerably higher than the effective mass, $0.07m$, deduced from a Faraday-rotation measurement on a sample of $N = 10^{16}\,\mathrm{cm}^{-3}$. The reason for this large difference is not clear.

The situation in GaSb is complicated by the fact that there are $\langle 111 \rangle$ minima in the conduction band that are close to the lowest minimum at $\mathbf{k} = 0$ with an energy separation $\Delta = 0.07\,\mathrm{eV}$. Except for low temperatures and low carrier concentrations, there will be carriers in the lowest and the $\langle 111 \rangle$ valleys. In this case, the expression for susceptibility is[26]

$$\chi_c = -\frac{1}{R_H ec}\frac{e^2}{m_{s1}\omega^2}\left[\frac{\mu_{H1}}{\mu_1}\frac{1 + xyy_H}{(1 + xy)^2}\left(1 + x\frac{m_{s1}}{m_{s2}}\right)\right], \tag{22}$$

where $x = n_2/n_1$, $y = \mu_2/\mu_1$, $y_H = \mu_{H2}/\mu_{H1}$, R_H is the Hall coefficient, and subscripts 1 and 2 refer to the central valley and the $\langle 111 \rangle$ valleys, respectively. Reflectivity measurements have been made by Spitzer[26] and by Cardona.[27] Becker *et al.*[26] obtained the values Δ, y, and m_{d2}/m_{d1} (the ratio of density-of-states masses) from other measurements, and calculated the ratio of m_{s2}/m_{d2} for the $\langle 111 \rangle$ valleys by using Spitzer's data. From m_{s2}/m_{d2}, the ratio of longitudinal and transverse masses was estimated for the $\langle 111 \rangle$ valleys.

4. Hole Susceptibility

On account of intervalence-band transitions, the problem of determining the free-carrier effect on susceptibility is more complicated for holes. The susceptibility contributed by interband transitions is related to the interband absorption by

$$\chi_{ij}(\nu) = \frac{1}{\pi^2}\int \frac{\sigma_{ij}(\nu_1)}{\nu_1^2 - \nu^2}\,d\nu_1, \tag{23}$$

where the subscripts i and j are indices for the two bands involved, and

[25] R. Newman, *Phys. Rev.* **111**, 1518 (1958).
[26] W. M. Becker, A. K. Ramdas, and H. Y. Fan, *J. Appl. Phys.* **32**, 2094 (1961).
[27] M. Cardona, *J. Phys. Chem. Solids* **17**, 336 (1961).

$\sigma_{ij}(\nu_1)$ is the conductivity corresponding to the interband absorption at frequency ν_1. Depending on the frequency ν, the susceptibility may be positive or negative. In order to obtain the contribution χ_c of the free-carrier effect, $\chi_{ij}(\nu)$ should be subtracted from the experimentally determined χ.

As discussed above, interband transitions dominate the carrier absorption in the p-type compounds. The free-carrier effects increase with wavelength, but within the convenient wavelength range, 10–30 microns, the absorption is still largely due to transitions between heavy-hole and light-hole bands. However, this does not mean that the susceptibility associated with interband transitions also overshadows the susceptibility due to free-carrier effects. Spitzer and Fan[22] showed that in a germanium sample, $4\pi\chi_{HL}$ of interband transitions was three to four times smaller in magnitude than $4\pi\chi_c$ of the free-carrier effect. The interband absorption α/N in the III–V compounds is close to that of germanium in magnitude, corresponding to about the same $4\pi\chi_{HL}$. At the same time, $4\pi\chi_c$ should be larger in magnitude than in germanium on account of generally smaller effective masses. By neglecting the interband $4\pi\chi_{HL}$, $m_s = 0.20m$ for InSb[22] and $m_s \sim 0.23m$ for GaSb[26] have been approximately estimated from reflectivity measurements.

CHAPTER 10

Free-Carrier Magnetooptical Effects*

Edward D. Palik and George B. Wright

I. INTRODUCTION 421

II. INDEX OF REFRACTION OF THE MAGNETOPLASMA 422
1. *Maxwell's Equations in a Tensor Medium* 422
2. *Magnetoconductivity of a System of Free Carriers* 423

III. FREE-CARRIER MAGNETOOPTICAL EFFECTS 425
3. *Effects Involving a Change of Intensity of the Incident Light* . . . 425
4. *Effects Involving a Change in the Polarization State of the Incident Light* 431
5. *Helicon and Alfvén Waves* 437
6. *Quantum Oscillatory Free-Carrier Effects* 438

IV. FREE-CARRIER MAGNETOOPTICAL EXPERIMENTS 439
7. *Magnetoreflection Experiments* 439
8. *Magnetotransmission Experiments* 441
9. *Summary of Experimental Results* 456

I. Introduction

The free-carrier magnetooptical experiments we wish to discuss have usually been performed in the infrared, where $\omega\tau \gg 1$, and the results are fairly insensitive to the type of scattering mechanism involved. In addition, the experiments are often performed on material in which the carrier distribution is degenerate, and the resulting simplification of the transport integrals allows one to describe the experiments with simple formulae derived from classical mechanics and Maxwell's equations.[1] In semiconductors, however, one deals with an effective mass, which may be small and anisotropic, and there is an important contribution from the background dielectric constant of the lattice. In addition, in contrast to free-carrier experiments on gaseous plasmas, one has the possibility of attaining relatively high carrier concentrations, low temperatures, and a well-defined boundary condition. A few of the experiments—e.g., the optical

* This work was performed at the Naval Research Laboratory and the Lincoln Laboratory (a center for research operated by M.I.T., with support of the U.S. Air Force).

[1] J. A. Ratcliffe, "Magneto-ionic Theory." Cambridge Univ. Press, London and New York, 1959.

de Haas–Shubnikov effect—exhibit quantum effects and cannot be described in the classical manner.

II. Index of Refraction of the Magnetoplasma

1. Maxwell's Equations in a Tensor Medium

We shall treat the system of free carriers in a semiconductor as a plasma of negative charges moving together in a uniform background of compensating positive charge. For this purpose, we need solutions of Maxwell's equations for plane waves propagating in the medium.

For fields varying as $e^{i\omega t}$, we may write Maxwell's equations in rationalized MKS units as

$$\nabla \times \mathbf{E} = -\frac{\partial \mathbf{B}}{\partial t} = -i\omega\mu_0\mathbf{H}, \tag{1}$$

$$\nabla \times \mathbf{H} = \frac{\partial \mathbf{D}}{\partial t} + \mathbf{J} = (i\omega\varepsilon_0\boldsymbol{\kappa} + \boldsymbol{\sigma})\cdot\mathbf{E}. \tag{2}$$

Here we have made use of the constitutive equations

$$\mathbf{B} = \mu_0\mathbf{H} \qquad \mathbf{D} = \varepsilon_0\boldsymbol{\kappa}\cdot\mathbf{E} \qquad \mathbf{J} = \boldsymbol{\sigma}\cdot\mathbf{E}, \tag{3}$$

where $\mu_0 = 4\pi \times 10^{-7}$ H/m and $\varepsilon_0 = 1/4\pi c^2 \times 10^{-7}$ F/m are the *permeability* and *permittivity*, respectively, of free space. For our purposes, all interband processes are assigned to $\boldsymbol{\kappa}$, the background dielectric constant, while intraband processes are assigned to $\boldsymbol{\sigma}$, the conductivity. Since we are primarily interested in the latter type of process, κ will be treated as a real scalar, while $\boldsymbol{\sigma}$ is a complex tensor. For a cubic semiconductor in an external magnetic field $\mathbf{B}_0$ along axis 3 of the rectangular coordinate system, $\boldsymbol{\sigma}$ will have the form[2]

$$\boldsymbol{\sigma} = \begin{bmatrix} \sigma_{11} & \sigma_{12} & 0 \\ -\sigma_{12} & \sigma_{22} & 0 \\ 0 & 0 & \sigma_{33} \end{bmatrix} \tag{4}$$

if B is along the [100], [111], or [110] crystalline axis. For the first two cases $\sigma_{11} = \sigma_{22}$. The diagonal terms are even functions of B, while σ_{12} is an odd function of B. This result is obtained by inspection of the crystal symmetry operations, and application of Onsager's principle $[\sigma_{ij}(\mathbf{B}) = \sigma_{ji}(-\mathbf{B})]$.

Assuming plane-wave solutions to Maxwell's equations,

$$\mathbf{E} = \mathbf{E}_0 \exp\{i\omega[t - (n^*/c)\hat{\mathbf{s}}\cdot\mathbf{r}]\} \quad \text{and} \quad \mathbf{H} = \mathbf{H}_0 \exp\{i\omega[t - (n^*/c)\hat{\mathbf{s}}\cdot\mathbf{r}]\},$$

where $\hat{\mathbf{s}}$ is a unit vector in the direction of propagation and n^* is the complex

[2] B. Lax and L. M. Roth, *Phys. Rev.* **98**, 548 (1955).

index of refraction $(n - ik)$, we obtain

$$n^{*2}[\mathbf{E} - (\hat{\mathbf{s}} \cdot \mathbf{E})\hat{\mathbf{s}}] = \kappa \mathbf{E} - i\boldsymbol{\sigma} \cdot \frac{\mathbf{E}}{\omega \varepsilon_0}. \tag{5}$$

For certain directions of propagation and polarization relative to the external field, it is possible to write the index equation in terms of a scalar effective conductivity[2]

$$n^{*2} = \kappa - i\frac{\sigma_{eff}}{\omega \varepsilon_0}. \tag{6}$$

Expressions for σ_{eff} are given in Table I. To proceed further, we derive the electromagnetic properties in terms of a model involving the atomistic parameters of the medium.

TABLE I

EFFECTIVE CONDUCTIVITIES FOR THE SCALAR REFRACTIVE-INDEX EQUATION

Direction of propagation	Polarization	Effective conductivity
$\hat{\mathbf{s}} \parallel \mathbf{B}_0$	$\mathbf{E}_{\pm} \perp \mathbf{B}_0$	$\sigma_{eff} = \frac{1}{2}(\sigma_{11} + \sigma_{22}) \pm i[\sigma_{12}^2 - \frac{1}{4}(\sigma_{11} - \sigma_{22})^2]^{1/2}$
$\hat{\mathbf{s}} \perp \mathbf{B}_0$	$\mathbf{E} \parallel \mathbf{B}_0$	$\sigma_{eff} = \sigma_{33}$
$\hat{\mathbf{s}} \perp \mathbf{B}_0$	$\mathbf{E} \perp \mathbf{B}_0$	$\sigma_{eff} = \dfrac{\omega\kappa\varepsilon_0(s_2^2\sigma_{11} + s_1^2\sigma_{22}) - i(\sigma_{12}^2 + \sigma_{11}\sigma_{22})}{\omega\kappa\varepsilon_0 - i(s_1^2\sigma_{11} + s_2^2\sigma_{22})}$

2. MAGNETOCONDUCTIVITY OF A SYSTEM OF FREE CARRIERS

We consider the electromagnetic properties of a medium containing N particles of effective mass m^* and charge e to be the sum of individual particle properties. This is the plasma mode because all particles move together. The classical equations of motion of a particle subjected to external field $\mathbf{E}e^{i\omega t}$ and $\mathbf{B}$, and viscously damped with frequency ν, are

$$m\frac{d\mathbf{v}}{dt} + m\nu\mathbf{v} = e(\mathbf{E}\, e^{i\omega t} + \mathbf{v} \times \mathbf{B}). \tag{7}$$

For $\mathbf{v} \sim e^{i\omega t}$, taking coordinates along the principal axes of the effective-mass tensor, and recalling that $\mathbf{J} = Ne\mathbf{v} = \boldsymbol{\sigma} \cdot \mathbf{E}$, we obtain[3]

$$\boldsymbol{\sigma} = Ne^2 \begin{bmatrix} (i\omega + \nu)m_1 & -eB_3 & eB_2 \\ eB_3 & (i\omega + \nu)m_2 & -eB_1 \\ -eB_2 & eB_1 & (i\omega + \nu)m_3 \end{bmatrix}^{-1}. \tag{8}$$

[3] B. Lax, H. J. Zeiger, and R. N. Dexter, *Physica* **20**, 818 (1954).

The algebra for even this simple model becomes tedious, but explicit results have been worked out.[3] Further simplification results for a model with isotropic mass m^* and **B** oriented along axis 3. Then

$$\sigma = \omega_p^2 \varepsilon_0 \kappa \begin{bmatrix} \dfrac{-i(\omega - i\nu)}{(\omega - i\nu)^2 - \omega_c^2} & \dfrac{-\omega_c}{(\omega - i\nu)^2 - \omega_c^2} & 0 \\ \dfrac{\omega_c}{(\omega - i\nu)^2 - \omega_c^2} & \dfrac{-i(\omega - i\nu)}{(\omega - i\nu)^2 - \omega_c^2} & 0 \\ 0 & 0 & \dfrac{-i}{(\omega - i\nu)} \end{bmatrix}, \tag{9}$$

where $\omega_p^2 = Ne^2/m^*\varepsilon_0\kappa$ and $\omega_c = e\hat{\mathbf{s}} \cdot \mathbf{B}/m^*$. The resultant indices of refraction are given in Table II. The $\pm$ signs on $(n - ik)_\pm^2$ indicate right and left circularly polarized light, respectively. We follow Shurcliff[4] in designating the right-hand mode as that in which the tip of the electric vector describes a right-handed helix. This corresponds to $E_+ = E_x + iE_y$ for a time variation $\exp i\omega t$.

TABLE II

COMPLEX REFRACTIVE INDEX FOR AN ISOTROPIC MAGNETOPLASMA

Direction of propagation	Polarization	Complex refractive index
$\hat{\mathbf{s}} \parallel \mathbf{B}_0$	$\mathbf{E}_\pm \perp \mathbf{B}_0$	$(n - ik)_\pm^2 = \kappa\left[1 - \dfrac{\omega_p^2}{\omega(\omega \mp \omega_c - i\nu)}\right]$
$\hat{\mathbf{s}} \perp \mathbf{B}$	$\mathbf{E} \parallel \mathbf{B}$	$(n - ik)_\parallel^2 = \kappa\left[1 - \dfrac{\omega_p^2}{\omega(\omega - i\nu)}\right]$
$\hat{\mathbf{s}} \perp \mathbf{B}$	$\mathbf{E} \perp \mathbf{B}$	$(n - ik)_\perp^2 = \kappa\left[1 - \dfrac{\omega_p^2[\omega_p^2 - \omega^2(1 - i\eta)]}{\omega^2[\{\omega_p^2 - \omega^2(1 - i\eta)\}(1 - i\eta) + \omega_c^2]}\right]$
		$\eta \equiv \nu/\omega$

Energy will be dissipated from a plane wave only when the index of refraction of the medium is complex. When $k = 0$, the wave is not attenuated, and when $n = 0$, the electric and magnetic fields are 90° out of phase, so that no energy is dissipated. If either n or k vanishes, then $2nk$, the imaginary part of $(n - ik)^2$ vanishes, and from Eq. (6) we see that the requirement for no energy dissipation is that σ_{eff} be completely imaginary. An

[4] W. A. Shurcliff, "Polarized Light." Harvard Univ. Press, Cambridge, Massachusetts, 1962.

inspection of Eq. (9) and Table I reveals then that there will be no dissipation if $\nu = 0$. For a qualitative understanding of free-carrier magnetooptical phenomena, a discussion of this lossless case is very helpful, and Table III summarizes the loss-free index equations.

TABLE III

COMPLEX REFRACTIVE INDEX FOR A LOSSLESS ISOTROPIC MAGNETOPLASMA

Direction of propagation	Polarization	Complex refractive index
$\hat{\mathbf{s}} \parallel \mathbf{B}_0$	$\mathbf{E}_\pm \perp \mathbf{B}_0$	$(n^2 - k^2)_\pm = \kappa\left[\dfrac{\omega^2 \mp \omega_c\omega - \omega_p{}^2}{\omega(\omega \mp \omega_c)}\right]$
$\hat{\mathbf{s}} \perp \mathbf{B}_0$	$\mathbf{E} \parallel \mathbf{B}_0$	$(n^2 - k^2)_\parallel = \kappa\left[\dfrac{\omega^2 - \omega_p{}^2}{\omega^2}\right]$
$\hat{\mathbf{s}} \perp \mathbf{B}$	$\mathbf{E} \perp \mathbf{B}$	$(n^2 - k^2)_\perp = \kappa\left[\dfrac{\omega^4 - \omega^2(2\omega_p{}^2 + \omega_c{}^2) + \omega_p{}^4}{\omega^2(\omega^2 - \omega_p{}^2 - \omega_c{}^2)}\right]$

For the experimental phenomena we intend to consider, a knowledge of the value of ω for which the index of refraction becomes infinite, zero, or equal to unity is important. The first two values are simply the poles and zeros of the expressions in Table III. This information can be displayed conveniently in the form of graphs[5] (Figs. 1 and 2).

III. Free-Carrier Magnetooptical Effects

3. Effects Involving a Change of Intensity of the Incident Light

a. Zero-Field Reflectivity

When a plane wave is reflected at normal incidence from a medium with index of refraction $n - ik$, the amplitude ratio of the reflected wave E_r to the incident wave E_i is given by

$$\frac{E_r}{E_i} \equiv re^{i\theta} = \frac{1 - n + ik}{1 + n - ik}. \tag{10}$$

The reflectivity ordinarily measured is the square of the absolute value of E_r/E_i,

$$R = |r|^2 = \frac{(1 - n)^2 + k^2}{(1 + n)^2 + k^2}. \tag{11}$$

[5] G. B. Wright, *Solid State Res. Rept.* No. 1, p. 42. Lincoln Laboratory, M.I.T. (1964).

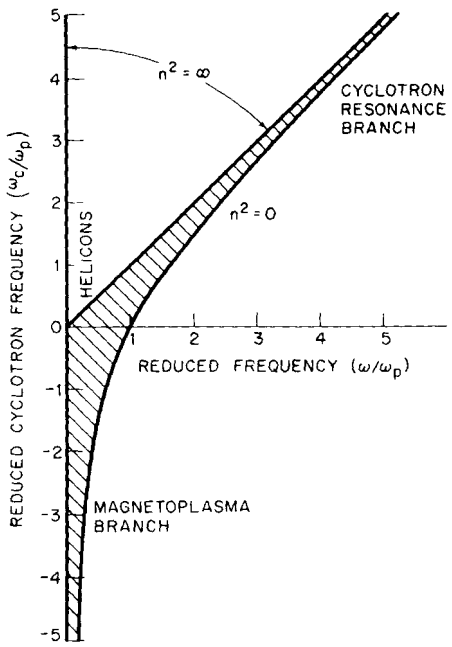


FIG. 1. Loci of the poles and zeros of the index of refraction for a lossless plasma in a longitudinal ($\hat{\mathbf{s}} \parallel \mathbf{B}$) magnetic field. The plasma is opaque in the cross-hatched region. $\omega_c = e\hat{\mathbf{s}} \cdot \mathbf{B}/m^*$, $\omega_p^2 = Ne^2/m^*\kappa\varepsilon_0$. (After G. B. Wright.[5])

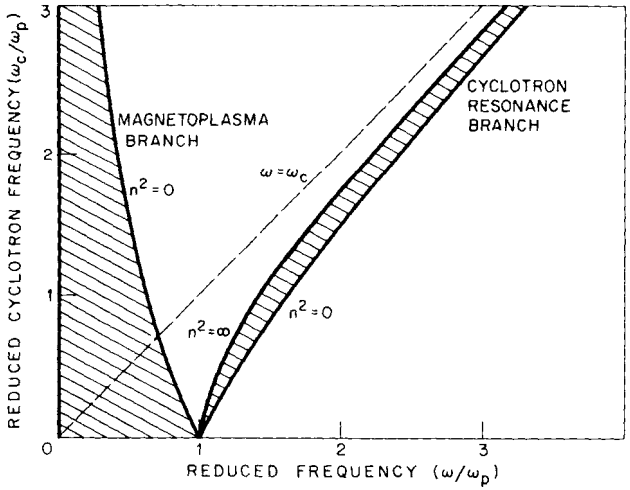


FIG. 2. Loci of the poles and zeros of the index of refraction for a lossless plasma in a transverse ($\hat{\mathbf{s}} \perp \mathbf{B}$) magnetic field. The plasma is opaque in the cross-hatched region. $\omega_c = e\hat{\mathbf{s}} \cdot \mathbf{B}/m^*$, $\omega_p^2 = Ne^2/m^*\kappa\varepsilon_0$. (After G. B. Wright.[5])

The phase shift on reflection is given by

$$\tan\theta = \frac{2k}{1 - n^2 - k^2}. \tag{12}$$

Since either n or k is zero for the lossless case, we see that the reflectivity will go to zero when $n = 1$, and will be unity when $n = 0$. Analytical expressions for the frequency at which these conditions occur are given in Table IV. These equations, applied to the magnetic-field–free case considered in this subsection, lead to a number of relationships discussed below.

The free carriers cause the dielectric constant to decrease at a rate $\kappa\omega_p^2/\omega^2$. When $\omega^2 = [\kappa/(\kappa - 1)]\omega_p^2$, $n^2 = 1$ and $R = 0$. When $\omega^2 = \omega_p^2$, $n^2 = 0$ and $R = 1$ (Fig. 3). For large κ, as we find in typical semiconductors, these frequencies will be quite close together, and the reflectivity will exhibit a steep rise known as the plasma reflection edge. From Fig. 3 we see that a plot of n^2 versus λ^2 will give a straight line with intercept κ at $\lambda = 0$ and slope $-\kappa\omega_p^2/4\pi^2c^2 = N(m/m^*)8.97 \times 10^{-22}$ (microns^{-2}-cm^3). A widely used method[6] of determining $N(m/m^*)$ from reflectivity is to assume $k^2 \ll 1$; then $n = (1 + \sqrt{R})/(1 - \sqrt{R})$. Deviation of the plot of n^2 versus λ^2 from a straight line will reveal the inadequacy of the assumption $k^2 \ll 1$.

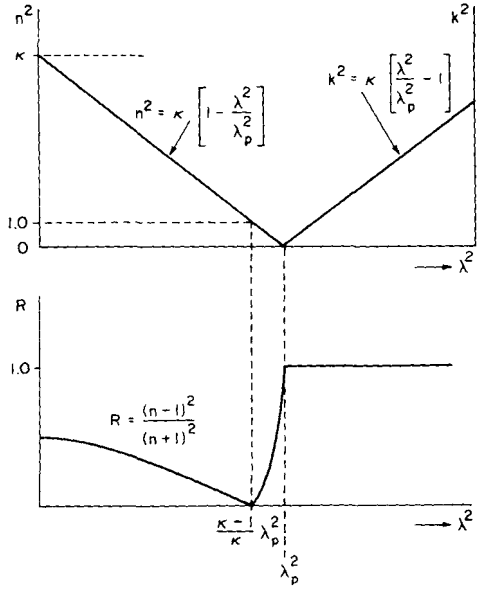


FIG. 3. Variation with wavelength of the index of refraction of a lossless solid-state plasma.

[6] W. G. Spitzer and H. Y. Fan, *Phys. Rev.* **106**, 882 (1957).

TABLE IV. CRITICAL FREQUENCIES FOR A LOSSLESS MAGNETOPLASMA[a]

Faraday Configuration: $\hat{\mathbf{s}} \parallel \mathbf{B}$

	$n^2 = 1, \quad R = 0$	$n^2 = 0, \quad R = 1$	$n^2 = \infty, \quad R = 1$
$\omega_c \ll \omega_p$	$\omega_\pm(1) = \pm\frac{1}{2}\omega_c + \left(\frac{\kappa}{\kappa-1}\right)^{1/2}\omega_p + \frac{1}{8}\left(\frac{\kappa-1}{\kappa}\right)^{1/2}\frac{\omega_c^2}{\omega_p}$	$\omega_\pm(0) = \pm\frac{1}{2}\omega_c + \omega_p + \frac{1}{8}\frac{\omega_c^2}{\omega_p}$	$\omega_\pm(\infty) = 0$
$\omega_c \gg \omega_p$	$\begin{cases}\omega_+(1) = \omega_c + \left(\frac{\kappa}{\kappa-1}\right)\frac{\omega_p^2}{\omega_c} \\ \omega_-(1) = \frac{\kappa}{\kappa-1}\frac{\omega_p^2}{\omega_c}\end{cases}$	$\begin{cases}\omega_+(0) = \omega_c + \frac{2\omega_p^2}{\omega_c} \\ \omega_-(0) = \frac{2\omega_p^2}{\omega_c}\end{cases}$	$\omega_+(\infty) = \omega_c$

Voigt configuration: $\hat{\mathbf{s}} \perp \mathbf{B}$

	$n^2 = 1, \quad R = 0$	$n^2 = 0, \quad R = 1$	$n^2 = \infty, \quad R = 1$
$\mathbf{E} \parallel \mathbf{B}$	$\omega_\parallel(1) = \left(\frac{\kappa}{\kappa-1}\right)^{1/2}\omega_p$	$\omega_\parallel(0) = \omega_p$	$\omega_\parallel(\infty) = 0$
$\mathbf{E} \perp \mathbf{B}$, $\frac{\omega_p^2}{\omega_c^2} \gg (2\kappa-2)(2\kappa-1)$	$\begin{cases}\omega_\perp^{+}(1)^2 = \frac{\kappa}{\kappa-1}\omega_p^2 + \kappa\omega_c^2 \\ \omega_\perp^{-}(1)^2 = \omega_p^2 - (\kappa-1)\omega_c^2\end{cases}$	$\omega_\perp^{\pm}(0) = \pm\frac{1}{2}\omega_c + \omega_p + \frac{1}{4}\frac{\omega_c^2}{\omega_p^2}$ $\begin{cases}\omega(\infty) = 0 \\ \omega(\infty) = \omega_p + \frac{1}{2}\frac{\omega_c^2}{\omega_p}\end{cases}$	
$\mathbf{E} \perp \mathbf{B}$, $(2\kappa-2)(2\kappa-1) > \frac{\omega_p}{\omega_c} > 1$	$\omega_\perp^{\pm}(1) = \left(\frac{2\kappa-1}{2\kappa-2}\right)^{1/2}\omega_p \pm \frac{1}{2}\omega_c$	$\omega_\perp^{\pm}(0) = \pm\frac{1}{2}\omega_c + \omega_p + \frac{1}{8}\frac{\omega_c^2}{\omega_p}$	
$\mathbf{E} \perp \mathbf{B}$, $\omega_c \gg \omega_p$	$\begin{cases}\omega_\perp^{+}(1) = \omega_c + \left(\frac{2\kappa-1}{2\kappa-2}\right)\frac{\omega_p^2}{\omega_c} \\ \omega_\perp^{-}(1) = \left(\frac{\kappa}{\kappa-1}\right)^{1/2}\frac{\omega_p^2}{\omega_c}\end{cases}$	$\begin{cases}\omega_\perp^{+}(0) = \omega_c + \frac{\omega_p^2}{\omega_c} \\ \omega_\perp^{-}(0) = \frac{\omega_p^2}{\omega_c}\end{cases}$	$\begin{cases}\omega(\infty) = 0 \\ \omega(\infty) = \omega_c + \frac{1}{2}\frac{\omega_p}{\omega_c}\end{cases}$

[a] Where $\omega_c = e\hat{\mathbf{s}}\cdot\mathbf{B}/m$ and $\omega_p^2 = Ne^2/m^*\kappa\varepsilon_0$.

b. $\hat{\mathbf{s}} \parallel \mathbf{B}$ *Longitudinal Magnetoplasma Reflection*

The application of a magnetic field in the direction of propagation of the incident wave changes the index of refraction as shown in Fig. 1 and Table IV. A typical magnetoplasma reflection experiment can be described by examining the indices of refraction encountered along a horizontal line in Fig. 1. The horizontal line corresponds to varying the frequency of the incident wave while the external magnetic field is held constant at a value corresponding to $\omega_c/\omega_p = \text{const}$. If we start with a small positive value of ω_c/ω_p (low-field region) and sweep ω/ω_p, we find that $n^2 = 0$ and $n^2 = 1$ at *higher* frequency than in the absence of the field (Table IV). Consequently, the plasma reflection edge moves to a higher frequency by approximately $\frac{1}{2}\omega_c$ for circularly polarized light. The edge would have shifted to lower frequencies for opposite polarity of the field or of the circular polarization. Recalling that $\omega_c = eB/m^*$, we can determine the effective mass from the shift of the reflection edge with field. Then from a plot of n^2 versus λ^2 for the zero-field data, one obtains κ and N, the carrier concentration. If a computer is available, the curves can be fitted to give a value of ν, the carrier scattering frequency, as well. Experimental data[7] and calculated curves for InSb are shown in Fig. 4.

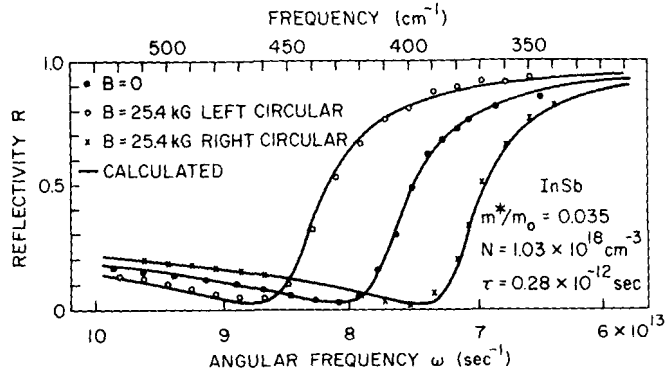


FIG. 4. Longitudinal magnetoplasma reflection in *n*-type InSb at room temperature. (After E. D. Palik *et al.*[7])

c. Cyclotron Resonance and Magnetoplasma Resonance

In the *high field* region, the critical points occur near ω_c, and we observe cyclotron resonance in reflection or transmission. The plasma reflection

[7] E. D. Palik, S. Teitler, B. W. Henvis, and R. F. Wallis, *Proc. Intern. Conf. Phys. Semicond., Exeter, 1962* p. 288. Inst. of Phys. and Phys. Soc., London, 1962.

minimum will be shifted from its zero field position to $\omega = \omega_c + [\kappa/(\kappa - 1)]\omega_p^2/\omega_c$. Cyclotron resonance is observed in the high-field region when the charge carrier rotates about the magnetic field in the same sense as the circularly polarized electric vector. If the rotation of the electric vector is opposite to that of the charge carrier, one observes magnetoplasma resonance[8] when the index of refraction goes to zero. There is no resonant absorption of power in this case, only a balancing of the charge-carrier electric susceptibility against the susceptibility of the lattice. The frequency at which this balance occurs *decreases* inversely with field.

d. $\hat{\mathbf{s}} \perp \mathbf{B}$ *Transverse Magnetoplasma Reflection*

For the case of $\hat{\mathbf{s}} \perp \mathbf{B}$, the diagram of Fig. 2 applies. If $\mathbf{E} \parallel \mathbf{B}$, we get no magnetic effect, corresponding to the fact that there is no longitudinal magnetoresistance for an isotropic carrier. With $\mathbf{E} \perp \mathbf{B}$, two reflection minima are found, starting in the low-field region. One minimum corresponds to the zero-field minimum at $[\kappa/(\kappa - 1)]^{1/2}\omega_p$, and the other develops at $\omega = \omega_p$. Experimental data[9] and calculated curves for InSb are shown in Fig. 5. Table IV gives analytical expressions for the motions of these

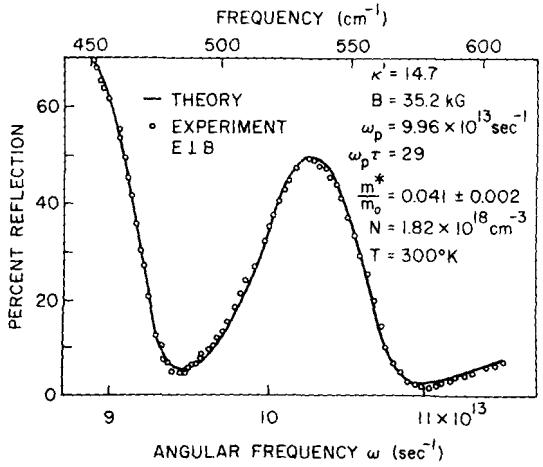


FIG. 5. Transverse magnetoplasma reflection in *n*-type InSb at room temperature. (After G. B. Wright and B. Lax.[9])

minima with field. The zero-field minimum develops into cyclotron resonance and the other minimum passes over to the magnetoplasma resonance at high field. The plasma shift of the cyclotron resonance is about 3% smaller for $\hat{\mathbf{s}} \perp \mathbf{B}$ than for $\hat{\mathbf{s}} \parallel \mathbf{B}$ when $\kappa \approx 16$. The effective mass, carrier

[8] G. Dresselhaus, A. F. Kip, and C. Kittel, *Phys. Rev.* **100**, 618 (1955).
[9] G. B. Wright and B. Lax, *J. Appl. Phys. Suppl.* **32**, 2113 (1961).

concentration, dielectric constant, and scattering frequency may be obtained from this experiment, just as for the longitudinal configuration.

e. Magnetointerference-Fringe Shift

In frequency regions where the crystal is transparent, a plane-parallel sample will exhibit interference fringes on transmission or reflection. Since the wavelength for constructive interference in transmission at normal incidence is given by $m\lambda = 2nd$, where m is the order of interference and d is the sample thickness, the fringes will shift if n is changed by the magnetic field. In most frequency regions the effect will be small, but it is the principal method used for the observation of Alfvén and helicon waves.

4. Effects Involving a Change in the Polarization State of the Incident Light

a. Elliptically Polarized Light

Elliptically polarized light is encountered in experiments that measure the rotation of the plane of polarization of the light. An elliptically polarized wave may be decomposed into two waves linearly polarized at right angles to each other by specifying the relative amplitudes and phases of the two waves. If the two waves are given by $E_1 = a_1 \cos(\tau + \beta_1)$ and $E_2 = a_2 \cos(\tau + \beta_2)$, it is convenient to choose the parameters

$$\alpha = \tan^{-1} \frac{a_2}{a_1}, \tag{13}$$

$$\beta = \beta_2 - \beta_1. \tag{14}$$

Then it is easy to show[10] that

$$\tan 2\gamma = \tan 2\alpha \cos \beta \tag{15}$$

and

$$\sin 2\delta = \sin 2\alpha \sin \beta. \tag{16}$$

The angle γ measures the rotation of the major axis of the ellipse from axis 1, and $\tan \delta = b/a$ is the ratio of the minor to major axis of the ellipse (Fig. 6). This ratio is also called the ellipticity, ε. We note that for $\sin \delta > 0$, the polarization is right handed, with the sense of rotation indicated by the arrow in the figure. In the right-handed coordinate system shown, the wave is propagating out of the plane of the paper.

To every polarization state of a light wave there corresponds one orthogonal polarization state. These two states then span the two-dimensional

[10] M. Born and E. Wolf, "Principles of Optics," 2nd ed., p. 26. Pergamon, New York, 1959.

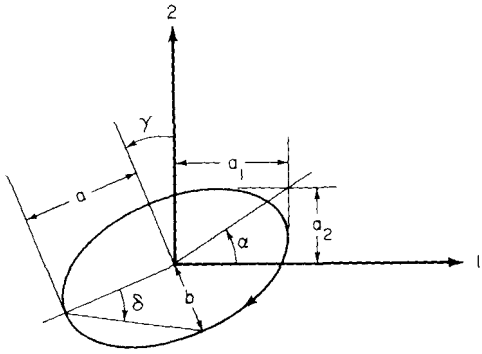


FIG. 6. The parameters of elliptically polarized light. The arrowhead on the ellipse indicates the direction of circulation for a right-hand polarized wave propagating out of the plane of the paper.

polarization space, so that any polarization state can be formed as a linear combination of the two orthogonal states. We need to consider the characterization of an optical element, which in general may transmit (or reflect) the orthogonal states differently, and introduce a phase shift between them. Such an element may be called a dichroic retarder. The *linear dichroic retarder* introduces a phase shift $\beta = \beta_2 - \beta_1$ between waves polarized linearly along axis 1 and axis 2, while transmitting them in the ratio $r_2/r_1 = r$. Incident light linearly polarized at 45° between axis 1 and axis 2 will emerge from such an element with a polarization specified by

$$\tan 2\gamma = \frac{2r}{1 - r^2} \cos \beta, \tag{17}$$

$$\sin 2\delta = \frac{2r}{1 + r^2} \sin \beta. \tag{18}$$

The angle of inclination of the major axis, γ, as well as the ellipticity, depends upon both the relative transmission and the relative phase shift of the two modes.

Free carriers in a magnetic field transverse to the direction of propagation (Voigt configuration) produce linear dichroic retardation. For propagation parallel to the magnetic field (Faraday configuration), the carriers produce *circular dichroic retardation.* One then chooses right and left circularly polarized light as the basis for expansion of an arbitrary polarization state. If linear horizontally polarized light passes through a circular dichroic retarder that introduces a phase shift $\beta = \beta_+ - \beta_-$ and a transmission ratio $r = r_+/r_-$ between the right and left circular components, the emergent

light will have a polarization characterized by

$$\tan 2\gamma = \tan \beta, \tag{19}$$

$$\sin 2\delta = \frac{r^2 - 1}{r^2 + 1}, \tag{20}$$

$$\tan^2 \delta = \left(\frac{r_+ - r_-}{r_+ + r_-}\right)^2 \equiv \varepsilon^2. \tag{21}$$

The inclination of the major axis depends only on the relative phase shift β, while the ellipticity is determined only by the relative transmission r.

b. Phase Shift on Reflection at Zero Field

We must begin our discussion of rotation of the plane of polarization on reflection by considering the variation of phase shift on reflection for the zero-field case. Equation (12) can be recast in the form[11]

$$(k + \cot \theta)^2 + n^2 = \csc^2 \theta. \tag{22}$$

The loci of constant θ in the $n - ik$ plane are thus circles centered at $(-\cot \theta)$ on the k axis with radii $\csc \theta$, all intersecting the n axis at $n = 1$. Some of these circles are shown in Fig. 7. For a discussion of the frequency

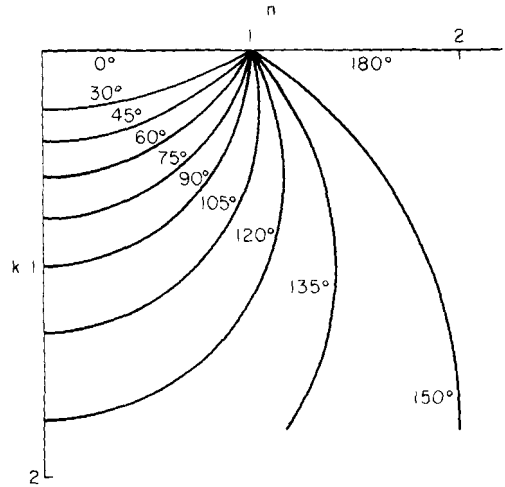


FIG. 7. The loci of constant phase shift for light reflected from a medium with complex refractive index $n - ik$. (After G. B. Wright.[11])

variation of the phase shift, we may consider the loss-free case, when the path of the index runs along the n and k axes. For the lossless plasma, $\theta = \pi$ for $n > 1$, which will be the case until $\omega = [\kappa/(\kappa - 1)]^{1/2}\omega_p$, at which

[11] G. B. Wright, *Appl. Opt.* **4**, 366 (1965).

time θ changes to zero. The phase shift remains zero until $n = k = 0$ at $\omega = \omega_p$, and then increases again, reaching $\theta = 90°$ at $\omega = [\kappa/(\kappa + 1)]^{1/2}\omega_p$, and finally approaches 180° as ω goes to zero. A calculated curve of the phase shift with losses is shown in Fig. 9. Here, the $\mathbf{E} \parallel \mathbf{B}$ case is equivalent to the $B = 0$ case. Note that θ does not reach 0° with losses included.

c. Longitudinal Magnetoplasma Rotation and Ellipticity

We have seen that in the Faraday configuration the refractive indices for the right and left circular modes are translated in frequency by $\pm\frac{1}{2}\omega_c$ while remaining very similar in form to the zero-field pattern. We thus expect the behavior shown in Fig. 8. According to Eq. (19), the polarization rotation is

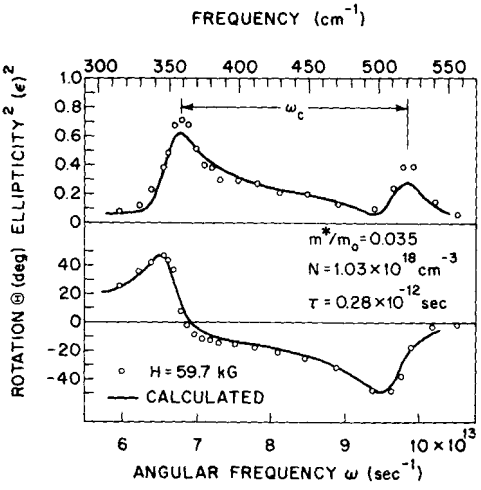


FIG. 8. Longitudinal magnetoplasma rotation and ellipticity in *n*-type InSb at room temperature. (After E. D. Palik *et al.*[7])

equal to half the phase-shift difference between the two modes. The square of the ellipticity, given by Eq. (21), should have maxima when the reflectivity difference of the two modes is greatest, and should become zero when the reflectivities are equal. The separation of the ellipticity maxima should be approximately equal to the cyclotron frequency.

d. Transverse Magnetoplasma Rotation and Ellipticity

In the Voigt orientation, the phase change with frequency for $\mathbf{E} \parallel \mathbf{B}$ is the same as in the zero field case. For $\mathbf{E} \perp \mathbf{B}$ there are two peaks in the phase shift, when $n \approx 1$, separated by a minimum in the phase shift when $n^2 = \infty$. A calculated curve including losses is shown in Fig. 9. In this configuration

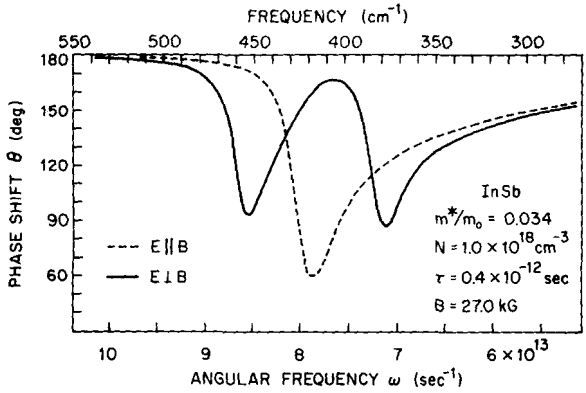


FIG. 9. Calculated magnetoplasma phase shift on reflection for InSb at room temperature for the transverse case. The curve for $\mathbf{E} \parallel \mathbf{B}$ is the same as the zero-field curve. Note that this is the lossy case, with $\nu \neq 0$.

the rotation and ellipticity both depend on the product of functions involving the dichroism and the relative phase shift. It is better to specify the rotation in terms of $\Theta = \gamma - \pi/4$. Then Eq. (17) becomes

$$\tan 2\Theta = \frac{1 - r^2}{2r} \sec \beta. \tag{23}$$

The rotation will become zero or π whenever $R_\perp = R_\parallel$, and peaks when $\beta \to \pi/2$, while the ellipticity should go to zero whenever $\beta = \theta_\perp - \theta_\parallel$, is zero. A calculated curve is shown in Fig. 10.

e. Faraday Rotation

We have seen in Eq. (19) that, for the longitudinal configuration, the angle of rotation of the plane of polarization will be given by one-half the phase shift β introduced by the sample between the right and left circular polarization components of the incident light. For transmission through a sample of thickness d, the rotation Θ is given by

$$\Theta = \frac{\omega d}{2c}(n_+ - n_-). \tag{24}$$

From Table III, where $\omega \gg \nu$, $2n \approx n_+ + n_-$,

$$\Theta = -\frac{\kappa \omega_p{}^2 \omega_c d}{2nc(\omega^2 - \omega_c{}^2)}. \tag{25}$$

For $\omega \gg \omega_c, \nu$,

$$\Theta = -\frac{Ne^3 B \lambda^2 d}{8\pi^2 c^3 n \varepsilon_0 m^{*2}}. \tag{26}$$

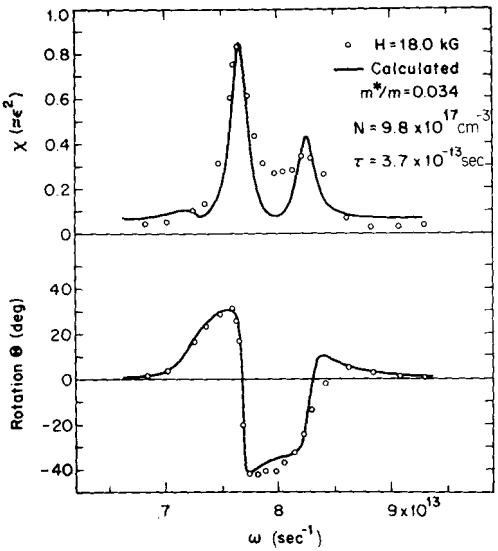


FIG. 10. Transverse magnetoplasma rotation and ellipticity in *n*-type InSb at room temperature. (After E. D. Palik *et al.*[7])

The rotation varies as the square of the incident wavelength, linearly with magnetic field, and as the inverse square of the effective mass, and its sign depends on the sign of the charge carrier. Equation (25) implies that rotation will have a sign reversal when $\omega_c \approx \omega$, and this is indeed true. In this case, however, the approximation $n_+ + n_- = 2n$ may not be true. A detailed description of the Faraday rotation in this region and a discussion of the ellipticity resulting from differential absorption have been given in several papers.[12–14]

f. Voigt Effect

For a transmission experiment transverse to the magnetic field through a sample of thickness d, the phase shift between waves with $\mathbf{E} \perp \mathbf{B}$ and $\mathbf{E} \parallel \mathbf{B}$ is given by

$$\beta = \frac{\omega d}{c}(n_\perp - n_\parallel). \tag{27}$$

If we operate in a region where the amplitude of transmission is equal for the two polarizations ($r = 1$), Eq. (23) tells us that there will be no rotation of the plane of polarization. An incident beam linearly polarized

[12] M. J. Stephen and A. B. Lidiard, *J. Phys. Chem. Solids* **9**, 43 (1959).
[13] B. Donovan and J. Webster, *Proc. Phys. Soc. (London)* **78**, 120 (1961).
[14] J. K. Furdyna and M. E. Brodwin, *Phys. Rev.* **124**, 740 (1961).

at 45° to the external magnetic field represents this case. An ellipticity will be introduced, however, which from Eq. (18) can be described by an angle $2\delta = \beta$. From Table III, we find

$$2\delta = -\frac{\kappa d}{2nc\omega} \frac{\omega_p{}^2 \omega_c{}^2}{(\omega^2 - \omega_p{}^2 - \omega_c{}^2)}; \tag{28}$$

for $\omega \gg \omega_p, \omega_c, \nu$,

$$2\delta = -\frac{Ne^4 B^2 \lambda^3 d}{16\pi^3 c^4 n \varepsilon_0 m^{*3}}. \tag{29}$$

From Eq. (28) we see that the ellipticity will change sign when $\omega^2 < \omega_p{}^2 + \omega_c{}^2$. Because of the different dependence of Voigt effect on magnetic field, mass, and wavelength, one may measure both Faraday rotation and Voigt effect on the same sample, to determine

$$\frac{2\delta}{\Theta} = \frac{\omega_c}{\omega}. \tag{30}$$

With this determination of ω_c, and hence of m^*, one can then go back to either Eq. (29) or Eq. (26) to find N, the carrier concentration.

5. Helicon and Alfvén Waves

Helicon waves and Alfvén waves are phenomena usually studied at low frequencies, but it is of interest to bring out their simple relation to the other effects we have described. Consider a system of N_1 isotropic carriers of mass $m_1{}^*$ and charge $+e$, and N_2 isotropic carriers of mass $m_2{}^*$ and charge $-e$. The index of refraction, neglecting scattering, for a longitudinal magnetic field is

$$(n^2 - k^2)_+ = \kappa \left[1 - \frac{\omega_{p1}^2}{\omega(\omega - \omega_{c1})} - \frac{\omega_{p2}^2}{\omega(\omega + \omega_{c2})}\right]. \tag{31}$$

For $B = 0$ and $\omega^2 < \omega_{p1}^2 + \omega_{p2}^2$, the medium is opaque ($n = 0$). When the field is turned on, the extinction coefficient k will increase because the denominator of the second term is decreasing. When $\omega_{c1} = \omega$, the medium becomes transparent, with very high index of refraction n_+. It remains cut off for the left circular polarization ($n_- = 0$). Aigrain[15] gave the name helicon to the quanta of the electromagnetic wave and its associated polarization wave in this frequency region. In fact, the presence of two types of charge carriers is not necessary for the observation of this transparency at low frequencies. The essential requirement is that $\omega_c \tau \gg 1$.

[15] P. Aigrain, *Proc. Intern. Conf. Semicond. Phys., Prague, 1960* p. 224. Czech. Acad. Sci., Prague, and Academic Press, New York, 1961.

If there is an equal concentration of positive and negative charge carriers ($N_1 = N_2$), the propagating waves are called Alfvén waves.[16] For this special case, the index equation becomes

$$(n^2 - k^2)_+ = \kappa\left[1 - \frac{Ne}{\kappa\varepsilon_0 B}\frac{(\omega_{c1} + \omega_{c2})}{(\omega - \omega_{c1})(\omega + \omega_{c2})}\right]. \tag{32}$$

The medium is again opaque at zero field, becoming transparent at $\omega_{c1} = \omega$. The difference between the Alfvén and helicon condition is only apparent at high fields ($\omega_{c1}, \omega_{c2} \gg \omega, \nu$). Then

$$n^2 \text{ (helicon)} \sim \frac{1}{\omega B} \tag{33}$$

and

$$n^2 \text{ (Alfvén)} \sim \frac{1}{B^2}. \tag{34}$$

These waves are usually observed as interference-fringe changes in a Fabry–Perot cavity as the field is swept.

6. Quantum Oscillatory Free-Carrier Effects

a. Harmonic Cyclotron Resonance

Up to this point we have ignored the quantization of the orbital motion of the free carriers in a magnetic field. In fact, the quantization of the motion normal to the field results in the discrete energy levels called "Landau levels,"[17]

$$E_l = (l + \tfrac{1}{2})\hbar\omega_c. \tag{35}$$

The ordinary $\Delta l = 1$ selection rule for harmonic-oscillator transitions may be broken down in the presence of scattering or of nonparabolic or warped energy bands. When the selection rule is broken, one may observe oscillatory absorption at photon energies $\hbar\omega$ given by

$$\hbar\omega \pm \hbar\omega_s = l\hbar\omega_c, \tag{36}$$

where the $\pm$ sign refers to absorption or emission of the energy $\hbar\omega_s$ in a scattering process.

b. Optical de Haas–Shubnikov Effect

Another oscillatory process may occur at low temperatures in degenerate materials. Thus, when the Fermi level E_F is given by

$$E_F = (l + p)\hbar\omega_c, \tag{37}$$

[16] H. Alfvén, *Arkiv. Mat. Astron. Fysik* **29B**, No. 2 (1942).

[17] L. D. Landau and E. M. Lifshitz, "Quantum Mechanics, Non-relativistic Theory" (English Transl.), p. 474. Addison-Wesley, Reading, Massachusetts, 1958 [Second Russian Edition, p. 492. Fizmatgiz, Moscow, 1963].

where p is a phase factor, the optical conductivity will be enhanced by the passage of a Landau level through the Fermi level.[18] This will be recognized as the optical analog of the de Haas–Shubnikov effect.[19] The field at which the maxima occur is independent of photon frequency for the optical de Haas–Shubnikov effect, while Eq. (36) indicates its variation for harmonic cyclotron resonance.

IV. Free-Carrier Magnetooptical Experiments

7. Magnetoreflection Experiments

a. Magnetoplasma Reflection

Although the preceding classical discussion is very useful in interpreting most free-carrier magnetooptical effects, many experiments show detailed effects that are explained on the basis of the quantum mechanical band structure. Some effects are nonparabolicity of the energy band, anisotropic effective mass, Landau levels, and effective g factors. In the experimental section that follows, we shall discuss specific interesting experiments in some detail and attempt to cite all the work that has been done on III–V semiconductors with each magnetooptical experiment.

The first measurements of magnetoplasma reflection were made by Lax and Wright[20] on n-type InSb and HgSe for the transverse orientation. Subsequent work on n-type InSb and InAs is discussed by Wright and Lax.[9] Measurements by Palik *et al.*[7] on n-type InSb in the longitudinal orientation with left and right circularly polarized radiation clearly showed the unequal shifts in the reflection minima, as given in Table IV. Results are shown in Fig. 4. The data have been fitted by adjustment of m^*/m, $\tau = 1/\nu$, and N in the equations in Table II to determine n and k and calculation of R by Eq. (11). Sniadower *et al.*[21] measured the transverse magnetoplasma effect in n-type InSb with $N \approx 10^{19}\ \text{cm}^{-3}$. Microwave transverse magnetoplasma reflection was measured in low carrier concentration InSb for $\omega < \omega_p$ by Mansfield.[21a]

Lax[22,23] has mentioned some far-infrared reflectivity measurements of Lipson[24] on room-temperature InSb, done at fixed frequencies as a function

[18] A. H. Kahn and H. P. R. Frederikse, *Solid State Phys.* **9**, 257 (1959).
[19] M. S. Dresselhaus and J. G. Mavroides, *Solid State Commun.* **2**, 297 (1964).
[20] B. Lax and G. B. Wright, *Phys. Rev. Letters* **4**, 16 (1960).
[21] L. Sniadower, J. Rauluszkiewicz, and R. R. Galazka, *Phys. Status Solidi* **6**, 549 (1964).
[21a] R. Mansfield, *Phys. Letters* **20**, 629 (1966).
[22] B. Lax and J. G. Mavroides, *Solid State Phys.* **11**, 261 (1960).
[23] B. Lax, *Solid State Phys. Electron. Telecommun., Proc. Intern. Conf. Brussels, 1958.* Vol. 3, p. 508. Academic Press, New York, 1960.
[24] H. G. Lipson, S. Zwerdling, and B. Lax, *Bull. Am. Phys. Soc.* **3**, 218 (1958).

of magnetic field. The results showed the general behavior of the reflectivity near ω_p, as may be deduced from Fig. 1. Edwards and Maker[25] have demonstrated that the plasma reflectivity edge is sensitive to N, and that the position of the edge can be used to determine the inhomogeneity in carrier concentration across the face of a sample.

Some magnetoplasma reflectivity measurements have been done with other semiconductors. A mention of the effect in n-type PbS was given by Palik *et al.*[7] The effective mass in $Cd_xHg_{1-x}Te$ samples has been determined by this technique by Harman *et al.*[26] Dresselhaus and Mavroides[27] have measured the effect in Ag in the ultraviolet. The transverse magnetoplasma effect is anisotropic in cubic semiconductors with ellipsoidal energy bands[20] and has been measured in n-type Ge.[28] An interesting variation of the experiment is suggested by the work of McAlister and Stern[29] who measured the resonant absorption at ω_p in thin films of Ag in zero field at oblique angles of incidence, where the incident electric field can couple to the plasma oscillation.

b. Magnetoplasma Rotation and Ellipticity

Lax and Zwerdling[30] suggested the measurement of this effect in the vicinity of ω_p, and it was subsequently measured by Palik *et al.*[7] on n-type InSb for both the longitudinal and transverse orientations. Some results are shown in Figs. 8–10. In the longitudinal orientation, the separation of the ellipticity peaks gives ω_c. Usually, the square of the ellipticity has been measured. The data have been fitted with the parameters shown. The rotation and ellipticity are sensitive functions of τ, which is assumed constant in the Drude model. The calculated results are in good but not complete agreement with the experimental data. This may be due to experimental errors introduced by the quality of the sample surface and by the spectral resolution and the failure of the simple model as regards a constant τ.

It is to be noted that the experiment gives no new information over that of the reflectivity experiment. The one advantage is that it does not require a measurement of absolute reflectivity. Stern *et al.*[31] have performed similar experiments on Al in the visible at frequencies considerably lower

[25] D. F. Edwards and P. D. Maker, *J. Appl. Phys.* **33**, 2466 (1962).
[26] T. C. Harman, A. J. Strauss, D. H. Dickey, M. S. Dresselhaus, G. B. Wright, and J. G. Mavroides, *Phys. Rev. Letters* **7**, 403 (1961).
[27] M. S. Dresselhaus and J. G. Mavroides, *Bull. Am. Phys. Soc.* **8**, 257 (1963).
[28] S. Teitler, B. W. Henvis, and E. D. Palik, *in* "Plasma Effects in Solids" (7th Intern. Conf.), p. 59. Dunod, Paris, and Academic Press, New York, 1965.
[29] A. J. McAlister and E. A. Stern, *Phys. Rev.* **132**, 1599 (1963).
[30] B. Lax and S. Zwerdling, *Progr. Semicond.* **5**, 223 (1960).
[31] E. A. Stern, J. C. McGroddy, and W. E. Harte, *Phys. Rev.* **135**, 1306 (1964).

than ω_p. Brodwin and Vernon[32] have measured the effect in semiconductors in the microwave region, again under the condition $\omega < \omega_p$.

8. Magnetotransmission Experiments

a. Cyclotron Resonance

Although cyclotron resonance has been measured in reflection,[33,34] usually it is measured in transmission as a change in extinction coefficient. It is noted—for example, from Table III—that for the longitudinal orientation, the absorption line is observed at ω_c, whereas for the transverse orientation it is observed at $(\omega_c^2 + \omega_p^2)^{1/2}$. From the absorption constant $\alpha = 4\pi k/\lambda$ and the appropriate equations in Table II, the peak absorption constant α_c for the longitudinal orientation with circular polarization is found to be

$$\alpha_c = \frac{\sigma_0}{\varepsilon_0 nc}, \tag{38}$$

where $\sigma_0 = Ne^2/m^*\nu$ is the d-c conductivity. For the transverse orientation with $\mathbf{E} \perp \mathbf{B}$, the peak absorption constant is half as large. When propagation is parallel to the magnetic field, electrons absorb left circular polarization while holes absorb right. The sharpness of the absorption line depends on the condition $\omega_c\tau = \mu B > 1$, where μ is the carrier mobility.

To explain the detailed results of cyclotron-resonance experiments in III–V-compound semiconductors, it is necessary to take into account band interactions that produce nonparabolicity and spin–orbit effects.[22,35–37] Among the results are an energy-dependent effective mass and an energy-dependent effective g factor. The conduction-band Landau levels of InSb in a magnetic field, calculated from the theory of Bowers and Yafet,[36] are shown in Fig. 11(a). Here the wave vector k_z parallel to the magnetic field is zero. The energies are determined from a knowledge of the energy gap E_g, m^*, and the spin–orbit splitting Δ. For this calculation, room-temperature parameters were used. Cyclotron resonance is just a transition between adjacent levels, governed by the selection rule $\Delta l = \pm 1$ and $\Delta m = 0$. The effective g factor determines the splitting of each Landau level into two spin states.

The original measurements for a III–V-compound semiconductor were done by Dresselhaus *et al.*[38] on n-type InSb in the microwave region.

[32] M. E. Brodwin and R. J. Vernon, *Phys. Rev.* **140**, A1390 (1965).
[33] E. Burstein, G. S. Picus, and H. A. Gebbie, *Phys. Rev.* **103**, 825 (1956).
[34] R. J. Keyes, S. Zwerdling, S. Foner, H. H. Kolm, and B. Lax, *Phys. Rev.* **104**, 1804 (1956).
[35] E. O. Kane, *J. Phys. Chem. Solids* **1**, 249 (1957).
[36] R. Bowers and Y. Yafet, *Phys. Rev.* **115**, 1165 (1959).
[37] B. Lax, J. G. Mavroides, H. J. Zeiger, and R. J. Keyes, *Phys. Rev.* **122**, 31 (1961).
[38] G. Dresselhaus, A. F. Kip, and G. Wagoner, *Phys. Rev.* **98**, 556 (1955).

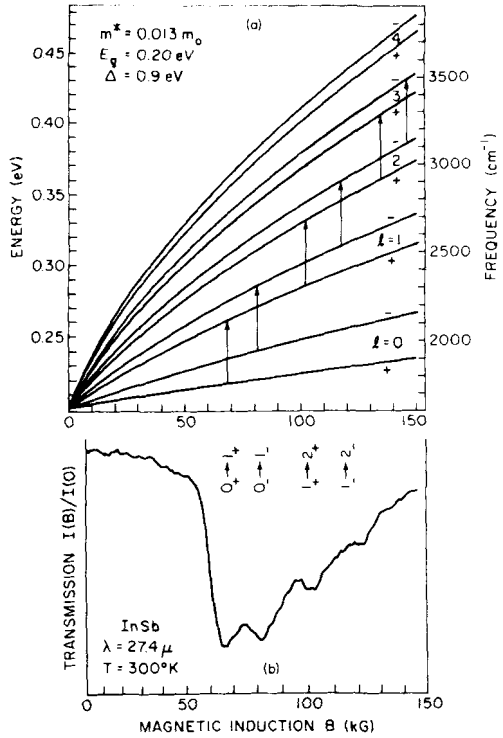


FIG. 11. (a) Calculated conduction-band Landau levels at $k_z = 0$ for room-temperature InSb, with allowed cyclotron-resonance transitions. (b) Observed cyclotron-resonance absorption in InSb. (After E. D. Palik *et al.*[39] and unpublished data.)

Subsequent measurements in the infrared were made by Burstein *et al.*[33] Keyes *et al.*[34,37] and Palik *et al.*[39] This work has established the mass at the bottom of the conduction band and the mass variation with magnetic field. Details of the energy levels of InSb at room temperature shown in Fig. 11(a) have been confirmed.[39] One example of cyclotron resonance in intrinsic InSb observed in the spectral region 20–30 microns is shown in Fig. 11(b). To fit the line positions, it was necessary to adjust E_g and m^* to the values given in Fig. 11(a). Consequently, the room-temperature effective mass is $0.013m_0$, as compared to a liquid-nitrogen–temperature mass of $0.0145m_0$. The energy gap was adjusted to 0.20 eV, while the room temperature optical gap is known to be 0.18 eV. The problem of the variation of effective mass with temperature has not been satisfactorily treated yet. Since the gap moves to higher energy as the temperature is lowered, it

[39] E. D. Palik, G. S. Picus, S. Teitler, and R. F. Wallis, *Phys. Rev.* **122**, 475 (1961).

follows from Kane's formula

$$\frac{m}{m^*} = P^2\left[\frac{1}{E_g} + \frac{1}{E_g + \Delta}\right] \tag{39}$$

that the effective mass should increase also as the temperature decreases. Such a change is found for data obtained at room temperature and liquid-nitrogen temperature, but is not as large as would be calculated from Eq. (39) when the optical gap change with temperature is used. The total gap change is due to dilation of the lattice and electron–lattice-vibration interactions. Equation (39) was derived including only dilation. In the absence of a more complete theory that includes effects of lattice vibrations, Eq. (39) has been used with only the dilational gap change and does appear to account for the mass variation with temperature somewhat better.

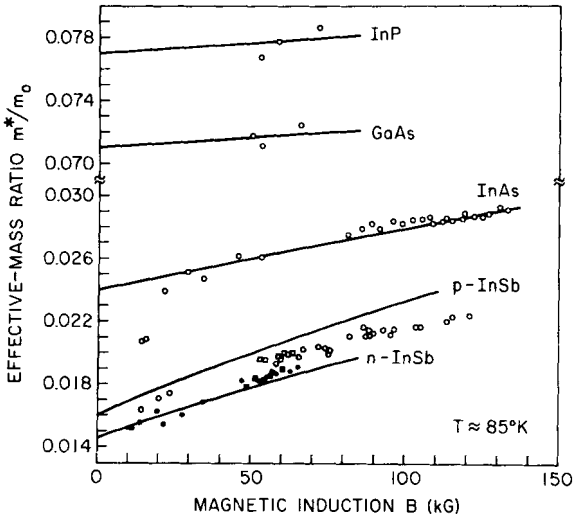


FIG. 12. Effective-mass variation with magnetic field for four III–V semiconductors near liquid-nitrogen temperature. The solid curves are calculated with the theory of Bowers and Yafet. (After E. D. Palik *et al.*[44] and unpublished data.)

Infrared cyclotron resonance has been measured in *n*-type InAs,[22,34,40,41] InP,[40] and GaAs.[42] Line structure due to spin effects similar to that observed in InSb has been observed in InAs.[41] Some results of mass variation with magnetic field for several III–V semiconductors near liquid-nitrogen temperature are shown in Fig. 12. The increasing mass is a direct measure

[40] E. D. Palik and R. F. Wallis, *Phys. Rev.* **123**, 131 (1961).
[41] E. D. Palik and J. R. Stevenson, *Phys. Rev.* **130**, 1344 (1963).
[42] E. D. Palik, J. R. Stevenson, and R. F. Wallis, *Phys. Rev.* **124**, 701 (1961).

of the nonparabolicity of the energy band. The solid lines are calculated with the use of the theory of Bowers and Yafet for the lowest-energy transition $l = 0 \rightarrow 1$.

Microwave cyclotron resonance of holes in p-type InSb has been measured by Bagguley *et al.*[43] Their result for the light hole is a spherical mass of $(0.021 \pm 0.005)m_0$. The heavy hole is slightly anisotropic with $m \approx 0.4m_0$.

Palik *et al.*[44] mention observing cyclotron resonance in p-type InSb containing $\sim 1 \times 10^{16}$ holes/cm^3 at liquid-nitrogen temperature. Measurements were made in the 20–40-micron and the 80–120-micron regions.

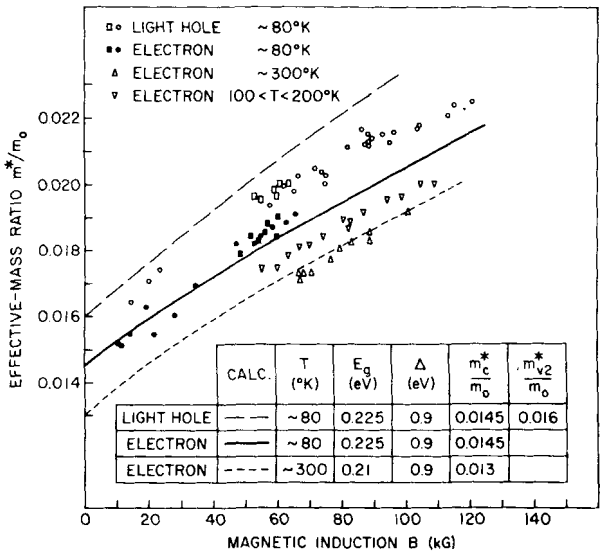


FIG. 13. Effective mass versus magnetic induction for n- and p-type InSb. Calculated curves are based on the theory of Bowers and Yafet. (After E. D. Palik *et al.*[44] and unpublished data.)

Circular polarization was used in the shorter-wavelength region. The sample 0.5 mm thick showed strong intrinsic electron cyclotron absorption at room temperature, with left circular polarization. This absorption almost disappeared upon cooling. A somewhat stronger hole absorption appeared (about 10% absorption), which was observed with right circular polarization at slightly higher magnetic fields. The results of the measurements are shown in Fig. 13. The hole data were fitted qualitatively with the Bowers and Yafet theory with $m_c^* = 0.0145$, since one of the solutions of the cubic equations is the light-hole energy V_2. The simplicity of the observed data is surprising,

[43] D. M. S. Bagguley, M. L. A. Robinson, and R. A. Stradling, *Phys. Letters* **6**, 143 (1963).
[44] E. D. Palik, S. Teitler, and R. F. Wallis, *J. Appl. Phys. Suppl.* **32**, 2132 (1961).

considering that the "quantum" effects in the valence bands of InSb[44a] should be quite marked and that only at higher l levels should the cyclotron spacing approach the value calculated from the Kane or Bowers and Yafet theory. The light-hole effective mass at the bottom of the band was determined to be $0.0155m_0$, only slightly heavier than the light electron in agreement with the Kane model. As there are only about 3×10^{14} light holes/cm^3, the observed cyclotron line should be the $l = 0 \rightarrow 1$ transition. In the experiment, magnetic fields as high as 140 kOe were used in the 20–40-micron region, and no other absorption lines were observed.

Microwave spin resonance of conduction electrons in InSb has been observed by Bemski,[45] confirming the light effective mass and large effective g factor. These lines correspond to spin transitions in a given l Landau level. Richards[46] has observed the same type of absorption in the far infrared. This is a magnetic-dipole transition, very weak compared to the electric-dipole cyclotron-resonance line.

An interesting new resonance has recently been observed that involves electric-dipole, spin-type transitions in InSb.[46a,b,c] Due to spin–orbit effects that produce k^3 nonparabolic effects, the conduction-band wave functions are mixed so that the spin states are not "pure"—i.e., for a given l, the states are not just + or − but mixed, a + state in Fig. 11(a) having a small − mixture and vice versa. Aside from the usual electric-dipole cyclotron-resonance transition and the magnetic-dipole spin-resonance transition, this leads to electric-dipole transitions such as $(0, +) \rightarrow (1, -)$ and $(0, -) \rightarrow (1, +)$ in Fig. 11(a), which, although weak compared to cyclotron resonance, are strong compared to spin-resonance transitions.

Boyle and Brailsford[47] observed absorption lines in the far infrared in InSb due to transitions between bound impurity levels that lie just below the Landau levels. The effective mass obtained is essentially the same as that for cyclotron resonance between the corresponding Landau levels. This type of transition has been studied by Wallis and Bowlden,[48] who predicted other impurity-level transitions also, which have recently been measured by Kaplan[48a] in the far infrared.

[44a] C. R. Pidgeon and R. N. Brown, *Phys. Rev.* **146**, 575 (1966).

[45] G. Bemski, *Phys. Rev. Letters* **4**, 62 (1960).

[46] P. L. Richards, *Japan. J. Appl. Phys. Suppl.* **4**, 417 (1965).

[46a] E. I. Rashba and V. I. Sheka, *Fiz. Tverd. Tela* **3**, 1863 (1961) [*English Transl.: Soviet Phys.-Solid State* **3**, 1357 (1961)].

[46b] R. L. Bell, *Phys. Rev. Letters* **9**, 52 (1962).

[46c] Y. A. Bratashevskii, A. A. Galkin, and Y. M. Ivanchenko, *Fiz. Tverd. Tela* **5**, 358 (1963) [*English Transl.: Soviet Phys.-Solid State* **5**, 260 (1963)].

[47] W. S. Boyle and A. D. Brailsford, *Phys. Rev.* **107**, 903 (1957).

[48] R. F. Wallis and H. J. Bowlden, *J. Phys. Chem. Solids* **7**, 78 (1958).

[48a] R. Kaplan, *Proc. Intern. Conf. Phys. Semicond., Kyoto, 1966* (*J. Phys. Soc. Japan* **21**, Suppl.) p. 249. Phys. Soc. Japan, Tokyo, 1966.

A novel application of cyclotron-resonance absorption in n-type InSb has been described by Richards and Smith.[49] The circular polarization absorption is utilized to make a circular polarizer, and the Faraday rotation is used to make a circulator—i.e., a device to pass a linearly polarized wave in one direction only.

A tunable, narrow-band, far-infrared detector based on cyclotron-resonance absorption in n-type InSb has been described.[49a,b] The detection is based on a change in the d-c conductivity of the sample when radiation of the cyclotron frequency is absorbed. The magnetic field is the variable that determines the wavelength at which the detector is sensitive.

b. Harmonics of Cyclotron Resonance

Breakdown in the selection rule $\Delta l = 0$ gives rise to harmonics of cyclotron resonance, which have been observed in germanium.[22] In n-type InSb in the carrier concentration range 10^{16}–10^{17} cm^{-3}, Palik and Wallis[50] have observed harmonics of cyclotron resonance at room temperature and liquid-nitrogen temperature. The effect was observed in both the longitudinal and transverse orientations. In a sample 1 mm thick, oscillations were observed at fixed photon energies in the 10–15-micron range as a function of magnetic field. The absorption maxima and minima labeled by integers and half-integers and plotted against $1/B$ are shown in Fig. 14. At lower fields, the lines were straight. At high fields, there were some deviations from linearity, probably due to nonparabolic effects. Also shown in Fig. 14 are curves calculated with room-temperature parameters used in the theory of Bowers and Yafet, except that the structure due to the spin levels specified by $m = \pm\frac{1}{2}$ is smoothed out. The calculated harmonics indicated by the solid dots arise, then, from transitions from the $l = 0$ level to the $l = 2$, $l = 3$, and higher levels. If spin is included, there should be two series of lines, but these were not resolved in the experiment. The calculations involve no consideration of phase. A comparison of the two sets of curves shows good qualitative agreement as to slope. The effective mass $0.0183m_0$ obtained from the slopes of the calculated lines at lower fields was in good agreement with the observed effective mass $0.0185m_0$. It is of interest to note that one measures an effective mass appreciably larger than the mass at the bottom of the band, $0.013m_0$, because of nonparabolic effects. The breakdown in the selection rule that allows harmonics may be due to phonon assistance in scattering the carrier to a final state.

[49] P. L. Richards and G. E. Smith, *Rev. Sci. Instr.* **35**, 1535 (1964).

[49a] M. A. C. S. Brown and M. F. Kimmitt, *Brit. Commun. Electron.* **10**, 608 (1963).

[49b] J. Besson, B. Philippeau, R. Cano, M. Mattiloli, and R. Papoular, *L'Onde Electrique* **45**, 107 (1965).

[50] E. D. Palik and R. F. Wallis, *Phys. Rev.* **130**, 41 (1963).

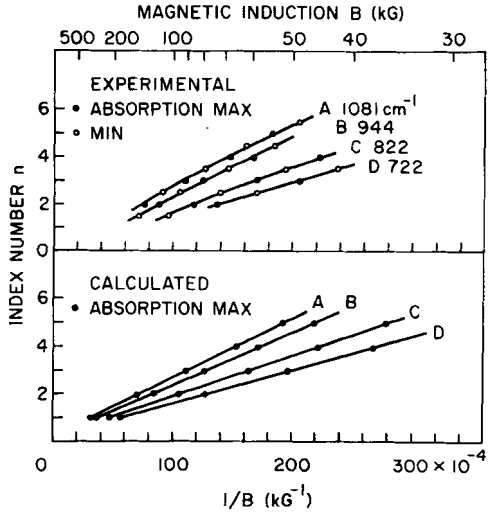


FIG. 14. Experimentally observed and calculated harmonics of cyclotron resonance in *n*-type InSb at room temperature. Calculations are based on the parameters $m^*/m_0 = 0.013$, $E_g = 0.20$ eV, and $\Delta = 0.9$ eV used in the Bowers and Yafet theory. No consideration was given to phase, and fine structure due to spin levels is averaged out. Solid lines are simply drawn through the points for clarity. (After E. D. Palik and R. F. Wallis[50] and unpublished data.)

The effect has also been observed in an *n*-type InAs specimen 1 mm thick at liquid-nitrogen temperature in the 10–15-micron region.[41] The carrier concentration was $2.3 \times 10^{16}\,\text{cm}^{-3}$. In the magnetic-field range 100–150 kOe, an effective mass of $0.028m_0$ was measured, in good agreement with results obtained from the fundamental cyclotron-resonance measurements in the same magnetic-field range.

Cyclotron resonance is the most direct way to measure the polaron mass. Below the lattice-vibration frequency, the electron interacts with the ion lattice to produce electric polarization that follows the electron. The resulting effective mass of the polaron (electron plus lattice polarization) is slightly heavier than the band effective mass. Above the lattice-vibration frequency, the electron has its normal effective mass. Measurement of cyclotron resonance on both sides of the reststrahlen band may reveal this mass change.[51] The calculated mass change for InSb and InAs is $\sim 1\,\%$ and has not been observed because of inadequate accuracy in the experiment.

An interesting type of cyclotron resonance proposed by Azbel' and Kaner for metals[52] has recently been observed in the microwave region in *p*-type

[51] F. C. Brown, *in* "Polarons and Excitons" (C. G. Kuper and G. B. Whitfield, eds.), p. 323. Plenum Press, New York, 1963.

[52] M. Ya. Azbel' and E. A. Kaner, *Zh. Eksperim. i Teor. Fiz.* **30**, 811 (1956) [*English Transl.: Soviet Phys. JETP* **3**, 772 (1956)]; *J. Phys. Chem. Solids* **6**, 113 (1958).

PbTe with large carrier concentration.[53,54] The effect is usually observed in reflection in the transverse orientation. The classical skin depth is $\delta = \lambda/4\pi k$, while the cyclotron orbit radius is $r = [2(l + \frac{1}{2})\hbar/eB]^{1/2}$. When the skin depth is small compared to the orbit radius, the radiation field is inhomogeneous over the extent of the orbit. The electric vector can couple to the electron for only a fraction of each orbit. This leads to a breakdown of the selection rule, so that now $\Delta l = 0, 1, 2, 3, \ldots$ transitions are allowed. Consequently, harmonics of cyclotron resonance are possible when $\omega \ll \omega_p$ at undisplaced frequencies. It is possible to observe the usual transverse cyclotron resonance also, in the same sample. For $\omega_c > \omega_p$ the radiation field is homogeneous across the orbit, and resonance will be observed at $(\omega_c^2 + \omega_p^2)^{1/2}$, as has already been discussed for the transverse orientation. The depolarization electric field in the direction of propagation is presumably screened out below ω_p, so that Azbel'–Kaner cyclotron resonance is unshifted from ω_c or integer multiples of ω_c.

The depolarization field due to the plasma motion which arises in the transverse (Voigt) orientation is responsible for the shift of the cyclotron resonance from ω_c in the longitudinal (Faraday) orientation to $(\omega_c^2 + \omega_p^2)^{1/2}$ in the transverse orientation. The Voigt resonance represents a coupling of the cyclotron and plasma modes of motion of the electrons. Recently, both Faraday and Voigt cyclotron resonance were observed[54a] in a 5-micron thick sample of *n*-type InSb containing about 2×10^{17} carriers/cm^3. Measurements were made in the spectral region 230–400 cm^{-1}, just above ω_p. In a plot of ω^2 versus B^2, the Faraday resonance was a straight line which extrapolated through zero, while the Voigt resonance was a straight line with the same slope but intersecting the ω^2 axis at ω_p^2. The slope yielded an effective mass ratio of 0.020.

c. Helicons

When $\omega < \omega_c \ll \omega_p$ and $\omega_c\tau \gg 1$ (Fig. 1) hold, a semiconductor in the longitudinal (Faraday) orientation becomes somewhat transparent to one of the two circular polarized waves. Helicons have been studied in the microwave region for InSb and InAs by Libchaber and Veilex,[54b] Flietner and

[53] P. J. Stiles, E. Burstein, and D. N. Langenberg, *Proc. Intern. Conf. Phys. Semicond., Exeter, 1962* p. 577. Inst. of Phys. and Phys. Soc., London, 1962.

[54] E. Burstein, P. J. Stiles, D. N. Langenberg, and R. F. Wallis, *Proc. Intern. Conf. Phys. Semicond., Exeter, 1962* p. 345. Inst. of Phys. and Phys. Soc., London, 1962.

[54a] S. Iwasa, Y. Sawada, E. Burstein, and E. D. Palik, *Proc. Intern. Conf. Phys. Semicond., Kyoto, 1966* (*J. Phys. Soc. Japan* **21**, Suppl.) p. 742. Phys. Soc. Japan, Tokyo, 1966.

[54b] A. Libchaber and R. Veilex, *Phys. Rev.* **127**, 774 (1962); *Proc. Intern. Conf. Phys. Semicond., Exeter, 1962* p. 138. Inst. of Phys. and Phys. Soc., London, 1962.

Kliefoth,[54c] and Furdyna.[54d] Since reflectivity of the sample is high in the helicon region, a plane-parallel slab acts as a Fabry–Perot cavity producing interference effects as the magnetic field is swept. The basic information obtained is the carrier concentration. From Table III for electrons the refractive index for the helicon is $n_-^2 \approx \kappa\omega_p^2/\omega\omega_c$. The interference condition is $n\lambda_0 = 2n_-d$ where λ_0 is the wavelength of the radiation in vacuum. Orders of interference n then follow the relation

$$n^2 = \frac{\kappa d^2\omega_p^2\omega}{\pi^2c^2\omega_c} = \frac{Ned^2\omega}{\varepsilon_0\pi^2cB} \tag{39a}$$

from which the carrier concentration is found.

d. Faraday Rotation

Mitchell[55] suggested the free-carrier Faraday effect to determine effective masses in semiconductors, and calculations were extended by Stephen and Lidiard.[12] The first measurements were made by Brown[56] in *n*-type InSb. As shown by Stephen and Lidiard for degenerate semiconductors with a spherical, nonparabolic energy band, the Faraday mass m_F^* is given by

$$\frac{1}{m_F^*} = \left[\frac{1}{\hbar^2k}\frac{dE}{dk}\right]_\zeta, \tag{40}$$

where the energy E is a function of the wave vector k. The right side of Eq. (40) is evaluated at the Fermi level ζ. Thus, the Faraday effect measures the mass at the Fermi level. As a function of carrier concentration, such measurements can give the shape of the E–k curve. This is true of the Faraday effect, Voigt effect, and magnetoplasma effects.

For cubic crystals with energy ellipsoids, the Faraday effect in the approximation of Eq. (26) gives an average mass independent of crystal direction. The particular average depends on the location and number of ellipsoids. Measurements on Ge by Walton and Moss[57] verified the calculations of Stephen and Lidiard. Near cyclotron resonance, however, the Faraday effect will show mass anisotropy.[58,59] The Faraday effect in III–V semiconductors has been interpreted on the basis of spherical bands, except in the case of *n*-type GaSb.[60]

[54c] H. Flietner and K. Kliefoth, *Phys. Status Solidi* **14**, 181 (1966).
[54d] J. K. Furdyna, *Phys. Rev. Letters* **16**, 646 (1966); *Rev. Sci. Instr.* **37**, 462 (1966).
[55] E. W. J. Mitchell, *Proc. Phys. Soc. (London)* **A68**, 973 (1955).
[56] R. N. Brown, Masters Thesis, M.I.T. (1958); R. N. Brown and B. Lax, *Bull. Am. Phys. Soc.* **4**, 133 (1959).
[57] A. K. Walton and T. S. Moss, *Proc. Phys. Soc. (London)* **78**, 1393 (1961).
[58] B. Donovan and J. Webster, *Proc. Phys. Soc. (London)* **79**, 46 (1962).
[59] I. G. Austin, *J. Electron. Control* **6**, 271 (1959).
[60] H. Piller, *J. Phys. Chem. Solids* **24**, 425 (1963).

Smith and co-workers[61,71] have measured the Faraday effect in many n-type InSb samples to determine the E–k curve. In this case, the mass was calculated from the data, taking into account the Fermi distribution of carriers in the nonparabolic band. The results are in substantial agreement with cyclotron-resonance data. The temperature dependence of the effective mass has also been studied by Ukhanov and Mal'tsev.[62]

Faraday rotation has also been measured in n-type InAs,[63–65a] InP,[63,66,67] GaAs,[64,68,69,69a] GaSb,[60] GaP,[70] and AlSb.[70] The observed variation of the Faraday effective mass with temperature was first explained by Cardona[64] on the basis of the distribution of carriers in a nonparabolic band and effective-mass dependence on band gap, and has subsequently been observed by others.[68,71,72] Kołodziejczak[73] has calculated the Faraday effect for nonparabolic energy bands in InSb.

Faraday rotation involving carriers distributed in two conduction bands has been measured by Piller[60] in GaSb. In this interesting case, for large carrier concentrations, carriers are distributed between a spherical [000] band and four [111] ellipsoidal bands. As a function of temperature, the carriers spill between the bands. Analysis of the data gave a spherical-band effective mass of $0.053m_0$ and implied germanium-like m_T^* and m_L^* for the ellipsoids.

Moss, Walton, and Ellis[70,74] have recently measured effective masses in GaP and AlSb. These materials have very low mobilities ($\sim 50\ \mathrm{cm^2/V\text{-}sec}$),

[61] S. D. Smith, T. S. Moss, and K. W. Taylor, *J. Phys. Chem. Solids* **11**, 131 (1959).

[62] Yu. I. Ukhanov and Yu. V. Mal'tsev, *Fiz. Tverd. Tela* **4**, 3215 (1962) [*English Transl.: Soviet Phys.-Solid State* **4**, 2354 (1963)].

[63] I. G. Austin, *J. Electron. Control* **8**, 167 (1960).

[64] M. Cardona, *Phys. Rev.* **121**, 752 (1961).

[65] Yu. I. Ukhanov and Yu. V. Mal'tsev, *Fiz. Tverd. Tela* **5**, 1548 (1963) [*English Transl.: Soviet Phys.-Solid State* **5**, 1124 (1963)].

[65a] S. A. Shulman and Yu. I. Ukhanov, *Fiz. Tverd. Tela* **7**, 952 (1965) [*English Transl.: Soviet Phys.-Solid State* **7**, 768 (1965)].

[66] F. P. Kesamanly, E. E. Klotyn'sh, Yu. V. Mal'tsev, D. N. Nasledov, and Yu. I. Ukhanov, *Fiz. Tverd. Tela* **6**, 134 (1964) [*English Transl.: Soviet Phys.-Solid State* **6**, 109 (1964)].

[67] T. S. Moss and A. K. Walton, *Physica* **25**, 1142 (1959).

[68] Yu. I. Ukhanov, *Fiz. Tverd. Tela* **5**, 108 (1963) [*English Transl.: Soviet Phys.-Solid State* **5**, 75 (1963).

[69] T. S. Moss and A. K. Walton, *Proc. Phys. Soc. (London)* **74**, 131 (1959).

[69a] W. M. De Meis and W. Paul, *Bull. Am. Phys. Soc.* **10**, 344 (1965).

[70] T. S. Moss, A. K. Walton, and B. Ellis, *Proc. Intern. Conf. Phys. Semicond., Exeter, 1962* p. 295. Inst. of Phys. and Phys. Soc., London, 1962.

[71] C. R. Pidgeon and S. D. Smith, *Infrared Phys.* **4**, 13 (1964).

[72] Yu. I. Ukhanov and Yu. V. Mal'tsev, *Fiz. Tverd. Tela* **5**, 2926 (1963) [*English Transl.: Soviet Phys.-Solid State* **5**, 2144 (1964)].

[73] J. Kołodziejczak, *Acta Phys. Polon.* **21**, 637 (1962).

[74] T. S. Moss and B. Ellis, *Proc. Phys. Soc. (London)* **83**, 217 (1964).

requiring some amendment of Eq. (26) because the assumption $(\omega - \omega_c)\tau \gg 1$, which implies $\omega\tau \gg 1$, no longer holds. Then Eq. (26) is modified by a multiplying factor $(1 - \omega^{-2}\tau^{-2})/(1 + \omega^{-2}\tau^{-2})$. Appropriate analysis of the data allowed both m^* and τ to be determined.

In Fig. 15 is shown the wavelength dependence of rotation in n-type InSb at room temperature and low temperature.[75] At short wavelengths an interband rotation of opposite sign to the free carrier causes a deviation from linearity. It is not shown here. It is vital in most experiments to measure θ versus λ^2 to correct for interband rotation and in some cases for inter-valence-band rotation, as in p-type Ge.[57]

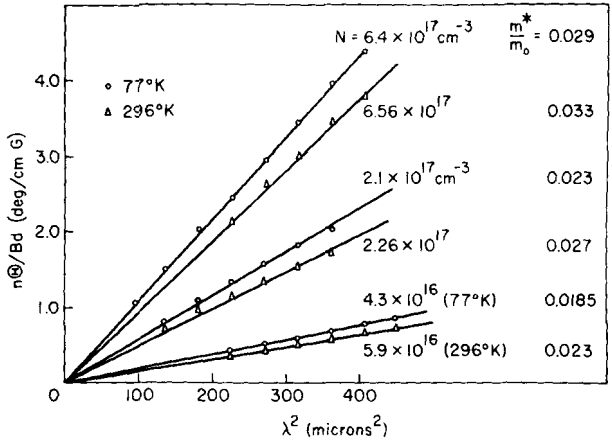


FIG. 15. Faraday rotation in n-type InSb. A negative interband rotation (not measured here) causes deviation from linearity at short wavelengths. (After C. R. Pidgeon.[75])

If there is a difference between the left and right circular extinction coefficients, there will be a slight differential absorption between left and right circular polarization, which produces a slight ellipticity to the beam. This has been measured by Smith and Pidgeon[76] and is a means of determining τ.

Faraday rotation can be measured through cyclotron resonance where absorption occurs.[77] Some results for n-type InSb are shown in Fig. 16. Near ω_c, θ is sensitive to τ. Attempts to fit the data with the Drude theory were reasonably successful, as the two calculated fits indicate. At small

[75] C. R. Pidgeon, Ph.D. Dissertation, University of Reading, Reading, England, 1962.
[76] S. D. Smith and C. R. Pidgeon, *Proc. Intern. Conf. Semicond. Phys., Prague, 1960* p. 342. Czech. Acad. Sci., Prague, and Academic Press, New York, 1961.
[77] E. D. Palik, *Appl. Opt.* **2**, 527 (1963).

fields, Eq. (26) held, while at the largest fields for $\omega_c \gg \omega$, the rotation is given by

$$\theta = \frac{eNd}{2c\varepsilon_0 nB}. \tag{41}$$

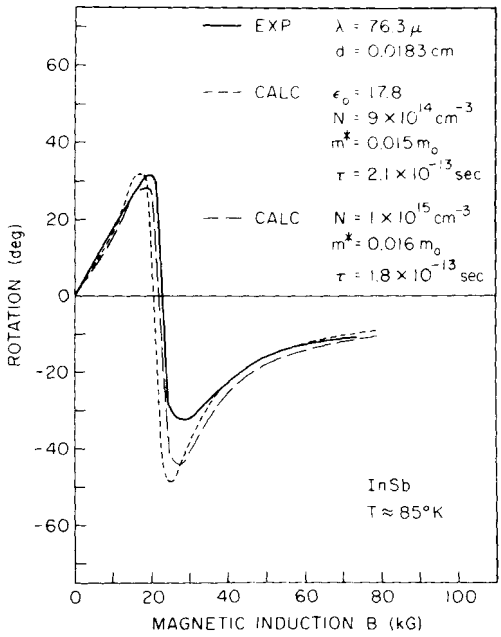


FIG. 16. Faraday rotation through cyclotron resonance in *n*-type InSb. The two calculated curves are based on the indicated parameters. (After E. D. Palik.[77])

From fitting these end regions, it was possible to determine m^* and N optically. Calculations indicate that even better results are obtained if the magnetic-field dependence of the mass is included.

The microwave Faraday rotation and ellipticity have been observed in low carrier concentration InSb for $\omega < \omega_c$ and accounted for with the Drude model.[77a]

The Faraday effect of free holes has not been studied in III–V semiconductors, but has been measured in *p*-type Ge by Walton and Moss[57] and discussed by Lax and Zwerdling.[30] The rotation is given by

$$\theta = -\frac{e^3 d\lambda^2 B}{8\pi^2 c^3 n\varepsilon_0}\left(\frac{N_h}{m_h^2} + \frac{N_l}{m_l^2}\right), \tag{42}$$

[77a]R. Mansfield and M. R. Borst, *Brit. J. Appl. Phys.* **16**, 570 (1965).

where the subscripts h and l refer to heavy and light holes. Since $N_l/N_h = (m_l/m_h)^{3/2}$ gives the distribution of carriers in the two bands, it is obvious that the effect of the two kinds of holes may be comparable, even though $N_l \ll N_h$. It follows that if m_l and m_h and the total concentration N are known, it is possible to determine the light- and heavy-hole densities. This has been done for Ge[57] and would be of interest in p-type InSb.

It has recently been pointed out by Walton and Moss,[57] Donovan and Medcalf,[78] and Piller[78a] that multiple reflections must be considered in analysis of Faraday rotation. De Meis and Paul[69a] report observing multiple-reflection effects in Faraday rotation in GaAs, which were eliminated by wedging of the sample.

Cardona has recently reviewed the Faraday effect in semiconductors[79] in some detail.

e. *Voigt Effect*

Magnetic double refraction was predicted by Voigt in 1899.[80] Shortly thereafter, he observed that sodium vapor exhibited a small double refraction in the vicinity of the D lines for the transverse orientation.[81] This diamagnetic phenomenon was demonstrated for free carriers in semiconductors by Teitler and Palik[82] and has further been discussed by Teitler *et al.*,[83] Cardona,[84] Webster and Donovan,[85] and Teitler.[86]

The Voigt effect is an optical analog to the magnetoresistance effect and, in the approximation of Eq. (29), will show anisotropy in cubic crystals with energy ellipsoids. This has been demonstrated in n-type Ge by Palik.[87]

To date, in III–V semiconductors, the Voigt effect has been measured in n-type InSb,[83] InAs,[82] and GaAs,[77] all of which have spherical, nonparabolic bands. The results demonstrate that the Voigt effective mass is the mass at the Fermi level, as in the case of Faraday rotation. Also, the temperature dependence of the effective mass is similar to that in the Faraday effect. Usually, both the Faraday and Voigt effects were measured in each sample from which both N and m^* were obtained. The results for N were within $\pm 15\%$ of the carrier concentration measured by the Hall effect.

[78] B. Donovan and T. Medcalf, *Phys. Letters* **7**, 304 (1963); *Brit. J. Appl. Phys.* **15**, 1139 (1964).
[78a] H. Piller, *J. Appl. Phys.* **37**, 763 (1966).
[79] M. Cardona, *Verhandl. Deut. Physik. Ges. Festkörper* **1**, 72 (1962).
[80] W. Voigt, *Weid. Ann.* **67**, 345 (1899).
[81] W. Voigt, "Electro- and Magneto-Optics." Teubner, Leipzig, 1907.
[82] S. Teitler and E. D. Palik, *Phys. Rev. Letters* **5**, 546 (1960).
[83] S. Teitler, E. D. Palik, and R. F. Wallis, *Phys. Rev.* **123**, 1631 (1961).
[84] M. Cardona, *Helv. Phys. Acta* **34**, 796 (1961).
[85] J. Webster and B. Donovan, *Phys. Letters* **2**, 330 (1962); *Brit. J. Appl. Phys.* **16**, 25 (1965).
[86] S. Teitler, *J. Phys. Chem. Solids* **24**, 1487 (1963).
[87] E. D. Palik, *J. Phys. Chem. Solids* **25**, 767 (1964).

The linear dependencies of β on λ^3 and B^2 are shown for InSb in Figs. 17 and 18. The λ^3 dependence is observable, although an interband Voigt effect seems to persist out to 18 microns. A small correction for the slight decrease in index of refraction to longer wavelengths has not been made. The linear dependence of β on B^2 is evident in Fig. 18, but a departure from linearity indicates that the condition $\omega \gg \omega_c$ is no longer valid, so that Eq. (29) does not hold.

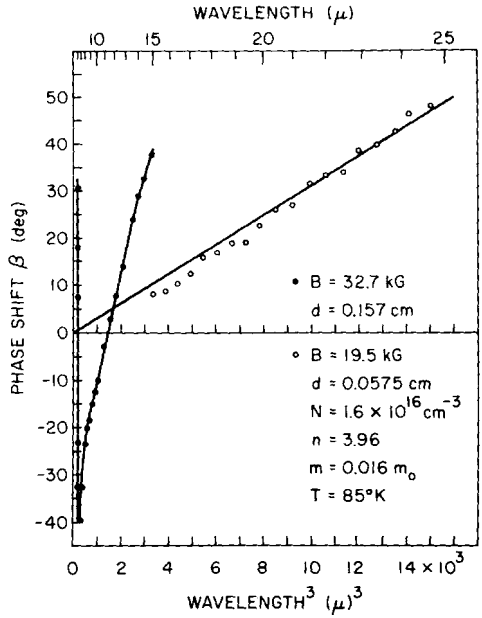


FIG. 17. Voigt effect in n-type InSb. An interband Voigt effect is shown at short wavelengths for different conditions. The straight line was calculated with the indicated parameters. The curve was simply drawn through the solid data points. (After S. Teitler *et al.*[83] and unpublished data.)

f. Interference Fringes

This effect has been measured by Palik[77] in intrinsic n-type InSb for left and right circular reflection and transmission fringes. Left and right circular fringes in the 20–40-micron region were observed to shift to higher and lower frequencies, respectively, by different amounts. With an assumed effective mass of $0.018m_0$ for intrinsic, room-temperature InSb, the calculated shifts of the fringes obtained from use of $n_\pm$ from Table III in the

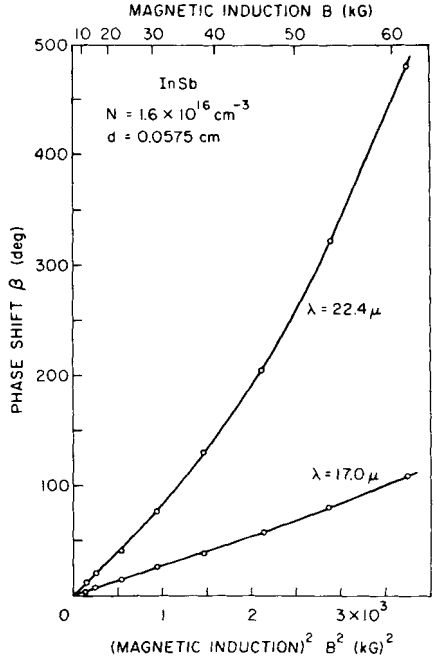


FIG. 18. Voigt effect in low-temperature *n*-type InSb, indicating departure of β from linearity in B^2. The solid curves are simply drawn through the data points. (After S. Teitler *et al.*[83] and unpublished data.)

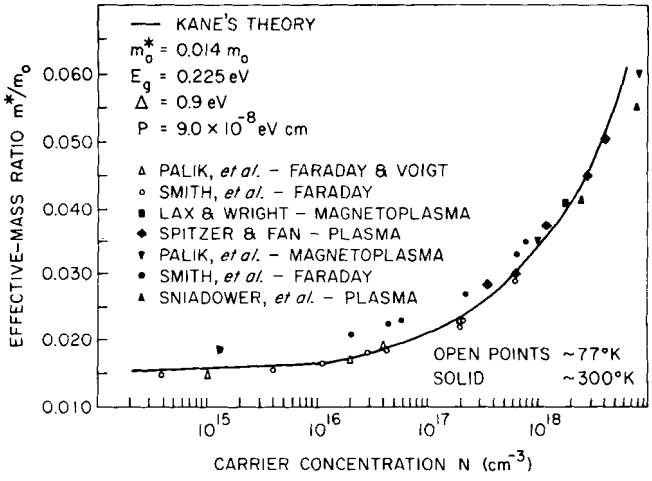


FIG. 19. Variation of the conduction-band effective mass in InSb with carrier concentration, plotted to emphasize agreement with theory at low concentrations.

equation $m\lambda = 2nd$ were in good agreement with the observed shifts. This experiment, although another way to measure effective mass, does not appear to have any advantage over other methods already discussed.

9. Summary of Experimental Results

Reviews of free-carrier magnetooptical effects not referred to before have been written by Moss[88] and Lax.[89]

In summary for InSb, we present Fig. 19, which shows the conduction effective-mass dependence on carrier concentration because of the nonparabolic band. For the condition $\Delta \gg E_g$, Wright and Lax[9] showed that Kane's equation for the conduction-band energy of InSb could be rewritten to show the linear dependence of $[(m^*/m_0)/(1 - m^*/m_0)]^2$ on $N^{2/3}$. All the known effective-mass data are collected in Fig. 20 to demonstrate this dependence.

Recently, more comprehensive plots, like Fig. 19, for both InSb and InAs have been given[90,91] based on more detailed calculations involving the formulas of Kane.

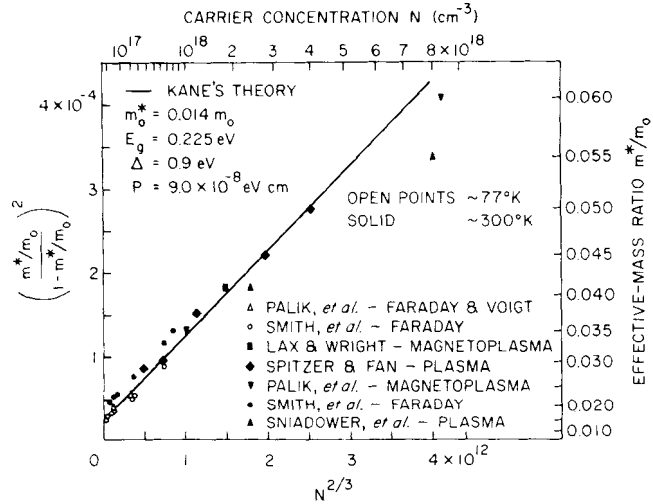


FIG. 20. Variation of the conduction-band effective mass in InSb with carrier concentration plotted to emphasize agreement with theory at high concentrations.

We have collected in Table V all the effective-mass data for III–V semiconductors, as obtained from each type of magnetooptical experiment, and displayed them as a function of temperature and carrier concentration.

[88] T. S. Moss, *Phys. Status Solidi* **2**, 601 (1962).

[89] B. Lax, *Proc. Intern. School Phys. "Enrico Fermi," Varenna, 1961*, Course XXII. Academic Press, New York, 1963.

[90] J. Kołodziejczak, S. Zukotyński, and H. Stramska, *Phys. Status Solidi* **14**, 471 (1966).

[91] J. Kołodziejczak and S. Zukotyński, *Phys. Status Solidi* **16**, K55 (1966).

TABLE V

EFFECTIVE MASSES OF III–V COMPOUNDS DETERMINED BY MAGNETOOPTICAL EXPERIMENTS

Compound	m^*/m_0	N (cm^{-3})	T (°K)	Experimental method[a]	Reference
InSb	0.0134	$0.2–3 \times 10^{15}$	4	CR	45
	0.0155	2×10^{14}	4	CR	47
	0.013	3×10^{14}	77	FR	61
	0.0148	3.8×10^{14}	77	FR	75
	0.0131	2.6×10^{15}	77	FR	61
	0.0145	10^{15}	77	CR	39
	0.0165	1.1×10^{16}	77	FR	61
	0.0178	2.9×10^{16}	77	FR	61
	0.019	4×10^{16}	77	FR, VE	75, 83
	0.0185	4.3×10^{16}	77	FR	75
	0.022	2.0×10^{17}	77	FR	61
	0.023	2.0×10^{17}	77	FR, VE	44, 83
	0.023	2.1×10^{17}	77	FR	75
	0.029	6.4×10^{17}	77	FR	61
	0.012	—	300	CR	37
	0.021	2.0×10^{16}	300	FR	71
	0.0225	4.5×10^{16}	300	FR	75
	0.023	5.9×10^{16}	300	FR	75
	0.035	7.8×10^{16}	300	FR	75
	0.035	1.0×10^{18}	300	MPR	7
	0.041	1.8×10^{18}	300	MPR	9
	0.038	2.4×10^{18}	300	MPR	21
	0.021	$p = 10^{14}$	4–65	CR	43
	0.0155	$p = 10^{16}$	80	CR	44
InAs	0.024	7×10^{15}	80	CR	40, 41
	0.026	7×10^{15}	80	FR	44
	0.030	1×10^{17}	80	FR, VE	44
	0.027	4.9×10^{16}	300	FR	64
	0.031	1.0×10^{17}	300	VE	82
	0.029	2.9×10^{17}	300	FR	65
	0.043	1.0×10^{18}	300	FR	63
	0.06	5.3×10^{18}	300	MPR	9
InP	0.077	6.1×10^{15}	80	CR	40, 44
	0.073	1×10^{16}	300	FR	67
	0.066	8.2×10^{16}	300	FR	66
	0.10	1.4×10^{17}	300	FR	63
GaP	0.35	3×10^{18}	300	FR	70, 74
GaSb	0.04	3.7×10^{17}	77	FR	60
AlSb	0.39	2×10^{18}	300	FR	70, 74

TABLE V—*continued*

Compound	m^*/m_0	N (cm^{-3})	T (°K)	Experimental method[a]	Reference
GaAs	0.071	3×10^{15}	80	CR	42, 44
	0.071	4.3×10^{16}	80	VE	44, 47
	0.076	4.3×10^{16}	80	FR	44
	0.067	4.1×10^{15}	300	FR	68
	0.061	1.2×10^{16}	300	FR	68
	0.071	4.6×10^{16}	300	FR	68
	0.072	5×10^{16}	300	FR	69
	0.069	1.0×10^{17}	300	FR	68
	0.067	1.4×10^{17}	300	FR	64
	0.072	2.4×10^{17}	300	FR	68
	0.083	2.3×10^{18}	300	FR	64
	0.078	2.6×10^{18}	300	FR	68
	0.080	5.5×10^{18}	300	FR	68
	0.089	7×10^{18}	300	FR	68
	0.081	9×10^{18}	300	FR	68

[a] CR = cyclotron resonance; FR = Faraday rotation; VE = Voigt effect; MPR = magnetoplasma reflection or rotation.

CHAPTER 11

Photoelectronic Analysis

Richard H. Bube

I. Concepts and Parameters 461
1. *Lifetime* 461
2. *Photosensitivity and Gain* 462
3. *Imperfection Sensitization* 463
4. *Trapping* 464
II. Techniques of Photoelectronic Analysis 464
5. *Spectral Response of Photoconductivity* 464
6. *Photoconductivity vs. Excitation Intensity* 465
7. *Thermal Quenching of Photoconductivity* 466
8. *Optical Quenching of Photoconductivity* 467
9. *Thermally Stimulated Conductivity* 468
10. *Hall Effects of Nonequilibrium Carriers* 471
11. *Photomagnetoelectric Effects* 473
III. Applications of Photoelectronic Analysis 474
12. *Majority- and Minority-Carrier Lifetimes* 474
13. *Properties of Trapping Imperfections* 476
14. *Properties of Sensitizing Imperfections* 478
15. *Giant Scattering Cross Sections* 481
16. *Imperfection Identification with Hall-Effect Measurements* . . . 486

I. Concepts and Parameters

The term "photoelectronic analysis," as applied to imperfections in insulators or high-resistivity semiconductors, embraces a variety of techniques involving the interaction between electrons, photons, electric fields, and magnetic fields in crystals. Growing out of the study of photoconductivity phenomena, particularly in II–VI compounds, it has come to have a wider application to many different materials. In this chapter the intent is to summarize rather briefly the nature of the techniques involved in photoelectronic analysis, with pertinent references to the literature, and to describe the results of applying these techniques to III–V compounds.

1. Lifetime

Photoexcitation of electron-hole pairs in a crystal results in an increased conductivity that is terminated either when the excited carriers recombine or when carriers are drawn out of the electrodes affixed to the crystal

without being replenished from the opposite electrode. The lifetime of a free carrier is the length of time that it is available to contribute to the conductivity. We may associate a lifetime with each of the carriers, so that it is possible to express

$$n = f\tau_n, \tag{1}$$

$$p = f\tau_p. \tag{2}$$

Here n is the density of photoexcited free electrons, τ_n is the electron lifetime, p is the density of photoexcited free holes, τ_p is the hole lifetime, and f is the rate of excitation per unit volume. Although τ_n may be equal to τ_p, as is most frequently the case in low-resistivity semiconductors, $\tau_n \neq \tau_p$ in a majority of the cases in which photoelectronic analysis is involved.

It is the lifetime that is the key parameter in photoelectronic analysis. The details of the recombination mechanisms involving imperfections in crystals manifest themselves through the lifetimes of the free carriers. It is usually possible over a wide range of imperfection densities to express the lifetime in terms of a capture cross section S. Thus the lifetime τ_n for electrons as determined by capture at centers with a capture cross section S_n is given by

$$\tau_n = \frac{1}{S_n v N_1^*}. \tag{3}$$

Here N_1^* is the density of unoccupied imperfection centers, and v is the electron thermal velocity. The magnitude and the temperature dependence of the cross section S_n are determined by the nature of the imperfection center and of the specific recombination mechanism.

It is common practice to refer to a majority-carrier lifetime and a minority-carrier lifetime. In the case of a high-resistivity semiconductor, the photoexcited carrier densities are in general much larger than the thermal-equilibrium densities, and therefore the majority carrier under photoexcitation is the carrier with the longer lifetime. Photoelectronic phenomena can be separated into two categories in general: (1) those for which the existence of electron-hole pairs is essential—here the minority-carrier lifetime is the critical lifetime; and (2) those for which the existence of free carriers of one type is sufficient—here the majority-carrier lifetime is the critical lifetime.

2. Photosensitivity and Gain

The photosensitivity of a crystal is defined as the change in conductivity under photoexcitation per electron-hole pair created. Thus the photosensitivity is proportional to the product of lifetime and mobility, and

photoexcitation effects resulting in a change in the mobility of free carriers are also observed as a change in the photosensitivity.

A practical measure of photosensitivity in a particular crystal with a specific applied electric field is the photoconductivity gain. The gain is defined as the number of charges passing between the electrodes of the crystal per electron-hole pair created. Thus, if a photocurrent ΔI is measured for an excitation rate of F sec^{-1}, the gain G is given by

$$G = \frac{\Delta I}{eF}. \tag{4}$$

The gain may be related to the lifetime by recognizing that the above definition of gain is equivalent to setting the gain equal to the ratio of lifetime to transit time:

$$G = \frac{\tau}{t_{tr}} = \frac{\tau \mu V}{l^2}. \tag{5}$$

Here τ is the lifetime of the carriers contributing to the gain, t_{tr} is the time required for these carriers to move under the effect of the applied electric field from one electrode to the other electrode, μ is the carrier mobility, V is the applied voltage, and l is the crystal length, the distance between electrodes. If the free-carrier lifetime exceeds the transit time, the gain may exceed unity by a large factor. Indeed, in the most sensitive materials, the gain reaches values in excess of 10^4. The achievement of such high gains requires that ohmic electrodes be used—i.e., electrodes that are able to replenish carriers drawn out at the opposite electrode—in order to maintain electrical charge neutrality in the crystal.

3. Imperfection Sensitization

In insulators and high-resistivity semiconductors for which the density of free carriers may under all practical conditions of photoexcitation be considered less than the density of imperfection centers controlling recombination, it is possible to increase the photosensitivity by incorporating suitable imperfections. Such sensitizing imperfections are characterized by a much larger capture cross section for one type of carrier than for the other. Thus their incorporation reduces the minority-carrier lifetime, but increases the majority-carrier lifetime. In order for such imperfections to be effective in increasing the sensitivity through this effect on the lifetimes, however, it is necessary that the operating conditions of photoexcitation intensity and temperature be such that the occupancy of these centers is determined by recombination kinetics (i.e., by the cross sections) and not by thermal-equilibrium conditions with the nearest band.

Photoelectronic effects associated with a change in the occupancy of such sensitizing centers from recombination-dominated to thermal-equilibrium-dominated may be used to determine the hole ionization energy (electrons being the majority carriers in the cases to be discussed) and the capture cross sections of these centers. Such effects are described further in Part II.

4. Trapping

Real crystals commonly contain imperfections with energy levels lying relatively close to the conduction or valence bands, the occupancy of which is determined by thermal-equilibrium interchange with the nearest band. Such levels are called trapping levels. As indicated in the previous section, a given type of imperfection may be a recombination center under one set of photoexcitation and temperature conditions and a trapping center under another. Thus the classification of an imperfection as a trapping or recombination center is more closely related to the type of analytical technique used to obtain information about its ionization energy, density, and cross sections than to some intrinsic property of the center itself.

Levels corresponding to compensated donors or acceptors in a high-resistivity semiconductor can often be profitably investigated in terms of their electron- or hole-trapping characteristics. The techniques described in Part II available for such investigation from photoelectronic effects frequently exceed other methods in their ability to detect and characterize very low imperfection densities.

II. Techniques of Photoelectronic Analysis

5. Spectral Response of Photoconductivity

The typical spectral response of photoconductivity for a pure material contains a maximum for photon energies slightly less than the absorption edge, with a very rapid decrease for smaller photon energies. The maximum usually occurs for an absorption constant approximately equal to the reciprocal thickness of the crystal and arises because of a volume photoconductivity lifetime larger than the surface photoconductivity lifetime.

The existence of imperfection centers in a crystal with ionization energies less than the band gap clearly results in the measurement of a photoconductivity for photon energies much less than the band gap. Thus just the qualitative observation of photoconductivity for such photon energies is evidence for the existence of imperfections. From the low-energy threshold for the imperfection photoconductivity, it is possible to obtain an estimate of the location of the imperfection level with respect to the energy bands of

the crystal, although a knowledge of the sign of the excited carrier is required to fix the location of the level uniquely. Over a certain range of imperfection densities the ratio of photoconductivity in the imperfection-excitation region to that at the maximum of the intrinsic-excitation region provides a relative measure of the imperfection density.

Although it is possible to obtain some quantitative information about the imperfection level location from the low energy threshold of the imperfection photoconductivity response, most of the information obtained from spectral response curves is essentially qualitative.

6. Photoconductivity vs. Excitation Intensity

In a crystal with one principal type of recombination center, as defined by its capture cross sections, the photoconductivity is found to vary as a power of the light intensity between one-half and unity. Some information about the nature of the trap distribution can be obtained from such curves, since the exact exponent in the power-law dependence of photoconductivity on excitation intensity depends on the particular distribution of trap density with trap depth.[1]

If two types of recombination center are present, and particularly if one of these has the cross sections suitable for its behavior as a sensitizing center, a region is found where the photoconductivity increases with a power of excitation intensity greater than unity. This phenomenon has been called superlinearity. It occurs in that region where the sensitizing centers are changing from hole traps to recombination centers with increasing excitation intensity. Because of this change in the occupancy-determining factor for the sensitizing centers, the crystal's photosensitivity increases with excitation intensity.[2]

The condition for the end of superlinearity with increasing excitation intensity, or conversely for the beginning of superlinearity—i.e., the beginning of sensitivity loss—with decreasing excitation intensity is that the sensitizing centers be "on the verge" of changing from hole traps to recombination centers or vice versa. This condition may be stated quantitatively in terms of an equality between the rate of electron capture by empty sensitizing centers and rate of thermal freeing of holes from sensitizing centers to the valence band.[3,4]

$$n(N_1 - n_1)v_n S_n = (N_1 - n_1)N_v v_p S_p e^{-E_1/kT}, \tag{6}$$

where n is the density of free electrons, N_1 is the total density of sensitizing

[1] A. Rose, *RCA Rev.* **12**, 362 (1951).
[2] A. Rose, *Phys. Rev.* **97**, 322 (1955).
[3] R. H. Bube, *J. Phys. Chem. Solids* **1**, 234 (1957).
[4] F. Cardon and R. H. Bube, *J. Appl. Phys.* **35**, 3344 (1964).

centers, n_1 is the density of sensitizing centers occupied by electrons, v_n is the thermal electron velocity, S_n is the capture cross section of an unoccupied sensitizing center for a free electron, N_v is the effective density of states in the valence band, v_p is the thermal hole velocity, S_p is the capture cross section of an occupied sensitizing center for a hole, and E_1 is the hole ionization energy for a sensitizing center. Solving Eq. (6) for n gives

$$\ln n' = -\frac{E_1}{kT'} + \ln\left(N_v \frac{S_p}{S_n}\left[\frac{m_e^*}{m_h^*}\right]^{1/2}\right). \tag{7}$$

Here n' and T' are the particular values of electron density and temperature occurring at the beginning of sensitivity loss, and m_e^* and m_h^* are the effective electron and hole masses, respectively. By making measurements of photoconductivity as a function of excitation intensity at different temperatures, a set of values for n' and T' may be obtained. It is then possible to obtain both E_1 and S_p/S_n from a plot of $\ln n'$ vs. $1/T'$.

An alternate way of expressing the result inherent in Eq. (7) is to substitute $n = N_c \exp(-E_{fn}/kT)$ into Eq. (6), where N_c is the effective density of states in the conduction band, and E_{fn} is the distance of the steady-state electron Fermi level below the bottom of the conduction band. Then an equivalent equation to Eq. (7) is obtained:

$$E'_{fn} = E_1 - kT' \ln\left(\frac{S_p}{S_n}\left[\frac{m_h^*}{m_e^*}\right]^{3/2}\right), \tag{8}$$

where the primes have the same significance as in Eq. (7). In this case a plot of E'_{fn} vs. T' yields values for E_1 and S_p/S_n.

7. Thermal Quenching of Photoconductivity

Thermal quenching of photoconductivity refers to a rapid decrease in photosensitivity in a crystal characterized by imperfection sensitization, when the temperature is raised beyond some critical temperature. The nature of this phenomenon is completely analogous to that of superlinearity discussed in the previous section. Indeed, the two phenomena are really two different ways of viewing the same mechanism. In superlinearity a change in the sensitizing centers from hole traps to recombination centers is observed with increasing excitation intensity at fixed temperature. In thermal quenching the same change in the sensitizing centers from recombination centers to hole traps is observed with increasing temperature at fixed excitation intensity. Data of n' or E'_{fn} and T', for the onset of thermal quenching, may be analyzed using Eqs. (7) and (8) in exactly the same way as data on superlinearity.

The use of either superlinearity or thermal-quenching data gives a value for the thermal hole-ionization energy of sensitizing centers, and an average value of the cross-section ratio over the temperature range of the measurements. By these techniques it is not possible to obtain either S_n or S_p alone, nor is it possible to measure either the cross sections or their ratio as a function of temperature.

8. Optical Quenching of Photoconductivity

Optical quenching of photoconductivity is analogous to thermal quenching, with the substitution of optical freeing of holes from sensitizing centers instead of thermal freeing of holes. Normally a steady-state photoconductivity is first established by photoexcitation with light of a suitable wavelength. Then quenching is observed when a second light is used to illuminate the crystal, if the photon energy of this second light is (1) small enough not to cause appreciable creation of free electrons, and (2) large enough to optically excite an electron from the valence band to a sensitizing center that has previously captured a photoexcited hole.

The optical hole-ionization energy of sensitizing centers is obtained by determining the smallest photon energy sufficient to cause optical quenching. A quenching spectrum is obtained by measuring the effectiveness of quenching as a function of the photon energy of the quenching light. For high photon energies near the absorption edge of the crystal, the effectiveness of quenching decreases because the same photons are active also in creating free electrons. Usually a fairly sharp threshold for quenching characterizes the spectrum at low photon energies.[5,6]

The measurement of the onset of sensitivity loss with optical quenching can be used to determine the electron-capture cross section and also its dependence on temperature. The onset of sensitivity loss, either with fixed quenching-light intensity and decreasing exciting-light intensity or with fixed exciting-light intensity and increasing quenching-light intensity, may be described quantitatively by replacing the thermal rate of hole freeing in Eq. (6) by the optical rate of hole freeing.

$$n(N_1 - n_1)v_n S_n = F_q, \tag{9}$$

where F_q is the rate per unit volume at which holes are optically freed from the sensitizing centers. For the weak absorption processes involved

$$F_q = f_q S_o(N_1 - n_1)d, \tag{10}$$

in optical quenching,

[5] R. H. Bube, *Phys. Rev.* **99**, 1105 (1955).

[6] R. H. Bube, "Photoconductivity of Solids," pp. 348–354. Wiley, New York, 1960.

where f_q represents the incident photon flux per unit volume, S_o is the optical cross section for quenching photon absorption, and d is the crystal thickness. Equations (9) and (10) may be combined to obtain a value for the electron capture cross section:

$$S_n = \frac{f_q' S_o d}{v_n n'}. \tag{11}$$

Once again the primes indicate that the values to be used correspond to the onset of sensitivity loss because of quenching. The value of S_n can be determined by this method at any desired temperature below that at which thermal quenching of photoconductivity occurs.

9. Thermally Stimulated Conductivity

If a crystal is subjected to photoexcitation at a low temperature, carriers will be trapped at imperfections in the crystal. The energy required to thermally free these carriers again—the electrons to the conduction band or the holes to the valence band—is not available at the low temperature. If, after such a photoexcitation, the crystal is heated in the dark, however, the trapped carriers will be freed when sufficient thermal energy is available. Their existence as free carriers may be detected by measuring the conductivity. The temperature at which the maximum thermally stimulated conductivity (TSC) in such a process is found may be correlated with the trap depth, and the total charge that is thermally freed may be correlated with the trap density.

The technique of TSC consists essentially of observing the decay of conductivity while this decay is being thermally stimulated by raising the temperature at a fixed rate. It is thus possible to cover a wide range of trap depths in a single measurement, as well as to measure the distribution of traps in density over this range. Operationally, the crystal is cooled to a low temperature and is then excited with light of such a wavelength as to produce homogeneous excitation. After a period of excitation sufficiently long to establish a steady-state condition, the radiation is removed, and the crystal is heated at a linear rate in the dark. The measured current, in excess of any normal dark current, is contributed by carriers being freed from trapping centers.

The density of traps of a given depth can be determined from the area A under the corresponding portion of the TSC curve:

$$N_t = \frac{A}{e\mathscr{V} G^*}. \tag{12}$$

Here $\mathscr{V}$ is the volume of the crystal, and G^* is the gain calculated from an independent measurement of the steady-state photocurrent with magnitude equal to the TSC at the same temperature. G^* indicates how many charges pass between the electrodes per emptied trap before recombination of the free carrier occurs. Its use assumes that the gain during the TSC measurement is the same as that during photoexcitation, if the location of the Fermi level is the same.[7]

Certain precautions must be observed in determining trap densities from TSC data:

(1) Such trap densities may represent only a lower limit to the total trap density if the steady-state excitation condition corresponds to only partly filled traps, or if it is possible that traps for one carrier may be partially emptied by recombination with carriers of the opposite type freed from shallower traps earlier in the TSC measurement.

(2) If imperfections are present that are compensated partially in the dark, the density derived from TSC measurements will be the density of the compensated imperfections only.

(3) The value of G^* obtained from steady-state photoexcitation will be related to the lifetime of the majority carriers under photoexcitation. If the traps being emptied correspond to the other carriers, then in general the density calculated from G^* will be too small.

The correlation of trap depth with the temperature of the maximum TSC, T_m, depends in some detail on the nature of the trapping and untrapping processes. The basic kinetic equations for a single trap depth are as follows:

$$\frac{dn_t}{dt} = -n_t N_c S_t v \exp(-E_t/kT) + n(N_t - n_t)S_t v, \tag{13}$$

$$\frac{dn}{dt} = -\frac{n}{\tau_n} - \frac{dn_t}{dt}. \tag{14}$$

Equation (13) describes the rate of change of trapped electrons n_t in terms of the effective density of states in the conduction band N_c, the capture cross section of an unoccupied trap for an electron S_t, the trap depth E_t below the conduction band, and the total trap density N_t. Equation (14) describes the rate of change of free electrons as affected by recombination corresponding to a lifetime τ_n and interaction between free and trapped electrons. Similar equations could be written for hole traps. A variety of

[7] R. H. Bube, *J. Appl. Phys.* **34**, 3309 (1963).

procedures have been suggested for the description of TSC phenomena in terms of Eqs. (13) and (14).[8–18]

The relationship between the trap depth E_t and the maximum of the TSC curve T_m can be readily obtained from Eqs. (13) and (14) in two physically significant limits. If recombination of freed electrons is much more probable than their being retrapped at empty traps—i.e., if $n(N_t - n_t)S_t v \ll n/\tau_n$—then

$$E_t = kT_m \ln\left[\frac{N_c S_t v k T_m^2}{bE_t}\right], \tag{15}$$

where b is the heating rate, $dT = b\,dt$. On the other hand, if recombination of freed electrons is much less probable than their being retrapped, virtual thermal equilibrium will persist between free and trapped electrons throughout the TSC measurement. Under these conditions,

$$E_t = kT_m \ln\left[\frac{N_c k T_m^2}{N_t b \tau_n E_t}\right]. \tag{16}$$

Since retrapping is in general a likely process once any appreciable fraction of the traps has been emptied, it is likely that Eq. (16) gives a more reliable value of E_t than Eq. (15) in most cases.

Since the approximation of strong retrapping is the same as assuming virtual thermal equilibrium in the TSC experiment between free and trapped electrons, it should also be possible to obtain the trap depth from the location of the steady-state Fermi level at the maximum of the TSC curve:

$$E_t = kT_m \ln\left[\frac{N_c}{n_m}\right], \tag{17}$$

where n_m is the free-electron density at the maximum of the TSC curve. For most practical cases the trap depth calculated from Eq. (17) is almost the same as that calculated from Eq. (16).

If either Eq. (15) or (16) is applicable, then measurements as a function

[8] J. T. Randall and M. H. F. Wilkins, *Proc. Roy. Soc.* (*London*) **A184**, 366 (1945).
[9] G. F. J. Garlick and A. F. Gibson, *Proc. Phys. Soc.* (*London*) **A60**, 574 (1948).
[10] L. I. Grossweiner, *J. Appl. Phys.* **24**, 1306 (1953).
[11] A. H. Booth, *Can. J. Chem.* **32**, 214 (1954).
[12] R. H. Bube, *J. Chem. Phys.* **23**, 18 (1955).
[13] W. Hoogenstraaten, *Philips Res. Rept.* **13**, 515 (1958).
[14] A. Halperin and A. A. Branner, *Phys. Rev.* **117**, 408 (1960).
[15] R. R. Haering and E. N. Adams, *Phys. Rev.* **117**, 451 (1960).
[16] P. N. Keating, *Proc. Phys. Soc.* (*London*) **78**, 1408 (1961).
[17] See Ref. 6, pp. 292–299.
[18] K. W. Böer, S. Oberländer, and J. Voigt, *Ann. Physik.* **2**, 131 (1958).

of heating rate should give the same trap depth regardless of whether the strong or weak retrapping approximation is used. In either case,

$$\ln\left[\frac{T_m^2}{b}\right] = \frac{E_t}{kT_m} - \ln A, \tag{18}$$

where A is a combination of constants independent of T or b.

Another method of determining the trap depth is to measure the TSC in the approach to the maximum, in that range where the traps are only slightly empty. If interference from other nearby maxima is not present, this approach will give a TSC that is proportional to $\exp(-E_t/kT)$. In the event that interference from nearby maxima is present, allowing the current to decay at some temperature in the midst of the maximum of interest, then cooling and reheating without further excitation permit determination of E_t from this procedure. It is also possible by this method to determine whether a broad TSC peak is composed of more than one component with different trap depths, by carrying the decay to different temperatures within the TSC peak.

10. Hall Effects of Nonequilibrium Carriers

Hall-effect measurements have been widely used in the study of imperfections and their effect on the conductivity of semiconductors. The incorporation of the Hall-effect technique into a scheme of photoelectronic analysis performs the useful service of allowing the experimenter to know the sign of the charge carriers involved and their mobility. The nonequilibrium carriers involved in the Hall effect are those produced either by photoexcitation or by thermal stimulation.

When the conductivity is dominated by carriers of one type, the conductivity σ is given by $\sigma = ne\mu$, where μ is the carrier mobility. The Hall constant in this case is $R = r/ne$, where r is a constant, of the order of unity, which is dependent on the specific scattering mechanism and the band structure. The Hall mobility $\mu_H = \sigma R = r\mu$. If the Hall mobility is observed to vary with photoexcitation under such conditions of one-carrier conductivity, the variation in Hall mobility may arise either because of an effect of photoexcitation on r or on μ. In general the possible effects of photoexcitation on r are both too small and of the wrong sign to explain experimental observations. A variation of mobility μ with photoexcitation can result from a decrease in ionized impurity scattering, as, for example, if photoexcitation resulted in the capture of electrons by ionized donors or in the capture of holes by ionized acceptors.[19,20]

If photoexcitation affects a particular species of charged imperfection characterized by an ionization energy E_I, a density N_I, and a scattering

[19] W. W. Tyler and H. H. Woodbury, *Phys. Rev.* **102**, 647 (1956).

[20] R. H. Bube and H. E. MacDonald, *Phys. Rev.* **121**, 473 (1961).

cross section S_I, we may express the mobility as

$$\frac{1}{\mu} = \frac{300m_e^*}{e}\left[\frac{1}{\tau_0} + vS_I(N_I - n_I)\right]. \tag{19}$$

Here we assume that the imperfections are charged when unoccupied and neutral when occupied; for specificity the free carriers will be assumed to be electrons. The first term on the right of Eq. (19) includes all scattering processes not involved in the motion of the Fermi level through the N_I levels with photoexcitation, the quantity τ_0 being therefore just a generalized relaxation time. The variation of the second term on the right of Eq. (19) with location of the Fermi level is given by

$$(N_I - n_I) = \frac{N_I}{1 + 2\exp[(E_I - E_{fn})/kT]}, \tag{20}$$

where E_{fn} is the energy difference between the bottom of the conduction band and the steady-state electron Fermi level. As E_{fn} varies from much greater than E_I to much less than E_I, $1/\mu$ passes through a single "step." The change in $1/\mu$ in this step, $\Delta(1/\mu)$, is given by

$$\Delta(1/\mu) = 10^4 m_e^{*1/2} T^{1/2} S_I N_I. \tag{21}$$

Thus, from the variation of $1/\mu$ with E_{fn}, it is possible to determine both the energy level of the scattering centers and the product of scattering cross section and density. If the value of N_I can be determined independently, as by knowing the density of chemical impurities present or from the analysis of TSC, a value for S_I can be calculated. Since both electrons and holes are generated by photoexcitation, the cross section calculated corresponds to the net change in scattering caused by the capture of both electrons and holes.

Another situation in which Hall-effect measurements are particularly helpful is that in which one-carrier conductivity is changed to two-carrier conductivity by the photoexcitation. If, in the case of multicarrier conduction, we still define the Hall mobility as the $R\sigma$ product, then when both electrons and holes are making an appreciable contribution to the conductivity, the Hall mobility for low magnetic fields is given by

$$\mu_H = \frac{p\mu_p^2 - n\mu_n^2}{p\mu_p + n\mu_n}. \tag{22}$$

In writing the expression in this form we have assumed that we may approximately consider $r_n = r_p = 1$. The Hall mobility goes to zero when $p\mu_p^2 = n\mu_n^2$, with R changing sign as this point is passed.[21–23]

[21] W. W. Tyler and R. Newman, *Phys. Rev.* **98**, 961 (1955).
[22] H. H. Woodbury and W. W. Tyler, *Phys. Rev.* **100**, 659 (1955).
[23] R. O. Carlson, *Phys. Rev.* **104**, 937 (1956).

11. Photomagnetoelectric Effects

If a magnetic field is applied to a crystal at right angles to the direction of photoexcitation by strongly absorbed radiation, a potential difference is produced at right angles to both radiation and magnetic-field directions. This effect may be considered as the Hall effect of the diffusion current of the photoexcited carriers. The photomagnetoelectric (PME) effect provides a technique for the determination of minority-carrier lifetimes.

In the small-magnetic-field approximation, the magnitude of the PME current will be proportional to the diffusion distance of the carriers, which in turn is proportional to $\tau^{1/2}$ if τ is the minority-carrier lifetime. Since the photoconductivity is proportional to the majority-carrier lifetime, the situation of equal majority- and minority-carrier lifetimes is a fortuitous one that permits the determination of the lifetime from a measurement only of photocurrent and PME current without absolute calibration of the photoexcitation:

$$\tau = D\left[\frac{B}{\mathscr{E}}\right]^2\left[\frac{i_{PC}}{i_{PME}}\right]^2. \tag{23}$$

Here B is the magnetic field used in the PME measurement and $\mathscr{E}$ is the electric field used in the photoconductivity measurement. D is the averaged diffusion constant for electrons and holes.

In many real materials, however, the majority- and minority-carrier lifetimes are not equal. It has been shown[24] that the analysis can be adapted for the situation in which trapping of carriers is important, by writing

$$\frac{\tau_p}{\tau_n} = \frac{p}{n} = 1 + \frac{n_t}{n}, \tag{24}$$

where n_t represents the density of trapped carriers, positive in sign for trapped electrons and negative for trapped holes. Under these conditions, two lifetimes are defined, one determined from the PME experiment and the other from the photoconductivity experiment.

$$\tau_{PME} = \frac{\tau_n + (n_0/p_0)\tau_p}{1 + (n_0/p_0)}, \tag{25}$$

$$\tau_{PC} = \frac{\tau_n + (\mu_p/\mu_n)\tau_p}{1 + (\mu_p/\mu_n)}. \tag{26}$$

Here n_0 and p_0 are, respectively, the density of electrons and holes in the

[24] R. N. Zitter, *Phys. Rev.* **112**, 852 (1958).

absence of photoexcitation. The measurement of τ_{PME} and of τ_{PC} permits the determination of τ_n and τ_p in terms of (n_0/p_0) and (μ_p/μ_n).

Since the PME effect involves strongly absorbed light, interaction with surface-recombination processes might be expected to play a significant role. Inclusion of the surface-recombination velocity s in a general calculation for large as well as small values of magnetic field[25] leads to the result

$$i_{PME} = \frac{eL\mu B(D\tau)^{1/2}}{(1 + \mu^2B^2)^{1/2}} \frac{1}{1 + [\tau s/(D\tau)^{1/2}](1 + \mu^2B^2)^{1/2}}, \tag{27}$$

where L is the excitation rate. Two limiting cases, depending on the importance of the surface recombination, can be delineated. For high surface recombination, $\tau s/(D\tau)^{1/2} \gg 1$,

$$i_{PME} = \frac{eL\mu BD}{(1 + \mu^2B^2)s}. \tag{28}$$

As a function of B, i_{PME} passes through a maximum for high values of s. For low surface recombination, $\tau s/(D\tau)^{1/2} \ll 1$,

$$i_{PME} = \frac{eL\mu B(D\tau)^{1/2}}{(1 + \mu^2B^2)^{1/2}}. \tag{29}$$

Under these conditions i_{PME} saturates with increasing magnetic field.

III. Applications of Photoelectronic Analysis

12. Majority- and Minority-Carrier Lifetimes

Many of the data resulting from the investigation of carrier lifetimes through measurements of photoconductivity and PME effect have been summarized through 1960 by Hilsum and Rose-Innes,[26] and need not be repeated here. Table I summarizes the quantitative data given in these earlier measurements.

Typical of the results obtained are those for InSb shown in Fig. 1, as published originally by Zitter *et al.*[27] The InSb crystal of Fig. 1 was p-type with 6×10^{15} acceptors cm^{-3}. Above about 200°K the photoconductivity lifetime was equal to the PME lifetime, indicating that trapping is unimportant at these temperatures. At low temperatures the electron lifetime was given by the PME lifetime, but the hole lifetime was found to be

[25] S. W. Kurnick and R. N. Zitter, *J. Appl. Phys.* **27**, 278 (1956).

[26] C. Hilsum and A. C. Rose-Innes, "Semiconducting III–V Compounds," pp. 181–192. Macmillan (Pergamon), New York, 1961.

[27] R. N. Zitter, A. J. Strauss, and A. E. Attard, *Phys. Rev.* **115**, 266 (1959).

TABLE I

TYPICAL MEASURED VALUES OF ROOM-TEMPERATURE LIFETIME[a]

Material	Conductivity type	Lifetime (sec)
InSb	*p*	3×10^{-10} to 3×10^{-8}
InSb	*n*	10^{-7}
InAs[b]	*n*	10^{-8} to 10^{-7}
InAs	*p*	5×10^{-10}
GaSb	*p*	10^{-6}
GaAs[c]	—	10^{-6} to 10^{-4}
GaAs[d]	—	10^{-12} to 10^{-9}

[a] As summarized by Hilsum and Rose-Innes.[26]
[b] Heat treatment has produced lifetime values as large as 10^{-5} sec.
[c] Majority-carrier lifetime.
[d] Minority-carrier lifetime.

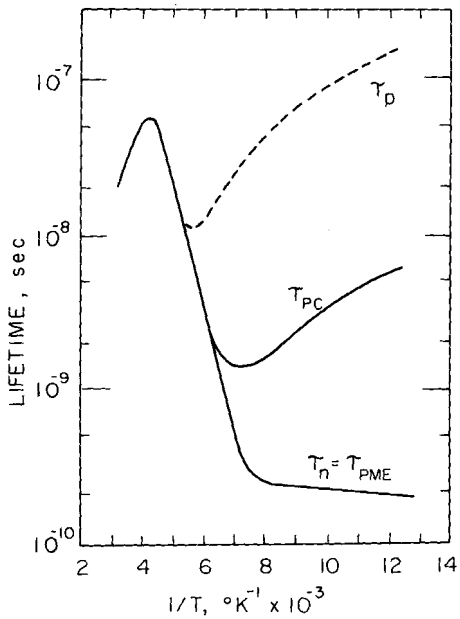


FIG. 1. Variation of electron and hole lifetimes as a function of temperature in *p*-type InSb, as determined by measurements of photoconductivity and PME lifetimes. (After Zitter *et al.*[27])

inversely proportional to the equilibrium hole concentration. For the data shown, the majority-carrier lifetime is some 500 times larger than the minority-carrier lifetime at 77°K.

Particular attention has been paid to the lifetimes in high-resistivity III–V compounds, such as GaP and GaAs. Measurements in GaP are few to date; a majority-carrier lifetime of 3×10^{-9} sec[28] may be compared with a minority-carrier lifetime of 10^{-10} sec measured in a surface-barrier junction.[29] A combination of photoconductivity and PME measurements on high-resistivity GaAs by Holeman and Hilsum[30] yields electron lifetimes between 5×10^{-9} and 2×10^{-7} sec, and hole lifetimes between 2×10^{-9} and 8×10^{-7} sec. In no case does the ratio of the lifetimes exceed a factor of 4. Majority-carrier lifetimes measured for high-resistivity GaAs by Bube[31] vary from 2×10^{-8} to 2×10^{-6} sec at room temperature, and from 2×10^{-9} to the order of 2×10^{-2} sec at 90°K. It was subsequently shown by Blanc *et al.*[32] that highly photosensitive GaAs crystals at low temperatures could be prepared by compensating high-conductivity *n*-type GaAs with diffused copper impurity. In such crystals the majority-carrier lifetime due to holes at room temperature of the order of 10^{-7} sec increases to a value of the order of 2×10^{-3} sec due to electrons at 90°K.

The problems of large-signal PME and photoconductivity effects, when the volume lifetime and the surface recombination velocity are functions of the excess carrier concentration, have been treated by Beattie and Cunningham[33] and applied to experimental studies with InSb.

13. Properties of Trapping Imperfections

Trap depths and densities in high-resistivity GaAs have been investigated by measurements of thermally stimulated conductivity.[31,32,34,35] An over-all summary of imperfection levels derived from a variety of photoelectronic techniques, including TSC, is given by Blanc *et al.*[36]

In this section only the properties of trapping centers derivable from TSC measurements themselves will be discussed. Further information on the identity of trapping centers obtained by the application of Hall effects is presented in Section 16 of this chapter.

[28] D. F. Nelson, L. F. Johnson, and M. Gershenzon, *Bull. Am. Phys. Soc.* **9**, 236 (1964).
[29] R. A. Logan and A. G. Chynoweth, *J. Appl. Phys.* **33**, 1649 (1962).
[30] B. R. Holeman and C. Hilsum, *J. Phys. Chem. Solids* **22**, 19 (1961).
[31] R. H. Bube, *J. Appl. Phys.* **31**, 315 (1960).
[32] J. Blanc, R. H. Bube, and H. E. MacDonald, *J. Appl. Phys.* **32**, 1666 (1961).
[33] A. R. Beattie and R. W. Cunningham, *Phys. Rev.* **125**, 533 (1962); *J. Appl. Phys.* **35**, 353 (1964).
[34] R. H. Bube and H. E. MacDonald, *Phys. Rev.* **128**, 2062 (1962).
[35] R. H. Bube and H. E. MacDonald, *Phys. Rev.* **128**, 2071 (1962).
[36] J. Blanc, R. H. Bube, and L. R. Weisberg, *J. Phys. Chem. Solids* **25**, 225 (1964).

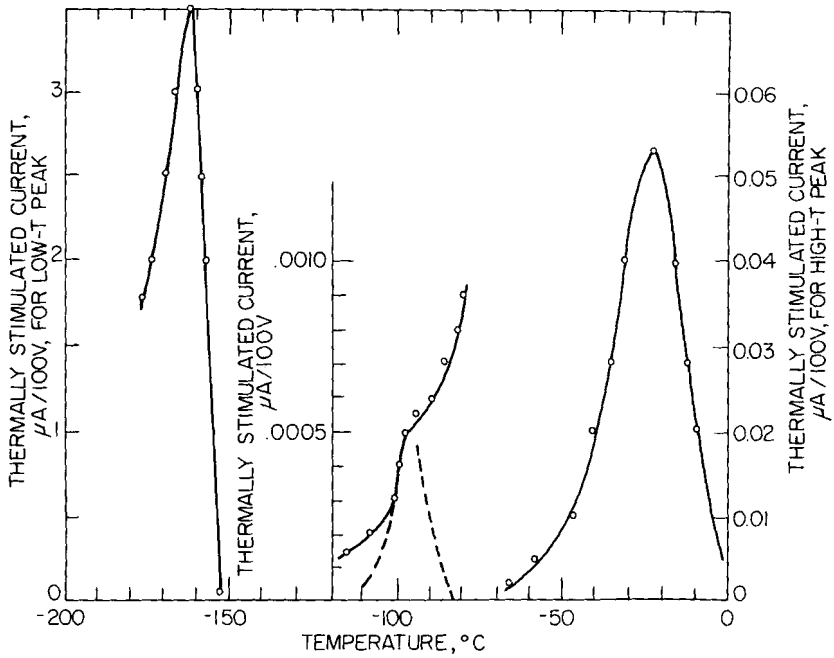


FIG. 2. Thermally stimulated current curves for a high-resistivity GaAs crystal. Note that each peak has its own current scale.

A typical TSC plot for high-resistivity GaAs is given in Fig. 2. This represents the general form of the trap distribution found in essentially all high-resistivity GaAs crystals. The principal trapping levels are one at about 0.2 eV and another at about 0.55 eV. Without measurements of the Hall effect of the TSC it is not possible to decide whether electron or hole traps are involved. In addition to these two principal trap depths, others have been measured with values between 0.2 and 0.4 eV—as, for example, the minor trap shown in this range in Fig. 2—and also with values about 0.7 eV. Trap densities in as-grown crystals range from 10^{14}, found in crystals grown by the floating-zone method, to $10^{18}\ cm^{-3}$. The three traps in Fig. 2 have densities of about 2×10^{18}, 3×10^{15}, and $2 \times 10^{17}\ cm^{-3}$, respectively, in order of increasing depth. TSC measurements make it quite clear that high-resistivity GaAs abounds with deep levels present in moderate to high densities.

Figure 3 shows the TSC curve obtained for another high-resistivity crystal of GaAs, showing a principal peak at $-33°C$ with a much smaller satellite peaking at higher temperatures. For the purposes of the present discussion, only the principal peak will be considered. This curve represents

a trap density of about 10^{18} cm^{-3}, with a depth calculated from the Fermi level according to Eq. (17) of 0.50 eV. Detailed comparison with Eq. (16) shows that this method of analysis would give a trap depth of 0.47 eV. When the heating rate in a subsequent TSC measurement was decreased by about a factor of 2, the trap depth calculated from Eq. (17) was 0.48 eV.

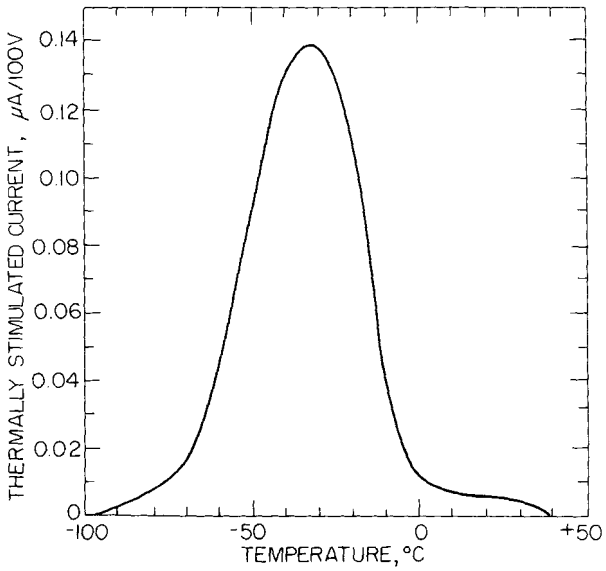


FIG. 3. Thermally stimulated current curve for a high-resistivity GaAs crystal.

The determination of trap depth for this same crystal by the method of decayed TSC is shown in Fig. 4. The results indicate that a single trap depth is involved in the major peak of Fig. 3, and the slopes of the straight portions of the curves indicate a trap depth of 0.44 eV.

14. PROPERTIES OF SENSITIZING IMPERFECTIONS

Highly photosensitive crystals of GaAs and InP can be prepared by diffusing copper into low-resistivity *n*-type material.[32] The high sensitivity of these materials corresponds to the introduction of imperfections that have a large capture cross section for photoexcited holes but a subsequently much smaller capture cross section for photoexcited electrons. At room temperature and above, the photoconductivity in such crystals is *p*-type (see Section 16 for further details); but it changes to *n*-type as the crystal is cooled, and holes may be stably captured in the sensitizing centers.

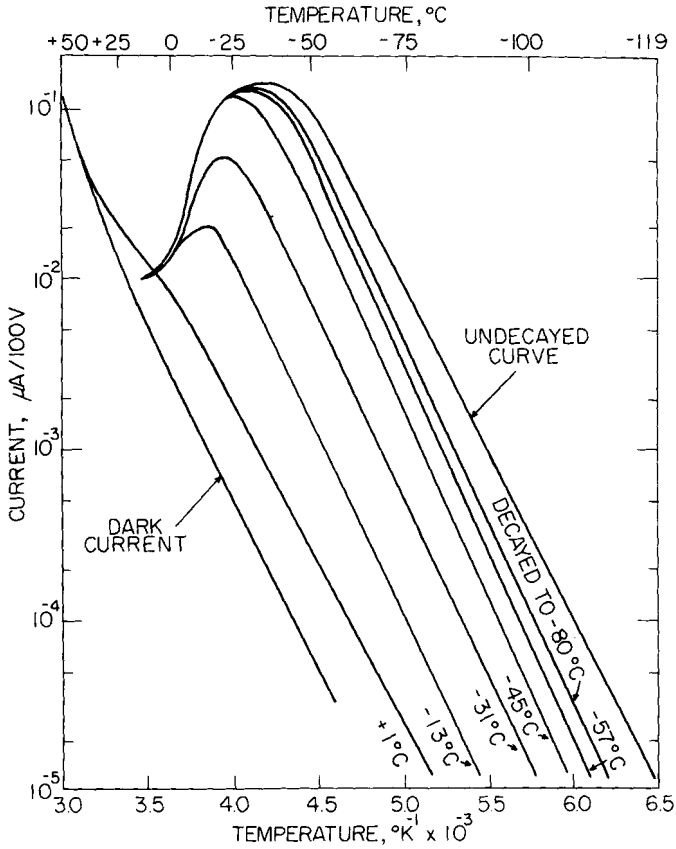


FIG. 4. Decayed thermally stimulated current curves for the crystal of Fig. 3.

Figure 5 shows the temperature dependence of photoconductivity in such a crystal of GaAs, for excitation by two different photoexcitation intensities. The excitation intensity for the upper curve is twenty-five times that for the lower curve. A variety of such data has been analyzed according to the discussion given in Section 7 to obtain values for the thermal hole-ionization energy and the capture cross-section ratio for the sensitizing centers.[37] Values obtained are 0.45 eV and 4×10^4, respectively, for GaAs, and 0.37 eV and 7×10^4 for InP.

Consistent with the value of hole-ionization energy obtained in this manner for GaAs is the observation that the imperfections act as sensitizing centers only when compensated—i.e., only in high-resistivity *p*-type material. If the thermal-equilibrium *p*-type conductivity of the crystal is increased by Cu diffusion at higher temperatures, no sensitizing action

[37] R. H. Bube, *J. Appl. Phys.* **32**, 1707 (1961).

is observed and in fact the photosensitivity is found to decrease with decreasing temperature. It is found that the sensitizing action of the imperfections is no longer observed if the thermal-equilibrium Fermi level lies closer than 0.47 eV to the valence band.

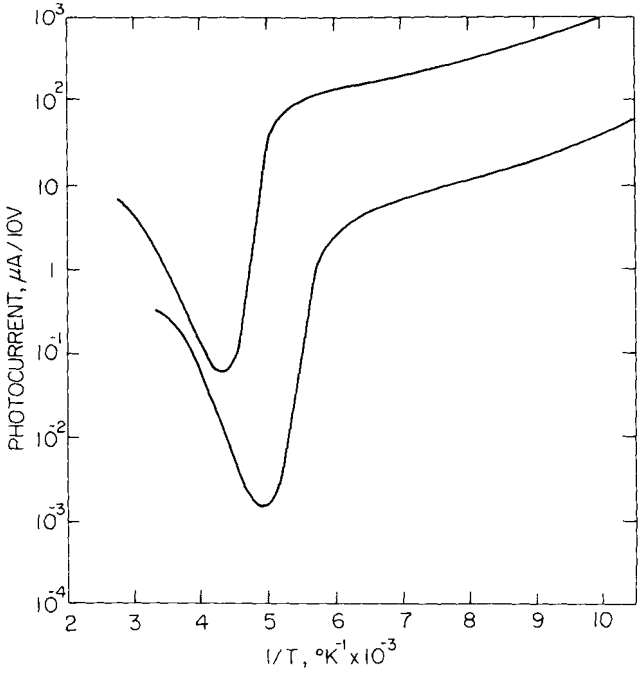


FIG. 5. Temperature dependence of photocurrent for a GaAs : Si : Cu crystal. The excitation intensity is 25 times greater for the upper curve than for the lower.

The magnitude of the electron-capture cross section and the temperature dependence of the cross section have been determined for the sensitizing centers in GaAs and InP using the optical quenching technique described in Section 8.[38] Typical results are shown in Fig. 6 for GaAs. Over the range of temperatures below the thermal quenching temperature, it is observed that the onset of optical quenching occurs for the same photoconductivity. Thus the only temperature-dependent variables entering into a calculation of the electron-capture cross section are the electron thermal velocity and the electron mobility. Photo-Hall measurements on this particular GaAs crystal indicated a temperature-independent electron mobility of 200 cm^2/V-sec over this temperature range.[34] Assuming a reasonable optical cross section S_o of 10^{-17} cm^2, the electron-capture cross section of sensitizing centers in GaAs is found to be of the order of

[38] R. H. Bube and F. Cardon, *J. Appl. Phys.* **35**, 2712 (1964).

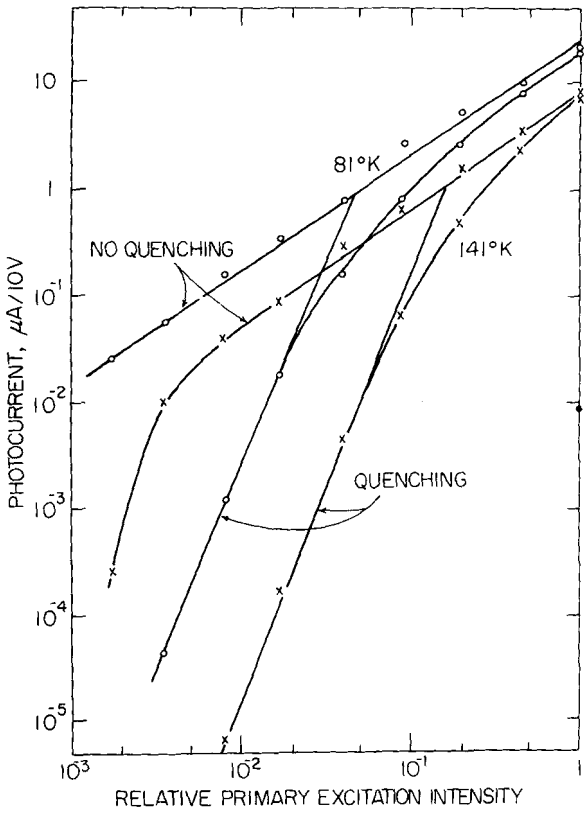


FIG. 6. Determination of the onset of optical quenching in a GaAs : Si : Cu crystal at 81° and 141°K.

5×10^{-22} cm^2 with a maximum temperature dependence as T^{-1}. The electron-capture cross section in InP was found to be about 4×10^{-21} cm^2.

The relative independence of these cross sections on temperature appears to rule out the possibility that the small magnitude of the cross section is caused by a Coulomb repulsive center surrounded by a potential barrier for electron capture. A consideration of the various mechanisms suggests that radiative capture at a neutral imperfection is the most likely recombination mechanism consistent with the magnitude of the cross section and its independence of temperature.[38]

15. GIANT SCATTERING CROSS SECTIONS

A variation of mobility with photoexcitation at fixed temperature has often been observed in high-resistivity GaAs.[34,39] The form of this variation

[39] R. H. Bube, H. E. MacDonald, and J. Blanc, *J. Phys. Chem. Solids* **22**, 173 (1961).

in those cases where one-carrier conductivity is predominant frequently is that of a "step" as discussed in Section 10. Figure 7 shows a typical single step in $1/\mu_H$ as a function of the steady-state Fermi-level position, as varied by photoexcitation. The experimental points may be fitted with a calculated curve derived from Eqs. (19) and (20), if values of τ_0 and $S_I N_I$ are properly chosen. The value of E_I obtained from Fig. 7 agrees within 0.01 eV with the value determined for a trapping level in the same crystal by measurements of TSC. Knowing the trap density from the TSC data, a value for S_I of 3×10^{-11} cm^2 is calculated.

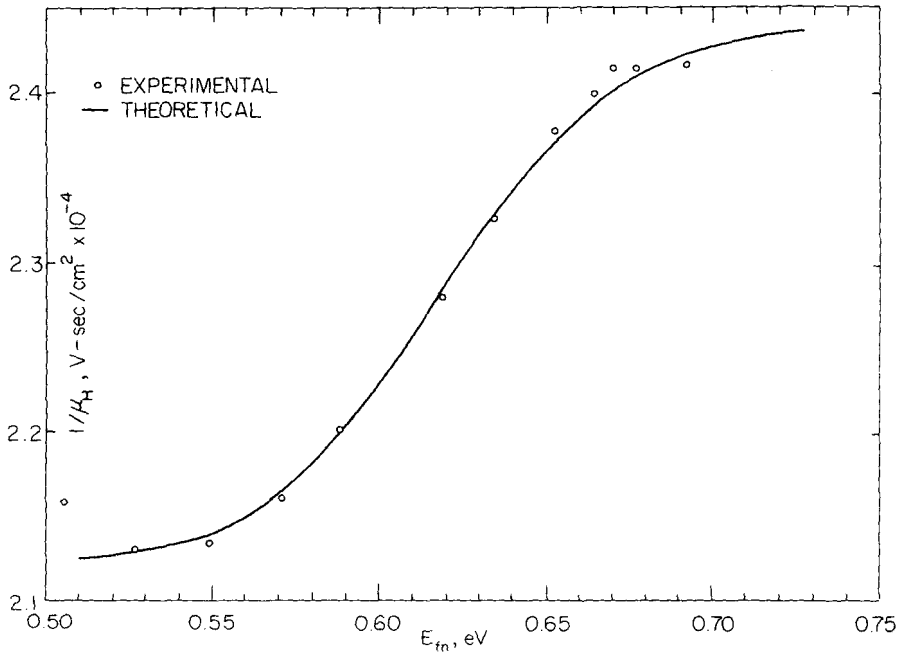


FIG. 7. The reciprocal Hall mobility as a function of the steady-state electron Fermi level, as varied by photoexcitation, for a high-resistivity GaAs crystal. Experimental points are compared with a theoretical curve calculated from Eqs. (19) and (20).

The behavior of another crystal of GaAs showing a single step in $1/\mu_H$ vs. Fermi-level position is shown in Fig. 8 as a function of temperature. The temperature dependence of mobility for photoexcitation of the highest intensity used in Fig. 8 and for the absence of photoexcitation is shown in Fig. 9. The independently measured TSC showed 6.5×10^{14} cm^{-3} traps with depth of 0.54 eV. As the temperature is increased, the effect of photoexcitation on the mobility decreases, until above 340°K no detectable effect remains. An analysis of the variation of mobility with photoexcitation

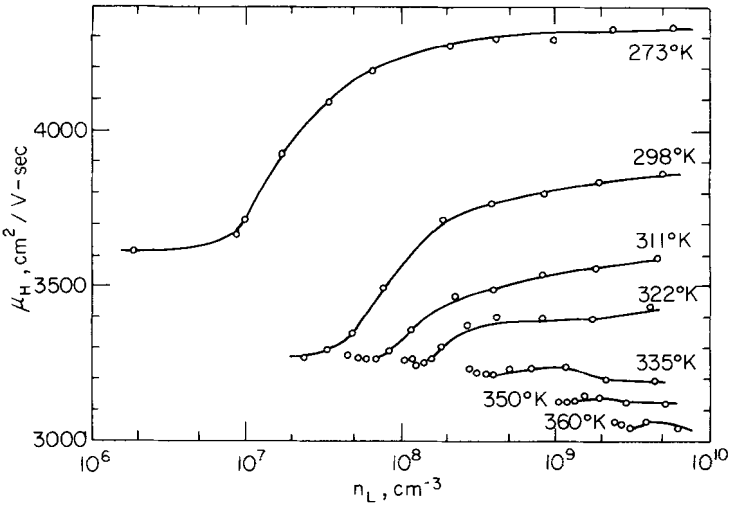


FIG. 8. Dependence of Hall mobility on density of photoexcited electrons, as varied by changing excitation intensity, at various temperatures for a "pure" high-resistivity GaAs crystal.

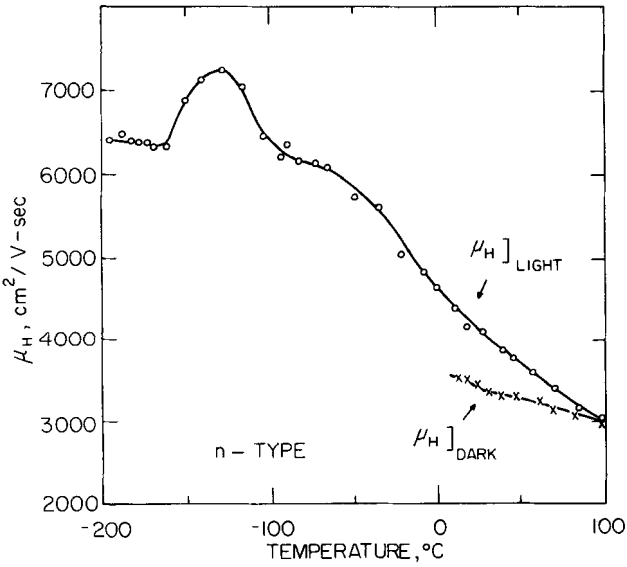


FIG. 9. Temperature dependence of photo-Hall mobility and dark Hall mobility for the crystal of Fig. 8.

for this crystal is summarized in Table II. Excellent agreement is found between the imperfection-level position determined directly from the

TABLE II

ANALYSIS OF VARIATION OF MOBILITY WITH PHOTOEXCITATION[a]

Temperature (°K)	Trap depth determined from mobility step (eV)	$\Delta(1/\mu)$ (V-sec/cm^2)	S_1 (cm^2)
273	0.53	4.6×10^{-5}	5.3×10^{-11}
298	0.54	4.8×10^{-5}	5.3×10^{-11}
311	0.55	2.8×10^{-5}	3.0×10^{-11}
322	0.57	1.4×10^{-5}	1.5×10^{-11}
335	—	$\sim 2 \times 10^{-6}$	$\sim 2 \times 10^{-12}$

[a] From data of Fig. 8.

mobility data and independently by the TSC measurement. The scattering cross section at room temperature is 5.3×10^{-11} cm^2, some fifty times larger than would be predicted for a singly charged Coulombic scattering center. As the temperature is increased, the apparent cross section decreases, until above 330°K the observed effect is compatible with a normal Coulomb scattering cross section. Thus the data show that an increase in temperature is able to remove the scattering effect associated with the large calculated values of S_1.

A proposed explanation for these observations is that scattering is due to an inhomogeneous distribution of imperfections with the resultant development of space-charge regions surrounding volumes with differing Fermi levels.[40] Photoexcitation removes the charge on these imperfections and therefore the space-charge regions as well. Increasing the temperature drives the conductivity toward intrinsic and by this means also removes the effect of these scattering regions. On this view it is supposed that the dark Hall mobility would have decreased much more rapidly with increasing temperature than actually observed in Fig. 9, if increasing temperature did not act to reduce the space-charge scattering. The coalescence of dark Hall mobility and light Hall mobility at elevated temperatures is attributed to an increase in the dark Hall mobility.

In certain cases much larger variations of mobility with photoexcitation are observed—so large, in fact, as to warrant the name anomalous. Figure 10 shows typical results for an InP crystal that had been made photosensitive by the diffusion of copper into high-conductivity *n*-type InP.[39] The apparent Hall mobility varies by over a factor of 10 with

[40] L. R. Weisberg, *J. Appl. Phys.* **33**, 1817 (1962).

photoexcitation. The data of Fig. 10 indicate, however, that the variations observed are not particularly affected by the region of the crystal being measured. It is believed that very large variations of Hall mobility of this type are probably to be attributed to gross imperfection inhomogeneity, resulting in "spurious" Hall-voltage readings. The method of preparation involving Cu diffusion favors this interpretation.

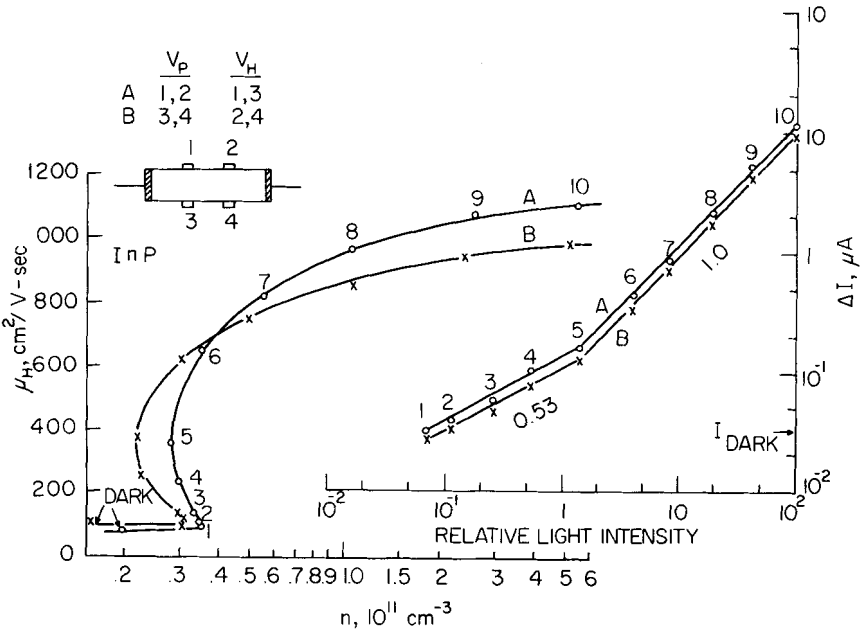


FIG. 10. Anomalously large variations of Hall mobility with photoexcitation for a crystal of InP diffused with Cu to make it photosensitive and give it high resistivity. The two curves are for two ways of calculating the Hall mobility from the possible combinations of conductivity and Hall constant.

Nelson *et al.*[28] have observed an effect in the spectral response of GaP that they have attributed to the removal of inhomogeneous space-charge effects by photoexcitation. Figure 11 shows spectral response of photoconductivity curves for several temperatures. Indirect-excitation transitions predominate between photon energies of 2.2 and 2.8 eV. At the high-energy end of this range all of the light entering the crystal is absorbed. In spite of this, the photoconductivity response increases by a factor of 10 to 100 when direct-excitation transitions become important, for photon energies greater than 2.8 eV. The effect is observed only in high-resistivity GaP whiskers. It is proposed that the effect is caused by the higher density of

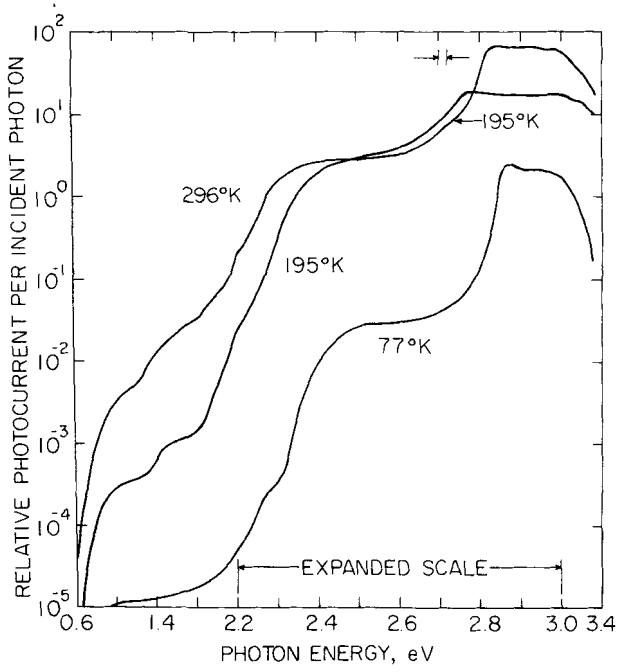


FIG. 11. Photoconductive spectra for an *n*-type, high resistivity GaP whisker. (After Nelson *et al.*[28])

excitation associated with the higher absorption constant found for direct excitations. This higher excitation density is suggested to be effective in removing the scattering caused by inhomogeneous imperfection distributions.

16. Imperfection Identification with Hall-Effect Measurements

In this final section of the chapter, a variety of effects will be summarized in which greater insight into the identity and properties of various imperfections in GaAs has been obtained through the application of Hall-effect measurements to nonequilibrium carriers.[34,35]

a. Traps in High-Resistivity n-Type GaAs

Trap densities in "pure" high-resistivity as-grown crystals of *n*-type GaAs are fairly low. Since the majority-carrier lifetimes are also low, the magnitude of TSC usually does not exceed 10^{-10} (ohm-cm)$^{-1}$. Under these conditions it is difficult to make meaningful Hall-effect measurements of the carriers released in a TSC experiment. An exception to this general limitation is the crystal used for the data of Fig. 12. For this crystal TSC

values in the 10^{-8} and 10^{-9} (ohm-cm)$^{-1}$ range were found, and it was possible to measure the Hall mobility of the carriers freed in the process of a TSC measurement. The measured Hall mobility corresponding to each TSC point is shown in Fig. 12. The indicated result—that only

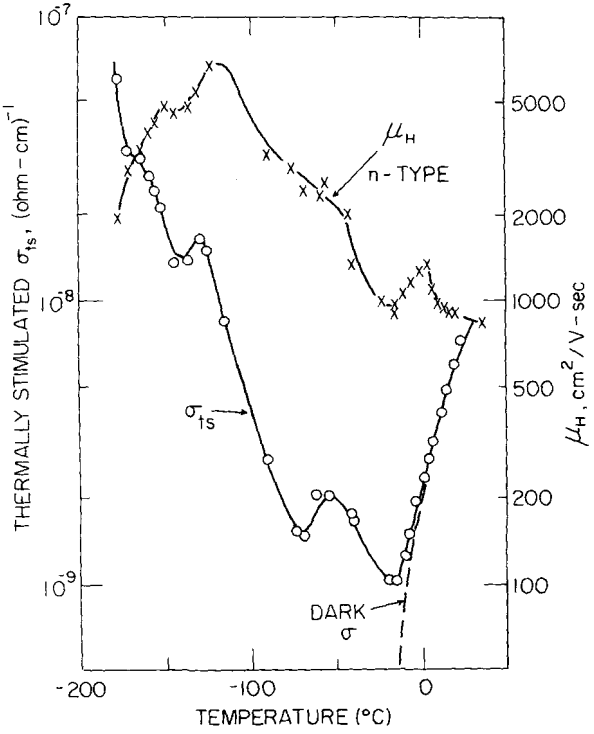


FIG. 12. Thermally stimulated conductivity and Hall effect of thermally freed carriers as a function of temperature for a "pure" high-resistivity GaAs crystal.

electron traps contribute significantly to the trapping in "pure" high-resistivity GaAs crystals— is typical of this kind of material. Such behavior is in contrast to the importance of hole traps in annealed crystals, as discussed further on in this section.

b. High Photosensitivity in "Pure" GaAs at Low Temperatures

In "pure" as-grown high-resistivity GaAs crystals, it is commonly found that the photoconductivity increases exponentially with increasing reciprocal temperature. Apparently a certain minimum purity is required before this effect is observed. Results of Hall-effect measurements on the

photoexcited carriers in a crystal of this type are shown in Fig. 13. It is found that the photoconductivity is n-type and that a plot of the density

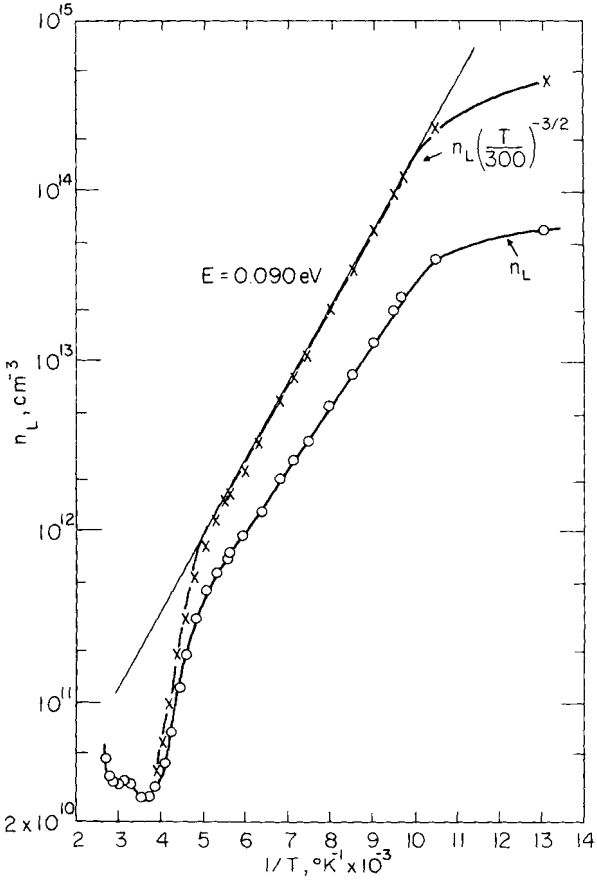


FIG. 13. Temperature dependence of density of photoexcited electrons in a "pure" high-resistivity GaAs crystal, as determined from photo-Hall measurements.

of photoexcited electrons, corrected for the temperature dependence of the density of states, as a function of $1/T$ yields a region extending over several orders of magnitude with an activation energy of 0.09 eV. The simplest interpretation calls for the existence of centers lying 0.09 eV above the valence band that act as sensitizing centers for electron conductivity to the extent that photoexcited holes may be stably held in them.

It appears that the sharp departure from an exponential variation of free-electron density with $1/T$, which occurs at about 200°K for the crystal in Fig. 13, can be correlated with thermal release of holes from sensitizing

centers lying 0.45 eV above the valence band. These appear to be the same as the centers discovered in Cu-diffused GaAs crystals, as discussed in Section 14. The occurrence of these sensitizing imperfections in both "pure" and impure GaAs suggests that they are to be associated with crystal defects rather than with specific impurities.

c. GaAs : Si : Cu Crystals with High Photosensitivity at Low Temperature

GaAs : Si : Cu crystals were discussed previously in Section 14. They are characterized by the presence of sensitizing centers for electron photoconductivity located 0.45 eV above the valence band, with a capture cross section for holes-to-electrons ratio of 4×10^4.

The temperature dependence of the photo-Hall effect for such a crystal is shown in Fig. 14. A high photosensitivity is found at low temperatures,

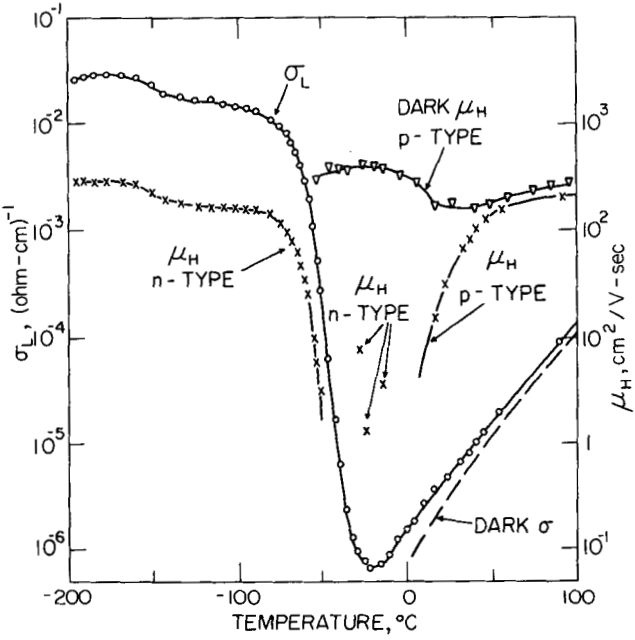


FIG. 14. Temperature dependence of photoconductivity, photo-Hall mobility, and dark Hall mobility for a GaAs : Si : Cu crystal.

with an abrupt thermal quenching of this photosensitivity by about four orders of magnitude when the temperature exceeds about -60°C at the excitation intensity used. The photoconductivity, which is *p*-type at room temperature and above, changes to *n*-type when the crystal is cooled below the minimum conductivity point at about -20°C. At this point photo-

excited holes begin to become stably held in the 0.45-eV sensitizing centers in appreciable densities, and as a result the electron lifetime and the photosensitivity rise rapidly. The Hall mobility measured in this range, however, is very low—of the order of 1 to 20 cm^2/V-sec. The Hall mobility reaches its maximum low-temperature value only after the photoconductivity has risen to its high low-temperature value. Even then it remains relatively low, of the order of 200 cm^2/V-sec. It was not possible to make continuous measurements of Hall mobility between about $-50°$ and 0°C, primarily because of a high noise background in the Hall-voltage circuit in this particular temperature range only.

The decrease in *n*-type Hall mobility in the thermal quenching range cannot be associated with two-carrier conductivity, but must be attributed to inhomogeneous scattering effects. Inhomogeneities would be expected to be particularly significant in this range, where the conductivity of the crystal as a whole must change by some four orders of magnitude over a relatively short temperature interval. Although the decrease in *n*-type Hall mobility with thermal quenching cannot be associated with two-carrier conductivity, it seems likely that the behavior of the Hall mobility above -50°C is at least partially associated with two-carrier effects. This conclusion is supported by the data of Fig. 14, where the *p*-type dark Hall mobility is compared with the measured Hall mobility in the light. Above 0°C, the *p*-type Hall mobility under photoexcitation is less than in the dark, and between $-50°$ and 0°C, the *p*-type Hall mobility in the dark is actually changed to an *n*-type Hall mobility in the light. The sporadic nature of the measurements of the Hall effect in this intermediate range is probably associated with the formation of local *p*-type regions in the otherwise *n*-type crystal under photoexcitation.

d. Optical Quenching in GaAs : Si : Cu Crystals

According to the mechanism of optical quenching described in Section 8, it should be possible to detect a change from *n*-type to *p*-type conductivity under strong optical quenching because of the optical freeing of holes from sensitizing centers. This has been confirmed experimentally with a crystal of GaAs : Si : Cu at low temperature, with the results shown in Fig. 15. A decrease in Hall mobility with decreasing free-carrier density alone, such as is caused by a decrease in photoexcitation intensity, occurs in such crystals because of inhomogeneous imperfection scattering. This is the curve shown in Fig. 15 as that for decreasing L with no quenching.

Two methods of quenching were used. In the first, quenching was by white light through a Corning 2540 filter. For the same conductivity the mobility is lower in the presence of quenching radiation. In the second, a Si filter was used for the quenching radiation, thus eliminating any

possibility of excitation by the transmitted quenching light. A change in conductivity type from *n*-type to *p*-type is observed for very strong quenching.

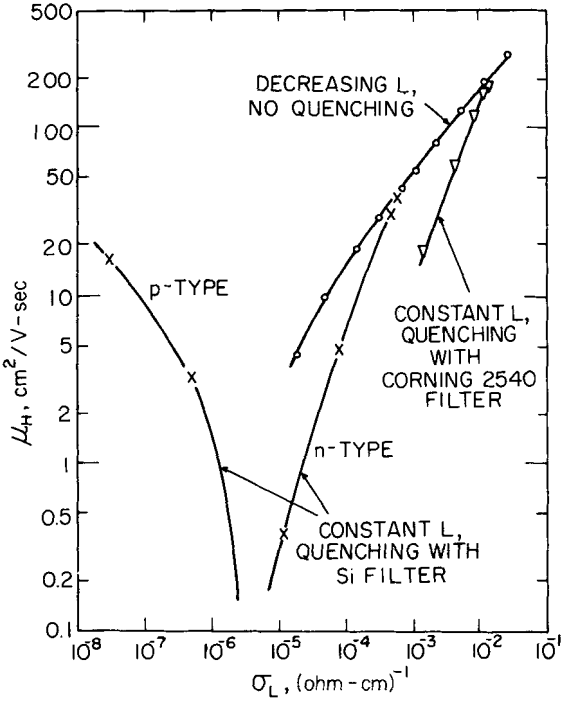


FIG. 15. Hall mobility as a function of photoconductivity during optical quenching, for a GaAs: Si: Cu crystal at 77°K.

e. Properties of Annealed GaAs Crystals with High Trap Densities[35,36,41]

If "pure" high-resistivity GaAs crystals are annealed for 16 hours at temperatures between 450° and 700°C, very high densities of traps (up to 10^{19} cm^{-3}) with depths of about 0.2 and 0.5 eV are introduced. Valuable insight into the nature of these traps has been obtained through the use of Hall-effect measurements.

Annealed crystals with such high trap densities are *n*-type in the dark at room temperature, become *p*-type at low photoexcitation intensities as the photoexcited electrons are trapped in the 0.5 eV traps, and then become *n*-type once more at higher photoexcitation intensities after the traps are filled. The examination of this behavior as a function of temperature is

[41] J. Blanc, R. H. Bube, and L. R. Weisberg, *J. Phys. Chem. Solids* **25**, 225 (1964).

shown in Fig. 16. The maximum p-type mobility shifts to higher photoconductivities at higher temperatures. If the reasonable assumption is made that the rate-determining step in this process is the thermal release of trapped electrons from the 0.5-eV traps, the depth of the traps may be determined from the temperature dependence of the maximum p-type mobility. A trap depth of 0.56 eV is found in this way.

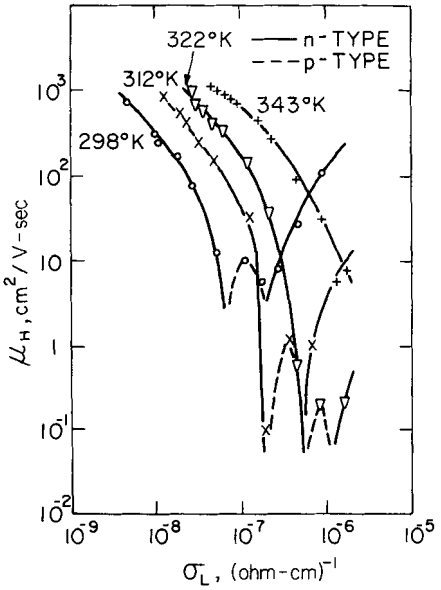


FIG. 16. Hall mobility as a function of photoconductivity, as varied by changing excitation intensity, at different temperatures for an annealed GaAs crystal.

The measurement of photoconductivity and photo-Hall mobility as a function of temperature for an annealed crystal is shown in Fig. 17, using the maximum light intensity of Fig. 16. Upon cooling, the n-type Hall mobility rises steeply, reaches a maximum value, and then drops off again as at low temperatures the photoconductivity abruptly changes to p-type. The rapid increase in n-type Hall mobility upon cooling, in view of the existence of a two-carrier regime, suggests the existence of a hole trap with depth between 0.4 and 0.5 eV that reduces the free-hole density, as the 0.56-eV electron trap had reduced the free-electron density at room temperature. The sudden change from n-type to p-type photoconductivity at low temperatures suggests the presence of a shallow electron trap that removes free electrons from the conduction band at low temperatures, as the 0.56-eV trap had done at room temperature.

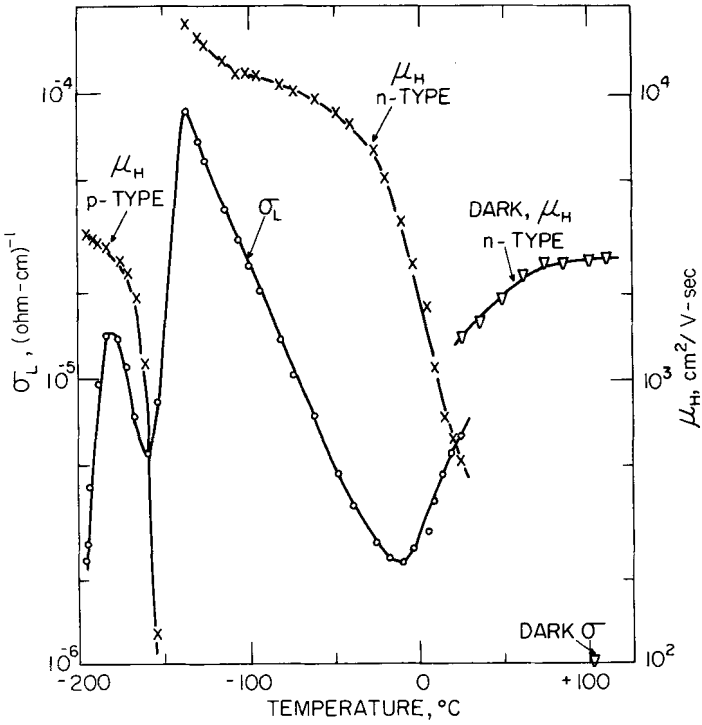


FIG. 17. Temperature dependence of photoconductivity, photo-Hall mobility, and dark Hall mobility for an annealed GaAs crystal.

Direct measurement of the trapping properties of these crystals through the Hall effect of carriers freed during a TSC measurement is shown for two different crystals in Figs. 18 and 19. Figure 18 is for a crystal grown by the floating-zone method, annealed for 16 hours at 700°C in molten KCN. Figure 19 is for a crystal grown by the Bridgman technique, annealed for 16 hours at 450°C in the presence of Cu corresponding to about 10^{16} cm^{-3} if completely incorporated. Both sets of data are included to show the close correlation between these two crystals in spite of the differences in their preparation and annealing processes.

The first traps to empty at the lowest temperatures are hole traps. Then the Hall mobility drops at about the center of the TSC peak to a minimum, more pronounced in Fig. 18 than Fig. 19. This drop may be associated with the emptying of an electron trap with slightly larger ionization energy than the hole trap. Except for this transient decrease, however, the measured hole mobility retains the same high value throughout the temperature range between $-200°$ and $-150°$C, both before and after trap emptying,

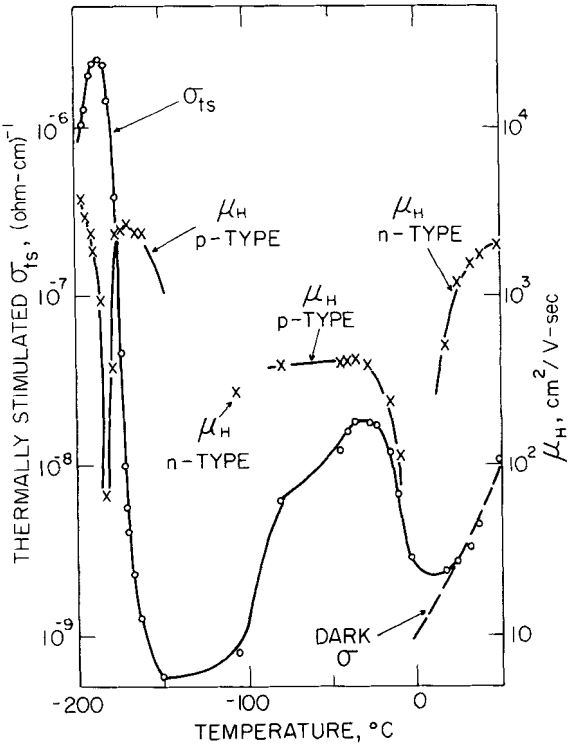


FIG. 18. Temperature dependence of thermally stimulated conductivity and the Hall effect of thermally freed carriers for an annealed crystal of GaAs grown by the floating-zone method.

a value between 2000 and 3000 cm^2/V-sec. After the principal low-temperature peak has been passed, there is an indication of electron-trap emptying at the foot of the current peak of the deeper traps. Then holes empty from the deeper traps, the Hall effect finally becoming *n*-type at high temperatures as the dark conductivity dominates.

Thus the information on the high-density traps may be summarized as follows: (1) a high density of 0.56-eV electron traps, as indicated by Fig. 16; (2) a high density of 0.4–0.5-eV hole traps indicated by Fig. 17, to be identified with the 0.45-eV hole traps measured directly in Figs. 18 and 19; (3) a high density of 0.2-eV electron traps as indicated by Fig. 17; and (4) a high density of 0.15-eV hole traps indicated in Figs. 18 and 19. The absence of direct measurement of the 0.2-eV and 0.56-eV electron traps in the Hall effect of the TSC measurement is not contradictory, since in each case it might be expected that holes freed from the shallower trap would recombine with electrons at the deeper trap. It may be noted that the only photoelectronic information available without the Hall effect of nonequilibrium

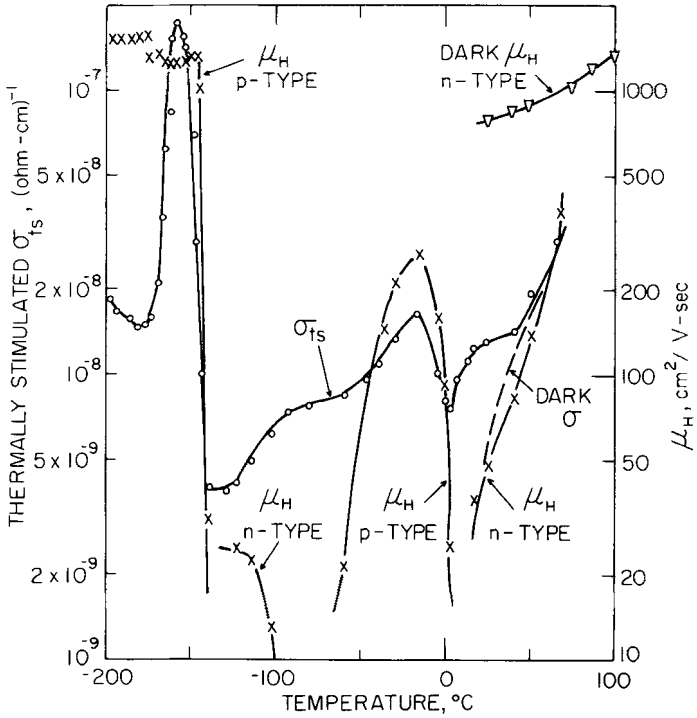


FIG. 19. Temperature dependence of thermally stimulated conductivity and the Hall effect of thermally freed carriers for an annealed crystal of GaAs grown by the Bridgman method.

carriers was that there were two traps with depths of about 0.2 and 0.5 eV of unknown type.

The additional information that the low-temperature hole mobility is essentially the same high value both before and after the 10^{19} cm^{-3} shallow hole and electron traps have emptied implies that there is Coulomb scattering from these traps neither when they are filled nor empty. It would seem that this condition can be fulfilled only by the hypothesis that these hole and electron traps exist in pairs. Then, when occupied by a hole and an electron, respectively, they are each neutral. When unoccupied, the hole trap has a negative charge and the electron trap a positive charge, but because of their proximity their effect in scattering is still only the relatively weak effect of a dipole.

The judicious use of the Hall effect of nonequilibrium carriers can be expected to provide valuable additional tools in the techniques of photoelectronic analysis.

CHAPTER 12

Optical Constants

B. O. Seraphin and H. E. Bennett

	INTRODUCTION	499
I.	BORON PHOSPHIDE	503
II.	ALUMINUM ANTIMONIDE	505
III.	GALLIUM PHOSPHIDE	509
IV.	GALLIUM ARSENIDE	513
V.	GALLIUM ANTIMONIDE	524
VI.	INDIUM PHOSPHIDE	527
VII.	INDIUM ARSENIDE	532
VIII.	INDIUM ANTIMONIDE	536

Introduction

The optical behavior of a material is completely determined if its optical constants are known. The index of refraction, n, and the extinction coefficient, k, may thus be regarded as a summary of the experimental results of optical measurements made on the material. They arise in the solution of the wave equation, which cannot be satisfied unless

$$\bar{n}^2 = \varepsilon_1 - j\varepsilon_2, \tag{1}$$

where $\bar{n} = n - jk$ is the complex index of refraction and ε_1 and ε_2 are the real and imaginary parts of the complex dielectric constant. Both n and k are dimensionless parameters. However, k is directly related to the absorption coefficient α, usually given in cm^{-1}, which arises in the Lambert–Bouguer law. The relationship is

$$\alpha = 4\pi k/\lambda, \tag{2}$$

where λ is the wavelength of the incident radiation.

Compared to the wealth of information accumulated on other aspects of the III–V compounds in the 14 years since Welker[1] first reported their

semiconductive properties, relatively few measurements of the optical constants have been reported, and no extensive compilation of n and k in tabular form has been available. Most of the work so far has been directed towards determining the major features in the optical spectra of the various compounds. Values of the optical constants have in most cases been only a by-product of these investigations and cannot be judged by the same standards one would apply to those found, for example, in a glass catalog. One must also remember that the optical properties of the III–V compounds, particularly in the free-carrier region, are very sensitive to impurity concentration, and hence, unless sophisticated sample preparation and testing techniques are available, measurements of the optical constants are somewhat meaningless. In addition to impurity concentration, a two-component material such as a III–V compound is much more susceptible to lattice distortion and crystal disorder than is a material composed of only one kind of atom. Such effects can have a pronounced effect on the optical properties. Closely related to such defects is the problem of surface damage developed in a sample by optical polishing. It is difficult to make accurate optical measurements on samples that are not smooth and flat; but if mechanical polishing techniques are used, the crystal structure at the surface is distorted[2,3] with consequent changes in the observed optical properties of the material.[4,5] Such changes have even been used to determine the depth of surface damage produced by mechanical polishing.[6] The effect on the optical properties is most pronounced in wavelength regions where sufficiently strong absorption occurs that the penetration depth $\lambda/2\pi k$ of the light is comparable to or smaller than the depth of the distorted surface layer. Thus, although surface damage may affect the optical properties of materials even in the far infrared, it becomes particularly troublesome in the visible and ultraviolet regions of the spectrum.[5] This problem of avoiding surface damage is accentuated by the contradictory necessity of keeping the surface roughness at a low value in this part of the spectrum. For a Gaussian height distribution of surface irregularities, the fraction of light that is diffusely reflected increases initially as $1/\lambda^2$ and is more than 1% even for surfaces having an rms roughness of 0.01λ (i.e., about 25 Å in the ultraviolet region).[7] An additional problem in the ultraviolet is the presence of oxide films, which, although usually only a few tens of angstroms thick, can have a drastic effect on the reflectance.[8,9] Recent work[10–12] has shown that even surface adsorption beyond any kind of detection except field-effect measurements may also change the optical properties of a semiconductor through the electroreflectance effect, making it futile to perform accurate optical measurements near either initial or higher-energy band edges unless the surface state can be accurately specified.

With few exceptions, the optical constants of III–V compounds have

been determined in the past by essentially only four different methods: (1) measurement of reflection at normal incidence and application of a Kramers–Kronig analysis, (2) measurement of reflection and transmission at normal incidence, (3) prism measurements of refractive index, and (4) reflectance measurements at normal incidence and application of a classical dispersion analysis. The Kramers–Kronig analysis has been used primarily at wavelengths shorter than the absorption edge, where transmission measurements become impractical. Some use of this technique has also been made in the lattice-absorption region, but classical dispersion analyses give more reliable results, since requirements on the accuracy of the experimental reflectance measurements are not so great. Unfortunately, although the optical constants are a by-product of every dispersion analysis and there are a large number of papers on lattice-absorption characteristics, only a few authors tabulate n and k. In many cases, therefore, the measured reflectance values are listed in the tables together with the reported characteristic frequencies, oscillator strengths, and other dispersion parameters required to calculate n and k. In all cases where the optical constants have been determined from normal-incidence reflectance measurements alone, the experimental reflectance values are tabulated. Thus, in the event that more precise reflectance values in some wavelength region become available or that an extension of the region covered becomes possible, the new reflectance data can be combined with tabulated reflectance values in other regions.

Measurement of the reflectance over an extended wavelength range is particularly important if a Kramers–Kronig analysis is to be used. The Kramers–Kronig integral extends formally from zero to infinity. In practice, it is not necessary to make measurements over this entire wavelength range, but the extrapolation procedures that must then be used cannot be expected to give accurate optical-constant data at a given wavelength unless neighboring regions where considerable optical activity is present are measured experimentally. For example, the optical constants obtained for absorbing media in the visible region, using a Kramers–Kronig analysis, often depend strongly on measurements made in the 500–1000 Å region of the vacuum ultraviolet. It is mostly for this reason that the results of Philipp and Ehrenreich[13] are given preference in the tables over the results of other not less precise measurements that did not extend as far into the vacuum ultraviolet. In addition, the reflectance values they report are in general higher than values reported by others, indicating, by application of a rather empirical criterion, that the surface treatment of their samples is probably superior to treatments which produce lower reflectance values.

In semitransparent wavelength regions, the results of direct measurements

of n or k are given preference in the tables over values obtained from a dispersion analysis. Prism measurements of the refractive index are reported where possible, since very high accuracy can be obtained using this technique, and surface properties of the sample are relatively unimportant. In many cases, no values of the extinction coefficient are listed in the semitransparent region between the absorption edge and the lattice-absorption region. The absorption in this region is extremely sensitive to the type and concentration of impurities, and can differ for different samples by orders of magnitude even if careful sample preparation techniques are used.

The majority of the entries in the tables were compiled from original data, which most authors supplied on request. Their cooperation is gratefully acknowledged. Frequently, they supplied their data in the form of large-scale graphs rather than in tabular form, in which case it was reduced to numerical values using a type 25-105 C2 Telereader.[14] Only in a small number of cases was it necessary to read the data off of the graphs printed in the journal articles.

In the literature, the popularity of wavelengths, wave numbers, and electron volts as units for the frequency scale appears to be roughly equal. Since it was necessary to settle on one unit for the tables, all photon energies and electron volts were converted to wavelengths and are given in microns. No interpolation was applied to values available in numerical form—i.e., if given in a unit other than the wavelength, the conversion of wavelength was made at the point at which the original values were reported. However, data given in graphical form were read out directly in wavelength intervals. Conversion from other units, when necessary, was readily accomplished by using the Telereader. In one case, data from a set of prism measurements were available in both tabular and graphical form. Comparison showed that the graphs could be read out with the Telereader at an uncertainty of about 0.1%. This is less than that of the original measurement in most cases.

No experimental values are given to more than four significant figures, and in most cases only two or three significant figures are reported. The number of significant figures does not represent our evaluation of the quality of the measurement. In most cases such a restriction was imposed by the author. If in doubt, we have reported too many rather than too few significant figures. One may assume, therefore, that at least the last figure reported is in most cases uncertain.

A fundamental difficulty faced in compiling tables of optical constants is the repeated necessity to choose which of several measurements of equal quality to include in the tables. Since there have been great improvements in sample preparation techniques of III–V compounds in the past few

years, one of the guidelines used was to report more recent work in preference to earlier work of equal, or in some cases even better, quality from an optical point of view. Similarly, measurements on carefully specified samples were given preference over others made on samples whose characteristics were not given in detail. In spite of such guidelines, it occasionally became necessary to choose one of several equally careful investigations to tabulate. When this situation occurred, all that could be done was to tabulate one of them and reference the others with appropriate comments that the different investigations did or did not agree. Every attempt was made, however, to reference all the papers in which optical-constant data were reported. With this aim, a systematic literature survey was carried out, including all papers published before July 1, 1964. In a somewhat less systematic way, the literature was followed and pertinent data were included in the tables up to July 1, 1965.

REFERENCES

1. H. Welker, *Z. Naturforsch.* **7a**, 744 (1952).
2. T. M. Buck, *in* "The Surface Chemistry of Metals and Semiconductors" (H. C. Gatos, ed.), p. 107. Wiley, New York, 1960.
3. E. P. Warekois, M. C. Lavine, and H. C. Gatos, *J. Appl. Phys.* **31**, 1302 (1960).
4. J. R. Beattie and G. K. T. Conn, *Phil. Mag.* **46**, 989 (1955).
5. T. M. Donovan, E. J. Ashley, and H. E. Bennett, *J. Opt. Soc. Am.* **53**, 1403 (1963).
6. C. E. Jones and A. R. Hilton, *J. Electrochem. Soc.* **112**, 908 (1965).
7. H. E. Bennett and J. O. Porteus, *J. Opt. Soc. Am.* **51**, 123 (1961).
8. R. P. Madden and L. R. Canfield, *J. Opt. Soc. Am.* **51**, 838 (1961).
9. R. P. Madden, L. R. Canfield, and G. Hass, *J. Opt. Soc. Am.* **53**, 620 (1963).
10. B. O. Seraphin and R. B. Hess, *Phys. Rev. Letters* **14**, 138 (1965).
11. B. O. Seraphin and N. Bottka, *Phys. Rev. Letters* **15**, 104 (1965).
12. B. O. Seraphin, *J. Appl. Phys.* **37**, 721 (1966).
13. H. R. Philipp and H. Ehrenreich, *Phys. Rev.* **129**, 1550 (1963).
14. Manufactured by Telecomputing Corporation, Pasadena, California.

I. Boron Phosphide

Although the promising aspect of extending injection luminescence to materials with large band gaps has stimulated interest in BP, the extreme difficulty of preparing crystals sufficiently large for optical work has limited the number of investigations.

An indirect fundamental edge at 0.6 micron gives the transparent crystal a reddish appearance. Toward larger photon energies, the absorption levels off before reaching higher values. This is presumably caused by the presence of pinholes, which cannot be avoided even in single-crystal specimens.

Archer *et al.*[1] as well as Wang *et al.*[2] have used small single crystals grown

from metal solvents under phosphorous pressure to make absorption measurements. Using a reflectance value of 0.3, the results of these measurements agree in the region of the fundamental absorption edge. The interband nature of this edge is confirmed by a square-root dependence of the absorption coefficient upon photon energy. The values of the extinction coefficient in the wavelength region 0.422 to 0.710 micron are listed in Table I.

Stone and Hill[3] have measured the absorption coefficient on thin-film samples deposited on quartz by vapor phase reaction. They have found values slightly larger than those previously mentioned, shifting the whole edge to longer wavelengths by 0.03 micron. The films could be stripped off their backing and the absorption coefficient measured in the infrared. The absorption remaining below the edge decreases gradually, except for a spike at 12.1 microns, which is attributed to lattice absorption.

Table II lists Stone and Hill's values for the extinction coefficient at 77°K. The displacement of an image by a crystal with parallel faces is used by Stone and Hill to give a rough estimate of 3.0 to 3.5 for the refractive index in the visible region.

REFERENCES

1. R. J. Archer, R. Y. Koyama, E. E. Loebner, and R. C. Lucas, *Phys. Rev. Letters* **12**, 538 (1964).
2. C. C. Wang, M. Cardona, and A. G. Fischer, *RCA Rev.* **25**, 159 (1964).
3. B. Stone and D. Hill, *Phys. Rev. Letters* **4**, 282 (1960).

TABLE I

EXTINCTION COEFFICIENT k OF BORON PHOSPHIDE AS A FUNCTION OF WAVELENGTH λ AT 300°K[a]

λ (microns)	k	λ (microns)	k
0.422	6.5×10^{-4}	0.540	1.8×10^{-4}
0.428	6.5×10^{-4}	0.550	1.5×10^{-4}
0.432	6.6×10^{-4}	0.560	1.2×10^{-4}
0.435	6.6×10^{-4}	0.570	1.0×10^{-4}
0.440	6.6×10^{-4}	0.580	8.7×10^{-5}
0.443	6.5×10^{-4}	0.590	8.0×10^{-5}
0.448	6.4×10^{-4}	0.600	7.1×10^{-5}
0.454	6.1×10^{-4}	0.620	7.8×10^{-5}
0.460	5.8×10^{-4}	0.630	6.3×10^{-5}
0.470	4.7×10^{-4}	0.640	6.2×10^{-5}
0.480	4.3×10^{-4}	0.650	6.2×10^{-5}
0.490	3.7×10^{-4}	0.660	6.3×10^{-5}
0.500	3.1×10^{-4}	0.670	6.4×10^{-5}
0.510	2.7×10^{-4}	0.680	6.7×10^{-5}
0.520	2.4×10^{-4}	0.710	7.4×10^{-5}
0.530	2.1×10^{-4}		

[a] After Refs. 1 and 2.

TABLE II

EXTINCTION COEFFICIENT k OF BORON PHOSPHIDE AS A FUNCTION OF WAVELENGTH λ AT 77°K[a]

λ (microns)	k	λ (microns)	k
0.470	4.45×10^{-3}	0.517	1.15×10^{-3}
0.478	3.61×10^{-3}	0.530	6.33×10^{-4}
0.486	2.92×10^{-3}	0.546	9.12×10^{-5}
0.497	2.27×10^{-3}	0.561	8.04×10^{-5}
0.506	1.68×10^{-3}	0.577	$< 5.00 \times 10^{-5}$

[a] After Ref. 3.

II. Aluminum Antimonide

Because chemically polished surfaces of AlSb react rapidly with water vapor in the air, optical measurements on this material are extremely difficult. Even when common polishing techniques are used, the sample must be kept from contact with moisture, since humidity alters the surface and covers it with a brown film that decreases the reflectance.

Fischer[1] has circumvented this problem by measuring the reflectance on (110) surfaces of p-type samples of $N_A = 2 \times 10^{17}\,\text{cm}^{-3}$ that have been freshly cleaved in an ultrahigh vacuum of less than 10^{-8} Torr. Examination under the optical microscope proves the cleavage planes to be nearly perfect (110) surfaces. Fischer's reflectance data are listed in Table IV for wavelengths from 0.22 to 0.58 micron. Cardona[2] reports a reflectance measurement over approximately the same wavelength region, but gives the results only in arbitrary units.

Although values for the energy gap have been discussed in a number of papers, a detailed measurement of the region of the fundamental absorption edge has not been reported. Turner and Reese[3] report structure in the center of the steep rise of the absorption coefficient at 0.93 micron, measured on n-type samples of $10^{17}\,\text{cm}^{-3}$ tellurium and selenium doping, which was substantiated by measurements at high resolution. This structure, as well as peaks in the absorption coefficient of n-type samples at 4.3 microns and of p-type samples at 1.6 microns, both previously reported by Blunt *et al.*,[4] are assigned to transitions within the conduction band. No values for the absorption coefficient in the region between the absorption edge and the lattice-absorption band are listed, since the results vary by orders of magnitude, depending upon type and density of the impurities present in the material.

Oswald and Schade[5] have measured, in the wavelength region between the fundamental absorption edge of most of the III–V compounds and

15 microns, the reflected and transmitted intensities and have calculated the optical constants from a combination of these two data. Provisions were made to suppress reflections from the back surface of the specimens. Interference effects were eliminated by choosing a thickness of more than 100 wavelengths and polishing the samples under a slight wedge angle. The sample thickness was determined by a measuring microscope. Reference was the sample itself, after it had been coated with aluminum. This provided the same effective aperture for the incident beam and eliminated imperfections of the sample surface.

The values for the refractive index from 1.1 to 15.6 microns in Table III are taken from Oswald and Schade.[5] Their measurements represent the most comprehensive study of the optical constants of the III–V compounds; their method is exemplary. In 1954, when their studies were conducted, however, the preparation of pure samples had not been developed to its present stage. It is only for this reason that their results are used to such a limited extent in this compilation. Later measurements on better-defined materials are given preference, even in cases where the method is slightly inferior.

Turner and Reese[6] have measured transmission and reflection of some 20 samples of both *n*- and *p*-type AlSb and have computed values of n and k for the wavelength range from 15 to 40 microns, using a classical dispersion[7] analysis that adjusts four dispersion parameters for the best least-squares fit of the data to a single resonance. The fit is within the accuracy of the reflection measurement except at the region of the reflection minimum and maximum, where the difference is still only 2%. The calculated n and k values are listed in Table III, the reflectance data in Table V.

REFERENCES

1. T. E. Fischer, *Phys. Rev.* **139**, A1228 (1965).
2. M. Cardona, *J. Appl. Phys.* **32**, 2151 (1961).
3. W. J. Turner and W. E. Reese, *Phys. Rev.* **117**, 1003 (1960).
4. R. F. Blunt, H. P. R. Frederickse, J. H. Becker, and W. R. Hosler, *Phys. Rev.* **96**, 578 (1954).
5. F. Oswald and R. Schade, *Z. Naturforsch.* **9a**, 611 (1954).
6. W. J. Turner and W. E. Reese, *Phys. Rev.* **127**, 126 (1962).
7. W. G. Spitzer, D. Kleinman, and D. Walsh, *Phys. Rev.* **113**, 127 (1959); D. A. Kleinman and W. G. Spitzer, *ibid.* **118**, 110 (1960).

TABLE III

REFRACTIVE INDEX n AND EXTINCTION COEFFICIENT k OF ALUMINUM ANTIMONIDE AS A FUNCTION OF WAVELENGTH λ[a]

λ (microns)	n	k	λ (microns)	n	k
1.1	3.445	—	30.1	0.232	2.365
1.5	3.382	—	30.2	0.246	2.643
2.0	3.300	—	30.3	0.266	2.940
2.5	3.291	—	30.4	0.293	3.261
3.0	3.245	—	30.5	0.330	3.616
4.0	3.182	—	30.6	0.381	4.017
6.0	3.173	—	30.7	0.453	4.482
8.0	3.127	—	30.8	0.557	5.036
10.0	3.100	—	30.9	0.719	5.722
15.0	3.080	—	31.0	0.990	6.612
16.0	3.068	—	31.1	1.509	7.838
17.0	3.054	—	31.2	2.710	9.627
18.0	3.037	—	31.3	6.278	11.73
19.0	3.018	—	31.4	12.23	8.261
19.5	3.007	—	31.5	11.29	3.291
20.0	2.995	0.001	31.6	9.541	1.633
20.5	2.981	0.001	31.7	8.373	0.984
21.0	2.966	0.001	31.8	7.581	0.666
21.5	2.949	0.002	31.9	7.012	0.485
22.0	2.931	0.002	32.0	6.583	0.372
22.5	2.910	0.002	32.1	6.247	0.295
23.0	2.886	0.002	32.2	5.977	0.241
23.5	2.859	0.003	32.3	5.753	0.202
24.0	2.828	0.004	32.5	5.406	0.148
24.5	2.792	0.004	32.7	5.148	0.114
25.0	2.750	0.005	33.0	4.863	0.082
25.5	2.699	0.007	33.5	4.547	0.053
26.0	2.637	0.009	34.0	4.338	0.037
26.5	2.561	0.011	34.5	4.190	0.028
27.0	2.464	0.015	35.0	4.080	0.022
27.5	2.336	0.021	35.5	3.994	0.018
28.0	2.158	0.031	36.0	3.926	0.015
28.5	1.893	0.051	36.5	3.870	0.013
29.0	1.435	0.102	37.0	3.823	0.011
29.2	1.125	0.157	37.5	3.784	0.010
29.4	0.623	0.349	38.0	3.750	0.008
29.6	0.273	1.001	38.5	3.721	0.008
29.8	0.224	1.572	39.0	3.695	0.007
30.0	0.223	2.097	40.0	3.652	0.006

[a] After Ref. 5 (1.1–10 microns) and Ref. 6 (15–40 microns).

TABLE IV

REFLECTANCE R OF ALUMINUM ANTIMONIDE AS A FUNCTION OF WAVELENGTH λ[a]

λ (microns)	R	λ (microns)	R	λ (microns)	R
0.22	0.29	0.36	0.17	0.50	0.14
0.24	0.30	0.38	0.17	0.52	0.13
0.26	0.32	0.40	0.17	0.54	0.13
0.28	0.34	0.42	0.17	0.56	0.12
0.30	0.30	0.44	0.18	0.58	0.12
0.32	0.26	0.46	0.16		
0.34	0.22	0.48	0.15		

[a]After Ref. 1.

TABLE V

REFLECTANCE R OF ALUMINUM ANTIMONIDE AS A FUNCTION OF WAVELENGTH λ[a]

λ (microns)	R	λ (microns)	R	λ (microns)	R
15.0	0.255	29.0	0.058	31.8	0.580
16.0	0.252	29.2	0.027	31.9	0.558
17.0	0.250	29.4	0.095	32.0	0.541
18.0	0.247	29.6	0.610	32.1	0.522
19.0	0.245	29.8	0.754	32.2	0.517
19.5	0.243	30.0	0.850	32.3	0.492
20.0	0.242	30.1	0.877	32.5	0.473
21.0	0.238	30.2	0.888	32.7	0.454
21.5	0.237	30.3	0.895	33.0	0.436
22.0	0.236	30.4	0.899	33.5	0.412
22.5	0.234	30.5	0.902	34.0	0.392
23.0	0.232	30.6	0.903	34.5	0.378
23.5	0.229	30.7	0.904	35.0	0.368
24.0	0.226	30.8	0.906	35.5	0.359
24.5	0.222	30.9	0.906	36.0	0.353
25.0	0.217	31.0	0.906	36.5	0.344
25.5	0.212	31.1	0.904	37.0	0.338
26.0	0.205	31.2	0.901	37.5	0.331
26.5	0.196	31.3	0.878	38.0	0.326
27.0	0.187	31.4	0.808	38.5	0.320
27.5	0.172	31.5	0.731	39.0	0.318
28.0	0.153	31.6	0.664	40.0	0.317
28.5	0.120	31.7	0.609		

[a]After Ref. 6.

III. Gallium Phosphide

The optical properties of GaP, as well as several other III–V compounds, have been determined by Philipp and Ehrenreich[1–4] from a Kramers–Kronig analysis of normal-incidence reflectance data over the wavelength range from 0.05 to approximately 10 microns. Experimental procedures and the theoretical framework of the analysis are described in Chapter 4 and are briefly summarized in the GaAs section of this chapter.

No other measurements are available for GaP between the vacuum ultraviolet and the short-wavelength side of the fundamental absorption edge, so that Philipp and Ehrenreich's values are listed throughout this spectral region.

Approaching the fundamental absorption edge, more direct methods for the determination of the optical constants are available, and their results are given preference.

Spitzer *et al.*[5] report transmission measurements on polycrystalline *n*-type specimens of $1 \times 10^{18}\,\mathrm{cm}^{-3}$ carrier concentration. The absorption coefficient α is obtained from the transmission T through a sample of thickness d, using the equation[6]

$$T = \frac{(1 - R)^2 e^{-\alpha d}}{1 - R^2 e^{-2\alpha d}}, \tag{3}$$

where the reflectance R is measured separately. The values listed for the extinction coefficient k above 0.452 micron are taken on the samples with the smallest absorption tail on the bottom of the edge.

The broad absorption band found in this measurement between 1 and 4 microns increases with the electron concentration and does not occur in *p*-type material. The absorption at longer wavelengths is typical of normal free-carrier absorption.

Values for the extinction coefficient k between 25 and 30 microns and for the refractive index n between 16 and 30 microns are taken from Kleinman and Spitzer's work on the infrared lattice absorption of GaP.[7] The reflectance from 13 to 42 microns is fitted within the experimental error by classical dispersion theory. As a by-product of this procedure, the optical constants are calculated and checked against transmission measurements in the regions outside the fundamental band. The samples were of *n*-type with a carrier density of about $10^{17}\,\mathrm{cm}^{-3}$. Consideration was given to the proper etching treatment of the samples, and it was determined that differences in the free-carrier concentration had no effect on the reflectance measurement.

The refractive index listed between 0.52 and 10 microns was obtained by

Oswald[8,9] from a combination of reflection and transmission measurements[10] on *p*-type samples. Between 0.52 and 0.77 micron the results are checked against measurements of the refraction through a GaP prism.

REFERENCES

1. H. R. Philipp and H. Ehrenreich, *Phys. Rev. Letters* **8**, 92 (1962).
2. H. R. Philipp and H. Ehrenreich, *Phys. Rev.* **129**, 1550 (1963).
3. H. Ehrenreich, H. R. Philipp, and J. C. Phillips, *Phys. Rev. Letters* **8**, 59 (1962).
4. H. R. Philipp and H. Ehrenreich, Chapter 4 of this volume.
5. W. G. Spitzer, M. Gershenzon, C. J. Forsch, and D. F. Gibbs, *J. Phys. Chem. Solids* **11**, 339 (1959).
6. H. Y. Fan, *Rept. Progr. Phys.* **19**, 107 (1956).
7. D. A. Kleinman and W. G. Spitzer, *Phys. Rev.* **118**, 110 (1960).
8. O. G. Folberth and F. Oswald, *Z. Naturforsch.* **9a**, 1050 (1954).
9. H. Welker, *J. Electron.* **1**, 181 (1955).
10. F. Oswald and R. Schade, *Z. Naturforsch.* **9a**, 611 (1954).

TABLE VI

REFRACTIVE INDEX n AND EXTINCTION COEFFICIENT k OF GALLIUM PHOSPHIDE AS A FUNCTION OF WAVELENGTH λ

λ (microns)	n	k	Reference	λ (microns)	n	k	Reference
0.049	1.028	0.168	(1–4)	0.165	1.187	1.841	(1–4)
0.050	1.000	0.201	(1–4)	0.177	1.390	2.119	(1–4)
0.052	0.991	0.231	(1–4)	0.180	1.479	2.188	(1–4)
0.054	0.999	0.280	(1–4)	0.188	1.727	2.125	(1–4)
0.056	1.023	0.290	(1–4)	0.190	1.732	2.073	(1–4)
0.059	1.026	0.278	(1–4)	0.194	1.696	2.085	(1–4)
0.063	0.972	0.243	(1–4)	0.207	1.709	2.353	(1–4)
0.065	0.901	0.286	(1–4)	0.229	2.246	3.295	(1–4)
0.069	0.839	0.362	(1–4)	0.234	2.631	3.472	(1–4)
0.073	0.797	0.474	(1–4)	0.239	3.191	3.462	(1–4)
0.077	0.801	0.588	(1–4)	0.264	4.130	2.102	(1–4)
0.083	0.825	0.691	(1–4)	0.288	3.862	1.481	(1–4)
0.089	0.854	0.796	(1–4)	0.295	3.785	1.494	(1–4)
0.095	0.896	0.905	(1–4)	0.302	3.743	1.541	(1–4)
0.103	0.951	1.023	(1–4)	0.310	3.770	1.649	(1–4)
0.113	1.025	1.138	(1–4)	0.318	3.906	1.801	(1–4)
0.124	1.143	1.303	(1–4)	0.330	4.653	1.959	(1–4)
0.135	1.250	1.230	(1–4)	0.335	5.078	1.710	(1–4)
0.139	1.195	1.234	(1–4)	0.344	5.192	—	(1–4)
0.146	1.116	1.331	(1–4)	0.354	4.848	—	(1–4)
0.157	1.075	1.639	(1–4)	0.375	4.252	—	(1–4)

TABLE VI—*continued*

λ (microns)	n	k	Reference	λ (microns)	n	k	Reference
0.452	—	3.12×10^{-2}	(5)	0.850	3.24	—	(9)
0.454	—	2.36×10^{-2}	(5)	0.900	3.20	—	(9)
0.456	—	1.87×10^{-2}	(5)	0.950	3.17	—	(9)
0.457	—	1.59×10^{-2}	(5)	1.00	3.17	—	(9)
0.459	—	1.43×10^{-2}	(5)	1.10	3.13	—	(9)
0.463	—	1.16×10^{-2}	(5)	1.20	3.10	—	(9)
0.464	—	9.49×10^{-3}	(5)	1.30	3.07	—	(9)
0.470	—	7.68×10^{-3}	(5)	1.40	3.07	—	(9)
0.473	—	6.37×10^{-3}	(5)	1.60	3.04	—	(9)
0.477	—	5.47×10^{-3}	(5)	1.60	—	4.99×10^{-4}	(5)
0.480	—	4.66×10^{-3}	(5)	1.80	3.03	—	(9)
0.482	—	4.29×10^{-3}	(5)	1.80	—	7.56×10^{-4}	(5)
0.488	—	3.41×10^{-3}	(5)	2.00	3.02	—	(9)
0.492	—	3.06×10^{-3}	(5)	2.00	—	1.03×10^{-3}	(5)
0.496	—	2.54×10^{-3}	(5)	2.50	2.99	—	(9)
0.500	—	2.47×10^{-3}	(5)	2.50	—	2.11×10^{-3}	(5)
0.501	—	2.18×10^{-3}	(5)	3.00	2.97	—	(9)
0.504	—	1.85×10^{-3}	(5)	3.00	—	2.53×10^{-3}	(5)
0.510	—	1.42×10^{-3}	(5)	3.50	2.95	—	(9)
0.514	—	1.19×10^{-3}	(5)	3.50	—	2.23×10^{-3}	(5)
0.519	—	1.04×10^{-3}	(5)	4.00	2.95	—	(9)
0.520	3.65	—	(9)	4.00	—	2.57×10^{-3}	(5)
0.521	—	8.57×10^{-4}	(5)	4.50	2.95	—	(9)
0.530	—	5.34×10^{-4}	(5)	4.50	—	3.21×10^{-3}	(5)
0.534	—	3.34×10^{-4}	(5)	5.00	2.94	—	(9)
0.538	—	2.41×10^{-4}	(5)	5.00	—	4.22×10^{-3}	(5)
0.544	—	1.18×10^{-4}	(5)	6.00	2.92	—	(9)
0.547	—	6.90×10^{-5}	(5)	6.00	—	7.26×10^{-3}	(5)
0.553	—	3.44×10^{-5}	(5)	7.00	2.95	—	(9)
0.555	—	2.19×10^{-5}	(5)	7.00	—	1.11×10^{-2}	(5)
0.561	—	1.39×10^{-5}	(5)	8.00	2.94	—	(9)
0.565	—	9.38×10^{-6}	(5)	8.00	—	1.64×10^{-2}	(5)
0.571	—	6.88×10^{-6}	(5)	9.00	2.91	—	(9)
0.574	—	5.70×10^{-6}	(5)	9.00	—	2.69×10^{-2}	(5)
0.579	—	4.96×10^{-6}	(5)	10.00	2.90	—	(9)
0.582	—	4.71×10^{-6}	(5)	16.00	2.750	—	(7)
0.600	3.46	—	(9)	16.65	2.714	—	(7)
0.620	3.42	—	(9)	17.23	2.679	—	(7)
0.640	3.36	—	(9)	18.00	2.643	—	(7)
0.660	3.34	—	(9)	18.87	2.600	—	(7)
0.680	3.34	—	(9)	20.00	2.529	—	(7)
0.700	3.33	—	(9)	20.87	2.500	—	(7)
0.750	3.28	—	(9)	21.72	2.386	—	(7)
0.800	3.27	—	(9)	22.51	2.207	—	(7)

TABLE VI—*continued*

λ (microns)	n	k	Reference	λ (microns)	n	k	Reference
23.29	1.979	—	(7)	27.34	—	10.84	(7)
24.01	1.650	—	(7)	27.36	15.19	—	(7)
24.57	1.129	—	(7)	27.37	—	8.20	(7)
24.82	—	0.064	(7)	27.44	—	5.13	(7)
25.00	0.100	—	(7)	27.45	13.47	—	(7)
25.26	—	1.379	(7)	27.46	—	2.57	(7)
25.42	0.043	—	(7)	27.53	—	1.04	(7)
26.23	—	3.400	(7)	27.54	10.87	—	(7)
26.51	0.129	—	(7)	27.57	—	0.68	(7)
26.66	—	5.000	(7)	27.65	—	0.45	(7)
26.89	—	6.614	(7)	27.69	8.50	—	(7)
26.98	0.457	—	(7)	27.82	—	0.200	(7)
27.04	—	8.893	(7)	28.09	—	0.114	(7)
27.14	—	11.50	(7)	28.21	6.19	—	(7)
27.18	1.83	—	(7)	28.64	—	0.107	(7)
27.19	4.07	—	(7)	29.12	—	0.050	(7)
27.21	7.62	—	(7)	29.34	4.67	—	(7)
27.26	13.12	—	(7)	29.69	—	0.050	(7)
27.26	—	14.68	(7)	29.94	4.39	—	(7)
27.29	—	17.33	(7)	30.00	4.36	0.021	(7)
27.32	16.58	13.89	(7)				

TABLE VII

REFLECTANCE R OF GALLIUM PHOSPHIDE AS A FUNCTION OF WAVELENGTH λ

λ (microns)	R	Reference	λ (microns)	R	Reference	λ (microns)	R	Reference
0.049	0.007	(1–4)	0.095	0.188	(1–4)	0.194	0.416	(1–4)
0.050	0.010	(1–4)	0.103	0.216	(1–4)	0.207	0.469	(1–4)
0.052	0.013	(1–4)	0.113	0.240	(1–4)	0.229	0.580	(1–4)
0.054	0.019	(1–4)	0.124	0.273	(1–4)	0.234	0.583	(1–4)
0.056	0.020	(1–4)	0.135	0.239	(1–4)	0.239	0.568	(1–4)
0.059	0.019	(1–4)	0.139	0.246	(1–4)	0.264	0.463	(1–4)
0.063	0.015	(1–4)	0.146	0.286	(1–4)	0.288	0.402	(1–4)
0.065	0.025	(1–4)	0.157	0.385	(1–4)	0.295	0.398	(1–4)
0.069	0.045	(1–4)	0.165	0.419	(1–4)	0.302	0.398	(1–4)
0.073	0.077	(1–4)	0.177	0.455	(1–4)	0.310	0.408	(1–4)
0.077	0.108	(1–4)	0.180	0.459	(1–4)	0.318	0.428	(1–4)
0.083	0.134	(1–4)	0.188	0.422	(1–4)	0.330	0.480	(1–4)
0.089	0.161	(1–4)	0.190	0.411	(1–4)	0.335	0.491	(1–4)

TABLE VII—*continued*

λ (microns)	R	Reference	λ (microns)	R	Reference	λ (microns)	R	Reference
0.344	0.468	(1–4)	19.44	0.195	(7)	27.14	0.921	(7)
0.354	0.435	(1–4)	20.00	0.188	(7)	27.19	0.903	(7)
0.375	0.384	(1–4)	20.43	0.183	(7)	27.26	0.875	(7)
0.413	0.331	(1–4)	21.25	0.172	(7)	27.33	0.846	(7)
0.459	0.302	(1–4)	22.34	0.144	(7)	27.40	0.806	(7)
0.517	0.280	(1–4)	23.18	0.107	(7)	27.46	0.771	(7)
0.620	0.263	(1–4)	23.87	0.069	(7)	27.54	0.736	(7)
0.689	0.257	(1–4)	24.19	0.029	(7)	27.64	0.700	(7)
0.885	0.251	(1–4)	24.66	0.016	(7)	27.76	0.669	(7)
1.240	0.247	(1–4)	24.80	0.077	(7)	27.89	0.646	(7)
1.377	0.246	(1–4)	24.86	0.269	(7)	28.02	0.627	(7)
2.066	0.244	(1–4)	24.95	0.550	(7)	28.49	0.467	(7)
3.099	0.244	(1–4)	25.00	0.669	(7)	29.16	0.421	(7)
6.198	0.243	(1–4)	25.03	0.736	(7)	30.00	0.385	(7)
13.17	0.228	(7)	25.03	0.824	(7)	31.30	0.352	(7)
14.00	0.226	(7)	25.22	0.906	(7)	32.64	0.331	(7)
14.88	0.222	(7)	25.26	0.925	(7)	33.95	0.321	(7)
15.75	0.219	(7)	25.39	0.957	(7)	35.00	0.315	(7)
16.00	0.220	(7)	25.79	0.966	(7)	35.44	0.313	(7)
16.59	0.217	(7)	26.22	0.971	(7)	36.27	0.307	(7)
17.40	0.210	(7)	26.56	0.973	(7)	37.39	0.302	(7)
18.00	0.207	(7)	26.80	0.966	(7)	38.16	0.299	(7)
18.55	0.202	(7)	27.05	0.956	(7)	38.95	0.299	(7)

IV. Gallium Arsenide

Philipp and Ehrenreich's[1–4] measurement of the reflectance at normal incidence extends down to 0.05 micron, including most of the structure at higher energies. The Kramers–Kronig analysis of the reflectance data evaluates the real and imaginary parts of the dielectric constant, from which the optical constants can be obtained in a straightforward manner. Careful consideration is given to extrapolation procedures in the high-energy end of the region. The contribution from this extrapolated region is evaluated by checking the calculated value against measured optical data below the threshold for direct optical transitions. The electropolished samples are not identified, but the reflectivities at extremely short wavelengths should be an intrinsic property of the material and should be relatively insensitive to the impurities present.

In the near ultraviolet and visible wavelength region, Philipp and

Ehrenreich's results overlap the measurements on mechanically polished samples by Tauc and Abraham[5] and Morrison.[6] While all three curves agree as to structure, Philipp and Ehrenreich's data are slightly (1 to 3%) higher than Morrison's and well above (up to 8%) what Tauc and Abraham report for the reflectance. One possible explanation for these discrepancies is differences in surface treatment, of importance in this wavelength region.[7,8]

Morrison[6] has used a similar dispersion analysis to evaluate his careful reflectance measurements between 0.2 and 15 microns, extending his study into the influence of different surface treatments on material of defined impurity content. Philipp and Ehrenreich's data are given preference in Table VIII for the simple reason that their Kramers–Kronig analysis is based on measurements that extended to 0.05 micron, which makes it superior by definition to a similar analysis based on a more restricted wavelength interval.

In the wavelength region where k is sufficiently small to permit the optical constants to be determined by a combination of transmission and reflection measurements, values obtained by this more direct method are more accurate than the results of a Kramers–Kronig analysis and are therefore given preference.

Sturge,[9] for instance, has determined the absorption coefficient from 0.46 to 2.07 microns at 21, 90, 185, and 294°K from transmission measurements through thin samples, using Morrison's[6] data to calculate the reflectivity correction to the absorption. The samples were "semi-insulating" with carrier concentrations of less than 10^{10} cm^{-3} and ionized impurity concentrations as concluded from mobility data of 3×10^{16} to 1×10^{17} cm^{-3}. Extreme care was taken to fulfill the severe requirements for high resolution and spectral purity imposed by the steepness of the absorption edge, especially at low temperatures. A prism–grating combination monochromator in which the scattered light was minimized by the use of baffles provided a resolution of up to 2×10^{-4} eV. For the thinnest samples, which could not be measured freely suspended, the effect of strain due to the backing by the substrate was corrected. The thickness of the samples was measured interferometrically, with some criticism voiced against the assignment of the order of interference in this determination.[10]

Moss and Hawkins's[11] measurements of the absorption coefficient complement Sturge's data in the wavelength region of the absorption edge. The material is described as containing 3×10^{16} electrons per cm^3, with the thickness of the polished wafers determined interferometrically for the thinner samples. The agreement with Sturge[9] is within the same order of magnitude only, which is satisfactory in a wavelength region where the absorption is drastically dependent upon the doping parameters.

Marple[10] has measured the index of refraction around the absorption

edge, using the very precise prism refraction method. The prism material consisted of boat-grown GaAs, free of intentional doping and containing 6×10^{16} donors per cm^3 in one case, and intentionally doped with 5.5×10^{17} cm^{-3} tellurium in the other case. No difference greater than the possible systematic error could be observed between the two prisms. The probable systematic error in the index values is estimated to be ± 0.002, the random error, ± 0.001. The temperature may be in error by $\pm 3°K$ and the wavelength by ± 0.001 micron.

Marple[10] has performed a least-squares analysis of his data, using a first-order Sellmeier equation:

$$n^2 = A + B\left(\frac{\lambda^2}{\lambda^2 - C^2}\right). \tag{4}$$

The computer-determined constants for the three different temperatures at which the measurements were performed are shown in the accompanying tabulation. $(A + B)$ gives the high-frequency dielectric constant.

Temperature	A	B	$(A + B)$	C^2
103°K	8.720	2.053	10.773	0.358
185°K	8.598	2.242	10.840	0.353
298°K	8.950	2.054	11.004	0.390

From his results, Marple[10] also has calculated $[n + \nu(dn/d\nu)]$ as a function of photon energy for 300°K and 103°K. This parameter determines the frequency spacing $\delta\nu$ of successive elementary modes in a Fabry–Perot resonator of length l, according to the relation

$$\delta\nu = \frac{1}{2l[n + \nu(dn/d\nu)]}, \tag{5}$$

and is frequently used in the interpretation of the line spectrum of GaAs in injection lasers.

The same prism refraction method has been used by Hambleton *et al.*[12] for the determination of the refractive index at four wavelengths in the near infrared. The material is described as of high resistivity with a carrier concentration of less than 10^8 cm^{-3}. The error in n is estimated as ± 0.007.

An isolated value for n and k has been determined by Zaininger and Revesz,[13] using ellipsometry at $\lambda = 5461$ Å. The value for k is in excellent agreement with Sturge.[9] The value for n is slightly above the results of other authors, but it is pointed out that this value represents only an upper limit for n.

Oswald and Schade[14] have measured the reflected and transmitted intensity in the wavelength region between the fundamental absorption edge and 15 microns, and have calculated the optical constants from a combination of these two data. Provisions were made to suppress reflections from the back surface of the specimen. Interference effects were eliminated by choosing a thickness of more than 100 wavelengths and polishing the wafers under a slight wedge angle. The sample thickness was determined by a measuring microscope. Reference was the sample itself, after it had been coated with aluminum. This provided the same effective aperture for the incident beam and eliminated imperfections of the sample surface. No information on the material is given except that it was of high resistivity.

Barcus *et al.*[15] have determined both the index of refraction and the extinction coefficient between wavelengths of 2 and 22 microns by measuring the percentage of plane polarized light reflected at two angles of incidence from the surface. The GaAs was *n*-type and polycrystalline with a Hall-effect carrier concentration of $6.9 \times 10^{17}\,\mathrm{cm}^{-3}$. Throughout this spectral region the extinction coefficient was found to be less than 0.1, so it was disregarded in order to simplify the calculations for the index of refraction.

Several authors have measured reflection spectra in the infrared region in order to study the lattice vibration characteristics of GaAs.[16–19] The observed reflection data can be analyzed according to classical dispersion theory and can, in the case of GaAs, be well represented by a single dispersion oscillator. Using a method of successive trials and adjustment, the three dispersion parameters—the oscillator strength, the dispersion frequency, and the damping constant—can be determined within reasonable uncertainties by the requirement of fitting the experimental reflection curve. Once these three parameters are found, the two optical constants can be calculated. It must be kept in mind, however, that this process is very sensitive to small variations in the maximum reflectivity due to surface effects, which can lead to wide variations in the values of the optical constants. This adds to the experimental difficulties encountered in this wavelength region.

Piriou and Cabannes[18] present the results of their analysis in terms of n and k in the wavelength range between 1 and 40 microns. The material on which the reflectance was measured is not specified, nor are the details of the experimental procedure. The dispersion frequency in their analysis agrees within 2% with the values given by Hass and Henvis[16] and Picus *et al.*[17]

Although slightly different from each other, the results of four different measurements are carried in Table VIII for the refractive index on the long-wavelength side of the fundamental absorption edge. Since these results were obtained by four entirely different methods, the difference between the

values might present additional information, although the prism method used by Marple[10] and Hambleton *et al.*[12] is certainly more indicative for the properties of the bulk material than the methods that are influenced by properties of surface layers.

No values for the extinction coefficient are tabulated between 0.904 and 30 microns, although a number of absorption measurements are published in this wavelength region between the fundamental absorption edge and the onset of the lattice-vibration absorption band. The results of these measurements often do not even agree as to the order of magnitude, because of different doping conditions. Because of interest generated by the increasing importance of GaAs as material for injection lasers, several papers[20–28] have discussed absorption mechanisms as related to the impurity content of the material. In general, the absorption can be understood as the result of two competing processes: (1) the process relating to the change of the Fermi level with doping (Burstein shift), shifting the absorption edge toward higher energies for increasing density of doping, and (2) the process that shifts the edge toward lower energies and can be explained as an effective decrease in the energy gap due directly to the presence of impurities or to a change in the lattice parameters due to doping. Which of these two processes dominates, and to what extent, depends upon the type to which the material was doped, the kind of dopant used, and its interaction with and compensation of the impurities already present. The present data on this complex balance are not extensive enough to make a complete analysis possible and to tabulate the extinction coefficient as a function of a few parameters. On the other hand, measurements on materials of an uncompensated impurity content of less than $10^{17}\,\mathrm{cm}^{-3}$, for which the dopant-induced absorption seems to be less effective, are not available.

We conclude the section on GaAs with Cardona's[29] measurement of the temperature dependence of the refractive index between 5 and 20 microns, obtained from interferometric measurements on thin layers:

$$\frac{1}{n}\frac{dn}{dT} = (4.5 \pm 0.2) \times 10^{-5}\,^{\circ}\mathrm{C}^{-1}. \tag{6}$$

REFERENCES

1. H. R. Philipp and H. Ehrenreich, *Phys. Rev. Letters* **8**, 92 (1962).
2. H. R. Philipp and H. Ehrenreich, *Phys. Rev.* **129**, 1550 (1963).
3. H. Ehrenreich, H. R. Philipp, and J. C. Phillips, *Phys. Rev. Letters* **8**, 59 (1962).
4. H. R. Philipp and H. Ehrenreich, Chapter 4 of this volume.
5. J. Tauc and A. Abraham, *Proc. Intern. Conf. Semicond. Phys., Prague, 1960* p. 375. Czech. Acad. Sci., Prague and Academic Press, New York, 1961.
6. R. E. Morrison, *Phys. Rev.* **124**, 1314 (1961).
7. H. E. Bennett and J. O. Porteus, *J. Opt. Soc. Am.* **51**, 123 (1961).

8. J. O. Porteus, *J. Opt. Soc. Am.* **53**, 1394 (1963).
9. M. D. Sturge, *Phys. Rev.* **127**, 768 (1962).
10. D. T. F. Marple, *J. Appl. Phys.* **35**, 1241 (1964).
11. T. S. Moss and T. D. H. Hawkins, *Infrared Phys.* **1**, 111 (1961).
12. K. G. Hambleton, C. Hilsum, and B. R. Holeman, *Proc. Phys. Soc. (London)* 77, 1147 (1961).
13. K. H. Zaininger and A. G. Revesz, *J. Phys. (France)* **25**, 208 (1964).
14. F. Oswald and R. Schade, *Z. Naturforsch* **9a**, 611 (1954).
15. L. C. Barcus, A. Perlmutter, and J. Callaway, *Phys. Rev.* **111**, 167 (1958).
16. M. Hass and B. W. Henvis, *J. Phys. Chem. Solids* **23**, 1099 (1962).
17. G. Picus, E. Burstein, B. W. Henvis, and M. Hass, *J. Phys. Chem. Solids* **8**, 282 (1959).
18. B. Piriou and F. Cabannes, *Compt. Rend.* **255**, 2932 (1962).
19. S. J. Fray, F. A. Johnson, J. E. Quarrington, and N. Williams, *Proc. Phys. Soc. (London)* **77**, 215 (1961).
20. W. G. Spitzer and J. M. Whelan, *Phys. Rev.* **114**, 59 (1959).
21. M. V. Hobden and M. D. Sturge, *Proc. Phys. Soc. (London)* **78**, 615 (1961).
22. L. J. Vieland and I. Kudman, *J. Phys. Chem. Solids* **24**, 437 (1963).
23. R. Braunstein, J. I. Pankove, and H. Nelson, *Appl. Phys. Letters* **3**, 31 (1963).
24. W. J. Turner and W. E. Reese, *J. Appl. Phys.* **35**, 350 (1964).
25. D. E. Hill, *Phys. Rev.* **133**, A 866 (1964).
26. G. Lucovsky, *Appl. Phys. Letters* **5**, 37 (1964).
27. I. Kudman and T. Seidel, *J. Appl. Phys.* **33**, 771 (1962).
28. G. Lucovsky, A. J. Varga, and R. F. Schwarz, *Solid State Commun.* **3**, 9 (1965).
29. M. Cardona, *Proc. Intern. Conf. Semicond. Phys., Prague, 1960* p. 388. Czech. Acad. Sci., Prague and Academic Press, New York, 1961.

TABLE VIII

REFRACTIVE INDEX n AND EXTINCTION COEFFICIENT k OF GALLIUM ARSENIDE AS A FUNCTION OF WAVELENGTH λ AT 300°K

λ (microns)	n	k	Reference	λ (microns)	n	k	Reference
0.049	1.049	0.156	(1–4)	0.115	0.923	0.881	(1–4)
0.051	1.033	0.203	(1–4)	0.124	0.913	0.974	(1–4)
0.054	1.037	0.228	(1–4)	0.138	0.901	1.136	(1–4)
0.056	1.043	0.243	(1–4)	0.155	0.899	1.435	(1–4)
0.058	1.051	0.250	(1–4)	0.177	1.063	1.838	(1–4)
0.059	1.058	0.245	(1–4)	0.188	1.247	2.047	(1–4)
0.062	1.025	0.212	(1–4)	0.197	1.441	1.988	(1–4)
0.065	0.981	0.234	(1–4)	0.200	1.424	1.976	(1–4)
0.069	0.936	0.267	(1–4)	0.207	1.395	2.048	(1–4)
0.073	0.889	0.324	(1–4)	0.216	1.402	2.203	(1–4)
0.078	0.850	0.411	(1–4)	0.225	1.451	2.416	(1–4)
0.083	0.836	0.503	(1–4)	0.236	1.561	2.722	(1–4)
0.089	0.840	0.602	(1–4)	0.248	1.882	3.279	(1–4)
0.096	0.864	0.709	(1–4)	0.258	2.726	3.388	(1–4)
0.103	0.895	0.791	(1–4)	0.270	3.291	2.860	(1–4)

TABLE VIII—*continued*

λ (microns)	n	k	Reference	λ (microns)	n	k	Reference
0.282	3.486	2.527	(1–4)	0.820	—	0.632×10^{-1}	(11)
0.295	3.526	2.074	(1–4)	0.825	—	0.615×10^{-1}	(11)
0.310	3.513	1.857	(1–4)	0.830	—	0.593×10^{-1}	(11)
0.318	3.451	1.827	(1–4)	0.835	—	0.578×10^{-1}	(11)
0.326	3.389	1.845	(1–4)	0.840	—	0.556×10^{-1}	(11)
0.344	3.391	1.906	(1–4)	0.845	—	0.535×10^{-1}	(11)
0.365	3.514	2.017	(1–4)	0.850	—	0.676×10^{-1}	(9)
0.400	4.149	2.137	(1–4)	0.852	—	0.661×10^{-1}	(9)
0.409	4.320	1.999	(1–4)	0.854	—	0.648×10^{-1}	(9)
0.419	4.459	1.930	(1–4)	0.856	—	0.640×10^{-1}	(9)
0.425	4.755	1.934	(1–4)	0.858	—	0.627×10^{-1}	(9)
0.443	4.929	1.195	(1–4)	0.860	—	0.620×10^{-1}	(9)
0.459	4.748	—	(1–4)	0.862	—	0.615×10^{-1}	(9)
0.460	—	0.510	(9)	0.864	—	0.606×10^{-1}	(9)
0.465	—	0.506	(9)	0.866	—	0.605×10^{-1}	(9)
0.470	—	0.500	(9)	0.868	—	0.601×10^{-1}	(9)
0.475	—	0.490	(9)	0.870	—	0.483×10^{-1}	(9)
0.480	—	0.464	(9)	0.872	—	0.318×10^{-1}	(9)
0.485	—	0.442	(9)	0.874	—	0.207×10^{-1}	(9)
0.490	—	0.425	(9)	0.876	—	0.105×10^{-1}	(9)
0.495	—	0.412	(9)	0.878	—	7.140×10^{-3}	(9)
0.495	4.427	—	(1–4)	0.880	—	4.549×10^{-3}	(9)
0.500	—	0.400	(9)	0.882	—	2.783×10^{-3}	(9)
0.505	—	0.387	(9)	0.884	—	1.808×10^{-3}	(9)
0.510	—	0.375	(9)	0.886	—	1.177×10^{-3}	(9)
0.515	—	0.363	(9)	0.888	—	0.664×10^{-3}	(9)
0.520	—	0.351	(9)	0.890	—	0.416×10^{-3}	(9)
0.525	—	0.339	(9)	0.892	—	0.262×10^{-3}	(9)
0.530	—	0.330	(9)	0.894	—	0.173×10^{-3}	(9)
0.535	—	0.320	(9)	0.895	3.603	—	(10)
0.540	—	0.313	(9)	0.896	—	0.112×10^{-3}	(9)
0.540	4.127	—	(1–4)	0.898	—	0.082×10^{-3}	(9)
0.590	3.888	—	(1–4)	0.900	—	0.639×10^{-4}	(9)
0.653	3.746	—	(1–4)	0.900	3.595	—	(10)
0.729	3.627	—	(1–4)	0.902	—	0.518×10^{-4}	(9)
0.775	—	0.697×10^{-1}	(11)	0.904	—	0.433×10^{-4}	(9)
0.780	—	0.696×10^{-1}	(11)	0.910	3.581	—	(10)
0.785	—	0.693×10^{-1}	(11)	0.920	3.569	—	(10)
0.790	—	0.692×10^{-1}	(11)	0.940	3.550	—	(10)
0.795	—	0.688×10^{-1}	(11)	0.960	3.534	—	(10)
0.800	—	0.682×10^{-1}	(11)	0.980	3.520	—	(10)
0.805	—	0.666×10^{-1}	(11)	1.000	3.509	—	(10)
0.810	—	0.658×10^{-1}	(11)	1.000	3.326	—	(18)
0.815	—	0.643×10^{-1}	(11)	1.000	3.500	—	(14)

TABLE VIII—*continued*

λ (microns)	n	k	Reference	λ (microns)	n	k	Reference
1.02	3.498	—	(10)	7.0	3.217	—	(15)
1.04	3.488	—	(10)	8.0	3.315	—	(18)
1.06	3.479	—	(10)	8.0	3.250	—	(14)
1.10	3.463	—	(10)	8.0	3.183	—	(15)
1.15	3.446	—	(10)	9.0	3.312	—	(18)
1.20	3.433	—	(10)	9.0	3.250	—	(14)
1.40	3.394	—	(10)	9.0	3.143	—	(15)
1.50	3.381	—	(10)	10.0	3.309	—	(18)
1.70	3.362	—	(10)	10.0	3.095	—	(15)
2.0	3.314	—	(15)	11.0	3.305	—	(18)
2.0	3.325	—	(18)	11.0	3.047	—	(15)
2.0	3.410	—	(14)	12.0	3.300	—	(18)
3.0	3.324	—	(18)	12.0	2.991	—	(15)
3.0	3.350	—	(14)	13.0	3.295	—	(18)
3.0	3.303	—	(15)	13.0	2.933	—	(15)
3.0	3.313	—	(12)	14.0	3.289	—	(18)
4.0	3.323	—	(18)	14.0	2.863	—	(15)
4.0	3.300	—	(14)	15.0	3.283	—	(18)
4.0	3.289	—	(15)	15.0	2.790	—	(15)
4.0	3.302	—	(12)	16.0	2.707	—	(15)
5.0	3.322	—	(18)	17.0	2.621	—	(15)
5.0	3.290	—	(14)	18.0	2.521	—	(15)
5.0	3.269	—	(15)	19.0	2.409	—	(15)
5.0	3.298	—	(12)	20.0	2.287	—	(15)
6.0	3.320	—	(18)	20.0	3.234	—	(18)
6.0	3.280	—	(14)	21.0	2.151	—	(15)
6.0	3.246	—	(15)	22.0	2.029	—	(15)
7.0	3.318	—	(18)	23.0	3.182	—	(18)
7.0	3.250	—	(14)	25.0	3.133	—	(18)

TABLE IX

REFRACTIVE INDEX n AND EXTINCTION COEFFICIENT k OF GALLIUM ARSENIDE AS A FUNCTION OF WAVELENGTH λ AT 185°K

λ (microns)	n	k	Reference	λ (microns)	n	k	Reference
0.834	—	6.31×10^{-2}	(9)	0.868	—	5.01×10^{-5}	(9)
0.836	—	6.17×10^{-2}	(9)	0.870	—	3.83×10^{-5}	(9)
0.838	—	6.26×10^{-2}	(9)	0.870	3.581	—	(10)
0.840	—	6.89×10^{-2}	(9)	0.872	—	3.46×10^{-5}	(9)
0.842	—	5.21×10^{-2}	(9)	0.874	—	3.22×10^{-5}	(9)
0.844	—	2.07×10^{-2}	(9)	0.876	—	3.05×10^{-5}	(9)
0.846	—	9.17×10^{-3}	(9)	0.878	—	2.94×10^{-5}	(9)
0.848	—	3.43×10^{-3}	(9)	0.880	3.567	—	(10)
0.850	—	1.86×10^{-3}	(9)	0.900	3.544	—	(10)
0.852	—	1.06×10^{-3}	(9)	0.920	3.526	—	(10)
0.854	—	7.37×10^{-4}	(9)	0.950	3.501	—	(10)
0.856	—	5.03×10^{-4}	(9)	0.950	3.504	—	(10)
0.858	—	2.88×10^{-4}	(9)	1.000	3.474	—	(10)
0.860	—	2.01×10^{-4}	(9)	1.100	3.433	—	(10)
0.862	—	1.41×10^{-4}	(9)	1.300	3.384	—	(10)
0.864	—	8.89×10^{-5}	(9)	1.500	3.355	—	(10)
0.866	—	6.63×10^{-5}	(9)	1.700	3.337	—	(10)

TABLE X

REFRACTIVE INDEX n OF GALLIUM ARSENIDE AS A FUNCTION OF WAVELENGTH λ AT 103°K[a]

λ (microns)	n	λ (microns)	n
0.845	3.589	0.900	3.519
0.850	3.578	1.000	3.455
0.855	3.570	1.100	3.415
0.860	3.562	1.200	3.387
0.870	3.549	1.400	3.351
0.880	3.538	1.600	3.329

[a]After Ref. 10.

TABLE XI

EXTINCTION COEFFICIENT k OF GALLIUM ARSENIDE AS A FUNCTION OF WAVELENGTH λ AT 90°K[a]

λ (microns)	k	λ (microns)	k
0.820	6.23×10^{-2}	0.836	2.81×10^{-4}
0.822	6.75×10^{-2}	0.838	1.90×10^{-4}
0.824	5.95×10^{-2}	0.840	1.16×10^{-4}
0.826	1.55×10^{-2}	0.842	8.52×10^{-5}
0.828	4.96×10^{-3}	0.844	6.33×10^{-5}
0.830	1.44×10^{-3}	0.846	5.36×10^{-5}
0.832	7.95×10^{-4}	0.848	4.56×10^{-5}
0.834	5.08×10^{-4}		

[a] After Ref. 9.

TABLE XII

EXTINCTION COEFFICIENT k OF GALLIUM ARSENIDE AS A FUNCTION OF WAVELENGTH λ AT 21°K[a]

λ (microns)	k	λ (microns)	k	λ (microns)	k
0.450	0.497	0.570	0.245	0.690	0.133
0.460	0.465	0.580	0.235	0.700	0.126
0.470	0.428	0.590	0.225	0.710	0.122
0.480	0.394	0.600	0.219	0.720	0.117
0.490	0.370	0.610	0.208	0.730	0.113
0.500	0.344	0.620	0.201	0.740	0.110
0.510	0.321	0.630	0.194	0.750	0.101
0.520	0.303	0.640	0.187	0.760	0.096
0.530	0.291	0.650	0.178	0.770	0.091
0.540	0.281	0.660	0.168	0.780	0.085
0.550	0.265	0.670	0.146	0.790	0.076
0.560	0.253	0.680	0.137	0.800	0.070

[a] After Ref. 9.

TABLE XIII

REFLECTANCE R OF GALLIUM ARSENIDE AS A FUNCTION OF WAVELENGTH λ

λ (microns)	R	Reference	λ (microns)	R	Reference	λ (microns)	R	Reference
0.049	0.006	(1–4)	0.590	0.350	(1–4)	31.91	0.186	(18)
0.051	0.010	(1–4)	0.653	0.335	(1–4)	32.08	0.180	(18)
0.054	0.013	(1–4)	0.729	0.323	(1–4)	32.25	0.173	(18)
0.056	0.014	(1–4)	0.827	0.314	(1–4)	32.43	0.164	(18)
0.058	0.015	(1–4)	1.00	0.289	(18)	32.60	0.155	(18)
0.059	0.015	(1–4)	2.00	0.289	(18)	32.78	0.144	(18)
0.062	0.011	(1–4)	3.00	0.289	(18)	32.96	0.132	(18)
0.065	0.014	(1–4)	4.00	0.289	(18)	33.14	0.117	(18)
0.068	0.020	(1–4)	5.00	0.289	(18)	33.33	0.100	(18)
0.073	0.032	(1–4)	6.00	0.288	(18)	33.52	0.080	(18)
0.077	0.053	(1–4)	7.00	0.288	(18)	33.70	0.059	(18)
0.083	0.077	(1–4)	8.00	0.287	(18)	33.89	0.046	(18)
0.089	0.104	(1–4)	9.00	0.288	(18)	34.09	0.080	(18)
0.096	0.131	(1–4)	10.00	0.287	(18)	34.28	0.255	(18)
0.103	0.151	(1–4)	11.00	0.287	(18)	34.48	0.473	(18)
0.115	0.175	(1–4)	12.00	0.286	(18)	34.68	0.617	(18)
0.124	0.208	(1–4)	13.00	0.266	(18)	34.88	0.704	(18)
0.138	0.265	(1–4)	14.00	0.285	(18)	35.08	0.756	(18)
0.155	0.365	(1–4)	15.00	0.284	(18)	35.29	0.788	(18)
0.177	0.443	(1–4)	15.78	0.283	(18)	35.50	0.806	(18)
0.188	0.460	(1–4)	16.66	0.283	(18)	35.71	0.812	(18)
0.197	0.419	(1–4)	17.64	0.282	(18)	35.92	0.804	(18)
0.200	0.418	(1–4)	18.75	0.280	(18)	36.14	0.769	(18)
0.207	0.438	(1–4)	20.00	0.278	(18)	36.36	0.699	(18)
0.225	0.510	(1–4)	21.42	0.276	(18)	36.58	0.628	(18)
0.248	0.605	(1–4)	23.07	0.272	(18)	36.81	0.576	(18)
0.253	0.598	(1–4)	25.00	0.266	(18)	37.03	0.539	(18)
0.276	0.494	(1–4)	27.27	0.256	(18)	37.26	0.510	(18)
0.318	0.404	(1–4)	30.00	0.230	(18)	37.50	0.487	(18)
0.326	0.402	(1–4)	30.15	0.228	(18)	37.73	0.469	(18)
0.344	0.408	(1–4)	30.30	0.225	(18)	37.97	0.454	(18)
0.365	0.425	(1–4)	30.45	0.223	(18)	38.21	0.442	(18)
0.400	0.466	(1–4)	30.61	0.220	(18)	38.46	0.431	(18)
0.409	0.465	(1–4)	30.76	0.217	(18)	38.71	0.422	(18)
0.419	0.468	(1–4)	30.92	0.214	(18)	38.96	0.414	(18)
0.425	0.484	(1–4)	31.08	0.210	(18)	39.21	0.407	(18)
0.443	0.461	(1–4)	31.25	0.206	(18)	39.47	0.401	(18)
0.459	0.436	(1–4)	31.41	0.202	(18)	39.73	0.395	(18)
0.496	0.402	(1–4)	31.57	0.197	(18)	40.00	0.390	(18)
0.539	0.373	(1–4)	31.74	0.192	(18)			

V. Gallium Antimonide

Cardona[1] reports the results of a reflectance measurement on mechanically polished *n*-type samples of a carrier concentration of 10^{18} cm^{-3} in the wavelength region from 0.245 to 2.38 microns. Although this range is not sufficiently large for a Kramers–Kronig analysis, particularly on the short-wavelength side, the reflectance values are listed in Table XV. Should future measurements extend this wavelength range, these values can be used in conducting a Kramers–Kronig analysis with respect to the optical constants.

In a limited range in the ultraviolet, Lukeš and Schmidt[2] report reflectance values that are in excellent agreement with Cardona's. Slightly smaller values for the reflectance are reported by Tauc and Abraham.[3]

In connection with an infrared study of the double-conduction-band model of GaSb, Becker *et al.*[4] have measured the intrinsic absorption edge of pure *p*-type samples, for which a Hall coefficient of 55 cm^3/C at 300°K is given. The *k* values for this sample are listed in Table XIV. The same authors report curves for the absorption edge at 80°K and 4.2°K, measured on *n*-type samples of higher carrier concentration, for which, presumably, degeneracy effects as well as the existence of the second conduction band must be taken into account. A measurement of the absorption edge at 1.4°K is reported by Johnson *et al.*[5]

The values for the extinction coefficient in the wavelength region from 1.73 to 14 microns are taken from the measurement of Roberts and Quarrington[6] on mechanically polished material of approximately 10^{17} impurity centers per cm^3. A prism monochromator was used for the "sample-in–sample-out" technique, based on Eq. (3). The reflectance is assumed to be the one that is calculated from the refractive index as measured by Oswald and Schade[7] on *p*-type material of a specific resistivity of 0.08 ohm-cm and a hole mobility of 650 cm^2/V-sec. Their values are listed in Table XIV between 2 and 14.9 microns.

The index of refraction was measured by Edwards and Hayne[8] in the wavelength region 1.8 to 2.5 microns, using the prism method. Hall-effect measurements indicate a carrier concentration of only 7.5×10^{16} cm^{-3} in the *p*-type material from which the prism was cut. An error of 0.3% is estimated for the data measured by this prism method. An interesting feature of this work is that two independent techniques for the determination of the refractive index are compared for the same material and the same polishing treatment. In addition to the prism method, *n* was determined with an error of less than 2% from a reflectance measurement, and the resulting data were found to be consistently lower, by more than 0.21, or 6%, over the whole wavelength range. These lower values agreed with Oswald and

Schade's[7] results obtained by a similar reflectance technique, so that the source of the discrepancy apparently lies in the method: Prism measurements indicate the properties of the bulk, while reflectance measurements depend upon the qualities of a thin surface layer only, making the results highly dependent upon the surface treatment.

Using the same method as he used for a number of other III–V compounds, Cardona[9] has determined the temperature coefficient of the refractive index for p-type samples of 10^{17} cm^{-3} carrier concentration as

$$\frac{1}{n}\frac{dn}{dT} = (8.2 \pm 0.2) \times 10^{-5}\,^{\circ}\mathrm{C}^{-1}. \tag{7}$$

REFERENCES

1. M. Cardona, *Z. Physik* **161**, 99 (1960).
2. F. Lukeš and E. Schmidt, *Proc. Intern. Conf. Semicond. Phys., Exeter, 1962* p. 389. Inst. Phys. and Phys. Soc., London, 1962; *Phys. Letters* **2**, 288 (1962).
3. J. Tauc and A. Abraham, *Proc. Intern Conf. Semicond. Phys., Prague, 1960* p. 375. Czech Acad. Sci., Prague and Academic Press, New York, 1961.
4. W. M. Becker, A. K. Ramdas, and H. Y. Fan, *J. Appl. Phys.* **32**, 2094 (1961).
5. E. J. Johnson, I. Filinski, and H. Y. Fan, *Proc. Intern. Conf. Semicond. Phys., Exeter, 1962* p. 375. Inst. Phys. and Phys. Soc., London, 1962.
6. V. Roberts and J. E. Quarrington, *J. Electron.* **1**, 152 (1955).
7. F. Oswald and R. Schade, *Z. Naturforsch.* **9a**, 611 (1954).
8. D. F. Edwards and G. S. Hayne, *J. Opt. Soc. Am.* **49**, 414 (1959).
9. M. Cardona, *Proc. Intern. Conf. Semicond. Phys., Prague, 1960* p. 388. Czech. Acad. Sci., Prague and Academic Press, New York, 1961.

TABLE XIV

REFRACTIVE INDEX n AND EXTINCTION COEFFICIENT k OF GALLIUM ANTIMONIDE AS A FUNCTION OF WAVELENGTH λ

λ (microns)	n	k	Reference	λ (microns)	n	k	Reference
1.49	—	9.70×10^{-2}	(4)	1.62	—	6.80×10^{-2}	(4)
1.51	—	9.45×10^{-2}	(4)	1.63	—	6.49×10^{-2}	(4)
1.53	—	9.06×10^{-2}	(4)	1.64	—	6.14×10^{-2}	(4)
1.55	—	8.67×10^{-2}	(4)	1.65	—	5.82×10^{-2}	(4)
1.56	—	8.52×10^{-2}	(4)	1.66	—	5.47×10^{-2}	(4)
1.57	—	8.16×10^{-2}	(4)	1.68	—	5.10×10^{-2}	(4)
1.58	—	7.90×10^{-2}	(4)	1.69	—	4.70×10^{-2}	(4)
1.59	—	7.68×10^{-2}	(4)	1.70	—	4.06×10^{-2}	(4)
1.60	—	7.39×10^{-2}	(4)	1.71	—	2.51×10^{-2}	(4)
1.61	—	7.10×10^{-2}	(4)	1.72	—	7.48×10^{-3}	(4)

TABLE XIV—*continued*

λ (microns)	n	k	Reference	λ (microns)	n	k	Reference
1.73	—	6.68×10^{-3}	(4)	3.5	—	7.46×10^{-4}	(6)
1.73	—	2.14×10^{-3}	(6)	3.5	3.861	—	(7)
1.74	—	3.05×10^{-3}	(4)	3.7	—	9.25×10^{-4}	(6)
1.75	—	1.83×10^{-3}	(4)	4.0	—	1.26×10^{-3}	(6)
1.76	—	1.24×10^{-3}	(4)	4.0	3.833	—	(7)
1.77	—	9.18×10^{-4}	(4)	4.5	—	1.88×10^{-3}	(6)
1.77	—	1.23×10^{-3}	(6)	5.0	—	2.53×10^{-3}	(6)
1.80	—	5.40×10^{-4}	(4)	5.0	3.824	—	(7)
1.80	—	5.51×10^{-4}	(6)	5.4	—	3.13×10^{-3}	(6)
1.80	3.820	—	(8)	5.8	—	3.66×10^{-3}	(6)
1.82	—	3.56×10^{-4}	(4)	6.0	—	3.94×10^{-3}	(6)
1.82	—	3.55×10^{-4}	(6)	6.0	3.824	—	(7)
1.84	—	4.96×10^{-4}	(6)	6.2	—	4.22×10^{-3}	(6)
1.85	—	2.52×10^{-4}	(4)	6.7	—	4.90×10^{-3}	(6)
1.88	—	2.00×10^{-4}	(4)	7.0	—	5.33×10^{-3}	(6)
1.88	—	1.41×10^{-4}	(6)	7.0	3.843	—	(7)
1.90	3.802	—	(8)	7.4	—	5.90×10^{-3}	(6)
1.91	—	1.41×10^{-4}	(4)	8.0	—	6.68×10^{-3}	(6)
1.94	—	1.18×10^{-4}	(4)	8.0	3.843	—	(7)
1.97	—	1.10×10^{-4}	(4)	8.4	—	7.21×10^{-3}	(6)
2.00	—	1.08×10^{-4}	(4)	9.0	—	7.99×10^{-3}	(6)
2.00	—	9.87×10^{-5}	(6)	9.0	3.843	—	(7)
2.00	3.789	—	(8)	9.5	—	8.63×10^{-3}	(6)
2.03	—	1.09×10^{-4}	(4)	10.0	—	9.26×10^{-3}	(6)
2.07	—	1.13×10^{-4}	(4)	10.0	3.843	—	(7)
2.1	3.780	—	(8)	10.6	—	9.95×10^{-3}	(6)
2.2	3.764	—	(8)	11.1	—	1.06×10^{-2}	(6)
2.3	3.758	—	(8)	12.0	—	1.16×10^{-2}	(6)
2.4	3.755	—	(8)	12.0	3.843	—	(7)
2.4	—	1.43×10^{-4}	(6)	12.4	—	1.21×10^{-2}	(6)
2.5	—	1.65×10^{-4}	(6)	12.8	—	1.26×10^{-2}	(6)
2.5	3.749	—	(8)	13.4	—	1.41×10^{-2}	(6)
2.8	—	2.65×10^{-4}	(6)	14.0	—	1.40×10^{-2}	(6)
3.0	—	3.65×10^{-4}	(6)	14.0	3.861	—	(7)
3.0	3.898	—	(7)	14.9	3.880	—	(7)
3.4	—	6.66×10^{-4}	(6)				

TABLE XV

REFLECTANCE R OF GALLIUM ANTIMONIDE AS A FUNCTION OF WAVELENGTH λ[a]

λ (microns)	R	λ (microns)	R	λ (microns)	R
0.245	0.385	0.351	0.434	0.64	0.454
0.246	0.386	0.360	0.422	0.65	0.456
0.249	0.393	0.365	0.418	0.66	0.453
0.252	0.409	0.370	0.414	0.68	0.438
0.256	0.419	0.380	0.406	0.70	0.432
0.260	0.430	0.390	0.402	0.75	0.419
0.265	0.451	0.400	0.400	0.80	0.410
0.269	0.473	0.409	0.400	0.85	0.399
0.272	0.500	0.415	0.406	0.90	0.391
0.276	0.511	0.420	0.405	0.95	0.380
0.280	0.521	0.423	0.403	1.00	0.370
0.282	0.526	0.427	0.409	1.06	0.358
0.285	0.535	0.430	0.413	1.09	0.351
0.288	0.540	0.440	0.411	1.20	0.346
0.291	0.536	0.450	0.420	1.26	0.346
0.295	0.532	0.460	0.425	1.30	0.343
0.300	0.522	0.470	0.430	1.40	0.340
0.302	0.520	0.480	0.434	1.55	0.340
0.303	0.513	0.490	0.439	1.60	0.339
0.308	0 503	0.500	0.435	1.68	0.338
0.309	0.497	0.520	0.435	1.80	0.335
0.311	0.490	0.540	0.434	1.86	0.334
0.315	0.486	0.560	0.436	2.00	0.333
0.320	0.475	0.58	0.442	2.15	0.330
0.327	0.463	0.60	0.448	2.38	0.329
0.333	0.452	0.62	0.454		
0.340	0.448	0.63	0.453		

[a]After Ref. 1.

VI. Indium Phosphide

The reflectance values in Table XVII are taken from a measurement of Cardona[1] on etched samples. The wavelength range from 0.062 to 1.24 microns in this measurement is sufficient for a calculation of the optical constants by Kramers–Kronig analysis. Their values are listed in Table XVI for the wavelengths between 0.062 and 0.885 microns.

The absorption coefficient in the region of the fundamental absorption edge is measured at a resolution of better than 1×10^{-3} eV by Newman.[2] The absorption depends upon the impurity content of the material below

$\alpha \sim 500\ \text{cm}^{-1}$. The results obtained at the purest sample, an n-type specimen of $5 \times 10^{15}\ \text{cm}^{-3}$ carrier concentration, are listed in Table XVI.

Indium phosphide is practically transparent between the edge and approximately 13 microns. The doublet absorption band beyond this region has been studied in transmission by Reynolds *et al.*[3] Using polycrystalline wafers cut from n-type 30 ohm-cm material, the absorption coefficient was calculated from the ratio of transmitted to incident intensity, allowing for reflection losses.

A very recent measurement by Pettit and Turner[4] presents values for the refractive index obtained by the prism method between 1 and 2 microns and at 298° and 77°K. A prism with an apex angle of approximately 15 degrees was cut from n-type material of a carrier concentration of $5 \times 10^{16}\ \text{cm}^{-3}$, and the refractive index was determined from the minimum deviation. A precision of ± 0.0003 in the index values is claimed. A least-squares fit of the data can be obtained to within 0.0007, using the equation

$$n^2 = \frac{A + B\lambda^2}{(\lambda^2 - C^2)}, \tag{8}$$

where $A = 7.255$ (7.781), $B = 2.316$ (1.661), and $C^2 = 0.3922 \times 10^8$ (0.4397×10^8) must be used for 298°K (77°K), if the wavelength λ is expressed in angstroms.

From 5 to 15 microns, Oswald's[5] values for the refractive index are used in Table XVI.

Cardona[6] has determined the temperature dependence of the refractive index by measuring the interference patterns of thin single-crystal films at different temperatures. He finds for an n-type sample of $10^{17}\ \text{cm}^{-3}$ carrier concentration

$$\frac{1}{n}\frac{dn}{dT} = (2.7 \pm 0.3) \times 10^{-5}\ ^\circ\text{C}^{-1}. \tag{9}$$

REFERENCES

1. M. Cardona, *J. Appl. Phys.* **36**, 2181 (1965); **32**, 958 (1961).
2. R. Newman, *Phys. Rev.* **111**, 1518 (1958).
3. W. N. Reynolds, M. T. Lilburne, and R. M. Dell, *Proc. Phys. Soc.* (*London*) **71**, 416 (1958).
4. G. D. Pettit and W. J. Turner, *J. Appl. Phys.* **36**, 2081 (1965).
5. F. Oswald, *Z. Naturforsch.* **9a**, 181 (1954).
6. M. Cardona, *Proc. Intern. Conf. Semicond. Phys., Prague, 1960* p. 388. Czech. Acad. Sci., Prague and Academic Press, New York, 1961.

TABLE XVI

REFRACTIVE INDEX n AND EXTINCTION COEFFICIENT k OF INDIUM PHOSPHIDE AS A FUNCTION OF WAVELENGTH λ

λ (microns)	n	k	Reference	λ (microns)	n	k	Reference
0.062	0.793	0.494	(1)	0.159	0.984	1.627	(1)
0.064	0.815	0.499	(1)	0.161	1.000	1.664	(1)
0.065	0.834	0.493	(1)	0.163	1.022	1.700	(1)
0.067	0.843	0.487	(1)	0.165	1.046	1.736	(1)
0.069	0.846	0.477	(1)	0.167	1.072	1.771	(1)
0.071	0.840	0.469	(1)	0.170	1.100	1.812	(1)
0.073	0.824	0.454	(1)	0.172	1.136	1.847	(1)
0.075	0.785	0.457	(1)	0.175	1.174	1.882	(1)
0.077	0.742	0.491	(1)	0.177	1.215	1.915	(1)
0.079	0.719	0.529	(1)	0.180	1.261	1.941	(1)
0.083	0.695	0.574	(1)	0.182	1.307	1.966	(1)
0.085	0.675	0.645	(1)	0.185	1.354	1.986	(1)
0.089	0.688	0.706	(1)	0.188	1.402	2.004	(1)
0.092	0.701	0.765	(1)	0.191	1.453	2.010	(1)
0.095	0.726	0.820	(1)	0.194	1.496	2.008	(1)
0.099	0.754	0.861	(1)	0.197	1.526	1.991	(1)
0.103	0.771	0.899	(1)	0.200	1.525	1.982	(1)
0.108	0.781	0.946	(1)	0.203	1.508	2.005	(1)
0.113	0.793	0.996	(1)	0.207	1.500	2.063	(1)
0.118	0.797	1.056	(1)	0.210	1.516	2.130	(1)
0.124	0.806	1.154	(1)	0.214	1.544	2.191	(1)
0.125	0.820	1.172	(1)	0.217	1.573	2.267	(1)
0.126	0.832	1.185	(1)	0.221	1.616	2.349	(1)
0.128	0.840	1.198	(1)	0.225	1.668	2.442	(1)
0.129	0.847	1.210	(1)	0.229	1.737	2.553	(1)
0.130	0.852	1.225	(1)	0.234	1.834	2.675	(1)
0.132	0.859	1.237	(1)	0.238	1.960	2.801	(1)
0.133	0.861	1.253	(1)	0.243	2.132	2.982	(1)
0.135	0.865	1.269	(1)	0.248	2.451	3.166	(1)
0.136	0.868	1.287	(1)	0.253	2.885	3.144	(1)
0.138	0.872	1.304	(1)	0.258	3.335	3.039	(1)
0.139	0.874	1.324	(1)	0.264	3.729	2.635	(1)
0.141	0.875	1.346	(1)	0.269	3.849	2.117	(1)
0.142	0.877	1.375	(1)	0.275	3.655	1.691	(1)
0.144	0.885	1.403	(1)	0.282	3.473	1.549	(1)
0.146	0.894	1.433	(1)	0.288	3.347	1.468	(1)
0.148	0.909	1.458	(1)	0.295	3.248	1.415	(1)
0.149	0.919	1.486	(1)	0.302	3.162	1.389	(1)
0.151	0.934	1.512	(1)	0.310	3.105	1.392	(1)
0.153	0.947	1.539	(1)	0.318	3.054	1.401	(1)
0.155	0.960	1.566	(1)	0.326	3.027	1.440	(1)
0.157	0.973	1.594	(1)	0.335	3.024	1.489	(1)

TABLE XVI—*continued*

λ (microns)	n	k	Reference	λ (microns)	n	k	Reference
0.344	3.047	1.550	(1)	0.965	—	3.92×10^{-5}	(2)
0.354	3.082	1.622	(1)	0.968	—	2.46×10^{-5}	(2)
0.364	3.192	1.747	(1)	0.970	3.351	—	(4)
0.375	3.441	1.857	(1)	0.972	—	1.66×10^{-5}	(2)
0.387	3.835	1.804	(1)	0.975	3.346	—	(4)
0.399	4.100	1.439	(1)	0.975	—	1.13×10^{-5}	(2)
0.413	4.083	1.056	(1)	1.00	3.327	—	(4)
0.427	3.982	0.816	(1)	1.10	3.268	—	(4)
0.443	3.833	0.670	(1)	1.20	3.231	—	(4)
0.459	3.754	0.599	(1)	1.30	3.205	—	(4)
0.477	3.675	0.531	(1)	1.40	3.186	—	(4)
0.496	3.621	0.480	(1)	1.50	3.172	—	(4)
0.517	3.567	0.430	(1)	1.60	3.161	—	(4)
0.539	3.521	0.389	(1)	1.70	3.152	—	(4)
0.563	3.472	0.358	(1)	1.80	3.145	—	(4)
0.590	3.450	0.334	(1)	1.90	3.139	—	(4)
0.620	3.430	0.298	(1)	2.00	3.134	—	(4)
0.652	3.410	0.253	(1)	5.00	3.08	—	(5)
0.689	—	0.206	(1)	6.00	3.07	—	(5)
0.729	—	0.176	(1)	7.00	3.07	—	(5)
0.775	—	0.163	(1)	8.00	3.06	—	(5)
0.826	—	0.140	(1)	9.00	3.06	—	(5)
0.885	—	9.06×10^{-2}	(1)	10.00	3.05	—	(5)
0.921	—	5.71×10^{-2}	(2)	12.00	3.05	—	(5)
0.925	3.396	—	(4)	12.00	—	5.27×10^{-4}	(3)
0.925	—	3.55×10^{-2}	(2)	13.08	—	6.67×10^{-4}	(3)
0.928	—	2.04×10^{-2}	(2)	14.00	3.04	—	(5)
0.930	3.390	—	(4)	14.00	—	8.86×10^{-4}	(3)
0.930	—	1.09×10^{-2}	(2)	14.40	—	1.28×10^{-3}	(3)
0.935	3.385	—	(4)	14.85	3.03	—	(5)
0.935	—	5.90×10^{-3}	(2)	14.85	—	3.00×10^{-3}	(3)
0.940	3.379	—	(4)	15.00	—	3.71×10^{-3}	(3)
0.940	—	3.18×10^{-3}	(2)	15.24	—	5.25×10^{-3}	(3)
0.942	—	1.71×10^{-3}	(2)	15.32	—	6.17×10^{-3}	(3)
0.945	3.374	—	(4)	15.45	—	6.26×10^{-3}	(3)
0.945	—	9.67×10^{-4}	(2)	15.52	—	5.63×10^{-3}	(3)
0.950	3.369	—	(4)	15.74	—	5.22×10^{-3}	(3)
0.950	—	5.27×10^{-4}	(2)	15.85	—	6.13×10^{-3}	(3)
0.953	—	2.81×10^{-4}	(2)	16.00	—	7.12×10^{-3}	(3)
0.955	3.364	—	(4)	16.14	—	7.46×10^{-3}	(3)
0.957	—	1.45×10^{-4}	(2)	16.21	—	6.67×10^{-3}	(3)
0.960	3.359	—	(4)	16.28	—	5.16×10^{-3}	(3)
0.960	—	7.39×10^{-5}	(2)	16.39	—	3.33×10^{-3}	(3)
0.965	3.355	—	(4)	16.55	—	2.31×10^{-3}	(3)

TABLE XVI—*continued*

λ (microns)	n	k	Reference	λ (microns)	n	k	Reference
17.00	—	1.77×10^{-3}	(3)	20.00	—	7.94×10^{-3}	(3)
18.00	—	1.81×10^{-3}	(3)	20.19	—	9.49×10^{-3}	(3)
18.93	—	2.32×10^{-3}	(3)	20.34	—	1.08×10^{-2}	(3)
19.51	—	3.84×10^{-3}	(3)	20.42	—	1.15×10^{-2}	(3)
19.62	—	4.73×10^{-3}	(3)	20.57	—	1.30×10^{-2}	(3)
19.78	—	6.02×10^{-3}	(3)				

TABLE XVII

REFLECTANCE R OF INDIUM PHOSPHIDE AS A FUNCTION OF WAVELENGTH λ[a]

λ (microns)	R	λ (microns)	R	λ (microns)	R
0.059	0.091	0.133	0.316	0.194	0.417
0.060	0.087	0.135	0.320	0.197	0.410
0.062	0.083	0.136	0.325	0.200	0.408
0.064	0.080	0.138	0.330	0.203	0.415
0.065	0.075	0.139	0.336	0.207	0.429
0.067	0.072	0.141	0.343	0.210	0.442
0.069	0.069	0.144	0.359	0.214	0.452
0.071	0.068	0.146	0.366	0.217	0.465
0.075	0.075	0.148	0.370	0.221	0.477
0.077	0.094	0.149	0.376	0.225	0.490
0.079	0.111	0.151	0.380	0.229	0.504
0.083	0.132	0.153	0.385	0.234	0.517
0.085	0.162	0.155	0.390	0.238	0.528
0.089	0.178	0.157	0.395	0.243	0.544
0.093	0.194	0.159	0.407	0.248	0.553
0.095	0.205	0.161	0.409	0.253	0.538
0.099	0.210	0.163	0.414	0.258	0.524
0.103	0.218	0.165	0.419	0.264	0.491
0.108	0.232	0.167	0.423	0.269	0.450
0.113	0.246	0.170	0.428	0.275	0.404
0.118	0.266	0.172	0.430	0.282	0.380
0.124	0.298	0.175	0.432	0.288	0.364
0.125	0.300	0.177	0.433	0.295	0.352
0.126	0.301	0.180	0.432	0.302	0.343
0.128	0.303	0.182	0.431	0.310	0.339
0.129	0.305	0.185	0.429	0.318	0.336
0.130	0.309	0.188	0.427	0.326	0.338
0.132	0.311	0.191	0.422	0.335	0.343

TABLE XVII—*continued*

λ (microns)	R	λ (microns)	R	λ (microns)	R
0.344	0.351	0.477	0.336	0.729	0.290
0.354	0.361	0.496	0.329	0.775	0.286
0.375	0.406	0.517	0.322	0.826	0.285
0.387	0.424	0.539	0.316	0.885	0.282
0.399	0.416	0.563	0.310	0.953	0.273
0.413	0.394	0.590	0.307	1.033	0.269
0.427	0.375	0.620	0.304	1.126	0.265
0.443	0.356	0.652	0.301	1.240	0.263
0.459	0.346	0.689	0.295		

[a] After Ref. 1.

VII. Indium Arsenide

As in the case of GaAs, Philipp and Ehrenreich have determined the optical constants of InAs in the wavelength region from 0.05 to 2.5 microns from reflectance measurements, using a dispersion relation between the phase and the magnitude of the reflectance.[1–4] The computation of both optical constants requires the reflectance spectrum to be known for all wavelengths. Reasonably accurate values for n and k can be obtained, however, if the measurement includes most of the strong structure at higher photon energies and if proper consideration is given to extrapolation procedures beyond this range. Both conditions seem fulfilled for Philipp and Ehrenreich's measurements. Morrison[5] has used a similar analysis to evaluate his careful reflectance measurements over a wavelength region that extends to only 0.2 micron. As a result of a range that is limited especially toward higher photon energies, the optical constants are sensitive to the extrapolation procedure, which suggests that plasma absorption in particular contributes to the dispersion integral outside the range of Morrison's measurement.

Philipp and Ehrenreich do not identify their material. It can be assumed, however, that in the wavelength range between 0.05 and 1.38 microns in which their results are listed, the optical constants do not depend upon type and density of the carriers. The surface treatment is of importance. As an empirical rule, the surface treatment that produces the highest reflectance over a wide spectral range can be considered the best. This rule is confirmed by Morrison's study of different polishing procedures with respect to the resulting reflectance. His highest reflectance data, after polishing on a silk lap, are only 3 to 5% lower than Philipp and Ehrenreich's results on

etched samples, but are, on the average, 4 to 5% higher than the values Tauc and Abraham[6] report.

The wavelength region of the fundamental absorption edge is the subject of a number of optical investigations.[7–11] Since the type and density of impurities affect the shape and the position of this edge, it is essential to measure the optical constants on the purest material available. Dixon and Ellis[12] have been able to explain many of the previous contradictory results by measuring the absorption properties of material that contained only 3.8×10^{16} carriers per cm^{-3}, as determined from room-temperature Hall measurements. The absorption coefficient α was calculated from the transmission T, using the relationship given as Eq. (3) in the GaP section. Dixon and Ellis have found that for nondegenerate material, absorption coefficients larger than $10^3\ cm^{-1}$ obey satisfactorily the following functional relation to the photon energy E:

$$\alpha^2 = 3.0 \times 10^8(E - 0.35) \quad cm^{-2}. \tag{10}$$

Absorption coefficients below $10^3\ cm^{-1}$ and down to at least $3\ cm^{-1}$ depend exponentially upon E in the following form:

$$\alpha = C \exp(E/kT_{\text{eff}}), \tag{11}$$

where 80°K should be used for the effective temperature T_{eff}, if room-temperature values for α are to be calculated.

Electron transitions between the light- and the heavy-hole band contribute to the optical absorption in p-type InAs on the long-wavelength side of the fundamental absorption edge. The peak of the absorption occurs at 7.3 microns, and its magnitude is proportional to the hole concentration, the absorption coefficient per hole being $5.4 \times 10^{-16}\ cm^2$.

In n-type material, electron transitions within the conduction band control the optical absorption from the edge region on to around 23 microns, where the first lattice-absorption band occurs. The absorption coefficient is proportional to the carrier concentration, every electron contributing $4.7 \times 10^{-17}\ cm^{-1}$ to the absorption coefficient at 9 microns.[13]

Lorimor and Spitzer[14] have analyzed transmission interference fringes with classical dispersion theory and have plotted the peak position of each fringe on an ordinary order-number scale. Assuming that the following equation for the order number p holds, the refractive index is determined from

$$p = \frac{2nt}{\lambda}, \tag{12}$$

where t is the thickness (0.0138 cm) of the n-type sample $2 \times 10^{16}\,\mathrm{cm}^{-3}$ carrier concentration. Good fit is reported between experimental data and the following relation derived from classical dispersion theory:

$$n^2 = 11.1 + \frac{0.71}{1 - (1/3922\lambda)^2} + \frac{2.75}{1 - (1/218.9\lambda)^2} - 6 \times 10^4 \lambda^2 \qquad (13)$$

where λ is in cm and the three last terms result from the contribution of (1) the band-edge resonance, (2) the reststrahlen band, and (3) the free-carrier susceptibility.

REFERENCES

1. H. R. Philipp and H. Ehrenreich, *Phys. Rev. Letters* **8**, 92 (1962).
2. H. R. Philipp and H. Ehrenreich, *Phys. Rev.* **129**, 1550 (1963).
3. H. Ehrenreich, H. R. Philipp, and J. C. Phillips, *Phys. Rev. Letters* **8**, 59 (1962).
4. H. R. Philipp and H. Ehrenreich, Chapter 4 of this volume.
5. R. E. Morrison, *Phys. Rev.* **124**, 1314 (1961).
6. J. Tauc and A. Abraham, *Proc. Intern. Conf. Semicond. Phys., Prague, 1960* p. 375. Czech. Acad. Sci., Prague and Academic Press, New York, 1961.
7. H. J. Hrostowski and M. Tanenbaum, *Physica* **20**, 1065 (1954).
8. F. Oswald, *Z. Naturforsch.* **10a**, 927 (1955); **14a**, 374 (1959).
9. F. Stern and R. M. Talley, *Phys. Rev.* **100**, 1638 (1955).
10. W. G. Spitzer and H. Y. Fan, *Phys. Rev.* **106**, 882 (1957).
11. F. Matossi, *Z. Naturforsch.* **13a**, 767 (1958).
12. J. R. Dixon and J. M. Ellis, *Phys. Rev.* **123**, 1560 (1961).
13. J. R. Dixon, *Proc. Intern. Conf. Semicond. Phys., Prague, 1960* p. 366. Czech. Acad. Sci., Prague and Academic Press, New York, 1961.
14. O. G. Lorimor and W. G. Spitzer, *J. Appl. Phys.* **36**, 1841 (1965).

TABLE XVIII

REFRACTIVE INDEX n AND EXTINCTION COEFFICIENT k OF INDIUM ARSENIDE AS A FUNCTION OF WAVELENGTH λ

λ (microns)	n	k	Reference	λ (microns)	n	k	Reference
0.049	1.139	0.168	(1–4)	0.451	3.980	1.865	(1–4)
0.051	1.135	0.195	(1–4)	0.459	4.087	1.748	(1–4)
0.054	1.135	0.207	(1–4)	0.468	4.119	1.644	(1–4)
0.056	1.133	0.215	(1–4)	0.477	4.192	1.618	(1–4)
0.059	1.131	0.222	(1–4)	0.496	4.489	1.452	(1–4)
0.062	1.125	0.225	(1–4)	0.517	4.558	1.047	(1–4)
0.064	1.120	0.224	(1–4)	0.563	4.320	0.554	(1–4)
0.067	1.110	0.215	(1–4)	0.620	4.101	0.348	(1–4)
0.070	1.047	0.189	(1–4)	0.689	3.934	0.231	(1–4)
0.077	0.948	0.272	(1–4)	0.775	3.800	0.157	(1–4)
0.082	0.894	0.336	(1–4)	0.885	3.696	0.109	(1–4)
0.089	0.829	0.426	(1–4)	1.03	3.613	0.076	(1–4)
0.095	0.766	0.563	(1–4)	1.24	3.548	0.051	(1–4)
0.103	0.745	0.727	(1–4)	1.38	3.516	0.047	(1–4)
0.108	0.751	0.830	(1–4)	1.68	—	0.200	(12)
0.112	0.775	0.905	(1–4)	1.80	—	0.185	(12)
0.123	0.835	1.071	(1–4)	2.00	—	0.168	(12)
0.136	0.890	1.260	(1–4)	2.07	—	0.162	(12)
0.153	0.967	1.552	(1–4)	2.25	—	0.149	(12)
0.172	1.184	1.889	(1–4)	2.50	—	0.133	(12)
0.180	1.332	1.998	(1–4)	2.76	—	0.119	(12)
0.188	1.483	2.020	(1–4)	3.00	—	0.102	(12)
0.195	1.583	2.120	(1–4)	3.35	—	0.064	(12)
0.211	1.782	2.011	(1–4)	3.40	—	0.052	(12)
0.225	1.765	2.202	(1–4)	3.44	—	0.037	(12)
0.248	1.987	2.647	(1–4)	3.50	—	0.018	(12)
0.259	2.288	3.086	(1–4)	3.65	—	0.002	(12)
0.264	2.617	3.264	(1–4)	3.74	3.52	—	(14)
0.269	3.060	3.274	(1–4)	4.00	3.51	—	(14)
0.282	3.800	2.735	(1–4)	5.00	3.46	—	(14)
0.310	3.678	1.508	(1–4)	6.67	3.45	—	(14)
0.335	3.359	1.340	(1–4)	10.0	3.42	—	(14)
0.344	3.271	1.363	(1–4)	14.3	3.39	—	(14)
0.354	3.227	1.411	(1–4)	16.7	3.38	—	(14)
0.387	3.184	1.547	(1–4)	20.0	3.35	—	(14)
0.413	3.331	1.787	(1–4)	25.0	3.26	—	(14)
0.443	3.817	1.954	(1–4)	33.3	2.95	—	(14)

TABLE XIX

REFLECTANCE R OF INDIUM ARSENIDE AS A FUNCTION OF WAVELENGTH λ[a]

λ (microns)	R	λ (microns)	R	λ (microns)	R
0.049	0.010	0.153	0.384	0.443	0.435
0.052	0.012	0.172	0.432	0.451	0.437
0.054	0.013	0.180	0.435	0.459	0.435
0.056	0.014	0.188	0.421	0.468	0.430
0.059	0.015	0.195	0.433	0.477	0.433
0.062	0.015	0.211	0.395	0.496	0.443
0.064	0.014	0.225	0.435	0.517	0.430
0.067	0.013	0.248	0.501	0.563	0.396
0.070	0.009	0.259	0.550	0.620	0.373
0.077	0.020	0.264	0.559	0.689	0.355
0.082	0.034	0.269	0.550	0.775	0.341
0.089	0.060	0.282	0.502	0.885	0.330
0.095	0.108	0.310	0.391	1.033	0.321
0.103	0.166	0.335	0.354	1.240	0.314
0.108	0.200	0.344	0.349	1.377	0.311
0.112	0.219	0.354	0.350	2.066	0.305
0.123	0.260	0.387	0.360	3.099	0.302
0.136	0.310	0.413	0.393	6.198	0.300

[a] After Refs. 1–4.

VIII. Indium Antimonide

Selected values of the optical constants of indium antimonide are given in Table XX. Table XXI gives the reflectance values in regions where n and k were determined using a dispersion analysis. In the vacuum ultraviolet, ultraviolet, visible, and near infrared wavelength regions, n and k were obtained from the normal-incidence reflectance measurements of Philipp and Ehrenreich.[1–3] At wavelengths longer than 0.2 micron, where a comparison can be made with other reflectance data,[4–6] the values reported by Philipp and Ehrenreich are in general slightly higher than other values. It is probable that this difference, which becomes more pronounced at the shortest wavelengths at which comparisons can be made, is caused primarily by the different sample-preparation techniques used. Philipp and Ehrenreich made their measurements on etched single-crystal samples. In this way samples can be obtained whose surface structure is virtually undistorted.[7] However, surface roughness and the very thin oxide film present may still cause the reported reflectance values to be somewhat too low in the vacuum ultraviolet. Fortunately, the positions of the various peaks and shoulders in

the reflectance spectrum, which are of particular theoretical interest, should be relatively unaffected. Of these peaks, the splitting of the 2-eV peak has received the most study.[3,5,8–10]

The values of n given in Table XX in the 0.05- to 2-micron region, and those of k in the 0.05- to 1.5-micron region, were obtained by Philipp and Ehrenreich from their reflectance data by use of a Kramers-Kronig analysis. Although no values of n are tabulated between 2.07 and 7.87 microns, where the first direct measurements of n begin,[11] the agreement between the values of n obtained from the dispersion analysis and that directly measured is good and interpolation is thus possible.

Direct measurements of k have been reported at considerably shorter wavelengths than for n. Values reported by Moss *et al.*[11] and at longer wavelengths by Kurnick and Powell[12] are tabulated for k in Table XX. Moss *et al.* describe their samples as having a carrier concentration of $2.0 \times 10^{16}\,\mathrm{cm}^{-3}$ at 293°K. Kurnick and Powell determined the p-type impurity concentration of their samples at 78°K as $2.75 \times 10^{16}\,\mathrm{cm}^{-3}$ from the Hall coefficient. Somewhat higher k values differing from those tabulated by about a factor of two, have been reported by Gobeli and Fan,[13] and slightly lower values have been reported by Moss *et al.*,[11] Roberts and Quarrington,[14] and Oswald and Schade.[15] The value of k in this region is extremely sensitive to impurity concentration, sample preparation, and temperature. In addition to the usual free-carrier effects, InSb shows a pronounced Burstein shift of the absorption edge.[16–18] Conversely, for heavily doped compensated samples a shift to longer wavelengths can occur.[12,14] In the attempt to understand these and other questions, rather extensive studies of the dependence of the absorption coefficient on temperature and doping in the neighborhood of the absorption edge have been carried out.[4,11–31] Measurements from 5°K to 500°K have been reported, and material of a wide range of doping of either type has been studied. An emittance study has been made,[32] neutron-irradiated InSb has been studied,[33] and investigations of the absorption edge of InSb–GaSb alloys have been carried out.[34–37] Recently, the nonlinear optical susceptibility describing the second polarization of InSb was also measured within the fundamental absorption edge.[38]

In contrast to k, the value of n is relatively insensitive to moderate impurity concentrations at wavelengths longer than the absorption edge, and good agreement is found between the different measurements.[11,15] The data reported by Moss *et al.*,[11] which are given in Table XX, were obtained using an interferometric fringe counting technique. The uncertainty in n is given as $\pm 0.5\%$. The change in n with temperature in this region has been investigated by Cardona.[39] It is more complicated than that typically found for III–V compounds, since the variation of the number of free

carriers with temperature causes $(1/n)\,dn/dT$ to have a spectral dependence. Since $n \gg k$, the index of refraction is given by

$$n^2 = 1 + 4\pi\chi - \frac{4\pi Ne^2}{m^*\omega^2}, \tag{14}$$

where χ is the electric polarizability arising from other than free carriers, N is the carrier concentration, e the electronic charge, m^* the carrier effective mass, and ω the angular frequency of the radiation. Since both electrons and holes are present, $1/m^* = 1/m_e + 1/m_h$ where m_e and m_h are the electron and hole effective masses respectively. For InSb, $m_h = 10\,m_e$, so that m^* is primarily determined by m_e. At 419°K and 368°K, m^* was found to be $0.024m$, and at 297°K, $0.0225m$, where m is the free-electron mass. From Eq. (14),

$$\frac{1}{n}\frac{dn}{dT} = \frac{2\pi}{n^2}\frac{d\chi}{dT} - \frac{2\pi e^2}{n^2\omega^2}\frac{d(N/m^*)}{dT}. \tag{15}$$

Cardona found that $(2\pi/n^2)(d\chi/dT) = (11.9 \pm 0.2) \times 10^{-5}\,°C^{-1}$, independent of wavelength or temperature in the region tested. Since the dependence of the intrinsic carrier concentration N on temperature can be assumed,[40] the temperature variation of n can then be calculated.

At wavelengths longer than 20 microns the optical constants of InSb are determined primarily by lattice and free-carrier absorption. Numerous investigations in this region have been reported, many of them at cryogenic temperatures where the contribution from free carriers and thermal broadening of the lattice absorption lines is reduced.[23,24,41–45] Several studies at room temperature, however, have also been reported.[23,24,41,45,46] Values of n and k given in Table XX for the 20–45 micron wavelength region were reported by Yoshinaga and Oetjen[41] from room-temperature reflection and transmission measurements on n-type material of $6 \times 10^{15}\,cm^{-3}$ carrier concentration at 83°K.

The values of R given in Table XXI in the 20–45 micron wavelength region were reported by Yoshinaga and Oetjen. At wavelengths longer than 45 microns, where scattered light is extremely difficult to eliminate in conventional far-infrared spectrometers, Sanderson's[45] reflectance data are given. These data were obtained using the same samples used by Yoshinaga and Oetjen but making the measurements with an interferometric modulation spectrometer. Much better spectral purity in the far infrared may be obtained in this way than is possible using more conventional techniques. Sanderson found that his reflectance data could be fit quite well by a classical dispersion analysis. The following equations were used:

$$n^2 - k^2 = \varepsilon_\infty + (\varepsilon_0 - \varepsilon_\infty)\frac{1 - (\nu/\nu_t)^2}{[1 - (\nu/\nu_t)^2]^2 + (\gamma\nu/\nu_t)^2} - \frac{A}{\nu^2 + G^2}, \quad (16)$$

$$2nk = (\varepsilon_0 - \varepsilon_\infty)\frac{\gamma\nu/\nu_t}{[1 - (\nu/\nu_t)^2]^2 + (\gamma\nu/\nu_t)^2} + \frac{AG}{\nu(\nu^2 + G^2)}, \quad (17)$$

where ν is the frequency in cm^{-1} and $A = 10.28 \times 10^4\ cm^{-2}$, $G = 10.7\ cm^{-1}$, $\nu_t = 179.1\ cm^{-1}$, $\varepsilon_0 = 17.72$, $\varepsilon_\infty = 15.68$, and $\gamma = 0.016$. By substituting these parameters in Eqs. (16) and (17) the optical constants n and k can be calculated at any desired wavelength in the 50–500 micron wavelength region.

REFERENCES

1. H. R. Philipp and H. Ehrenreich, *Phys. Rev.* **129**, 1550 (1963).
2. H. R. Philipp and H. Ehrenreich, *Phys. Rev. Letters* **8**, 92 (1962).
3. H. Ehrenreich, H. R. Philipp, and J. C. Phillips, *Phys. Rev. Letters* **8**, 59 (1962).
4. R. E. Morrison, *Phys. Rev.* **124**, 1314 (1961).
5. J. Tauc and A. Abraham, *Proc. Intern. Conf. Semicond. Phys., Prague, 1960* p. 375. Czech. Acad. Sci., Prague and Academic Press, New York, 1961.
6. N. I. Kurdiani, *Fiz. Tverd. Tela* **5**, 1797 (1963) [*English Transl.: Soviet Phys.-Solid State* **5**, 1310 (1964)].
7. T. M. Donovan and B. O. Seraphin, *J. Electrochem. Soc.* **109**, 877 (1962).
8. J. Tauc and E. Antončik, *Phys. Rev. Letters* **5**, 253 (1960).
9. F. Lukeš and E. Schmidt, *Proc. Intern. Conf. Phys. Semicond., Exeter, 1962* p. 389. Inst. of Phys. and Phys. Soc., London, 1962.
10. M. Cardona and G. Harbeke, *Phys. Rev. Letters* **8**, 90 (1962).
11. T. S. Moss, S. D. Smith, and T. D. F. Hawkins, *Proc. Phys. Soc. (London)* **B70**, 776 (1957).
12. S. W. Kurnick and J. M. Powell, *Phys. Rev.* **116**, 597 (1959).
13. G. W. Gobeli and H. Y. Fan, *Phys. Rev.* **119**, 613 (1960).
14. V. Roberts and J. E. Quarrington, *J. Electron.* **1**, 152 (1955).
15. F. Oswald and R. Schade, *Z. Naturforsch.* **9a**, 611 (1954).
16. M. Tanenbaum and H. B. Briggs, *Phys. Rev.* **91**, 1561 (1953).
17. E. Burstein, *Phys. Rev.* **93**, 632 (1954).
18. H. J. Hrostowski, G. H. Wheatley, and W. F. Flood, Jr., *Phys. Rev.* **95**, 1683 (1954).
19. D. G. Avery, D. W. Goodwin, W. D. Lawson, and T. S. Moss, *Proc. Phys. Soc. (London)* **67B**, 761 (1954).
20. R. G. Breckenridge, R. F. Blunt, W. R. Hosler, H. P. R. Frederikse, J. H. Becker, and W. Oshinsky, *Physica* **20**, 1073 (1954).
21. R. G. Breckenridge, R. F. Blunt, W. R. Hosler, H. P. R. Frederikse, J. H. Becker, and W. Oshinsky, *Phys. Rev.* **96**, 571 (1954).
22. T. S. Moss, *Proc. Phys. Soc. (London)* **67B**, 775 (1954).
23. W. Kaiser and H. Y. Fan, *Phys. Rev.* **98**, 966 (1955).
24. W. G. Spitzer and H. Y. Fan, *Phys. Rev.* **99**, 1893 (1955).
25. E. Blount, J. Callaway, M. Cohen, W. Dumke, and J. Phillips, *Phys. Rev.* **101**, 563 (1956).
26. W. Goodwin, *Rept. Meeting Semicond., Rugby, 1956* p. 137. Inst. of Phys. and Phys. Soc., London, 1956.

27. T. S. Moss, T. Hawkins, and S. D. Smith, *Rept. Meeting Semicond., Rugby, 1956* p. 133. Inst. of Phys. and Phys. Soc., London, 1956.
28. W. G. Spitzer and H. Y. Fan, *Phys. Rev.* **106**, 882 (1957).
29. G. Bate and K. N. R. Taylor, *J. Appl. Phys.* **31**, 991 (1960).
30. F. R. Kessler and E. Sutter, *Z. Naturforsch.* **16a**, 1173 (1961).
31. R. F. Potter and G. G. Kretschmar, *J. Opt. Soc. Am.* **51**, 693 (1961).
32. T. S. Moss and T. D. H. Hawkins, *Proc. Phys. Soc. (London)* **72**, 270 (1958).
33. N. I. Kurdiani, *Fiz. Tverd. Tela* **5**, 2022 (1963) [*English Transl.*: *Soviet Phys.-Solid State* **5**, 1477 (1964)].
34. J. S. Blakemore, *Can. J. Phys.* **35**, 91 (1957).
35. V. I. Ivanov-Omskii and B. T. Kolomiets, *Dokl. Akad. Nauk SSSR* **127**, 135 (1959) [*English Transl.*: *Proc. Acad. Sci. USSR, Phys. Chem. Sect.* **127**, 553 (1959)].
36. V. I. Ivanov-Omskii and B. T. Kolomiets, *Fiz. Tverd. Tela* **1**, 568 (1959) [*English Transl.*: *Soviet Phys.-Solid State* **1**, 512 (1959)].
37. J. C. Woolley, J. A. Evans, and C. M. Gillet, *Proc. Phys. Soc. (London)* **74**, 244 (1959).
38. N. Bloembergen, R. K. Chang, J. Ducuing, and P. Lallemand, *in* "Physics of Semiconductors" (Proc. 7th Intern. Conf.), p. 121. Dunod, Paris, and Academic Press, New York, 1964.
39. M. Cardona, *Proc. Intern. Conf. Semicond. Phys. Prague, 1960* p. 388. Czech. Acad. Sci., Prague and Academic Press, New York, 1961.
40. H. J. Hrostowski, F. J. Morin, T. H. Geballe, and G. H. Wheatley, *Phys. Rev.* **100**, 1672 (1955).
41. H. Yoshinaga and R. A. Oetjen, *Phys. Rev.* **101**, 526 (1956).
42. S. J. Fray, F. A. Johnson, and R. H. Jones, *Proc. Phys. Soc. (London)* **76**, 939 (1960).
43. F. A. Johnson, S. J. Fray, and R. H. Jones, *Proc. Intern. Conf. Semicond. Phys., Prague, 1960* p. 349. Czech. Acad. Sci., Prague and Academic Press, New York, 1961.
44. M. Hass and B. W. Henvis, *J. Phys. Chem. Solids* **23**, 1099 (1962).
45. R. B. Sanderson, *J. Phys. Chem. Solids* **26**, 803 (1965).
46. H. Yoshinaga, *Phys. Rev.* **100**, 753 (1955).

TABLE XX

REFRACTIVE INDEX n AND EXTINCTION COEFFICIENT k OF INDIUM ANTIMONIDE AS A FUNCTION OF WAVELENGTH λ

λ (microns)	n	k	Reference	λ (microns)	n	k	Reference
0.049	1.15	0.15	(1)	0.656	4.71	1.88	(1)
0.052	1.15	0.18	(1)	0.677	5.08	1.65	(1)
0.054	1.15	0.19	(1)	0.689	5.13	1.37	(1)
0.056	1.16	0.20	(1)	0.708	5.06	1.07	(1)
0.059	1.17	0.21	(1)	0.775	4.72	0.60	(1)
0.062	1.17	0.21	(1)	0.886	4.40	0.40	(1)
0.065	1.18	0.20	(1)	1.03	4.24	0.32	(1)
0.069	1.15	0.18	(1)	1.24	4.15	0.26	(1)
0.073	1.11	0.16	(1)	1.55	4.08	0.20	(1)
0.080	1.02	0.17	(1)	1.60	—	0.18	(11)
0.083	0.97	0.19	(1)	1.80	—	0.17	(11)
0.089	0.88	0.26	(1)	2.00	—	0.17	(11)
0.095	0.80	0.37	(1)	2.07	4.03	—	(1)
0.103	0.75	0.51	(1)	2.50	—	0.15	(11)
0.113	0.72	0.69	(1)	3.00	—	0.13	(11)
0.124	0.74	0.88	(1)	3.50	—	0.12	(11)
0.138	0.80	1.08	(1)	4.00	—	0.11	(11)
0.155	0.88	1.32	(1)	4.50	—	0.10	(11)
0.163	0.94	1.41	(1)	5.00	—	0.091	(11)
0.182	1.06	1.61	(1)	6.00	—	0.074	(11)
0.207	1.23	1.91	(1)	6.10	—	0.072	(11)
0.218	1.36	1.97	(1)	6.20	—	0.070	(11)
0.221	1.38	2.00	(1)	6.30	—	0.068	(11)
0.234	1.48	2.11	(1)	6.40	—	0.066	(11)
0.238	1.53	2.14	(1)	6.50	—	0.063	(11)
0.243	1.57	2.13	(1)	6.60	—	0.059	(11)
0.248	1.56	2.15	(1)	6.70	—	0.055	(11)
0.282	1.73	2.70	(1)	6.80	—	0.049	(11)
0.302	2.19	3.26	(1)	6.90	—	0.037	(11)
0.310	2.62	3.36	(1)	7.00	—	0.025	(12)
0.344	3.51	2.44	(1)	7.50	—	5.2×10^{-3}	(12)
0.365	3.51	2.15	(1)	7.87	4.001	—	(11)
0.413	3.37	1.81	(1)	8.00	3.995	—	(11)
0.428	3.32	1.86	(1)	8.00	—	2.3×10^{-3}	(12)
0.443	3.32	1.91	(1)	8.50	—	2.0×10^{-3}	(12)
0.477	3.42	2.06	(1)	9.00	—	1.9×10^{-3}	(12)
0.517	3.82	2.25	(1)	9.01	3.967	—	(11)
0.539	4.05	2.09	(1)	9.50	—	1.9×10^{-3}	(12)
0.564	4.18	1.94	(1)	10.06	3.953	—	(11)
0.590	4.22	1.82	(1)	11.01	3.937	—	(11)
0.620	4.29	1.83	(1)	12.06	3.920	—	(11)

TABLE XX—*continued*

λ (microns)	n	k	Reference	λ (microns)	n	k	Reference
12.98	3.912	—	(11)	26.0	3.74	7.5×10^{-3}	(41)
13.90	3.902	—	(11)	27.0	3.66	9.7×10^{-3}	(41)
15.13	3.881	—	(11)	28.0	3.56	1.1×10^{-2}	(41)
15.79	3.873	—	(11)	29.0	3.50	1.0×10^{-2}	(41)
16.96	3.866	—	(11)	30.0	3.47	1.0×10^{-2}	(41)
17.85	3.850	—	(11)	31.0	3.44	1.0×10^{-2}	(41)
18.85	3.843	—	(11)	32.0	3.39	1.0×10^{-2}	(41)
19.98	3.826	—	(11)	33.0	3.34	1.1×10^{-2}	(41)
20.0	—	2.0×10^{-3}	(41)	34.0	3.30	1.2×10^{-2}	(41)
21.15	3.814	—	(11)	35.0	3.25	1.4×10^{-2}	(41)
22.20	3.805	—	(11)	40.0	2.98	2.6×10^{-2}	(41)
25.0	3.78	5.1×10^{-3}	(41)	45.0	2.57	5.4×10^{-2}	(41)

TABLE XXI

REFLECTANCE R OF INDIUM ANTIMONIDE AS A FUNCTION OF λ

λ (microns)	R	Reference	λ (microns)	R	Reference	λ (microns)	R	Reference
0.049	0.010	(1)	0.238	0.442	(1)	1.24	0.376	(1)
0.052	0.012	(1)	0.243	0.436	(1)	1.55	0.369	(1)
0.054	0.013	(1)	0.248	0.441	(1)	2.07	0.364	(1)
0.056	0.014	(1)	0.282	0.530	(1)	20.0	0.35	(41)
0.059	0.016	(1)	0.302	0.579	(1)	25.0	0.34	(41)
0.062	0.016	(1)	0.310	0.570	(1)	30.0	0.31	(41)
0.065	0.015	(1)	0.344	0.466	(1)	35.0	0.29	(41)
0.069	0.012	(1)	0.365	0.438	(1)	40.0	0.25	(41)
0.073	0.009	(1)	0.413	0.398	(1)	45.0	0.21	(41)
0.080	0.007	(1)	0.428	0.400	(1)	50.0	0.19	(45)
0.083	0.009	(1)	0.443	0.405	(1)	50.3	0.18	(45)
0.089	0.023	(1)	0.477	0.425	(1)	50.5	0.17	(45)
0.095	0.053	(1)	0.517	0.460	(1)	50.8	0.15	(45)
0.103	0.100	(1)	0.539	0.458	(1)	51.0	0.14	(45)
0.113	0.160	(1)	0.564	0.454	(1)	51.3	0.12	(45)
0.124	0.222	(1)	0.590	0.448	(1)	51.5	0.13	(45)
0.138	0.274	(1)	0.620	0.453	(1)	51.8	0.17	(45)
0.155	0.332	(1)	0.656	0.479	(1)	52.1	0.27	(45)
0.163	0.348	(1)	0.677	0.488	(1)	52.4	0.42	(45)
0.182	0.380	(1)	0.689	0.480	(1)	52.6	0.59	(45)
0.207	0.430	(1)	0.708	0.466	(1)	52.9	0.70	(45)
0.218	0.424	(1)	0.775	0.430	(1)	53.2	0.76	(45)
0.221	0.429	(1)	0.886	0.400	(1)	53.5	0.79	(45)
0.234	0.442	(1)	1.03	0.385	(1)	53.8	0.81	(45)

TABLE XXI—*continued*

λ (microns)	R	Reference	λ (microns)	R	Reference	λ (microns)	R	Reference
54.1	0.83	(45)	74.0	0.35	(45)	130.0	0.13	(45)
54.3	0.83	(45)	76.9	0.34	(45)	132.0	0.16	(45)
54.6	0.83	(45)	80.0	0.33	(45)	133.0	0.20	(45)
54.9	0.82	(45)	83.3	0.32	(45)	135.0	0.25	(45)
55.2	0.81	(45)	87.0	0.31	(45)	137.0	0.31	(45)
55.6	0.78	(45)	90.9	0.30	(45)	139.0	0.38	(45)
55.9	0.75	(45)	95.2	0.28	(45)	141.0	0.45	(45)
56.2	0.70	(45)	100.0	0.26	(45)	143.0	0.50	(45)
56.5	0.66	(45)	105.0	0.23	(45)	145.0	0.54	(45)
56.8	0.61	(45)	111.0	0.20	(45)	147.0	0.58	(45)
57.1	0.58	(45)	112.0	0.19	(45)	149.0	0.61	(45)
57.5	0.56	(45)	114.0	0.18	(45)	152.0	0.63	(45)
57.8	0.54	(45)	115.0	0.18	(45)	154.0	0.66	(45)
58.1	0.52	(45)	116.0	0.17	(45)	167.0	0.75	(45)
58.5	0.50	(45)	118.0	0.16	(45)	182.0	0.80	(45)
58.8	0.49	(45)	119.0	0.15	(45)	200.0	0.83	(45)
60.6	0.44	(45)	120.0	0.14	(45)	222.0	0.86	(45)
62.5	0.41	(45)	122.0	0.13	(45)	250.0	0.88	(45)
64.5	0.40	(45)	123.0	0.12	(45)	286.0	0.90	(45)
66.7	0.38	(45)	125.0	0.11	(45)	333.0	0.91	(45)
69.0	0.37	(45)	127.0	0.11	(45)	400.0	0.92	(45)
71.4	0.36	(45)	128.0	0.11	(45)	500.0	0.93	(45)

Author Index

Numbers in parentheses are footnote numbers and are inserted to enable the reader to locate those cross references where the author's name does not appear at the point of reference in the text.

Abagyan, S. A., 126
Abraham, A., 98, 110 (21), 129, 131 (11), 132, 140 (11), 514, 524, 533, 536 (5), 537 (5)
Adams, E. N., 309, 342, 396, 470
Adler, S. L., 101, 119 (49)
Aggarwal, R. L., 257, 398, 400
Aigrain, P., 251, 437
Alfvén, H., 438
Allen, J. W., 411
Antončík, E., 98, 110 (20), 129, 131 (11), 132 (11), 140 (11), 537 (8)
Aoyagi, K., 323
Arai, T., 326
Archer, R. J., 503
Argyres, P. N., 396
Aronov, A. G., 333, 334, 338
Ashley, E. J., 97, 98 (16), 110 (16), 500 (5)
Aspnes, D. E., 246
Attard, A. E., 474, 475 (27)
Austin, I. G., 169, 326, 449, 450
Aven, M., 61, 64
Avery, D. G., 537 (19)
Azbel', M. Ya., 447

Bagguley, D. M. S., 150, 151 (47), 180, 364, 380, 383, 384, 395 (97), 444
Balkanski, M., 31, 35 (24), 57, 60, 85
Balslev, I., 8, 257
Barcus, L. C., 516
Bardeen, J., 156, 188, 196, 197, 294, 295 (68), 327, 354 (72)
Barker, A. S., 10
Basov, N. G., 399
Bassani, F., 101, 129, 132 (16), 144 (16)
Bate, G., 537 (29)
Bate, R. T., 210, 241 (90)
Batz, B., 257
Baxter, R. D., 210, 241
Beattie, A. R., 476
Beattie, J. R., 500 (4)
Becker, J. H., 178, 191, 314, 505 (4), 537 (20, 21)
Becker, W. M., 183, 253, 406, 409 (26), 414 (1, 26), 418, 419 (26), 524
Bell, R. L., 445
Bemski, G., 445
Bennett, H. E., 97, 98, (16), 110 (16), 500 (5, 7), 514 (7)
Bennett, H. S., 325
Benoit a la Guillaume, C., 399
Berglund, C. N., 257
Bergstresser, T. K., 132
Bernstein, J. B., 72
Besson, J., 446
Besson, J. M., 57, 60
Berreman, D. W., 134
Bethe, H. A., 281, 282 (39), 338
Biellmann, J., 266
Birman, J. L., 24, 56, 84, 298
Blakemore, J. S., 537 (34)
Blanc, J., 476, 478 (32), 481, 484 (39), 491
Blatt, F. J., 156, 188, 223, 294, 295 (68), 323, 327, 354 (72)
Bloembergen, N., 15, 537 (38)
Blount, E., 537 (25)
Blunt, R. F., 173, 178, 191, 314, 505, 537 (20, 21)
Bode, H., 98
Böer, K. W., 248, 470
Bogdankevich, O. V., 399
Bonch-Bruevich, V. L., 251
Bond, W. L., 30
Booth, A. H., 470
Born, M., 5, 13, 15, 268, 431

Borst, M. R., 452
Boswarva, I. M., 325, 326, 347, 359 (59), 361, 364, 365, 366, 367, 368, 379, 383, 384, 385, 392, 394, 395
Bottka, N., 256, 500 (11)
Bowers, R., 224, 441
Bowlden, H. J., 201, 228, 309, 445
Boyle, W. S., 309, 324, 445
Brailsford, A. D., 445
Branner, A. A., 470
Bratashevskii, Y. A., 445
Braunstein, R., 41, 42, 44, 137, 141 (29), 142 (29), 143, 175, 251, 314, 398, 413, 414, 517 (23)
Breckenridge, R. G., 178, 537 (20, 21)
Briggs, H. B., 31, 176, 398, 537 (16)
Britsyn, K. I., 248
Brockhouse, B. N., 32, 33, 35
Brodsky, M. H., 15
Brodwin, M. E., 436, 441
Brout, R., 27, 86
Brown, F. C., 447
Brown, M. A. C. S., 446
Brown, R. N., 323, 324, 379, 380, 381, 382, 383, 399, 445, 449
Brust, D., 129, 132 (16), 144 (16)
Bube, R. H., 211, 465, 467, 469, 470, 471, 476, 478 (32), 479, 480, 481, 484 (39), 486 (34, 35), 491
Buck, T. M., 500 (2)
Bulyanitsa, D. S., 243
Burns, G., 210, 343, 393
Burstein, E., 8, 13, 15, 23, 31, 176, 223, 270, 322, 323, 328 (13), 379, 441, 442, 448, 516 (17), 537
Butler, J. F., 345
Button, K. J., 151, 290, 298 (58), 314, 323, 329, 354 (74), 355 (74), 371 (74), 372 (74), 373, 388 (20), 389 (20), 401

Cabannes, F., 516
Calawa, A. R., 225, 227 (112), 345, 385, 386 (118)
Callaway, J., 146, 201, 243, 246, 252, 516 (15), 537 (25)
Callen, H. B., 14
Canfield, L. R., 97, 500 (8, 9)
Cano, R., 446
Cardon, F., 465, 480, 481 (38)
Cardona, M., 95, 98, 100, 110 (22, 23, 24), 113, 125, 126, 128 (2), 129, 130, 131, 132, 133 (9, 10), 135 (2), 136 (2), 137 (2, 8, 19), 138, 139 (2, 10, 19), 140, 141 (8, 9), 143 (8, 14), 144, 145 (10), 146 (9, 10, 14, 22), 147 (9, 10), 148, 149 (44), 150, 151, 183, 256, 264, 311, 312, 314, 326, 387, 392, 416, 417, 418, 450, 453, 503 (2), 505, 517, 524, 525, 527, 528, 537
Carlson, R. O., 472
Casella, R. C., 266
Celli, V., 101
Certier, M., 323
Chalikyan, G. A., 221
Champion, F. C., 200
Chang, R. K., 537 (38)
Cheeseman, I. C., 188, 294
Chen, Y. S., 10
Chester, M., 248
Choyke, W. J., 40, 232
Chynoweth, A. G., 476
Cochran, W., 16, 17, 20, 21, 24 (3), 26 (3), 33 (3), 35, 44, 45, 47, 81, 86 (9)
Cohen, M. H., 101, 537 (25)
Cohen, M. L., 132
Collins, R. J., 31, 32, 88, 406, 407 (2), 408 (2), 409 (2)
Condon, E. U., 305
Conn, G. K. T., 500 (4)
Conwell, E. M., 130
Cunningham, R. W., 476

Darwin, C. G., 324
Dash, W. C., 97, 98 (17), 100, 110 (17)
De Bever, T. M., 399
Deiss, J. L., 266, 323
Dell, R. M., 528 (3)
De Meis, W. M., 450, 453
Des Cloizeaux, J., 251
Deutsch, T., 60, 61, 62
Devyatkov, A. G., 399
Dexter, D. L., 156
Dexter, R. N., 322, 423, 424 (3)
Dickey, D. H., 255, 324, 440
Dietz, R. E., 193, 212 (70), 218 (70), 232 (70), 242 (70), 243 (70), 298
Dimigen, H., 100, 118 (42), 119
Dimmock, J. O., 293, 301 (65), 308 (65), 323
Dingle, R. B., 304, 358, 367
Dixon, J. R., 78, 172, 181, 200, 408, 409, 533
Dolling, G., 12, 33, 47, 48

Donovan, B., 436, 449, 453
Donovan, T. M., 97, 98 (16), 110 (16), 500 (5), 536 (7)
Dresselhaus, G. F., 149, 165, 178, 213, 257, 283, 285 (43), 288, 302 (43), 312, 316 (98), 322, 357, 366, 369, 380, 396, 398, 400 (134a), 412, 430, 441
Dresselhaus, M. S., 257, 323, 324, 398, 400 (134a), 439, 440
Drickamer, H. G., 200
Drilhon, G., 399
Ducuing, J., 537 (38)
Dumke, W. P., 194, 195, 201, 369, 537 (25)
Duncan, W., 151
Dunlap, W. C. Jr., 116, 151

Eagles, D. M., 201
Edwards, A. L., 200
Edwards, D. F., 291, 309, 310, 371, 440, 524
Effer, D., 210
Ehrenreich, H., 14, 93, 94, 95, 97, 98, 100, 101, 105 (19), 110 (17), 113 (5), 119 (8), 120 (4), 121, 126, 129 (4), 133, 134 (5), 140 (24), 141 (24), 142, 144 (4), 151, 156, 186, 187 (60), 199, 314, 390, 410, 501, 509, 513, 532, 536, 537
Elliot, R. J., 145, 213, 215, 217 (101), 223, 228, 262, 269 (15), 288, 289 (15, 51), 290 (15), 293, 295 (15), 296 (15, 51), 297 (15), 298, 305, 306 (88, 89), 307 (88, 89), 308 (88, 89), 309, 312, 323, 359 (16), 371, 395
Ellis, B., 325, 326, 394, 450
Ellis, J. M., 172, 181, 200, 533
Engeler, W., 12, 257, 324
Etter, P. J., 210
Evans, J. A., 537 (37)

Fan, H. Y., 8, 31, 32, 35 (23), 43 (23), 52, 65 (23), 88, 151, 156, 169, 170, 172, 173, 175, 176 (6), 178, 179, 180, 181, 183, 194, 200, 205, 206, 207, 208, 209, 210, 211 (85), 219, 224, 225, 226, 227, 228, 229, 232, 237 (88), 238, 239, 240, 241, 250 (47), 253, 257, 291, 323, 387, 390 (19), 391 (19), 406, 407 (2, 3), 408 (2), 409 (2, 22, 26), 414, 415, 416, 417, 418, 419, 427, 509 (6), 524 (4, 5), 533 (10), 537, 538 (24)
Faraday, M., 321
Faust, J. W., 97
Feher, G., 374
Feinleib, J., 256, 400
Ferrell, R. A., 120
Filinski, I., 151, 208, 237 (88), 291, 323, 390 (19), 391 (19), 524 (5)
Firsov, Yu. A., 397
Fischer, A. G., 140 (43), 148, 503 (2)
Fischer, T. E., 140, 505, 508 (1)
Fletcher, R. C., 398
Fleury, P. A., 400
Flietner, H., 449
Flood, W. F., 178, 537 (18)
Folberth, O., 151, 174, 510
Foner, S., 322, 323 (12), 441, 442 (34), 443 (34)
Forsch, C. J., 509 (5)
Fowler, A. B., 343
Franz, W., 243, 247, 340
Fray, S. J., 44 (40), 45 (40), 47, 55, 56, 81, 86 (9), 516 (19), 538 (42, 43)
Frederikse, H. P. R., 173, 178, 191, 314, 439, 505 (4), 537 (20, 21)
Frenkel, J., 213, 260
Frisch, H. L., 400
Fritsche, L., 248
Fritzsche, H., 257
Fröhlich, H., 119, 253
Frosch, C. J., 38, 174, 175 (30), 190 (30), 191 (30), 193 (30), 211 (30), 314, 409 (13), 410, 411 (13)
Frova, A., 247, 248
Fuller, C. S., 49, 51
Furdyna, J. K., 436, 449

Galazka, R. R., 439
Galeener, F. L., 387, 388 (121), 392, 393, 399
Galkin, A. A., 445
Garfinkel, M., 257
Garlick, G. F. J., 470
Gatos, H. C., 500 (3)
Gauthe, B., 100, 118 (43)
Geballe, T. H., 538 (40)
Gebbie, H. A., 322, 379 (11), 441, 442 (33)
Geick, R., 6
Gere, E. A., 374
Gerlich, D., 85
Gershenzon, M., 174, 175 (30), 190 (30), 191 (30), 193, 211 (30), 212 (70), 218, 232, 242, 243, 298, 314, 394, 409 (13), 410, 411 (13), 476, 485 (28), 486 (28), 509 (5)

Gibbs, D. F., 174, 175 (30), 190 (30), 191 (30), 193 (30), 211 (30), 314, 409 (13), 410, 411 (13), 509 (5)
Gibson, A. F., 470
Gielisse, P. J., 8
Gill, D., 15
Gillett, C. M., 537 (37)
Gobeli, G. W., 169, 170, 178, 179, 180, 250 (47), 257, 414, 537
Goodman, R. R., 360, 361, 362
Goodwin, D. W., 537 (19)
Goodwin, W., 537 (26)
Greenaway, D. L., 98, 100, 110 (26), 126, 129, 130, 131 (9), 132 (9, 19), 133 (9), 137 (19), 139 (19), 140 (9, 19), 141 (9), 143 (14), 146 (9, 14), 147 (9), 148 (9, 14), 411
Griffis, R. C., 8
Grosmann, M., 266, 323
Gross, E. F., 193, 218, 232, 242, 262, 323
Grossweiner, L. I., 470
Groves, S. H., 256, 399, 400
Grun, J. B., 266, 323
Guertin, R. F., 15
Gurevich, V. L., 397
Gutsche, E., 248

Habegger, M., 208, 241 (87)
Haering, R. R., 342, 470
Haga, E., 410
Hagstrum, H. D., 114
Haken, H., 269
Hall, L. H., 156, 188, 294, 295 (68), 327, 354
Hall, R. N., 12
Halperin, A., 470
Halpern, J., 323, 326, 347 (61), 352, 353, 354, 356, 374, 375, 376, 379, 380, 389
Hambleton, K. G., 14, 515, 517
Hamilton, D. R., 232
Hanamura, E., 323, 377, 378, 401
Handler, P., 247, 248
Hänsch, H. J., 248
Harbeke, G., 125, 126 (2), 128 (2), 132 (2), 135 (2), 136 (2), 137 (2), 139 (2), 144, 264, 537 (10)
Hardy, J. R., 31, 36, 37 (22), 63, 65
Harman, T. C., 324, 440
Harte, W. E., 440
Hartmann, B., 324
Hasegawa, H., 228, 309, 323, 377, 378 (109)
Hass, G., 97, 500 (9)
Hass, M., 8, 9, 52, 79, 82 (8), 99, 117 (36), 270, 516, 538 (44)
Hawkins, T. D. H., 72, 172, 174, 514, 537 (11, 27, 32)
Hayne, G. S., 524
Haynes, J. R., 232, 241
Hebel, L., 324
Heckart, P. G., 211
Heller, W. R., 260
Hensel, J. C., 338
Henvis, B. W., 8, 9, 52, 79, 82 (8), 99, 117 (36), 270, 429, 434 (7), 436 (7), 440, 516, 538 (44)
Herman, F., 115, 121 (54), 124, 131, 146, 357
Hess, R. B., 256, 398, 500 (10)
Hill, D., 10, 174, 182, 251 (55), 504, 517 (25)
Hilsum, C., 14, 16, 99, 100 (35), 117 (35), 474, 475, 476, 515 (12), 517 (12)
Hilton, A. R., 500 (6)
Hobden, M. V., 13, 126, 128, 218, 226, 231, 314, 392, 517 (21)
Hodby, J. W., 141, 411, 414
Holeman, B. R., 14, 476, 515 (12), 517 (12)
Holstein, T. D., 396
Hoogenstraaten, W., 470
Hopfield, J. J., 232, 236, 237 (121), 242, 252 (121), 257, 270, 287, 293, 298, 304, 308 (64), 323, 394
Hosler, W. R., 173, 178, 191, 314, 505 (4), 537 (20, 21)
Howard, R. E., 228, 309, 325, 326 (52), 365 (52), 367 (52)
Hrostowski, H., 49, 51, 178, 181, 533 (7), 537 (18), 538 (40)
Huang, K., 5, 13, 15, 268
Hunter, W. R., 97

Ichikawa, Y. H., 120
Ishiguro, K., 98, 110 (27)
Ivanchenko, Y. M., 445
Ivanov-Omskii, V. I., 537 (35, 36)
Iwasa, S., 8, 448
Iyengar, P. K., 35

Jacobus, G. F., 97
Jahoda, F. C., 93, 99
James, H. M., 314, 316
Jeffreys, B. S., 245
Jeffreys, H., 245
Jensen, J. D., 323
Johnson, E. J., 151, 181, 182, 205, 206, 207,

208, 209, 210, 211 (85), 219, 224, 225, 226, 227, 228, 229, 232, 237 (88), 238, 239, 240, 241, 254, 255, 257, 291, 323, 387, 390, 391, 400, 524
Johnson, F. A., 12, 17 (3), 18, 20, 21, 24 (3), 26 (3), 32, 33, 35, 42, 44 (40), 45 (40), 47, 55 (48), 56, 65, 81, 86 (9), 516 (19), 538 (42, 43)
Johnson, L. F., 476, 485 (28), 486 (28)
Johnson, M. H., 304
Johnson, P. D., 95
Jones, C. E., 500 (6)
Jones, G. O., 11
Jones, R. H., 55 (48), 56, 538 (42, 43)

Kahn, A. H., 175, 330, 439
Kaiser, R., 209, 210 (89)
Kaiser, W., 30, 31 (19), 32 (18), 175, 178, 537 (23), 538 (23)
Kaluzhnaya, G. K., 193, 218 (69), 232 (69), 242 (69)
Kane, E. O., 130, 137, 141 (29), 142 (17, 29), 143, 149 (17), 150, 163, 164, 170, 171, 172, 175, 251, 257, 269, 282, 312, 315 (40), 357, 380, 382, 396, 398, 412, 413, 414 (21), 441
Kaner, E. A., 447
Kaplan, R., 445
Kaplyansky, A. A., 323
Karplus, R., 102
Kauer, E., 174
Keating, P. N., 470
Keck, P. H., 30, 32 (18)
Keldysh, L. V., 243, 248, 340
Kesamanly, F. P., 450
Keyes, R. J., 225, 227 (112), 322, 323, 380, 382, 385, 386 (118), 441, 442, 443 (34)
Keyes, R. W., 26, 200, 309
Kharitonov, E. V., 325
Khás, Z., 237
Kimmitt, M. F., 446
Kimura, H., 410
Kip, A. F., 149, 178, 312, 322, 357, 366 (89), 369 (89), 380, 430, 441
Kireev, P. S., 248
Kirk, D. D., 72
Kittell, C., 149, 178, 187, 188, 280, 312, 322, 357, 366 (89), 369 (89), 380, 430
Kleiner, W. H., 151, 181, 205, 225 (86), 226 (86), 230 (86), 314, 364, 373, 377, 379, 382, 383, 384 (98)
Kleinman, D. A., 4, 8, 9, 10 (11), 14 (11), 23, 31, 38, 39 (35), 48, 49, 79, 82 (8), 193, 506, 509
Kleinman, L., 101, 114
Kleman, B., 324
Kliefoth, K., 449
Klotyn'sh, E. E., 450
Knox, R. S., 262, 267, 287
Kohn, W., 159, 201, 202 (84), 204 (84), 217, 269, 271, 277, 278 (36), 280, 281, 282 (38), 312, 314, 316, 357, 380
Kolm, H. H., 322, 323 (12), 441, 442 (34), 443 (34)
Kolodziejczak, J., 325, 326 (51), 331 (55), 345 (51), 348 (51), 364 (51), 377, 378 (108), 384 (55), 450, 456
Kolomiets, B. T., 537 (35, 36)
Korovin, K. I., 325
Kosicki, B. B., 389
Koyama, R. Y., 503 (1)
Krag, W. E., 392, 393 (126)
Kramers, H. A., 98
Kretschmar, G. G., 537 (31)
Kröger, F. A., 38
Kronig, R. de L., 98, 322
Kudman, I., 172, 173, 182, 517 (22, 27)
Kümmel, U., 248
Kurdiani, N. I., 536 (6), 537 (33)
Kurnick, S. W., 89, 195, 409, 474, 537
Kuwabara, G., 323

Lallemand, P., 537 (38)
Lamb, W. E., 284, 285 (44)
Lampert, M. A., 232
Landau, L. D., 244, 304, 327, 438
Lange, C. F., 30, 32 (18)
Lange, H., 248
Langenberg, D. N., 448
Larsen, D. M., 254, 255, 400
Lavine, M. C., 500 (3)
Lawson, W. D., 537 (19)
Lax, B., 129, 130 (15), 151, 156, 223, 225, 227 (112), 257, 290, 298 (57, 58), 313, 314, 322, 323, 324, 325, 326, 328 (14, 15, 17), 329, 331, 335, 340, 341, 344, 345 (46, 51), 347 (61), 348 (51), 352 (61), 353 (61), 354, 355 (74), 356 (61), 363, 364 (51), 368 (15), 369 (15), 370, 371, 372, 373, 374, 375, 376, 377, 378 (108), 379, 380, 381 (15), 382, 384, 385, 386 (118), 387 (15, 107), 388 (20), 389 (20), 397 (37), 398, 400 (134a), 401, 422, 424 (3), 430, 439, 440, 441, 442 (34, 37), 443 (22, 34), 446 (22), 449, 456
Lax, M., 23, 31, 298, 407

Lazazzera, V. J., 291, 309, 310, 371
Leder, L. B., 134
Leifer, H. N., 151
Lely, J., 38
Levinger, B. W., 130
Levinstein, H., 12
Libchaber, A., 448
Lidiard, A. B., 324, 325, 326 (52), 347, 359 (59), 361, 364, 365 (52), 366, 367, 368, 392, 394, 395, 436, 449
Lifshitz, E. M., 244, 438
Lilburne, M. T., 528
Lippman, B. A., 304
Lipson, H. G., 439
Liu, L., 114, 133
Loebner, E. E., 503 (1)
Logan, R. A., 476
Long, D., 200
Lord, R. C., 31
Lorentz, H. A., 321
Lorimor, O. G., 14, 51, 52 (45), 533
Loudon, R., 228, 298, 305, 306 (88), 307 (88), 308 (88), 309, 314, 316, 317, 371, 395
Lucas, R. C., 503 (1)
Lucovsky, G., 252, 517 (26, 28)
Lukeš, F., 137 (31), 140, 143 (31), 524, 537 (9)
Luttinger, J. M., 159, 280, 281, 282 (38), 283, 312, 315 (41), 316 (41), 357, 380
Lyddane, R. H., 6, 14, 20

MacDonald, H. E., 471, 476, 478 (32), 480 (34), 481 (34), 484 (39), 486 (34, 35), 491 (35)
Macfarlane, G. G., 223, 249, 290, 298, 305, 306 (89), 307 (89), 308 (89), 323, 329, 359 (16)
Madden, R. P., 97, 500 (8, 9)
Madelung, O., 156, 200 (7)
Magid, L., 175
Maker, P. D., 440
Mal'tsev, Yu. V., 326, 450
Mansfield, R., 439, 452
Mansur, L. C., 8
Marcus, A., 260
Marple, D. T. F., 61, 64 (56), 100, 121, 126, 129 (4), 144(4), 514, 515, 517
Marshall, R., 8, 27, 28, 29 (13), 57, 60, 61, 62
Martin, D. H., 11
Marton, L., 95, 119 (7)
Massey, H. S. W., 214
Matossi, F., 78, 151, 172, 175, 314, 533 (11)
Mattiloli, M., 446
Mavroides, J. G., 257, 313, 323, 324, 375, 376 (107), 380, 382, 387 (107), 398, 400 (134a), 439, 440, 441, 442 (37), 443 (22), 446 (22)
Mawer, P. A., 11
Mazerewics, W., 31, 35 (24)
McAlister, A. J., 440
McClure, D. S., 262
McClymont, D. R., 169
McGroddy, J. C., 440
McClean, T. P., 156, 218 (3), 223, 249, 290, 292, 298, 305, 306 (89), 307 (89), 308 (89), 314, 316, 317, 323, 359 (16), 371, 373
Mead, C. A., 155, 190, 191, 192
Medcalf, T., 453
Melngailis, I., 387, 388
Mendelson, K. S., 314, 316
Meyer, H. J. G., 88, 396, 407, 408 (5)
Misu, A., 323
Mitchell, A. H., 280
Mitchell, D. L., 323, 325, 377, 384, 399
Mitchell, E. W. J., 31, 36 (22), 37 (22), 65 (22), 449
Mitra, S. S., 8, 27, 28, 29 (12, 13), 50, 56, 57, 60, 61, 62, 86
Mooradian, A., 6, 12, 13
Moore, A. R., 139, 144 (30)
Moore, C. E., 121, 123 (60)
Morgan, T. N., 252
Morin, F. J., 538 (40)
Morrison, R. E., 98, 110 (25), 514, 532, 536 (4), 537 (4)
Moss, T. S., 4, 14 (2), 72, 99, 125, 151, 172, 174, 182, 247, 251 (54), 314, 324, 325, 326, 368 (64), 394, 449, 450, 451 (57), 452, 453, 456, 514, 537
Mott, N. F., 214

Nanney, C., 72
Nasledov, D. N., 151, 450
Nathan, M. I., 210, 343, 393
Nelson, D. F., 476, 485, 486
Nelson, H., 251, 517 (23)
Newman, R., 56, 57, 100, 173, 314, 409 (25), 418, 472, 527
Nikitine, S., 262, 266, 323
Nishina, Y., 325, 326, 331 (55), 345 (51), 347 (61), 348 (51), 352 (61), 353 (61), 354 (61), 356 (61), 364 (51), 377, 378, 384, 385
Nodzvetskii, D. S., 193, 218 (69), 232 (69), 242 (69)
Nozieres, P., 94, 108 (6)

Oberländer, S., 470
Oetjen, R. A., 8, 538
Okazaki, M., 377, 378 (109)
Orlova, N. N., 248
Oshinsky, W., 178, 537 (20, 21)
Oswald, F., 51, 169, 174, 200, 505, 506, 507 (5), 510, 516, 524, 528, 533 (8), 537
Overhauser, A. W., 213
Owens, E. B., 210

Page, L., 304
Palik, E. D., 323, 392, 429, 434, 436, 440, 442, 443, 444, 446, 447, 448, 451, 452, 453, 454, 455 (83)
Pankove, J. I., 251, 517 (23)
Papoular, R., 446
Parmenter, R. H., 251, 412
Parratt, L. G., 121
Pascoe, E. A., 8
Patel, C. K. N., 400
Patrick, L., 40, 232
Patton, V. A., 326, 389 (65), 391 (65), 394
Paul, W., 131, 198, 199, 200 (76, 77), 389, 399, 411, 412, 450, 453
Pauling, L., 288
Pearson, G. L., 10
Peierls, R. E., 260
Pekar, S. I., 287
Pelzer, H., 119
Penchina, C. M., 248
Perlmutter, A., 516 (15)
Perry, C. H., 11
Pettit, G. D., 218, 221 (104), 251 (104), 291, 528
Phelan, R. J., 225, 227, 385, 386, 399 (119)
Philipp, H. R., 93, 94, 95, 97, 98, 100, 105 (19), 110 (17), 113 (5), 119 (8), 120 (4), 126, 133, 134 (5), 140 (24), 141 (24), 374, 501, 509, 513, 532, 536, 537
Philippeau, B., 446
Phillips, J. C., 24, 94, 101, 113 (5), 114, 129, 132 (13, 16), 133, 140 (24), 141, 144 (16), 145, 509 (3), 513 (3), 532 (3), 536 (3), 537 (3, 25)
Picus, G. S., 8, 223, 270, 322, 323, 328 (13), 379 (11), 441, 442, 516
Pidgeon, C. R., 151, 256, 325, 326, 379, 380, 381, 382, 383, 384 (48), 399, 400, 445, 450, 451
Piller, H., 325, 326, 332, 368, 389 (65, 66), 391 (65), 394, 449, 450, 453
Pines, D., 94, 101, 108 (6)
Piriou, B., 516
Plendl, J. N., 8
Pollak, F. H., 140, 256
Porteus, J. O., 500 (7), 514 (7, 8)
Potter, R. F., 10, 12, 30, 56 (17), 68, 72, 73, 76, 77, 78, 79, 84 (5, 7), 86 (5, 7), 89, 325, 332, 537 (31)
Powell, C. J., 100, 118 (41), 119
Powell, J. M., 89, 195, 409, 537
Pratt, G., 269
Prior, J. R., 200
Prosser, V., 151, 325, 379 (48), 383 (48), 384 (48)
Putley, E. H., 225

Quarrington, J. E., 44 (40), 45 (40), 47, 81, 86 (9), 173, 194, 195, 200, 249, 290, 298, 516 (19), 524, 537
Quist, T. M., 392, 393 (126)

Rabenau, A., 174
Racette, J. H., 12
Ramdas, A. K., 31, 35 (23), 43 (23), 65 (23), 173, 175 (25), 183, 409 (26), 414 (26), 418, 419 (26), 524 (4)
Randall, J. T., 470
Rasba, E. I., 445
Ratcliffe, J. A., 421
Rauluszkiewicz, J., 439
Redfield, D., 246
Rediker, R. H., 225, 227 (112), 385, 386, 387, 388, 399 (119)
Reese, W. E., 8, 10, 56, 58, 183, 191, 218, 221 (104), 251 (104), 291, 314, 409 (17), 412, 505, 506, 507 (6), 508 (6), 517 (24)
Reid, F. J., 210, 241 (90)
Reine, M., 341, 401
Revesz, A. G., 515
Reynolds, W. N., 528
Richards, P. L., 445, 446
Rigaux, C., 399
Ringeissen, J., 266
Ritchie, R. H., 119
Roberts, V., 173, 194, 195, 200, 249, 290, 298, 329, 524, 537
Robins, J. L., 123
Robinson, M. L. A., 150, 151 (47), 180, 444
Robinson, T. S., 93, 98
Rodgers, K. F., 324
Rodriguez, S., 257, 258

Rose, A., 465
Rose-Innes, A. C., 99, *100* (35), *117* (35), 474, 475
Rosenberg, R., 407
Rosenblum, E. S., 322
Rosenfeld, L., 322
Rosenstock, H. B., 28, 86
Rosi, F. D., 211
Roth, L. M., 129, 130 (15), 151, 223, 269, 290, 298 (57, 58), 300, 314, 322, 323, 325, 328 (15, 17), 329, 331, 347, 354 (74), 355 (74), 363, 364, 365, 367, 368 (15), 369 (15), 370, 371, 372, 373, 374, 376, 377, 379 (15), 381 (15), 382, 387 (15), 388 (20), 389 (20), 392, 396, 422
Rubin, L., 257, 398, *400* (134a)
Rubinstein, M., 132
Russell, J. P., 13
Rustgi, O. P., 121

Sachs, R. G., 6, 14 (6), 20
Sagar, A., 183
Salpeter, E. E., 281, 282 (39)
Salzberg, C., *100*, *116* (38)
Sanderson, R. B., 6, 538
Sasaki, T., 98, 110 (27)
Saurin, V. N., 248
Sawada, Y., 448
Schade, R., 169, 174 (18), 505, 506, 507 (5), 510, 516, 524, 537
Schechter, D., 314, 316
Schiff, L. I., 288, 304
Schmidt, E., 137 (31), 140, 143 (31), 524, 537 (9)
Schneider, E. E., 151
Schoolar, R. B., 323
Schwab, C., 266
Schwartz, R. F., 252, 517 (28)
Schwinger, J., 102
Scouler, W. J., 133, 141 (23)
Segall, B., 61, 64 (56), 140
Seidel, T., 172, 173, 182, 517 (27)
Seitz, F., 158, 160, 232
Seraphin, B. O., 256, 398, 500 (10, 11, 12), 536 (7)
Shaklee, K. L., 132, 140, 256
Sharma, R. R., 257, 258
Sheka, V. I., 445
Shiff, L. I., 160
Shindo, T., 338
Shockley, W., 10, 196, 197, 357
Shortley, G. H., 305
Shulman, S. A., 450
Shurcliff, W. A., 424
Sieskind, M., 266
Skillman, S., 115, 121 (54), 124 (54), 131
Slater, J. C., 261
Slobodchikov, S. V., 151
Slusher, R. E., 400
Slykhouse, T. E., 200
Smith, G. E., 324, 446
Smith, S. D., 31, 36, 37, 63, 65, 151, 324, 325, 326, 379, 384, 450, 451, 537 (11, 27)
Sniadower, L., 439
Snyder, H., 304
Sommers, H. S. Jr., 98, 110 (24), 129, 130 (12), 132 (12)
Sorokin, O. M., 121
Spitzer, W. G., 4, 8, 9, 10 (11), 12, 14, 31, 38, 39, 47, 48, 49, 51, 52, 61 (41), 79, 82, 88, 155, 172, 174, 175, 179, 181, 190, 191, 192, 193, 194, 211 (30), 314, 406, 407 (2), 408 (2), 409 (2, 13, 18, 22), 410, 411, 412, 415, 416, 417, 418, 419, 427, 506, 509, 517 (20), 533, 537 (24, 28), 538 (24)
Stannard, C., Jr., 12
Stephen, M. J., 324, 436, 449
Stern, E. A., 325, 440
Stern, F., 13, 78, 100, 151, 156, 172, 175, 181, 314, 398, 533 (9)
Stern, R., 15
Stevenson, J. R., 392, 443, 447 (41)
Stierwalt, D. L., 10, 12, 30, 56 (17), 68, 72, 73, 76, 77, 78, 79, 84 (5, 7), 86 (5, 7), 89
Stiles, P. J., 448
Stone, B., 10, 174, 504
Stradling, R. A., 150, 151 (47), 180, 364, 380, 383, 384, 389, 395 (97), 444
Stramska, H., 456
Strauss, A. J., 210, 324, 440, 474, 475 (27)
Strel'tsov, L. N., 248
Sturge, M. D., 126, 134 (6), 135 (6), 142 (6), 173, 210, 211, 212, 218, 219, 220, 252 (24), 267, 291, 392, 514, 515, 517 (21)
Subashiev, V. K., 126, 221
Suffczynski, M., 325
Sugano, S., 323
Summers, C. J., 326
Sutter, E., 537 (30)
Suzuki, K., 377, 378 (109)
Szigeti, B., *15*, *26*

Taft, E. A., 93, 374
Talley, R. M., 175, 181, 398, 533 (9)
Tanenbaum, M., 176, 181, 533 (7), 537 (16)
Tauc, J., 98, 110 (20, 21), 129, 131 (11), 132, 140 (11), 514, 524, 533, 536 (5), 537 (5, 8)
Taylor, J. H., 200
Taylor, K. N. R., 537 (29)
Taylor, K. W., 324, 450
Teitler, S., 429, 434 (7), 436 (7), 440, 442, 443 (44), 444, 453, 454, 455
Teller, E., 6, 14 (6), 20
Tharmalingam, K., 243, 244, 246 (127), 340, 341
Theriault, J. P., 151, 181, 205, 225 (86), 226 (86), 230 (86), 314, 364, 379, 382, 383, 384 (98)
Thomas, D. E., 99
Thomas, D. G., 193, 212 (70), 218 (70), 232, 242, 243 (70), 293, 298, 304, 308 (64), 323, 394
Thompson, A. G., 132
Thouless, D. J., 267
Thurmond, C., 30, 31 (19)
Tiemann, J. J., 257
Toll, J. S., 98
Tousey, R., 97
Turner, W. J., 8, 10, 56, 58, 183, 191, 218, 221, 251 (104), 291, 314, 409 (17), 412, 505, 506, 507 (6), 508 (6), 517 (24), 528
Tyler, W. W., 471, 472

Ukhanov, Yu. I., 326, 450

Van Doorn, C. Z., 252
Van Hove, L., 24, 144
Van Vleck, J. H., 102
Varga, A. J., 252, 517 (28)
Vavilov, V. S., 248
Veilex, R., 448
Verleur, H. W., 10
Vernon, R. J., 441
Vieland, L., 182, 517 (22)
Villa, J., 100, 116 (38)
Vink, A. T., 252
Visvanathan, S., 408, 410
Voigt, J., 470
Voigt, W., 322, 453
Vrehen, Q. H. F., 323, 335, 336, 337, 338, 339, 341, 392, 398 (29)

Wagner, V., 8
Wagoner, G., 178, 380, 441
Walker, W. C., 121
Wallis, R. F., 223, 228, 309, 323, 325, 377, 384, 392, 429, 434 (7), 436 (7), 440 (7), 442, 443, 444, 445, 446, 447, 448, 453, 454 (83), 455 (83)
Walsh, D., 38, 39 (35), 506
Walters, R. L., 116
Walton, A. K., 151, 325, 326, 368 (64), 449, 450, 451 (57), 452, 453
Wang, C. C., 140 (43), 148, 503
Wannier, G. H., 213, 246, 261, 264 (5)
Warekois, E. P., 500 (3)
Warren, J. L., 65
Watson, W. H., 324
Waugh, J. L. T., 12, 47, 48
Weber, M., 401
Webster, J., 436, 449, 453
Weisberg, L. R., 211, 476, 484, 491
Weiss, W., 151
Weisskopf, V., 102
Weissler, G. L., 121
Welker, H., 499, 510
Wendland, P. H., 248
Wengel, R. G., 65
Wheatley, G. H., 178, 537 (18), 538 (40)
Wheeler, R. G., 293, 301 (65), 308 (65), 323
Whelan, J. M., 314, 409 (18), 412, 416, 517 (20)
White, H. E., 322
Wilkins, M. H. F., 470
Willardson, R. K., 225
Williams, E. W., 132
Williams, N., 44 (40), 45 (40), 47, 81, 86 (9), 516 (19)
Williams, R., 248
Wilson, D. K., 374
Wilson, E. B., 288
Wolf, E., 431
Wolf, H. C., 262
Wolfe, R., 408
Wolff, P. A., 251, 339
Wood, R. W., 322
Woodbury, H. H., 471, 472
Woolley, J. C., 132, 537 (37)
Wright, G. B., 6, 12, 13, 133, 156, 324, 379, 387, 388 (121), 392, 393, 397 (37), 399, 425, 426, 430, 433, 439, 440, 456
Wursteisen, L., 266

Yafet, Y., 224, 283, 309, 441
Yahoda, F. C., 126, 134 (5)
Yarnell, J. L., 65
Yoshinaga, H., 8, 538

Zacharcenja, B. P., 323
Zaininger, K. H., 515
Zak, J., 340
Zallen, R., 131, 199, 200
Zawadzki, W., 340, 401
Zeeman, P., 321
Zeiger, H. J., 322, 323, 380, 382, 392, 393 (126), 423, 424 (3), 441, 442 (37)
Zemel, J. N., 323
Ziman, J. M., 186, 297
Zitter, R. N., 473, 474, 475
Zukotyński, S., 456
Zwerdling, S., 151, 181, 205, 223, 225 (86), 226, 230, 290, 298, 313, 314, 322, 323, 328 (14, 15, 17), 329, 331 (17), 354 (74), 355 (74), 363, 364, 368 (15), 369, 370, 371, 372, 373, 379, 381, 382, 383, 384, 387, 388 (20), 389, 439, 440, 441, 442 (34), 443 (34)

Subject Index

A

Absorption, *see also* Fundamental absorption, Magnetoabsorption, Magnetic field, listings of specific materials
  edge, 73, 153–258
  electric field, 243–249
    magnetic field, *see* Crossed field effects
    modulation technique, 255–257
  exciton, 18, 287–289, 311
    magnetic field, 226–231
  free carrier, 19, 73, 405ff.
  impurity, 181, 196, 201–212, 251, 252
    heavy doping, 251, 252
    magnetic field, 223–226
  indirect gap, 188–191
  intrinsic, 125–151
  lattice, 17–69
  probability, 162
Absorption coefficient, 72, 125ff., 157, 163, 346, 406, 499, 509
  indirect transition, 190
  interband, 327–330
Absorption edge, 73, 153–258, *see also* Fundamental absorption, listings of specific materials
  exciton effects, 311
  fundamental, 125ff., 153ff., 405
  phonon broadening, 194–196
  pressure effect, 196–200
  shift, *see* Edge shift
  strain effect, 196–200
  tail, 195, 196
  temperature effect, 196–200
Acoustic mode vibrations, *see* Scattering
Adsorption, *see* Surface damage
Alfvén waves, 437, 438
Aluminum antimonide
  absorption, 56–59, 174, 175, 190, 191, 505
    free-carrier, 409
    interband, 412–414
  band parameters, 137–141, 151, 314
    pressure dependence, gap, 200
  Brout sum rule, 29
  critical-point analysis, phonon energies, 68
  dielectric constants, 14
  effective ionic charges, 14, 27
  effective mass, 151, 457
  exciton states, binding energy, 314
  extinction coefficient, 507
  Faraday rotation, 394, 450
  indirect transitions, 190, 191
  magnetooptical effects, interband, 326
  phonon assignments, 58, 59
  phonon frequencies, 29, 58, 59
  Raman spectra, 11, 12
  reflection, 9–11, 137–139, 505, 506, 508
  refractive index, 506, 507
  Reststrahlen band, 82, 84
  spin–orbit splitting, 141, 314, 414
  symmetry-forbidden transitions, 175
Aluminum arsenide
  absorption, 174, 190, 191
  emittance spectra, 84
  indirect transitions, 190, 191
Aluminum phosphide, complex dielectric constant, 105
Anharmonicity, 11
Anharmonic mechanism, absorption, 23
Azbel'-Kaner resonance, 447, 448

B

Band approximation, 158–160
  dispersion relations, 139, 163–167
  k · **p** theory, 163
Band degeneracy, 163–167, 280
Band parameters
  calculation, 148–151
  determination, magnetooptical effects, 359, 369

dispersion relations, 159, 163–167
heavy doping, 250, 251
InSb, 177–181
Kane model, 163–167
nonparabolicity, 163–167, 380–382
InSb, 178, 179, 380–382
pressure dependence, gap, 196–200
subsidiary minima, 183
tabulation, 151
temperature dependence, gap, 196–199
warping, 165, 380–383
InSb, 179, 180, 380–383
Band structure, 127, 163–167, 178, 311, *see also* Band parameters, listing of specific materials
magnetooptical effects, 357–368
Birefringence, *see* Voigt effect
Born approximation, 407
Born–Oppenheimer approximation, 268
Boron nitride
complex dielectric constant, 105
reflection spectra, 8, 11
Boron phosphide
absorption coefficient, 504
band parameters, 140
extinction coefficient, 504, 505
indirect fundamental edge, 503
lattice absorption, 504
transmission spectra, 10, 11
Bremsstrahlung, 408
Broadening effects, 105, 121, 186
electron interactions, 121
exciton peak, GaSb, 230, 389
impurity level, 252
phonon, 194–196
scattering, 186, 194
Brout sum rule, 27–29, 86
Burstein shift, *see* Edge shift

C

Cadmium sulfide
absorption, electric field, 248
Brout sum rule, 29
effective ionic charges, 27
exciton-impurity complexes, 232
transition probability, 293
exciton states, 278
magnetooptical effects, interband, 323
phonon assignments, 60
phonon frequencies, 29, 60
Cadmium telluride
band gaps, 130
spin-orbit splitting, 126, 133
Capture, charge carrier
cross section, 462, 478–481
photoexcited holes, 478
photoexcited electrons, 478
radiative, 481
rate, 465
Carbon, *see* Diamond
Center-of-mass coordinates, 303
Characteristic frequencies, 501
Characteristic phonon energies, *see* Phonon frequencies
Circulator, 446
Compressibility, 198
Conductivity, 405, 415
effective, 423
thermally stimulated, 468–471
Conductivity tensor, 423, 424
complex, 345–354
Covalent bonding, 16
Critical-point analysis, 12, 18
AlSb, 68
Diamond, 66
GaAs, 68
GaP, 68
InSb, 68
Si, 67, 68
SiC, 68
ZnS, 68
Crossed-field effects, 398–400, *see also* Magnetotunneling
magnetoabsorption, 333–338, 392
Cuprous halides, spin-orbit splitting, 126, 131
Cyclotron frequency, 345, 346, 375, 376, 424
Cyclotron resonance, 255, 322, 429, 430, 441–446, *see also* Magnetotransmission, Magnetoreflection
Azbel'-Kaner, 447, 448
harmonics, 446–448
infrared, 322
microwave, 322

D

d-bands, 106–110, 114–118, 121–124, 133
Degenerate band, *see* Band degeneracy

de Haas-Shubnikov effect, optical, 422, 438, 439
Density matrix, 101
Density of states, 171, 176, 189, 289, 290, 346
  exciton, 217
  heavy doping, 251
  magnetic field, 222, 305, 355, 385
  optical, 204
Depolarization field, 448
Diamagnetic effects, 302, 308
  acceptor state, 224
Diamond
  band parameters
    pressure dependence, gap, 200
  Brout sum rule, 29
  critical-point analysis
    energies, 66
    phonon assignments, 66
  multiphonon absorption, 36
  phonon assignments, 36–38
  phonon frequencies, 29, 37, 38
Dichroic retardation, 432–435
Dielectric constant, 405, 406, 414, 421
  complex, 5, 93, 94, 101ff., 111–113, 499
  effective, 116
  free carrier, 427
  high frequency, 14, 108–110, 270, 515
  low frequency, 14, 108–110, 117
  optical, 108–110
  static, 108–110, 270
Dilatation, 443, 500
Dipole scattering, 495
Dirac equation, 338
Disorder, *see* Lattice distortion
Dispersion, 4, 405, *see also* Band parameters
  lattice mode
    GaAs, 48
    InAs, 89
    InP, 88
  parameters, 501
Dispersion formula, 534, 539
Dispersion relations, 159, 163–167

E

Edge, fundamental, *see also* Absorption
  absorption, 153–258
  resonance, 534
Edge shift, carrier degeneracy, 130, 176, 181, 517, 537
Effective ionic charge, 3, 13–16
  Born, 13, 14
  Callen, 14
  Szigeti, 14–16, 26, 27
Effective mass, *see also* Mass, effective and listing of specific materials
  energy dependent, 441
  susceptibility, 415–418
    carrier distribution, 417
    lattice dilatation, 417, 443
  tensor, 300, 423
    exciton, 301, 302
  total, exciton, 303
Effective-mass eigenfunction, 159
Effective-mass equation, 326
  exciton states, 259, 261, 270–287, 297, 299–305, 311–317
Effective-mass theory, 159
  exciton states, 267
Electric field, fundamental absorption, 243–249
  oscillatory behavior, 246
Electroabsorption, 243–249, 255
Electron-electron interactions, 118, 249, 251
  broadening effects, 121
Electron-hole pairs, 201, 212ff., *see also* Excitons
  interaction potential, 269, 270
    screening, 270, 278
Electroreflection, 256, 400, 500
Ellipsometry, 515
Ellipticity, 431–437
Emittance, 12, 71–90, *see also* listing of specific materials
  free carrier, 87
  spectra, 76–84
Energy gap, 154, 164, 369–373, 381, 382
  direct
    III-V compounds, 314
    Ge, 314, 369–371
    InAs, 387
    InSb, 381–383
    Si, 314
  indirect
    Ge, 372
  pressure effect, 196–200
  temperature coefficient, 196–199
Energy-loss function, 110–113, 118–120, 123
Energy surfaces, *see also* Band parameters
  warped, 165

InSb, 179, 180
Excitation
imperfection, 465
intensity, 465
intrinsic, 465
Excited states
optical creation, 160–163
wave functions, 158–160
Exciton, 144, 171, 193, 212–222, 259–319, *see also* listing of specific materials
absorption, 18, 287–289
magnetic field, 226–231, 305–310
allowed transition, 293, 294
binding energy, 217, 218, 265, 278, 312–317
GaAs, 219, 314, 394
GaSb, 219, 314
Ge, 314
InP, 221, 314
other III-V compounds, 314
silicon, 314
bound states, 216, 217
creation operator, 270ff.
degenerate band, 218
density of states, 217
direct, 288, 370–372
direct transitions, 215, 279, 288–294
electron-hole interaction screening, 266, 267
forbidden transition, 293, 294
first, 293, 294
second, 294
Frenkel, 260, 265
impurity complexes, 231–237, 257, 258
indirect, 288, 373
indirect transitions, 217, 280, 288
ionic crystals, 262
magnetic field, 299–310, 323, 395
molecular crystals, 262
nonparabolic band, 218
reduced mass, 265, 306
spectrum
continuous, 265, 289, 290
discrete, 265, 289, 290, 295
strain effect, 219
strain shift, 220
total mass, 276, 303
absorption, indirect, 298
unbound states, 214–216
Wannier, 261, 265, 266
Extinction coefficient, 4–7, 98, 99, 157, 405, 406, 499

F

Faraday effect, 321–326, 330–332, 347, 348, 428, 434–437, 449–453
AlSb, 394, 450
band-structural considerations, 357–368
calculated rotation
GaAs, 367, 368
GaSb, 367
Ge, 368
InAs, 367
InSb, 367, 368
circulator, 446
cyclotron resonance, 448
GaAs, 392, 450
GaP, 394, 450
GaSb, 391, 449, 450
Ge
direct transition, 377–379
indirect transition, 374, 379
InAs, 450
reflectivity technique, 387
InP, 450
InSb, 383–385, 449–452
line shape
direct transition, 352
indirect transition, 356
oscillatory effects, 325, 331, 351
quantum theory
direct transition, 350, 352
indirect transition, 356
sign of rotation, 364
Free-carrier absorption, 19, 405ff.
interband, 405, 406, 410ff.
tabulation, 409
Free-carrier optical effects, 405–419
dielectric constant, 427, *see also* Dielectric constant
magnetooptical, 421–458
Fresnel coefficient, *see* Reflection
f-sum rule, 104, 110, 282
Fundamental absorption, 405ff.
absence of interactions, 167–183
crossed field, 244
electric field, 243–249
heavy doping, 249–252
tail absorption, 250, 251

G

Gain, photoconductivity, 463

Gallium antimonide
absorption, 49–51, 82, 135–137, 173–175, 237–242, 524
free-carrier absorption, 409
interband, 413, 414
alloys (*see* Mixed crystals)
band parameters, 130, 137–141, 151, 200, 314, 389
Brout sum rule, 29
carrier lifetime, 475
dielectric constants, 14
direct transitions, exciton states, 291
edge shift, 183
effective ionic charges, 14, 27
effective mass, 151, 183, 238, 389, 418, 457
susceptibility, 419
emittance spectra, 81, 84
free carriers, 87
energy gap, 314, 389
pressure dependence, 200
exciton effects, 218, 219, 222, 237–242, 389, 390
binding energy, 238, 314
magnetic field, 226–230, 239–241
exciton-impurity complexes, 232, 238–242, 257, 258, 390
extinction coefficient, 525, 526
Faraday rotation, 391, 450
g-factor, 229, 390
impurity absorption, 196, 205–210
impurity levels, 240–242
magnetoabsorption, 388–391
magnetooptical effects, interband, 323–326
nonparabolic effects, 390
phonon assignments, 50
phonon frequencies, 29, 50
photoconductivity, 208
photoluminescence, 237
recombination emission, 208
reflection, 8, 9, 11, 137–139, 524, 527
electroreflection, 256
refractive index, 524–526
temperature coefficient, 525
spin-orbit splitting, 141, 229, 230, 314, 390
subsidiary band, 183, 418
symmetry-forbidden transitions, 175
Gallium arsenide
absorption, 134–137, 172–175, 182, 514, 516, 517
Burstein shift, 182, 517
electric field, 247, 248
free-carrier, 409
heavy doping, 251
interband, 411–414
alloys (*see* Mixed crystals)
band parameters, 130, 137–141, 151, 200, 314
band structure, 127, 311–317
Brout sum rule, 29
carrier lifetime, 475, 476
critical-point analysis, phonon energies, 68
d-bands, 114–118, 121, 123
dielectric constants, 14, 112, 115, 513, 515
direct transitions, exciton states, 291
edge shift, 182, 517
effective dielectric constant, 117
effective ionic charges, 14, 27
effective mass, 151, 394, 414, 443, 458
magnetic field, 443
susceptibility, 416, 417
emission diode, anomalous dispersion, 343
emittance spectra, 83
energy gap
direct, 314
pressure dependence, 200
energy-loss function, 112, 118
exciton effects, 218–220, 222
binding energy, 291, 314, 394
diamagnetic shift, 231
high magnetic fields, 399
extinction coefficient, 516–522
Faraday rotation, 392, 417, 450
impurity absorption, 196, 210–212, 252
lattice absorption, 43–45, 81
magnetoabsorption, 391, 392
crossed field, 392
magnetodispersion, 343
magnetoemission, 392–394
magnetooptical effects, interband, 323, 326
mobility, photoexcitation, 482–484
nonparabolic effects, 172
optical quenching, 481, 490, 491
phonon assignments, 46, 47
phonon frequencies, 29, 47, 48
photo Hall mobility, 482–484, 486–495
plasma frequencies, 118
Raman spectra, 11, 12
reflectance, 112
reflection, 8, 9, 11, 137–139, 141, 513, 514, 516, 523

electroreflection, 256
refractive index, 515–521
temperature coefficient, 517
Reststrahlen band, 82, 84
sensitizing centers, 488–490
split-off valence band, 398
spin-orbit splitting, 126, 131, 141, 314, 414
symmetry-forbidden transitions, 175
thermally stimulated conductivity, 477–480, 487, 493–495
transmission spectra, 8, 11
trapping, 486, 491–495
Voigt effect, 453
Gallium phosphide
absorption, 48, 49, 174, 175, 190, 191, 242, 243, 509
free-carrier, 409
interband, 410–414
alloys (*see* Mixed crystals)
band parameters, 131, 139–141, 151, 200, 314
Brout sum rule, 29
carrier lifetime, 476
critical-point analysis, phonon energies, 68
d-bands, 114–118, 121, 123
dielectric constants, 14, 113, 115
effective dielectric constant, 117
effective ionic charges, 14, 27
effective mass, 151, 457
energy gap
direct, 314
pressure dependence, 200
energy-loss function, 113, 118
exciton effects, 218, 221
indirect absorption spectrum, 298
exciton-impurity complexes, 232, 242, 243, 394
luminescence, 242, 243
strain, 242
exciton states, binding energy, 314
extinction coefficient, 509–512
Faraday rotation, 394, 450
impurity absorption, 211, 212, 252
impurity levels, 242
indirect transitions, 190, 191
magnetooptical effects, interband, 325, 326
phonon assignments, 48, 50, 193
phonon frequencies, 29, 48, 50
photoconductive spectra, 486
plasma frequencies, 118
Raman spectra, 11
reflectance, 113
reflection, 8–11, 141, 509, 512, 513
refractive index, 509–512
Reststrahlen band, 82, 84
spin-orbit splitting, 141, 314
Gallium selenide
magnetooptical effects, interband, 323
Germanium
absorption, 291
electric field, 248
free-carrier, 409
absorption edges, 128–134
allowed direct transitions, statistical weights, 363
alloys (*see* Mixed crystals)
band parameters, 200, 249, 314, 369–372
band structure, 127
Brout sum rule, 29
complex dielectric constant, 106, 111, 115
d-bands, 114–118, 121, 123
direct transitions
exciton states, 290, 291
magnetoabsorption, 368–372
effective dielectric constant, 117
effective ionic charges, 27
effective mass, 369, 372, 376
energy gap
direct, 249, 314, 369–371
indirect, 372, 373
pressure dependence, 200
energy-level diagram, 360–362
energy-loss function, 111, 118, 120
exciton states, 290, 291, 315, 370–372
binding energy, 314, 315, 317
Faraday rotation, 451–453
direct transition, 377–379
indirect transition, 379
g-factor, 129, 374, 376
indirect transition, magnetoabsorption, 372–376
lattice absorption, 32
magnetooptical absorption, 310, 355, 368–375
magnetooptical effects
crossed-field, 338
interband, 322, 325, 326, 328
oscillatory Faraday rotation, 354

nonparabolic correction, 372
phonon assignments, 35, 36
phonon frequencies, 29, 36
piezoabsorption, 257
plasma frequencies, 118
reflection
electroreflection, 256
reflectance, 111
spin-orbit splitting, 126, 314
symmetry-forbidden transitions, 175
Voigt effect, 453
Germanium-silicon alloys
lattice absorption, 41–43
phonon assignments, 43
phonon frequencies, 43, 44
g-factor, 299, 365, 366, 374
energy dependent, 441
GaSb, 229, 390
germanium, 129, 374, 376
InSb, 225, 230
Greek peaks, 232

H

Hall effect, 471, 472, 486–495
multicarrier, 472
Hall mobility, 471, 472, 487–495
photoexcitation, 481–485, 489–495
Hamiltonian
conduction band, 312ff.
one-electron, crystal, 281ff., 299ff.
magnetic field, 282–287, 299, 303, 304
relativistic term, 281, 283
spin-orbit term, 281, 283, 300
valence band, 312ff.
Hartree–Fock theory, 267–269
Helicon waves, 437, 438, 448, 449
InAs, 448, 449
InSb, 448, 449
Horizontal sequence, 147
energy gaps, 147

I

Imperfection centers, 462, 469
excitation, 465
ionization energy, 464, 466, 479
sensitizing, 478–480, 488–490, *see also* Sensitization
trapping, 476–478
Imperfection sensitization, *see* Sensitization
Impurity-exciton complex, 231–237, 257, 258
dissociation energy, 232–237, 257
Greek peaks, 232
ionized, 232
neutral, 232
Index of refraction, *see* Refractive index
Indium antimonide
absorption, 54, 55, 89, 122, 135–137, 169–172, 175–181, 194–196, 537
free-carrier, 409, 538
interband, 413, 414
lattice, 538
band parameters, 137–141, 151, 177–181, 199, 200, 314, 380–383
Brout sum rule, 29
Burstein shift, 537
carrier lifetime, 474–476
complex dielectric constant, 106, 115
critical-point analysis, phonon energies, 68
cyclotron-resonance absorption, 442
harmonic, 446–448
d-bands, 114–118, 121
dielectric constants, 14, 122
edge shift, 80
effective dielectric constant, 117
effective ionic charges, 14, 27
effective mass, 151, 382, 383, 414, 442–444, 446, 448, 456, 457, 538
magnetic field, 443, 444
susceptibility, 416, 419
emittance spectra, 80
energy gap
direct, 314, 381
pressure dependence, 200
temperature dependence, 199
energy-loss function, 118
exciton absorption, magnetic field, 230
exciton states, binding energy, 314
extinction coefficient, 539–542
Faraday rotation, 383–385, 446, 449–452
g-factor, 225, 230, 382
heavy doping, 250, 251
tail absorption, 250
impurity absorption, 181, 196, 205–207
magnetic field, 224–227
magnetodispersion, 345
magnetoemission, 385–387

magnetooptical effects, interband, 322–326, 328, 379–387
magnetoplasma
ellipticity, 434
phase shift, 435
rotation, 434
multiphonon absorption, 400
phonon assignments, 53
phonon frequencies, 29, 53
plasma frequencies, 118
reflection, 8, 9, 11, 137–139, 141, 179, 416, 417, 536, 537, 542, 543
electroreflection, 256
magnetoplasma, 429, 430
refractive index, 538–542
temperature coefficient, 538
screening effects, 194
spin-orbit splitting, 131, 141, 314
symmetry-forbidden transitions, 175
transmission spectra, 8, 11
Voigt effect, 453–455
Indium arsenide
absorption, 51, 52, 78, 88, 122, 135–137, 172, 175, 181, 182, 533
free-carrier, 409
heavy doping, 251
interband, 413, 414
band parameters, 130, 137–141, 151, 200, 314
carrier lifetime, 475
d-bands, 121
dielectric constants, 14, 112, 115, 122
edge shift, 181
effective ionic charges, 14
effective mass, 151, 181, 387, 414, 418, 443
magnetic field, 443
susceptibility, 417, 418
emittance spectra, 77, 84
energy gap, 314, 387
pressure dependence, 200
temperature dependence, 200
energy-loss function, 112
exciton states, binding energy, 314
extinction coefficient, 535
Faraday rotation, 387, 418, 450
impurity absorption, 196, 211
interference fringes, 533, 534
intervalence-band transitions, 88
magnetoabsorption, 387, 399
magnetodispersion, 345
magnetoemission, 387, 388
magnetooptical effects, interband, 323, 326
nonparabolic band, 387
phonon assignments, 52, 86
phonon frequencies, 52, 87
plasma absorption, 532
reflectance, 112
reflection, 8, 9, 11, 137–139, 141, 532, 536
surface treatment, 532
refractive index, 533–535
spin-orbit splitting, 141, 314, 414
symmetry-forbidden transitions, 175
Voigt effect, 453
Indium phosphide
absorption, 57, 173, 174, 527, 528
free-carrier, 409
band parameters, 137–141, 151, 200, 314
Brout sum rule, 29
dielectric constants, 14
direct transitions, exciton states, 291
effective ionic charges, 14, 27
effective mass, 151, 418, 443, 457
magnetic field, 443
susceptibility, 417, 418
emittance measurements, 56
emittance spectra, 79, 84
energy gap, 314
pressure dependence, 200
exciton effects, 218, 220–222
binding energy, 221, 314
extinction coefficient, 529–531
Faraday rotation, 450
impurity absorption, 211
mobility, photoexcitation, 485
phonon assignments, 56, 85
phonon frequencies, 29, 56, 87
photo Hall mobility, 485
Raman spectra, 11, 12
reflection, 8, 9, 11, 137, 138, 141, 418, 527, 531, 532
refractive index, 528–531
temperature coefficient, 528
Reststrahlen band, 79
spin-orbit splitting, 141, 314
Inhomogeneities
edge shift, 252
electric field, 448
imperfections, 484–486, 490
plasma edge, 440
scattering, *see* Scattering

Interactions
Coulomb, 212
electron-hole pairs, 201, 212ff., *see also* Excitons
fundamental absorption
charged impurity, 159
lattice dilatation, 159
screened Coulomb, 159
uniform electric field, 159
Interband matrix element, 292
Interband mixing, 278
Interband optical effects, definition, 405, 406
Interband transitions, *see* Transitions
Interferometric modulation spectrometer, 538
Intermediate states, 296
Intraband optical effects, definition, 405, 406
Intrinsic absorption, 125–151
Inversion symmetry, 313, 316
Ionic bonding, 16
Ionicity, 142, *see also* Effective ionic charge
Ionized impurity scattering, *see* Scattering

K

Kane band model, 163–167, 410, 443
dilatation, 443
lattice vibrations, 443
Klein–Gordon equation, 338, 340
k · p perturbation, 130
Kramers–Heisenberg relations, 331, 332, 345, 347, 354
Kramers–Kronig analysis, 4, 93, 94, 98, 99, 108, 126, 331, 345, 501

L

Lambert–Bouguer law, 499
Landau level, 144, 223, 299, 304–310, 327, 377, 438, 439, 441, 442
Landau shift, 144
spin splitting, 350
Landau wave functions, *see* Wave functions
Laser diode, *see* Magnetoemission
Lattice absorption
multiphonon, 17–69
mechanisms, 23
phonon assignment, 26ff.
phonon branch, 19–21
selection rules, 23–25
temperature dependence, 21–23
Lattice distortion, 500, *see also* Dilatation
Lattice reflection, 3–16
Lead selenide
magnetooptical effects, interband, 323
Lead sulfide
magnetooptical effects, interband, 323
Lead telluride
magnetooptical effects, interband, 323
multiphonon absorption, 400, 401
Lifetime, carrier, 461–463
majority, 462, 473–476
minority, 462, 473–476
Line width, absorption, 203
Liouville equation, 101
linearized, 102
Lorentz polarization factor, 15

M

Magnetic field, *see also* Magnetoabsorption, Magnetooptical effects
absorption, 222–231
impurity, 223
acceptor ground state split, 224
crystal Hamiltonian, 282–287
density of states, 222–305, 385
diamagnetic shift, 224
electron-phonon coupling, 400
exciton absorption, 226–231, 305–310
excitons, 226ff., 299–310, 323, 395
g-factor, *see g*-factor
impurity level shift, 224
Landau level, 144, 223, 299, 304–310, 327, 438, 439, 441, 442
Landau shift, 144, 224
lifetime, 396
operator, 292, 293
piezoreflection, 398
quantum limit, 396
recombination, 397
strong-field effects, 395–399
Zeeman effect, *see* Zeeman effect
Magnetoabsorption, 222–231, 305–310, 326–330
band structural considerations, 357–363
direct transition
Ge, 368–372

InAs, 387
InSb, 379–383
electric field, *see* Crossed-field effects, Magnetotunneling
exciton effects, 311
indirect transition, Ge, 372–376
effective masses, 376
Landau level versus exciton, 309, 365
quantum theory
direct transitions, 349, 350
indirect transitions, 354, 355
Magnetodispersion, 343–345
GaAs, 343
InAs, 345
InSb, 345, 386
Magnetoemission phenomena, laser diodes
GaAs, 392–394
InAs, 387
InSb, 385–387
Magnetointerference fringe shift, 431, 454, 456
Magnetooptical effects, *see also* Magnetoabsorption, Magnetoreflection
free carrier, 421–458
interband, 321–401
Magnetoplasma
critical frequencies, 428
reflection, 429, 430, 439, 440
ellipticity, 440
rotation, 440
refractive index, 422–431
resonance, 429, 430
Magnetoplasma resonance, definition, 430
Magnetoreflection, *see also* Magnetoplasma
Faraday rotation, InAs, 387
Ge, 440
InAs, 489
InSb, 324, 379, 489
HgSe, 439
HgTe-CdTe, 324, 440
Magnetotransmission, 441–458
cyclotron resonance, 441–446, *see also* Cyclotron resonance
harmonic, 446–448
Magnetotunneling
electromagnetoabsorption, 341
photon assisted, 338–343
Mass-difference effect, phonon branches, 28
Mass, effective, 149–151, 223, *see also* Effective mass, listing of specific materials
electron-hole pair, 265
germanium, 129, 369, 372, 376
InSb, 178, 179, 382, 383
polaron, 254, 447
reduced, 328, 346
exciton, 265
susceptibility, 415, 418
tabulation, 151
total exciton mass, 276
Maxwell's equations, tensor medium, 422
Mercury telluride
band gaps, 130
magnetoabsorption, 399
spin-orbit splitting, 133, 141
Metallic region, 114
dielectric constant, 95
Mixed crystals
GaAs-GaP
band gaps, 131, 132
interband absorption, 411–414
lattice frequencies, 8, 9
GaAs-GaSb, lattice frequencies, 8, 9
Ge-Si alloys
lattice absorption, 41–43
phonon assignments, 43
phonon frequencies, 43, 44
HgTe–CdTe, magnetoreflection, 324
Mobility, *see* Hall mobility
Modulation techniques, 255–257
Multiphonon lattice absorption, 17–69, 73
Multiphonon processes, *see also* listings of specific materials
diamond structure, 24, 25
zinc-blende structure, 24, 25
Multiphoton absorption
InSb, 400
PbTe, 400, 401

N

Neutron scattering, lattice frequencies, 12, 17
GaAs, 48
Nonparabolic bands, 144, 163–167, 224, 372, 380–383, 387, 390, 441, 444, 446

O

Onsagar relationship, 422
Optical constants, 499–543

Optical matrix element, 161, 162, 171, 183–186, 194
indirect transitions, 188
tail absorption, 251
Optical mode vibrations, *see also* Scattering
longitudinal, 3
transverse, 3
Optical selection rule, *see* Selection rule
Oscillations, *see also* Oscillatory effects
absorption, electric field, 334
Oscillator strength, 104, 110, 346, 501
Oscillatory effects, *see also* Quantum effects
Faraday rotation, 325, 354
interband magnetoabsorption, 322–325, 328–331, 369
electric field, 334–338
Ge, 369–375
Voigt effect, 325, 332, 333

P

Periodicity, destruction, 295
Permeability, 422
Phonon assignments, *see* listing of specific materials
Phonon frequencies, *see* listing of specific materials
characteristic, 26–29
Phonon structure, 191–193
Photoconductivity, 12, 155, 461, 466, 473, 474
gain, 463
GaSb, 208
spectral response, 464, *see also* Spectral response
surface, 464
volume, 464
Photoelectronic analysis, 461–495
Photo Hall effect, 471, 472, 480, 486–495
GaAs, 486–495
Photoluminescence, 155
Photomagnetoelectric effect, 473, 474
Photon absorption, *see also* Absorption
probability, 162
Photon-assisted tunneling, 338–343
Photon capture cross section, free carriers, 406–410
Photosensitivity, 462, 463
GaAs, 478–480
InP, 478–480
Photovoltaic response, 155, 190–192
Piezoreflectivity, 257
magnetic field, 398, 400
Planck equation, 71
Plasma, 422
magnetic field, *see* Magnetoplasma
refractive index, 426–431
Plasma frequency, 100, 105, 118, 424
effective, 107, 118
Plasma mode, 423–425
Plasma oscillations, 95, 119, 120, 134
lifetime, 120
Polar character, 3, 13
Polarization state, 431–435
depolarization field, 448
Polaron effects, 253–255
doublets, InSb, 255
effective mass, 254, 447
self energy, 253
energy gap shift, 253
Pseudomomentum matrix element, 281
Pseudomomentum operator, 273, 288

Q

Quantum effects, 422
harmonic cyclotron resonance, 438, 439, 446–488
optical de Haas–Shubnikov effect, 422, 438, 439
Quantum limit, 396
Quasi-momentum operator, 281, *see also* Pseudomomentum operator
Quenching, photoconductivity
optical, 467, 480, 490
thermal, 466

R

Raman spectra, 12, 13
Random-phase approximation, 101
Recombination, 462
magnetic field, 397
surface, 474
Recombination emission, GaSb, 208
Reflectance, 72, 73, 93, 94, 98, 111–113
Reflection, 156
coefficient, 72, 98
free-carrier, 5, 10, 414–419

Fresnel coefficient, 72
Fresnel equation, 72, 98
lattice, 3–16
magnetic field, *see* Magnetoreflection
phase shift, 427, 433–435
Reflectivity, 157, 414, 425–431, *see also* Reflectance
magnetic field, *see* Magnetoreflection
Refractive index, 347, 405, 422–429, 499, 502
complex, 4–8, 72, 98, 157, 422–425, 438, 499
extinction coefficient, 4–7, 98, 99, 157, 495
magnetic field, *see* Magnetodispersion, *Magnetoplasma*
ordinary, 4–7
plasma, 426–431
Relaxation time, 118
electron-electron scattering, 118
magnetic field, 396, 397
Umklapp processes, 118
Relaxation-time approximation, 102
Release rate, charge carrier
optical, 467, 490
thermal, 467
Reststrahlen, 72, 73, 194, 270, 447, 534, *see also* listing of specific materials

S

Scattering
acoustic mode, optical absorption, 406, 407
giant cross sections, 480
dipole, 495
electron-electron, 118, 249
impurity, 249, 471, 472
inhomogeneous distributions, 484, 485, 490
intervalley, optical absorption, 407–410
ionized impurity, 186, 187
optical absorption, 407–410
magnetic field, 396, 397, 400
matrix elements
acoustic phonon, 188
ionized impurity, 186, 187
optical phonon, 187, 188
optical effects, 415, 421, 471, 472
optical phonon, optical absorption, 407–410
polar mode, optical absorption, 408–410
space-charge regions, 484, 485
threshold broadening, 186
Umklapp processes, 118
Screening, 194
Debye length, 186
electron-hole interaction, 266, 267, 270, 278
heavy doping, 252
ionized impurity, 407, 408
Selection rule, 168, 186
cyclotron resonance, 438
exciton states, 293, 294
indirect transitions, 297, 298
magnetoabsorption, 328
optical, 168, 186
Self energy
electron, 185, 194, 200
polaron, 253
energy gap shift, 253
Sellmeier equation, 515
Sensitization, imperfection, 463, 464, 466, 478–480
Shell model, 17, 33
Silicon
absorption, electric field, 248
alloys (*see* Mixed crystals)
band parameters, 314
Brout sum rule, 29
complex dielectric constant, 105, 111, 115
critical-point analysis
energies, 67, 68
phonon assignments, 67, 68
effective dielectric constant, 117
effective ionic charges, 27
effective-mass complexes, 232
energy gap
direct, 314
pressure dependence, 200
energy-loss function, 111, 118, 120
exciton states, 315
binding energy, 314, 315, 317
lattice absorption, 32, 33
magnetooptical effects
crossed field, 338
interband, 325
metallic effects, 114
phonon assignments, 34, 35
phonon frequencies, 29, 35
plasma frequencies, 118

reflection
electroreflectance, 256
reflectance, 111
spin-orbit splitting, 314
Silicon carbide
absorption, 39
Brout sum rule, 29
complex dielectric constant, 105
critical-point analysis, phonon energies, 68
effective ionic charges, 27, 38
exciton-impurity complexes, 232
exciton recombination, 40
phonon assignments, 40, 41
phonon frequencies, 29
reflectivity, 38
Silver iodide, spin-orbit splitting, 126, 131
Skew sequence, 148
energy gaps, 148
Skin depth, 448
Space-charge regions, 484, 485
Spectral response, 464
GaP, 485
Spin operator, 284, 300
Spin-orbit coupling, 346, 347, 358, *see also* Spin-orbit splitting
Spin-orbit splitting, 126, 133, 140–143, 149, 164, 257, 312, 313, 316, 359, 374, 382, 441
III-V compounds, 137, 141, 314
GaSb, 390
germanium, 129, 314
silicon, 314
Spin resonance
germanium, 130
InSb, 445
Spin splitting, 282, 386
Landau levels, 350
Splitting
band, 283
orbital contribution, 283
magnetic field, 224
spin, 282, 350
spin-orbit, 126, 133, 140–143, 149, 164
Sum rules, 108, 302, 303, 348
Brout, 27–29, 86
f-sum rule, 104, 110, 282
Strain, 196–200
absorption edge shift, 252
absorption line splitting, 242
exciton shift, 220
Faraday rotation, 377
inhomogeneities, edge shift, 252
magnetoabsorption, 338, 339, 389
crossed field, 338, 339
Subsidiary band minima, 316
GaSb, 183, 418
Superlinearity, 465
Surface damage, 500
adsorption, 500
oxide films, 500
roughness, 500
Susceptibility
carrier, 414–419, 534
degenerate carriers, 416
electric, 405, 406, 415
intervalence band, 418, 419
Susceptibility effective mass, 415–418
carrier distribution, 417
degenerate bands, 415
lattice dilatation, 417
multivalley ellipsoids, 415
nonquadratic bands, 416
spherical bands, 415

T

Thermal expansion coefficient, 198
Thermally stimulated conductivity, 468–471, 476–478, 482–484, 486, 487, 493–495
Thermal reflectance, 400
Time-reversal operator, 271, 288
Transitions
allowed, 162, 184, 293
Ge, 363
InSb, 169
direct, 154, 264, 279, 288–294
magnetic field, 306, 309, 328, 332, 349, 350, 369–372
exciton, 215–218, 279, 280, 288–299
forbidden, 162, 185, 186, 191–193, 293, 294
first, 293, 294
magnetic field, 307, 308, 329, 330, 332
second, 294
impurity, 196
indirect, 154, 188–191, 264, 280, 294–299
absorption coefficient, 190
AlAs, 190
AlSb, 191
GaP, 190, 242, 243

magnetic field, 306–308, 332, 372–376
piezoabsorption, 257
interband, 94, 95, 109, 120
magnetic field, 310, 328, 329, 370
intermediate state, 185
symmetry-forbidden, 162
Transit time, carrier, 463
Transmission, 8, 155, 157, 509
magnetic field, *see* Magnetoabsorption, Magnetoreflection, Magnetotransmission
spectra, 8
transmittance, 72
Zeeman effects, 240
Trapping, 464, 468–471, 473, 486, 487, 491
density, 468, 469
depth, 468–471, 491–495
distribution, 477
imperfection, 476–478
Tunneling, 12

U

Ultraviolet optical properties, 93–124
Umklapp processes, 118

V

Verdet constant, 377
Voigt effect, 322, 325, 332, 333, 347, 349, 428, 434–437, 453, 454
cyclotron resonance, 448
line shape, direct transition, 353
quantum theory
direct transitions, 352, 353
indirect transitions, 356, 357

W

Wave functions
excited-state, 158–160
exciton states, 275, 287, 293, 294
Landau, 304, 305, 326, 338
modulating function, 275

Z

Zeeman effect, 223, 308 309, 321, 322, 374, 385
exciton peak, GaSb, 228
GaSb, 239–241
germanium
direct exciton, 370–372
indirect exciton, 373
Zinc selenide
absorption spectra, 64
Brout sum rule, 29
d-band excitation, 123
effective ionic charges, 27
phonon assignments, 61, 62, 64
phonon frequencies, 29, 64
spin-orbit splitting, 126
Zinc sulfide
band gaps, 131
Brout sum rule, 29
critical-point analysis, phonon energies, 68
effective ionic charges, 27
exciton states, 278
phonon assignments, 61–63
phonon frequencies, 29, 62, 63
Zinc telluride
band gaps, 130
spin-orbit splitting, 126